

UNCLASSIFIED

AD NUMBER
AD876677
NEW LIMITATION CHANGE
TO Approved for public release, distribution unlimited
FROM Distribution authorized to U.S. Gov't. agencies and their contractors; Administrative/Operational Use; SEP 1969. Other requests shall be referred to Navy Weather Research Facility, Norfolk, VA 23511.
AUTHORITY
NWRF ltr, 14 Aug 1974

THIS PAGE IS UNCLASSIFIED

THIS DOCUMENT IS SUBJECT TO SPECIAL EXPORT CONTROLS  
AND EACH TRANSMITTAL TO FOREIGN GOVERNMENTS OR  
OTHER NATIONALS MAY BE MADE ONLY WITH PRIOR  
APPROVAL OF NAVY WEATHER RESEARCH FACILITY.

NWRF 09-0969-146

Norfolk, Va 23511



AD 876677

# Proceedings of the CONFERENCE ON THE SUMMER MONSOON OF SOUTHEAST ASIA

Colin S. Ramage, Editor

Conducted 7-9 April 1969 at

Department of Geosciences, University of Hawaii

Sponsored by



AIR FORCE CAMBRIDGE RESEARCH LABORATORIES

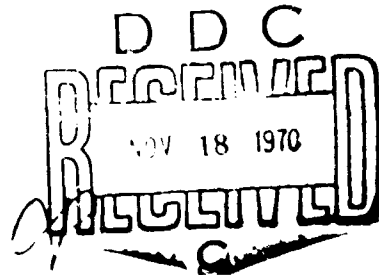


and

NAVY WEATHER RESEARCH FACILITY

AD No. \_\_\_\_\_

DDC FILE COPY



**NAVY WEATHER RESEARCH FACILITY**  
BUILDING R-48, NAVAL AIR STATION  
NORFOLK, VIRGINIA 23511

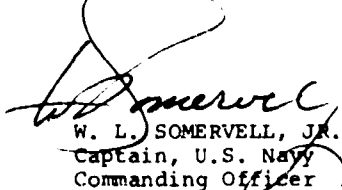
September, 1969

**Best  
Available  
Copy**

## FOREWORD

In recognition of the necessity for augmentation and acceleration of research on weather phenomena associated with the Southwest Monsoon, Air Force Cambridge Research Laboratories and the Navy Weather Research Facility jointly sponsored a Conference on the Summer Monsoon of Southeast Asia (SEASIA) at the University of Hawaii from 7 through 18 April 1969, with Professor Colin S. Ramage as Scientific Director. A digest of the operationally significant findings and conclusions from that conference was published earlier<sup>1</sup>, for the sake of timely dissemination to organizations to which the prediction of variations in SEASIA summer weather are a matter of day-to-day concern. By publication herewith of the Proceedings for the 7-9 April 1969 seminar phase of the conference in their entirety, it is hoped that both familiarization on the part of forecasters newly arrived in the WESTPAC area and research by scientists interested in SEASIA summer-season atmospheric processes will be enhanced.

To all who participated in this conference, and particularly the invited attendees who presented papers on relevant research results, it is desired to extend the appreciation of Commander, Air Force Cambridge Research Laboratories and this command. Judging by correspondence received from a number of the field participants and comments received relative to the publication cited below, it appears that conference objectives were met to the extent of contemporary feasibility and that participants are to be congratulated for the pertinence and comprehensiveness of their contributions. The rather extensive work of readying these Proceedings for publication was accomplished under the direction of Mr. L. R. Brody, Mr. S. D. Case, Jr., Mr. J. L. Bean and Mrs. J. L. Estes of the Navy Weather Research Facility staff.



W. L. SOMERVELL, JR.  
Captain, U.S. Navy  
Commanding Officer

U.S. Navy Weather Research Facility

---

<sup>1</sup> "A Diagnosis of the Summer Monsoon of Southeast Asia," NAVWEARSHFAC Tech. Paper No. 10-69, June 1969.



## PREFACE

The problems of forecasting summer weather over southeast Asia, where continental and maritime influences interact on the edge of the south Asian monsoon, defy easy solution. To bring together representatives of the scattered groups working on these problems, a conference on the summer monsoon of southeast Asia was held at the University of Hawaii from 7 through 9 April 1969. The U. S. Navy Weather Research Facility and the U. S. Air Force Cambridge Research Laboratories sponsored the conference, which was organized and directed by the Department of Geosciences of the University of Hawaii.

The 55 participants, whose interests ranged from the esoterically theoretical to the severely practical, presented and discussed 19 papers. Copies of almost all the papers were distributed ahead of the presentations. As a result argument was more to the point and idea exchange more effective than might otherwise have been the case.

Since the conference significantly added to my knowledge of the southeast Asian summer monsoon, I optimistically assume that the other participants also benefited and that distribution of these proceedings will help many more tropical meteorologists.

Besides their forthright opening remarks, Captain W. L. SOMERVELL, Jr., Commanding Officer of the Navy Weather Research Facility and Colonel D. J. FLINDERS, Commander of Air Force Cambridge Research Laboratories, directly contributed to the conference and through their organizations supported publication of these proceedings.

The names of many who helped make the conference a success appear in the following pages. In addition I gratefully commend Michie Hamao, Louis Oda, James Nasuti, John Pitko, Robert Barang, and the staff of the University Conference Center.

C. S. RAMAGE  
Scientific Director and Editor

TABLE OF CONTENTS

	Page
FOREWORD . . . . .	i
LOCATOR CHART. . . . .	iii
PREFACE. . . . .	v
TABLE OF CONTENTS. . . . .	vii
LIST OF PARTICIPANTS . . . . .	x

PAPERS AND DISCUSSIONS

LARGE-SCALE FEATURES

	1
THE SETTING OF THE SOUTHEAST ASIA SUMMER MONSOON - C. S. Ramage. . . . .	3
MEAN CIRCULATION AND CLOUDINESS DURING THE DEVELOPMENT OF THE SOUTHWEST MONSOON OVER INDIA AND SOUTHEAST ASIA - J. C. Sadler. . . . .	13
ESTABLISHMENT OF THE SOUTHWEST MONSOON OVER SOUTH VIETNAM - K. M. Nguyen. . . . .	29
INDIAN OCEAN CLOUD PATTERNS FROM SATELLITE PICTURES - J. H. Conover . . . . .	35
CLIMATOLOGY OF ESSA CLOUD PICTURES OVER SOUTHEAST ASIA IN 1967 - T. T. Fujita . . . . .	37
NUMERICAL SIMULATION OF THE MONSOON ALONG 80° E. - T. T. Murakami, R. V. Godbole and R. R. Kelkar. Presented by T. Murakami. . . . .	39

SYNOPTIC METEOROLOGY

	53
FORMATION AND STRUCTURE OF EQUATORIAL ANTICYCLONES CAUSED BY LARGE-SCALE CROSS EQUATORIAL FLOWS DETERMINED BY ATS-1 PHOTOGRAPHS - T. T. Fujita, K. Watanabe and T. Izawa. Presented by T. T. Fujita . . . . .	55
FORECASTING FINE WEATHER OVER NORTH VIETNAM - W. R. Brett. . . . .	79
THE MONSOON TROUGH NEAR THE SOUTH CHINA COAST - G. J. Bell . . . . .	83
CASES OF HEAVY PRECIPITATION AND THEIR FORECAST IN SOUTH VIETNAM - H. H. Nguyen. . . . .	107
MID-TROPOSPHERIC CYCLONES OF THE SOUTHWEST MONSOON - T. N. Krishnamurti and R. S. Hawkins. Presented by T. N. Krishnamurti . . . . .	127
USE OF NUMERICAL PRODUCTS IN THE TROPICAL PACIFIC - R. E. Hughes. . . . .	151

CONVECTION

	153
SUMMER MONSOON STUDIES OF CLOUDS AND WEATHER OVER SOUTHEAST ASIA UTILIZING SATELLITE DATA - J. H. Conover . . . . .	155
FIFTEEN-DAY CYCLES IN SOUTHEAST ASIA RADAR DATA - J. T. Bunting. Presented by J. H. Conover. . . . .	207
AN OBJECTIVE METHOD OF FORECASTING CHANGES IN CONVECTION ACTIVITY IN SOUTHEAST ASIA - F. R. Valovcin. . . . .	215
INTERPRETATION AND APPLICATION OF NIMBUS HIGH RESOLUTION INFRARED RADIOMETER DATA - R. S. Hawkins. Presented by F. R. Valovcin. . . . .	

TABLE OF CONTENTS (CONTINUED)

	Page
DERIVATION OF CONVECTIVE FORECASTING MODELS OF NORTHERN AUSTRALIA FROM A CLIMATOLOGY OF LIGHTNING DISCHARGES - R. L. Southern, W. R. Kininmonth and N. R. Pescod. Presented by R. L. Southern . . . . .	239
THE INFLUENCE OF THE SYNOPTIC SCALE ON CONVECTION OVER SOUTHEAST ASIA DURING THE SUMMER MONSOON - B. E. Harris . . . . .	255
MESOSCALE AND DIURNAL VARIATIONS DEDUCED FROM THE SAIGON AREA RAWINSONDE DATA - C. W. Kreitzberg, F. W. Endlich and J. R. Sweeney. Presented by C. W. Kreitzberg . . . . .	271
VARIATIONS IN CONVECTIVE ACTIVITY OVER SOUTHEAST ASIA DURING THE SUMMER OF 1967 - R. F. Adler . . . . .	283
A NOTE ON APPLICATION OF A CUMULUS MODEL TO SOUTHEAST ASIA SOUNDING DATA - J. T. Bunting (not presented at Conference) . . . . .	295
GENERAL DISCUSSION . . . . .	297



LIST OF PARTICIPANTS

C. W. ADAMS, University of Hawaii  
R. F. APLER, Navy Weather Research Facility, NAS, Norfolk, Virginia  
CDR H. W. ALBERS, USN, Staff, Commander, SEVENTH Fleet  
Maj. G. D. ATKINSON, USAF, Air Weather Service, Scott AFB, Illinois  
G. J. BELL, Royal Observatory, Hong Kong  
S. BRAND, Navy Weather Research Facility, NAS, Norfolk, Virginia  
Maj. W. R. BRETT, USAF, 1st Weather Wing, Honolulu  
L. R. BRODY, Navy Weather Research Facility, NAS, Norfolk, Virginia  
CDR A. T. BUCKMASTER, USN, Staff, Commander in Chief, Pacific  
E. M. CARLSTEAD, ESSA Weather Bureau, Honolulu  
W. C. CHIU, University of Hawaii  
J. H. CONOVER, Air Force Cambridge Research Laboratories  
LCDR G. D. DELANO, USN, Naval Air Forces, U. S. Pacific Fleet and Fleet Weather Facility, San Diego, California  
R. L. ELSBERRY, Naval Postgraduate School, Monterey  
Col. D. J. FLINDERS, USAF, Air Force Cambridge Research Laboratories  
T. T. FUJITA, University of Chicago  
Maj. P. GANNON, USAF, 1st Weather Wing, Honolulu  
L. HACKER, ESSA Weather Wing, Honolulu  
LCDR J. S. HARDIE, USN, Fleet Weather Facility, Sangley Point  
Maj. B. E. HARRIS, USAF, 1st Weather Wing, Honolulu  
CAPT W. E. HUBERT, USN, Fleet Weather Central, Pearl Harbor  
CDR R. E. HUGHES, USN, Fleet Weather Central, Pearl Harbor  
Capt. R. M. HUGHES, USAF, 20th Weather Squadron, Fuchu Air Station, Japan  
LT D. L. JONES, USN, Amphibious Forces, U. S. Pacific Fleet and Amphibious Forces, U. S. Seventh Fleet  
Capt. R. E. KATZ, USMC, Fleet Marine Force, Pacific  
LCDR W. O. KERMAN, USN, Fleet Weather Central, Guam  
Capt. P. V. KOSMO, USMC, 1st Marine Aircraft Wing  
C. W. KREITZBERG, Pennsylvania State University  
T. N. KRISHNAMURTI, Florida State University  
P. H. KUTSCHENREUTER, ESSA Weather Bureau, Honolulu  
LT F. K. MARTIN, USN, U. S. Naval Support Activity, Da Nang  
CAPT H. A. MCCREREY, USN, Staff, Commander in Chief, U. S. Pacific Fleet and Naval Weather Service Command Representative, Pacific  
LT D. A. MILLS, USAF, Air Technical Training Center, Lakehurst  
Maj. A. MELLA, USAF, Air Weather Service, Washington, D. C. 1st Weather Group, Saigon. (from August 1969)

LIST OF PARTICIPANTS (CONTINUED)

T. MURAKAMI, University of Hawaii  
CAPT J. H. NEGELE, USN, U. S. Fleet Weather Central/Joint Typhoon Warning Center,  
Guam  
H. H. NGUYEN, DOM, RVN  
K. M. NGUYEN, DOM, RVN  
Maj. H. NISHIMOTO, USAF, 1st Weather Wing, Honolulu  
C. S. RAMAGE, University of Hawaii  
R. J. RENARD, Naval Postgraduate School, Monterey  
D. F. REX, University of Hawaii (National Center for Atmospheric Research)  
J. C. SADLER, University of Hawaii  
LCDR R. C. SCHIFFNER, USN, Fleet Weather Central, Guam  
Lt. Col. F. SHAY, USAF, 6th Weather Wing, Washington, D. C., 1st Weather Group,  
Saigon (from July 1969)  
CAPT W. L. SOMERVELL, Jr., USN, Navy Weather Research Facility, NAS, Norfolk,  
Virginia  
R. L. SOUTHERN, Australian Bureau of Meteorology, Darwin  
LTJG C. D. THORMEYER, USNR, Fleet Numerical Weather Central, Monterey  
F. R. VALOVGIN, Air Force Cambridge Research Laboratories  
J. VEDERMAN, ESSA Weather Bureau, Honolulu  
Maj. V. VON, USAF, 1st Weather Wing, Honolulu  
Capt. T. WANN, USAF, 1st Weather Wing, Honolulu  
Capt. R. B. WELDON, USAF, Air Training Command, Chanute AFB, Illinois  
Lt. Col. S. WITHROW, USAF, 1st Weather Wing, Honolulu  
Maj. J. ZIMMERLEE, USAF, 1st Weather Wing, Honolulu

## **LARGE-SCALE FEATURES**

## THE SETTING OF THE SOUTHEAST ASIA SUMMER MONSOON \*

Colin S. Ramage  
University of Hawaii

### ABSTRACT

The role of the Himalayan-Tibetan Massif in the Southeast Asia summer monsoon is described. Then discussion shifts to the changes leading to onset of the early summer rains, the mid-summer dry spell, and the late summer rains. Hypotheses are advanced to account for the rainfall regime over the neighboring seas and for "breaks" in the monsoon rains.

### 1. INTRODUCTION

Southeast Asia is conveniently defined as that part of Asia east of Tibet and the Bay of Bengal and south of the Yangtze River. It includes the East and South China Seas.

In this paper I propose to concentrate on describing, and trying to account for, the large-scale changes accompanying onset, persistence and cessation of the summer monsoon of Southeast Asia. This will involve comparing conditions in this region with conditions over India to the south of the Himalayas. The great Himalayan/Tibetan Massif powerfully but quite differently affects these two monsoon regions and a study of the differences throws significant light on the nature of the Southeast Asia branch of the phenomenon.

In the broadest sense, monsoonal Asia might be divided into three parts: east of Tibet, where significant winter precipitation falls and spring and summer are wet; west of Tibet, where deserts dominate; and south of Tibet, where winters are desert like and summers are wet. Figures 1 and 2, showing the 200-mb. mean resultant winds for January and July, reflect this distribution. East of Tibet they are divergent in both seasons, west of Tibet convergent in both seasons, and south of Tibet, convergent in winter and divergent in summer. These distributions derive from the combined mechanical-thermal effect of Tibet, and in what follows I make considerable use of the excellent data published by Flohn [5].

Figure 3 shows that upper-tropospheric pressure heights over southeast Tibet (Lhasa) are greater than pressure heights to the west throughout the year and than pressure heights to the east during summer.

Flohn has demonstrated from weather satellite pictures that central and southeast Tibet are almost snow free during winter and act as a high-level radiational heat source. Air subsides east of the plateau, is further warmed by compressional heating, and over central China flows alongside very cold air which has swung around the northern edge of the massif. Here the extremely large temperature gradients produce an exceptionally strong jet stream. West of Tibet, smaller pressure heights, resulting from absence of a mid-tropospheric heat source, accompany larger gradients and a stronger subtropical jet than to the south of Tibet.<sup>1</sup>

During the summer central and southeast Tibet continue to act as a heat source with condensation along the Himalayas powerfully aiding the effects of radiation. Now, however, the heating instead of acting to weaken a S. - N. temperature gradient as in winter, acts to increase the N. - S. temperature gradient of the summer monsoon and to produce a speed maximum in the upper-tropospheric easterlies over India [11]. Upstream to the east, the easterlies are divergent and downstream to the west are convergent. Since a high-pressure ridge overlies Tibet and winds over the massif are weak, no compressional warming occurs over west Pakistan and so the year-long upper-tropospheric convergence persists over the great deserts of Southwest Asia and north Africa.

In the remainder of this paper, I emphasize the summer monsoon of Southeast Asia, discussing in turn the changes leading to onset of the early summer rains, the mid-summer dry spell, the late summer rains and onset of the winter monsoon.

\*Research sponsored by Air Force Cambridge Research Laboratory and National Science Foundation

<sup>1</sup> I assume that pressure heights along 15° N. vary longitudinally much less than along higher latitudes.

The peculiar rainfall regime of the adjacent seas is also described. The summer monsoon can be considered as a regional reversal of the Hadley cell where, instead of heat being transported poleward from a near-equatorward source, it is transported both poleward and equatorward from a source displaced 20 degrees or more from the equator.

It is in the zone between the normal position of the near-equatorial trough (5° N. - 10° N.) and the summer location of the monsoon/heat trough that the major monsoon changes occur.

## 2. SLOW ONSET, RAPID RETREAT OF THE SUMMER MONSOON

The summer monsoon circulation results from development of a heat source over the continent, well poleward of the equator. The circulation starts in the surface layers and only gradually extends through the troposphere, becoming truly established in late June when upper-tropospheric east-northeasterlies complete the reverse Hadley cell. According to Kao, et al. [6], the sequence over east Asia starts in March and is completed in June. At the end of summer, the reverse sequence again starts at the surface by September (cooling), but by mid-October is complete throughout the troposphere. The reason for such a relatively sudden reversal is simply that the normal temperature gradient instead of being opposed by a summer monsoonal effect is now reinforced by a winter monsoonal effect.

## 3. EARLY SUMMER

Over south China and northern North Vietnam summer monsoon rains do not set in suddenly. From mid-January onward rain on the average steadily increases. The polar front is maintained over south China through early summer by weak surges of cool air to the east of Tibet [6]. When troughs in the upper-tropospheric westerlies, frequently intensifying along about 105° E., activate the polar front, heavy rain falls beneath the overriding warm air [9]. In early spring air above the front is usually modified Polar Maritime, but by early summer it is almost always Tropical Maritime. As the year advances, although air-mass discontinuity across the front diminishes, available moisture increases (table 1) and average rainfall also increases.

Table 1. Annual Variations of Surface Temperature, Tropospheric Shear and 300-mb. Wind at Calcutta, Hong Kong and Naha. Annual Variation of 850-mb. Mixing Ratio at Hong Kong.

	Jan	Feb	Mar	Apr	May	Jun	July	Aug	Sept	Oct	Nov	Dec
<i>Calcutta (22°39'N.; 88°27'E.)</i>												
Surface temperature (°C.)	20	24	28	31	32	31	29	29	29	28	24	21
850 - 300-mb. resultant shear (m. sec. <sup>-1</sup> )	262 27	256 29	262 26	265 18	253 13	96 8	83 13	75 7	81 3	234 11	257 25	253 22
300-mb. resultant wind (m. sec. <sup>-1</sup> )	270 31	262 33	266 31	265 22	252 19	108 6	92 11	94 7	111 4	242 12	264 26	264 23
<i>Hong Kong (22°18'N.; 114°10'E.)</i>												
Surface temperature (°C.)	15	15	17	21	25	27	28	28	27	25	21	17
850 - 300-mb. resultant shear (m. sec. <sup>-1</sup> )	263 33	266 34	266 29	276 21	305 9	21 6	57 9	47 4	82.2	270 14	263 22	260 30
300-mb. resultant wind (m. sec. <sup>-1</sup> )	260 35	262 37	259 31	266 23	273 10	2 2	85 6	84 5	76 4	279 8	266 18	260 29
<i>Kadena (26°21'N.; 127°45'E.)</i>												
Surface temperature (°C.)	16	17	19	21	24	26	28	28	27	24	21	18
850 - 300-mb. resultant shear (m. sec. <sup>-1</sup> )	259 47	263 49	271 43	275 24	281 13	321 5	45 6	40 3	283 3	262 19	259 31	258 42
300-mb. resultant wind (m. sec. <sup>-1</sup> )	264 50	265 52	269 47	271 27	271 17	266 8	87 4	89 3	283 1	268 15	263 30	262 42
<i>Hong Kong mixing ratio at 850 mb. (gm. kg.<sup>-1</sup>)</i>	5.4	6.9	8.3	10.0	11.7	12.9	13.0	13.0	12.2	8.7	7.3	5.5

Tibet prevents surface outbreaks of cold air from reaching Burma and Thailand. Thus, with neither polar front nor upper trough affecting the area, very little rain falls during spring north of  $10^{\circ}$  N. South of  $10^{\circ}$  N. the near-equatorial trough is active during spring.

Beginning usually in late April, the situation over Burma and Thailand changes dramatically.

### 3.1 Upper Tropospheric Westerlies

As mentioned earlier, the wintertime subtropical jet stream speeds up downstream from Tibet. Although meridional temperature gradients diminish through spring, this distribution does not change. In the weather satellite pictures considerable cloudiness over south China contrasts with nearly clear skies over northeast India and northern Burma, where as a result, insolation heating by the end of April increases the meridional temperature gradient and establishes a local jet stream maximum (table 1).

### 3.2 Near-Equatorial Trough

The trough begins to move irregularly north in April and by early May fluctuates between  $10^{\circ}$  and  $15^{\circ}$  N. Tropical storms developing in the trough and moving north or northeast may bring the first monsoon rains to Burma. However, interaction between the trough and the upper-tropospheric westerlies seems to be the most common cause of the rains. Detailed information is scanty, but the upper winds at Port Blair ( $11^{\circ} 40' N.$ ;  $92^{\circ} 43' E.$ ) supply some clues. When southwesterlies overlie the station from the surface up to 7 to 10 km., the Burma coast experiences a monsoon burst. The deep southwesterlies at Port Blair indicate that the near-equatorial trough is north of the station and that a middle- or upper-tropospheric trough or cyclone lies to the northwest. The consequent upper divergence superimposed on a surface vorticity center could lead to deep widespread convection and heavy rain.

Over south China and northern North Vietnam, May rainfall is about double April rainfall. Over most of Burma and Thailand, however, the increase ranges from 500 to 1200 per cent.

June is uniformly wet in Southeast Asia. To the east, the polar trough shifts slightly northward from its May position [17]. Rain over North Vietnam and parts of Kuangtung diminishes slightly, but elsewhere the "plum rains" increase. To the west, the southwest monsoon is well established, flowing into a surface monsoon/heat trough lying along the Ganges valley and extending into the northern Bay of Bengal. Monsoon depressions and subtropical cyclones cause torrential rains along the Arakan coast; on the average Akyab ( $20^{\circ} 08' N.$ ;  $92^{\circ} 53' E.$ ) receives 1143 mm. in June.

## 4. MID-SUMMER TRANSITION

By mid-June, sensible and condensation heating over northern India and Tibet have reversed the meridional temperature gradient to the south, and the summer monsoon circulation extends throughout the troposphere. Upper-tropospheric easterlies now prevail south of the Himalayas and extend eastward (table 1). Over China the polar front moves north [17] and over south China rainfall decreases to a secondary minimum during the first half of July [8] (see fig. 4) -- the best-defined weather singularity of the whole year. With the decrease in rain and cloudiness [15] insolation heating now acts to extend the monsoon trough eastward from northern India. The rainfall minimum moves north, affecting the Ryukyus and Japan during the second half of July (fig. 4).

## 5. LATE SUMMER

From mid-July through September, the summer monsoon dominates Southeast Asia (table 1). Steered by the N. - S. temperature gradient, western Pacific typhoons, which during early summer tend to recurve east of the continent, now move westward across the South China Sea, contributing to a rainfall maximum over south China around the end of July. In September typhoons most often travel across or to the south of Hainan Island [2].

Burma, lying east of a cyclogenetic region, is affected somewhat differently. From mid-June onward, tropical cyclones and monsoon depressions developing in the Bay of Bengal invariably travel west-northwest across India, and only remnants of South China Sea typhoons reach Burma. Consequently, rains in the interior valley are somewhat less in July and August than in June.

## 6. SUMMER MONSOON RAINS OFFSHORE

Figure 4 indicates that rain zones and intervening clear zones move northward with the sun. However, figure 5, showing mean monthly rainfalls at four small islands in the South China Sea, and at two island stations in the Bay of Bengal reveals no such thing. Although rates of change vary, the curves are in phase; the rainfalls increase to maxima in June and then decrease to minima in July. Mean monthly cloudiness [15] and daily synoptic and weather satellite charts never show single weather systems extending over the 2300 km. separating Terempa from Pratas let alone into the Bay of Bengal, nor do daily rainfalls at the six stations fluctuate in unison. Apart from the local effects of orographic shadowing, India, Burma and the Indochina Peninsula display a well-defined rainfall maximum in July, coinciding with a secondary minimum at the island stations. Continent and adjacent seas are in the same monsoon system. Why the difference?

I think the answer lies in a scale of land-ocean interaction not previously considered. The summer monsoon reaches peak strength in July, when the heat trough and the overlying upper-tropospheric ridge are most intense (fig. 3 and table 1). Since upward motion and rainfall are at a maximum over land, subsidence over the oceans to south and west must also be at a maximum. Over the South China Sea and the Bay of Bengal rains are enhanced as the monsoon strengthens, but a brake -- over-ocean subsidence -- is also being applied. Even though the brake acts weakly and fitfully so close to the continent, it apparently becomes strong enough on the average in July to produce a secondary rainfall minimum.

## 7. FLUCTUATIONS IN THE SUMMER MONSOON

Typhoons and monsoon depressions are obviously associated with bad weather and their movements can be forecast with some confidence particularly in July, August and September. However, during these months massive changes with periods of about a week may occur in the distribution of weather, apparently unconnected with or preceding development of surface lows or troughs. For example, lower-tropospheric southwesterlies have been observed to strengthen over south India and the Andamans and monsoon rains to increase along the Burma coast before development of a monsoon depression at the head of the Bay of Bengal [3, 12].

Much work needs to be done, but a hypothesis based on research over India [10, 13] could serve as a starting point.

Along the foothills of the Himalayas and over south China in May, precipitation is quite heavy and falls beneath the upward moving branch of a circulation in the vertical plane in which heat of condensation is transported to higher latitudes through the agency of upper-tropospheric westerlies. Between this rain area and another associated with the near-equatorial trough to the south, relative cloudiness and rainfall minima [15] (fig. 5) suggest subsidence.

In August, rain is heavy across central India and south China but now it falls beneath the upward moving branch of a summer monsoon circulation in which heat of condensation is transported to and across the equator through the agency of upper-tropospheric easterlies.

During "breaks" in the summer monsoon rains of central India, precipitation becomes heavy along the Himalayan foothills, while Kao [14] reported that the monsoon season rainfall of Assam is negatively correlated with the monsoon season rainfall over central India. Yoshino [17] found a similar negative correlation between July rainfalls for stations bordering and west of the Porosua Strait and for stations on a line between Wuhan (30° 35' N.; 114° 18' E.) and Tokyo.

Perhaps then, "breaks" in the monsoon rains occur when the vertical circulation cell on the north side of the heat equator becomes dominant over the monsoon cell to the south and a "pre-monsoon" condition temporarily supervenes. The rains resume when the monsoon cell is reinvigorated.

A staggering number of possibilities might put this sequence in train. Ramaswamy [13] suggested that southward protrusion of a large amplitude trough in the polar westerlies leads to a break over central India. Certainly one effect would be to increase the S. - N. temperature gradient and so favor intensification of the northern vertical cell. On the other hand, Dixit and Jones [4], ascribed the break to extension of a mid-tropospheric ridge from Indochina across central India. Koteswaram [7] associated breaks with weak 700- or 500-mb. lows moving slowly westward across south India (also remarked on by Dixit and Jones). These three ideas, which may have validity east of the Indian region, are not necessarily contradictory. Taken together they provide a picture of "pre-monsoon" conditions, with upward motion at the polar front in the north and at the near-equatorial trough in the south, and with subsidence in between.

The monsoon rains return when the westerly trough weakens or moves off, but this is by no means the only way in which the cycle might be advanced. Qualitative arguments cannot profitably be pursued much further; sophisticated numerical modelling through which the effects of varying individual synoptic components could be measured will be needed before we can hope to understand these complex interactions.

## 8. END OF SUMMER

The monsoon/heat trough lies over south China in August, and the near-equatorial trough lies along 5° N. in October. In a climatological sense, a trough shifts southward between these two months. However, figures 5 and 6 suggest neither a simple southward movement of a trough-associated zone of bad weather nor any apparent relation between rainfall and typhoon frequency variations. Transformation from summer to winter is sudden, except for disruption from an occasional late typhoon (see table 1).

## DISCUSSION

KREITZBERG: Is the July minimum in island rainfall due primarily to decreases in daytime rainfall rather than to decreases throughout the entire day?

RAMAGE: We have no data yet on diurnal variation of rainfall over these island stations.

SOMERVELL: You indicated that cold air did not get into Thailand and Burma during winter. Surely it can intrude at low levels from the northeast. The winter air over Thailand, Burma and northern India during winter is certainly not tropical.

RAMAGE: True polar outbreaks can't penetrate, although north India is a local source of relatively cool air.

CONOVER: May maximum rainfalls are observed in Florida and Central America -- distribution on islands are uncertain -- possibly similar influence as in Southeast Asia.

RAMAGE: A comparison of continental rainfall and rainfall on offshore islands could usefully be made throughout the tropics.

HAU: Which do you think is the most important factor contributing to the intensification of the winter-time subtropical jet stream:

- (a) The role of the Tibet Plateau;
- (b) The role of the Indonesia-Carolines area; or
- (c) The daily synoptic situation accompanying an active cold front?

RAMAGE: All are important and interact complexly.

SOMERVELL: If I interpret you correctly, you've said that by and large throughout Southeast Asia the precipitation maximum occurs in July, and that the double maximum evidenced by the island records in figure 5 is an exception. On the contrary, it is my impression that almost all stations show a double precipitation maximum -- one in late spring or early summer and another in late summer or early fall, and that the single mid-summer precipitation maximum is the exception.



RAMAGE: Overall, through south and Southeast Asia, July is the wettest month although in some areas (inland Burma; Madras), June is somewhat wetter.

SOUTHERN:

- (a) Drawing a parallel with the situation south of the equator where the effect of orography is much less, cold air does not reach well into the tropics in the pre-monsoon period and yet there is no Tibetan type plateau to prevent it. Possibly the effect of topography in the Northern Hemisphere is slightly overrated.
- (b) Possibly the apparent rainfall minimum in mid-summer represents a period of suppressed convective activity between periods when both strong convection and early or late synoptic scale systems are superimposed.

RAMAGE:

- (a) Southeast Asia cold polar outbreaks seldom reach latitudes as low as Darwin's (12° S.; 131° E.).
- (b) The distribution of early, mid- and late summer rain producers over south and Southeast Asia is quite similar to those you describe for northern Australia.

BELL: Sea temperature off Hong Kong shows a minimum in July. I have recently examined sea temperature at four stations in the South China Sea and they show a maximum in June and decrease thereafter. Convective activity will depend to some degree on the land/sea temperature difference and also on the sea temperature itself. Could not this result in some diminution of rainfall over the islands of the South China Sea? I am not sure what happens to sea temperature further to the west.

RAMAGE: This represents the weakened eastward limit of a mid-summer sea temperature minimum which is best developed over the Arabian Sea. There may be an effect on rainfall, although the two may be hard to separate since decreased cloudiness leads to increased insolation and increased sea-surface temperatures.

MILLS: You stated: "Polar front passage in Saigon once every 10 years". What happened 6 through 10 June 1967?

RAMAGE: Lt. Mills and I are going to study this case with the workshop material.

#### REFERENCES

1. ANANTHAKRISHNAN, R., "Tracks of Storms and Depressions in the Bay of Bengal and the Arabian Sea 1877-1960." India Meteorol. Dept. New Delhi, 166 charts, 1964.
2. CHIN, P. C., "Tropical Cyclones in the Western Pacific and the China Sea Area." Roy. Obsy. Hong Kong Tech. Mem., 7, 85 charts, 1958.
3. DESAI, B. N., "On the Development and Structure of Monsoon Depressions in India." Mem. Ind. Meteorol. Dept., 28, pp. 217-228, 1951.
4. DIXIT, C. M. and D. K. JONES, "A Kinematic and Dynamical Study of Active and Weak Monsoon Conditions Over India During June and July, 1964." International Meteorological Center, Bombay (prepub.), 28 pp., 1965.
5. FLOHN, H., "Contributions to a Meteorology of the Tibetan Highlands." Dept. Atmos. Sci. Colorado State University, Atmos. Sci. Paper No. 130, 120 pp., 1968.
6. FAO, Y. -H., et al., "Some Problems on the Monsoons of East Asia." Coll. Papers Inst. Geophys. and Meteorol., Acad. Sinica, 5, 106 pp., Translated by Oriental Science Library, Emmanuel College, Boston (Translation Emm-66-124), 1962.

REFERENCES (CONTINUED)

7. KOTESWARAM, P., "Upper Level 'Lows' in the Indian Area During SW Monsoon Season and 'Breaks' in the Monsoon." *Ind. J. Meteorol. Geophys.*, 1, pp. 162-164, 1950.
8. RAMAGE, C. S., "Variation of Rainfall Over South China Through the Wet Season." *Bull. Am. Meteorol. Soc.*, 33, pp. 308-311, 1952.
9. \_\_\_\_\_, "The Cool-Season Tropical Disturbances of Southeast Asia." *J. Meteorol.*, 12, pp. 252-262, 1955.
10. RAMAMURTHY, K. M., R. N. KESHAVAMURTHY and R. GAMBUNATHAN, "Some Distinguishing Features of Strong and Weak Monsoon Regimes Over India and Neighbourhood." in "Proceedings of the Symposium on Meteorological Results of the International Indian Ocean Expedition." (P.R. Pisharoty, ed.), pp. 350-361, Indian Meteorol. Dept., New Delhi, 1967.
11. RAMAN, C. R. V. and Y. RAMANATHAN, "Interaction Between Lower and Upper Tropical Tropospheres." *Nature*, 204, pp. 31-35, 1964.
12. RAMANATHAN, K. R. and K. P. RAMAKRISHNAN, "The Indian Southwest Monsoon and the Structure of Depressions Associated With It." *Mem. Ind. Meteorol. Dept.*, 26, pp. 13-36, 1932.
13. RAMASWAMY, C., "Breaks in the Indian Summer Monsoon as a Phenomenon of Interaction Between the Easterly and the Subtropical Westerly Jet Streams." *Tellus*, 14, pp. 337-349, 1962.
14. RAO, K. N., Personal communication, 1964.
15. SADLER, J. C., "Average Cloudiness in the Tropics From Satellite Observations." *International Indian Ocean Expedition Meteorol. Monogr.*, 2, 22 pp., 12 plates, 1969.
16. WORLD METEOROLOGICAL ORGANIZATION, "Research Work in Tropical Meteorology." Eighth report, Geneva, 1968.
17. YOSHINO, M. M., "Rainfall, Frontal Zones and Jet Streams in Early Summer Over East Asia." *Bonner Meteorol. Abhand.* No. 3., 1963.

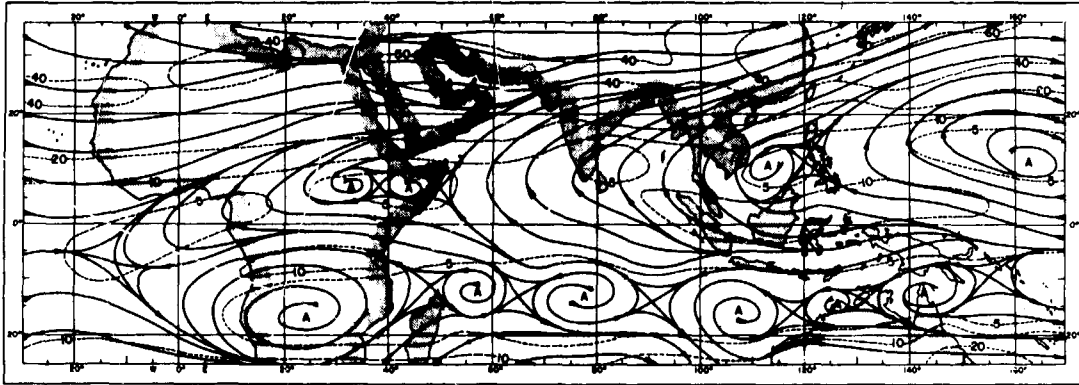


Figure 1. January Mean Resultant Winds at 200 mb. Solid lines are streamlines, dashed lines are isotachs labelled in m. sec. <sup>-1</sup>.

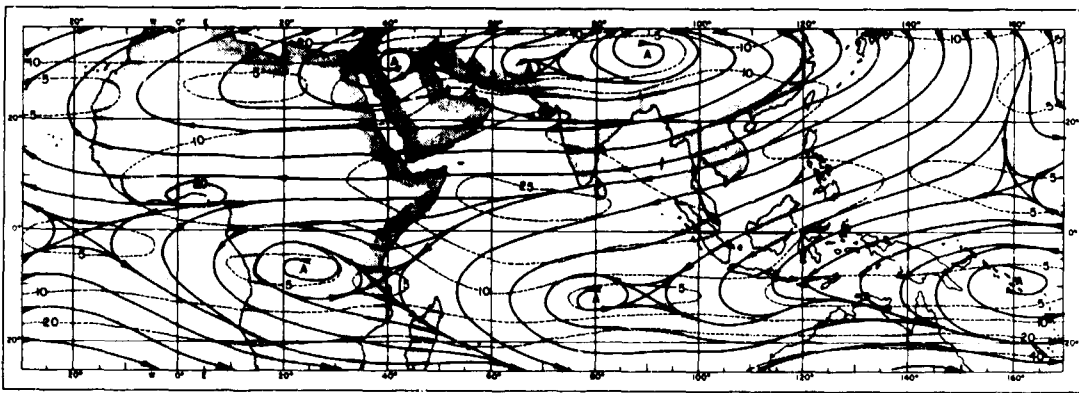


Figure 2. July Mean Resultant Winds at 200 mb. Solid lines are streamlines, dashed lines are isotachs labelled in m. sec. <sup>-1</sup>.

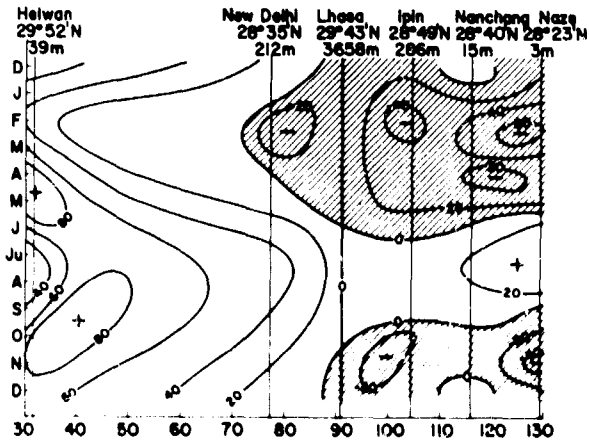


Figure 3. Differences Between Mean-Monthly 300-mb. Pressure Heights (gdm.) at Lhasa in Southern Tibet and Stations to East and West. Negative areas (Lhasa less) stippled. Patterns at 200 mb. are similar, although complicated during winter by presence of the tropopause. Temperatures recorded by Indian radiosondes are higher than those recorded by other radiosondes [5, 16]. Accordingly the New Delhi pressure heights have been adjusted.

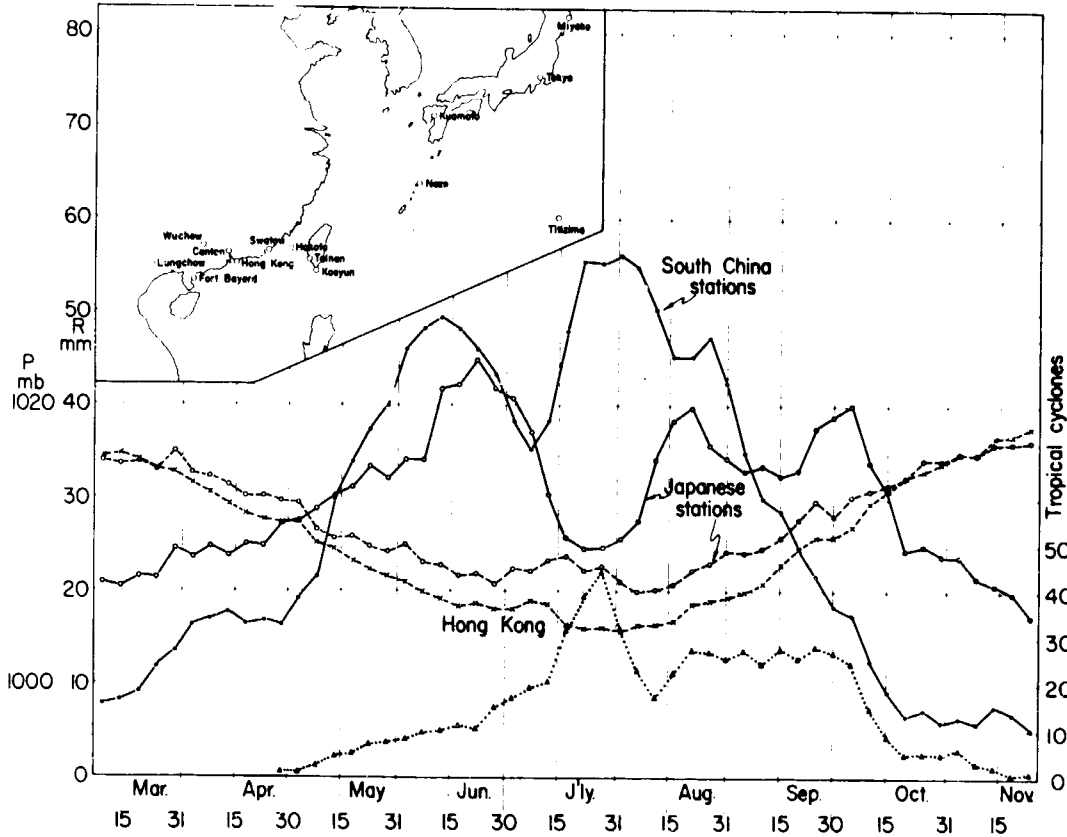


Figure 4. 5-day Means of Rainfall (solid lines) for Nine Stations in South China and Five Stations in and South of Japan, Pressure (dashed lines) for Hong Kcong and the Five Japanese Stations, and Tropical Storm Frequencies (dotted line) for South China.

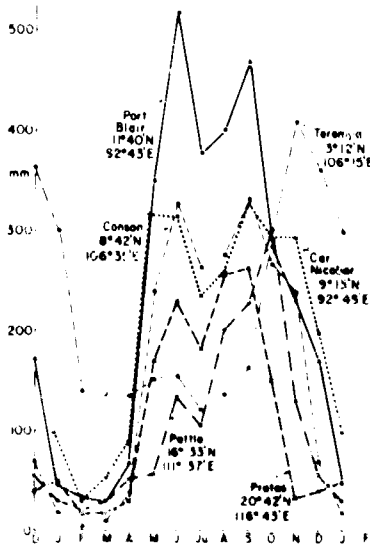


Figure 5. Mean Monthly Rainfalls in mm. for Pratas, Pattle, Con San and Terempa in the South China Sea and for Port Blair and Car Nicobar in the Bay of Bengal.

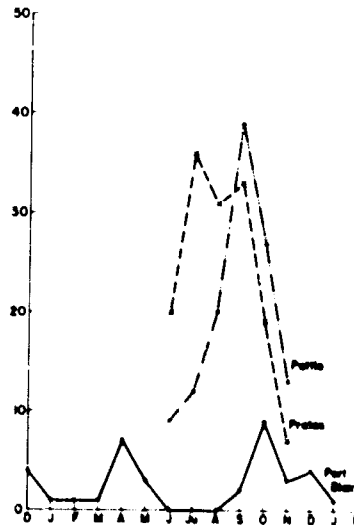


Figure 6. 70-year Frequencies of Tropical Storm Center Occurrences Within 250 km. of Pratas, Pattle and Port Blair. From Chin [2], Ananthakrishnan [1].

MEAN CIRCULATION AND CLOUDINESS DURING THE DEVELOPMENT  
OF THE SOUTHWEST MONSOON OVER INDIA AND SOUTHEAST ASIA \*

James C. Sadler  
University of Hawaii

ABSTRACT

For the months of April, May, June, and July, updated long term monthly mean wind climatology at standard pressure levels is discussed in relation to detailed cloud climatology prepared from 3 years of satellite data. A deep tropical southwesterly current flows into southern Burma in May and brings the monsoon rains to Rangoon a month earlier than at the same latitude on the west coast of India which in May is still dominated by a strong anticyclonic cell in the subtropical ridge. The rains over southern South Vietnam, which are persistent from the first of May, occur within a mean May southeasterly flow such that the onset of the southwesterly monsoon over Saigon cannot be determined from a rainfall analysis alone.

PREFACE

I am the first speaker representing a group at the University of Hawaii which has been working for the past two years on the Air Force forecast problem in Southeast Asia. The University complement of three professionals is supported under a contract with the Air Force Cambridge Research Laboratories. An integral part of the group is a complement of two Air Weather Service meteorologists from the 1st Weather Wing. More detail on the project's concept and operation is contained in the preface to our first scientific report (Sadler, et al. [10]) which has been included in the Conference hand-out material. An operational research project is somewhat unusual in a University program and I want to stress the point that, to be effective, it must be a cooperative effort and contain the vital link to the operational forecaster. We also work closely with the "in-house" personnel of the Air Force Cambridge Laboratories and are able to share the data gathering and processing chore.

The data and techniques used in our research studies are essentially those available to the field, i.e., conventional surface and upper-air data for subjective analyses, radar coverage over some areas and daily satellite photographs. Our approach has been to attempt to relate cloudiness and synoptic flow patterns, recognizing that if any results are to be of aid to the field forecaster they must meet the minimum criteria of:

- (a) the synoptic patterns and changes must have sufficient definition and continuity to be recognizable from his analyses, and
- (b) recurring synoptic patterns and changes should produce similar cloudiness and convective conditions.

The synoptic patterns over Southeast Asia can appear rather strange to the newly-arrived and inexperienced tropical meteorologist who is accustomed to the moving weather producing systems of temperate latitudes. We find it saves time and removes some of the frustrations if he is shown the simplified lower tropospheric flow patterns which are associated with the summer monsoon regions. Since my presentation and those of Major Brett and Major Harris will be discussing flow patterns over Southeast Asia, I take the liberty of assuming that some of you would benefit by an introductory discussion and definition of terms.

Diagram A of figure 1 depicts the well-known trade wind regime between the subtropical ridges of the Northern and Southern Hemispheres. In diagram B an east-west pressure trough (noted as a dotted line) of sufficient intensity to produce a westerly current on the equatorward side has been introduced in the Northern Hemisphere. Concurrent with the establishment of the tropical westerlies is the necessary appearance of a clockwise rotating wind system between the westerlies and the easterly trade wind regime. In B this clockwise system (noted as a dash-dot line) is located in the Northern Hemisphere and is anticyclonic and therefore a ridge system. In diagram C, only the latitudinal width of the tropical westerlies has been expanded southward and the same clockwise wind system is now located over the equator. In diagram D, only slight adjustments have

\* Research sponsored by Air Force Cambridge Laboratory

been made to introduce more reality and produce flow patterns similar to the mean low-level flow of the summer season from India through the Philippines with the longitude of Southeast Asia near the center of the diagram. The tropical westerlies extend across the equator on the western portion but not on the eastern portion of the diagram. The clockwise rotating wind system is now south of the equator in the region of India and north of the equator in the region of the Philippines.

There is general agreement on the terminology of the subtropical ridges but not of the other circulation systems. The trough system has been noted by a variety of names such as equatorial trough, near-equatorial trough, equatorial front, intertropical front, intertropical convergence zone, equatorial convergence zone, northern intertropical convergence zone, monsoonal trough and cyclonic directional shear zone. The term front is losing favor in application to tropical systems and the satellite observations have shown that it is incorrect to note the trough as an intertropical convergence zone if the definition implies maximum cloudiness for the trough is most apt to be a zone of minimum cloudiness. We will normally refer to it as the monsoonal trough or shear zone.

The equatorial clockwise wind system is also denoted by a variety of terms probably due to the fact that it crosses back and forth over the equator and is not generally recognized or treated as a continuous system. The portion in the longitudes of India and the Bay of Bengal, which is climatically south of the equator, and therefore cyclonic, is variously called the Southern Hemisphere near-equatorial trough, southern intertropical convergence zone, secondary intertropical convergence zone and clockwise equatorial eddy. During occasions when the system is located north of the equator in the Indian region it has been referred to as the sub-equatorial ridge. The portion of the system in the region of Borneo and the Philippines, which is climatically over or slightly north of the equator, has been called equatorial eddy, clockwise eddy or near-equatorial clockwise eddy with implications that the eddies may somehow be caused by the orography of the larger island. We prefer to view this system synoptically as one which is demanded by the opposing persistent flows of the tropical westerlies associated with the monsoon low system of Africa and Asia and the easterly trade wind regimes. We refer to it as the buffer system in the analogous sense of a buffer state. It is continuous in space and time and responds in position to the fluctuations in the intensity and configuration of the two basic currents. It is not anchored orographically, can move back and forth across the equator, and can have a synoptic scale cellular structure with the cyclonic or anticyclonic rotational sense being determined by the position with respect to the equator.

## 1. INTRODUCTION

The term monsoon in a broad descriptive sense applies to regions experiencing mean-wind currents which have a marked seasonal reversal. Operationally, however, the term onset of the monsoon has become more associated with the beginning of some specified rainfall regime. Each specification of the regime leads to a different date of onset such that in the literature, or in practice, there is no common method of identifying the date of onset. Most of Southeast Asia, experiences a gradual increase of rainfall during the pre-monsoon period and it is impossible from the rainfall data alone to determine the date of onset of the southwest monsoon rains. If rainfall is of prime operational consideration, it is only academic to consider the flow pattern except to answer the constant query of "Has the southwest monsoon started yet?"

Bombay, India has very little pre-southwest monsoon rainfall and the average date of the onset of monsoon rains has been determined by Kandas, et al. [6], to be 8 June from a simple plot of daily rainfall values. Rangoon, Burma experiences some premonsoon rainfall during most years and Neralla [4] used a plot of 3-day moving averages to determine the southwest monsoon rain onset for the years 1965-1967. The arrow in figure 2 indicates the date of onset by his definition. The 3-year average is near 5 May. Huke [1] used an 11-year period of record and a different definition, which was also based on rainfall amount and persistence, and obtained an average onset date at Rangoon of 5 May with a range of 25 days. The average date of onset of southwest monsoon rain at Rangoon is more than a month earlier than the average onset date at Bombay. Figure 1 is a plot of the 5-day moving average of rainfall for 3 stations southwest of Saigon as produced by Lund [3].

I have added the heavy vertical line at 1 May to clearly show that, on the average, persistent rainfall occurs by this date. The wind flow patterns, to be discussed later, will show that this date cannot be considered as the onset of the southwest monsoon rains.

In an attempt to better define the onset of the southwest monsoon over Southeast Asia, Riehl [8] used as a definition of onset the date when equatorial westerlies at 10,000 feet penetrate to 15° N. over central Southeast Asia. From 29 years of data the mean date was 17 May with a range of 33 days. This method is highly subjective in determining whether the westerlies are a branch of the southwest monsoon or a part of the mid-latitude westerlies and, in addition, has little operational utility without concurrent rainfall analyses.

The purpose of this paper is to present recently up-dated wind and cloud climatology during April, May, June, and July to serve as the large scale (time and space) setting within which to consider the daily, monthly and interannual variability of the monsoon from India through Southeast Asia.

## 2. MEAN FLOW PATTERNS AND AVERAGE CLOUDINESS

The data for the mean resultant wind analyses at the standard pressure levels were compiled by the International Indian Ocean Expedition (Ramage and Raman [5]). The period of record averages near 12 years (through 1965) for stations in India and Southeast Asia.

The gradient or 2000-ft. level data are a conglomerate from many sources and varying periods of record. They are mainly from a publication of the Thailand Meteorological Department [11] which covered only the 5-year period from 1956 to 1960. In addition to the short period of record, the data are mostly from pilot balloon observations and probably contain a good-weather bias in the cloudy regions. Considerable smoothing was used in the analysis of this level.

The cloud data were extracted from the operational nephanalyses of satellite observations in a manner described by Sadler [9]. The average monthly cloudiness will be shown for the individual years of 1965, 1966 and 1967, and for the 3 years combined. The April 1965 cloudiness will not be shown because some areas had less than 10 observations; however, the data have been used for the 3-year April average. The discussions of cloudiness will pertain to the 3-year averages unless otherwise noted.

### 2.1 April

#### A. Mean Circulation (fig. 4)

The gradient-level analysis (fig. 4) shows the tropical westerlies confined to the equatorial regions. The subtropical ridge is continuous from Southeast Asia through central India at this level and above (analyses not shown). An anticyclone covers the central Bay of Bengal. There is no organized current of 10 knots or greater except in the subtropical westerlies over northern India. The differential heating of land and sea shows as a weakening of the ridge (or conversely as an increased troughing), over India and over the region of Burma and western Thailand.

#### B. Cloud Distribution (fig. 5)

During this month, and the subsequent months to be discussed, the maximum and minimum cloudiness zones tend to be positioned in the same general areas from year to year; however, within the general areas there are significant year-to-year variations in cloud pattern and amount.

The northern Bay of Bengal and northwestern and western India southward along the coast are essentially cloud free. Some moisture is fed into central and eastern India by the southeasterly flow between the Bay of Bengal anticyclone and the heat low over southern India resulting in slightly greater cloudiness. This is shown best in 1966. Moisture is also entering Southeast Asia, as far west as Bangkok, from the southeasterly and southerly flow over the South China Sea and Gulf of Siam resulting in a land-locked convective cloudiness of greater than 4/8. A relative minimum extends across the Gulf of Siam into the South China Sea.

## 2.2 May

### A. Mean Circulation (figs. 6, 7, 8, and 9)

The increased heating of the land masses and the general decrease of surface pressures over the region of India and Southeast Asia has eliminated the low-level (fig. 6) closed anticyclone over the Bay of Bengal and the continuous ridge from Southeast Asia through India although weak relative ridging remains over the northern portion of the Bay of Bengal between the heat troughs of central India and Burma. Westerly winds cover all of India and Southeast Asia except extreme southern South Vietnam where the subtropical ridge lies through the Saigon region. Speeds of 10 to 15 knots are indicated in the southwesterlies over Ceylon and the western Bay of Bengal. The speeds over the Andaman Islands and Southeast Asia are less than 10 knots.

There is considerable change in the flow pattern between the near-surface levels and 700 mb. (fig. 7). Over the surface-heat trough of central India lies a strong anticyclonic cell in the subtropical ridge. The subtropical ridge is also sharp across Southeast Asia and lies just north of Saigon. The monsoon trough is between 5° N. and 10° N. from northern Borneo through southern India. The troughing in the central Bay of Bengal is of sufficient intensity to break the subtropical ridge and permit the tropical westerlies to flow onto the southern Burma coast. The high 58% steadiness of the wind at Port Blair in contrast to 39% at Bangkok, 32% at Songkla and 7% at Saigon supports this interpretation.

The monsoon trough weakens with height. It extends vertically through the 500-mb. level (fig. 8) over southern India and southern Bay of Bengal but not over Borneo and Malaya. The 49% wind steadiness at Port Blair, in contrast to the 24% steadiness at both Bangkok and Songkla, indicates that the tropical westerlies are frequently 500-mb. deep flowing onto the south Burma coast.

### B. Cloud Distribution

The May cloudiness (fig. 10) reflects these changing flow patterns. The change from a low-level southerly flow into eastern India during April to the broad westerly current in May results in a decrease in cloudiness from April to May over central India north of 15° N. However, the most significant change in cloudiness occurs along the south Burma coast and through the Gulf of Siam across southern Southeast Asia. The cloudiness along the south Burma coast increases from less than 3/8 in April to greater than 5/8 in May and the 5/8 isopleth extends northward to Rangoon. In May a relative maximum covers the Gulf of Siam and the South China Sea off the south coast of South Vietnam, replacing the minimum of April. Cloudiness in this region was rather intense during May 1965, with one area of greater than 7/8 cover.

## 2.3 June

### A. Mean Circulation (figs. 11, 12, 13, and 14)

In June the monsoon westerlies continue to grow in strength, depth, and area. At 2000 feet (fig. 11) the monsoon trough extends from the southern Philippines through Hainan, North Vietnam, Burma, and northern India. The tropical westerly current attains a speed of 25-30 knots in the region of Ceylon and decreases in strength downstream to less than 10 knots over the coastal region of the Vietnam north of 10° N. The 700-mb. flow (fig. 12) is little changed from that at 2000 feet except for a slight decrease in the speed of the tropical westerlies. Slight ridging is evident over north central India. The monsoon westerlies decrease in area and strength with altitude. At 500 mb. (fig. 13) the subtropical ridge lies near 23° N. across India and Burma, and the monsoon trough is near 19° N. Southeast Asia is near the eastern edge of the southwest monsoon system at this level and the buffer ridge is just south of Saigon. The westerlies reach a maximum depth of near 400 mb. over India and the Bay of Bengal (Ramage and Raman [5]). At 200 mb. (fig. 14) the subtropical ridge is well positioned near 25° N. This is a northward movement of 10° between May (fig. 9) and June. Strong, steady, and speed-divergent easterlies overlie Southeast Asia and India. The highest speed of 61 knots is observed over the southern tip of India.

### B. Cloud Distribution (fig. 15)

There is a general increase of cloudiness between May and June over India and Southeast Asia north of 10° N. In the Indian region the maximum cloudiness belt moves from near 3° N. to 12° N. along the west coast and 18° N. on the east coast. The maximum cloudiness along the Burma coast spreads northward and increases to greater than 6/8 coverage over a large area.



## 2.4 July

### A. Mean Circulation (figs. 16, 17, and 18)

There is a slight increase in the overall depth, area, and intensity of the southwest monsoon system between June and July. The low-level westerlies (fig. 16) become stronger across central India. The monsoon trough moves slightly northward through the South China Sea and the Philippines and extends further eastward into the western North Pacific. The subtropical ridge at 500 mb. (fig. 17) and 200 mb. (fig. 18) moves another 5° northward. There is a considerable change in the speed distribution within the 200-mb. northeasterly flow over Southeast Asia and India. The speed-minimum wedge, which is attributed to the tropical upper tropospheric trough, moves about 5° northward and the wind speeds decrease over Clark, Southeast Asia, Port Blair and southern India between June and July. However, the speeds increase considerably over northern India (from 20 to 53 knots at Bombay) and over the equatorial region (from 30 to 42 knots at Gan Island).

### B. Cloud Distribution (fig. 19)

The greatest change in cloudiness from June to July occurs over India. During July, 5/8 cloudiness covers all of India with the exception of the north-orth-western section and the southern tip with a greater than 6/8 strip across central India near 18° N. Cloudiness decreases slightly along the Burma coast from June to July and in fact the plotted data (not shown) indicates a slight decrease over all of Southeast Asia. A complete analysis of the month-to-month areal changes in cloudiness, using the 3-year data file, has not been completed.

## 2.5 Conclusions

The long term mean flow patterns in combination with the satellite viewed 3-year cloud distribution show well the orderly evolution of the monsoon system. The changing flow patterns also relate well to the observed average time separation between the onset of the monsoon rains over India and over Burma and Southeast Asia.

The general regions of maximum and minimum cloudiness have little inter-annual shift in position; however, there is a significant interannual variation in the pattern and amount of cloudiness within those regions. This is only another way of stating that the monsoon system will develop each year in response to the annual differential heating cycle between land and sea but that the timing and intensity of the circulation changes are slightly different each year. We do not have monthly mean circulations for individual years to compare with the cloud data, yet they are necessary ingredients for an increased understanding of the differences in monsoon onset and intensity from year to year. As examples, it might be revealing to know what the differences were in the mean monthly circulation of May 1965 versus May 1966, which produced the significant differences in the average cloudiness over the Gulf of Siam and the South China Sea off the southern coast of South Vietnam; or between the two Junes of 1965 and 1966 which show an equally drastic change in cloud cover over most of Southeast Asia. I feel that indices developed from such studies could be more successful in predicting the timing and intensity of the monsoon rains than some of the more external (to the monsoon) indices now being used (Rao and Ramamurthy [7]; Lund [3]).

Suggestions have been made that tropical storms in the Bay of Bengal usher in the southwest monsoon over Southeast Asia. Riehl [8] states that storm development is an important aspect of monsoon onset at 15° N. over Southeast Asia. However, his data for the 29-year period of 1936 through 1964 do not seem to substantiate the statement. Only 12 of the years had simultaneous storm occurrence and monsoon onset, while 11 years had storms in early May with no simultaneous onset and 6 years experienced no storms in early May prior to or during onset. Two of the earliest dates of onset (2 May 1956 and 3 May 1942) had no concurrent storm development and the year of latest onset (3 June 1958) experienced two storms in the Bay of Bengal during May.

We have studied the daily synoptic charts and satellite photographs during the onset period of 1966, 1967 and 1968 and found no useful relationship between storm occurrence and monsoon onset. In 1966 there were no storms. In 1967 a typhoon developed north of the Andaman Islands on 16 May, or about a week after the monsoon onset at Rangoon as determined by Neralla [4] (fig. 2).

In 1968 a typhoon developed near the Andaman Islands on 8 May and moved northward through the Bay of Bengal. Even though the dates of the storm were near the average date of monsoon onset at Rangoon (fig. 2), the flow pattern reverted to a premonsoon condition by 11 May and the onset was delayed until late May.

Developing storms in the Bay of Bengal do influence the weather over Southeast Asia and are a factor in the forecast problem. Each will either initiate a temporary westerly current or increase the strength and depth of the existing westerlies for a few days over portions of Southeast Asia. A general increase in cloudiness should be anticipated in this tropical westerly current.

## DISCUSSION

RENARD: Does your June-July cloud distribution in the Bay of Bengal area have distinct relation to the relative minimum of rainfall during the seasonal maximum (Ref. Ramage's discussion)? Would a biweekly cloud distribution bring this relation out more clearly?

SADLER: We have not looked for it in monthly averages but feel that shorter period averages would show it more clearly. It should show in the large scale difference patterns between June and July which we are not preparing.

WANN: How many satellite pictures were analysed per day?

SADLER: Once-a-day coverage from the operational nephanalyses.

SOUTHERN: Does the incidence of cirrus (either independent from passage of upper tropospheric westerly troughs or dependent cirrus from convective systems) interfere seriously with the analysis of mean cloudiness relating rainfall incidence to monsoonal wind influences?

SADLER: Most cirrus is not resolved by the satellite unless very thick. Thick cirrus does occur in the monsoon region but, since it is usually associated with the large convective systems, I feel it affects the analysis very little.

KREITZBERG: Do you attribute the cloud minimum in July in the valley north of Bangkok to orographic subsidence over the mountains to the west?

SADLER: Yes.

HAU: In your averaging of cloudiness in June and July, it seems that 1966 constitutes a very particular case in which we have a relatively clear area (less than 5/8) over the western side of the central mountains in Vietnam. The 3-year mean is therefore more or less influenced by this anomaly, if there is any. Have you studied what happened in 1966?

SADLER: No. There are no routine monthly averaged circulation analyses for the tropics and in fact there are no routine averages of any meteorological parameter over the tropics. Such analyses must be done to better understand the inter-annual variations on the monthly scale.

## REFERENCES

1. HUKU, R. E., "Rainfall in Burma." Geography Publication No. 2 at Dartmouth. 1965.
2. LUND, I.A., "Estimating the Date of Onset of the Rainy Season in Southern South Vietnam." Pro. Fifth Technical Conference on Hurricanes and Tropical Meteorology. Caracas, Venezuela. 1967.
3. LUND, I.A., and D. D. GRANTHAM, "Estimating the Date of Retreat of the Rainy Season in Southern Vietnam." Air Force Cambridge Research Labs. Report No. AFCRL-68-0229. 1968.
4. NERALLA, V. R., "The Burma Monsoon." University of Hawaii thesis. (In preparation). 1969.
5. RAMAGE, C. S. and C. R. V. RAMAN, "International Indian Ocean Expedition Meteorological Atlas." Vol. 2, Upper Air. Honolulu, East-West Center Press. (In preparation). 1969.

REFERENCES (CONTINUED)

6. RAMDAS, L. A., JAGANNATHAN, P. and S. Gopal RAO, "Prediction of Date of Establishment of Southwest Monsoonal on the West Coast of India." Ind. J. Meteorol. Geophys. 5, 305-314. 1954.
7. RAO, K. N. and K. S. RAMAMURTHY, "Monsoon Rainfall Forecasting in India." Pro. of Symposium on Monsoons of the World. India Meteorological Department. 1958.
8. RIEHL, H., "Cumulus Convection and Orographic Convection Cells." Final Report on Contract No. DA 36-039-SC-89080. Colorado State University. 39 pp. 1965.
9. SADLER, J. C., "Average Cloudiness in the Tropical From Satellite Observations." International Indian Ocean Expedition Meteorol. Monogr. 2, 22 pp., 12 plates. 1968.
10. SADLER, J. C., BRETT, W. R., HARRIS, B. E. and F. P. HO, "Forecasting Minimum Cloudiness Over the Red River Delta During the Summer Monsoon." Sci. Rept. No. 1 on Contract No. F19628-67-C-0232, Hawaii Insitute of Geophysics Rept. HIG 68-16 and AFCRL-68-0487, 104 pp. 1968.
11. THAILAND METEOROLOGICAL DEPARTMENT, "Upper Winds Over Southeast Asia and Neighboring Areas." Bangkok, Thailand, 12 pp. 1965.

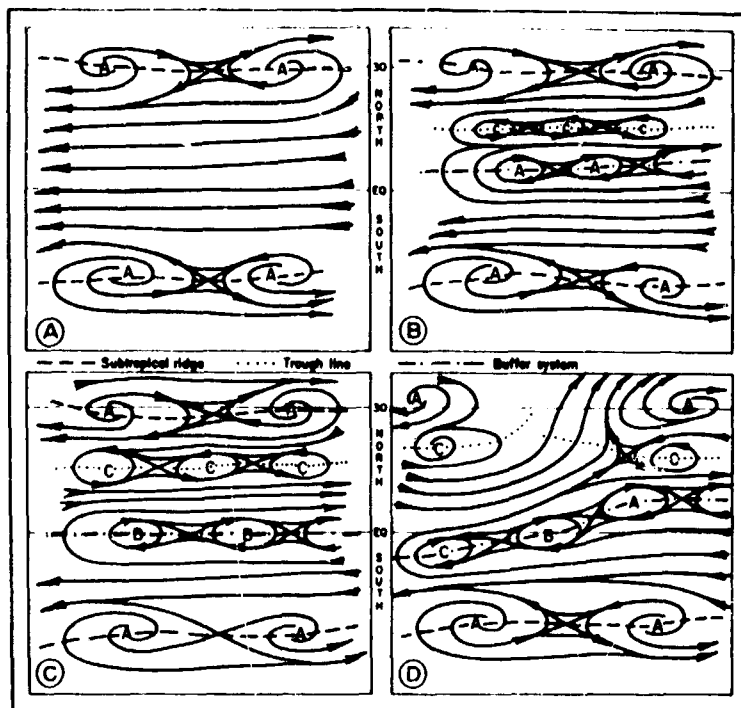


Figure 1. Schematic of the Low-Level Flow Patterns of a Maritime Tropical Trade Wind Region Versus a Northern Summer Monsoon Region.

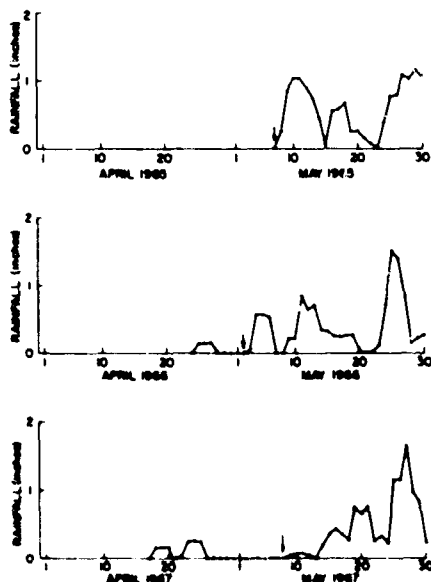


Figure 2. Three-Day Moving Averages of Rainfall at Rangoon, Burma (from Neralla [4]).

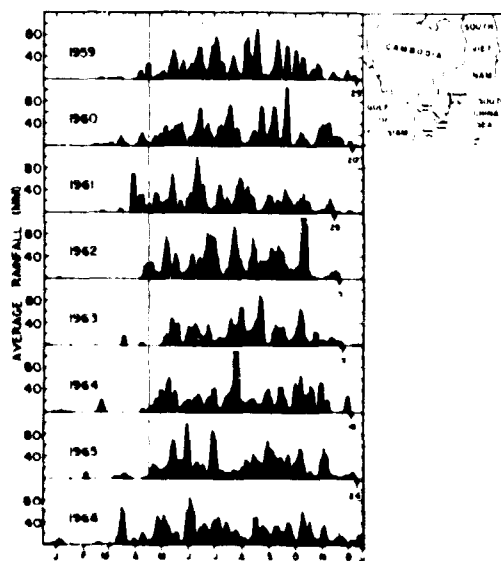


Figure 3. The 5-Day Moving Average Total Rainfall Observed at Rach Gai, Khanh Hung, and Quan Long (from Lund [3]).

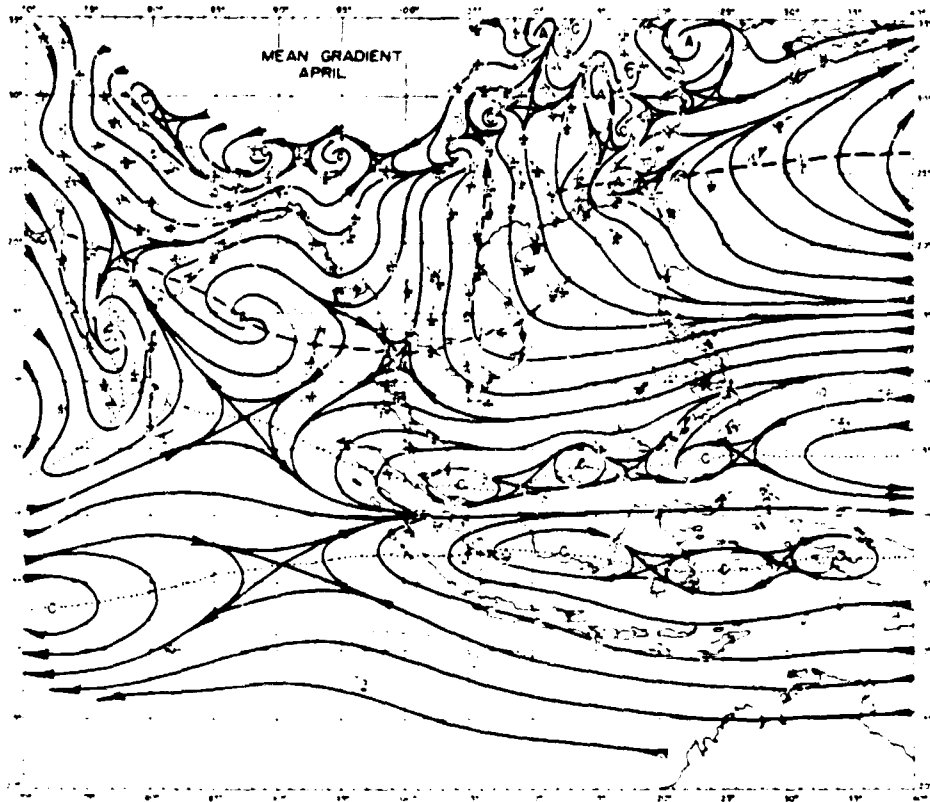


Figure 4. Mean 2000-ft. Flow for April. Trough position shown as dotted line; subtropical ridge as dashed line.

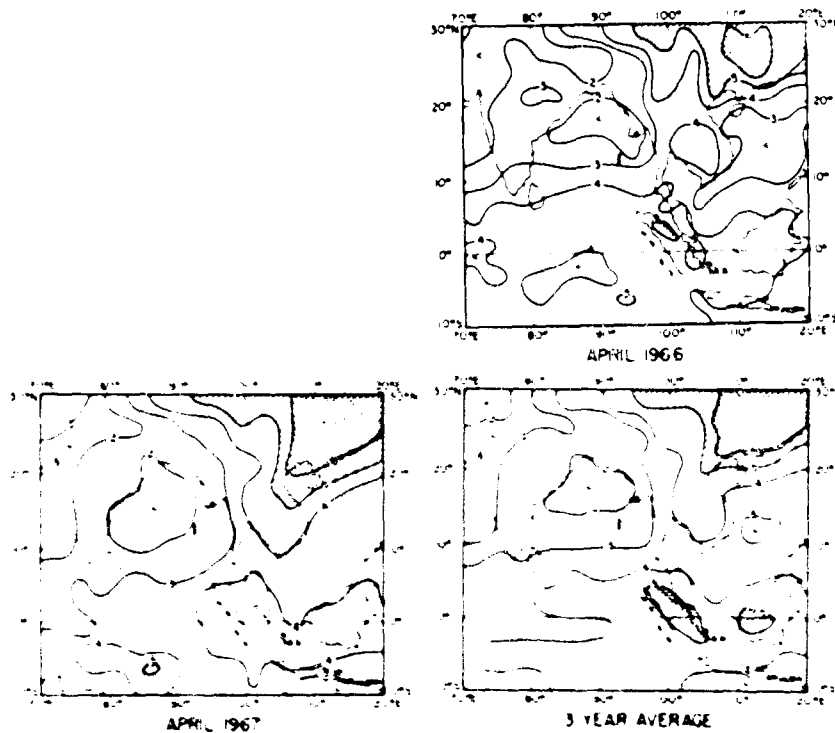


Figure 5. Average April Cloudiness From Satellite Observations. Isolines are total cloud cover in octans. From 5/8 to 6/8 is hatched; 6/8 to 7/8 is cross-hatched; and greater than 7/8 is black.

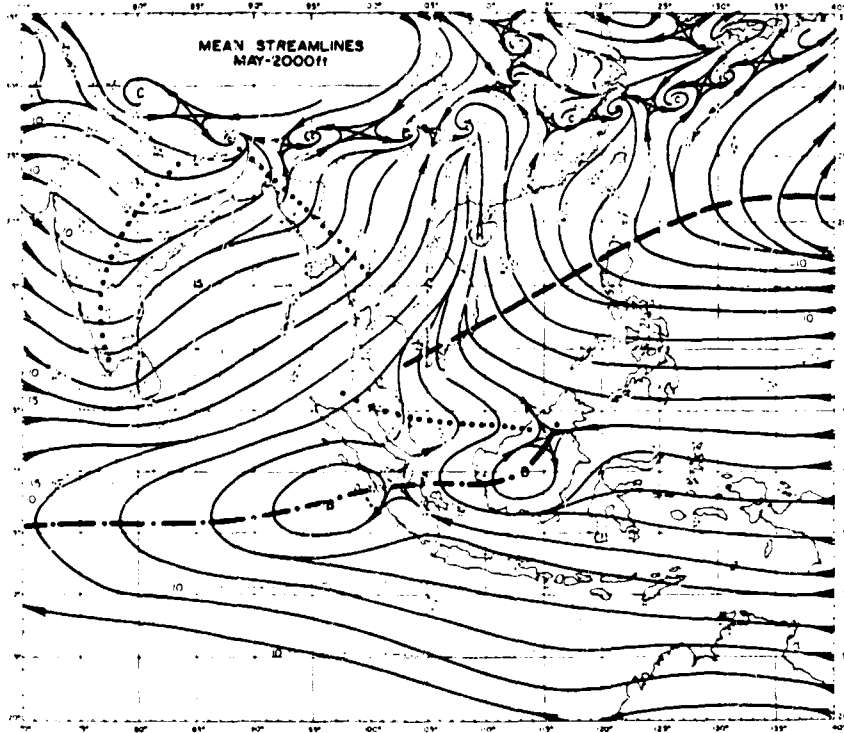


Figure 6. Mean 2000-ft. Flow for May. Trough position shown as dotted line; subtropical ridge as dashed line; buffer system as dash-dot line.

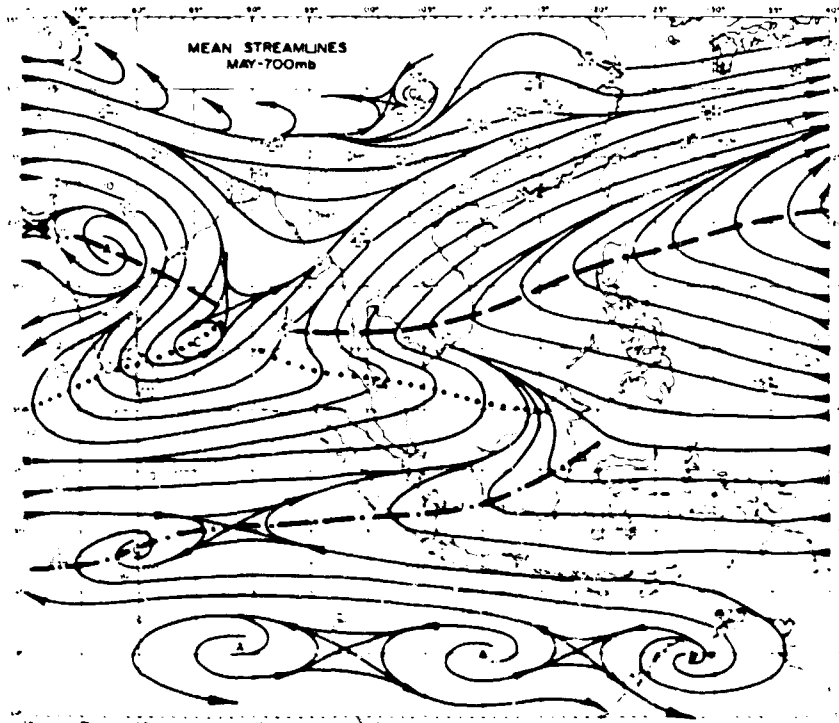


Figure 7. Mean 700-mb. Flow for May. Trough position shown as dotted line; subtropical ridge as dashed line; buffer system as dash-dot line.

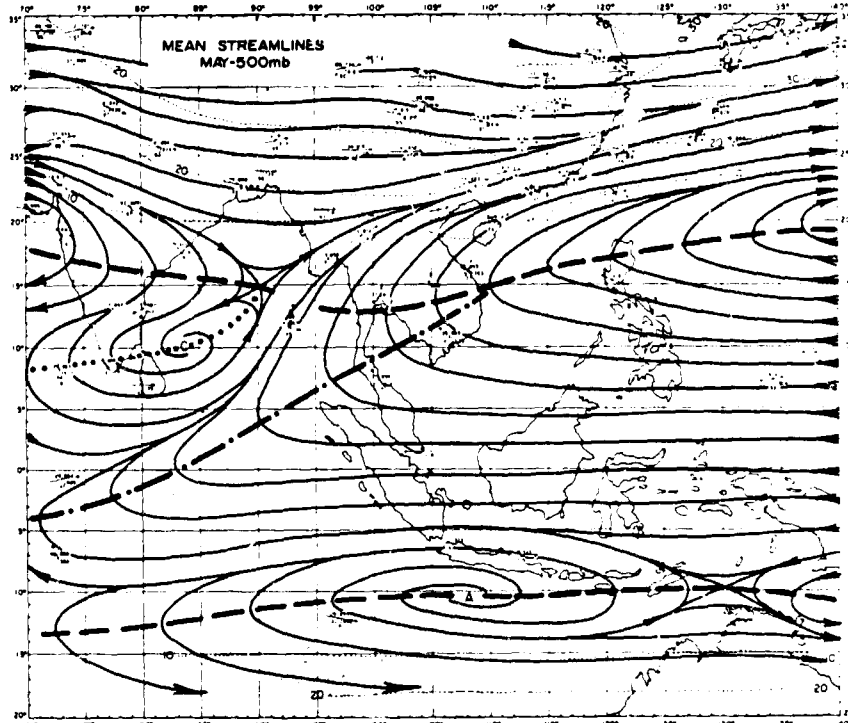


Figure 8. Mean 500-mb. Flow for May. Trough position shown as dotted line; subtropical ridge as dashed line; buffer system as dash-dot line.

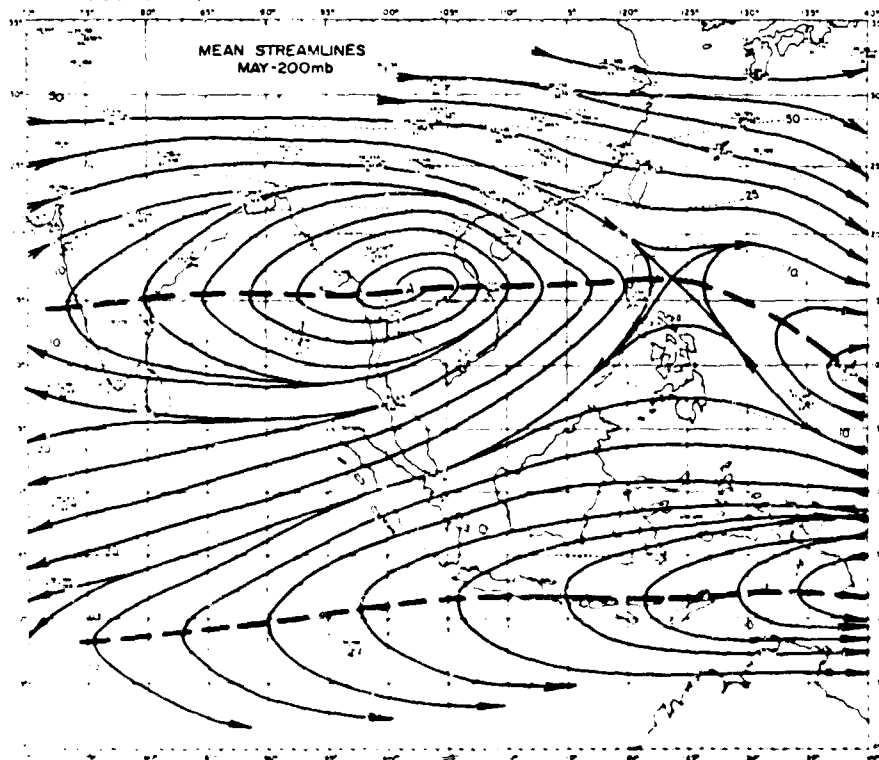


Figure 9. Mean 200-mb. Flow for May. Subtropical ridge position shown as dashed line.

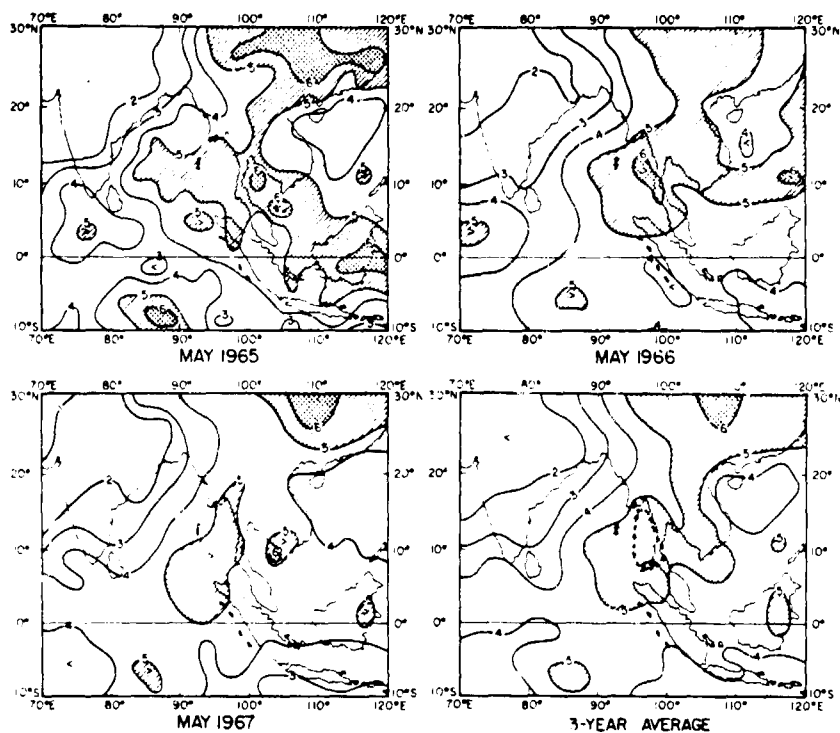


Figure 10. Average May Cloudiness From Satellite Observations. Isolines are total cloud cover in octas. From 5/8 to 6/8 is hatched; 6/8 to 7/8 is cross-hatched; and greater than 7/8 is black.

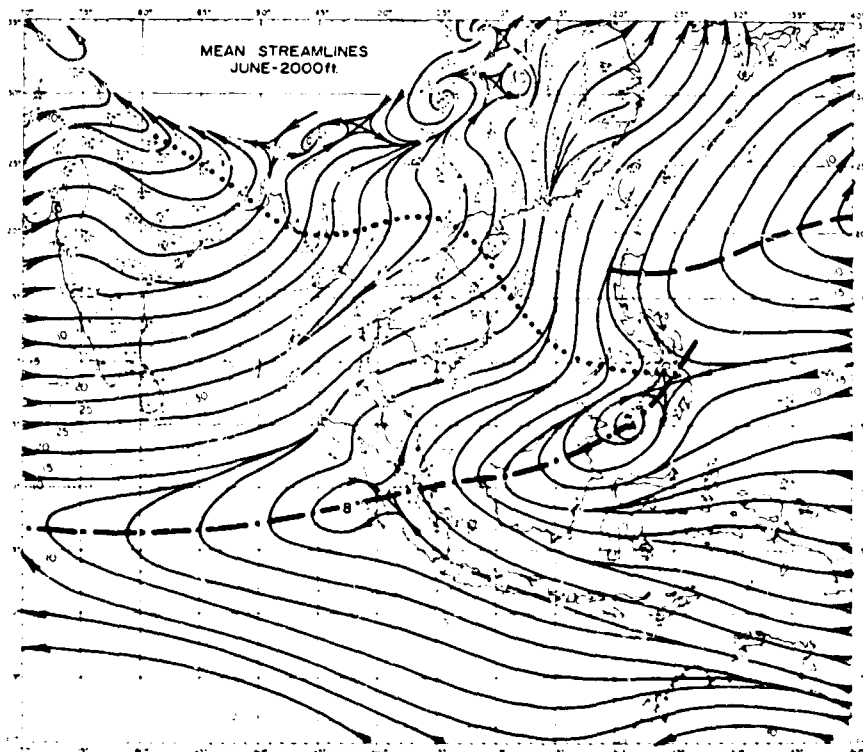


Figure 11. Mean 2000-ft. Flow for June. Trough position shown as dotted line; subtropical ridge as dashed line; buffer system as dash-dot line.



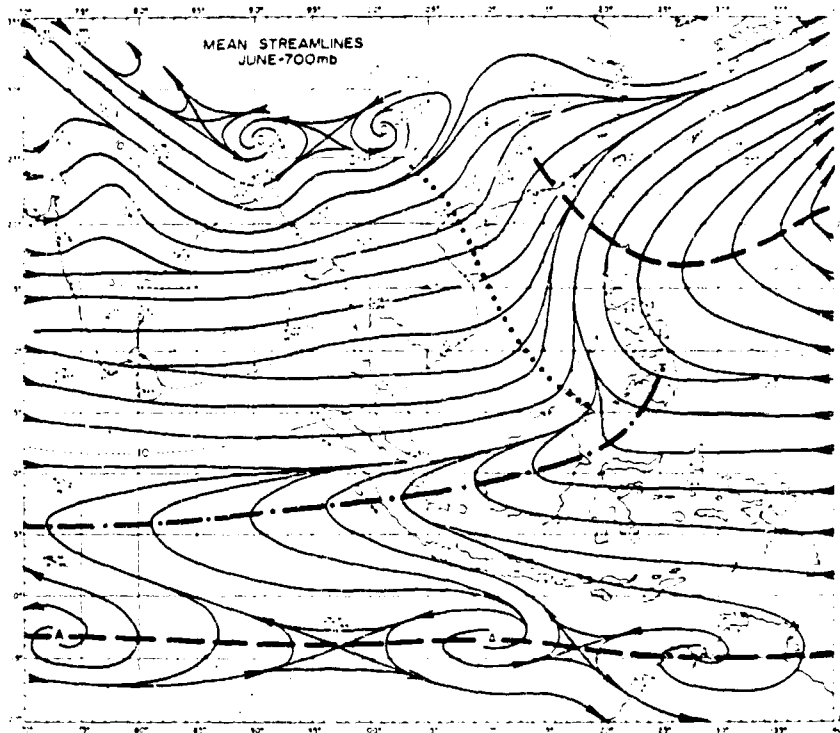


Figure 12. Mean 700-mb. Flow for June. Trough position shown as dotted line; subtropical ridge as dashed line; buffer system as dash-dot line.

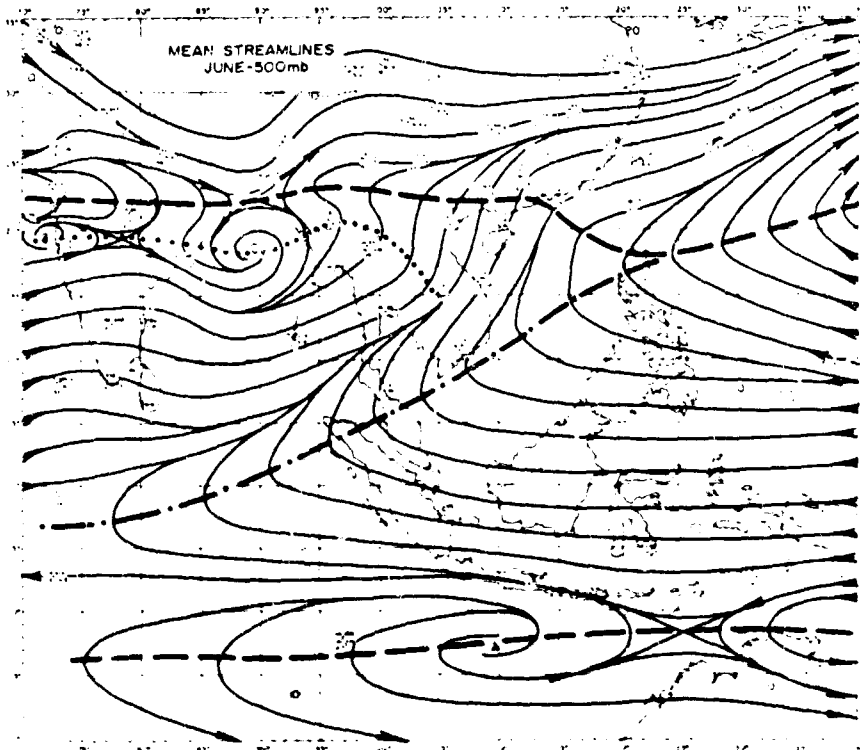


Figure 13. Mean 500-mb. Flow for June. Trough position shown as dashed line; subtropical ridge as dashed line; buffer system as dash-dot line.

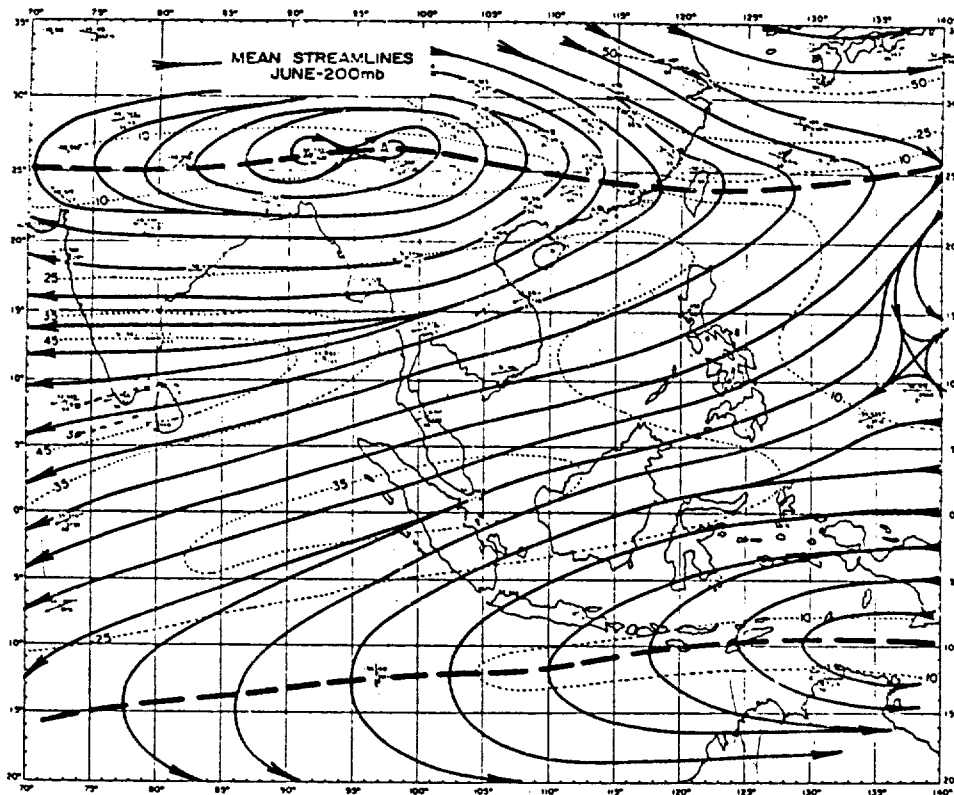


Figure 14. Mean 200-mb. Flow for June. Subtropical ridge position shown as dashed line.

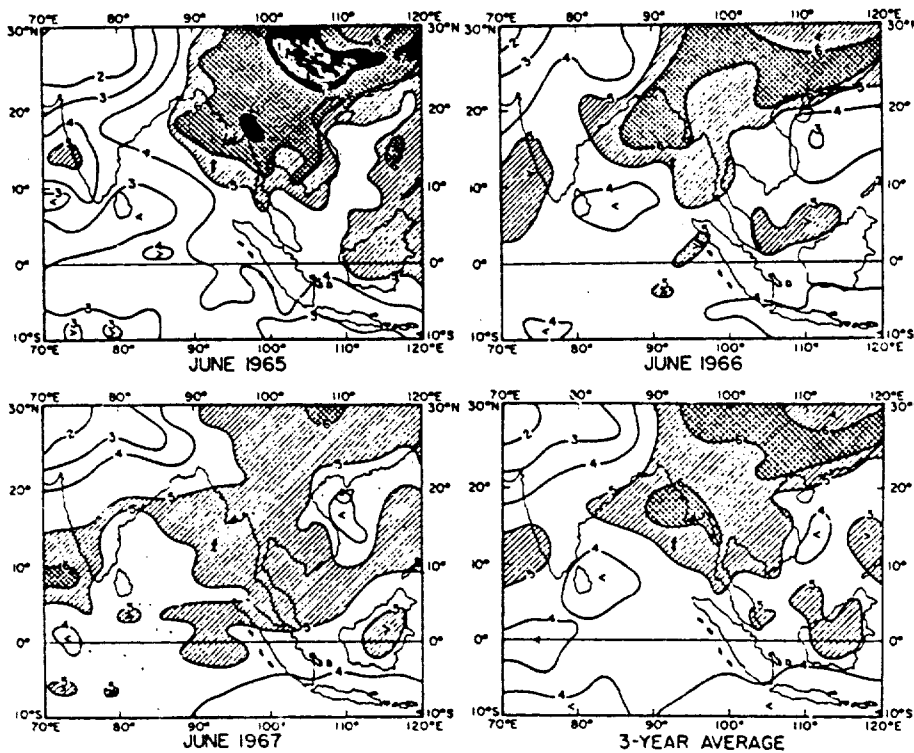


Figure 15. Average June Cloudiness From Satellite Observations. Isolines are total cloud cover in octas. From 5/8 to 6/8 is hatched; 6/8 to 7/8 is cross-hatched; and greater than 7/8 is black.

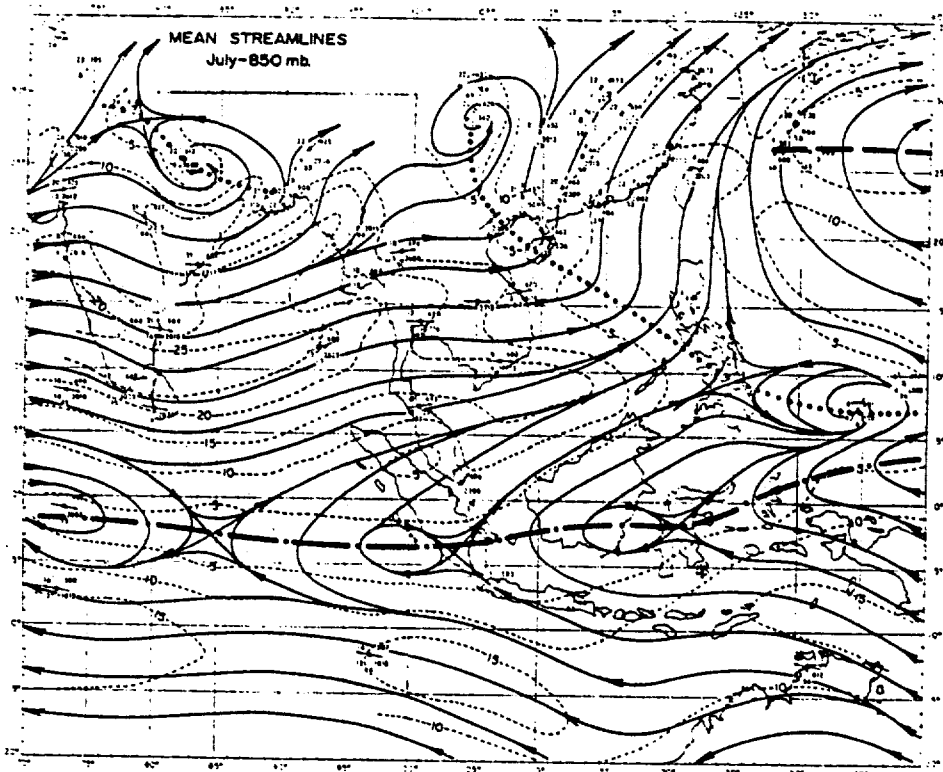


Figure 16. Mean 850-mb. Flow for July. Trough position shown as dotted line; subtropical ridge as dashed line; buffer system as dash-dot line.

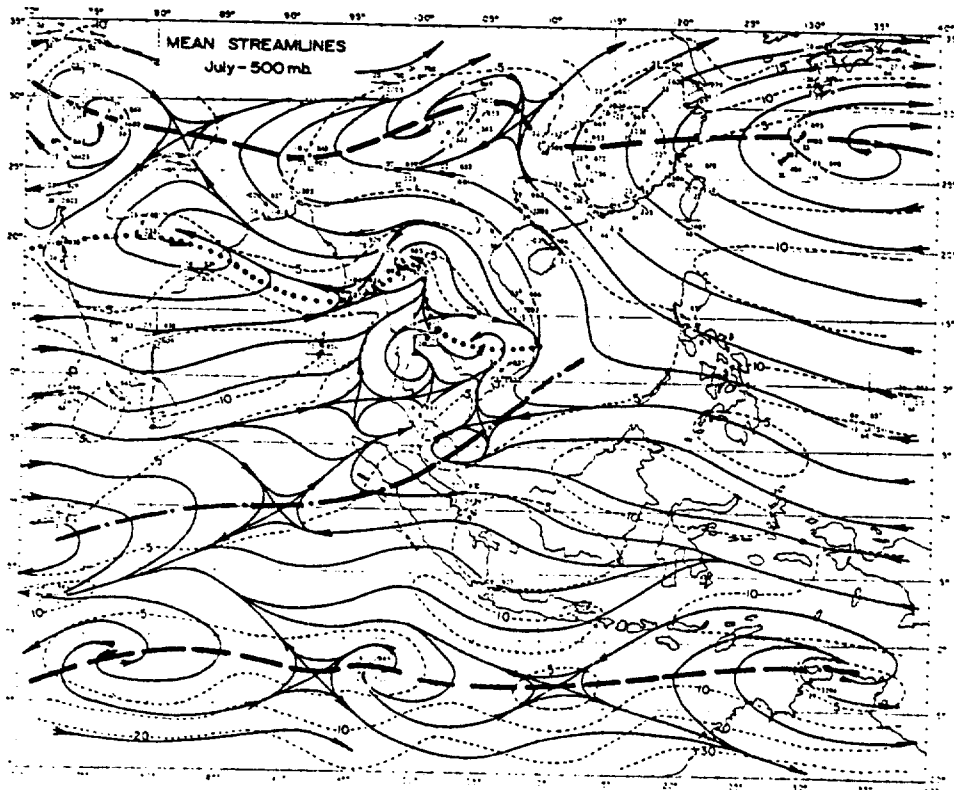


Figure 17. Mean 500-mb. Flow for July. Trough position shown as dotted line; subtropical ridge as dashed line; buffer system as dash-dot line.

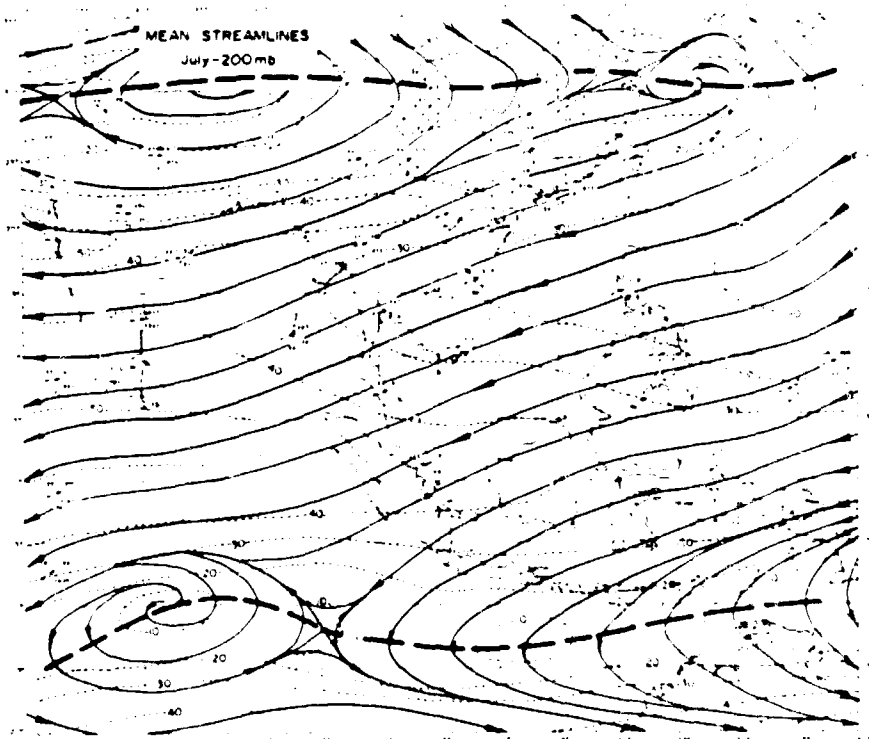


Figure 18. Mean 200-mb. Flow for July. Subtropical ridge position show as dashed line.

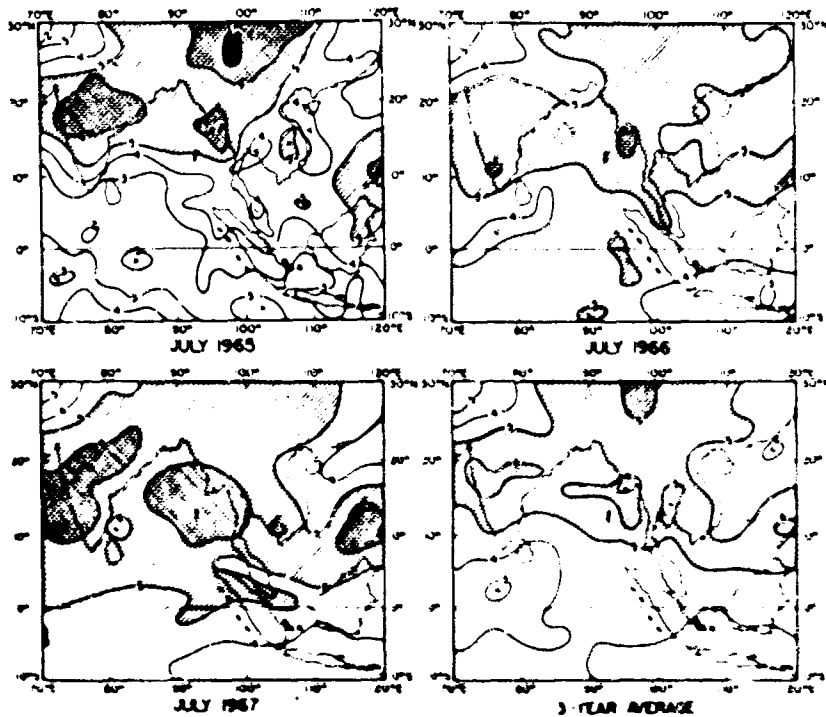


Figure 19. Average July Cloudiness From Satellite Observations. Isolines are total cloud cover in octas. From 5/8 to 6/8 is hatched; 6/8 to 7/8 is cross-hatched; and greater than 7/8 is black.

## ESTABLISHMENT OF THE SOUTHWEST MONSOON OVER SOUTH VIETNAM\*

Nguyen-Kim Mon  
Directorate of Meteorology, Republic of Vietnam

### ABSTRACT

The onset of the southwest monsoon may be tracked objectively by using streamline analysis for the lower troposphere (300 m., 1000 m. and 1500 m. levels) and following the changes in general circulation. For practical purposes, flow patterns during onsets are classified according to four types. Climatology shows that the first onset of the southwest monsoon over Saigon marks the date of its establishment over South Vietnam. This date is generally announced by the shift of the subtropical ridge axis to north of 16° N.

### 1. INTRODUCTION

While the typhoon is considered as the greatest tropical weather phenomenon in terms of damage it causes to human lives and property, the southwest monsoon is of chief importance to the agricultural economy of Vietnam. Advance information about the arrival date of the monsoon will be helpful to the public. However, the problem of forecasting the march of the forward edge of the southwest monsoon is difficult because the starting mechanism has not been completely understood so far. And, as mentioned by Riehl [2], the advance of the monsoon is difficult to trace and define. In fact, the continuity principle cannot be applied to its jumping movement. The change from easterly trade to equatorial westerlies is not always clear. There is often confusion between equatorial westerlies and the pre-monsoon westerlies or westerly counter-trade winds. Rainfall cannot be used to identify the monsoon because the amount of rain in the pre-monsoon period is comparable with the monsoon rainfall.

The following sections will attempt to present the characteristics of the onset of the summer monsoon and the relationship between the change in the upper troposphere circulation and the establishment of the summer monsoon over South Vietnam.

### 2. DEFINITION AND GENERAL CHARACTERISTICS OF THE ONSET OF THE SUMMER MONSOON

For analysis convenience, the following definition of the onset of southwest monsoon is commonly adopted in Vietnam:

The onset of the southwest monsoon over South Vietnam is considered as a replacement of the lower-troposphere trade winds by the equatorial westerlies originating in the Indian Ocean. This change in flow pattern results in the increase in cloudiness and frequency and amount of rainfall. The trade winds would be easterly winds or southwesterly counter-trade winds. This definition implies the idea of disappearance of the influence of the Pacific subtropical ridge on South Vietnam.

The leading edge of the southwest monsoon is identified as the intertropical convergence zone (ITCZ) or equatorial trough.

General characteristics of an onset of southwest monsoon over South Vietnam are indicated in the following example. Figure 1 shows the sequence of the ITCZ positions during an onset of the southwest monsoon.

On 12 May 1960, the ITCZ overlies Southern Malaysia from Sabang to Tarempa Island. The Pacific subtropical ridge extends roughly from Hong Kong to Phu Quoc Island and then west-northwestward up to 91° E.

On 14 May the Indian Ocean portion of the ITCZ moves north to the Adaman Islands. The heat low intensifies and extends as a deep trough across Burma to western Gulf of Thailand, reducing the strength of the Bay of Bengal anticyclonic cell and the western end of the Pacific subtropical ridge. This situation persists for the next three days.

\*Research sponsored by Directorate of Meteorology, Republic of Vietnam

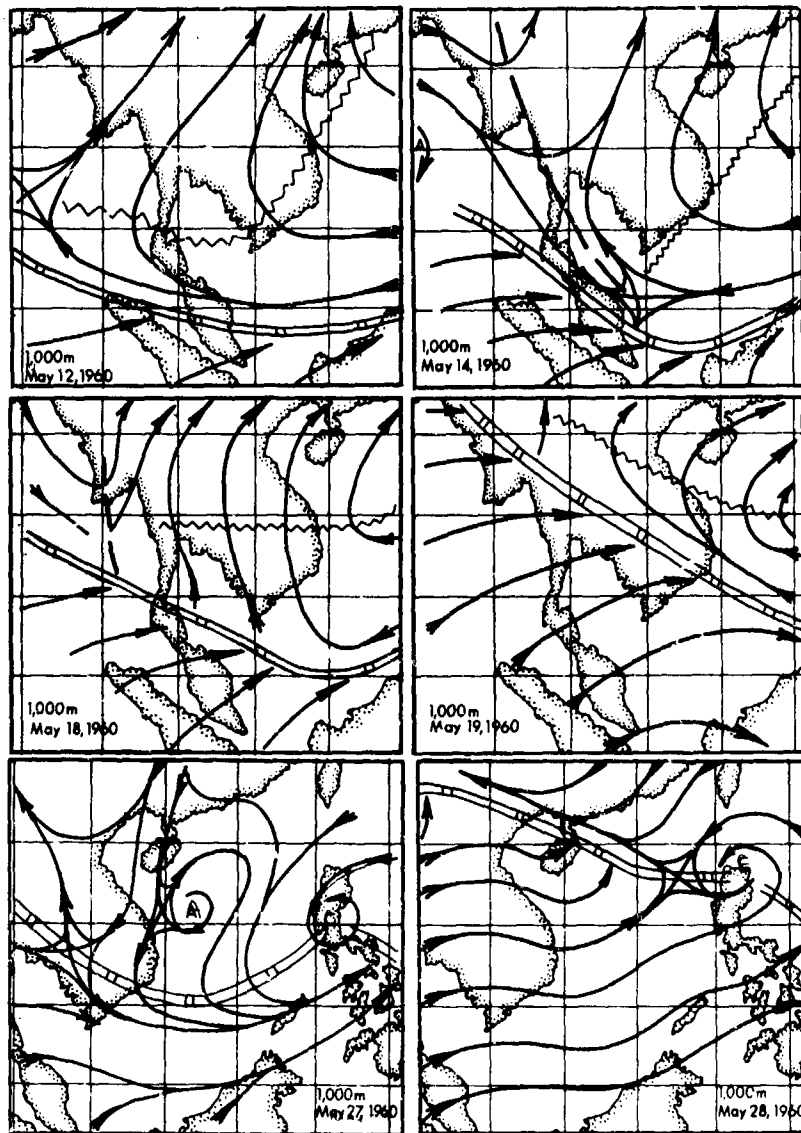


Figure 1. 1000 Meter Streamline Charts During an Advance of the Southwest Monsoon.

▬ ITCZ    — — — Trough line    ~~~ Ridge axis

On 18 May the South China Sea portion of the ITCZ moves northwards to the southern Gulf of Thailand and northern tip of Borneo. The Pacific subtropical ridge seems to retreat to the east. Over South Vietnam the trade winds veer from east-southeast to south-southeast or south. The Bay of Bengal anticyclonic cell disappears.

On the next day, 19 May, the west-southwest monsoon conjugates with the pre-monsoon west-northwesterlies over the Bay of Bengal and western Burma. The ITCZ jumps to north of Saigon. And thus the southwest monsoon is established over South Vietnam.

On the subsequent days, the ITCZ remains quasi-stationary over South Vietnam with small fluctuations around Saigon. A tropical cyclone is formed over the Pacific. On 27 May the Philippines portion of the ITCZ displaces northward in conjunction with the tropical cyclone movement; whereas, the South Vietnam portion of the ITCZ is blocked by a ridge from the continental anticyclone. (The outcoming north-northeast flow is shallow. It is only observed in the lowest layers from the surface up to 1000 m.)

On 28 May the continental ridge disappears and the tropical cyclone moves northward. The ITCZ jumps to a new position lying from northern Hainan Island to northern Luzon Island.

The above analysis and experience have shown the following main features:

- (a) The development of the heat low circulation over northern Burma and Pakistan with associated weakening of the Bay of Bengal anticyclonic cell and the western end of the Pacific subtropical ridge occurs before the progress of the southwest monsoon.
- (b) The displacement of the ITCZ is not continuous. It is characterized by advances, retreats and jumping movements.
- (c) The northward movement of a cyclone and the disappearance of the Pacific subtropical ridge are accompanied by the advance of ITCZ. The retreat of the ITCZ is related to:
  - (1) the southward migration of the continental anticyclone often giving rise to the formation of a shallow and ill-developed anticyclone over the Indochina Peninsula,
  - (2) the extension of the Pacific subtropical ridge to the west, and
  - (3) the westward movement of the tropical cyclone in the Philippines area, notably the typhoon circulation, favoring the progress of the divergent northeast flow far to the south.

By inspection of various weather maps, flow patterns during onsets of the southwest monsoon over Saigon are classified into four types as seen in figure 2.

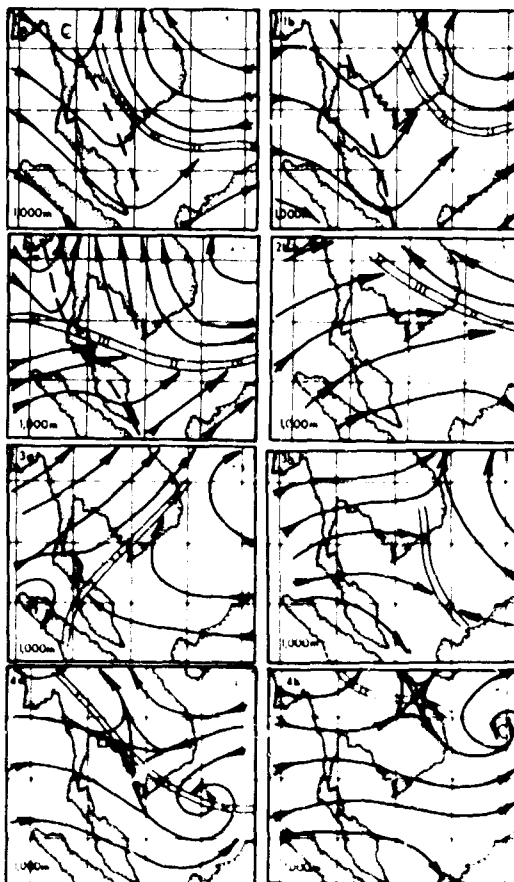


Figure 2. Types of Flow Patterns at 1000 M. Level During Onset of Southwest Monsoon Over Saigon.

— ITCZ      - - - - Trough line      a: before onset      b: after onset.





#### 4. CHANGES IN UPPER TROPOSPHERE CIRCULATION IN RELATION WITH THE MONSOON ESTABLISHMENT

Figure 3 indicates the normal change of the upper-troposphere subtropical ridge during the transition season from northeast monsoon to southwest monsoon. The normal subtropical ridge axis lies over the latitude of Saigon in April. It moves to Hainan Island in May corresponding to the period of onset of the summer monsoon.

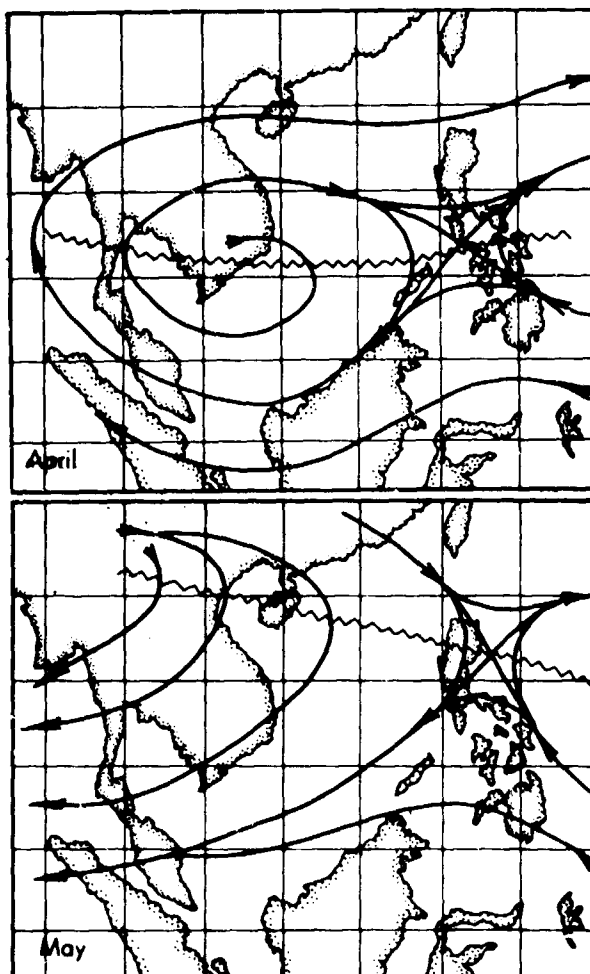


Figure 3. Normal Subtropical Ridge Axis Position at the 200 Mb. Level Over Vietnam for April and May (after Wiederanders [3]).

In general, the upper-troposphere subtropical ridge moves northwards with the seasonal inclination of the sun, with temporary north-south oscillations.

Orçill [1] has shown that late and early onsets are respectively associated with late and early latitudinal shifts of the subtropical ridge axis.

Inspection of 7-year radiosoundings over Danang has also revealed that a relationship between upper-level wind reversal over Danang and the southwest monsoon establishment over South Vietnam is very suggestive.

Figure 4 shows that the upper-level westerlies are very steady in April, north of 16° N. The change from westerly winds to easterly winds takes place around May and is accompanied by onset of southwest monsoon over Saigon. Apart from 1968, when the prolonged onset of the southwest monsoon is late, the first persistent appearance of the upper-level easterlies over Danang occurs generally 4 to 12 days before the onset of southwest monsoon over Saigon.

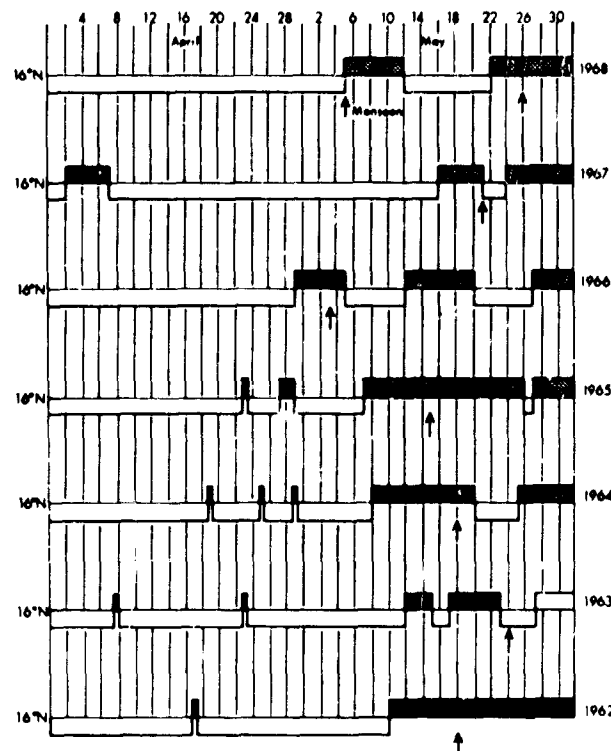


Figure 4. Relationship Between First Dates of Wind Reversal From West to East at 150 Mb. Level Over Danang ( $16^{\circ}$  N.) and Dates of Southwest Monsoon Establishment Over Saigon.

West Winds
  East winds
 ↑ Date of Southwest Monsoon Establishment Over Saigon.

## 5. CONCLUSION

Awaiting further investigations on the starting mechanism of the summer monsoon, forecasting the date of the establishment of the southwest monsoon over South Vietnam may be made by considering:

- (a) The heat-low circulation over northern Burma and Pakistan.
- (b) Tropical cyclone movement.
- (c) Continental anticyclone progress.
- (d) Changes in the lower-troposphere Pacific subtropical ridge.
- (e) Upper-level wind reversal from west to east over Danang.

## DISCUSSION

RAMAGE: Do you use this system to forecast monsoon onset each year? How many days in advance do you make the forecast?

MON: Yes, we do. We can forecast 2 or 3 days in advance.

## REFERENCES

1. ORGILL, M. M., "Some Aspects of the Onset of the Summer Monsoon Over South-east Asia." Colorado State Univ., Dept of Atmo. Science, 1967.
2. RIEHL, H., "Tropical Meteorology." McGraw-Hill, New York, pp. 256-257, 1954.
3. WIEDFRANDERS, C. J., "Analyses of Monthly Mean Resultant Winds for Standard Pressure Levels Over the Pacific." Hawaii Institute of Geophysics, Report No. 13, 1961.

INDIAN OCEAN CLOUD PATTERNS FROM  
SATELLITE PICTURES \*

J. H. Conover

Mr. Conover presented a movie--"Indian Ocean Cloud Patterns; ESSA Digital Product, May 1, 1967 - September 30, 1967."

The movie, made by the Walter A. Bohan Co., features a fade-in--fade out sequence.

DISCUSSION

RAMAGE: Are you planning to make a statistical analysis of the relative frequencies of moving and "pulsating" weather systems?

CONOVER: Mr. James Bunting of our laboratory plans to make such an analysis around the globe over tropical latitudes. Some of the observed pulsations may be related to atmospheric tides caused by the sun and moon.

CLIMATOLOGY OF ESSA CLOUD PICTURES OVER  
SOUTHEAST ASIA IN 1967\*

T. T. Fujita

Dr. Fujita presented slides showing computer-integrated cloudiness over southeast Asia and the Indian Ocean for each month of 1967 and for the 3-month periods: January-March, April-June, July-September and October-December. For the 6-month period July-December 1967 he compared the Pacific, Indian and Atlantic Oceans.

DISCUSSION

RAMAGE: It appears where the winds are light and moisture is available; the integrated pictures show evidence of seabreezes.

FUJITA: I noticed this phenomenon along the South China Sea coast in summer. If we had had an ATS-type picture, it would have been possible to see such sea-breeze cloud fronts in motion.

SOMERVELL: Three observations regarding your winter-season, monthly, cloud-summary slides upon which I'd appreciate your comments:

- (a) There appeared to be extensive cloudiness over southeastern Tibet which would seem to disagree with Flohn's conclusion that this area is a radiative heat source in winter.
- (b) The very marked winter-season cloud shadow west of the Annam and Burmese Mountains would seem to indicate a rather pronounced flow of low-level northeasterlies and, therefore, be at variance with earlier statements that cold air does not enter Thailand, Burma or India from China during the winter.
- (c) You did not take note of cold-air surges from China into Southeast Asia until November; yet there is a suggestion of the cloud shadow west of the Annams in September, which becomes very marked in October. I can assure you that cold-air intrusions into north Vietnam are common in September and occur in late August.

FUJITA:

- (a) Brightness in an integrated picture does not mean that clouds were in existence during the integration period. If bright clouds were only there for a total of 10 days or so, the area might act as a heat source as Flohn assumed.
- (b) My explanation should be limited to the case of blocking of low-level moisture by mountain ranges.
- (c) I would like to study my monthly averaged picture in the light of your comments.

CONOVER: Use of digital data will help reduce problem of adding thin cloudiness or weak reflectance from land or sea. Any threshold of brightness can be set up, i.e., the brightest levels will most likely show the active clouds. Patterns deduced in this fashion are quite different from those made by summing the photography.

FUJITA: You are right in this regard. In fact, ESSA is now producing various composite time integrations by integrating only above a certain intensity level. By doing so, it is feasible to eliminate as much as possible the effects of sand dunes, sun glint, etc.

SOUTHERN: I would like to comment on an extensive zone of cloudiness extending from the central Indian Ocean at about 60° - 80° E. southeastward to the southwest coast of Australia for the whole period April to October. This appears similar to the situation in the South Pacific southeastward from the Solomons-Fiji area. I was previously unaware of this link in mean cloudiness between the equator and southern cold fronts.

\* Research sponsored by National Environmental Satellite Center, Environmental Scientific Services Administration

FUJITA: I haven't studied closely the relationship between southern cold fronts and equatorial cloudiness. It would be interesting to study detailed motion of southern cold fronts in connection with satellite pictures.

SADLER: We have found that tracks of typhoons are not necessarily associated with maximum monthly cloudiness, and in fact many of your diagrams (November in the South China Sea and also in the eastern Pacific) show storm tracking along minimum monthly cloudiness.

FUJITA: Swaths of typhoon tracks on monthly average pictures are pronounced when storms move slowly over a relatively cloud-free area. I noticed one or two swaths along typhoon tracks. In general, however, it would be necessary to study case by case.

## NUMERICAL SIMULATION OF THE MONSOON ALONG 80° E.\*

Takio Murakami  
University of Hawaii

R. V. Godbole and R. R. Kelkar  
Institute of Tropical Meteorology, Poona, India

### 1. INTRODUCTION

The monthly mean geostrophic zonal wind speed along 80° E. in July 1967 is presented in figure 1. In a region south of 30° N., where the monsoon circulation prevails, a westerly current is encountered in the lower troposphere with its maximum speed (14 m. sec.<sup>-1</sup>) near 2.5 km., whereas the upper-flow pattern is characterized by the existence of strong easterlies (33 m. sec.<sup>-1</sup>) at about 16 km. Corresponding to this strong negative vertical shear of the zonal wind, the temperature is warmer to the north than to the south throughout the troposphere, the temperature difference between 30° N. and 10° N. being about 5 degrees. The surface-pressure trough located near 30° N. is capped by the pronounced subtropical high that reaches its maximum intensity near the 100 mb. level. According to meteorological satellite data gathered in 1967, cloud amounts are largest near 20° N., presumably indicating that ascending motion is stronger there than near 30° N. where the monsoon trough is located at the earth's surface. These characteristic features of the monsoon along 80° E., mentioned above, will be simulated by numerical experiments described in the following sections.

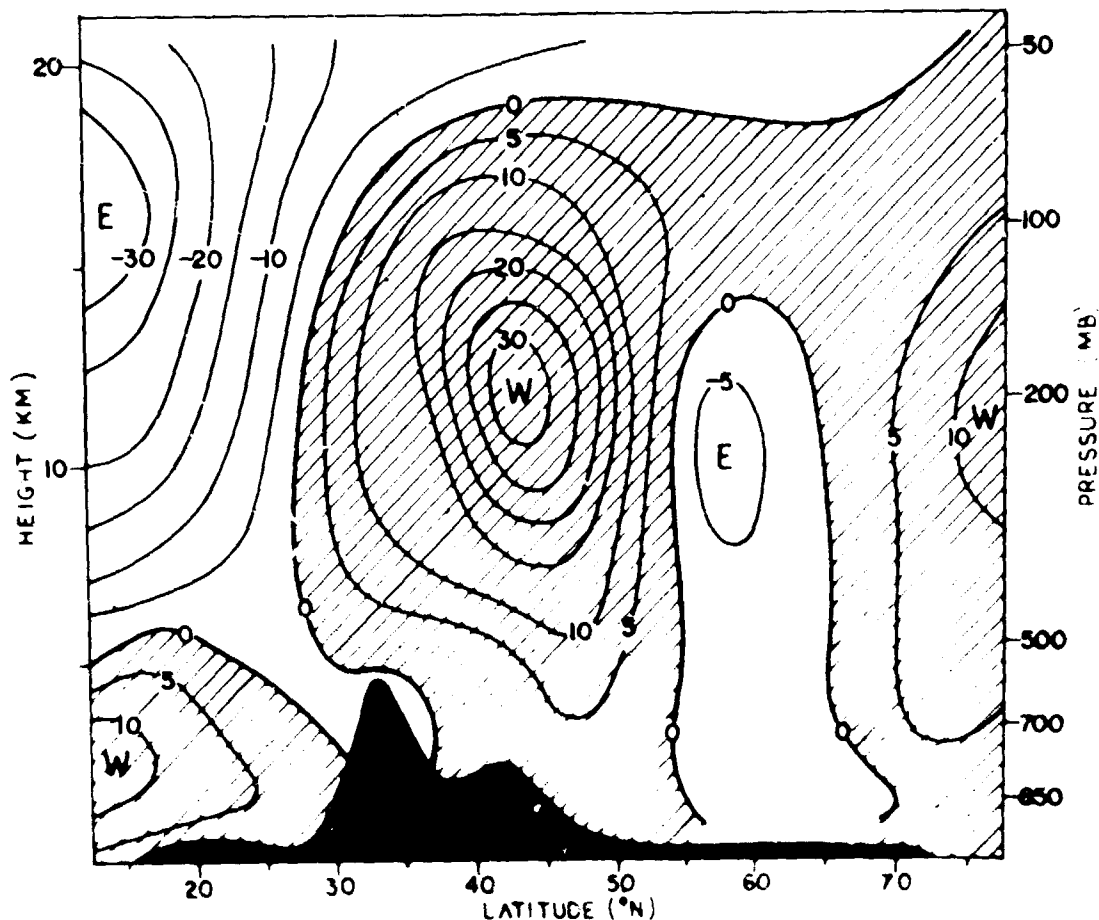


Figure 1. Monthly Mean Geostrophic Zonal Wind Along 80° E. in July 1967, Computed from Berliner Wetterkarte, Institute für Meteorologie und Geophysik der Freien Universität Berlin. Isolines are for 5 m. sec. intervals.

\* Research supported by the University of Hawaii and the Institute of Tropical Meteorology, Poona.

## 2. DESIGN OF THE EXPERIMENT

The monsoon develops over southeast Asia as a whole, extending roughly from 50° E. to 120° E. The main characteristics of the monsoon circulation are practically the same throughout this area. The essential geographic property of this area is relatively uniform in that it consists of a land mass to the north and oceans to the south. Under these circumstances, one may be allowed to introduce an idealized numerical model using a two-dimensional vertical plane along 80° E. from the equator to pole with the Indian Ocean extending from the equator to 15° N., the Asian continent from 15° N. to 80° N., and the Arctic Sea to the north of 80° N. This model considers only the meridional circulation and its associated zonal current and allows no disturbances to be superimposed upon the zonal motion. Observed vertical and horizontal wind shears, associated with the monsoon circulation shown in figure 1, are not considered strong enough to generate unstable barotropic and baroclinic waves because the stabilizing  $\beta$ -effect is substantial in the subtropics. It is our expectation that these disturbances do not play an important part in controlling the monsoon circulation.

In this first attempt at a numerical experiment, a few important factors are disregarded: (a) seasonal variation of the monsoon circulation by fixing the zenith angle of the sun to that in July and (b) the interaction between the northern and southern hemisphere by assuming that the meridional wind vanishes at the equator.

The  $\sigma$ -coordinate is used to facilitate an introduction of the dynamical and thermal effects of the Himalayas into the model. The  $\sigma$ -coordinate is defined by  $\sigma = P/P_0$ , where  $P_0$  denotes surface pressure. We divide the atmosphere into 8 layers as shown in table 1. We then apply the equations of motion to the levels 1 through 8, after replacing vertical derivatives with finite difference expressions. The finite difference scheme used was designed to conserve total energy in almost the same way as Kurihara [2] proposed.

Table 1. Vertical Location of the  $\sigma$ -Level Used:  $P_0$  Denotes the Surface Pressure.

K	1/2	1	2	3	4	5	6	7	8	8 1/2	9
$\sigma = P/P_0$	0.00	0.01	0.08	0.21	0.37	0.54	0.71	0.86	0.96	0.99	1.00

Following Manabe and Möller [3], the radiational heating due to both short- and long-wave effects are computed from an observationally determined distribution of water vapor, carbon dioxide and ozone, using the latest available data for the monsoon season. Condensation due to meridional circulation and convection are also considered. The convective effect is treated simply by adjusting the vertical distribution of temperature in any layer of a column to the dry (wet) adiabatic lapse rate whenever the distribution exceeds the dry (wet) adiabatic lapse rate for a humidity less (more) than 100 percent.

We assume constant vertical flux  $\kappa$  of momentum, heat and water vapor within the turbulence layer between the levels "8 1/2" and "9". The thickness of the surface-turbulence layer is assumed to be constant (about 80 m.) throughout the region considered. According to Deacon's empirical formula, the vertical eddy-diffusion coefficient is given by:

$$K = k_0 z_0^2 \left( \frac{z}{z_0} \right)^{-1} \frac{dU}{dz} \quad (1)$$

where  $U = (u^2 + v^2)^{1/2}$ ,  $k_0$  the Karman constant,  $z_0$  the roughness parameter;  $z_0 = 0.1$  cm. over the ocean,  $z_0 = 1$  cm. over the land and  $z_0 = 10$  cm. over the mountains. The value of  $\kappa$  is equal to 1.2 for unstable stratification and 1.0 for stable stratification.

The sensible and latent heat flux at the top of the turbulence layer may be obtained from:

$$-H = -\kappa k_0 z_0^2 (U^2) (T_8 - T_9) \quad (2)$$

$$-Q = -\kappa k_0 z_0^2 (U^2) (q_8 - q_9) \quad (3)$$

where  $h$  denotes the height of the turbulence layer,  $\rho_s$  the air density at the earth's surface,  $\theta(z)$  the potential temperature at the level "z",  $\theta_s$  the potential temperature at the surface,  $q(z)$  the mixing ratio at the level "z", and  $q_s$  the mixing ratio at the surface. The quantity  $m$  is defined by:

$$m = \left[ \frac{1}{1-\gamma} \left\{ \left( \frac{h+z_0}{z_0} \right)^{1-\gamma} - 1 \right\} \cdot \frac{\Delta z}{z_0} \left( \frac{h+z_0}{z_0} \right)^{-\gamma} \right]^{-1} \quad (4)$$

where  $\Delta z$  is the height difference between the level "z" and "z + 1/2".

Surface mixing ratio  $q_s$  is assumed to be proportional to the saturated mixing ratio at surface temperature,  $q_s(T_s)$ . That is:

$$q_s = a q_s(T_s) \quad (5)$$

where quantity  $a = 1.0$  over the ocean. Over the continent, we arbitrarily set quantity  $a = 0.4$  or  $0.8$  in order to examine the effect of surface humidity upon the intensity of the monsoon circulation.

By assuming an infinite heat capacity of the sea,  $T_s$  over the oceans can be considered constant. Temperature at the land surface is determined from the requirement of heat balance at the earth's surface. The balance equation of heat is:

$$S_d + D_s - U_s = -c_p (\gamma_s' \cdot \frac{1}{c_p} \mu_s') \quad (6)$$

where  $S_d$  and  $D_s$  are the net downward solar insolation and the downward long-wave radiation at the earth's surface respectively, and  $U_s = \sigma T_s^4$ , the upward long-wave radiation at the surface. Albedo at the earth's surface is determined empirically by considering cloud amounts, precipitation and surface conditions during the monsoon season. Due to the constraint of constant flux within the turbulence layer,  $\gamma_s'$  and  $\mu_s'$  at the earth's surface are assumed equal to  $\gamma'(h)$  and  $\mu'(h)$  in equation (2) and equation (3), respectively. The solution of equation (6) yields a value of  $T_s$  that satisfies the heat-balance condition at the earth's surface.

We start our numerical experiment by assuming a completely calm and dry atmosphere with the same vertical temperature distribution as that of the standard atmosphere. Therefore, there are no north-south temperature gradients along any constant pressure surface. It takes a very long time (about 150 days) before a state of quasi-equilibrium is reached. Wind, temperature, humidity, and surface-pressure distributions obtained in the quasi-equilibrium state are then compared with observed distributions along 80° E.

The object of this numerical simulation is to understand the basic mechanism responsible for maintaining the monsoon circulation. Even though our numerical model is very simple, it nevertheless includes many physical factors which can be examined individually. A complete and detailed attempt at the outset might give us some difficulty in obtaining a thorough understanding of the monsoon mechanism. Consequently, we start our experiment with the most simplified version of the model and then proceed to other models with fewer constraints. We planned the following series of experiments:

Experiment I assumes a completely dry model atmosphere having no evaporation at the earth's surface and no condensation in the atmosphere. We also disregard the effect of mountains by assuming a flat earth. Radiational heating and cooling, and the sensible heat transfer at the earth's surface are the main physical factors involved in this experiment. Surface temperatures over the continent, evaluated from the heat-balance condition, are much higher than surface temperatures over the oceans. The surface-temperature contrast between the continent and the oceans determines the direction and intensity of thermally induced circulations, as is the case in the sea-breeze circulation. However, there is a larger difference between the two circulations. The Coriolis force does not play an important part in the sea-breeze circulation because of its relatively small horizontal extent (of the order of 100 km.). On the other hand, the Coriolis force is one of the dominant factors controlling the monsoon circulation because of its relatively large north-south extent (of 1000 km. or more). The height of the sea breeze is generally 1 to 2 km. because of its small time scale of only one day, while the monsoon circulation extends perhaps even up to the stratosphere because its time scale is much larger than of one day.



We first carried out Experiment I by assigning 300° K. to the sea-surface temperature over the Indian Ocean and next by assigning 290° K. By comparing the two computed results thus obtained, it was possible to obtain quantitative information about the effect of the Indian Ocean surface temperature upon determining the intensity of the monsoon circulation.

Experiment II considers evaporation at the earth's surface and condensation in the atmosphere. The surface-temperature contrast between the continent and the oceans is appreciably lower than that in Experiment I, described above, because evaporation takes heat away from the ground surface of the continent. Due to this, the induced circulation is weakened. On the other hand, condensation may contribute to the intensification of the circulation. Our tentative conclusion is that these two effects almost cancel out each other so that the intensity of the monsoon circulation in Experiment II is nearly the same as that in Experiment I.

We assigned two different values for the surface humidity over the continent, i.e., 40% and 80%. Which surface-humidity value makes the monsoon circulation stronger? The answer to this question should provide some clue for understanding why the monsoon does not develop well in longitudes close to the Pacific Ocean where relative humidities over land there are presumably higher than those to the west. Two-condensation criterion, i.e., 80% and 100%, were examined in Experiment II. It was anticipated that the intensity of the monsoon circulation increases significantly according to the change of condensation criterion, i.e., from 100% to 80%.

Experiment III considers mountain effects. The east and elevated Himalayas could act as a heat source in the middle troposphere and could play a dominant role in intensifying the monsoon circulation. The importance of the thermal effect of the Himalayas has been discussed by Mohn [2] and Murakami [5]. A preliminary integration was carried out up to the time interval of 80 days. The computed zonal wind speed for an 80-day interval is presented in figure 2 as a function of latitude and height. One may at once notice a great similarity between the computed zonal wind distribution and the observed one, which are shown in figure 1. It may be possible to conclude that the essential feature of the monsoon circulation--existence of the westerlies in the lower troposphere capped by the strong easterlies aloft--can be simulated even by using the simplified two-dimensional model, in which several important factors are disregarded, such as the effects of disturbances superimposed upon the zonal motion and so on.

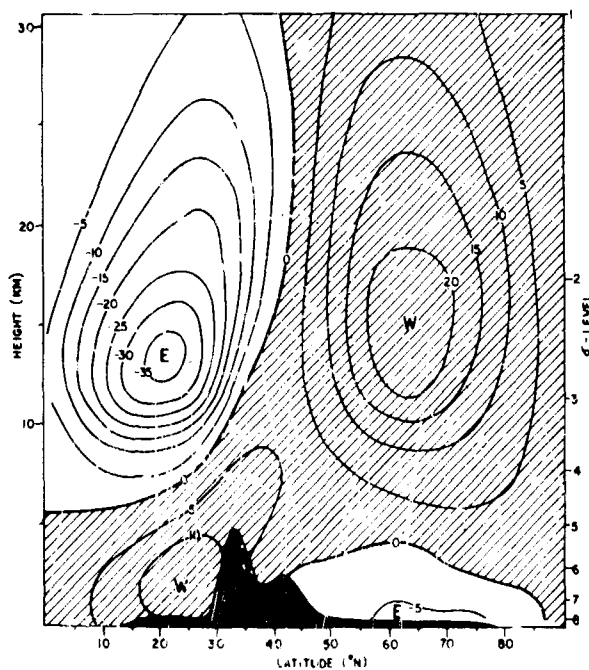


Figure 2. Computed Zonal Wind Along 80° E., Obtained After 80-day Time Integration in Experiment III. Isolines are for 5 m. sec.<sup>-1</sup> intervals.

In the course of the time integrations in Experiment III, however, we encountered some difficulty with the finite-difference scheme used. It was not possible to depress the so-called two-mesh irregularities caused primarily by steep mountains such as the Himalayas. We applied rather strong smoothing to extend computations up to 80 days. It was, therefore, necessary to revise our computational scheme before we continued Experiment III any further. This being the case, detailed discussions on Experiment III will not be given in this paper.

### 3. EXPERIMENT I

This section will be primarily devoted to discussions on the first subset of Experiment I, in which the sea-surface temperature was prescribed as being  $300^{\circ}$  K. over the Indian Ocean and  $270^{\circ}$  C. over the Arctic Sea.

Figure 3 demonstrates the latitudinal distribution of temperature at the  $\sigma$ -levels of "6", "7", "8", and "9". The level "9" is for the earth's surface as shown in table 1. Omission of evaporation in this experiment makes the surface temperature over the continent extremely high, the maximum being about  $323^{\circ}$  K. at  $27.5^{\circ}$  N. It is of interest here to add that the net solar insolation at the earth's surface, which is primarily related to the zenith angle of the sun and the duration of day time in a day, is maximum at  $32.5^{\circ}$  N. The surface temperature computed from the heat-balance requirement depends not only upon the net downward solar insolation but also dominantly upon the sensible heat flux at the top of the turbulence layer. The reason why the surface temperature computed in this experiment is maximum at  $27.5^{\circ}$  N., rather than at  $32.5^{\circ}$  N., is that the sensible heat flux is much larger at the latter latitude than at the former latitude as will be seen later. In other words, more heat is removed from the earth's surface at  $32.5^{\circ}$  N.

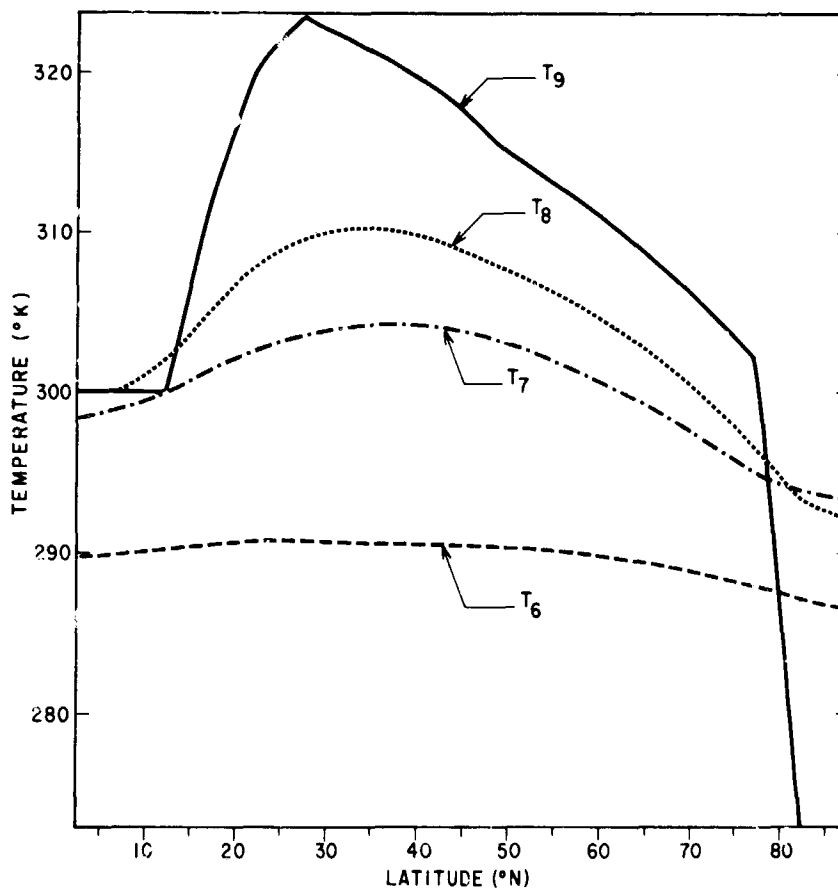


Figure 3. Latitudinal Temperature Distribution at Constant  $\sigma$ -level Obtained in Experiment I.  $T_9$  denotes the temperature at the earth's surface.  $T_6$ ,  $T_7$ , and  $T_8$  are the temperature at the  $\sigma$ -level "6", "7", and "8", respectively.

It also appears in figure 3 that the temperature difference between the continent and the Indian Ocean is about 23° C. at the earth's surface, about 5° C. at the level "7" (approximately 850 mb.), and only about 1° C. at the level "6" (roughly 700 mb.). The temperature difference appears to decrease almost exponentially with increasing height. This characteristic does not agree with observations. For example, the observed monthly mean-temperature difference between New Delhi (29° N., 77° E.) and Trivandrum (8° N., 77° E.) is 5.9° C. at 850 mb., 3.9° C. at 700 mb., 3.9° C. at 500 mb., 6.9° C. at 300 mb., 7.3° C. at 200 mb., and 2.0° C. at 100 mb. The mean temperature at New Delhi is substantially higher than that at Trivandrum throughout the entire troposphere with the maximum difference at the 200-mb. level. Referring to the thermal wind equation, one may guess that the computed vertical wind shear in Experiment I would be extremely weak as compared to the observed vertical wind shear associated with the westerlies in the lower troposphere and strong easterlies aloft. A question may be raised here as to what physical factor must be introduced into the numerical model so that even in the higher troposphere, computed north-south temperature gradients would compare favorably with observed ones. To answer this question, is one of the central problems in this study.

Now let us take a look at figure 4, which shows the latitudinal distribution of the computed surface pressure and the geopotential heights at several  $\sigma$ -levels. The surface pressure, considered constant (1013 mb.) initially at all latitudes, is minimum near 30° N., where the computed surface temperature is highest as shown in figure 3. It will be pointed out later that there is pronounced descending motion in the surface-pressure trough. These features are characteristic of the so-called heat low. In figure 4 we also present, by a dashed line, the observed monthly mean-surface pressure along 80° E. in July 1967, obtained from the Mittlere Luftdruck Verteilung, Hamburg. One may notice that the computed surface-pressure trough agrees fairly well in its location with the observed monsoon trough, although the computed trough is not as deep as the observed one.

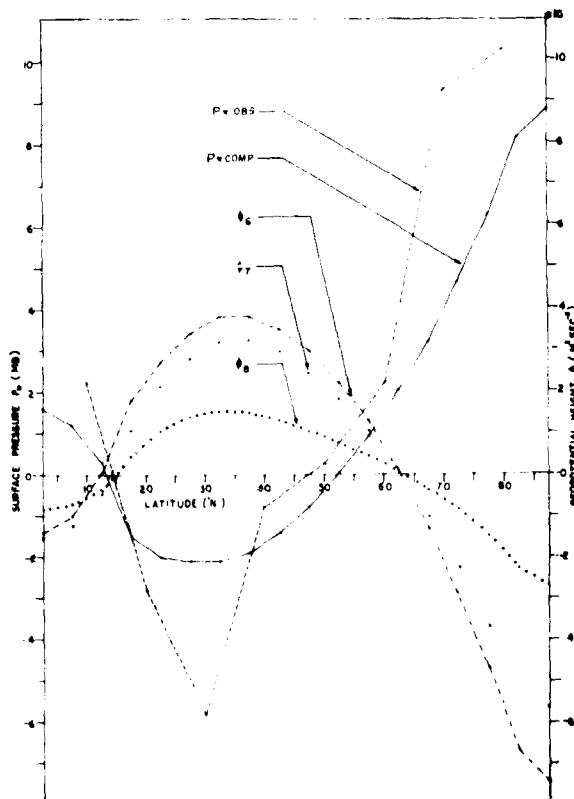


Figure 4. Latitudinal Distribution of the Surface Pressure and the Geopotential Height at Constant  $\sigma$ -level, Computed in Experiment I. The dashed line is for the observed monthly mean surface pressure along 80° E. in July 1967, extracted from Die Witterung in Obersee, Deutscher Wetterdienst, Hamburg. The unit is in mb. for the surface pressure, and in  $10^3 \text{ m}^2 \text{ sec}^{-2}$  for the geopotential height.

It appears in figure 4 that the geopotential height at any  $\sigma$ -surface is highest near  $35^\circ$  N., this latitude being only slightly north of the center of the computed surface-pressure trough. By using the geopotential height at  $\sigma$ -level and the surface pressure, it is possible to evaluate the north-south gradient of isobaric height as follows:

$$-\left(\frac{\partial \psi}{\partial \psi_p}\right) = \sigma \frac{\partial \phi}{\partial \sigma} \frac{\partial P_*}{\partial \psi} - P_* \left(\frac{\partial \phi}{\partial \psi_\sigma}\right) \quad (7)$$

where  $\psi$  is latitude,  $\phi$  is geopotential height and the subscripts "p" or " $\sigma$ " refers to the quantity at constant p or  $\sigma$  surfaces.

We next estimated the first and second terms on the right-hand side of equation (7). In the monsoon region to the south of  $30^\circ$  N., the first term is positive, decreasing as  $\sigma$  decreases, whereas the second term is negative with small (large) magnitude in the lower (upper) atmosphere. Consequently the sum of the two terms, which is identical to the north-south gradient of isobaric height, is positive in the lower atmosphere and negative in the upper atmosphere. Actual computation shows that the sum changes its sign somewhere around the  $\sigma$ -level "6" (approximately the 700-mb. surface). On the other hand, it has been long known among synoptic meteorologists that the north-south gradient of isobaric height changes its sign near 500 mb. since the monsoon trough extending generally up to 500 mb. is capped by the pronounced wedge in the upper atmosphere above 500 mb. At any rate, from Experiment I, it may be concluded that the monsoon trough extends only up to 700 mb., above which it is replaced by the wedge.

We prepared figure 5 to show the distribution of the computed zonal wind speed. In a region to the south of  $25^\circ$  N. a westerly current is encountered near the earth's surface with easterlies aloft. This feature is very similar to what we found in the observed zonal wind distribution shown in figure 1. However, the computed maximum speed of the easterlies is only about  $-8$  m. sec.<sup>-1</sup> as against the observed value of  $-33$  m. sec.<sup>-1</sup>. Likewise, the computed westerlies are appreciably weaker than the observed westerlies.

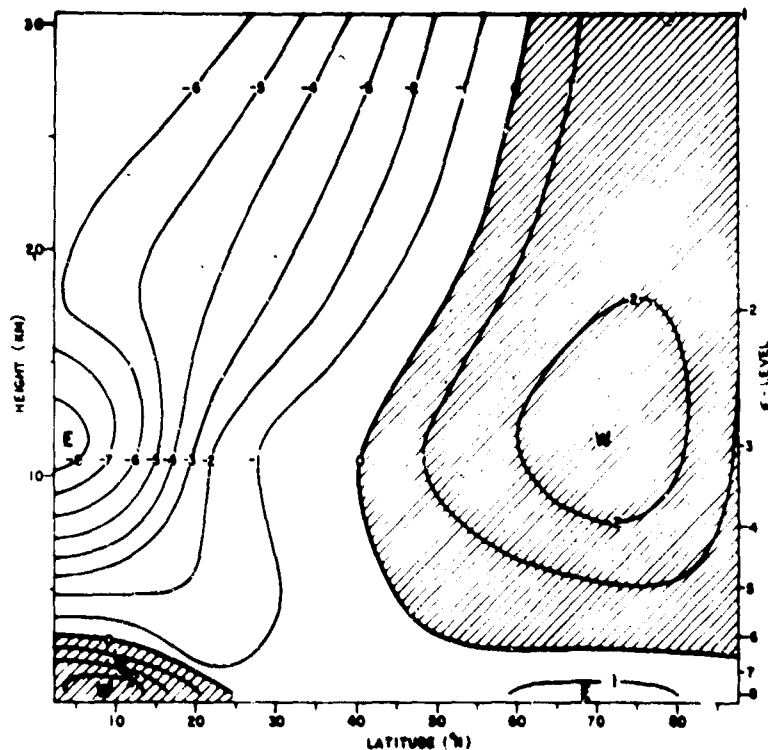


Figure 5. Computed Zonal Wind in Experiment I. Isolines are for 1 m. sec.<sup>-1</sup> intervals.

Let us now turn our attention to the distribution of the vertical velocity,  $\omega = dp/dt$ , shown in figure 6. A positive sign indicates descending motion and a negative sign ascending motion. The outstanding feature in the stratosphere is the presence of ascending motion in middle latitudes surrounded by descending motion to the north and south. This feature undoubtedly indicates existence of two meridional circulation cells in the stratosphere. One cell to the south of  $45^\circ$  N. is accomplished by ascending warm air in middle latitudes and descending cold air in lower latitudes with the northerly meridional current as a compensating flow. Another cell to the north of  $45^\circ$  N. is associated with ascending motion in middle latitudes and descending motion in higher latitudes, accompanied by the southerly meridional current. These two meridional circulation cells, each of about 45 degrees of latitude in horizontal extent, are perhaps induced by the geographical configuration--a flat continent overlies the central part of the region with the Indian Ocean to the south and the Arctic Sea to the north. These two meridional circulation cells can be discernible in the troposphere, also, although they are not as clearly defined as in the stratosphere. Tropospheric meridional circulation is more complicated. Near the southern edge of the continent, a marked region of strong ascending motion is surrounded by two bands of descending motion, one each to the north and south. The same situation, with less circulation intensity, can also be recognized near the northern periphery of the continent. In the monsoon region to the south of  $30^\circ$  N., we note the following:

- (a) Strong ascending motion exists near  $17.5^\circ$  N., about 10 degrees south of the surface-pressure trough (see fig. 3) and also of the maximum surface temperature (see fig. 2). This computed finding is supported by meteorological satellite observations taken in 1967 in that cloudiness is greatest about 10 degrees south of the monsoon trough. We will see later that the location of strong ascending motion coincides exactly with the location of maximum sensible heat flux at the top of the surface-boundary layer.
- (b) Strong descending motion is encountered near  $27.5^\circ$  N., which is the latitude of the surface-pressure trough and of the highest surface temperature.

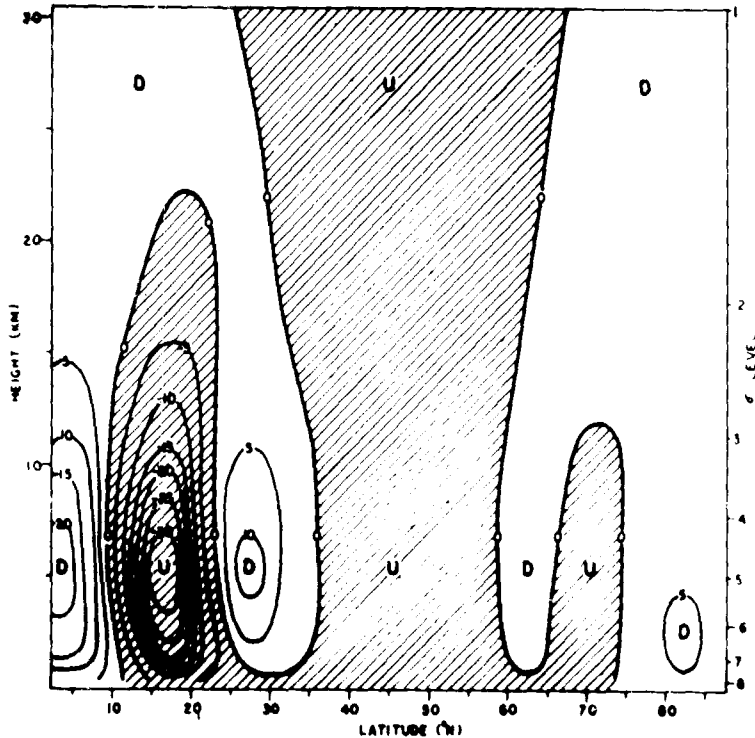


Figure 6. Vertical Velocity in the Unit of  $10^{-5}$  mb. sec.<sup>-1</sup> Obtained in Experiment I. Isolines are for  $5 \times 10^{-5}$  mb. sec.<sup>-1</sup> intervals. The ascending motion is indicated by minus, and the descending motion by positive.

- (c) Descending motion predominates over the Indian Ocean. This result agrees qualitatively with less cloudiness observed over the Indian Ocean by meteorological satellites.
- (d) At any level, the magnitude of the ascending motion is almost equal to the sum of the magnitude of descending motions to the north and south. At the level "5" for instance, the maximum value of ascending motion is about  $-30 \times 10^{-5}$  mb. sec.<sup>-1</sup> and the corresponding values for the descending motion are  $10 \times 10^{-5}$  mb. sec.<sup>-1</sup> (north) and  $20 \times 10^{-5}$  mb. sec.<sup>-1</sup> (south). This is due to the requirement of mass continuity.

In an effort to describe the process whereby balance is achieved among various forms of energy, we measured several interaction terms under Experiment I. In the quasi-equilibrium state, the energy equation may be expressed as follows:

$$0 = \langle K_z, K_m \rangle + \langle K_z, F_\lambda \rangle \quad (8)$$

$$0 = -\langle K_z, K_m \rangle + \langle K_m, P \rangle + \langle K_m, F_\psi \rangle \quad (9)$$

$$0 = -\langle K_m, P \rangle + \langle P, \dot{q} \rangle \quad (10)$$

where

$$\langle K_z, K_m \rangle = \frac{1}{g} \int_0^{\frac{\pi}{2}} \int_0^1 \rho_* u v \left( f + \frac{\tan \psi}{a} u \right) a^2 \cos \psi \, d\psi \, d\sigma \quad (11)$$

$$\langle K_m, P \rangle = \frac{1}{g} \int_0^{\frac{\pi}{2}} \int_0^1 \omega \frac{\partial \phi}{\partial \sigma} a^2 \cos \psi \, d\psi \, d\sigma \quad (12)$$

$$\langle P, \dot{q} \rangle = \langle P, \dot{q}_r \rangle + \langle P, F_T \rangle \quad (13)$$

$$\langle P, \dot{q}_r \rangle = \int_0^{\frac{\pi}{2}} [(S_0 - S_*) + (U_* - D_* - U_o)] a^2 \cos \psi \, d\psi \quad (14)$$

$$\langle P, F_T \rangle = -c_p \int_0^{\frac{\pi}{2}} \gamma_*^2 a^2 \cos \psi \, d\psi \quad (15)$$

in which  $S_0$  and  $S_*$  are the net solar radiation at the top and bottom of the atmosphere, respectively;  $U_*$  and  $D_*$  represent the upward and downward long-wave radiation at the earth's surface, and  $U_o$  the outgoing long-wave radiation at the top of the atmosphere.

The term  $\langle K_z, K_m \rangle$  represents a redistribution of kinetic energy between the zonal and meridional current,  $\langle K_m, P \rangle$  indicates a conversion of potential energy into kinetic energy of the meridional current,  $\langle P, \dot{q} \rangle$  signifies a generation of potential energy due only to radiational effect, and  $\langle P, F_T \rangle$  signifies a generation of potential energy due to sensible heat supply at the top of the turbulence layer. The quantity  $\langle P, \dot{q} \rangle$  indicates a net generation of potential energy and is equal to the sum of  $\langle P, \dot{q}_r \rangle$  and  $\langle P, F_T \rangle$ . The terms  $\langle K_z, F_\lambda \rangle$  and  $\langle K_m, F_\psi \rangle$  represent frictional dissipation of zonal and meridional kinetic energy, respectively. We evaluated the interaction terms in equations (11) through (15) at each 5-degree latitude band.

Figure 7 applies to  $\langle P, F_T \rangle$ . A positive sign represents an upward transfer of sensible heat at the top of the surface turbulence layer, i.e. the sensible heat is transferred into the atmosphere, and consequently potential energy is furnished through this process. Figure 7 reveals that the sensible heat transfer is upward over the entire continent, while it is slightly downward over the oceans. The net transfer of sensible heat over the whole region considered is obviously positive. Increase of potential energy through this process is eventually transformed into kinetic energy of the induced circulation. It would not be fortuitous to find in figures 6 and 7 that the strongest ascending motion is induced in a region where the sensible heat transfer is largest and that descending motion is induced in a region where the sensible heat flux is relatively small as compared with the surrounding area.

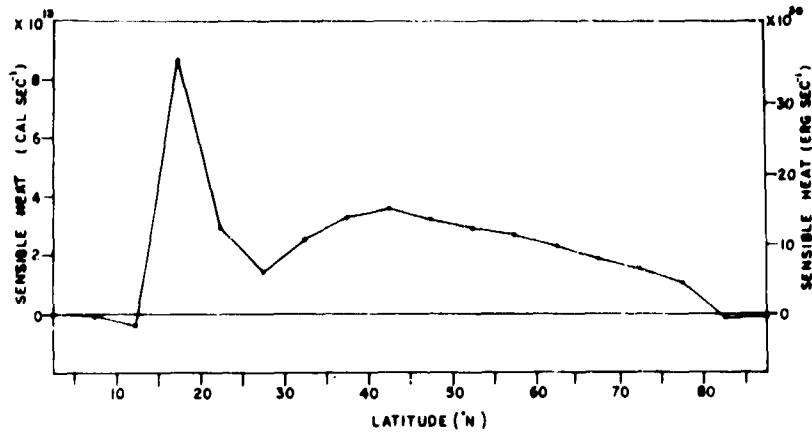


Figure 7. Sensible Heat Transfer at the Top of the Surface Turbulence Layer, Computed by (13) at each 5 degree Latitude Band. The unit is in either  $10^{20}$  ergs. sec.<sup>-1</sup> or  $10^{18}$  cal. sec.<sup>-1</sup>.

Let us next take a look at the latitudinal distribution of  $\langle P, \dot{q} \rangle$ , shown in figure 8 by the dashed line. The first term in the integrant of equation (14) represents the absorption of direct solar radiation and the second term the cooling due to long-wave radiation. It is clear in figure 8 that the net radiational effect,  $\langle P, \dot{q} \rangle$ , is negative (cooling) everywhere. The sum of the radiational effect and the sensible heat supply,  $\langle P, \dot{q} \rangle$ , is also shown in figure 8 by the solid line. There is a net heating over the continent due primarily to the sensible heat supply at the earth's surface and a net cooling over the oceans due mainly to radiational effects. This heat contrast between the continent and the oceans is an essential factor for determining the intensity of induced circulation. An excess of heat over the continent has to be transported through induced atmospheric circulation and on to the oceans to compensate for loss of heat there. There is a sharp gradient of diabatic heating near the latitude  $20^\circ$  N, where the monsoon circulation develops at its full intensity. It is our conclusion in this section that the monsoon circulation is caused principally by the heat contrast between the radiational cooling over the Indian Ocean and the sensible heat supply at the southern part of the continent.

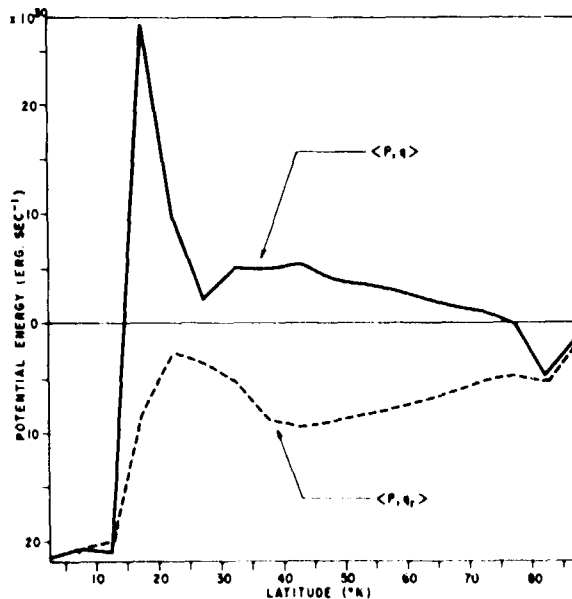


Figure 8. Generation of Potential Energy Due to Radiational Effect,  $\langle P, \dot{q} \rangle$  as Defined in (12), is Shown by Dashed Line. The full line is for  $\langle K, P \rangle$ , generation of potential energy due both to radiational effect and to sensible heat supply. The unit is in  $10^{20}$  ergs. sec.<sup>-1</sup>.

It would be worthwhile here to point out that  $\langle P, \dot{q} \rangle$  can be expressed in the following form:

$$\langle P, \dot{q} \rangle = \int_0^{\pi/2} [S_0 - U_0] a^2 \cos \psi \, d\psi \quad (16)$$

where use is made of the balance requirement of heat at the earth's surface. Since no evaporation is included in Experiment I, equation (16) becomes:

$$0 = U_0 - D_0 - S_0 - c_p \gamma_0^2 \quad (17)$$

By inserting equation (17) into equations (14) and (13), we can obtain the equation (16).

Figure 9 portrays  $\langle K_m, P \rangle$  and  $\langle K_z, K_m \rangle$ . As for  $\langle K_m, P \rangle$ , a large conversion of potential energy into meridional kinetic energy occurs near  $17.5^\circ \text{ N}$ , and the reverse is the case over the Indian Ocean. The dashed line gives the latitudinal distribution of  $\langle K_z, K_m \rangle$  and reveals that it is positive everywhere, a positive sign signifying kinetic energy transfer from the meridional to zonal current. The sign of  $\langle K_z, K_m \rangle$  is determined by the sign of a product of  $u$  and  $v$ , as is seen in equation (11). The computed wind field shows that the westerly zonal current ( $u > 0$ ) is generally associated with the southerly meridional flow ( $v < 0$ ), and the easterly ( $u < 0$ ) with the northerly ( $v > 0$ ). Accordingly, the product of  $u$  and  $v$  is found to be positive almost everywhere. This result presumably means that the coriolis force plays an important role in maintaining the monsoon circulation.

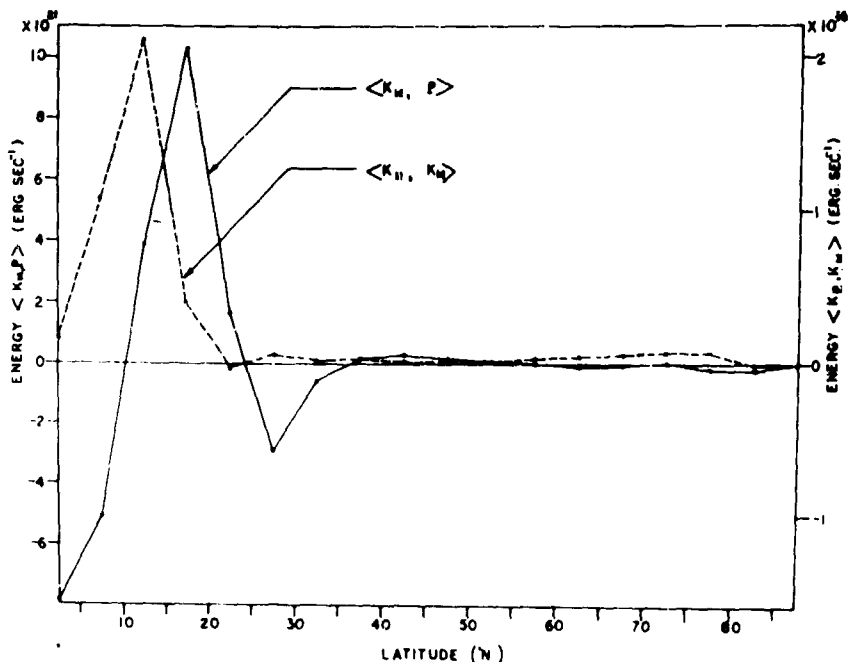


Figure 9. Conversion Between Potential Energy and Meridional Kinetic Energy (full line),  $\langle K_m, P \rangle$  as Defined by (10), is in the Unit of  $10^{21}$  ergs.  $\text{sec}^{-1}$ . The kinetic energy interaction between the meridional and zonal flow (dashed line),  $\langle K_z, K_m \rangle$  as defined in (9), is expressed in the unit of  $10^{19}$  ergs.  $\text{sec}^{-1}$ .

So much for the case where the sea-surface temperature over the Indian Ocean was assigned a value of  $300^\circ \text{ K}$ . In another case we changed it to  $290^\circ \text{ K}$ . The other parameters, such as the sea-surface temperature over the Arctic Sea, the surface albedo over the continent and so on, remained unchanged. In doing so, it is possible to isolate the effect of the Indian Ocean surface temperature upon the monsoon circulation. The results, obtained after 50-day time integrations, may be summarized as follows:

- (a) The surface pressure diminished over the continent as a whole; however, it increased over the Indian Ocean by about 1 mb.; the maximum decrease (about 0.5 mb.) occurred near  $50^\circ \text{ N}$ . This result means that a shift of mass took place between the continent and the Indian Ocean.



- (b) In spite of the extraordinarily large change (10° C.) of the Indian Ocean surface temperature, the magnitude of the westerlies and easterlies associated with the monsoon circulation remained basically the same; the maximum increase of the westerlies (easterlies) was only about 0.3 m. sec.<sup>-1</sup> (1.5 m. sec.<sup>-1</sup>).
- (c) Ageostrophic meridional flow developed rapidly at the initial stage to adjust to the sea-surface temperature change, but the flow died out soon.

These findings all lead us to conclude that the sea-surface temperature is not a dominant factor in controlling the intensity of the monsoon circulation.

#### 4. EXPERIMENT II

Only a brief discussion will be given in this section concerning Experiment II. It considers evaporation from the earth's surface and condensation in the atmosphere. Thermal and dynamical effects of the Himalayas are not taken into account, however.

Experiment II consists of three-subsets. In the first subset the humidity, at the earth's surface, defined in equation (3) as quantity  $a$ , is 40% over the continent and 100% over the oceans. The condensation criterion is prescribed as 100%. The second subset has a condensation criterion of 80%, while the surface-humidity criterion is the same as the first subset. In the third subset the surface-humidity value is changed to 80% over the continent, but the condensation value is held at 100%. For all subsets we use the same value (300° K.) for the Indian Ocean surface temperature. The remaining parameters, including the surface albedo, are the same as used in Experiment I.

The zonal wind speed obtained in the first subset was compared with that obtained in Experiment I. Surprisingly, the zonal wind speed remained practically unchanged. This result means that inclusion of evaporation and condensation in our model did not contribute significantly to intensify the monsoon circulation. A similar conclusion was reached by Manabe et al. [4]. In their three-dimensional simulation of the general circulation, using a nine-level model, they found that the jet stream did not appreciably intensify even when evaporation and condensation were incorporated. In order to consider this problem, we will examine the energetics of our present model. Instead of equation (11), we now obtain:

$$\langle P, \dot{q} \rangle = \langle P, \dot{q} \rangle + \langle P, F_T \rangle + \langle P, F_c \rangle \quad (18)$$

where  $\langle P, F \rangle$  represents a generation of potential energy due to condensation. It can be expressed as:

$$\langle P, F_c \rangle = -L \int_0^{\pi/2} c a^2 \cos \psi \, d\psi \quad (19)$$

in which quantity  $c$  denotes amount of condensation.

The continuity of water vapor in the atmosphere is given by:

$$\int_0^{\pi/2} c a^2 \cos \psi \, d\psi = \int_0^{\pi/2} \mu^2 a' \cos \psi \, d\psi. \quad (20)$$

Inserting equations (14), (15), and (19) into equation (18) and then using equations (6) and (20), we obtain:

$$\langle P, \dot{q} \rangle = \int_0^{\pi/2} [S_0 - U_0] a^2 \cos \psi \, d\psi. \quad (21)$$

which has exactly the same form as equation (16) under Experiment I. Since the albedo remains the same for both Experiment I and II, the net solar radiation at the top of the atmosphere,  $S_0$ , is also the same. The outgoing long-wave radiation at the top of the atmosphere,  $U_0$ , depends primarily upon atmospheric temperature, cloud amount and cloud height. In this study, however,  $U_0$  was simply assumed to be a function of temperature only. It was found that  $U_0$  remained practically unchanged in both Experiment I and II. In consequence of this, the net generation of potential energy,  $\langle P, \dot{q} \rangle$  estimated by equation (13) for Experiment I and by equation (18) for Experiment II, were also virtually equal. This result could be the reason why the intensity of the monsoon circulation did not change significantly even though evaporation and condensation were considered in the second experiment.

The second subset of Experiment II did not show any intensification of the monsoon circulation, either. We interpreted the findings as follows: The change of condensation criterion from 100% to 80% increased precipitation and at the same time increased evaporation at the earth's surface. The increase of condensation is favorable for intensifying the monsoon circulation, but the increase of evaporation over the land is unfavorable because it tends to diminish the temperature contrast between the continent and the oceans. In fact, these two effects seem to cancel each other out. It is our tentative conclusion in this paper that, unless we take the thermal and dynamical effects of the Himalayas into account, the computed monsoon circulation cannot be as strong as the observed one.

In the third subset we found that the monsoon circulation appreciably diminished in intensity as compared to the first subset. For instance, the easterly maximum centered near 12 km. decreased to about  $-3 \text{ m. sec.}^{-1}$ . This finding is to be compared with  $-8 \text{ m. sec.}^{-1}$  encountered in the first subset. Our speculation is that the monsoon circulation is weak in a region of high surface humidity.

## DISCUSSION

KRISHNAMURTI: Sadler's maps show large asymmetries in the zonal directions; hence, I would not expect a perfect simulation in a symmetric experiment. When you find some aspect of verification not working too well, you make another experiment by changing parameters such as relative humidity criteria, etc. I wonder if some of these large asymmetries may not be locally important in the Southeast Asia monsoon.

MURAKAMI: My contention concerning the large asymmetries in the zonal direction is not that they are unimportant factors of the monsoon, but that I neglected them in the preliminary experiment in order to examine other effects more closely. To include all possible factors at once makes physical understanding of the effect of each individual factor upon the monsoon quite difficult. We will consider east-west asymmetries in the future.

## REFERENCES

1. FLOHN, H., "Large-Scale Aspects of the "Summer-Monsoon" in the South and East Asia." 75th Anniversary of Volume of J. Meteorol. Soc. Japan, 180 pp., 1957.
2. KURIHARA, Y. and J. L. HALLOWAY, JR., "Numerical Integration of a Nine-Level Global Primitive Equations Model Formulated By the Box Method." Mon. Wea. Rev. 95, pp. 509-530, 1967.
3. MANABE, S. and F. MOLLER, "On the Radiative Equilibrium and Heat Balance of the Atmosphere." Mon. Wea. Rev. 80, pp. 503-532, 1961.
4. \_\_\_\_\_, J. SMAGORINSKY and R. F. STRICKLER, "Simulated Climatology of General Circulation with a Hydrologic Cycle." Mon. Wea. Rev. 93, pp. 769-798, 1965.
5. MURAKAMI, T., "The Sudden Change of Upper Westerlies Near the Tibetan Plateau at the Beginning of Summer Monsoon." J. Meteorol. Soc. Japan 36, pp. 239-247, 1958.
6. SMAGORINSKY, J., S. MANABE and J. L. HALLOWAY, JR., "Numerical Results From a Nine-Level General Circulation Model of the Atmosphere." Mon. Wea. Rev. 93, pp. 727-768, 1965.

**Preceding page blank**

**- 53 -**

# **SYNOPTIC METEOROLOGY**

FORMATION AND STRUCTURE OF EQUATORIAL ANTICYCLONES  
CAUSED BY LARGE-SCALE CROSS-EQUATORIAL FLOWS  
DETERMINED BY ATS-I PHOTOGRAPHS \*

Tetsuya T. Fujita  
The University of Chicago

and

Kazuo Watanabe and Tatsu Izawa  
Meteorological Research Institute, Tokyo

ABSTRACT

Because of poor coverage by synoptic stations, the tropical circulation over the eastern Pacific is not too well known. As a result of photographic experiments, using geosynchronous ATS-I, fields of cloud motion over the eastern equatorial Pacific were mapped in detail on a number of days in September 1967. It was found that a large-scale flow from the Southern Hemisphere recurves after crossing the equator to form an anticyclone centered around  $10^{\circ}$  N. Dynamical characteristics of this type of anticyclone were investigated by estimating the vorticity dissipating force from computed values of divergence and vorticity of low-cloud velocities determined from successive ATS-I pictures. The vorticity dissipating force seems to be closely related to the sea-surface temperature which would reduce the frictional coupling between the low-level atmosphere and the underlying sea surface. It was found that the anticyclone in its development stage results in a discontinuity of the intertropical band of cloudiness; then it travels westward, accompanying an active cloud band along its leading edge. Based upon evidence found through case studies, a model of an equatorial anticyclone is proposed in this paper. Numerical computations of cross-equatorial trajectories were made by using the divergence-vorticity relationships and the vorticity dissipating force, which were obtained through numerical analyses. This paper thus presents an initial step toward the further development of tropical synoptic meteorology, which is expected during the next few years as a result of photographic experiments by using ATS-I and III.

1. INTRODUCTION

Advanced knowledge of meteorological disturbances in high latitudes has been applied, during the past two decades, to the tropics so as to improve our understanding and subsequent forecasting of tropical weather systems. The lack of significant gradients in meteorological parameters in the deep tropics, except in the areas of tropical storms, made it very difficult for us to establish the fields of pressure and temperature related to the patterns of cloudiness. Meteorologists, therefore, tend to analyze streamlines based upon few island-station reports and those by ships.

Analyses of tropical flow patterns by Palmer [9] convincingly clarified the existence of equatorial and easterly waves which often develop into tropical storms. Extensive discussion by Riehl [11] in his book Tropical Meteorology also supported the existence of easterly waves in the Caribbean area.

In pre-satellite days, a band of cloudiness running parallel to the equator was studied both climatologically and synoptically. The band called the "intertropical convergence zone (ITCZ)" has been regarded as a zone in which the south-east trades and the northeast trades of the Southern and Northern Hemispheres, respectively, converge to form a well defined band.

Because the cloudiness associated with ITCZ broadens when easterly waves develop, the relationships between cloud patterns in satellite pictures and easterly waves in various stages were studied by a number of researchers, resulting occasionally in arguments leading to proposed revisions of the term ITCZ. There is no doubt that we see a climatological band or bands of cloudiness as studied by Godshall [6] and Kornfield, et al. [8]. In individual pictures,

\* Research sponsored by National Aeronautics and Space Administration, Environmental Scientific Services Administration, and Japan Cooperative Science Program

Examination of flow patterns in relation to nephosystems reveals that the cyclonic circulation center coincides with those of tropical storms. The cyclonic circulation centers seem to be related physically to large cloud clusters nearby. It is of interest to find that an anticyclone "A" is located over a clear area separating the intertropical cloud band into two. These subjects will be discussed later.

### 3. CORRECTION OF SEMIDIURNAL PRESSURE VARIATION AND SURFACE-MAP ANALYSES

After determining the field of low-cloud velocities in the previous section we shall compare the field with that of low-level winds. It is highly desirable to make such a comparison at several levels in the lower layer of the atmosphere; however, because of the lack of upper-air stations over the area of interest, only surface maps were available for comparison with the cloud-velocity field.

Shown in figure 3 is an example of these surface maps analyzed by plotting all available ship and station reports. In order to increase data over the ocean, surface winds reported by ships 6 hours before and after the synoptic time were also plotted at the ship positions without station circles.

Due to the fact that semi-diurnal pressure variation, decreasing poleward, reaches as large as 4 mb. in full amplitude at the equator, and that observed surface winds do not adjust themselves to this passing pressure wave of 20,000 km. wavelength travelling at about 1,700 km. hr., all surface pressures were plotted after correcting the semi-diurnal variations. No corrections to diurnal variation were made in this case because its amplitude was rather small over the ocean areas where diurnal temperature variation is insignificant.

Figure 3 illustrates the surface chart for 0000Z, 18 September 1967. The streamlines represent a surface-wind analysis and the isobars, a pressure analysis and the isobars, a pressure analyses after semi-diurnal variations had been corrected. Tropical storms, NANETTE and MONICA, and Hurricane BEULAH are clearly depicted. Since the period of cloud-velocity computed used in figures 1 and 2 is only 2 to 4 hours earlier than the time of the surface map in figure 3, we may compare these three figures for further meteorological interpretation. An anticyclone, centered at 10° N., 120° W., appears in all three figures. Note that the wind circling anticyclonically around the center can be traced back across the equator toward the region off Chile. This feature is the southeasterly wind from the mid-latitude high over the south Pacific.

Although it is not possible to estimate the height of the flow represented by low-cloud velocities determined from ATS pictures, the cloud-velocity field is very close to the surface-wind field. A number of other studies by Fujita<sup>1</sup> indicated that low-cloud velocities are very close to the winds at about 3,000 ft. In other words, cellular clouds in the tropics move with the wind approximately at the cloud base. Hubert and Whitney<sup>2</sup> found, on the other hand, that low-cloud velocity agrees best with the 6000-ft. wind. Figure 2 readily shows that these clusters, identified as b, c, and d are located, respectively, to the southeast of cyclonic circulation centers B, C, and D. These locations of cloud clusters are characterized by converging streamlines with cyclonic curvatures, suggesting that absolute vorticity will be very large. If we assume the conservation of

<sup>1</sup> Lectures on the use of ATS pictures entitled: Mesostructure of Subtropical Jet-Stream, Growth of Anvil Clouds, Modification of Jetstream by Large Convective Storms, Outflow from a Large Tropical Cloud Mass, Kinematic Analysis of Hurricane BRENDA, and Divergence and Vorticity at the Jetstream Level. Presented at the WMO Training Seminar on Interpretation of Meteorological Satellite Data, Melbourne, Australia, November - December, 1968.

<sup>2</sup> Wind estimate from geostationary satellites presented at New York, AMS Meeting, Jan., 1969. Their analysis of tropical and subtropical cumuli from five different days indicates that 68 percent are no more than 6 knots and 25° from the 6000-ft. wind.

potential vorticity while travelling inside each of the cyclonic disturbances,  $\Delta P$ , the pressure difference between the top and the base of the inflow layer would be very large where  $Q$ , the absolute vorticity, reaches a maximum. In light of such a simplified dynamical characteristic we may conclude that a band of intertropical cloudiness is composed of several cloud clusters each of which is closely related to the low-level disturbance such as B, C, and D, which are spaced more or less evenly. In this case, the spacing was about 1,100 km. which is about 1/2 of equatorial waves as introduced by Palmer [9].

#### 4. LOW-LEVEL WIND FIELD IN RELATION TO INTERTROPICAL CLOUD CLUSTERS

It was mentioned earlier that a cloud cluster is embedded inside a low-level wind disturbance extending much beyond its visual boundary. Unless a cirrus canopy obscures low clouds inside the area of the wind disturbance we are able to estimate the field of low-level air motion from computed low-level cloud velocities.

An attempt was made to compute both divergence and relative vorticity from the streamlines in figure 2 and isotachs drawn on separate charts. Both direction and speed at each grid point with spacing of 2.5-degree longitude square on a Mercator projection were read out for use as input data.

Divergence patterns of low-level flow, thus computed, are shown in figure 4. Isolines are drawn for every  $10^{-5}$  sec.<sup>-1</sup>. When the locations of maximum convergence are compared with those of cloud clusters and intertropical cloud bands, it is seen that the regions of the maximum convergence have shifted to the southeastern side of these nephysystems.

On the other hand, the regions of vorticity maxima shown in figure 5 coincide with the positions of cyclonic circulation centers which are located near the northwest edge of the nephysystems under consideration. This means that the locations of vorticity and convergence maxima associated with a cloud cluster are separated by a considerable distance. In the case of a tropical storm, however, both maxima are located near the storm's circulation center. Thus, the flow pattern accompanying a cloud cluster seems to be quite different from that of tropical storms. Instead it is rather similar to that of a so-called easterly or equatorial wave, although the latter is characterized by a much longer wave length.

To clarify the dynamical characteristics of a cloud cluster, figure 6 was prepared. Both low-level convergence and vorticity are schematically shown. The absolute vorticity with its maximum near the circulation center decreases both in the upwind and downwind directions while the maximum convergence is seen to the upwind side of the maximum vorticity. Such a distribution of convergence with respect to that of vorticity fits to the concept of vorticity advection in relation to divergence. Under the steady-state assumption we write the well-known equation by Petterssen [10],

$$-V \frac{\partial Q}{\partial s} = DQ \quad (1)$$

where  $V$  denotes the speed of air parcel moving toward the direction  $s$ ; the quantity,  $Q$ , represents the absolute vorticity and  $D$  the divergence. This equation shows that large convergence corresponds to the region where the vorticity advection, as defined by the left side of equation (1), shows large negative values. The maximum convergence in figure 6 is located where the vorticity advection is significant. Referring to this figure, we try to move low-level air enclosed by a rectangular box inside the friction layer toward the region of maximum convergence. The top of the inflow air moves upward while conserving the potential vorticity as soon as the air passes the top of the frictional layer. If the low-level air is sufficiently warm and humid, the top will soon reach the outflow layer at the cirrus level where diverging air spreads the cirrus canopy. Since the air parcel tends to conserve its potential vorticity while advecting into the region of varying absolute vorticity, the pressure difference between the top and the bottom of the parcel is more or less proportional to the absolute vorticity which increases toward the location of the maximum vorticity. Over the regions of decreasing absolute vorticity, where divergence dominates, convective clouds no longer receive moisture supply from the friction layer, resulting in the disintegration of cirrus canopy along with convective towers. The processes of cloud-cluster circulation are not reversible because it transports a significant amount of moisture, hydrometeors, and air from the friction layer to the outflow layer through condensation processes.

Although the locations of the centers of vorticity, convergence, and cloud clusters do not coincide precisely, the formation of cloud clusters is closely related to the frictional convergence by which the air inside the friction layer is pumped upward to form cirrus canopies. We may expect, therefore, that the grid-point values of vorticity and divergence plotted on a  $\zeta$  versus  $D$  diagram distribute systematically forming groups of points representing values inside or outside cloud clusters. A scatter diagram for these point values located inside tropical storms, inside cloud clusters, and outside cloud clusters appears in figure 7. The diagram reveals that clear areas are characterized by either divergence or very small convergence but mostly by anticyclonic relative vorticity. The areas of cloud clusters are where  $\zeta$  is positive and  $D$  is negative. Grid-point values inside hurricanes are also located inside the same domain where  $\zeta$  is positive and  $D$  is negative.

In connection with the dynamical properties accompanied by cloud clusters which often form a band of cloudiness, we shall discuss proper terms for the intertropical cloudiness which has long been called the "intertropical convergence zone" or ITCZ. In view of the evidence that the cloud band is characterized more by "vorticity" than "convergence", we may call it the "intertropical vorticity zone" or ITVZ. If we refer only to the pattern of clouds we may call it the "intertropical cloud band" ITCB. The ITCB in this definition may be a solid band of cloudiness or a band of cloudiness consisting of a number of cloud clusters.

## 5. EVALUATION OF VORTICITY DISSIPATING FORCE

So far we assumed that potential vorticity can be conserved against convergence. Cressman [2] computed trajectories of cross-equatorial flow assuming constant absolute vorticity, thus obtaining constant absolute vorticity trajectories (CAVT). These trajectories show significant anticyclonic curvatures as air parcels travel away from the equator.

In their computation of air trajectories over the Indian Ocean, Gordon and Taylor [7] introduced friction in a linear form,

$$\begin{aligned} \frac{du}{dt} - fv &= -\frac{1}{\rho} \frac{\partial P}{\partial x} - ku \\ \frac{dv}{dt} + fu &= -\frac{1}{\rho} \frac{\partial P}{\partial y} - kv \end{aligned} \quad (2)$$

where  $k$  is a constant of a dimension  $\text{sec}^{-1}$ . These expressions are very convenient for trajectory computations due to the fact that isobars over the Indian Ocean are more or less parallel to the equator. Computed trajectories revealed that they vary significantly with input values of  $k$  which increases with the frictional coupling between the sea surface and the friction layer.

Now that ATS pictures provide accurate methods of computing the cloud-velocity field, we shall try to determine the extent of the frictional coupling. Over the eastern tropical Pacific where equatorial anticyclones form as a result of cross-equatorial flow of the Southern Hemisphere air, there will be no pre-existing high-pressure centers. But the cross-equatorial flows under favorable conditions curve anticyclonically until they form an anticyclonic closed circulation.

To avoid unnecessary complications involving pressure fields, we will start from the vorticity equation but neglect the solenoid term because of insignificant gradient in temperature and pressure. We will also neglect the horizontal gradient of vertical motion since we deal only with the flow of the atmosphere inside the friction layer defined by low-cloud velocities. These assumptions were made by Riehl [11] to simplify vorticity equations. Now we shall write the vorticity equations under the above assumptions but will also include the frictional force between the sea-surface and the low-level flow, thus:

$$\dot{\zeta} = -QD + \text{rot } F \quad (3)$$

where  $F$  denotes the frictional force,  $Q$  and  $\dot{\zeta}$  are the absolute vorticity and its time derivative, and  $D$ , the divergence.

By using the expression of the frictional force in equation (2), we may write:

$$\begin{aligned}\dot{Q} &= -\dot{Q}D - \text{rot } k\vec{V} \\ &= -QD - k\zeta\end{aligned}\quad (4)$$

where  $\vec{V}$  is the velocity of low-level air or that of cellular low clouds,  $k$ , a positive constant,  $\zeta$ , the relative vorticity, and  $-k\zeta$ , the vorticity dissipating force.

In order to evaluate the magnitude of the frictional force we assume a steady-state flow and express the rotational part of the frictional force in equation (3) as:

$$\text{rot } \vec{F} = \vec{V} \cdot \nabla Q + QD \quad (5)$$

which should be proportional to the relative vorticity if equation (4) is applicable to the flow under discussion.

Because we already computed both  $D$  and  $\zeta$  for the flow at 0000Z, 18 September 1967, it would be useful to calculate  $\text{rot } \vec{F}$  from these values. The absolute vorticity and streamlines presented in figure 8 clearly show that the absolute vorticity is negative everywhere south of the equator. Due to cross-equatorial advection the area of the negative absolute vorticity invades northward beyond the equator as far north as about  $11^\circ$  N. near the  $120^\circ$  W. meridian. Due mainly to  $\text{rot } \vec{F}$ , the absolute potential vorticity is not conserved for such a low-level flow. From this figure,  $\vec{V} \cdot \nabla Q$  at each  $2.5^\circ$  grid point was obtained. Both  $Q$  and  $D$  are also read out of figures 4 and 8.

Figure 9 shows the pattern of  $\text{rot } \vec{F}$  thus computed. It should be noted that  $\text{rot } \vec{F}$  is negative mostly over the area of disturbances characterized by a large positive relative vorticity. A striking resemblance and negative correlation are found when figures 9 and 5 are compared. In other words, the areas of cloud clusters and tropical storms coincide with those of large negative value of  $\text{rot } \vec{F}$ . Namely, the rate of increase in the vorticity is suppressed inside cloud clusters where the frictional convergence tends to increase vorticity. The rotational part of the frictional force inside cloud clusters, therefore, acts as a vorticity dissipating force.

Such an important effect of the vorticity dissipating force can be evaluated by a scatter diagram of  $\text{rot } \vec{F}$  against relative vorticity,  $\zeta$ . Figure 10 was obtained by plotting computed values of  $\text{rot } \vec{F}$  and  $\zeta$  at  $2.5^\circ \times 2.5^\circ$  grid points located between  $5^\circ$  N. and  $25^\circ$  N. latitudes. The corresponding mesh size is about 280 km. Drawn also in the figure are the isolines of  $k$  for 1.0, 2.0, 3.0, and  $5.0 \times 10^{-5} \text{ sec.}^{-1}$ . The elongated distribution as outlined by an elliptic boundary indicates that the proper  $k$  would be about  $3 \times 10^{-5} \text{ sec.}^{-1}$ .

The value shows a good agreement with  $k = 1.7 \times 10^{-5} \text{ sec.}^{-1}$  as estimated earlier by Gordon and Taylor [7] based upon an entirely different method applied to Indian Ocean data. Through mesoscale analysis of heavy rain situations over Japan, Matsumoto and Akiyama<sup>1</sup> determined  $k$  to be  $4.2 \times 10^{-5} \text{ sec.}^{-1}$ .

## 6. COMPUTATIONS OF CROSS-EQUATORIAL TRAJECTORIES

In order to reveal the mechanism of the formation of equatorial anticyclones due to the cross-equatorial flow of low-level wind, we shall compute trajectories in a similar manner to that by Cressman [2] and Riehl [11]. The only difference is that we added a vorticity dissipating force introduced in the previous section.

The basic equations for computation are derived from equation (4) under the steady-state assumption, thus

$$\vec{V} \cdot \nabla Q = -QD - k\zeta \quad (6)$$

<sup>1</sup> Personal communication on the result of mesoscale analysis of heavy rainfalls of 9 July 1967.



Then we rewrite this equation in the natural coordinates with the  $s$  axis directed toward the direction of motion and  $n$  axis pointing left, perpendicular to the axis in a form:

$$V \frac{\partial}{\partial s} (f + \zeta) + (f + \zeta)D + k\zeta = 0. \quad (7)$$

where  $f + \zeta = Q$  denotes absolute vorticity.

To carry out a step-by-step computation we write equation (7) in a different form by using the relation  $V\Delta t = \Delta s$ , thus:

$$-\frac{\Delta \zeta}{\Delta t} = \frac{\Delta f}{\Delta t} + fD + \zeta D + k\zeta.$$

The increment of Coriolis parameter:

$$\Delta f = \beta \Delta y = \beta V \sin a \Delta t \quad (8)$$

is then put into this equation to obtain:

$$\frac{\Delta \zeta}{\Delta t} = -(\beta V \sin a + fD + \zeta D + k\zeta) \quad (9)$$

where  $\beta$  denotes Rossby parameter,  $V$ , the wind speed, and  $a$ , the direction of the flow measured counterclockwise from local east. It will be feasible to compute the rate of change in the relative vorticity from this equation after making a few further assumptions.

Although equation (9) gives the impression that vorticity and divergence can be independent of each other, their relationship presented in a scatter diagram in figure 7 does imply that divergence decreases with increasing vorticity, thus:

$$D = -0.48\zeta \quad (10)$$

The coefficient,  $-0.48$ , applies for the equatorial Pacific between  $10^\circ$  N. and  $25^\circ$  N. where statistics were made. In the southern hemisphere the sign of the coefficient should be reversed because negative vorticity is associated with convergence. A generalized but simplified relationship between  $\zeta$  and  $D$  may be written as:

$$D = -c\zeta \quad (11)$$

where  $f$  is Coriolis parameter and  $c$ , a constant. The latter may be affected by  $\beta$ ,  $V$ ,  $a$ , and  $k$  in equation (9), but we will be keeping this a constant in this paper in order to avoid further complications. From equation (10) and the mean value of  $\zeta$  at  $15^\circ$  N., we have:

$$c = \frac{0.48}{f \text{ at } 15^\circ \text{ N.}} = \frac{0.48}{3.78 \cdot 10^{-5}} = 0.13 \cdot 10^5 \text{ sec.} \quad (12)$$

Although the divergence-vorticity relationship expressed by equation (11) needs further modification, it would be considerably better than simply assuming either non-divergence or specific divergence values in the low-level atmosphere. By putting equation (11) into equation (9) we eliminate divergence, thus:

$$\frac{\Delta \zeta}{\Delta t} = c\zeta^2 + (cf^2 - k)\zeta - \beta V \sin a. \quad (13)$$

This equation will permit us to compute the rate of change in relative vorticity if initial conditions of flow are given.

Since our primary interest is to compute cross-equatorial trajectory, we form rectangular coordinates with the origin at the equator-crossing point,  $x$  axis pointing east, and  $y$  axis pointing north. Each trajectory then starts from  $x_0 = 0$  and  $y_0 = 0$ .

The initial vorticity at the equator may be chosen as a function of the equator-crossing angle  $\alpha_0$  measured from  $x$  axis to the velocity vector. A simplified equation can be written as:

$$\zeta_0 = -b_0 V_0 \sin \alpha_0 \quad (14)$$

because a southerly flow tends to be characterized by a negative absolute vorticity advected from the Southern Hemisphere while a northerly flow will have a positive absolute vorticity. Equation (14) indicates that the initial vorticity is proportional to the north-south component of cross-equatorial wind velocity. From the empirical relationship that  $\zeta_0 = -1.0 \times 10^{-5} \text{ sec.}^{-1}$  when  $V_0 = 10 \text{ m. sec.}^{-1}$  and  $\alpha_0 = 135^\circ$ , we estimate  $b_0$  being:

$$b_0 = \frac{-\zeta_0}{V_0 \sin \alpha_0} = \frac{1.0 \times 10^{-5} \text{ sec.}^{-1}}{10 \sin 135^\circ \text{ m. sec.}^{-1}} \approx 0.14 \times 10^{-5} \text{ m.}^{-1}. \quad (15)$$

Complete solutions of equation (13) require further assumptions of the wind speed and its lateral gradient. Using Riehl's [11] justification, we made the following two assumptions:

$$V = \text{constant} = V_0 \quad (16)$$

$$\text{and } \frac{\partial V}{\partial n} = 0,$$

so as to express relative vorticity:

$$\zeta = \frac{V}{r} - \frac{\partial V}{\partial n} \approx \frac{V_0}{r} \quad (17)$$

where  $r$  denotes the radius of curvature of the flow.

Through standard procedure we compute both  $\Delta x$  and  $\Delta y$  from

$$x_{n+1} - x_n = \Delta x_n = V_0 \Delta t \cos \alpha_n \quad (18)$$

$$y_{n+1} - y_n = \Delta y_n = V_0 \Delta t \sin \alpha_n$$

where the suffix  $n$  is changed 0, 1, 2, 3 ... to  $j$  for each time-interval  $\Delta t$ . The increment of  $\alpha$  is expressed by:

$$\alpha_{n+1} - \alpha_n = \Delta \alpha_n = \frac{V_0 \Delta t}{r} = \zeta_n \Delta t. \quad (19)$$

A number of trajectories of cross-equatorial air under the influence of various parameters were computed in order to determine the air motion after crossing the equator. Presented in figure 1' are these trajectories with the cross-equatorial speed of 20 knots which was kept constant as expressed in equation (16). The equator crossing angle  $\alpha$  was varied as  $10^\circ$ ,  $50^\circ$ ,  $90^\circ$ ,  $130^\circ$ ,  $150^\circ$ , and  $170^\circ$ . It should be noted, however, that the trajectories for  $\alpha = 0^\circ$  and  $180^\circ$  follow the equator eastward and westward, respectively.

The coefficient  $k$  was selected as  $2 \times 10^{-5} \text{ sec.}^{-1}$  in obtaining the upper figure in which trajectories extend up to about  $20^\circ \text{ N.}$  before returning gradually toward the equator in an oscillatory fashion while travelling eastward. It is of interest to find that the maximum northward penetration of the Southern Hemisphere air occurs when the equator-crossing angle is  $170^\circ$ . If it increases by  $10^\circ$  to  $180^\circ$  the air will travel along the equator without deviating either north or south. When  $\alpha$  decreases to less than  $90^\circ$ , trajectories reach only up to about  $8^\circ$ .

By decreasing the coefficient  $k$  to zero, trajectories show dramatic changes resulting in the formation of loops when  $\alpha$  exceeds about  $150^\circ$  and also in the returning of the air to the Southern Hemisphere where it started from. A group of such trajectories with varying  $\alpha$  is presented in the lower diagram of figure 11.

In view of significant changes in the shapes of trajectories when  $k$  was changed from zero to  $2 \times 10^{-5} \text{ sec.}^{-1}$ , we may postulate that the equatorial anticyclone presented earlier will form only if the value of  $k$  is approximately equal to  $1 \times 10^{-5} \text{ sec.}^{-1}$  which is very small compared with other estimated values. It is likely that a suppressed low-level overturning over the South Equatorial cold current results in such a small value of  $k$ . Over the equatorial regions with warm ocean-surface temperature, the large value of  $k$  would not permit a cross-equatorial trajectory to recurve for the formation of an equatorial anticyclone.

In order to evaluate the influence of the cross-equatorial velocity,  $V_0$  upon the shape and the maximum northward penetration of trajectories, figure 12 was produced by changing  $V_0$  into 10, 20, and 30 knots. It is of extreme interest to find that the size of the anticyclonic loop appearing when  $k = 0$  increases significantly with  $V_0$ , while three trajectories with three different velocities remain almost identical when  $k$  exceeds  $2 \times 10^{-5} \text{ sec.}^{-1}$ . That is to say, the cross-equatorial air will follow a trajectory determined mainly by  $k$  and not by  $V$  when  $k$  is larger than  $2 \times 10^{-5} \text{ sec.}^{-1}$ .

The northward penetration increases significantly with increasing  $k$ . This would be a partial reason why Southern Hemisphere air in northern summer penetrates far into northern latitudes over the warm western Pacific and western Atlantic especially when the equator crossing angle is close to  $170^\circ$ . However, the mean crossing angle over the region of the anticyclone formation is about  $135^\circ$ .

Although the results of these numerical computations of trajectory are rather preliminary, they have a potential value in studying cross-equatorial cloud motion which can now be determined from a series of ATS pictures.

## 7. A MODEL OF MIGRATORY EQUATORIAL ANTICYCLONES

It was revealed in the previous sections that an organized cross-equatorial flow from the Southern Hemisphere in winter gains its relative anticyclonic vorticity. The effect of  $B$  or the northward increase in Coriolis parameter  $f$  will overcome that of the vorticity dissipating force especially when  $k$  is small. Areas of small  $k$  would naturally coincide with oceanic regions with cold sea-surface temperatures. The eastern equatorial Pacific is really qualified for one of the most favorable regions of the formation of equatorial anticyclones.

Presented in figure 13 is a model of a migratory equatorial anticyclone which was established after studies of cloud patterns and velocities over the eastern equatorial Pacific.

During the "Pushing Stage", a large scale flow from the Southern Hemisphere pushes northward, thus producing a convex band of intertropical cloudiness. During this pushing stage the band is pushed as far as 1,000 km. to the north. We often observe formation of tropical storms along the zone in which Northern and Southern Hemisphere air begins interacting with large horizontal wind shear and cyclonic relative vorticity.

Within 1 to 3 days the flow from the Southern Hemisphere gains sufficient anticyclonic relative vorticity. The flow starts returning southward, thus entering the "recurring stage". The intertropical cloud band shows little change. Tropical depressions formed in the pushing stage tend to move out from the region of the tropical cloud band in this stage.

After a day or so the equatorial anticyclone is characterized by an enclosed circulation, forming an anticyclone. This stage is called the "Cut-off Stage". During this stage, the anticyclone center is encircled entirely by the air from the Southern Hemisphere.

As soon as a break in the intertropical cloud band takes place, the Northern Hemisphere trade starts flowing to the south of the anticyclonic flow. Then the Northern trade and the flow from the Southern Hemisphere start mixing around the anticyclone center. This stage is called the "Mixing Stage."

After a day or so a significant amount of the northern trade is transported through the southern sectors of the equatorial anticyclone migrating toward the west-northwest. Meanwhile the flow from the Southern Hemisphere keeps pushing the cloud band along the leading edge of the anticyclone. Such a joint push by both northern trade and the flow from the Southern Hemisphere often results in a very intense zone of convergence with cyclonic vorticity. An intense band of intertropical cloudiness located in this zone may be called the "burst band". This proposed term is related to the northwesterly expansion of an intertropical cloud band. In order to emphasize this phenomenon, we call this stage the "Burst Stage". This stage lasts only 1 or 2 days, and then the burst band disintegrates quickly into small fragments or isolated cloud clusters.

After the disintegration of the burst band there still remains a rather intense flow to the south of the equatorial anticyclone center moving in a north to northwesterly direction. This anticyclonic flow is still strong enough to prevent the southeasterly movement of a middle-latitude cold front in the summer hemisphere. A wave on the cold front is observed in the "Interacting Stage." The interaction takes place between a cold front and an equatorial anticyclone which has advected into middle latitudes.

The entire life cycle of an equatorial anticyclone requires about a 2-week period. Depending upon the frequency of the anticyclone formation, we often see two anticyclones in different stages of development at the same time over the equatorial northern Pacific, especially in August or September.

## 8. STRUCTURE OF A BURST BAND

Because the equatorial anticyclones under discussion form over the equatorial eastern Pacific where no upper-air observations are available, it would be very difficult to establish their three-dimensional models. When a burst stage is reached, however, a burst band is located over the equatorial central Pacific where several upper-air stations are in existence.

We shall examine the passage of a strong burst band over Johnston Island located at 16.7° N., 169.5° W. Shown in figure 14 is a time section of various meteorological parameters recorded at the surface. A burst band moved over the station on 24 September 1967. Heavy rain occurred in five separate periods identified in the figure as R1 through R5. The heaviest hourly rain occurring between 0600 and 0700 local time was 0.75 inches followed by 0.65 inches during the following hour. The wind direction shifted to southerly at the onset of the first rain R1, thus placing most of the burst band inside the southeasterly flow just behind the leading edge of the band. This position of the band coincides with that of the intertropical cloud band in figure 2 already discussed. In both cases, therefore, it is the southeasterly flow which converges into cloud bands while the easterly ahead of the line acts more or less as a barrier to initiate both convergence and cyclonic vorticity.

Surface pressures are not affected by the passage of the burst band. They could be a few tenths of a millibar higher than the average semi-diurnal variation. Surface temperatures are affected considerably especially during the rain periods. During the five rain periods, the temperature dropped by 3° C. to 5° C. As explained by Riess [11], these drops are due to cooling by rain. The fact that the pressure variation is insignificant strongly suggests that it is the shallow layer above the ground that is chilled by rain.

The vertical cross section of winds aloft from Johnston Island for about a 10-day period in September 1967 is shown in figure 15. Two burst bands, a weak one on September 17 and the other a strong one on 24 - 25 September Greenwich days, passed over the station as indicated in the figure. It is important to find that each band moving westward was followed by an anticyclonic circulation at about the 10,000-ft. level. The anticyclone center at sea level passed to the northeast of the station. Rather intense outflows associated with these burst bands are seen between 25,000 and 50,000 ft. They are identified as outflow 1 and outflow 2. The latter is combined with another outflow 3 from a large cloud cluster located near the equator at the southwest end of the strong burst band. It is of interest to see that burst band 2 was accompanied by a significant anticyclonic center at about 30,000 ft. identified in the figure as #2.

The 300-mb. chart in figure 16 was completed by plotting rawin winds with black station circles, aircraft winds with square boxes, and high-cloud velocities in arrows with open circles. Large areas of convective clouds are stippled. Groups of streamlines drawn in the chart reveal five centers of outflows, H<sub>1</sub>, H<sub>2</sub>, H<sub>3</sub>, H<sub>4</sub>, and H<sub>5</sub>. Both H<sub>1</sub> and H<sub>2</sub> are the highs associated with long-wave patterns, however, H<sub>3</sub>, H<sub>4</sub>, and H<sub>5</sub> are closely related to the accumulative outflow from groups of convective clouds or cloud clusters inside the boundary of each outflow system. Outflows 2 and 3 are more or less inseparable because intense convective activities near the southwest and the northwest ends of the burst band are contributing to the maintenance and intensification of these combined outflow systems. It would be highly desirable to compare the relative position of H<sub>1</sub> and H<sub>2</sub>.

in both figures 15 and 16 for better understanding of four-dimensional characteristics of these outflow systems, which need to be expressed in x, y, z, and t coordinates.

Returning to figure 15, we must recognize that the vertical transport of low-level momentum takes place only inside convective systems in which moist-adiabatic ascent takes place. A dry-adiabatic process does not permit low-level air to transport its horizontal momentum upward against the more or less moist adiabatic stratification of tropical atmosphere. Strong southerly winds in burst band 2 were measured probably when balloons were under the influence of such convective clouds.

It should be emphasized that the time variation of winds aloft at a single station is related to: (1) the synoptic flow patterns of wind systems, (2) their development and decay, and (3) their migratory velocities.

## 9. AN EXAMPLE OF EQUATORIAL ANTICYCLONES OVER THE TROPICAL PACIFIC

To verify the proposed model of equatorial anticyclones, efforts are being made to complete analyses of surface and 300-mb. charts over the equatorial Pacific for the entire month of September 1967.

Tracks of two major equatorial anticyclones,  $A_1$  and  $A_2$ , appear in figure 17. Note that each anticyclone lived over 10 days while travelling with the westward velocity component. The travelling speed varied between about 5 to 10 degrees per day, which is comparable to that of hurricanes and easterly waves.

A question might arise as to why the eastern tropical Pacific is favorable for such anticyclone formation. One reason being the cold ocean-surface temperature as studied extensively by Bjerknes [1] who pointed out the importance of the South Equatorial cold current extending from off the Pacific coast of South America to the equator. To confirm the existence of the cold current during the period of our analysis all ship reports during the 3-day period, 17 - 19 September 1967, were plotted on a composite chart of figure 18. It will be seen that a tongue of cold surface water was dominating the equatorial region.

Such a cold ocean-surface temperature would suppress vertical mixing of the air inside the friction layer. That is to say, the value of  $k$  in figure 10 and equation (4) is expected to be very small over the region of this cold current. This expectation means that the cross-equatorial flow will quickly gain anticyclonic relative vorticity as it travels with a northerly component, thus decreasing  $\zeta$  with time. Over the area of high ocean-surface temperature, however, the resulting convection and vertical mass exchange inside the friction layer tend to dissipate the relative vorticity so that an anticyclone development will be suppressed.

We shall now examine surface analyses corresponding to the six stages of an anticyclone development. Figure 19, including six surface charts covering longitudes  $150^\circ$  E. through  $90^\circ$  W., was drawn by plotting all land-station reports for 0000Z and ship reports for 18000Z, 0000Z, and 0600Z. Areas of large nephsystems were copied from ESSA's mosaic pictures reduced to the map scale. Surface streamlines were then drawn taking surface winds and cloud velocities from ATS-I picture analysis into consideration. No cloud velocities were plotted in the figure because they were computed tentatively without correcting the mis-synchronization of ATS scan lines which occurred shortly before the spring and autumnal equinoxes of 1967. We have succeeded, however, in correcting the mis-synchronization for the 18 September case which was used extensively in this report.

The top chart for 12 September includes anticyclone  $A_1$  in its cut-off stage and  $A_2$  in the pushing stage. Two tropical storms N (NANETTE) and M (MONICA) are forming simultaneously inside an intertropical cloud band along the leading edge of the southwesterly flow from the Southern Hemisphere. Near the eastern end of the intertropical cloud band associated with anticyclone  $A_1$ , we find a very weak vortex identified as P. In these examples of vortex formations a large number of vortices were found to form in the cloud band accompanied by an anticyclone in its pushing stage. This mode of vortex formation will correspond to Fett's [4] second category and also to Erickson and Fritz's [3] type of formations.

A well developed storm S, hurricane SARAH, near Johnston Island, originated from a weak easterly-wave disturbance and is now travelling westward. SARAH's formation would be in Fett's second category studied intensively by Yanai [12, 13].

The second chart for 0000Z, 16 September shows anticyclone A<sub>1</sub>, already in the burst stage and A<sub>2</sub> in the recurving stage. It should be pointed out that both storms N and M are moving away from their nesting band of intertropical cloudiness. Due to their locations over warm equatorial counter current they are maintaining their features of tropical storms. Seen to the southwest of anticyclone A<sub>1</sub> is a weak burst band along which is observed moderate cyclonic curvature in streamlines. Hurricane SARAH is moving toward the western edge of the chart.

On the third chart for 0000Z, 20 September, SARAH is seen in the northwest corner of the chart and anticyclone A<sub>1</sub> is seen interacting with a cold front in the middle latitudes. A weak vortex P is still visible near Hawaii. Of interest is an evidence of complete separation of tropical storms N and M from the intertropical cloud band north of A<sub>1</sub>, which has been reestablished into a thin band. Anticyclone A<sub>1</sub> in its cut-off stage is moving westward steadily.

The fourth chart for 0000Z, 24 September indicates that anticyclone A<sub>2</sub> has entered its mixing stage characterized by an injection of northern trade into the anticyclone circulation. Two tropical storms N and M are weakening rapidly, while an intertropical cloud band to their south becomes wider, extending toward the south quadrant of hurricane BEULAH over Mexico.

The dramatic burst stage of anticyclone A<sub>2</sub> is seen in the fifth chart for 0000Z, 25 September. A burst band which has passed Johnston Island has already been discussed in the previous section. Seen behind the burst band is a well-defined anticyclonic circulation which might have been analyzed not as an anticyclone but as a noise if there were no satellite data and no circulation model. Over the eastern half of the chart, tropical storm N is weakening further. Meanwhile, the distance from her sister storm M increased considerably.

The last chart for 0000Z, 26 September, shows anticyclone A<sub>2</sub> in its interacting stage. Note that the southward movement of a cold front has been slowed down in the region of interaction. Both BEULAH and MONICA merged to form a large, but weak tropical vortex centered on the Pacific coast of Mexico. A dissipating tropical storm NANETTE is still seen near the center of the chart.

## 10. CONCLUSIONS

Detailed analyses of data-scarce regions of the eastern tropical Pacific revealed that satellite data can be effectively used in determining the scales and the modes of the tropical circulation. Particularly, the use of ATS pictures in determining fields of cloud velocities resulted definitely in a breakthrough in understanding dynamical aspects of tropical circulations.

As a result of this study, it is concluded that the tropical nephsystems larger than a cloud cluster are accompanied by definite flow fields. These fields are mostly cyclonic and convergent, giving an impression that the frictional convergence is one of the most important driving mechanisms for the formation and the maintenance of cloud clusters and intertropical cloud bands.

It should be emphasized also that the cloud velocities determined from ATS pictures can be used in evaluating various dynamical parameters such as advection, frictional coupling, etc.

In the light of these results, it would be proper to recommend an organized effort of tropical analyses by collecting all existing synoptic, land and ship data in addition to satellite pictures. These efforts might or are likely to develop into a second look at "tropical synoptic meteorology" as well as "tropical mesometeorology".

## DISCUSSION

WANN: Have you ignored propagational cloud movement in your wind flow calculations from satellite pictures?

FUJITA: By selecting small cellular clouds only, we can minimize errors which might result due to propagation. My studies indicate that small cellular, low clouds move with the 950- to 850-mb. winds.

RAMAGE:

- (a) The Johnston Island analysis might more probably be modified to indicate an eastward moving large-amplitude trough in the westerlies superimposed on a low level disturbance, thus causing deep upward motion and accounting for the cloud mass.
- (b) Over South and Southeast Asia, a simple single vertical tropospheric circulation cell is often replaced by a double cell with deep and significant middle clouds.

FUJITA:

- (a) I do not rule out the possibility, however, day-to-day analyses of cloud velocities also indicate that a local outflow could affect a single station at high levels for several days.
- (b) Over Southeast Asia, cloud cover seen from satellites may be contributed equally by three-layer nephosystems. Trackable clouds as tracers will, however, be largest at low levels with a secondary maximum at high levels.

HAU: Until the time you could move the ATS westward, do you think the same reasoning still stands with the southwest monsoon in the Southeast Asia area. Would the frictional coefficient reach a value very much higher than the maximum determined for the eastern Pacific or the Indian Ocean?

FUJITA: Over Southeast Asia the frictional coefficient is related closely to the land and sea distribution. The horizontal patterns of  $k$  would be quite complicated if it were possible to determine the value in mesoscale. Over the Indian Ocean  $k = 2 \times 10^{-5} \text{ sec.}^{-1}$  is a proper value for me.

## REFERENCES

1. BJERKNES, J., "A Possible Response of the Atmospheric Hadley Circulation to Equatorial Anomalies of Ocean Temperature." *Tellus*, 18, 820-829, 1966.
2. CRESSMAN, G. C., "Studies of Upper-Air Conditions in Low Latitudes." Dept. Meteor., Univ. Chicago, Misc. Rep. 24, Part II, 68-103, 1948.
3. ERICKSON, C. O. and S. FRITZ, "Early History of Tropical Storm Katherine, 1963." *Mo. Wea. Rev.*, 93, 145-153, 1965.
4. FETT, R. W., "Typhoon Formation Within the Zone of the Intertropical Convergence." *Mo. Wea. Rev.*, 94, 9-18, 1968.
5. FUJITA, T. and D. BRADBURY, "Computation of Height and Velocity of Clouds From Dual, Whole-Sky, Time-Lapse Picture Sequences." SMRP Research Paper No. 70, 17 pp., 1968. (Copies may be obtained from the Department of Geophysical Sciences, The University of Chicago.)
6. GODSHALL, F. A., "Intertropical Convergence Zone and Mean Cloud Amount in the Tropical Pacific Ocean." *Mo. Wea. Rev.*, 96, 172-175, 1968.
7. GORDON, A. H. and R. C. TAYLOR, "Lagrangian Dynamics and Low Latitude Weather." Hawaii Institute of Geophysics, Univ. of Hawaii, HIG-66-12, 32 pp., 1966. (Copies may be obtained from The University of Hawaii.)
8. KORNFELD, J., A. F. HASLER, K. J. HANSON and V. E. SUOMI, "Photographic Cloud Climatology From ESSA III and V Computer Produced Mosaics." *Bull. Amer. Meteor. Soc.*, 48, 878-883, 1967.

REFERENCES (CONTINUED)

9. PALMER, C. E., "Tropical Meteorology." Quart. J. R. Met. Soc., 78, 126-164, 1952.
10. PETERSSEN, S., "Weather Analysis and Forecasting." Vol. 1, McGraw-Hill Co., New York, 428 pp., 1956.
11. RIEHL, H., "Tropical Meteorology." McGraw-Hill Co., New York 392 pp., 1954.
12. YANAI, M., "A Detailed Analysis of Typhoon Formation." J. Meteor. Soc. Japan, 39, 186-214, 1961.
13. \_\_\_\_\_, "Evolution of a Tropical Disturbance in the Caribbean Sea Region." J. Meteor. Soc. Japan, 46, 86-109, 1968.



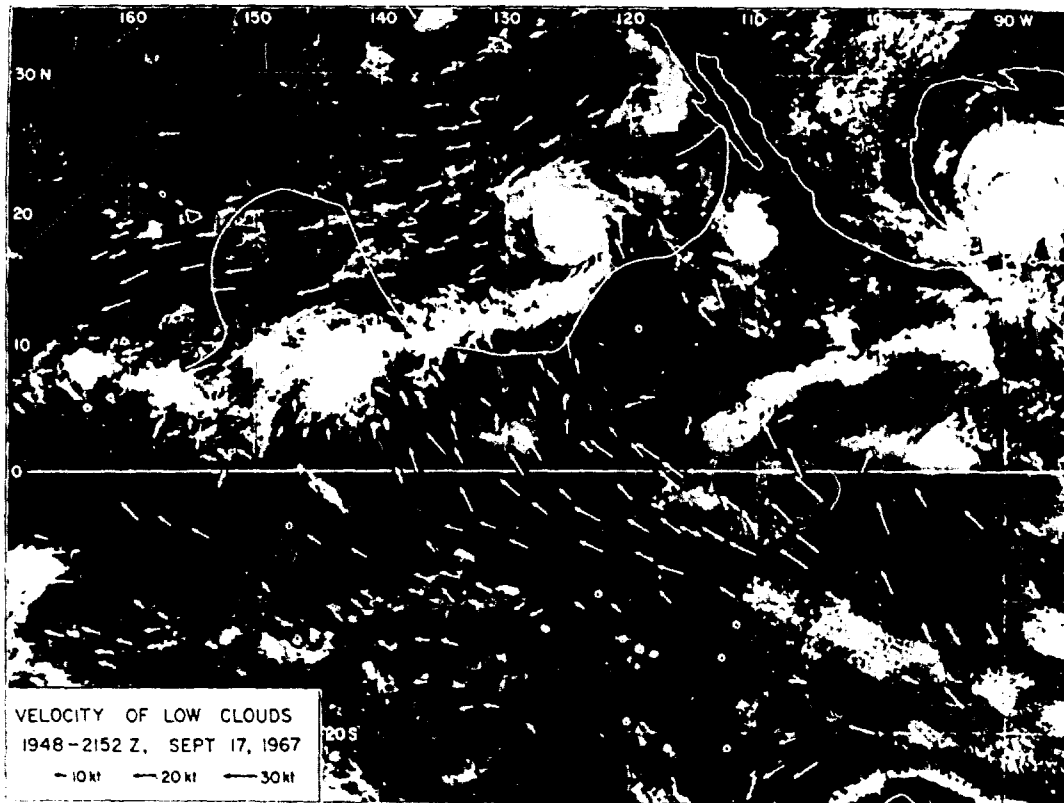


Figure 1. Velocities of Low Clouds Over the Eastern Pacific, Plotted on an ESSA Digital Mosaic on Mercator Projection. Velocities were obtained from six ATS-1 pictures taken at about 25-min. intervals.

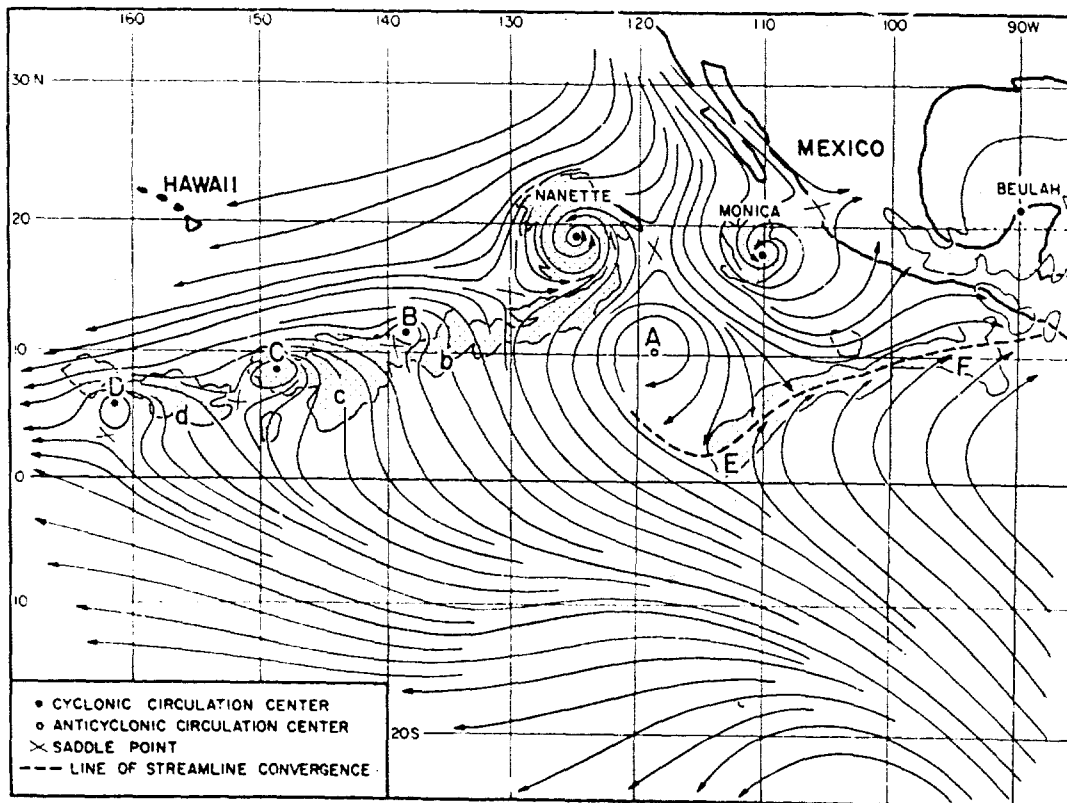


Figure 2. Streamlines of Low-Cloud Velocities Drawn From Velocity Vectors in Figure 1.

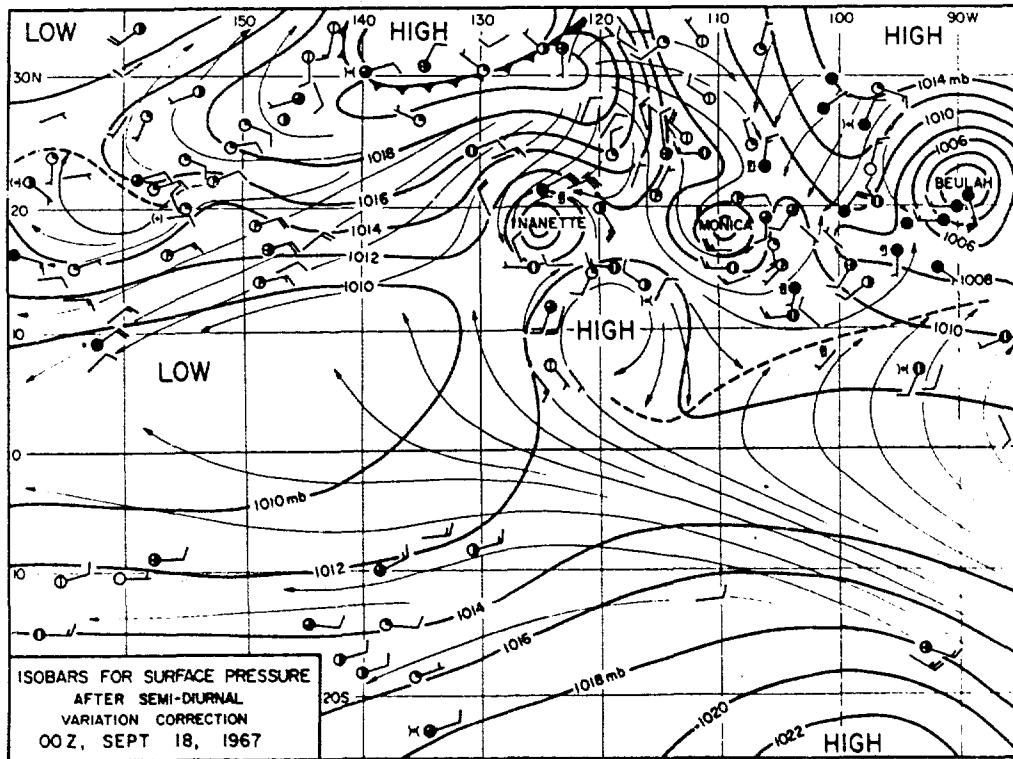


Figure 3. Surface Chart for 0000Z 18 September 1967, About 3 Hours After the Time of the Velocity Computation in Figure 1. Note that an anticyclone depicted by streamlines in figure 2 appears clearly in this surface map. Ship-reported winds at 1800Z on the 17th and 0600Z on the 18th were entered without station circles.

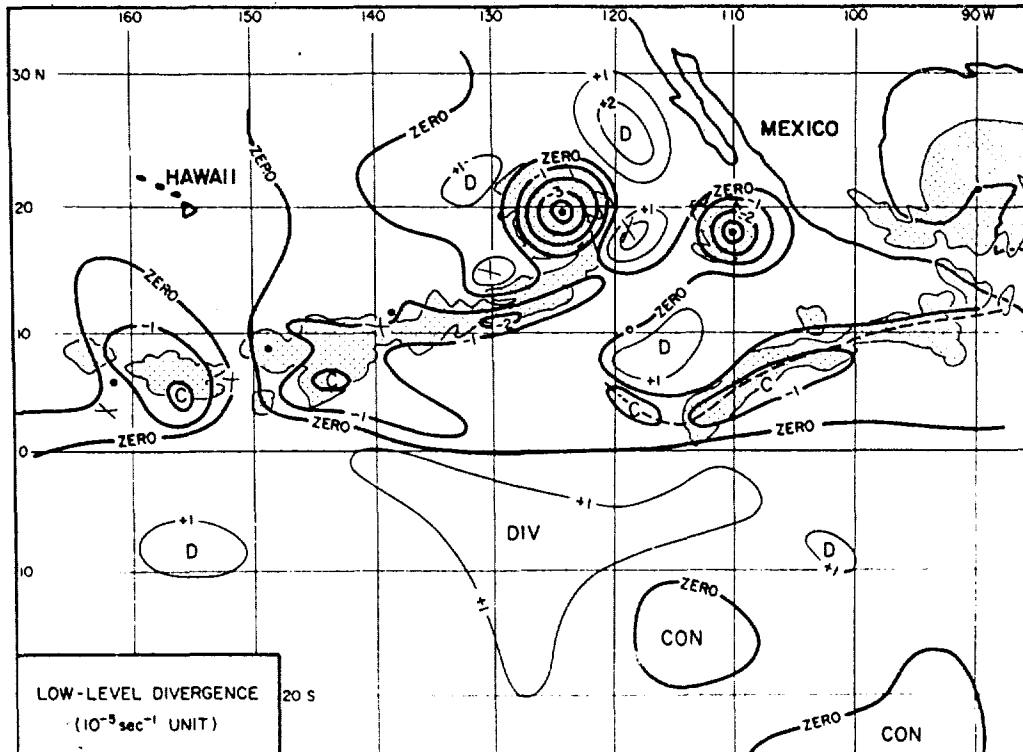


Figure 4. Divergence of Low-Cloud Velocities in Figure 1. As expected, the areas of intertropical nephsystems are characterized by fields of convergence.

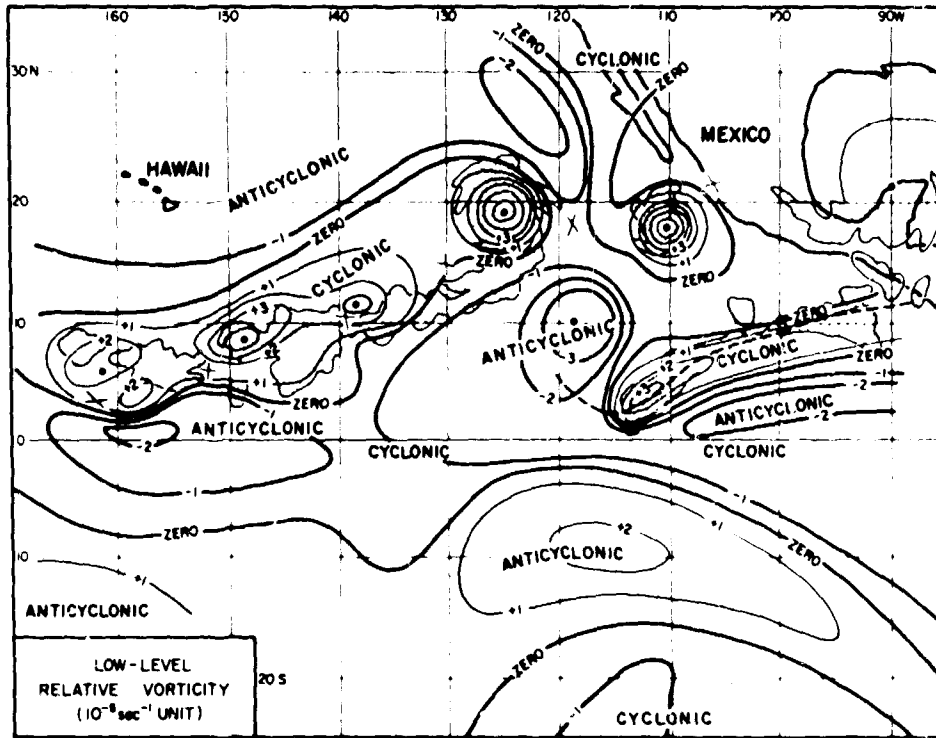


Figure 5. Relative Vorticity of Low-Cloud Velocities in Figure 1. Note that the areas of nephysystems correspond to those of large relative vorticity.

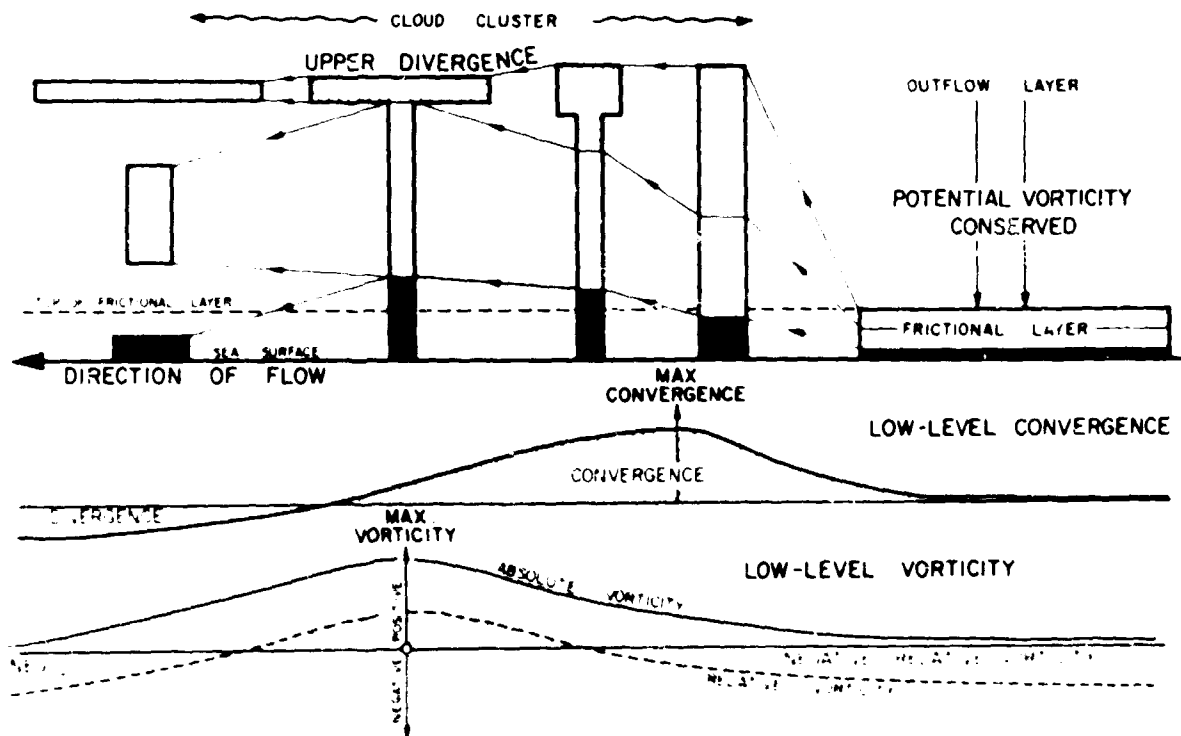


Figure 6. Mesoscale Correspondence between Convergence and Vorticity Advection Maxima. Since the frictional layer is mixed, the division of the layer into three sub-layers, top, middle, and bottom, is nearly schematic.

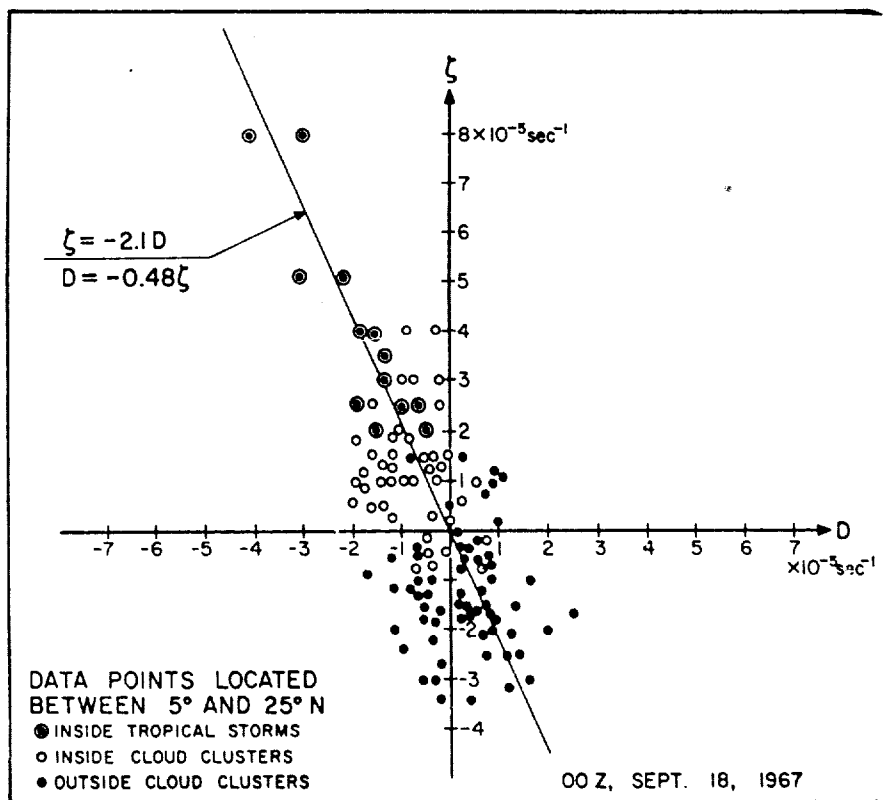


Figure 7. A Scatter Diagram Showing a Linear Relationship Between Divergence and Relative Vorticity. Data points are located inside a zonal belt between 5° N. and 25° N. bounded by 90° W. and 170° W.

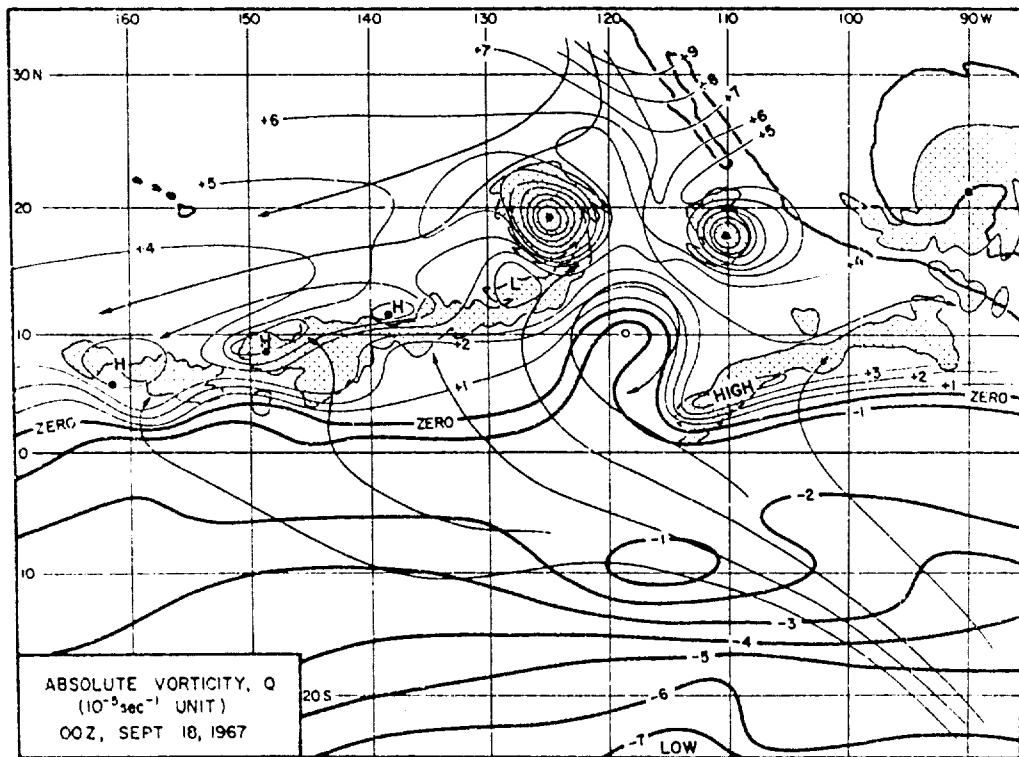


Figure 8. Absolute Vorticity Obtained by Adding Coriolis Parameter to the Relative Vorticity in Figure 5.

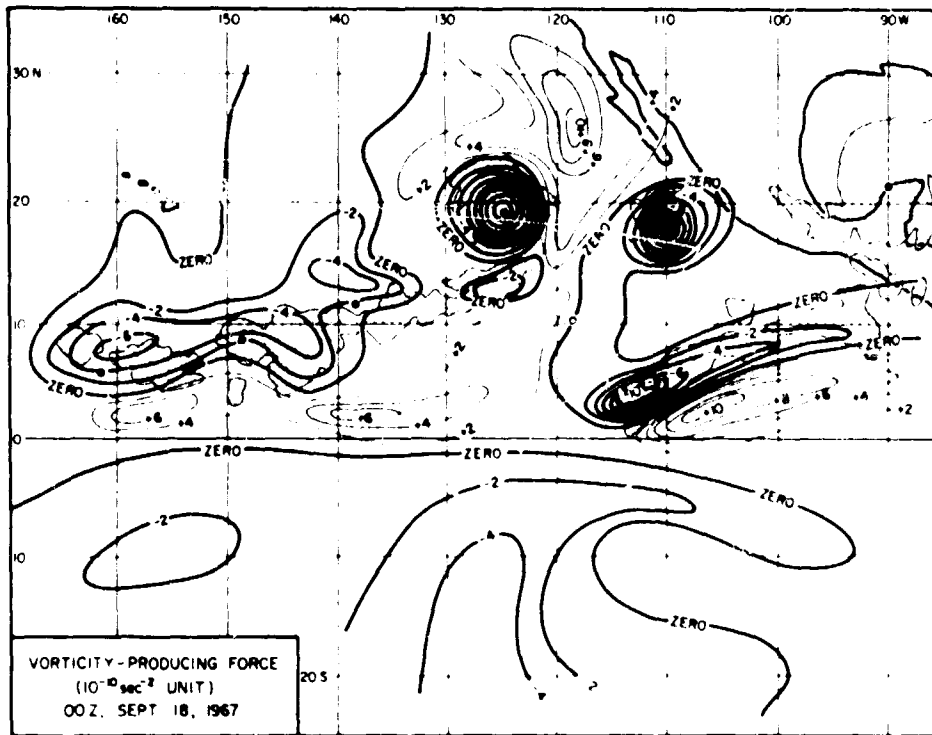


Figure 9. Vorticity-Dissipating Force Defined by Equation (3) and Computed Entirely From ATS Cloud Pictures. No synoptic data were used in the computation.

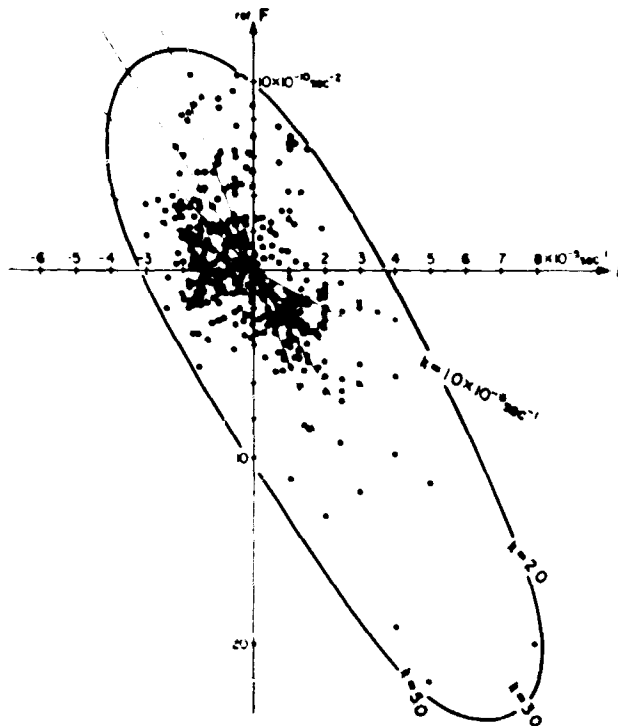


Figure 10. Scattered Diagram Relating the Vorticity-Dissipating Force With Relative Vorticity. The entire area of figure 1 was used in determining grid-point data appearing in this diagram. It should be emphasized that this diagram was constructed based on ATS pictures only.

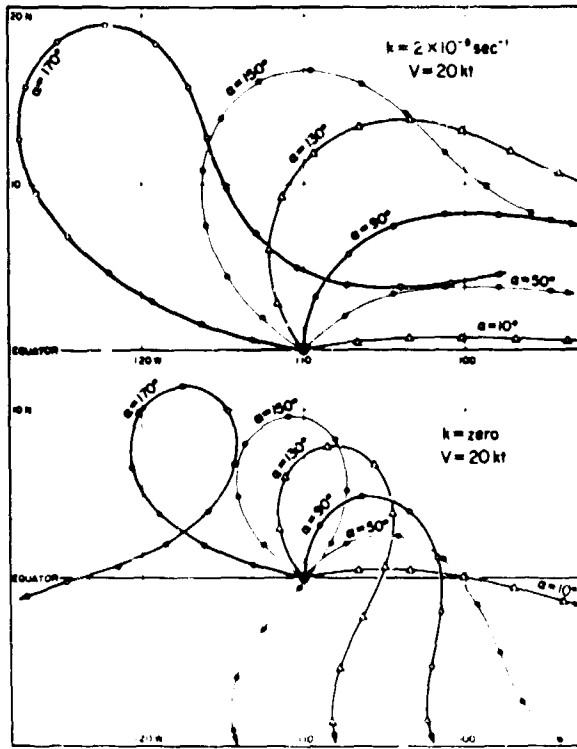


Figure 11. Trajectories of Cross-Equatorial Air Computed by Changing Both the Vorticity-Dissipating Force and the Equator Crossing Angle. Trajectories vary significantly with these input parameters.

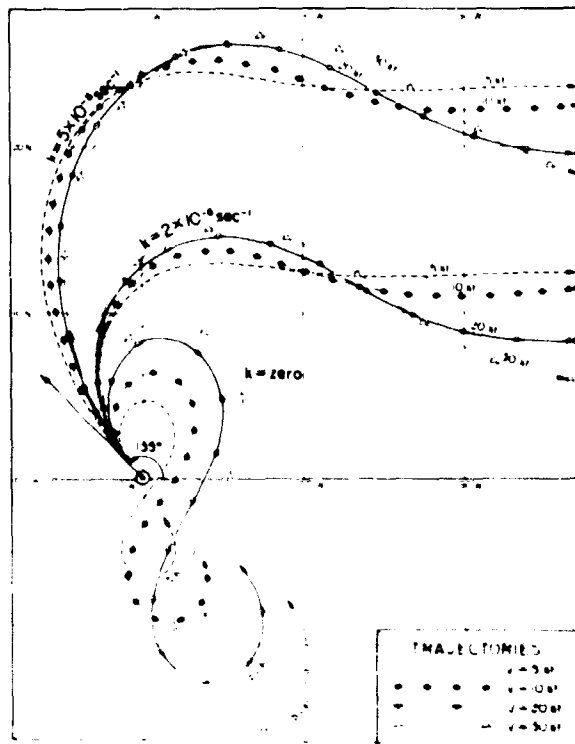


Figure 12. Influences of the Cross-Equatorial Velocity Which was Changed From 5 to 10 Kt. Unless  $k$  is very small, trajectories change very little according to the velocity variation within this range.

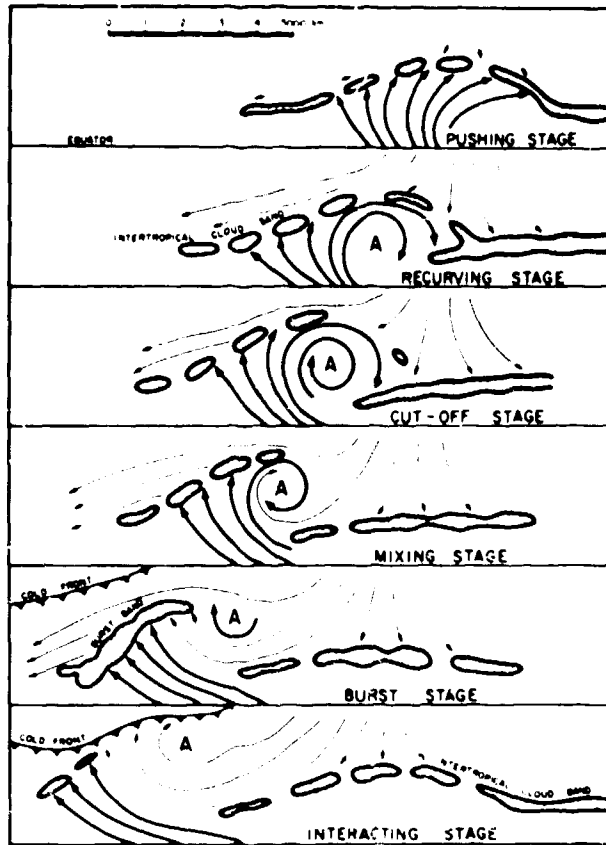


Figure 13. A Proposed Model of an Equatorial Anticyclone in Six Stages. An example corresponding to each stage is shown in Figure 19.

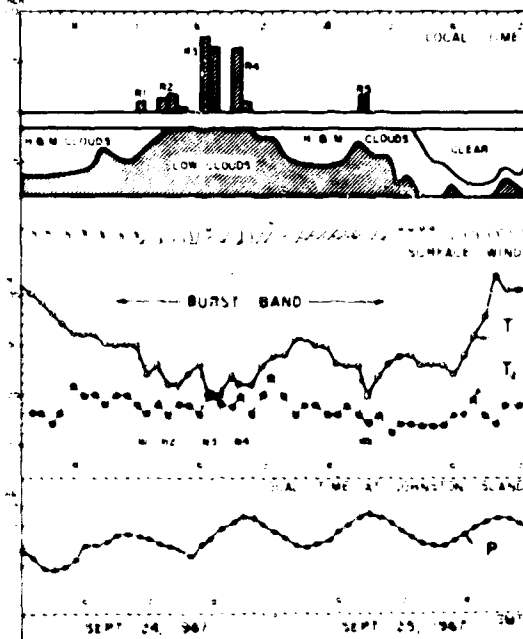


Figure 14. Passage of a Burst Band at Johnston Island, 16.7° N. and 169.5° W. on 24-25 September 1967. During the passage of the band, rain occurred in five separate periods, producing, 0.10, 0.31, 1.40, 0.73, and 0.15 inches, respectively, with a total of 2.69 inches. During each of these rain periods air temperature dropped several degrees.

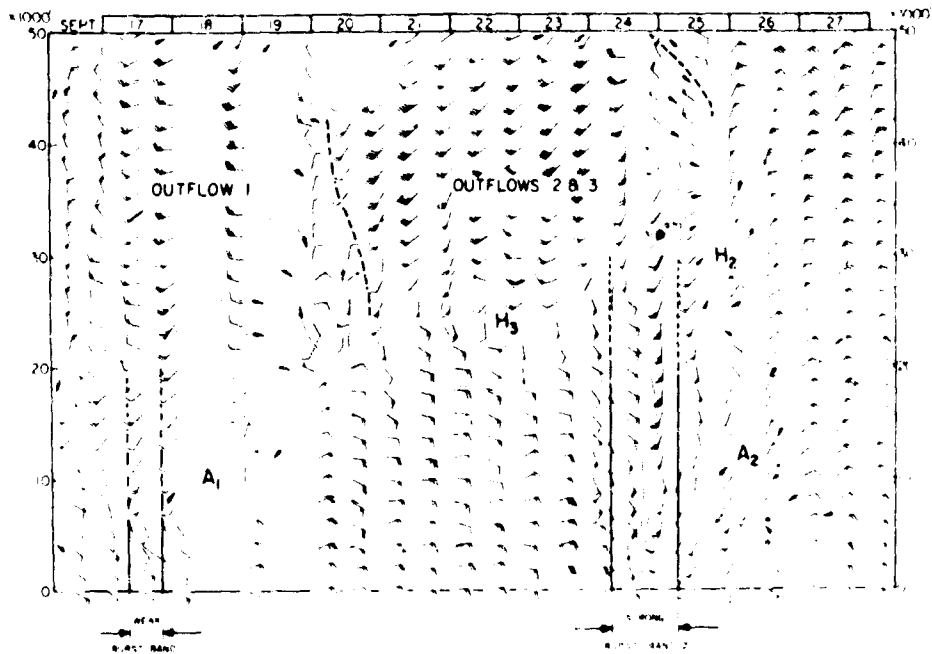


Figure 15. A Vertical Time Cross Section at Johnston Island Between 16 and 28 September 1967 When Two Burst Bands Passed Over the Station.

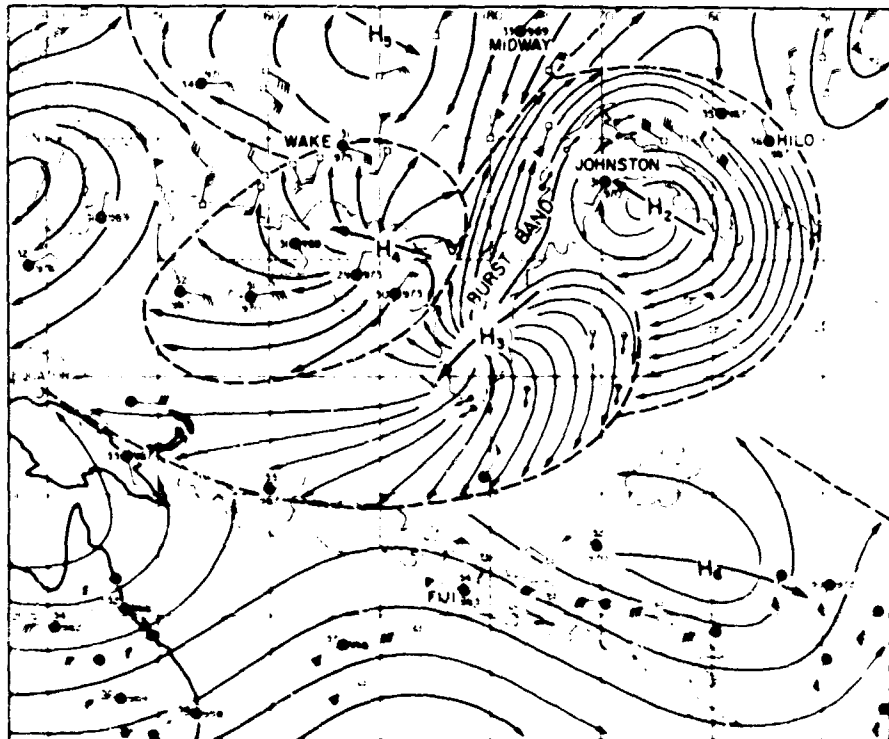


Figure 16. 300-mb. Chart for 0600Z 25 September 1967, When a Strong Burst Band Passed Over Johnston Island. There were three outflow highs,  $H_1$ ,  $H_2$ , and  $H_3$ , which were moving, respectively, from SE, NE, and ESE. Two anticyclone centers  $A_1$  and  $A_2$  were moving from WNW. Rawin and aircraft data were plotted with regular wind barsbs attached to black circles and open squares, respectively. ATS cloud velocities are shown with short arrows. Shown with curved lines with arrow heads are stream lines and the velocities of highs.



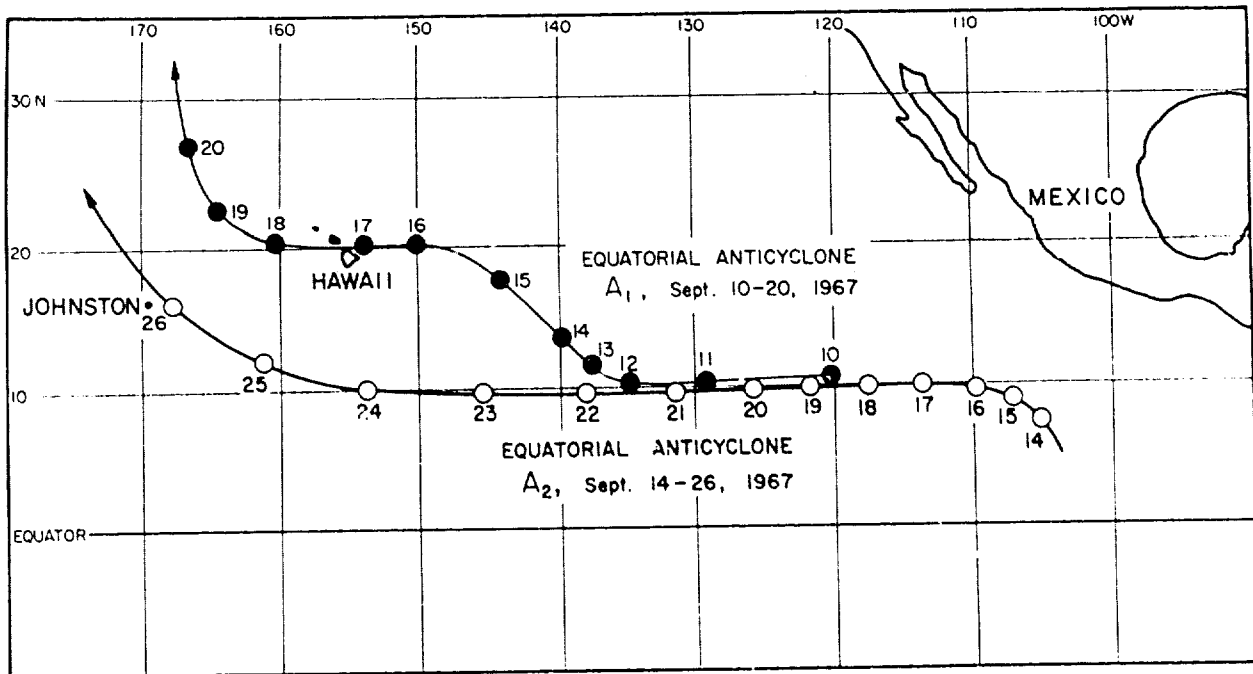


Figure 17. Tracks of Two Equatorial Anticyclones, A<sub>1</sub> and A<sub>2</sub>, Which Originated to the North of the Equator, South of Baja, California. They were tracked for 10 to 14 days until disappearing in the central Pacific.

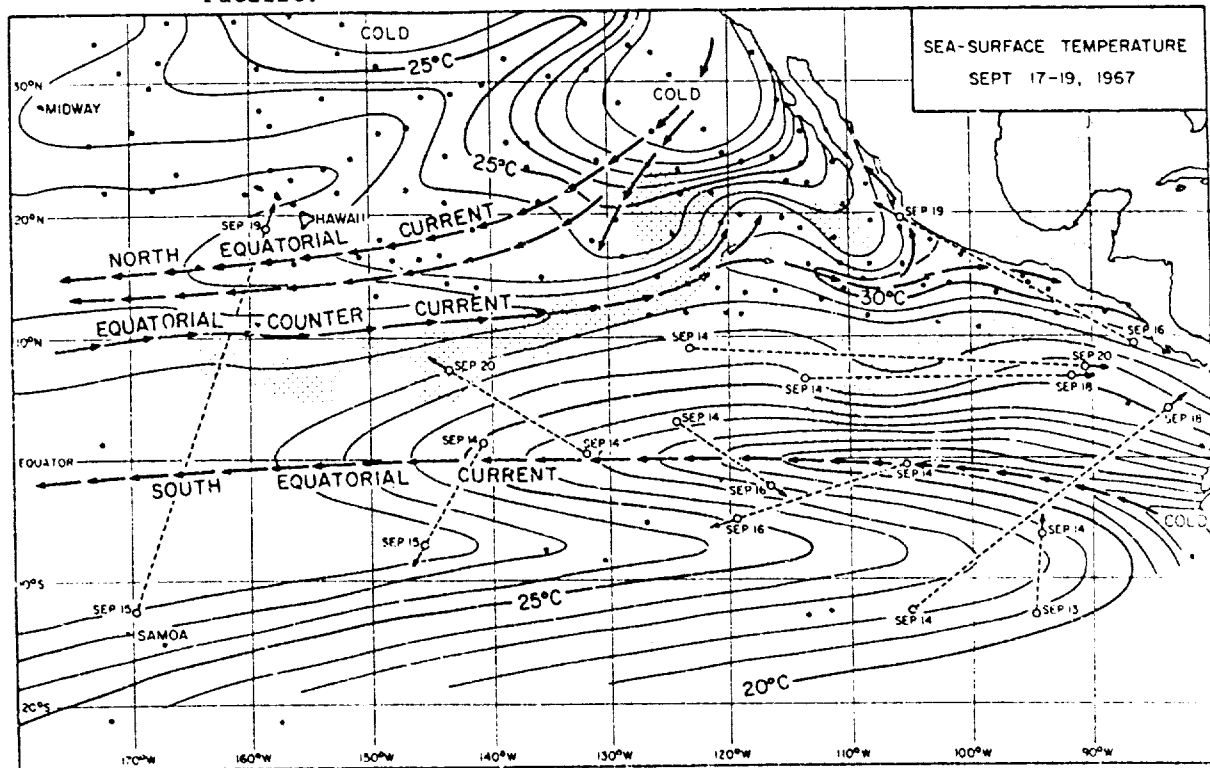


Figure 18. A Composite Sea-Surface Temperature Chart for a Three-Day Period, 17-19 September 1967. The temperature contrast between the South Equatorial Current and the Equatorial Counter Current, as large as 12° C. along 100° W., gradually decreases to about 2° C. to the south of Hawaii.

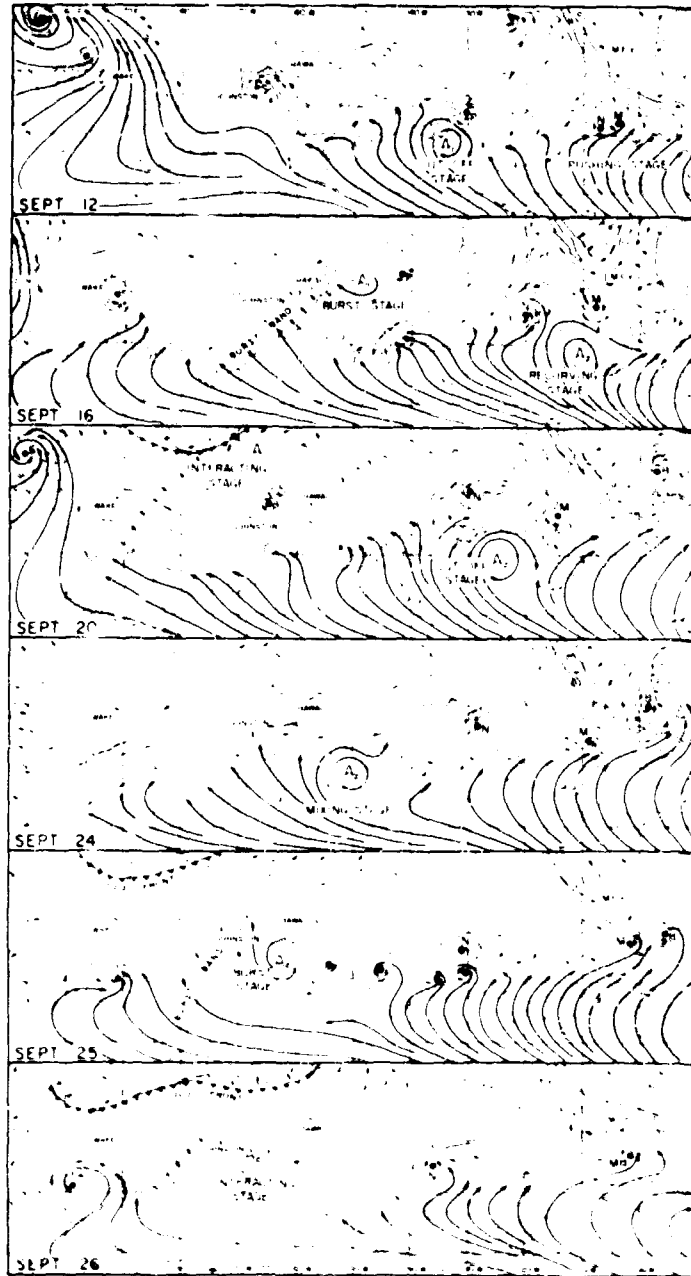


Figure 19. An Example of Six Stages of an Equatorial Anticyclone Over the North Equatorial Pacific. 12-26 September 1967.

## FORECASTING FINE WEATHER OVER NORTH VIETNAM\*

W. R. Brett  
1st Weather Wing

### ABSTRACT

Two distinct synoptic regimes, each possessing lower and middle tropospheric ridge systems and resultant fine weather over the Red River Delta of North Vietnam in summer, are examined.

- (1) Tropical storms entering or developing in the South China Sea have the effect of building, intensifying or reorienting a ridge in advance of the storm. Satellite photographs illustrate the minimum of cloudiness associated with sinking air through the advancing ridge system. A simple storm location versus cloudiness minimum relationship is suggested.
- (2) Movement of ridge system of near-equatorial origin across Southeast Asia in early July 1966 and mid-July 1967 was accompanied by dramatic clearing of the Red River Delta for several days. Kinematic analyses and satellite photographs document the July 1967 case. Rainfall data at three stations in central Southeast Asia reveals significant reduction of precipitation after passage of the ridge system.

Similar ridge associated clearing occurred in mid-July 1968 over Southeast Asia. Pisharoty and Asnam [2] and Dixit and Jones [1] observed similar 500-mb. ridge patterns during the "break" monsoon over India in mid-July of 1954 and 1955, and in 1964, respectively. However, they view differently events leading to the break. Ramage [3] documented a July dry spell singularity over southern China. These time related events over much of the monsoon region suggest a yearly recurrence, a circulation singularity that produces fine weather over a wide area.

Since this is not an original paper but instead, a presentation of cases already documented in Scientific Report No. 1 [4], figures published in that report will not be reproduced herein. With the exception of figure 1 (attached) slides used in this presentation are figures 8 through 17 (pp. 28-37) and figures 19 through 36 (pp. 39-56) of the publication. Pages 6-9 contain a discussion of the figures used. A copy of Scientific Report No. 1 will be distributed to conferees with this abstract.

### REFERENCES

1. DIXIT, C. M. and D. R. JONES, "A Kinematic and Dynamical Study of Active and Weak Monsoon Conditions Over India During June and July 1964." International Meteorological Center, Indian Meteorological Center, Indian Meteorological Department. 26 pages plus 17 figures and 5 tables. 1965.
2. PISHAROTY, P. R. and G. C. ASNAMI, "Flow Patterns Over India and Neighbourhood at 500 mb. During the Monsoon." Proc. of Symposium on Monsoons of the world, India Meteorological Department, pp. 112-117. 1958.
3. RAMAGE, C. S., "Variation of Rainfall Over South China Through the Wet Season." Bull. Amer. Meteorol. Soc., 33:308-311. 1952.
4. SADLER, J. C., W. R. BRETT, B. E. HARRIS and F. P. HO, "Forecasting Minimum Cloudiness Over the Red River Delta During the Summer Monsoon." Scientific Rept., No. 1, Contract No. F19628-67-C-0232, AFCRL-68-0487. Hawaii Institute of Geophysics Rept. HIG 68-16. University of Hawaii. 1968.

---

\*Research sponsored by Air Force Cambridge Research Laboratory

### DISCUSSION

ATKINSON: What happens to the vertical slope of the buffer zone as it moves northward?

BRETT: There is a pronounced northward slope with height as the buffer zone lies near the equator. As the buffer zone moves northward, the slope becomes more vertical.

BELL: Heywood found that at Hong Kong the weather clears ahead of typhoons when they are about 700 miles away, and clouds return when the storm is about 400 miles away. The fine weather ahead of the storm gives rise to the "Coppersky" mentioned by old mariners as the cirrus shield is illuminated by the setting sun.

- (a) Did you notice any effect due to recurving storms?
- (b) You mention that even weak storms give clear weather ahead; in south China we also get a clearing ahead of other westward moving disturbances such as easterly waves. Did you examine these situations?

BRETT:

- (a) The location relative to the recurving storm is important. North Vietnam is also affected by terrain, i.e., mountains to the west and north. Any light west-wind component tends to dissipate low level clouds. Ramage had noted that recurving storms give a longer period of clearing at Hong Kong.
- (b) Weak vortices also give reinforced ridging over the area (north Vietnam). We have examined only the two years 1966 and 1967.

ATKINSON: What happens to upper tropospheric flow as the storm develops?

SADLER: The westward moving cyclonic cell dissipates and the northeasterly flow at 200 mb. returns over the South China Sea.

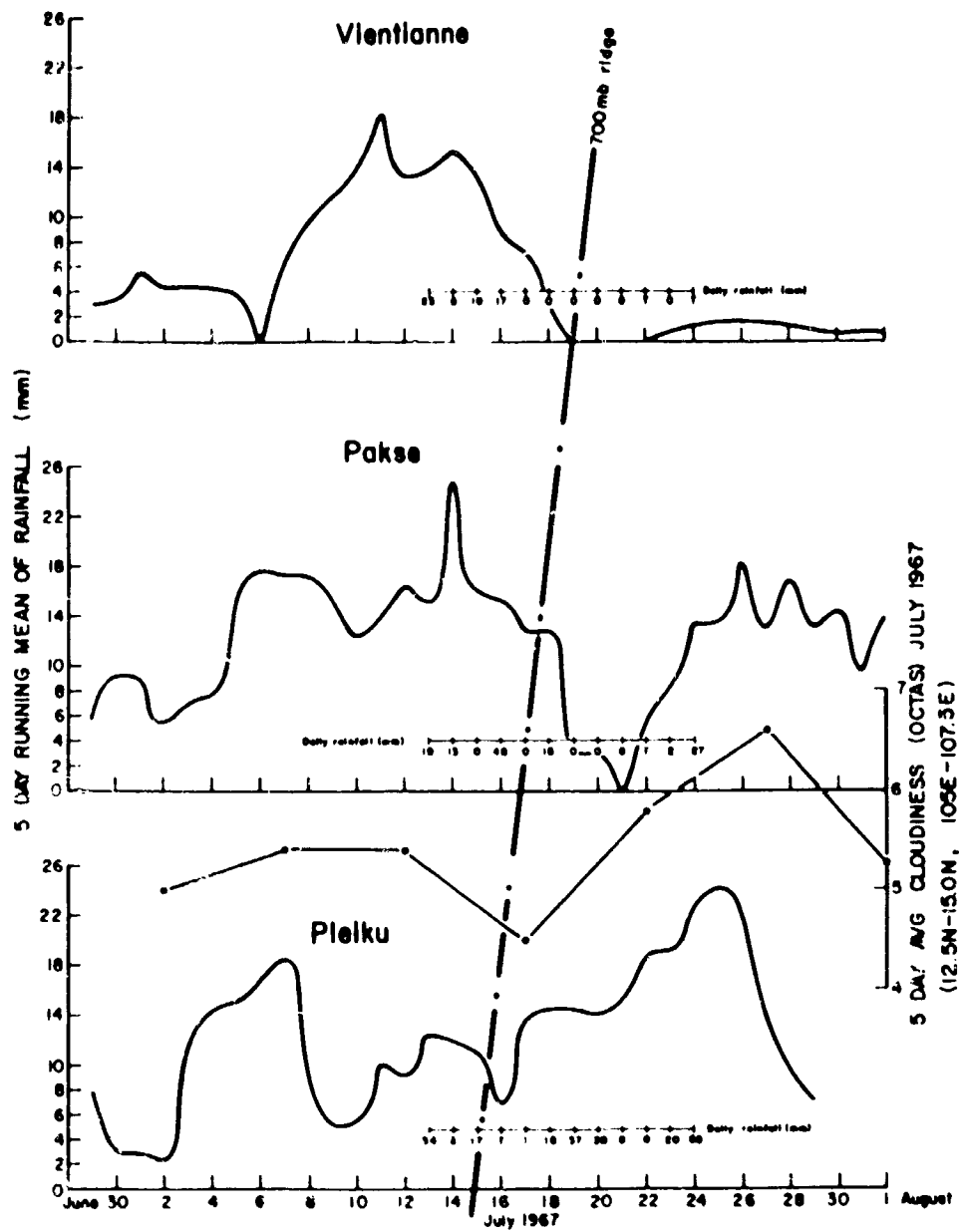


Figure 1. Depiction of Rainfall and Cloudiness Over Interior Southeast Asia as 700-mb. Ridge Passes.

## THE MONSOON TROUGH NEAR THE SOUTH CHINA COAST \*

Gordon T. Bell  
Royal Observatory, Hong Kong

### ABSTRACT

The frequency of the main synoptic patterns over south China during the summer season is determined. The frequency and duration of spells of southwest monsoon and trough situations are examined. The rainfall associated with the two meteorological situations during different summer months is examined, and a radar climatology of the southwest monsoon and associated troughs is given. Some rules are developed for predicting the location of the surface trough and its associated rainfall. The structure of the trough in the mean and at different times of the year is briefly discussed.

### 1. INTRODUCTION

At Hong Kong heavy rain associated with surface troughs that extend eastward from the southwest China low have, in recent years, caused a greater loss of life and more damage than tropical cyclones. In June 1966, the trough was particularly active and on the 12th of that month caused the loss of 64 lives and over 5 million dollars worth of damage. Chen [2] of the Royal Observatory produced a report on this storm in which the meteorological and hydrological aspects are examined in some detail. Rainfall rates as high as 161 mm. in 1 hour and 518 mm. in 24 hours were recorded. On the same day in 1968 - 12 June - a trough again caused loss of life and considerable damage in the territory.

In view of the importance of these troughs to people on the south China coast, I decided to look for techniques which would help in forecasting trough movement and intensity more accurately, especially insofar as they affect 5-day quantitative rainfall forecasts.

### 2. CLIMATOLOGY OF SYNOPTIC SITUATIONS

#### 2.1 Introduction

Several Chinese and Japanese authors have written extensively on the climatology of these troughs; for example, Asakura [1] has recently reviewed some of this work. The following treatment will concentrate on troughs near Hong Kong. These troughs have different structure and characteristics at different time of the year. It is doubtful whether the early season frontal troughs should bear the name Mai-yu (Japanese name BAIU) although this is sometimes done because they are found over China during the Mai-yu or Plum rains season.

Figure 1 portrays the surface chart for 0000Z, 12 June 1966, showing a typical trough situation. Ramage [6] has already described how the summer weather over the south China coastal region is mainly determined by the interplay between the ridge from the Pacific anticyclone, the summer monsoon, tropical cyclones and other westward moving disturbances. Ramage used the 10,000 ft. wind at Saigon as an indicator of ridge and monsoon dominance; if this wind is easterly then it usually indicates that the ridge dominates the area and that then anticyclonic flow occurs over the south China Sea with considerable subsidence and fine weather. Conversely, if this wind is westerly then south China is exposed to the southwest monsoon which turns cyclonically over the China Sea and reaches Hong Kong as a convergent humid south or southwest flow. At such times a monsoon low will be found over southwest China and frequently an associated trough will be encountered as shown in figure 1. The probability of showers at Hong Kong is high for both the trough and monsoon situations.

Satellite photographs show - as predicted by Riehl [10] - that the line of cloud on these troughs is usually linked to some extratropical line of cloud associated with extratropical depressions or westerly troughs. I have been surprised to see how highly correlated surface-pressure patterns and cloudiness are over China during the summer months. A pressure deficit over a region of the continent of one isobar (2-mb. interval) or so is immediately shown as an area of cloudiness on satellite pictures. The clouds and pressure falls seem to develop together. I know of no statistical treatment of this phenomenon.

\* Research sponsored by Royal Observatory of Hong Kong

2.2 Frequency of Occurrence

Table 1 lists the five main synoptic situations that are frequent during the summer months in the region. It will be seen that for the period May to September the summer monsoon plus its associated trough account for 52 percent of the days. The monsoon is most frequent, of course, in June when it attains a frequency of 77 percent. The definition of a trough day in this report has been limited to occasions when a surface trough is shown within 240 nm. of Hong Kong on the local printed Daily Weather Map for 1800Z. The maximum limit of range is usually 240 nm. at which the trough has any appreciable effect on Hong Kong rainfall; it is the rainfall with which we are most concerned.

Table 1. Percentage Frequency of Synoptic Situations at Hong Kong From R.O.H.K. Printed Daily Weather Map: 1800Z, 1958 - 1967.

Type of Situation \ Month	May	June	July	Aug.	Sept.	May-July	Aug.-Sept.	May-Sept.
T - Trough within 4° N. or S. of Hong Kong	45.2	53.7	10.3	14.5	18.3	36.2	16.4	28.3
S - Southerly or Southwesterly Flow	10.0	23.0	39.4	33.5	14.7	24.1	24.3	24.2
E - Easterly Flow	39.7	14.0	35.8	33.2	32.3	30.0	32.8	31.1
NE - Northeast monsoon	2.3	-	-	-	16.7	0.8	8.2	3.7
C - Tropical Cyclone	2.9	9.3	14.6	18.7	18.0	8.9	18.4	12.7
S+T - Summer monsoon	55.2	76.7	49.7	48.0	33.0	60.3	40.7	52.5

Table 2 shows the occurrence of "S" and "T" situations during the last 10 years. The number of "T" days in May is relatively stable, varying from 11 to 20. June is again seen to be the most active month for troughs, but with considerable variability. The number of "T" days varying from 8 to 24 in any one month. In July the number of "T" days is greatly reduced because the Mai-yu trough will normally be much further north, leaving south China under the influence of a Pacific ridge - a singularity which Ramage [7] has described.

Table 2. Number of Days With "S" and "T" Type Situations 1958 - 1967.

Year \ Month	May		June		July		Aug.		Sept.		May-July		Aug.-Sept.		May-Sept.	
	S	T	S	T	S	T	S	T	S	T	S	T	S	T	S	T
1958	6	15	11	9	17	1	9	1	6	1	34	25	15	2	49	27
1959	-	20	8	18	7	3	12	7	7	5	15	41	19	12	34	53
1960	8	16	6	9	6	1	7	5	2	8	20	26	9	13	29	39
1961	7	10	11	8	19	1	14	4	3	14	37	19	17	18	54	37
1962	3	17	6	21	10	2	14	6	3	4	19	40	17	10	36	50
1963	1	13	3	20	9	8	11	2	1	8	13	41	12	10	25	51
1964	-	11	8	17	20	2	7	13	-	3	28	30	7	16	35	46
1965	2	13	1	20	14	-	9	3	6	5	17	33	15	8	32	41
1966	-	11	4	24	9	4	13	4	11	-	13	39	24	4	37	43
1967	4	14	11	15	11	10	8	-	5	7	26	39	13	7	39	46
Mean	3.1	14.0	6.9	16.1	12.2	3.2	10.4	4.5	4.4	5.5	22.2	33.3	14.8	10.0	37.0	43.3

There does not appear to be any marked compensation of trough occurrence from one month to another; e.g., May, June and July can all have below normal "T" frequency as in 1961 (19 days), above normal occurrence as in 1963 (41 days) or 1959 (41 days). Incidentally, 1959 was a wet year and 1963, the driest in 105 years. The number of "S" + "T" days in the period May, June and July appears to be fairly conservative, varying from 46 to 56 apart from one year - 1967 with 65 days.

Table 3 shows the length of spells of "S" and "T" situations and it will be seen that in June the trough persisted within 4 degrees latitude of Hong Kong for as long as 24 days consecutively. It should also be noted that in June the trough occurs more frequently in 2-day spells than 1-day spells. During the ten years under review "S" and "T" situations together have persisted for 30 consecutive days from 27 May to 25 June, 1959 and for 29 days from 4 June to 2 July, 1962.

Table 3. Spells of Consecutive Days of "S" and "T" Type Situations 1958 - 1967.

Month No. of days	May*		June*		July*		Aug.*		Sept.*		May-July		Aug.-Sept.		May-Sept.	
	S	T	S	T	S	T	S	T	S	T	S	T	S	T	S	T
1	15	16	18	8	12	10	13	6	11	14	42	33	23	20	62	53
2	6	12	3	9	8	4	8	6	4	11	18	24	12	16	31	40
3	-	11	2	6	4	2	6	3	2	2	6	19	7	5	12	24
4	1	1	3	5	5	2	6	2	2	2	9	8	9	3	17	11
5	-	5	2	3	3	-	2	2	1	1	5	7	3	3	9	10
6	-	3	-	-	-	-	1	-	1	-	-	3	2	1	1	4
7	-	-	1	1	2	-	-	-	-	-	3	1	-	-	2	1
8	-	1	-	-	3	-	1	-	-	-	2	2	1	-	3	2
9	-	-	-	-	1	-	1	-	-	-	2	-	1	-	2	-
10	-	1	1	1	-	-	-	-	-	-	1	1	-	-	2	1
11	-	-	-	1	-	-	-	-	-	-	-	2	-	-	-	2
14	-	-	-	1	-	-	-	-	-	-	-	1	-	-	-	1
15	-	-	-	-	-	-	-	-	-	-	-	-	-	-	1	-
16	-	-	-	1	-	-	-	-	-	-	-	1	-	-	-	1
24	-	-	-	1	-	-	-	-	-	-	-	-	-	-	-	-
25	-	-	-	-	-	-	-	-	-	-	-	1	-	-	-	1
Longest Spell	4	10	10	24	9	4	9	5	6	5	10	25	9	6	15	25

\*A spell that continues from one month into the next is counted as two separate spells.

### 3. RAINFALL

#### 3.1 Introduction

On the average, approximately 25 percent of the annual rainfall at Hong Kong is attributable to tropical cyclones. Tropical cyclone rainfall is here defined as that which falls when a tropical cyclone of any intensity is centered within 300 nm. of the territory. Most of the annual rainfall is attributable to the southwest monsoon and its associated troughs.

Figures 2 and 3 show the variation of the instantaneous rate of rainfall (actually a 20 second mean) in a trough and in a typhoon; the records were taken from the same gauge. The appearance of the traces is typical for trough and typhoon rainfall respectively, but in both examples the intensity of the rainfall is extreme. The difference in appearance is attributable to wind effects. The typhoon gales cause extreme turbulence in the friction layer with changes in the relative fall speeds of raindrops. Rapid transit of rain cells over the gauge and turbulence around the gauge also cause variations in catch; however, the gauge in question is in a pit at ground level. The effects of gauge turbulence should be minimized. In contrast, the relative - sometimes absolute - calm that attends extreme rainfall from troughs is remarkable. Most troughs have higher instantaneous rates of rainfall than most tropical cyclones in this region. This fact is readily established by radar; the high power 10 cm. Plessey 43S, which has been in continuous operation at Hong Kong since August 1966, has not yet



(as of March 1969) seen a tropical cyclone with a "radar" rate of rainfall greater than 50 mm. hr.<sup>-1</sup> (equivalent to 35 db. of attenuation). Whereas troughs frequently contain cells with "radar" rates of rainfall in excess of 130 mm. hr.<sup>-1</sup> (40 db. of attenuation). It is to be expected that some typhoons will contain extreme short period rainfall rates; indeed, during the last 17 years rates of rainfall of 300, 301 and 307 mm. hr.<sup>-1</sup> have been recorded by the Jardi-gauge in tropical cyclones. The highest reading in a trough situation during the same period was 320 mm. hr.<sup>-1</sup>

Figure 4 shows the Z/R (radar reflectivity/rate of rainfall) relationship in different situations in 1968. It will be noted that typhoon SHIRLEY which passed directly over the radar and the 148 observatory rain-gauges had less intense rainfall than was recorded in troughs and the southwest monsoon.

### 3.2 Rainfall Climatology of Southwest Monsoon and Troughs

Table 4 gives information on the daily rainfall at Hong Kong associated with "S" and "T" situations. It will be seen that in May and June "S" rainfall is relatively light with 87 percent and 91 percent of the days having less than 5 mm. of rain, respectively.

Table 4. Percentage Frequency of Daily Rainfall at Hong Kong Associated With "S" and "T" Type Situations 1958 - 1967.

Month Rainfall mm.	May		June		July		Aug.		Sept.		May-July		Aug.-Sept.		May-Sept.	
	S	T	S	T	S	T	S	T	S	T	S	T	S	T	S	T
0 - Trace	48	51	46	20	43	28	50	27	43	35	45	34	48	31	46	33
0.1 - 5	39	30	15	29	25	28	25	18	23	31	33	29	24	25	29	28
6 - 10	3	5	4	12	10	6	6	4	7	11	7	9	6	8	7	8
11 - 15	3	4	-	6	5	19	5	16	5	4	3	6	5	9	4	7
16 - 20	-	1	-	2	2	6	4	-	7	2	1	2	5	1	2	2
>20	6	9	4	30	16	13	11	36	16	18	11	20	12	26	11	21
Total Rain mm.	187	860	173	3586	1232	333	853	829	506	680	1592	4779	1359	1508	2951	6287
Total Days	31	140	69	161	122	32	104	45	44	55	222	333	148	100	370	413
Average Rain per Day mm.	6.0	6.1	2.5	22.3	10.1	10.4	8.2	18.4	11.5	12.4	7.2	14.4	9.2	15.1	8.0	14.5
No. of Days with Measurable Rain	16	68	37	128	69	23	52	33	25	36	122	219	77	69	199	288
Average Rain on a Rain-Day mm.	11.7	12.6	4.7	26.0	17.9	14.5	16.4	25.1	20.2	18.9	13.0	21.9	17.6	21.9	14.8	21.8

Trough rainfall is very much more variable. In June 30 percent of "T" days have daily rainfall amounts in excess of 20 mm. and 20 percent have no rain at all. It will be noted that the average "T" rain-day in June has approximately six times more rain than the average "S" rain-day. During the summer as a whole, (i.e., May to September) the rainfall due to "T" days is more than twice that due to "S" days and, in June, trough rainfall is approximately 20 times as abundant as that from "S" situations. In July and August the frequency of "S" days increases and the "S" rain days also have more rain. By September the frequency of "S" days falls again, and the rainfall contribution of "S" and "T" days is similar in both amount and intensity. June, therefore, is the month when troughs are both most frequent and most active.

Figure 5 shows the mean daily rainfall from all troughs at given distances from Hong Kong during May to August. The individual values have been smoothed by taking moving averages over three points weighted 1, 2, 1. The indication that, on average, the heaviest rain falls when the surface trough is about 1° south of Hong Kong in May and June was not expected. The effect is probably due to lifting or "upslope" motion to the north of the early season troughs which retain frontal characteristics. In July and August frontal characteristics are nonexistent, or very weak. At this time the rainfall distribution shows a minimum on the trough axis with principal maxima 1 1/2 degrees north and 1 degree south of the trough axis. This finding is in accord with troughs found over the Indian Ocean and elsewhere in the tropics.

### 3.3 Forecasting Heavy Trough Rainfall

Although Chen [2] has determined the synoptic features associated with extreme rainfall in the June trough of 1966, we thought that it might be possible to devise some objective aids to assist in forecasting the heavier falls, given the necessary basic synoptic pattern.

Figure 6 shows the daily rainfall at Hong Kong plotted at the center of the southwest China surface low on occasions when surface troughs were within 60 nm. of Hong Kong in June. Data for the 12 years, 1958-1969, have been used. The rainfall was found to be independent of the Hong Kong pressure, the central pressure in the depression, and the pressure difference from the center of the depression to Hong Kong. The average pressure gradient between the center of the low and Hong Kong for all points within the 100 nm. isohyet varied from 1 mb./120 nm. to 1 mb./200 nm. The two points in the maxima were associated with a gradient of 1 mb./200 nm. i.e., 1.5-mb. pressure difference from the center of the low to Hong Kong.

If conditions over China, Indochina and the South China Sea modulate the rainfall of the monsoon and associated troughs over south China in May and June, then it seems likely that this modulation would be obtained through changes in surface temperature of the South China Sea. This possibility was examined for four selected sea areas, and it was found that the annual rainfall in June was correlated with the sea temperature over Nansha (11° - 13° N., 111° to 113° E.). However, the relationship was closer for the February and March sea temperatures. If annual rainfall less tropical cyclone rainfall had been considered as the variable, an even closer relationship would have resulted. Figure 7 shows a plot of the Hong Kong annual rainfall less tropical cyclone rainfall against Nansha sea temperature in March. The correlation coefficient of 0.76 is significant at a level better than 1 percent.

### 3.4 Upper Winds

When the westerly component at 200 mb. over Hong Kong is stronger and persists further than normal into the summer, then the year usually has more than normal rainfall. Neither the persistence of the westerly component nor the strength of the westerlies are in themselves closely related to the annual rainfall; however, an index which combines both the strength and persistence of the westerlies can be used as an index for seasonal rainfall forecasts. It has been found that the average west-wind component between 11 May and 20 June is satisfactory for this purpose. The relationship can be improved if tropical cyclone rainfall is discounted. The graph depicting the relationship is shown in figure 8; the correlation coefficient is 0.75, this value is significant at a level better than 1 percent. The relationship is not as useful as it appears because the relationship cannot be used until 21 June. Nine days later the rainfall for the first 6 months of the year will be available with the latter correlating well with the annual rainfall. The January to June rainfall for 1957 to 1968 has a correlation coefficient of 0.81 with the annual rainfall and 0.93 with the annual rainfall less tropical cyclone rainfall.

The correlation coefficient will rise to 0.80 if May plus June rainfall is used as the dependent variable and will rise to 0.88 if tropical cyclone rainfall in May and June is discounted. This latter relation is illustrated in figure 9. It probably could be further improved by removing the contribution to the west-wind component from passing tropical cyclones.

Wright [11] showed at Hong Kong, as at locations over India, that the west-wind component in some years falls steadily throughout May and June, and in other years there is a rapid fall. Frequently the west-wind component changes sign several times before finally becoming negative. The reasons for the relationship between the 200-mb. west-wind component and the annual rainfall have not been studied in detail. However, late season westerlies will be associated with surface troughs south of their normal position, having weak frontal characteristics. At such times the 200-mb. ridge will be south of the coast. Thus, with persistent westerlies, early troughs should contain frontal and be active over south China. Later troughs will also be active over the same region because the 200-mb. ridge will be late moving north and, consequently, will be superimposed upon the troughs.

Figure 10 illustrates the 200-mb. ridge over the surface trough in figure 1 on 12 June, 1966. Chen [2] demonstrated the importance of this superposition of the ridge on this occasion.

### 3.5 Albedo and Rainfall

Figure 11 shows the latitude of the trough during June 1966 as determined from original Royal Observatory 6-hourly working charts. Between the 1st and 15th of the month the trough was quasi-stationary near 22° N.; this location is reflected in the high rainfall amounts for that period over Hong Kong and Taiwan as shown in figure 12. The dashed isohyets have been entered in geometrical progression i.e., 100, 200, 400 and 800 mm. to bring out the pattern clearly. Chen [2] found that on 12 June the cloud cover, as depicted by satellites, did not correlate well with the rainfall pattern but did correlate well with the isopleth of 3° C. depression of the 200-mb. dew-point temperature. Since the trough was quasi-stationary for the 1st to 15th, it was thought worthwhile to examine the mean radiation pattern and the mean rainfall pattern. Raschke and Pasternak [9] have presented mean Nimbus II radiation data for this period.

Figure 13A shows that the albedo of 50 percent over the trough was greater than anywhere else between the latitudes 40° N. and 40° S. -- nearer the poles the reflectance is, of course, increased by the low elevation of the sun throughout the day. For completeness the outgoing long wave radiation and the radiation balance of earth-atmosphere system during this period are shown in figure 13B. These figures show that over the region of the trough the radiation balance is directed towards the earth and has a value of 0.08 cal. cm.<sup>-2</sup> min.<sup>-1</sup>. Figure 12 shows that the trough rainfall fell to the south of the area of highest albedo. The poor correlation between radiation and rainfall patterns in general has been observed previously by Radok [4] and Rainbird [5].

### 3.6 Diurnal Variation of Rainfall in the Southwest Monsoon

During 1967 and 1968 a radar climatology was prepared by recording all echoes within 60 nm. of Hong Kong at the main and intermediate synoptic hours. Figure 14 shows the area covered in the analysis. The high power 10 cm. radar used is sited 577 m. above sea level, and it has no difficulty in seeing rain near ground level to the limit of range employed. The radar was operated in swept-gain mode.

Figure 15 shows the percentage of the radar screen which was covered by echoes at each observation time when a trough was within 2° latitude of Hong Kong or when the southwest monsoon was prevailing. This figure, therefore, shows the diurnal variation of radar echo coverage irrespective of the location of the echoes. The maximum occurs at 1400 LT and is apparently determined by convection inland. The area of echoes then falls away rapidly until a minimum is reached in the early hours of the morning.

Ramage [8] has shown that, in those parts of east China, Japan and Korea that are affected by the southwest monsoon, a morning maximum of rainfall is experienced, and, in addition, if the location is favorable an afternoon maximum is also found. Frank, Moore and Fisher [3] have shown that over the Florida Peninsula clouds form offshore in the early morning and progress towards the coast with the basic windflow at a speed of approximately 11 knots and reach a maximum inland during the afternoon. Radar echoes in the rectangular area shown in figure 14 were studied to see if such a movement could be seen on the China coast during southwest monsoon days. The eastern area was chosen to reduce the effects of the estuary. Altogether there were 45 days in which the southwest monsoon prevailed for the whole 24 hours.

The rectangle was divided into 34 strips each 2.14 nm. wide and 47.08 nm. long. The percentage area of each strip covered by echoes at each observation time was obtained and smoothed by taking running means over three strips. The results are shown in figure 16. It will be seen that about dawn a maximum of approximately 10 percent appears offshore; it reaches a level of 15 percent at 0800 LT on the coast and about 10 nm. to seaward. There then follows a slight decrease in activity around mid day, rising to an afternoon maximum of 15 percent which appears about 10 nm. inland at 1400 LT. In the evening a lesser maximum is again found about 30 nm. offshore; this feature moves inland and reaches the coast at midnight.

In the 9 hours between 0500 LT and 1400 LT the location of the maximum shower activity progresses northwards at about 4 knots.

Figure 17 shows the number of observations of rain reported from Waqian Island and the Royal Observatory compared with the number of radar echoes from the same area. The top curve shows the number of rain observations at Canton - just off the northwest edge of the radar display in figure 14 - and the radar

echoes in the northernmost strip of the rectangle. These two curves are not, therefore, strictly comparable. It will be noted, however, that the observations show no morning maximum inland during the southwest monsoon. The rainfall observations from Canton during this period do not show the usual dawn maximum although a secondary maximum is apparent at 0200 LT.

#### 4. SOME SYNOPTIC CONSIDERATIONS

##### 4.1 Forecasting Movement of the Trough

During winter the southward penetration of outbreaks of polar continental air over China is usually related to the passage of waves in the westerlies at the 500-mb. level. Such waves, although further north in summer, also affect the position of the surface trough especially in the active month of June. The latitude of 125° E. for the 5,700 gpm. contour on the 500-mb. surface was used to crudely indicate passages and intensities of troughs in the westerlies over north-east China. The latitude of this contour was read off the printed series of Japanese Daily Weather Maps and it was found that its meridional movement tended to precede movement of the June surface trough - figure 11 - by approximately two days. Figure 18 shows the relationship between the latitude of the surface trough and the latitude of the 5,700 gpm. contour two days earlier. The latitude of the 5,700 gpm. contour at 125° E. is only a crude objective measure of trough activity. It is considered that a forecaster could identify troughs more precisely and so be able to improve on the relationship shown in figure 18. Furthermore, he will be able to make allowances for the short period variations in latitude of the surface trough which are caused by easterly moving vortices.

Northern hemisphere 500-mb. 48-hour forecast charts are generally available in the region of computer products. At the Royal Observatory both Japanese and Monterey charts are received. These products are usually available some 36 hours ahead of their time of validity and can therefore be used to enable a forecast of the movement of the surface trough to be made some 3 days and 12 hours ahead of time.

##### 4.2 The Structure of the Trough

In May and early June the trough retains some frontal characteristics. It is usually found below polar westerlies. By mid-June the frontal characteristics usually disappear, and the trough is found below the ridge at 200 mb. as shown in figure 10. Later still, upper easterlies prevail over south China and over any troughs that form there.

P. Li of the Royal Observatory is currently studying the three-dimensional structure of the trough in some detail by meaning all parameters located on a grid which moves with the trough. The grid covers an area of 20 degrees of latitude by 20 degrees of longitude. To reduce the effects of topography, the origin of the grid is always fixed on the trough at 100° E. The large square is divided into 50 boxes of 2° x 4°, and observations in each box are meaned and related to the central point of the box. Diagrams have been prepared for the trough which was located over south China during the first 15 days of May 1967.

Figure 19 shows the mean surface-pressure pattern. The monsoon low over southwest China was located at 24.5° N., 103.5° E., and the trough curved away to the east-northeast. In figure 20 the 850-mb. trough is found 2° north of the surface trough - a feature noted by Yoshino [12] as being peculiar to China, giving a slope of about 1 in 150. The trough is usually found still further north at 700 mb. See Chen [2].

Figure 21 shows the associated 500-mb. pattern. The westerlies of the monsoon current are relatively strong at this level, while those from the north are weak. There is a ridge in the flow over the trough and the strong 850-mb. flow near 116° E.

Figure 22 shows that westerlies are found on both sides of the trough at 200 mb. (see also fig. 10) and at 500 mb. The fields of surface dew point and surface temperature are shown in figures 23 and 24. As the data accumulate, P. Li hopes to be able to compute stable mean fields and follow changes in the structure and characteristics of the trough through the summer season.

Figure 25 shows isotherms and isopleths of wet-bulb potential temperature across the trough of 1 June 1967. Frontal characteristics are clearly seen. At the surface the dry-bulb temperature changes from 29° C. to 19° C. in 90 nm.

across the trough. The wet-bulb potential temperature changes from 26° C. to 19° C. over a similar distance. However, the mean 0000Z cross section for the first fifteen days of June, figure 26, during which the trough was quasi-stationary, seen in figure 11, shows a marked weakening of frontal characteristics. The isotherms showed that the atmosphere there was essentially barotropic.

## DISCUSSION

**SOUTHERN:** Is there a particular statistical method by which you distinguish between rainfall on a trough day and rainfall on a monsoon day?

**BELL:** Yes, trough rainfall is that which occurs when a surface trough is located within 4 degrees of Hong Kong.

**SADLER:**

- (a) In your definition of trough day and southwest monsoon day -- if the trough is north of Hong Kong and Hong Kong is in southwest flow, is it trough day or southwest monsoon day?
- (b) Is your southwest monsoon flow often anticyclonic around the western end of the Pacific anticyclone?

**BELL:** It is a trough day if the trough is within 4 degrees of Hong Kong because this is the approximate limit at which the trough significantly affects local rainfall. A southwest monsoon day has flow from the Indochina Peninsula and usually reaches Hong Kong as a southerly flow. Ramage in his summer weather over south China [6] showed that a ridge day was associated with 700-mb. easterly flow at Saigon; a monsoon day has westerly winds at Saigon; and, of course, the probability of rain at Hong Kong is greatly different for the two flows.

**RAMAGE:** Reference to your figure 6. Were there any cases in which no vortex could be detected in the trough? If so, what rainfall occurred at Hong Kong? It is my impression that the south China trough is very active with many vortices in contrast to over ocean near equatorial troughs. Perhaps this difference could account for the fact of trough/rain coincidence over south China as against the offsetting found by Sadler from satellite pictures.

**BELL:** I cannot say offhand whether there were any cases with no depression. It can be derived from the results by subtracting 107 from the total number of trough days. I will look into this.

**SOMERVELL:**

- (a) The torrential tropical trough precipitation during early June 1966 at Hong Kong occurred also at Kaohsiung, Taiwan, early in that month.
- (b) An operational application for the summer diurnal precipitation variation, which you described, may be found in the time of sailing or arrival of ships. It seems that noon would be preferable to the customary 0800 LST, or so. Not only would navigation be facilitated but also life would be better for line handling parties, and arrival honors for visiting dignitaries could be less inconvenienced.

## REFERENCES

1. ASAKURA, T., "Dynamic Climatology of Atmospheric Circulation Over East Asia Centered in Japan." *Papers in Met. & Geol.*, Vol. 19, No. 4, pp. 1-68, 1968.
2. CHEN, T. Y., "The Severe Rainstorm in Hong Kong During June 1966." Royal Observatory, Hong Kong, 1968.
3. FRANK, N. L., P. L. MOORE and E. G. FISHER, "Summer Shower Distribution Over the Florida Peninsula as Deduced From Digitized Radar Data." *J. Appl. Met.*, Vol. 6, No. 2, p. 109, 1967.
4. RADOK, U., "An Appraisal of TIROS III Radiation Data for Southeast Asia." Colo. St. U., Dept. of Atmos. Science Report No. 102, 1966.

REFERENCES (CONTINUED)

5. RAINBIRD, A. F., "Weather Disturbances Over Tropical Continents and Their Effect on Ground Conditions." Colo. St. U., Dept. of Atmos. Science Report No. 1, 1968.
6. RAMAGE, C. S., "Analysis and Forecasting of Summer Weather Over and in the Neighbourhood of South China." J. of Met., Vol. 8, 1951.
7. \_\_\_\_\_, "Diurnal Variation of Summer Rainfall Over East China, Korea and Japan." J. of Met., Vol. 9, pp. 83-86, 1952.
8. \_\_\_\_\_, "Variation of Rainfall Over South China Through the Wet Season." B.A.M.S., Vol. 33, pp. 308-311, 1952.
9. RASCHKE E. and M. PASTERNAK, "The Global Radiation Balance of the Earth Atmosphere System Obtained From Radiation Data of the Meteorological Satellite Nimbus II." Space Research VIII, North-Holland Publishing Co., Amsterdam, p. 1038, 1966.
10. RIEHL, H., "On the Role of the Tropics in the General Circulation of the Atmosphere." Tellus 2, pp. 1-17, 1950.
11. WRIGHT, P. B., "Changes in 200-mb. Circulation Patterns Related to the Development of the Indian Southwest Monsoon." Met. Mag., p. 302, 1967.
12. YOSHINO, M., "Four Stages of the Rainy Season in Early Summer Over East Asia (Part I)." J. Met. Soc. of Japan, Series II, Vol. 43, No. 5, p. 231, 1965.

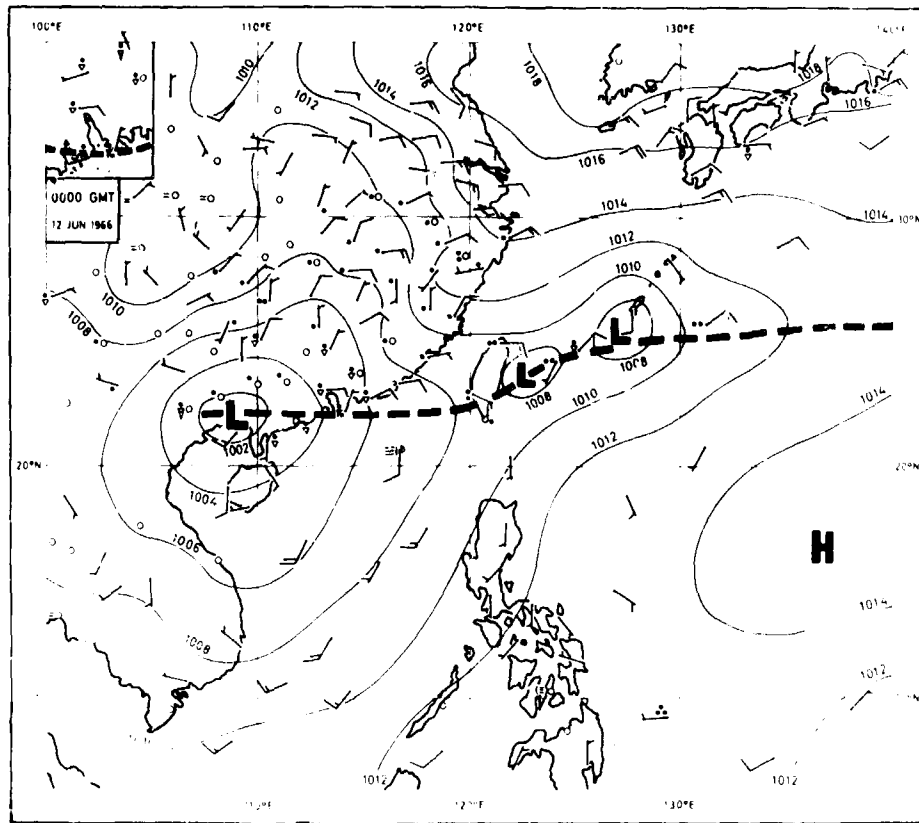


Figure 1. South East Asia-Surface Synoptic Chart.

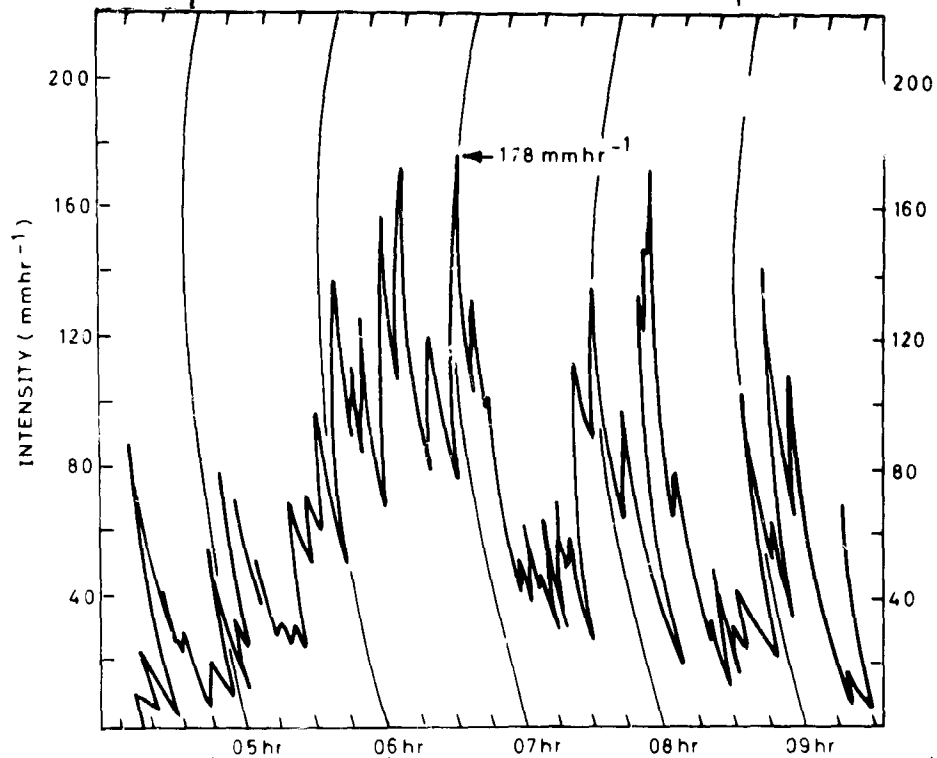


Figure 2. Jardi Trace Recorded on 12 June 1966 at King's Park (trough situation).

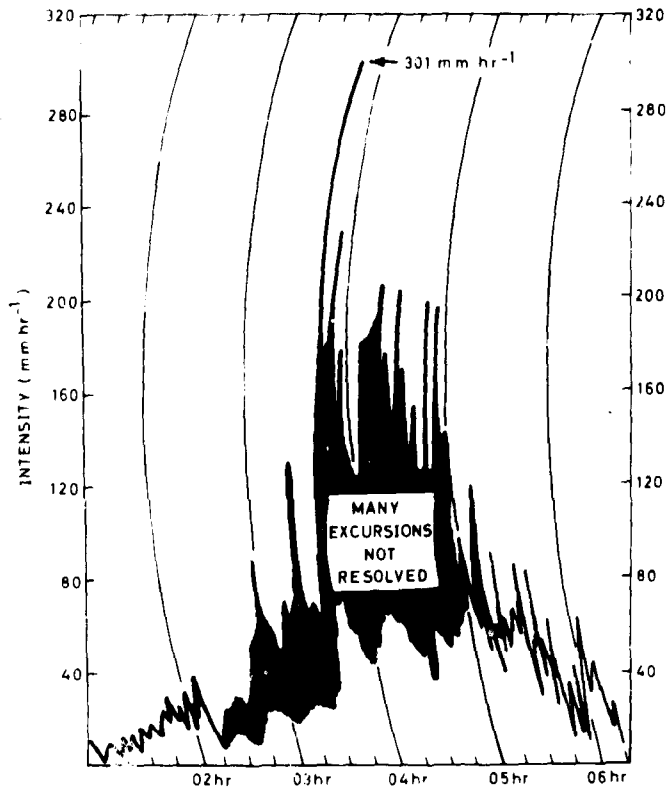


Figure 3. Jardi Trace Recorded on 13 October 1964 at King's Park (typhoon 'dot').

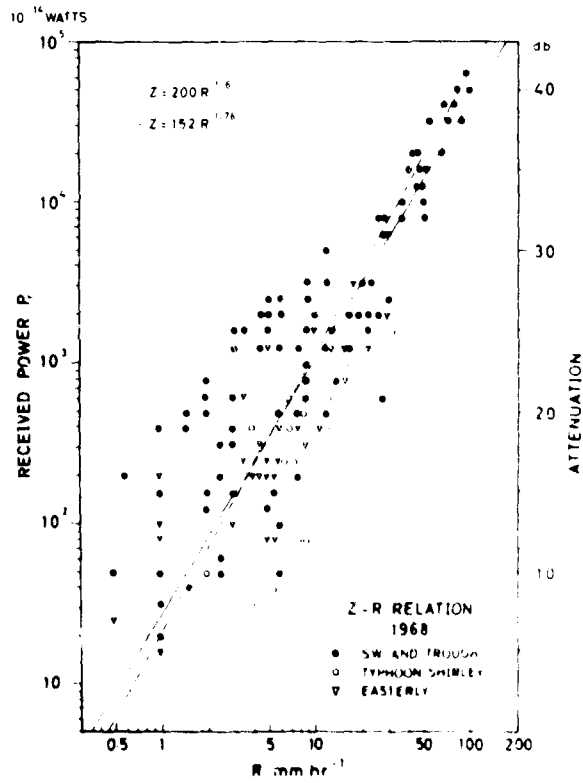


Figure 4. Z-R (radar reflectivity-rate of rainfall) Relationship for 1968.



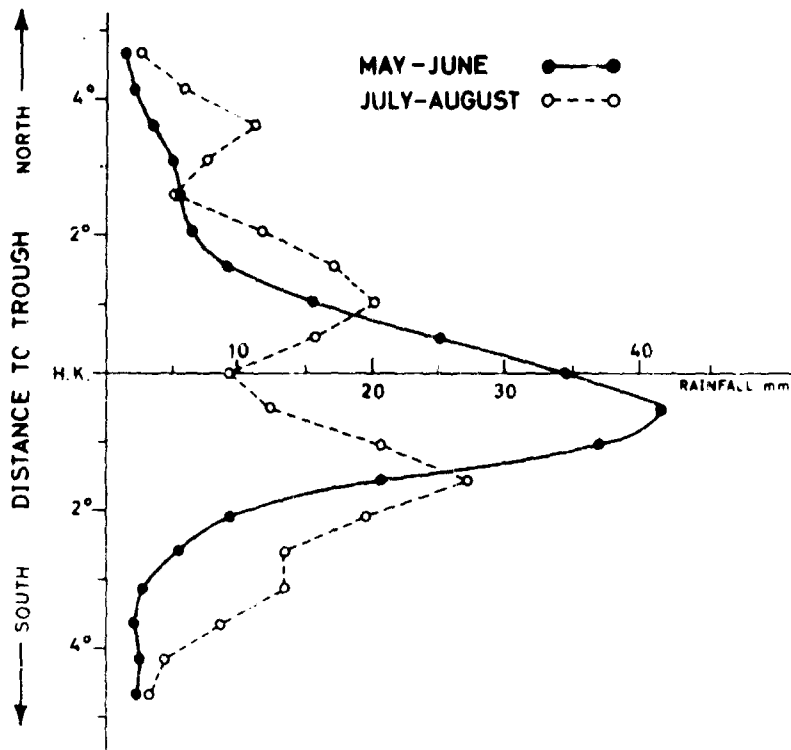


Figure 5. Mean Daily Rainfall Associated With Surface Troughs at Various Distances From Hong Kong at 1800Z, 1958-1967.

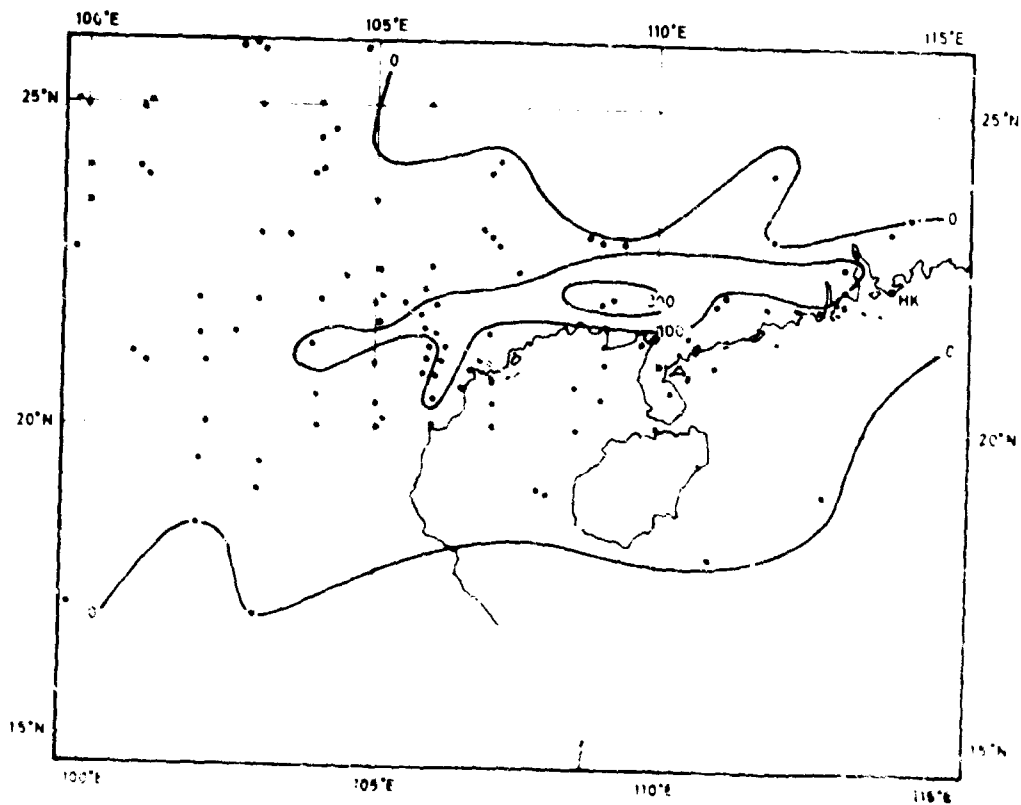


Figure 6. Hong Kong Daily Rainfall (mm) Plotted at the Centre of Associated Depressions on Occasions When Troughs Were Within 60 n.m. in June. Period 1951 to 1968-cases 107.

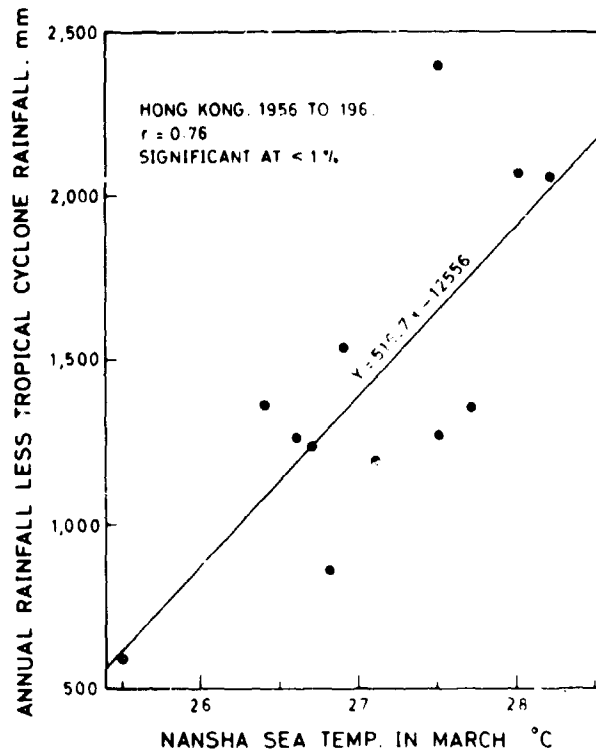


Figure 7. Hong Kong Annual Rainfall Less Tropical Cyclone Rainfall Versus Nansha Sea Temperature in March.

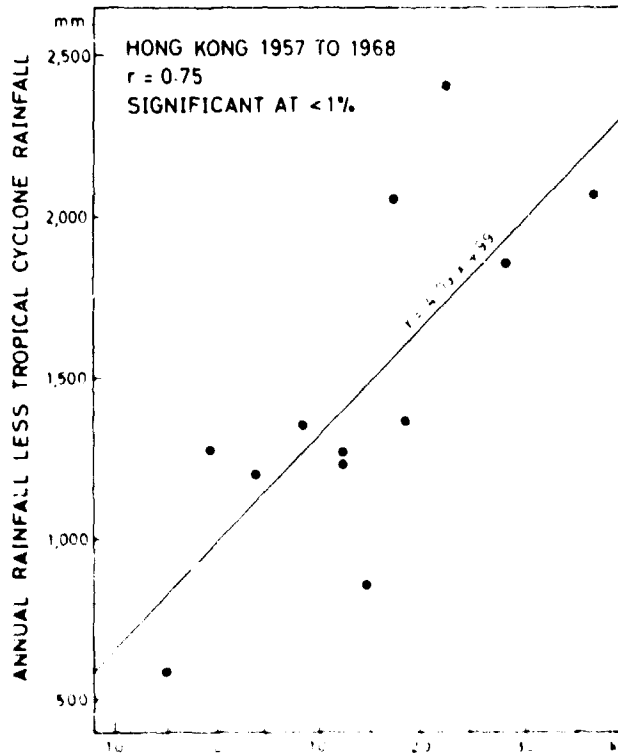


Figure 8. Hong Kong Annual Rainfall Less Tropical Cyclone Rainfall Versus Mean Westerly Wind Component at 200 mb. Over Hong Kong for Period 11 May to 20 June.

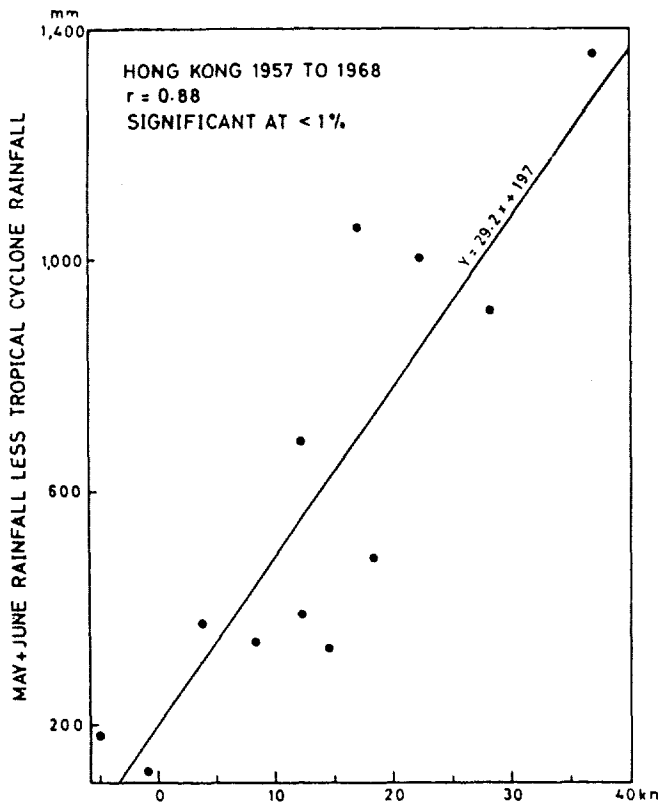


Figure 9. Hong Kong May and June Rainfall Less Tropical Cyclone Rainfall Versus Mean Westerly Wind Component at 200 mb. Over Hong Kong for Period 11 May to 20 June.

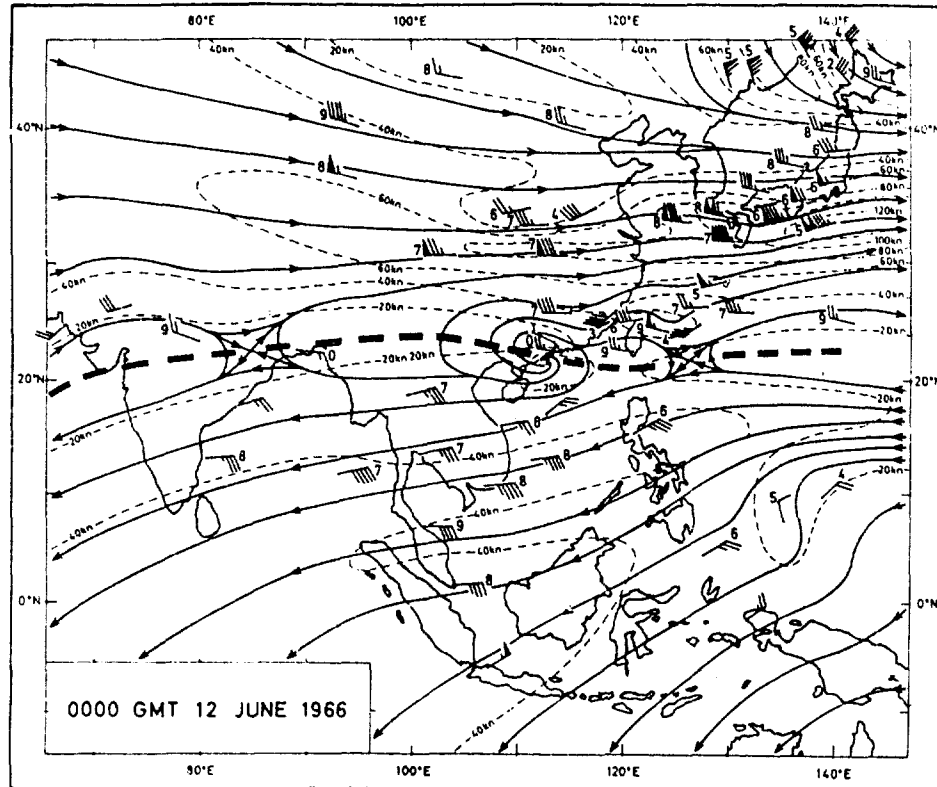


Figure 10. Southeast Asia 200-mb. Streamline Chart - 0000 GMT, 12 June 1966.

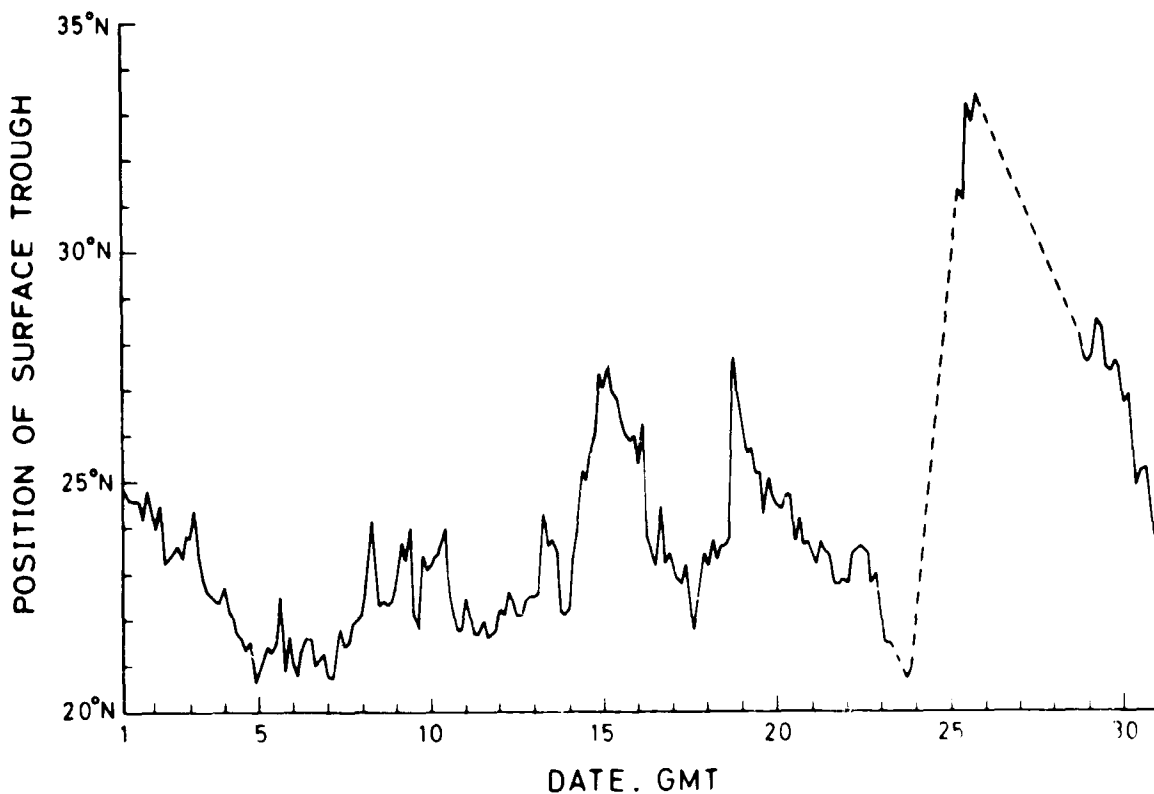


Figure 11. Position of Surface Trough at 114° E. Long. June, 1966.

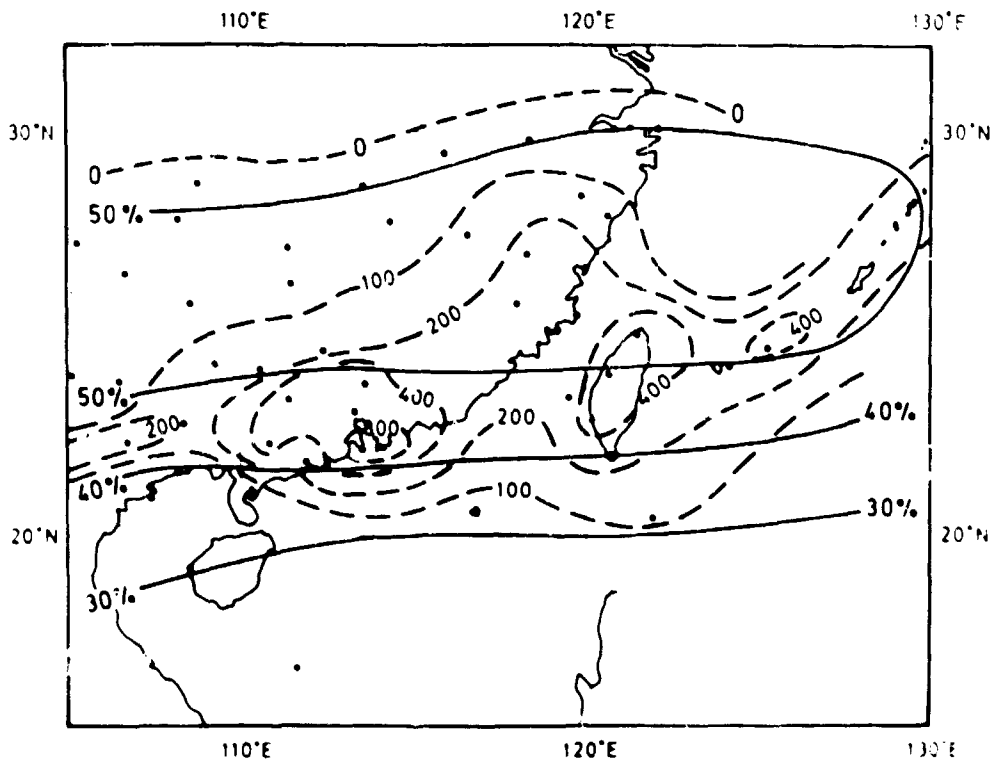


Figure 12. Total Rainfall (mm) From 1st to 15th June 1966 and the Albedo (%) of the Earth-Atmosphere System During the Same Period.

ALBEDO %  
NIMBUS II 1 - 15 JUNE 1966

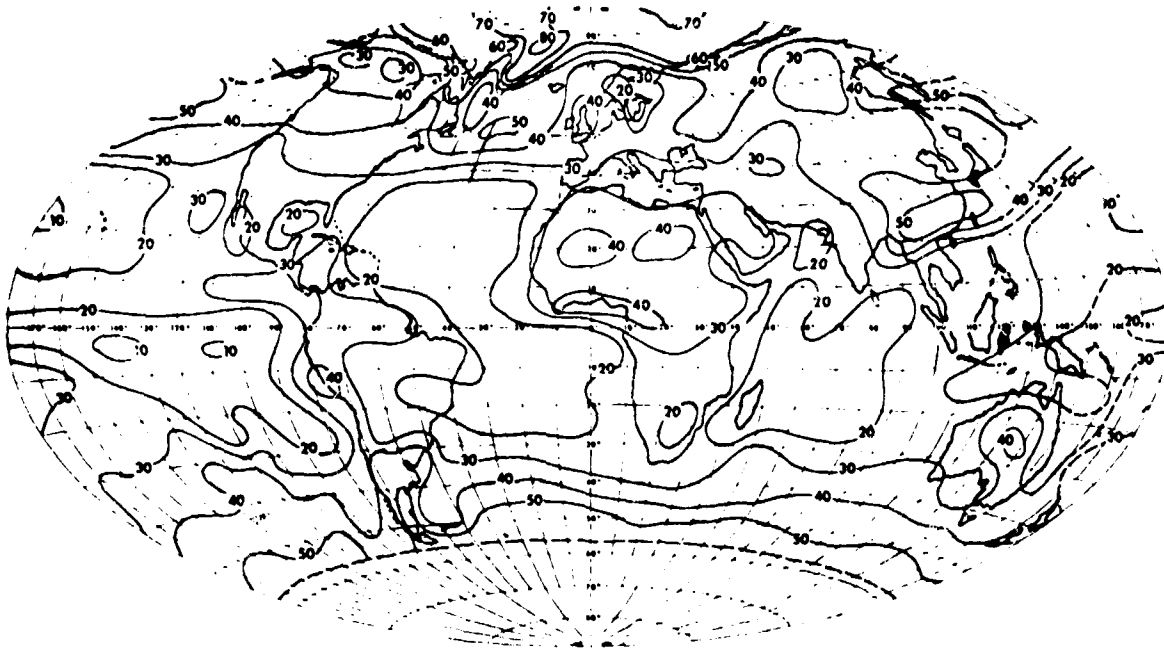


Figure 13A. The Albedo of the Earth-Atmosphere System During the Period 1-15 June, 1966. Values in %.

OUTGOING TOTAL LONGWAVE RADIATION [ $\text{LY MIN}^{-1}$ ]      NET RADIATION FLUX AT THE TOP OF THE ATMOSPHERE [ $\text{cal cm}^{-2} \text{min}^{-1}$ ]  
NIMBUS II 1 - 15 JUNE 1966                                      NIMBUS II 1 - 15 JUNE 1966

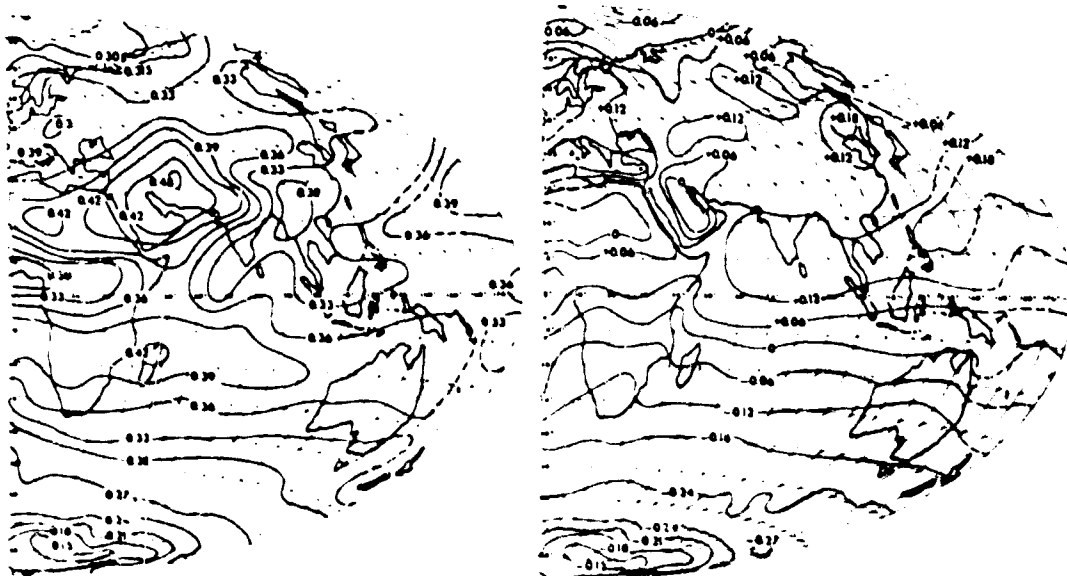


Figure 13B. Thermal Radiation Emitted Daily From the earth-Atmosphere System to Space and Radiation Balance of the Earth-Atmosphere System During the Period 1-15 June, 1966.

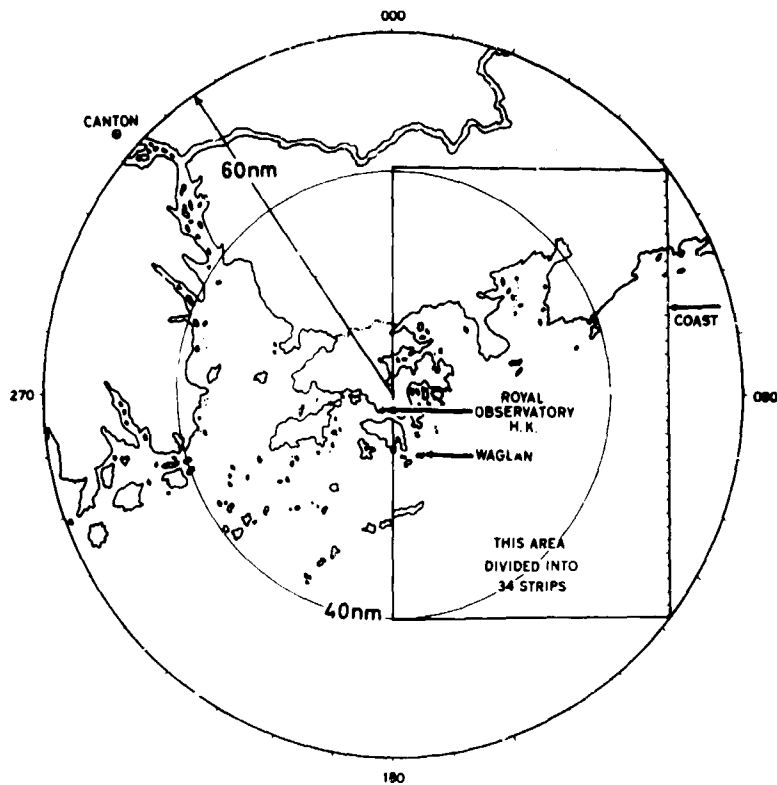


Figure 2.13

Figure 14. Area Surrounding Hong Kong Used in Radar Climatology.

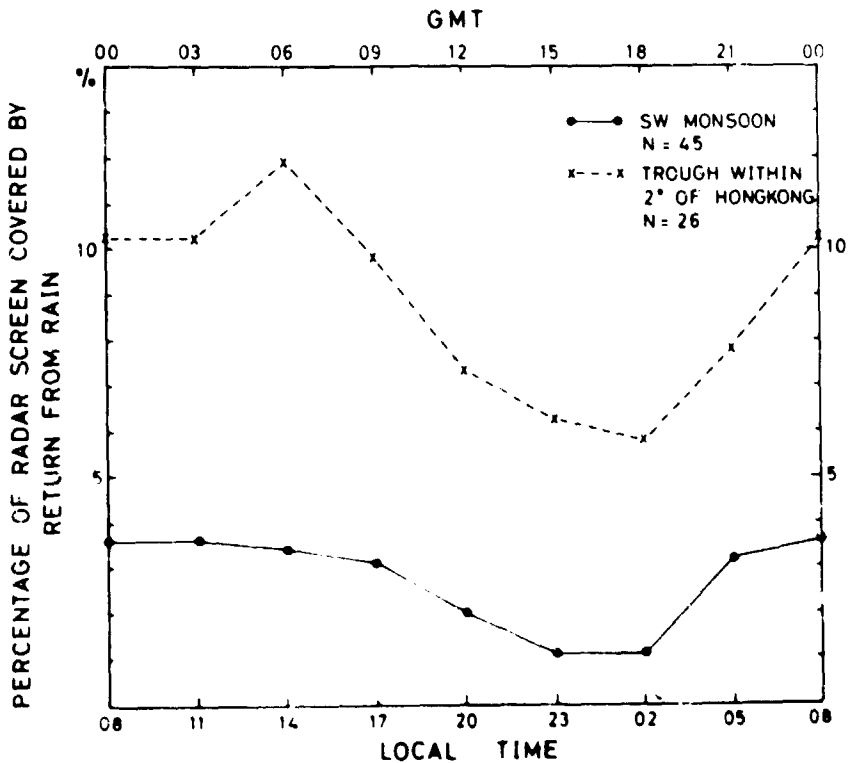


Figure 15. Diurnal Variation of Radar Echo Coverage Within Radius 60 n.m. of Hong Kong.

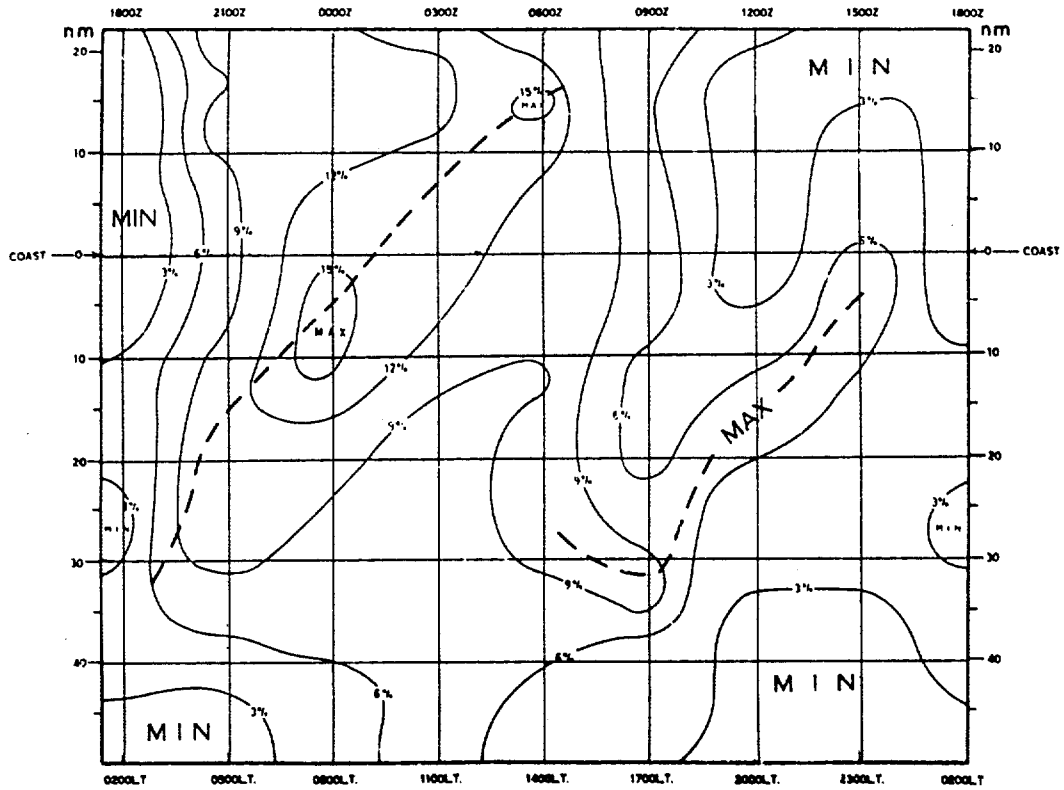


Figure 16. Variation of Rain Echoes in the S. W. Monsoon.

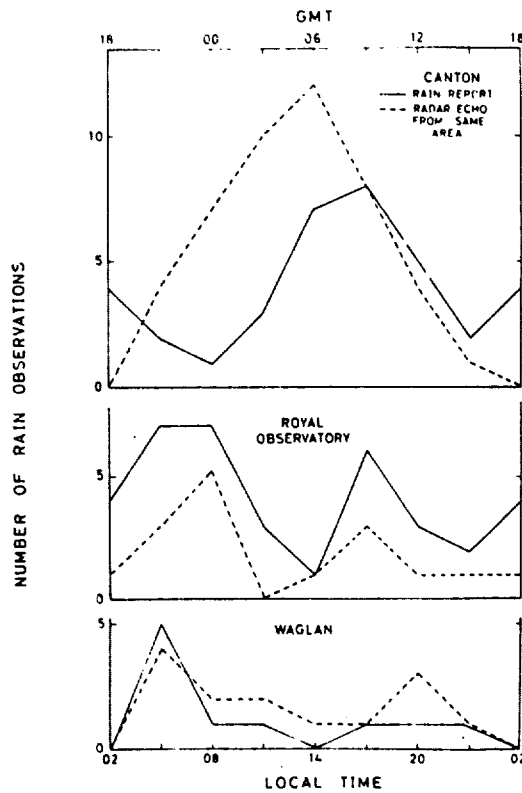


Figure 17. Observations of Rain and Radar Echoes Reported From Canton, Royal Observatory Hong Kong and Waglan Island.

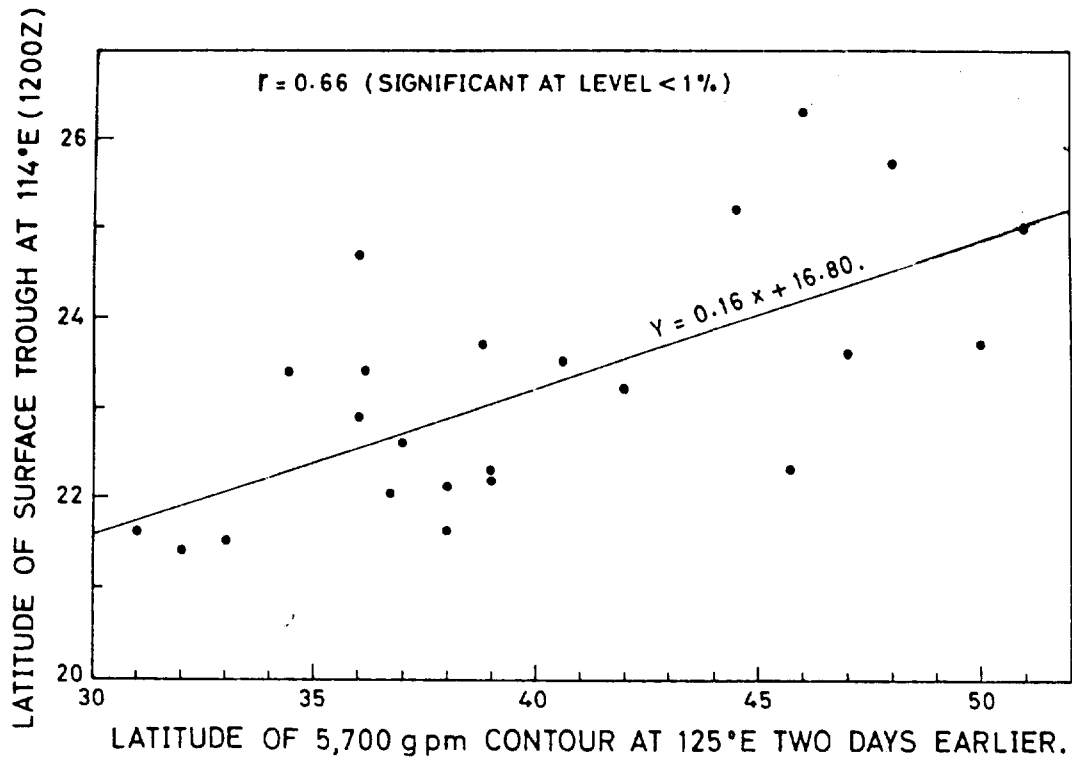


Figure 18. Latitude of Surface Trough at 114° E. Versus Latitude of 5,700 gpm. Contour at 125° E. Two Days Earlier.

ISOBARS 1 mb INTERVAL

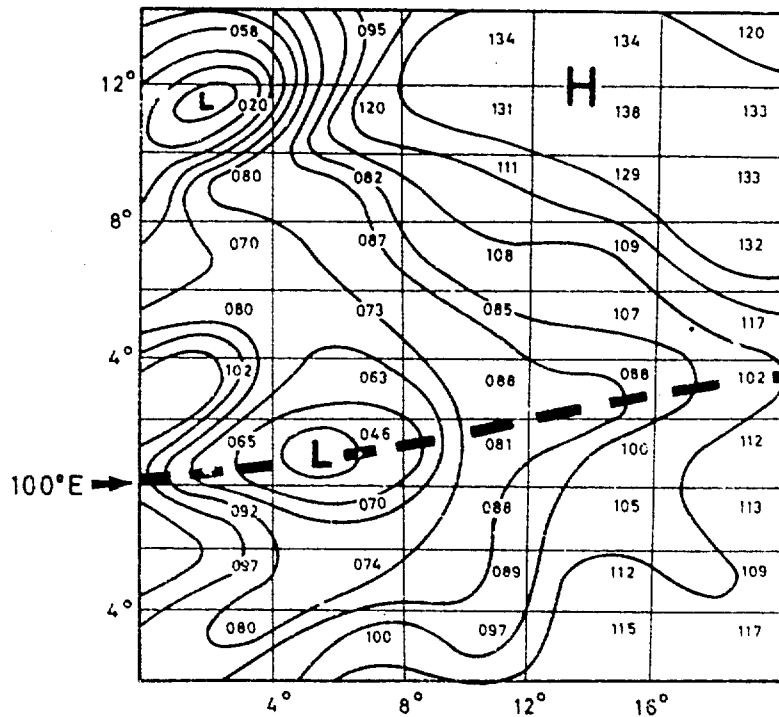


Figure 19. Mean Surface Pressure Pattern for the First 15 Days of May 1967 (note: 9th, 10th and 15th no surface trough)  
 Grid Size: 20° lat. x 20° long. Box Size: 2° lat. x 4° long.  
 Computed Mean value for monsoon Low = 1004.5 mb.  
 Computed Mean position of monsoon Low = 24.5° N.



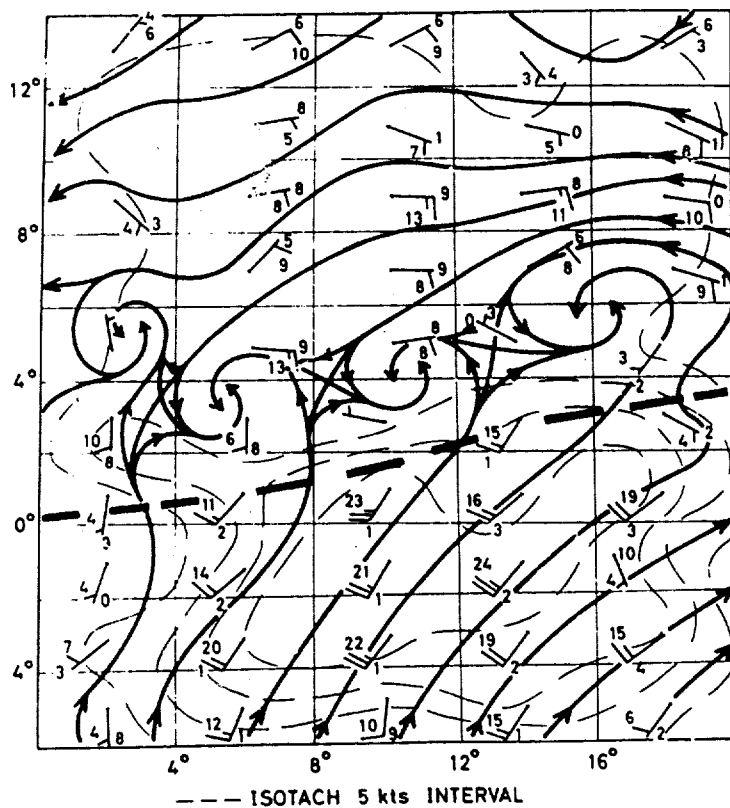


Figure 20. Mean 850-mb. Streamline Pattern for the First 15 Days of May 1967.  
---- Surface Trough

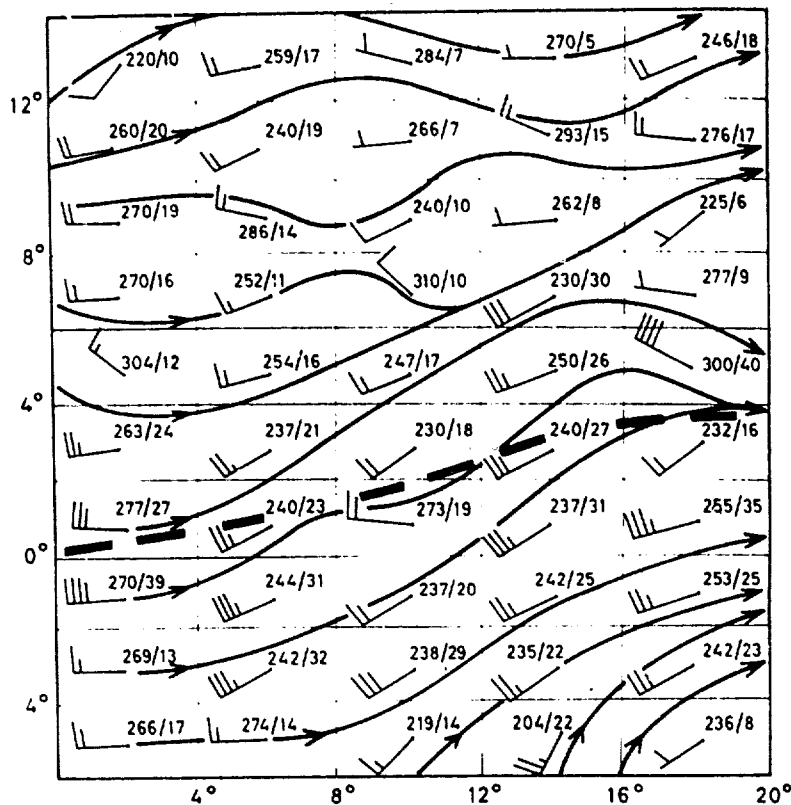


Figure 21. Mean 500-mb. Streamline Pattern for the First 15 Days of May 1967.  
---- Surface Trough.

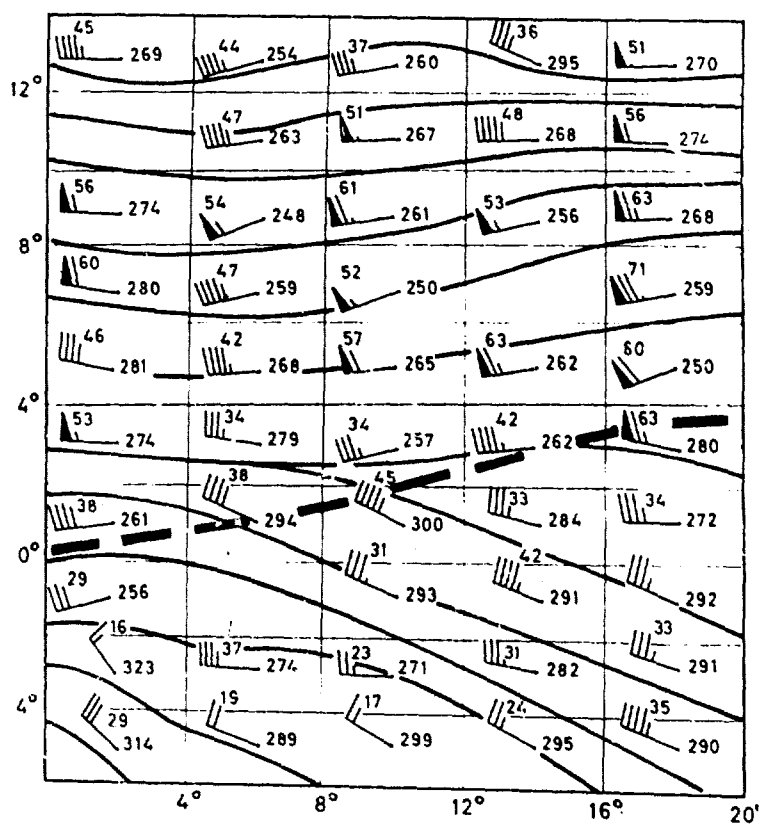


Figure 22. Mean 200-mb. Streamline Pattern for the First 15 Days of May 1967.  
 --- Surface Trough

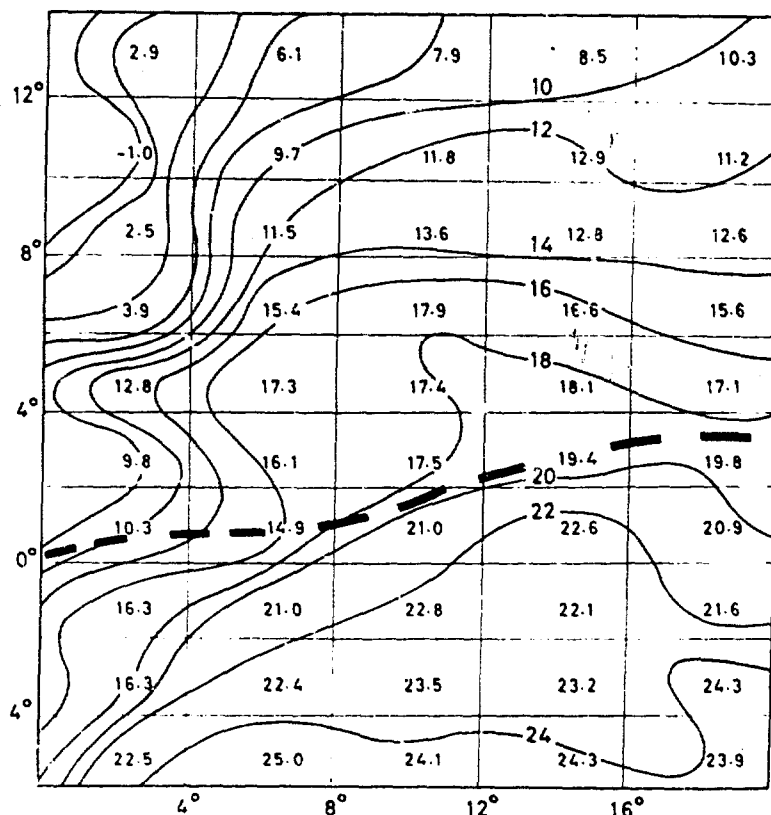


Figure 23. Mean Surface Dew Points for the First 15 Days of May 1967.  
 --- Surface Trough

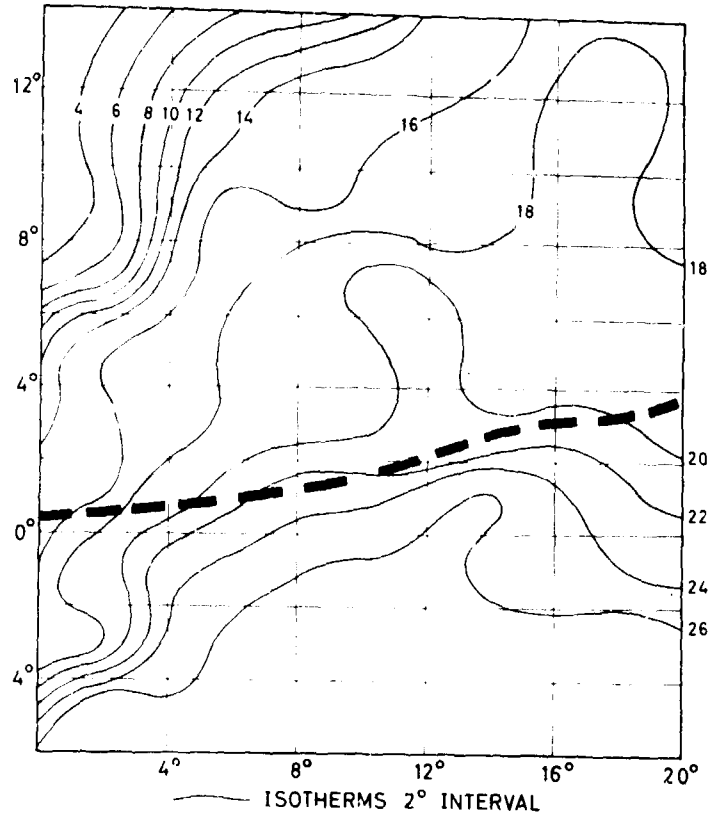


Figure 24. Mean Surface Temperatures for the First 15 Days of May 1967.  
— Isotherms 2° Interval  
--- Surface Trough

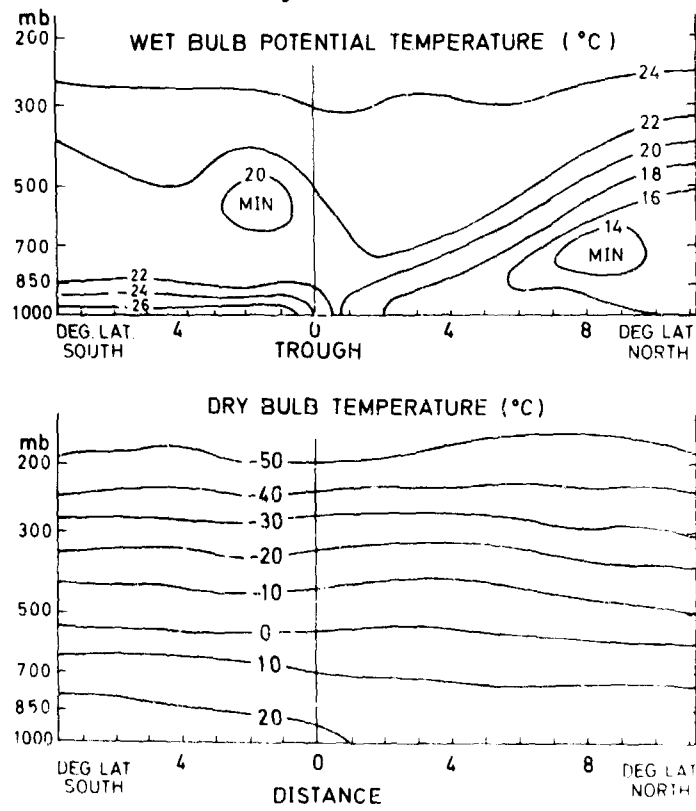


Figure 25. Cross Section of Trough at Lat. 24.5° N. 0000 GMT 1st June 1966.

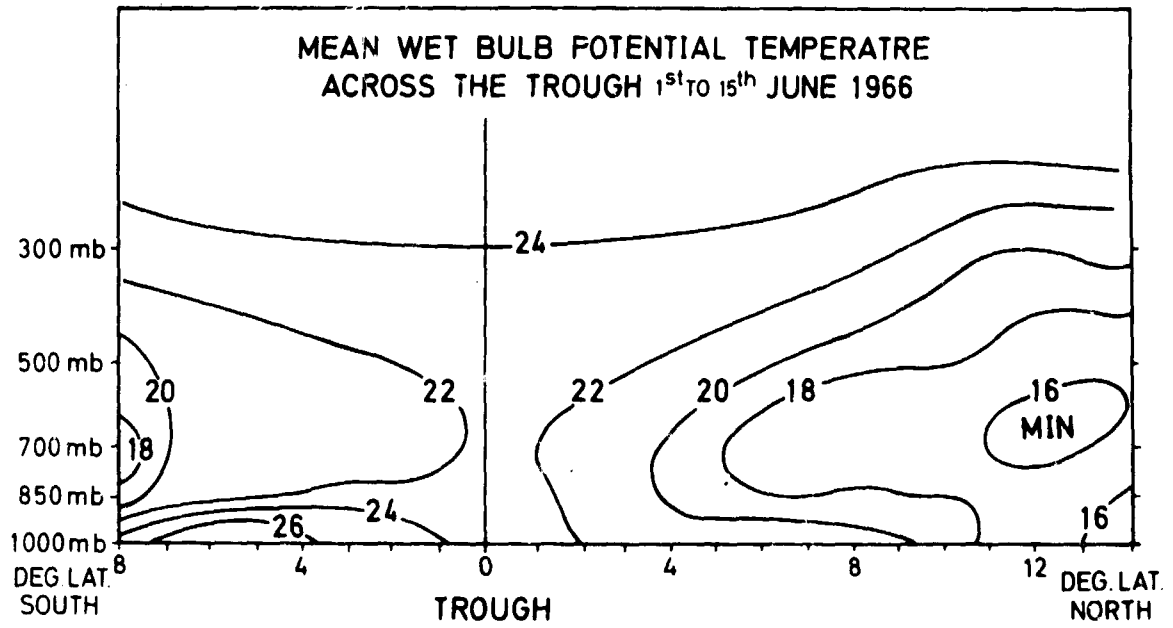


Figure 26. Mean Wet Bulb Potential Temperature Across the Trough 1st to 15th June 1966.

## CASES OF HEAVY PRECIPITATIONS AND THEIR FORECAST IN SOUTH VIETNAM\*

NGUYEN-HUU-HAU  
Directorate of Meteorology, Republic of Vietnam

### ABSTRACT

Statistical analysis of rainfall distribution in the III and IV Corps of the Republic of Vietnam represented by Saigon has shown that daily precipitations of 25 mm. or more occur only in 6 percent of all observed days.

The Darkow's "Total Energy Index" (EI) has been computed from Saigon radiosonde data during the 1968 summer monsoon and compared with synoptic considerations. A preliminary result is that an EI value more negative than -3.0, constitutes a good indication of heavy showers although the bulk of severe thunderstorms is derived from disturbances associated with higher EI.

The corresponding synoptic situations are classified into 5 types:

- A - Waves in the easterlies
- B - Low level convergence and westerly trough
- C - Trough associated with typhoon
- D - Upper easterly waves
- E - Tropical cyclones

In all types, the presence of some mid-level disturbance is striking.

Case studies 1968 are presented.

### 1. INTRODUCTION

To the weatherman in Vietnam, the war has brought the problem of heavy rain into a degree of acuteness never felt before. The tremendous increase in air operations and the influence of so many people from the countryside to the cities creating new difficulties in town planning are the two main factors sensitive to the intensity of precipitation.

On 17 September 1968, two thunderstorms lasting about four hours produced 112.9 mm. of rain in the Saigon area, creating an incredible traffic jam in the air as well as on the ground to the delight of newsmen. It took at least another four hours for the water to be completely drained off the streets. A record maximum of 179 mm. was received in 1942.

The purpose of this paper is to present some insight into the patterns and synoptic situations associated with those downpours in the southern part of the Republic of Vietnam.

### 2. DISTRIBUTION OF DAILY RAINFALL IN SOUTH VIETNAM

Due to the showery character of precipitation in this tropical part of the world, the best analysis of course would have to deal with the whole area of rain rather with data from one station alone. The assumption that Saigon could be representative of the III and IV Corps of the Republic of Vietnam in cases of heavy rain is based on the following:

- A. The III and IV Corps (and Saigon) are approximately within the same climatic boundaries.
- B. The very flat general topography excludes important variability in the local effects, especially regarding synoptic "rainstorm" producing disturbances. Their variations in frequency and intensity govern the rainfall variations [10].

Table 1 shows the repartition of daily amounts of rain in Saigon during the period from 1953 to 1968.

\*Research sponsored by Directorate of Meteorology, Republic of Vietnam

Table 1.

Rain in 24 hrs. (mm.)	Number of Observed Days
< 5	4474
5 - 14.9	688
15 - 24.9	306
25 - 34.9	151
35 - 44.9	80
45 - 54.9	53
55 - 64.9	30
65 - 74.9	24
75 - 84.9	13
85 - 94.9	6
95 - 104.9	6
105 - 114.9	7
115 - 124.9	1
125 - 134.9	1
135 - 144.9	1
145 - 154.9	1

Figure 1 is the corresponding frequency curve adjusted according to a modified form of the Poisson's distribution, in which 0, 1, 2 ... cm. respectively, represents intervals of daily amounts of <5, 5-14.9, 15-24.9 ... mm.

One can see that cases of 24-hour rainfall ( $R_{24}$ )  $\geq 25$  mm. represent only about 6 percent of all the observed cases or 13 percent of the rainy days. An average of 2 or 3 days with rain amount higher than or equal to 25 mm. is therefore, expected during the summer monsoon period from May through October. This will be our definition of heavy precipitation.

### 3. OBJECTIVE APPROACHES

Only eight soundings are available with a certain regularity for the whole of Southeast Asia (Song Khla, Bangkok, Udorn, Chiang Mai, Hongkong, Clark, Singapore, Saigon). Such a sparse density prevents successful analyses on horizontal charts and the only "objective" indices to look for, if there are any, are indeed through vertical time-cross sections.

#### 3.1 Vertical Distribution of Vorticity

One objective method for 24-hour forecasting of rainy areas has been proposed by Buajitti [3] using 24-hour wind change at 5000 ft. The method implies that for a triangular area with each side of about 200-300 km. there is a good possibility of rain when the change in the vertical component of vorticity at 5000 ft. (given by Bellamy's method) is larger than  $+5.0 \times 10^{-5} \text{ sec.}^{-1} \text{ day}^{-1}$ .

It seems that in consideration of the density of sounding stations and the assumption of linearity between stations, which could be in the proximity of vortices in the troughs, the simplest way to use the vertical change of vorticity as an aid in analysis (and forecasting) is still to interpret it qualitatively in terms of vertical wind profile at different locations. Thunderstorm areas are to be associated with upward vertical motion, i.e., as in case of divergence, the change of absolute vorticity must reverse sign; the lower air must gain and the upper air must lose positive vorticity [10].

A classification of different types of vertical wind profiles in Saigon has shown that precipitations of  $R_{24} \geq 25$  mm. are frequently preceded by the appearance of northwesterly winds at the top of the westerly monsoon between 700 and 500 mb. and north-northeasterly to northerly wind at the base of the upper easterlies [5]. Also, since the mean resultant winds over South Vietnam from 500 mb. upward, at this period of the year (June-October), are between  $070^\circ$  and  $160^\circ$ , the presence of a north-northeasterly wind at the mid-troposphere is a good sign of the approach of some disturbances from the east, most of them of wave type (fig. 2).

Exceptions to this rule are found when:

1. The low westerly layer is thin (below 700 mb.) indicating the proximity of the retreating thermal trough. Heavy rain could occur in association with upper easterly waves (fig. 3).

2. The transition zone is a thick layer of light variable winds denoting a large area of neutral flow. Fine weather is to be expected.

3. South Vietnam is under the influence of a tropical cyclone.

### 3.2 Total Energy Index

The notion of total energy  $E_T$  gives a combination of all parameters involved in any convective storm study. Per unit mass of air, it is:

$$E_T = c_p T + gZ + Lq + \frac{V^2}{2} . \quad (1)$$

where  $c_p$  is the specific heat of air at constant pressure,  $T$  the temperature,  $gZ$  the geopotential,  $L$  the latent heat,  $q$  the specific humidity and  $V$  the wind speed.

Considerations on the magnitude of the kinetic energy term and the normal allowable tolerances in upper air humidity measurement lead to the approximation:

$$E_T \approx c_p T + gZ + L_o w \quad (2)$$

$L_o$  and  $w$  being respectively the constant latent heat of condensation and the mixing ratio ( $c_p = 0.24 \text{ cal. gm.}^{-1} (\text{°A.})^{-1}$ ,  $L_o = 600 \text{ cal. gm.}^{-1}$ ,  $g = 980 \text{ cm. sec.}^{-2}$ ).

Darkow [4] uses the total energy profile to examine the ascent and descent of elements of air within an undisturbed environment and the degree of potential-convective instability of atmospheric layers according to the decrease of the total energy. As a practical application, he defines an Energy Index EI, as the algebraic difference between the total energy of air at the 500- and 850-mb. levels.

$$EI = E_{T500} - E_{T850} . \quad (3)$$

Since it seems to represent an improvement over other stability indices, taking into account both the ascending potentially warm air and the descending potentially cold air, the Darkow's Energy Index has been computed for the 1968 summer monsoon. Figure 4 presents some preliminary results in connection with heavy precipitation.

## 4. SYNOPTIC APPROACHES

It is well known that most of the rainfall in tropical areas results from disturbances and not from random convection.

Despite the complexity of the synoptic patterns associated with those disturbances, it is always convenient to group them around some basic situations. Seven synoptic models have been developed by Booz Allen Applied Research Inc. [2] to describe (and forecast) different types of "weather" over the Indochina Peninsula during the summer monsoon.

As far as heavy rain is concerned, daily synoptic analyses for over 10 years point out the predominance of the following five categories: (Samples are chosen from the 1968 summer which is considered as "wet" [164.4 mm. above the average from May through October]).

### A - Waves in the Easterlies

Waves in the easterlies represent major disturbances during the transition period in May. They show up quite well in vertical time section (fig. 5).

To the synoptic meteorologist, however, unlike the waves over the open ocean that can be seen over an area of nearly 1.000 sq. mi. and can be tracked over large distances day after day [7], most of the waves reaching South Vietnam in May are difficult to discover and trace on horizontal maps. (See figs. 6a and 6b and corresponding satellite pictures seen in figs. 7a and 7b.) The lack of data certainly plays a large part in this deficiency, but it is obvious that some deviation from Riehl's [10] or Frank's [7] model is to be expected in the South China Sea.

#### B - Low-Level Convergence and Upper Westerly Trough

As the season advances, with the northward migration of the thermal trough, the low-level wind veers gradually from easterly to southeasterly then to southerly forming a convergence area ahead of the trough. Convection becomes more and more developed, scattered thunderstorms start over South Vietnam in the afternoon. (See fig. 8a where Saigon received 50.7 mm. of rain in 45 minutes around 1300 local time.)

The pattern becomes typical of a heavy precipitation generating situation when a trough in the mid-troposphere, coming from Burma, overlays the lower convergence zone. (See fig. 8b where Saigon received 45 mm. of rain in 4 hours.) At 300 mb., a high cell generally covers the whole area in both cases. Later in the year, however, the westerly trough might occasionally extend up to 300 or 200 mb. It is only in this particular case that one can find the classical distribution of a mid-latitude trough with resulting severe convection on the eastern side. This seems to be the same as what happens in South India [1], but no correlation was found between this type of extensive trough and the onset of the monsoon.

#### C - Trough Associated with a Typhoon

A trough associated with a typhoon is considered a variation of Booz Allen's "pre-monsoon type", which is also typical for good weather over the Red River Delta in North Vietnam [11].

The trough extends southwestward from a typhoon in the northern part of the South China Sea and is generally best seen at the 500-mb. level (see fig. 9 together with satellite photo, fig. 10).

In the upper troposphere, easterlies strengthen over Southeast Asia with a relative maximum over Borneo and Malaysia. This seems to be a reverse process of what happens in winter when a correlation is found between the "wet" weather in the maritime continent of Indonesia with the vigorous subtropical jet stream through cross-latitudinal transport of energy [8].

#### D - Upper Easterly Waves

Upper-easterly waves are considered mid-level transverse waves in the easterlies overlying the lower monsoon. The disturbed wind field is frequently between 700 and 400 mb. so that charts at low levels are of little use in their analyses and forecasts. The 700-mb. level is either within the monsoon or near the transition layer.

Toward the end of the summer, with the regression of the thermal trough, the effect of this type of disturbance could be enhanced by the proximity of the lower intertropical convergence zone. This is, when it occurs on a shallow layer of convergent westerly wind. The most severe precipitation in South Vietnam is concomitant to this combination (see figs. 11 and 12).

#### E - Tropical Cyclones

Heavy rain resulting from the direct influence of tropical cyclones is rather rare in South Vietnam due to their small number. Most of the South China Sea cyclones have a track more toward the north in the direction of central North Vietnam and south China.

### 5. CONCLUSION

Because the 500-mb. level is considered the transition level in the tropical region in summer, difficulties exist in keeping time and space consistency at this level. Yet, as far as South Vietnam is concerned from the previous considerations, this level is of the utmost importance in locating disturbances which, in combination with low-level convergence, produces the heaviest rainfall in summer.

Vertical time sections constitute another big help, efficiently supplemented by the Darkow's Energy Index.



## DISCUSSION

SOMERVELL: A comment concerning upper-air data availability. You mentioned that you had but eight reporting stations for the entire Southeast Asia area. As most of us here know, there are approximately 3 times that many artillery GMD stations in the Republic of Vietnam--mostly Army but including a few USMC stations--which take observations daily but for which the reports are seldom operationally available to units such as the Fleet Weather Central at Guam or Detachment 14 of the 1st Weather Group. They are even difficult to obtain for research purposes such as ours or yours. It would seem that so long as we are aware of this problem, that some responsible organization would get out into the field and find a solution to the data-collection problem.

HAU: Amen!

KREITZBERG: Would Maj. Brett comment on the availability of the Army artillery data on a real time basis for operational use.

BRETT: In 1966, Army Met. soundings were turned over to the nearest AWS weather station for transmission to the weather editing unit in Saigon. Stations like Chu Chi, Tay Ninh and Bien Hoa do support Army Artillery Gun Battalions in the III Corps. Communications breakdown is frequent in the handling of such data. Hq. 1st Weather Group (Saigon) would know the current handling of Army Met. data.

SOMERVELL: Much more upper-air data are available in Southeast Asia than the eight stations mentioned in Mr. HAU's talk.

WITHROW: Many of the extra stations (Army upper-air soundings) are in the Saigon area. All Army upper-air data are subject to considerable delay and breakdown in communications. Continuing difficulty exists in Southeast Asia Weather Centrals in obtaining these upper-air data.

RAMAGE: Your statement that the 500-mb. chart is the best for detecting rain-producing disturbances agrees with experience over western India. Referring to your 28 July 1968 situation, I have observed that typhoons going inland are not infrequently followed by development of mid-tropospheric cyclones to the south. This might be worth keeping in mind by forecasters.

HAU: The development of the mid-tropospheric cyclone south of the surface position of the typhoon is not always observed but this is a deepening of the associated trough which is frequently observed when the cyclone reaches the northern part of the South China Sea.

SADLER: The changes are more apparent at 500 mb. because at this level (near the transition level) small changes in circulation features show as wind changes, and the intrusion of the ridge ahead of the typhoon is more apparent at this level. The easterlies associated with the 500-mb. intruding ridge in combination with the deep westerlies to the south produce a more apparent and sharper trough line with cyclonic cells embedded.

MILLS: Does the trough (500 mb.) deepen over South Vietnam (causing heavy rain) when the typhoon crosses the Philippines about 15° N. instead of through the Bashi Channel? Does the mountain chain of Luzon cause a disruption to allow the deepening to occur? If so, the upper-air soundings from Clark AFB Luzon could be a valuable tool.

HAU: The 500-mb. trough associated with typhoons is generally north-south oriented so that, if the typhoon comes from the Pacific either across the Philippines or through the Bashi Channel, it will be somewhat influenced by the land effects. I don't think we can find any rule about the deepening of that trough over South Vietnam. It seems that it is more related to the strength of the typhoon.

## REFERENCES

1. ANJANEYULU, T. S. S. and D. R. SIKKA, "Equatorward Extension of Troughs in the Upper Westerlies and the Relation of Upper Tropospheric Flow to Onset of Monsoon Rains Over India." In "Preliminary Results and Future Plans of the International Indian Ocean Expedition Meteorology Programme." pp. 68-81. Bombay (copies available from Dept. of Geosciences, University of Hawaii). 1963.

REFERENCES (CONTINUED)

2. BOOZ, ALLEN APPLIED RESEARCH, INC., "Progress Report on the Development of a BCW Forecast System." Washington, D. C. 1963.
3. BUAJITTI, K., "The Use of Vertical Vorticity of 24-Hour Wind Changes for Weather Forecasting." In "Proceedings of the Symposium on Tropical Meteorology." p. 393-402. New Zealand Meteorological Service, Wellington. 1964.
4. BARKOW, G. L., "The Total Energy Environment of Severe Storms." J. Appl. Meteorol. 7, 199-205. 1968.
5. DINH, D. P., "Note Sur Les Precipitations au Vietnam." Notes Tech. Meteorol. 2, 27-30. 1965.
6. \_\_\_\_\_, "Profile Verticaux de Vents et Precipitations Intenses a Tanson-Nhut." Notes Tech. Meteorol. 4, 1-4. 1966.
7. FRANK, N. L., "The "Inverted v" Cloud Pattern--An Easterly Wave?" Mon. Wea. Rev. 97, 130-140. 1969.
8. RAMAGE, C. S., "Role of a Tropical "Maritime Continent" in the Atmospheric Circulation." Mon. Wea. Rev. 96, 365-370. 1968.
9. RAMAN, C. R. V. and C. M. DIXIT, "Analyses of Monthly Mean Resultant Winds for Standard Pressure Levels Over the Indian Ocean and Adjoining Continental Areas." India Meteorological Department, New Delhi. 1964.
10. RIEHL, H., "Tropical Meteorology (pp. 93-97; 198-209). McGraw-Hill, New York. 1954.
11. SADLER, J. C., BREET, W. R., HARRIS, B. E., F. P. HO, "Forecasting Minimum Cloudiness Over the Red River Delta During the Summer Monsoon." Hawaii Inst. Geophys. HIG 68-16, 104 pp. 1968.

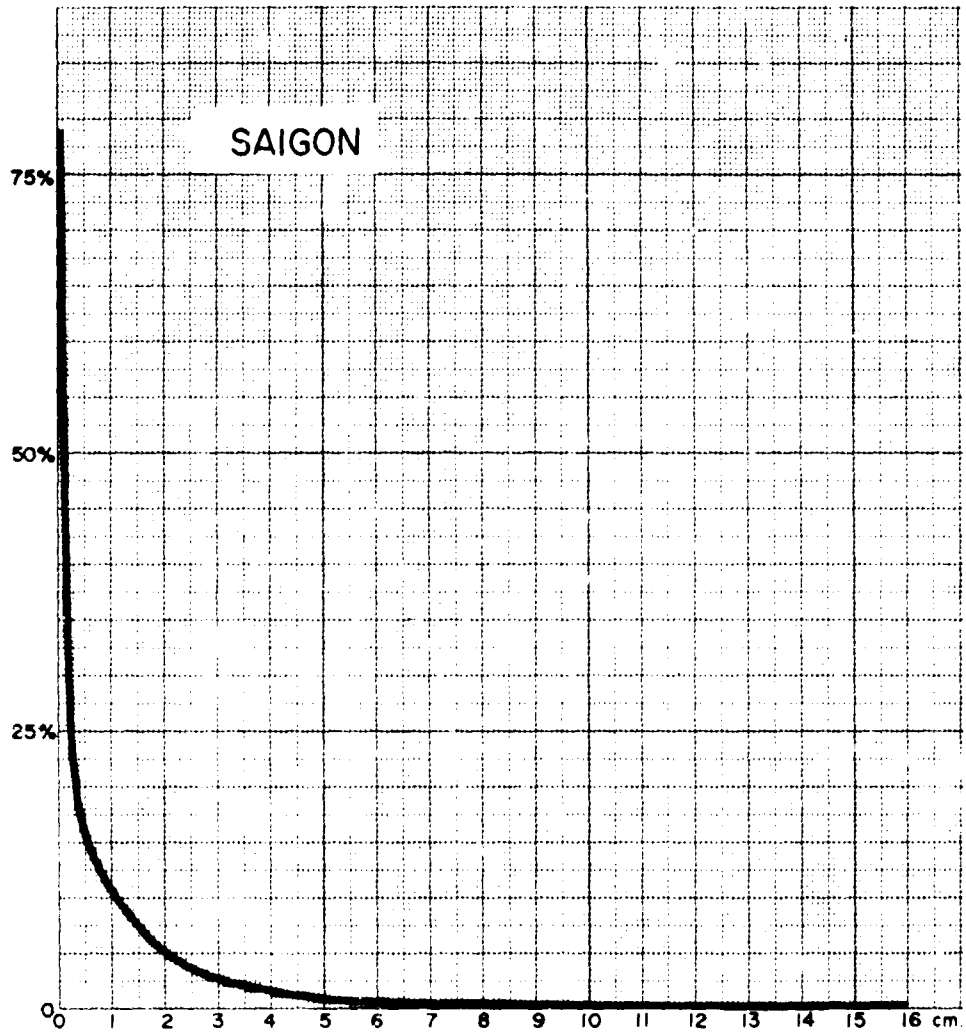


Figure 1. Frequency of Daily Precipitation.

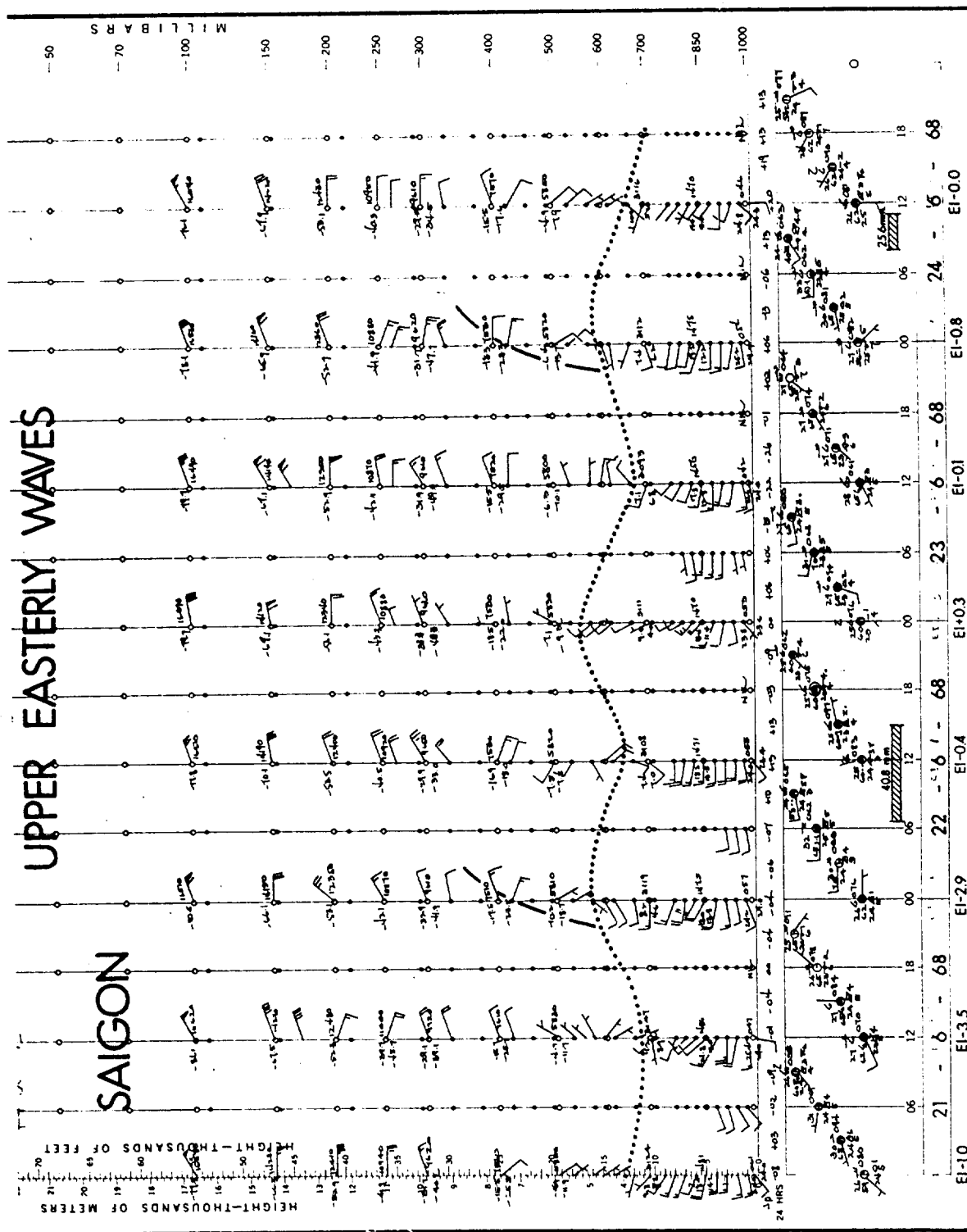


Figure 2. Upper Easterly Waves.

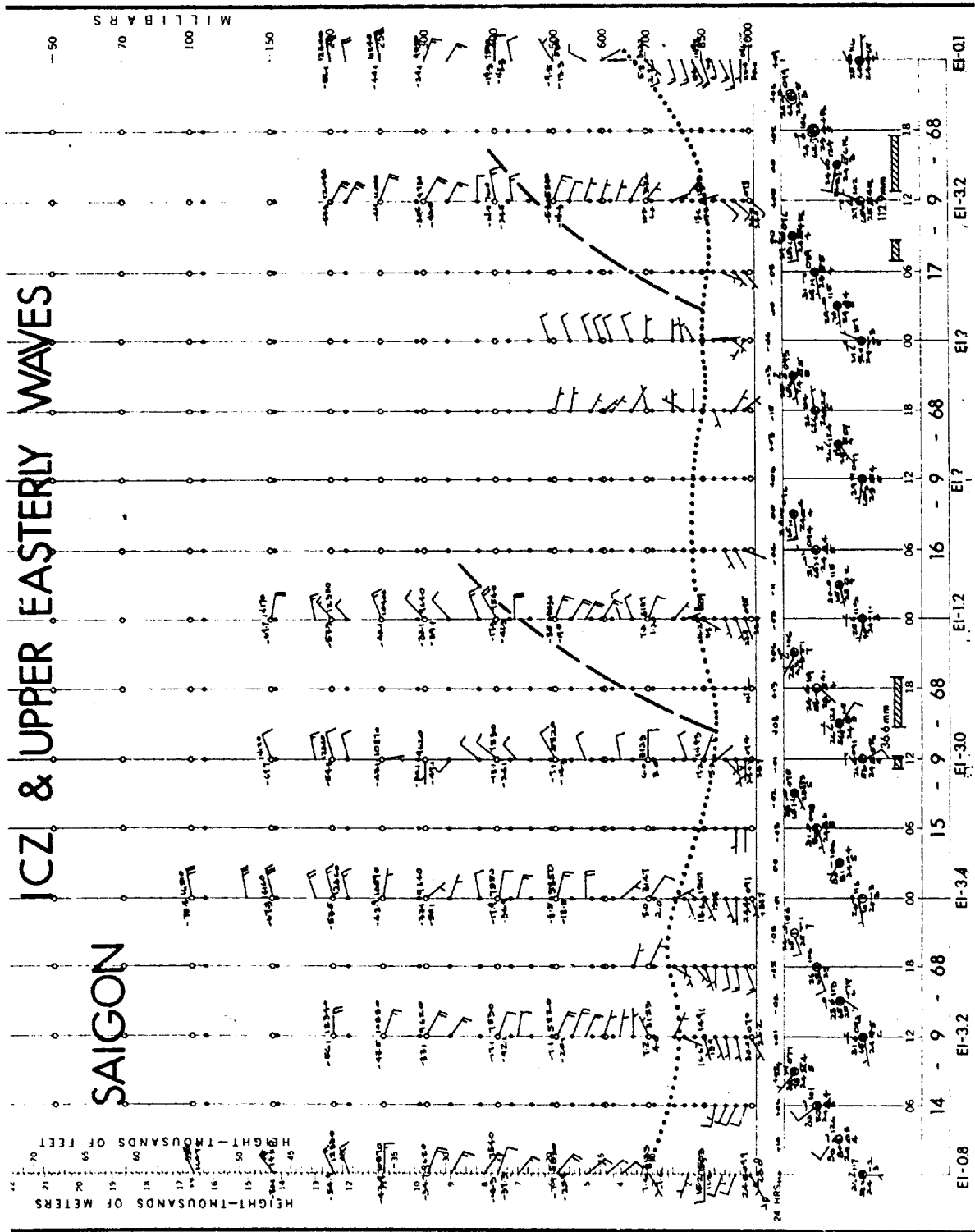


Figure 3. ICZ and Upper Easterly Waves.

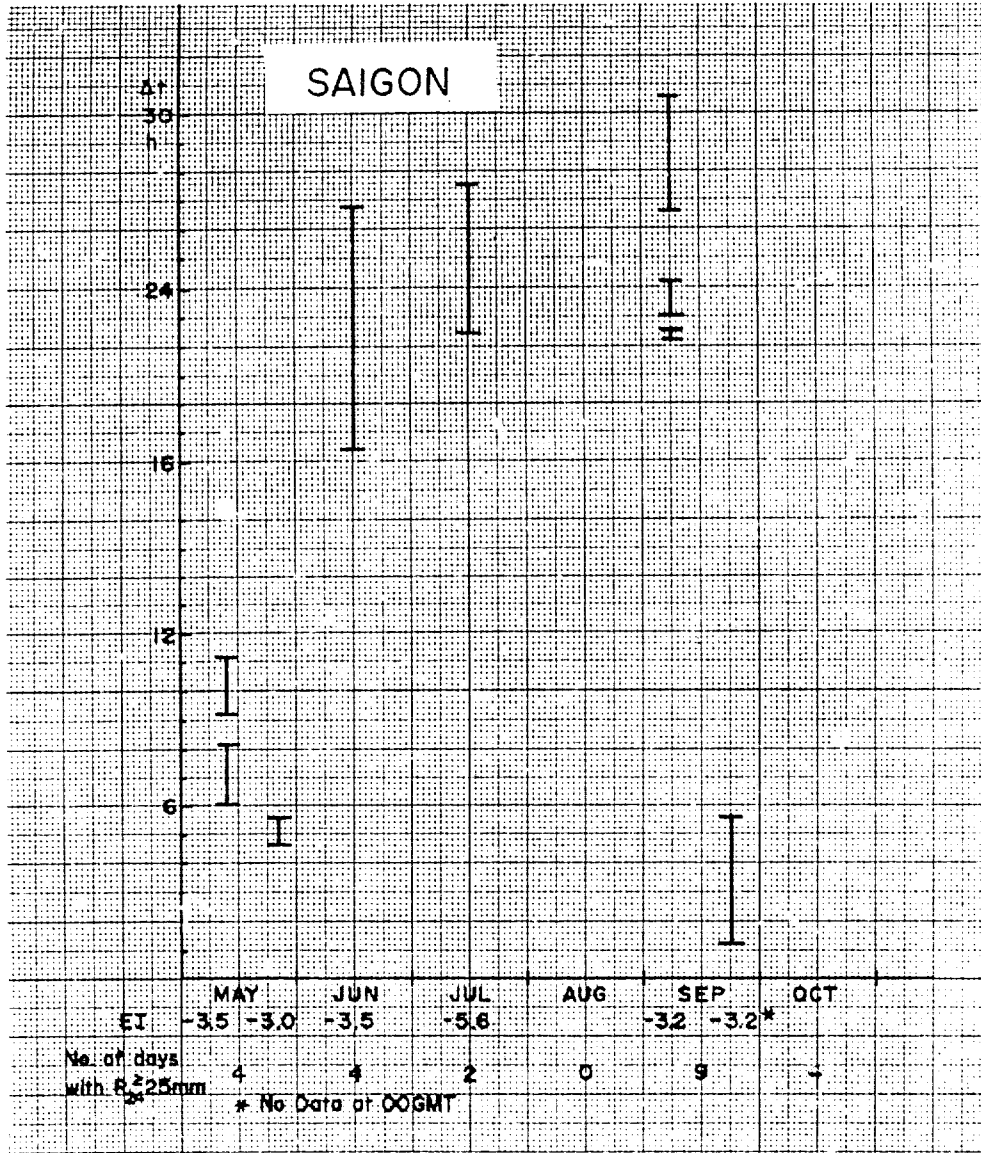


Figure 4. Total Energy Index  $EI < -3.0$  and Precipitation  $R_{24} \geq 25$  mm. in 1968.

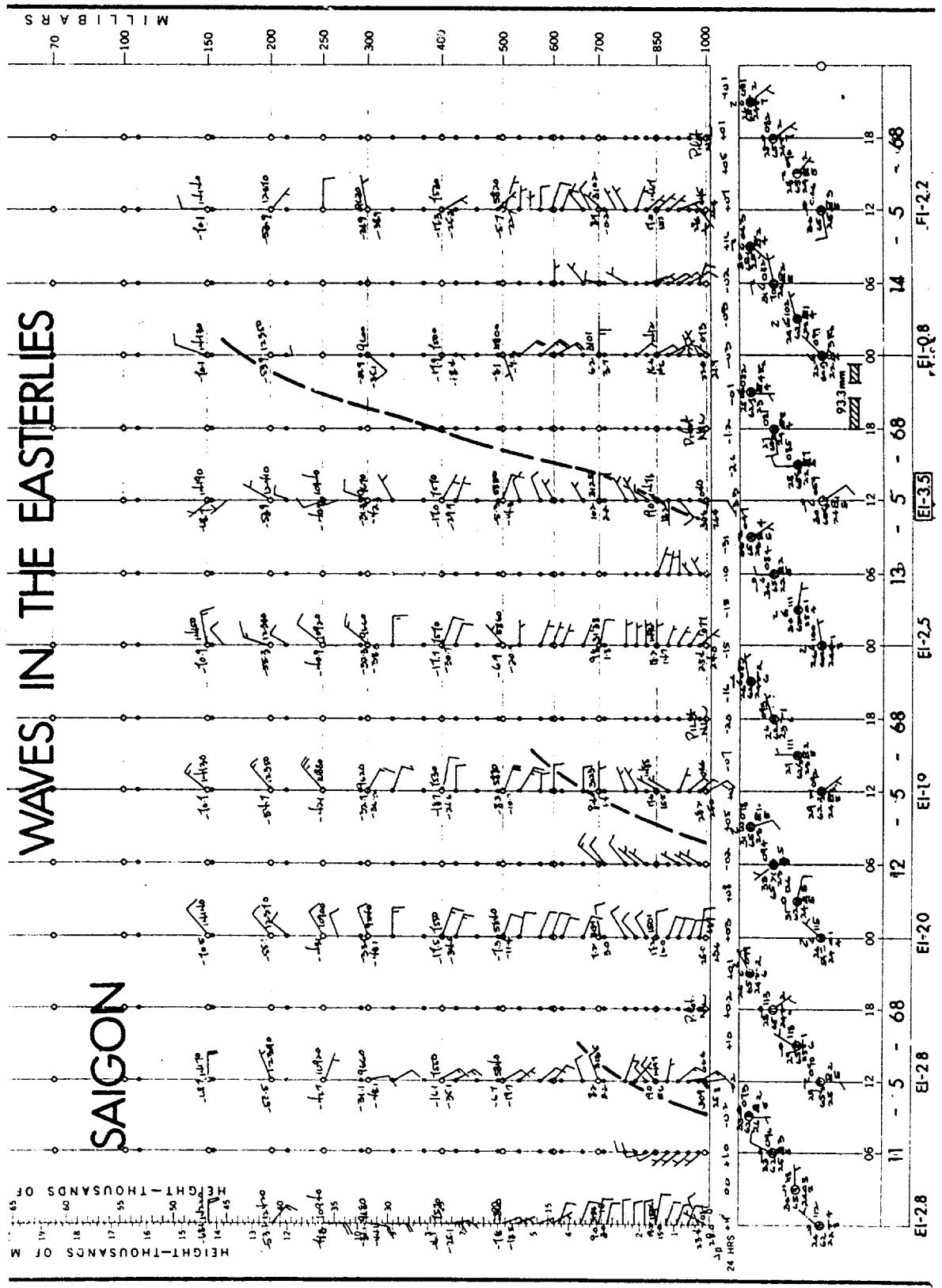


Figure 5. Waves in the Easterlies.

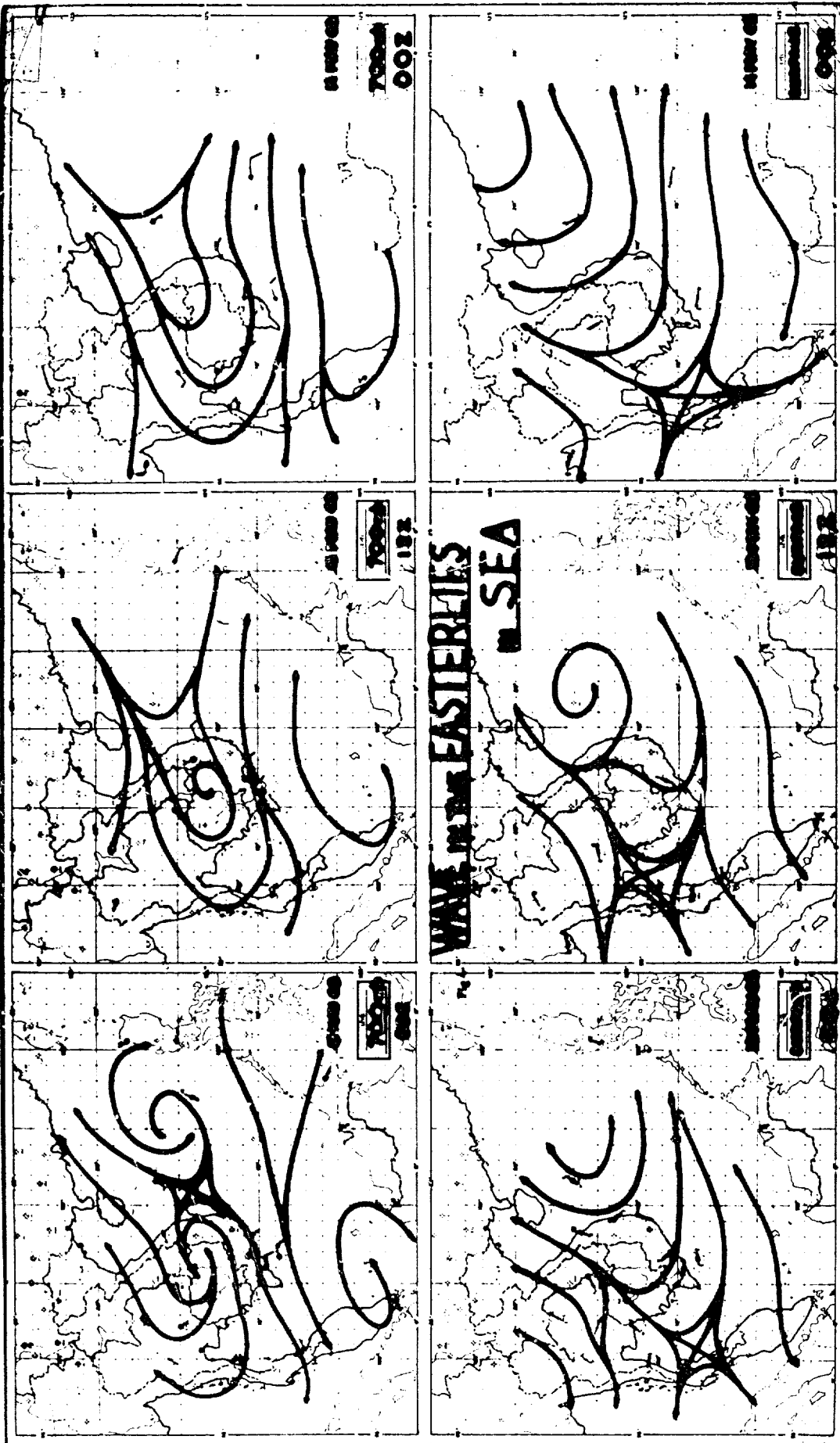


Figure 6(a). Wave in the Easterlies in Sea.



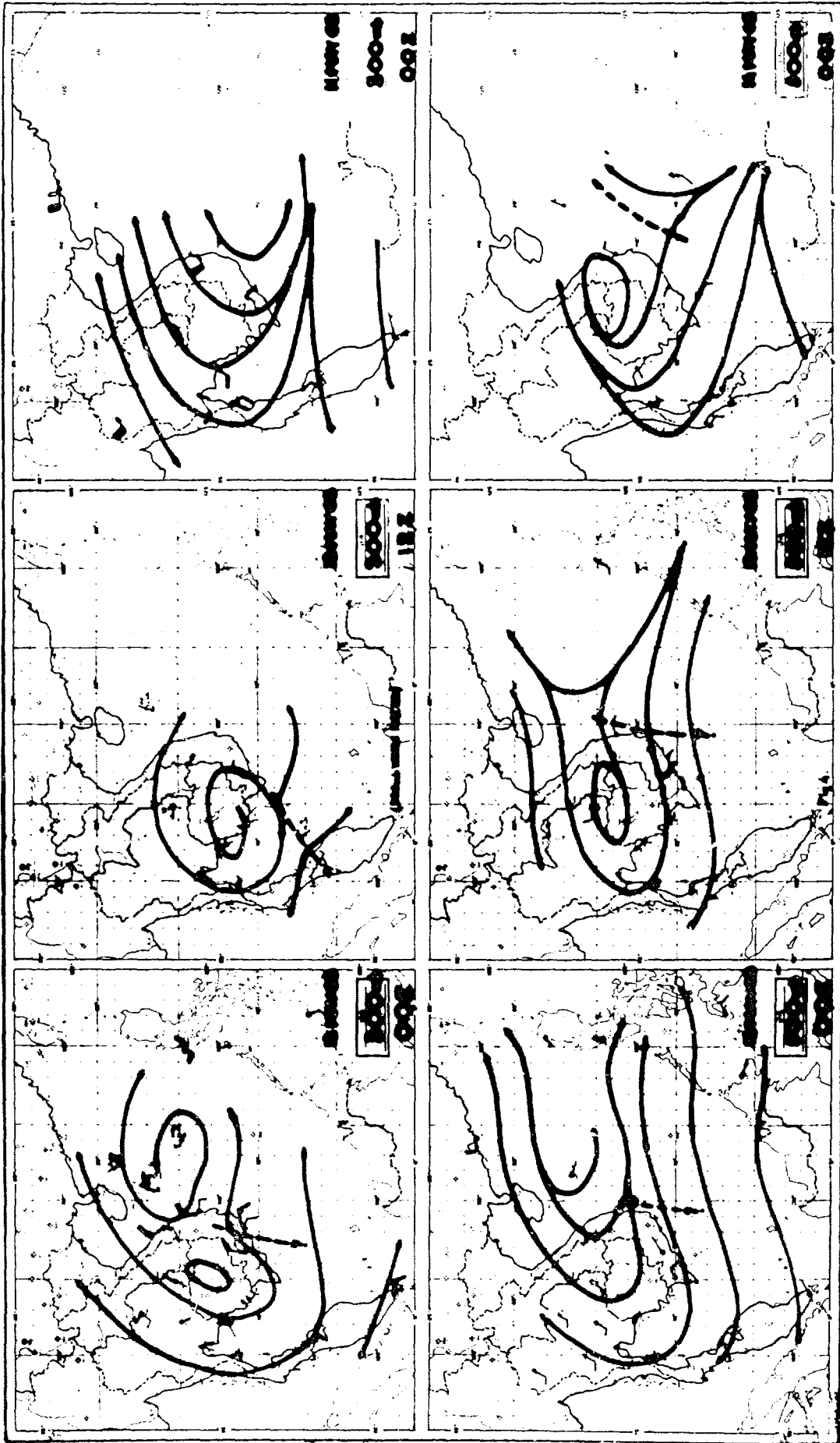


Figure 6 (b). 200-mb. Wind Plotted.



Figure 7(b). ESSA VI View of Possible Wave in the Easterlies, 1115 H, 13 May 1968.



Figure 7(a). ESSA VI View of Possible Wave in the Easterlies, 1013 H, 12 May 1968.

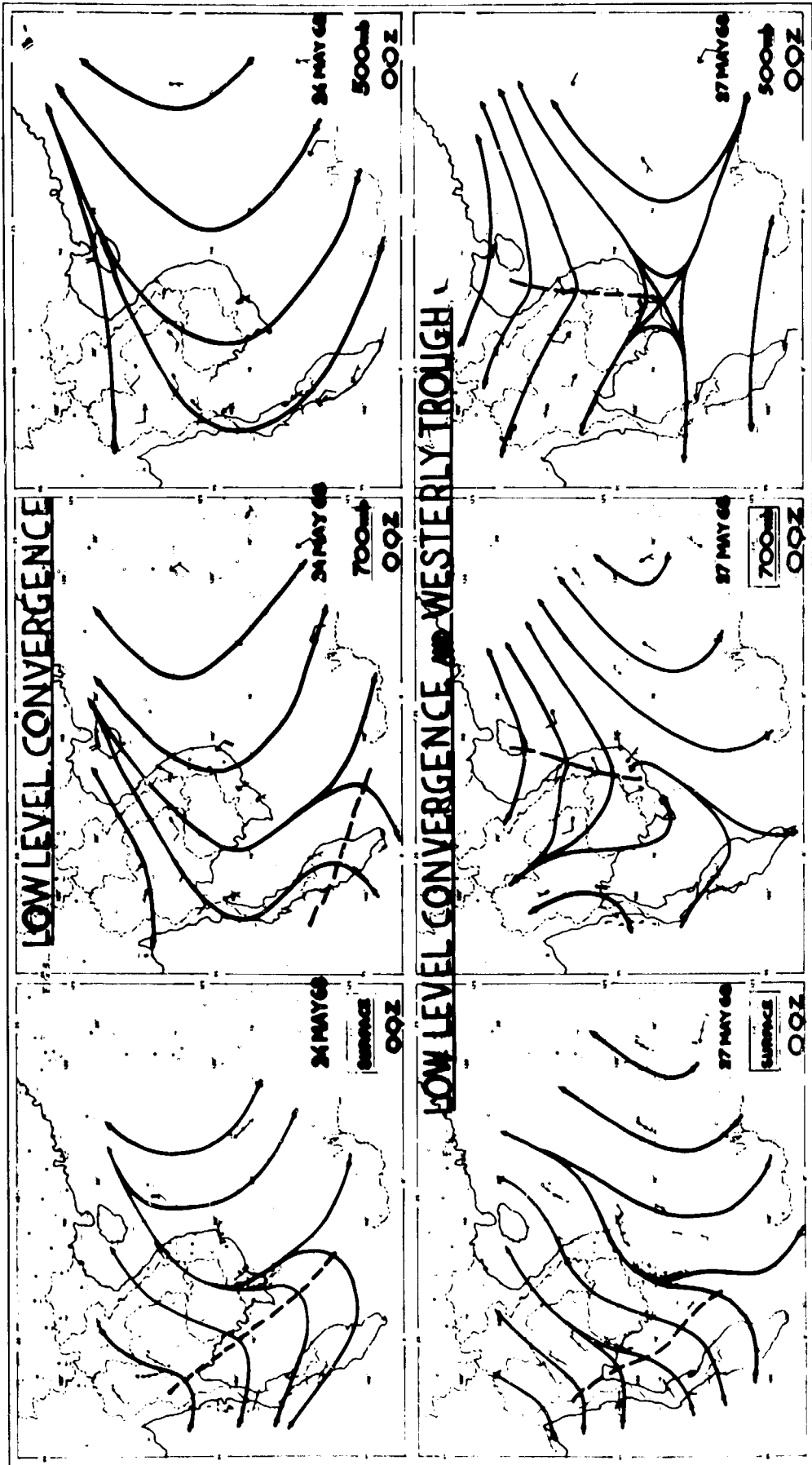


Figure 8(a). Low Level Convergence, 0000 GMT, 24 May 1968.  
(b). Low Level Convergence and Upper Westerly Trough, 0000 GMT  
27 May 1968.

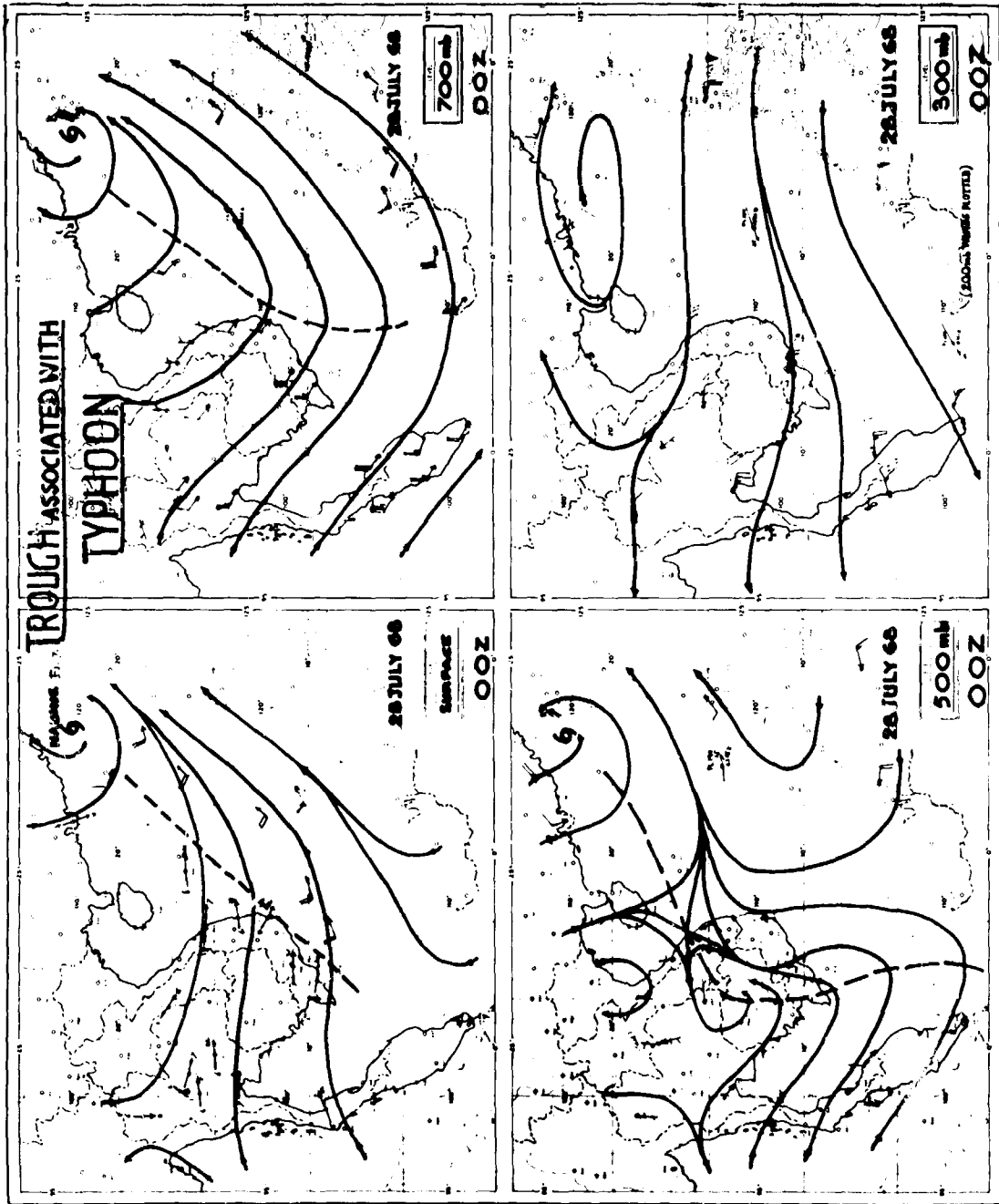


Figure 9. Trough Associated With Typhoon.



Figure 10. ESSA VI View of Trough Associated With Typhoon NADINE at 1100 H, 27 July 1968.

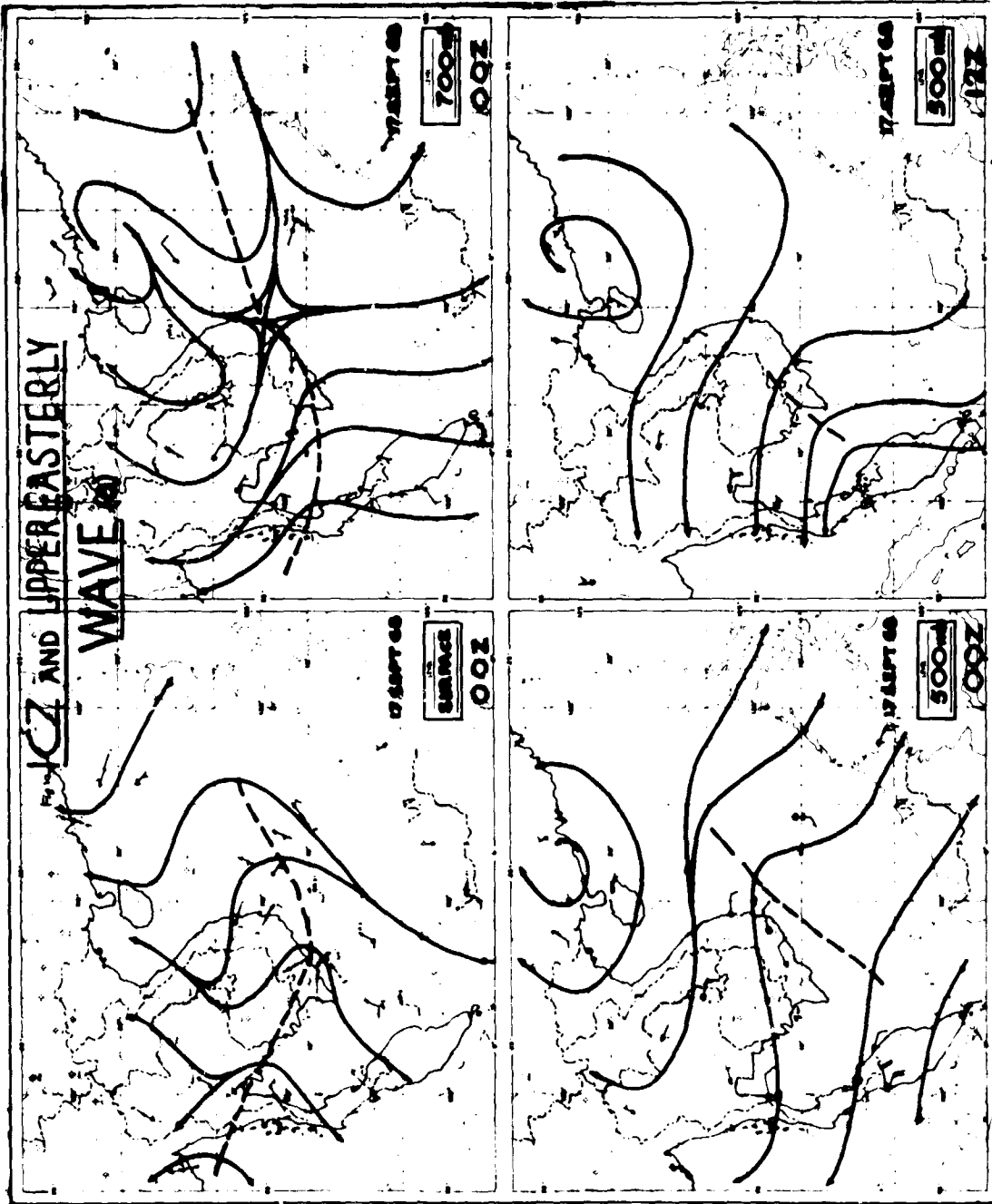


Figure 11(a). ICZ and Upper Easterly Wave, 0000 GMT 17 September 1968.

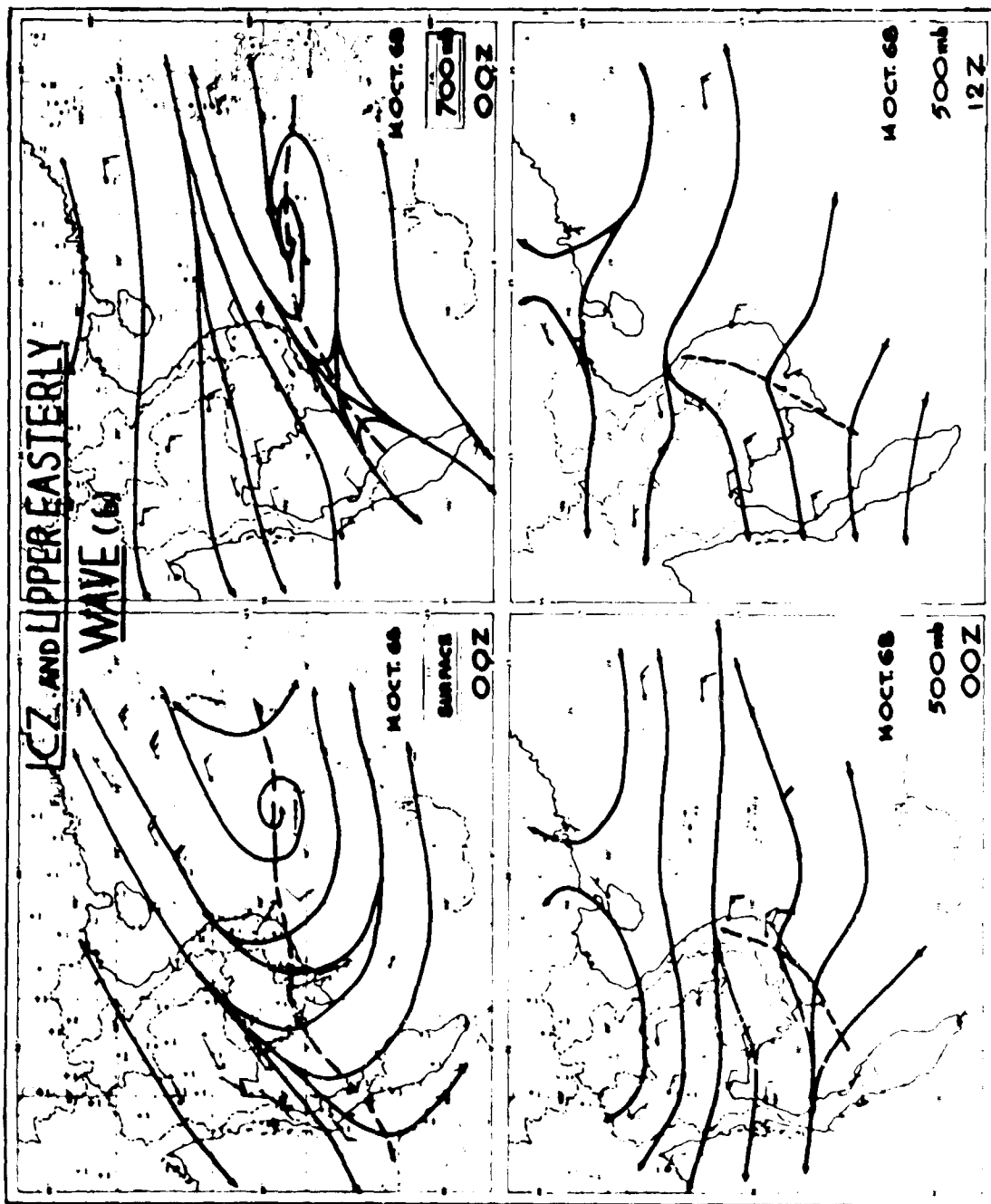


Figure 11(b). ICZ and Upper Easterly Wave, 0000 GMT 14 October 1968.

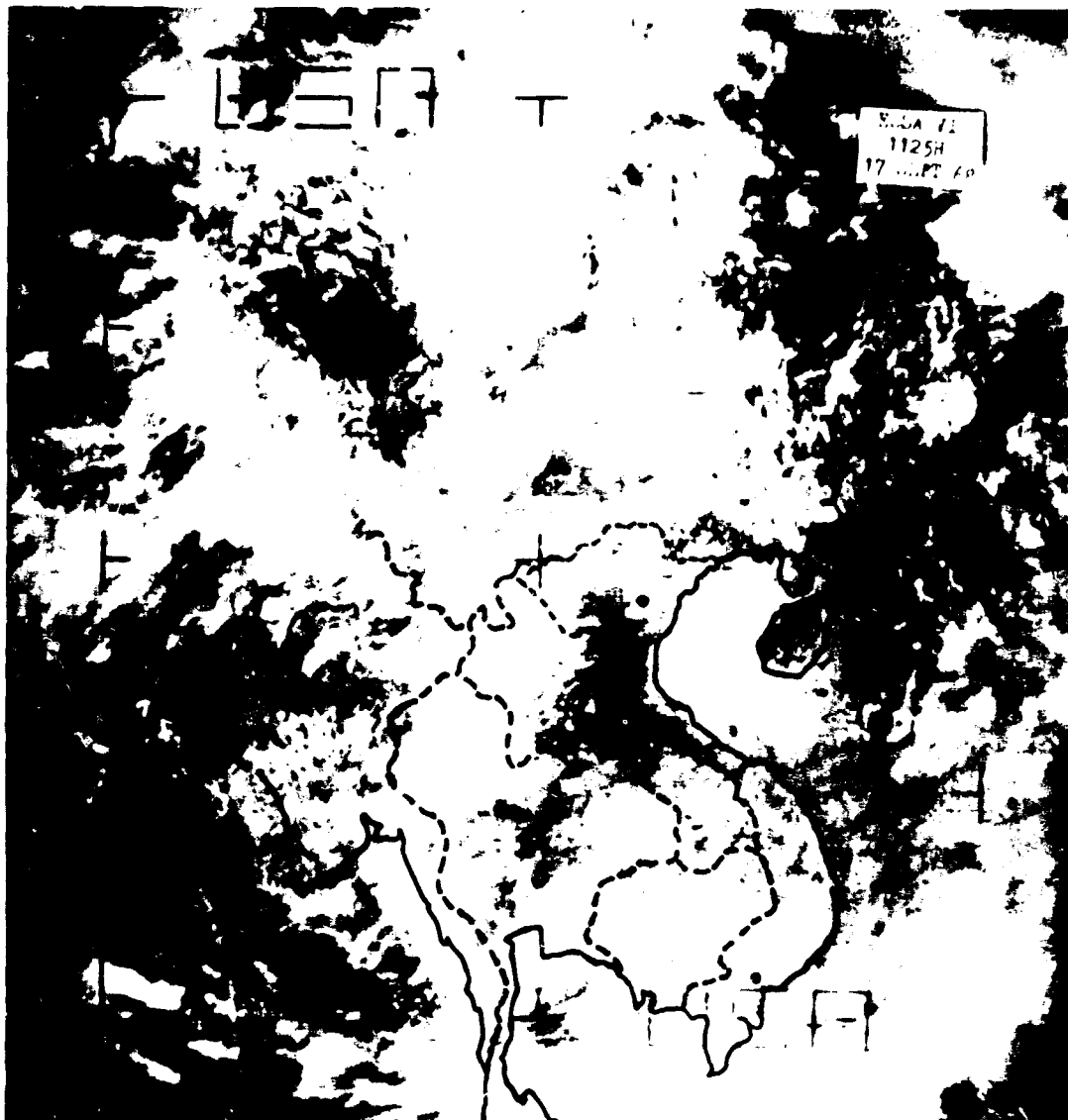


Figure 12. ESSA VI View of ICE and Upper Easterly Wave at 1125 H, 17 September 1968.



## MID-TROPOSPHERIC CYCLONES OF THE SOUTHWEST MONSOON\*

T. N. Krishnamurti  
Florida State University

and

R. S. Hawkins  
Air Force Cambridge Research Laboratories

### ABSTRACT

Mid-tropospheric cyclones are an important part of the tropical general circulation of the summer season. These are synoptic-scale disturbances that appear in the daily and monthly mean circulation maps with greatest intensity at levels near 500 mb. The structure and energetics of this type over south-east Asia are discussed in this paper. Interesting features include a warm anomaly above the cyclone and a cold anomaly below.

A five-level non-geostrophic balanced model is used in this study to obtain the distribution of vertical motion. The model includes a parameterization of cumulus-scale convection. In the middle levels rising motions are found west of the cyclone and sinking motions to the east. This is primarily due to the thermal structure of the atmosphere and associated advection of colder air from the oceanic regions and warmer air from land regions. A marked diurnal change in the vertical velocity,  $|\omega|$ , is noted in the computations; large  $|\omega|$  at 0700 local time compared to 1900. This diurnal change is primarily due to changes in the wind direction and speed. The important result of this study is that both the cumulus and synoptic-scale motions exhibit dual roles in the maintenance of this mid-level system.

- (1) Both scales contribute to a net warming of the air above the cyclone, diabatic warming by cumulus-scale motions and adiabatic warming by the descent of synoptic-scale motions.
- (2) The two scales oppose each other in the transformation of eddy available potential energy into eddy kinetic energy. Cumulus-scale con-tributes to a net generation, while the synoptic-scale motions trans-form kinetic energy into potential energy. This latter result is consistent with item (1) because the areas of descent are somewhat closer to the warm temperature anomaly than to the areas of ascent.

### 1. MID-LEVEL CYCLONES AS A FEATURE OF MONTHLY MEAN CIRCULATION

During the summer southwest monsoon season several quasi-stationary mid-tropospheric cyclones (wavelength  $\approx 1000$  km.) are observed over southeast Asia. These cyclones are frequently found north of the Bay of Bengal, over the north-eastern part of the Arabian Sea and over southern Indochina. References to these are found in the works of Miller and Keshavamurthy [14] and Sadler [18].

Figure 1 is a normal map from the "Climatological Atlas for Airmen" prepared by C. W. B. Normand [16]. It is a mean map based on more than 10 years of data for July at the 4-km. level. The mean streamlines rather clearly demonstrate the existence of mid-level cyclonic circulation over the northwestern part of the Bay of Bengal. A cyclonic trough is found over the northeastern part of the Arabian Sea.

On the larger scale, there is no clear evidence of an organized cyclonic circulation in the middle levels over southern Indochina. July means maps prepared by Miller and Keshavamurthy [14], based on the International Indian Ocean Expedition data, show the presence of these mid-level cyclones. There is also some evidence of a mid-level cyclone over southern Indochina in the recent mean maps prepared for July by Sadler [18]. It is, however, not as clearly defined as those found over the Arabian Sea and the Bay of Bengal. Figure 2 depicts a monthly mean map for July at the 500-mb. level based on the above mentioned references. The heavy dashed line connects the three major mid-level cyclones of the southwest monsoon. Solid lines represent streamlines, and thin dashed lines represent isotachs of the monthly mean wind-speed field.

\* Research sponsored by Air Force Cambridge Research Laboratory

JULY -  $\frac{4.0 \text{ km.}}{13,000 \text{ Ft.}}$

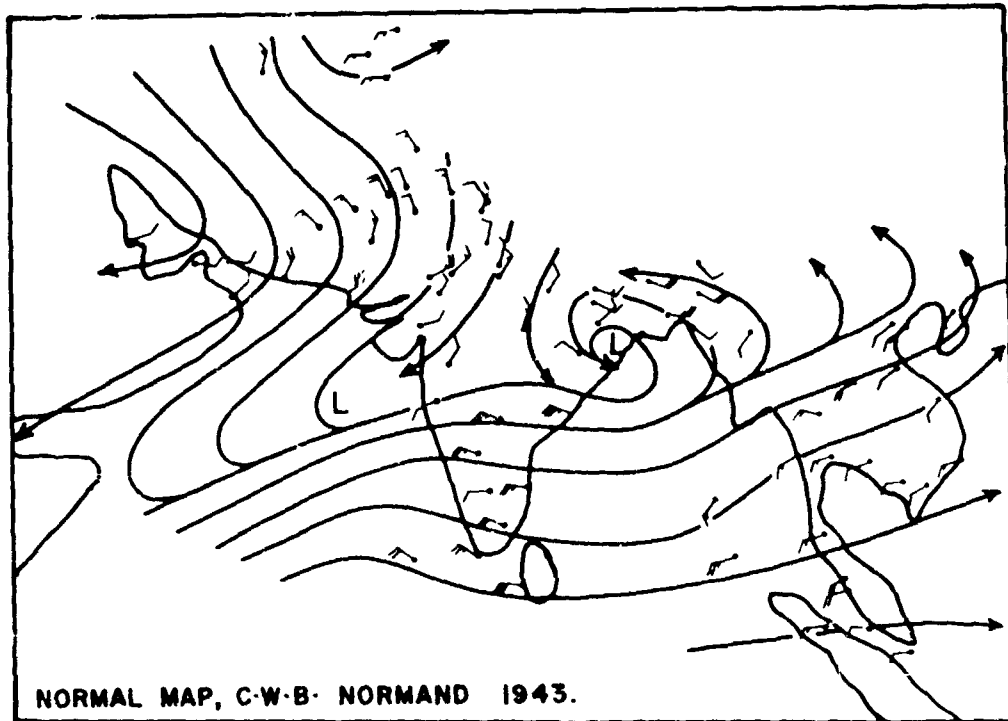


Figure 1. Normal Map for July at 4 km. (from Normand [16]).

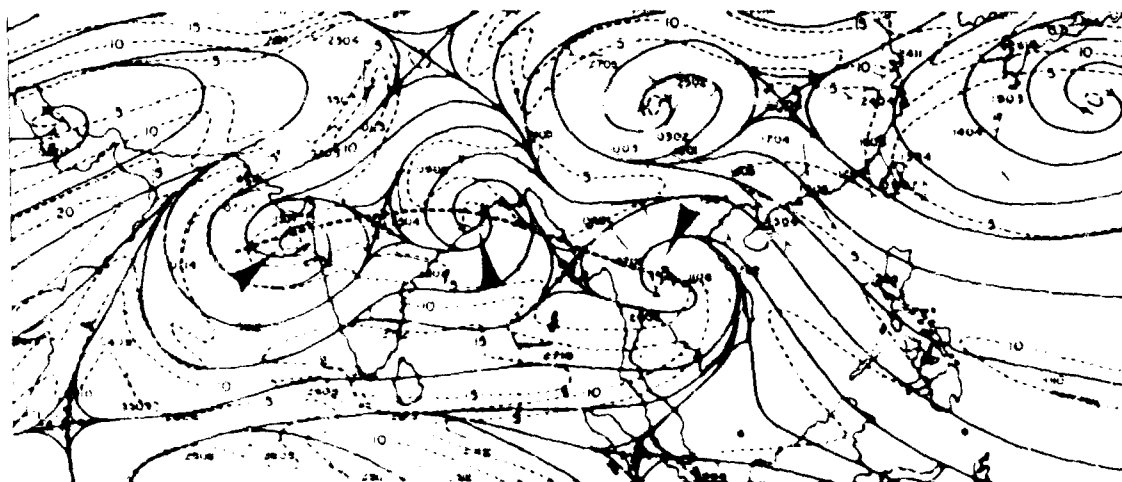


Figure 2. July Mean Map, Based on More Recent Data, at 500 mb. Showing the location of Mid-level Cyclones.

The problem.

In an intense mid-level cyclone ( $\zeta > 0$ ),  $\partial\zeta/\partial p$  is greater than zero above the level of maximum intensity and  $\partial\zeta/\partial p$  is less than zero below. Throughout an appreciable depth,  $\partial^2\zeta/\partial p^2$  is less than zero. A consequence of such a vertical distribution of  $\zeta$  is that a warm temperature anomaly  $T'$  will be found above such a cyclone and a cold anomaly will be observed below the cyclone. This type of structure, as illustrated by figure 3, can be viewed in terms of hydrostatic balance or from the thermal wind relationship.

Figures 3a, b, and c show a schematic diagram of the typical pressure distribution over southeast Asia during the summer months. A vertical cross section along lines A-B, intersecting the mid-level cyclone (fig. 3b), is illustrated in figure 3d. From point A to point B, a decrease in geopotential height is observed at 900 mb., and an increase is observed at 200 mb. and at 500 mb. where the mid-level cyclone is intersected. The warm anomaly above and cold anomaly below the middle-level cyclone are clearly illustrated in this figure.

The question as to how the vorticity of the mid-level cyclone is maintained is therefore intimately related to the question of maintenance of the vertical distribution of these temperature anomalies. In this paper we shall present results of computations of three-dimensional vertical motions based on a non-linear balanced model (including effects of terrain, cumulus-scale heating, and parameterized air-sea interaction). By constructing backward trajectories (passing through the mid-level cyclone), we will make an attempt to determine mechanisms that maintain observed temperature anomalies. It is hoped that this preliminary study will eventually lead to a formulation of a prediction model and achieve a better understanding of this phenomenon.

Recently, Charney [2] and Yanai et al. [19] have stressed the importance of a lack of coupling between lower- and upper-level systems in the tropics. Several earlier investigators, including Riehl [17], also pointed out that most of the eddy motions in the tropics are in the lower and upper troposphere. In this study, however, observations show that synoptic-scale cyclones are present in individual and monthly mean maps of the middle levels. A large part of the eddy kinetic energy at the middle levels in this region is in association with cyclonic systems that are a part of the summer monsoon complex of southeast Asia. There are large zonal asymmetries in the tropics, and mid-level features over the oceanic regions are quite different than observed over southeast Asia. Furthermore, seasonal differences in scales of motions are also quite large in the tropics. These intriguing features make the tropics a complicated and challenging area for large-scale meteorological research.

## 2. ON THE COMPUTATIONS OF VERTICAL VELOCITY

The procedure used for computation of vertical velocity,  $\omega$ , is similar to that described by Krishnamurti [9]. In order to obtain a three-dimensional distribution of  $\omega$  the following fields are required at several levels: streamlines, isotachs, isotherms, relative humidity, ocean temperatures (monthly mean), terrain heights (tabulations). The model contains the influence of air-sea interaction, terrain upslope and downslope motions, cumulus-scale heating and several other features. A one-degree latitude by one-degree longitude mesh on a mercator map projection is used for computations. While the model is internally consistent, the most serious drawback is the lack of meso-scale data. As a result, some of the details may not be quite representative on the smaller scale.

The non-divergent part of the wind  $V_\psi$  is obtained from a solution of the following equations:

$$V^2\psi = \zeta \quad (1)$$

and

$$W_\psi = k \times V\psi \quad (2)$$

where  $\zeta$  is the relative vorticity of the observed wind. Boundary conditions for  $\psi$  are obtained by the procedure outlined by Hawkins and Rosenthal [7]. This particular choice of boundary condition permits no net mass flux from the domain; however,  $\psi$  varies along the boundaries.

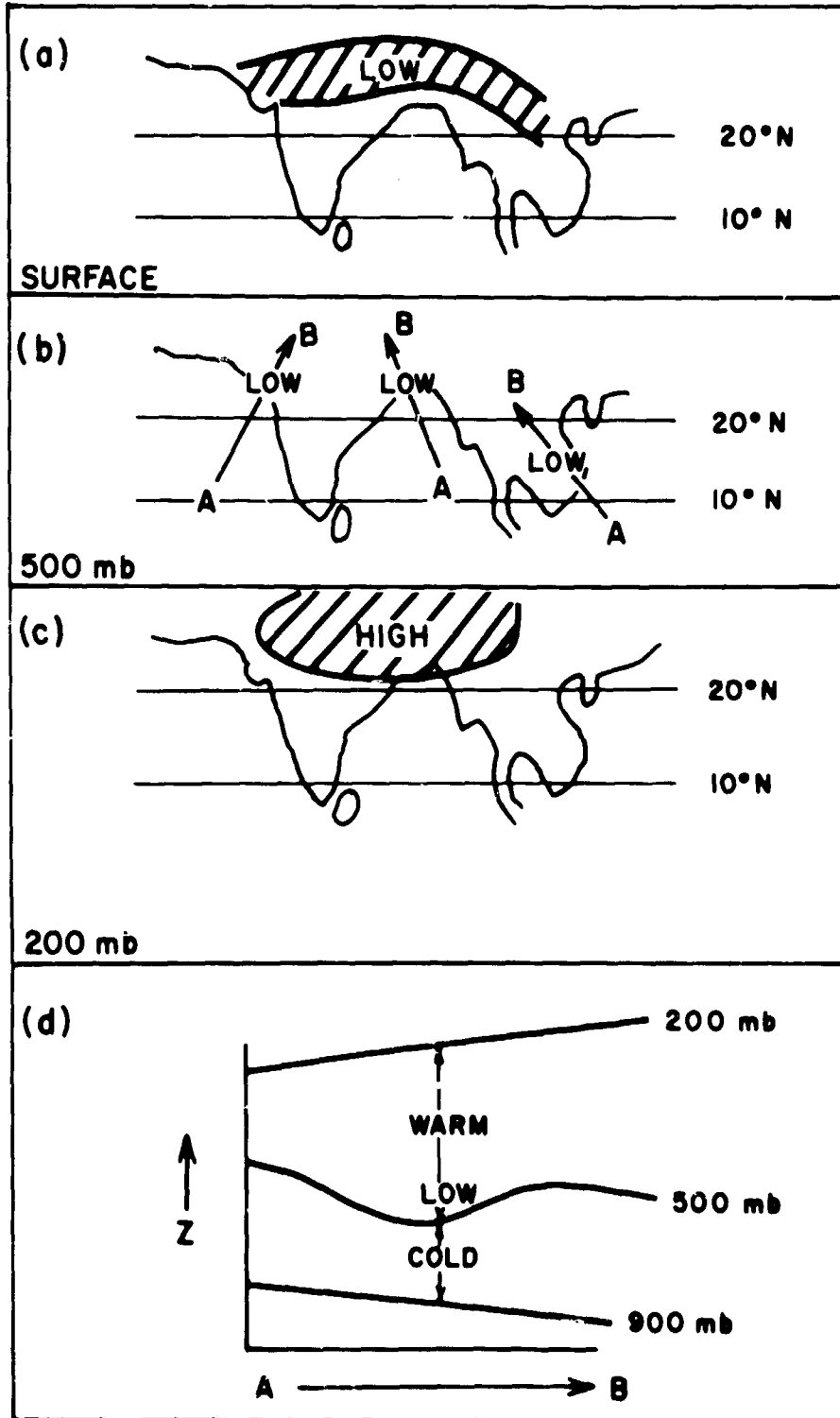


Figure 3. Schematic Diagram Showing Pressure Distribution at Lower (a), Middle (b) and Upper Troposphere (c). The bottom drawing (d) shows the slopes of 900-, 500- and 200-mb. surfaces and temperature anomalies in a vertical cross section.

The following other equations are used in the present study:

Omega equation

$$\begin{aligned} \nabla^2 \sigma \omega + f^2 \frac{\partial^2 \omega}{\partial p^2} = f \frac{\partial}{\partial p} J(\psi, \zeta_a) + HV^2 J(\psi, \theta) = f \frac{\partial}{\partial p} g \frac{\partial}{\partial p} \left[ \frac{\partial r_y}{\partial x} - \frac{\partial r_x}{\partial y} \right] - 2 \frac{\partial}{\partial t} \frac{\partial}{\partial p} J \left( \frac{\partial \psi}{\partial x}, \frac{\partial \psi}{\partial y} \right) - f \frac{\partial}{\partial p} (\zeta \nabla^2 \chi) \\ - \frac{R}{C_p P} \nabla^2 H + f \frac{\partial}{\partial p} \left( \omega \frac{\partial}{\partial p} \nabla^2 \psi \right) + f \frac{\partial}{\partial p} (\nabla \omega \cdot \nabla \frac{\partial \psi}{\partial p}) - f \frac{\partial}{\partial p} (\nabla \chi \cdot \nabla \zeta_2) \\ - \pi \nabla^2 (\nabla \chi \cdot \nabla \theta) - \beta \frac{\partial}{\partial p} \frac{\partial}{\partial y} \frac{\partial \psi}{\partial t} \end{aligned} \quad (3)$$

Continuity equation

$$\nabla^2 \chi = \frac{\partial \omega}{\partial p} \quad (4)$$

Vorticity equation

$$\begin{aligned} \nabla^2 \frac{\partial \psi}{\partial t} = -J(\psi, \zeta_2) + \nabla \chi \cdot \nabla \zeta_a + \zeta_a \nabla^2 \chi \\ - \omega \frac{\partial}{\partial p} \nabla^2 \psi - \nabla \omega \cdot \nabla \frac{\partial \psi}{\partial p} - g \frac{\partial}{\partial p} \left[ \frac{\partial r_y}{\partial x} - \frac{\partial r_x}{\partial y} \right] \end{aligned} \quad (5)$$

Boundary conditions

At  $p = 100$  mb.,  $\omega = 0$

At southern wall,  $y = y_1$ ,  $\omega = \chi = \frac{\partial \psi}{\partial t} = 0$

At northern wall,  $y = y_2$ ,  $\omega = \chi = \frac{\partial \psi}{\partial t} = 0$

At  $p = 1000$  mb.,  $\omega = -g \frac{1000}{Rr\theta_0} [J(\psi, h) - \nabla \chi \cdot \nabla h]$

The solutions for  $\omega$ ,  $\chi$  and  $\partial \psi / \partial t$  are obtained by a successive approximation procedure from equations (3), (4) and (5). This involves three-dimensional relaxation for  $\omega$  and two-dimensional relaxation for  $\chi$  and  $\partial \psi / \partial t$ .

In this diagnostic model diabatic heating rate per unit mass of air is split into two components:

$$H = H_s + H_l \quad (6)$$

where  $H_s$  is the transfer of sensible heat from the ocean;  $H_l$  is the release of latent heat. Radiative effects have not been included.

The sensible heat at 900-mb. surface is expressed by the following relationship (see Krishnamurti, [9]):

$$H_s = 0.00323 V (T_w - T_a) \quad (7)$$

Here  $H_s$  has units  $m.^2 \text{ sec.}^{-1}$ ,  $V$  being the wind speed in  $m. \text{ sec.}^{-1}$  at anemometer level and  $(T_w - T_a)$  the difference ( $^{\circ}C.$ ) between the water temperature and the air temperature at anemometer level.

The procedure for parameterization of the cumulus scale as a function of the large-scale motion with the mutual modification of the two scales is carried out using the approach used by Kuo [11] for a tropical storm.

Heat is released if the following criteria are met:

- (1)  $-\frac{\partial\theta}{\partial p} < 0$  at any level above 1000 mb. This parameter measures the moist conditional instability.
- (2) Net moisture convergence,  $l$ , exceeds zero in vertical columns. The column extends from the top of the friction layer to the top of atmosphere (100 mb.).

The heating function,  $H_L$ , is defined by the relation:

$$H_L = C_p \frac{a}{\Delta t} (T_c - T) \quad (8)$$

where  $(T_c - T)$  is the temperature difference between cloud element and tropical environment;  $C_p$  is the specific heat of air at constant pressure; and  $t$  is a cloud-time scale.

Surface frictional stresses  $\tau_x$  and  $\tau_y$  are defined in terms of a surface roughness constant applied at the lower level,  $p = 1000$  mb.

### 3. MID-LEVEL CYCLONE OVER SOUTHERN INDOCHINA

A few selected maps for June 1966 will be presented from the large number of cases prepared during this investigation. Maps at the surface, 500-mb. and 200-mb. levels are shown in figure 4 for four-map times over the period June 16-18. In all, six-case studies over this region were prepared.

#### 3.1 Surface Winds

Because of orography, the analyzed features only represent surface flows over oceans and the central plains of Cambodia. At  $10^\circ$  N. there is a marked diurnal change in surface winds between 1200 GCT (westerly) and 0000 GCT (southerly). Time continuity is not very clear in the surface-wind field. The flow is fairly typical of the southwest monsoon. The monsoon low-pressure trough is located around  $17^\circ$  to  $22^\circ$  N. The circulation around the heat low is more organized at 1200 GCT (1900 local time) than at 0000 GCT.

#### 3.2 500 Millibars

The mid-level cyclone is located near  $10^\circ$  N. and moves slowly westward during the four-map times. A warm temperature feature ( $-2^\circ$  C., 16 June, 1200 GCT) gradually moves westward; isotherms are represented by dashed lines (interval  $1^\circ$  C.). Marked intersection of streamlines and isotherms clearly indicates regions of cold advection east of the mid-level cyclone and warm advection west of the cyclone. This turns out to be an important aspect of the mid-level cyclones although advective effects are usually considered small in the tropics. Exceptions to this may be found in the vicinity of hurricanes, monsoon circulations and tropical cold-lows over oceanic areas. Temperature gradients are not always negligible in the tropics (see Erickson, [5]), and whenever temperature gradients greater than about  $1^\circ$  C./300 km. are found there are important synoptic-scale regions of rising and sinking motions, primarily resulting from warm and cold horizontal advection. This does not, however, lead to the inference that in these disturbances there is a net ascent of warm air and a descent of colder air. On the contrary, we find that maximum cold advection occurs closer to the axis of warmest temperature anomaly and maximum warm advection occurs some distance away from the warm anomaly. The implication of this finding to the energetics will be discussed later.

#### 3.3 200 Millibars

The mid-level cyclone of Indochina lies southeast of the upper-tropospheric position of the large upper anticyclone of the summer season. Winds at the 200-mb. level over the mid-level cyclone are very steady with easterlies around 20-40 kts. increasing steadily westward. Also noted is convergence at 200 mb. which is consistent with a gradual descending motion on the planetary scale, and this feature is confirmed by our dynamical calculations. Temperature increases gradually westward over this region with the warmest air near the Tibetan plateau. No local warm or cold temperature anomalies are observed at this level.

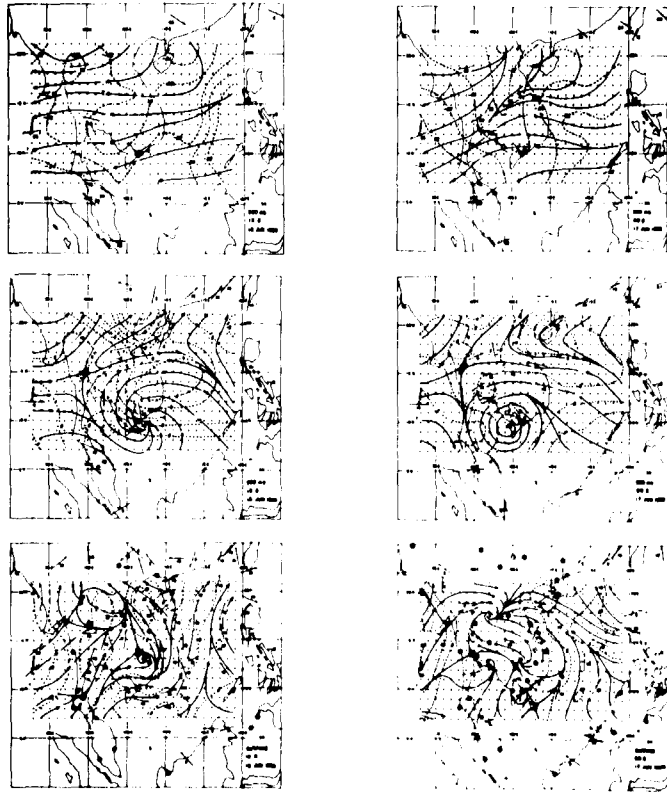
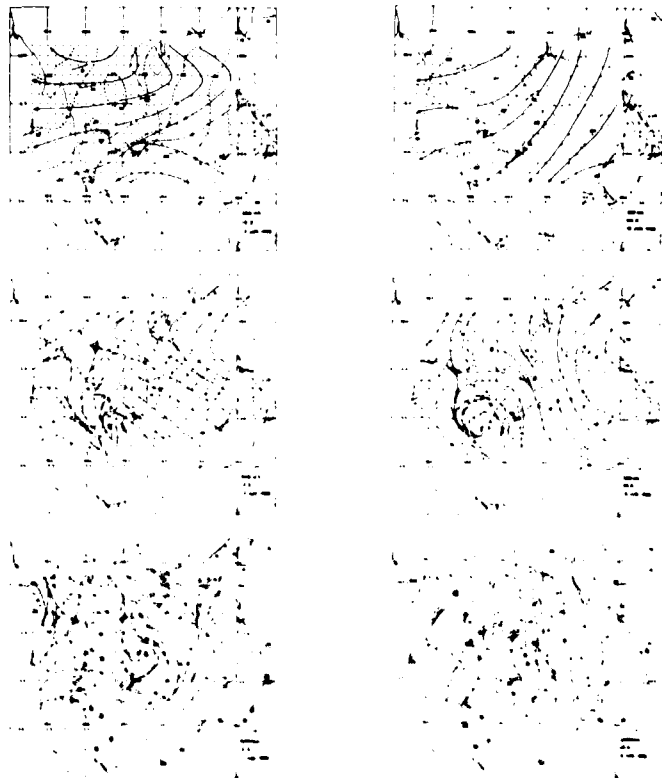


Figure 4. (a) Streamlines and Isotherms at 200 mb., 500 mb. and Surface Map for 12Z, 16 June and 00Z, 17 June 1966.



(b) Streamlines and Isotherms at 200 mb., 500 mb. and Surface Map for 12Z, 17 June and 00Z, 18 June 1966.

#### 4. MID-LEVEL CYCLONES OVER INDIA

Results of computations of dynamical parameters over southern Indochina have been compared with those obtained from mid-level cyclones over India. Computations have been made for a case presented by Miller and Keshavamurthy [4] for which considerable detail could be provided by the Indian Ocean expedition aircraft data. The case selected, 1200 GCT, July 7, 1963, has an intense mid-level cyclone present over the northeastern Arabian Sea and a weaker system over northern Bay of Bengal. The locations of these cyclones, at about 20° N., are shown at the 500-mb. level in figure 5. At 200 mb. (fig. 6) the flow is from the east with a weak easterly jet. Observed circulation patterns at other levels are shown in Miller and Keshavamurthy [14].

#### 5. VERTICAL STRUCTURE OF MID-LEVEL CYCLONES

Figure 7 depicts three examples of west-to-east vertical cross sections passing through the mid-level cyclones illustrated in figures 4a and 4b. Figures 7a and 7b present a cross section along 10° N. which passes through the cyclones of southern Indochina shown in figure 4. Finally figure 7c is a cross section along 20° N. through the cyclones portrayed in figure 5. The center of the cyclone is well marked in each case by a maximum in the absolute vorticity field. The cross sections also contain the distributions of temperature anomaly  $T'$ , and vertical velocity  $\omega$ . Values of  $\zeta_0$  in the mid-level cyclones were as high as  $80 \times 10^{-6} \text{ sec}^{-1}$ . This "trapped" mid-level vorticity is a puzzling phenomenon of the Asian southwest monsoon circulations. Above the center of the maximum vorticity, a warm anomaly is found in each of these cross sections. The intensity of the warm anomaly is greater over India than over southern Indochina. Rising motions are found to the west of the cyclone and sinking motions to the east. The rising air has a northerly component with associated advection of warm and dry air. In some portions of the cross sections the boundary-layer convergence is large, and maxima in the vertical velocity field are found near 900 mb. The vertical motion of the upper-level systems appears to couple and uncouple with the lower-level rising and sinking motion distributions. These zonal cross sections show a vertical tilt of the vorticity maxima towards the west. In the north-south plane (cross sections) the vorticity maxima have a southward tilt with height towards colder air. The greatest tilt is found near the surface and in the upper troposphere.

The cross sections show the warmest temperature anomaly is near the location where the upper easterlies change their sign of vertical motion. This result was found to be the case in almost all of the examples that were investigated. This is an observational evidence of the role of subsidence warming in maintaining the warm anomaly.

#### 6. HORIZONTAL DISTRIBUTION OF VERTICAL MOTION

The non-linear balanced model used in the present study resolves vertical velocity into a number of components (Krishnamurti [9]). An examination of the details of the vertical motion revealed that thermal advection was a primary contributor to the total vertical motion in the vicinity of the mid-level cyclone. This is not surprising in view of the thermal structure of the disturbance and its relation to the motion field. Air over the oceanic regions is cooler than that over land, and strong thermal advection is observed in some regions. Flow from the land areas is associated with warm advection and rising motions, and the converse is true for flow from the oceanic areas. Figure 8 shows the horizontal distribution of vertical motion at 700 mb. for four-map times over southern Indochina. Largest magnitudes of vertical velocity are of the order of 1 cm./sec. but these appear to have physical importance since the regions of rising motions correlate reasonably well with the cloud cover during these periods (fig. 9). We are also extending these studies over larger areas including Southeast Asia and India. The results of these studies will be reported later.

#### 7. DIURNAL CHANGES IN VERTICAL VELOCITY

Remarkable diurnal differences in the magnitude of lower tropospheric vertical velocity  $\omega$  were noted in the computed fields. The magnitudes of  $|\omega|$  were systematically lower at 1200 GCT (1900 local time) as compared to 0000 GCT (0700 local time). A further examination of the distribution of the dependent variables (fig. 4) revealed that this diurnal change in  $|\omega|$  was



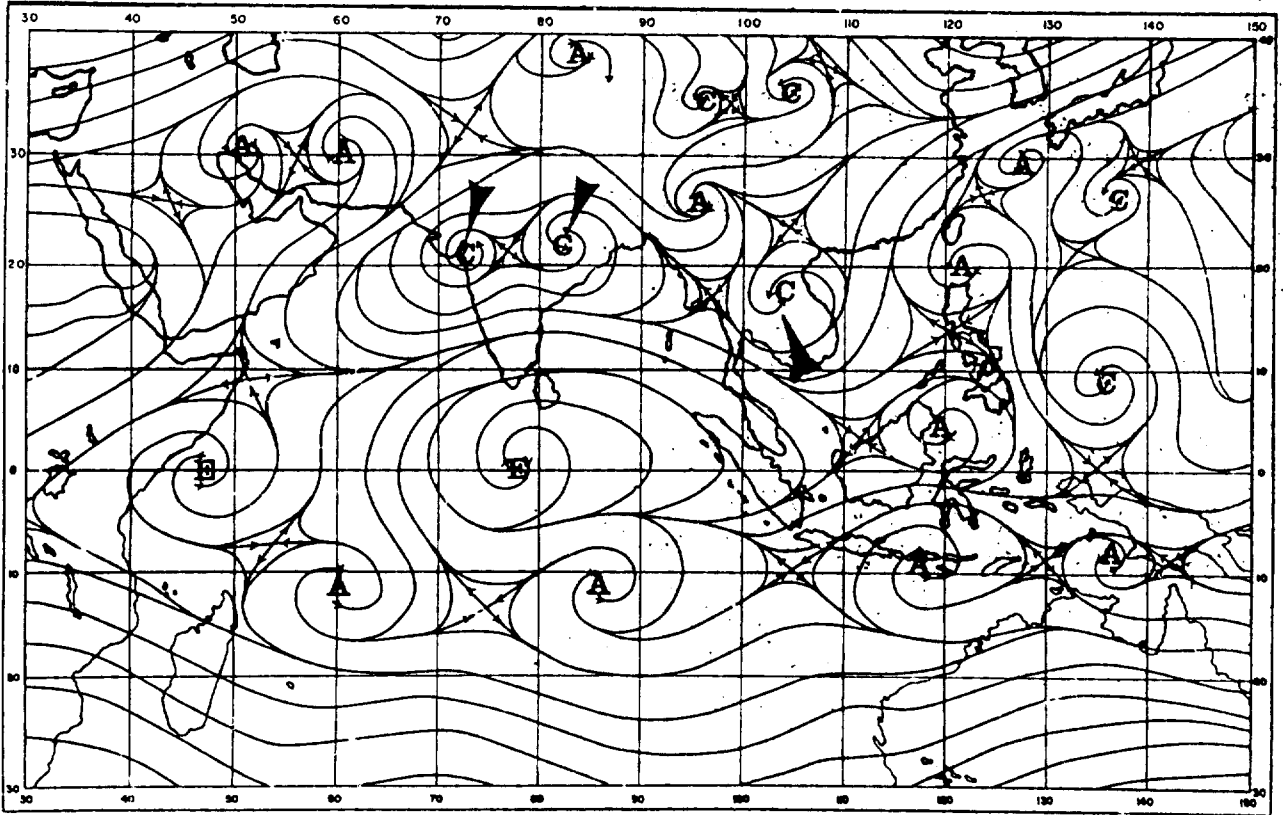


Figure 5. Streamlines at 500 mb., 12Z, 7 July 1963.

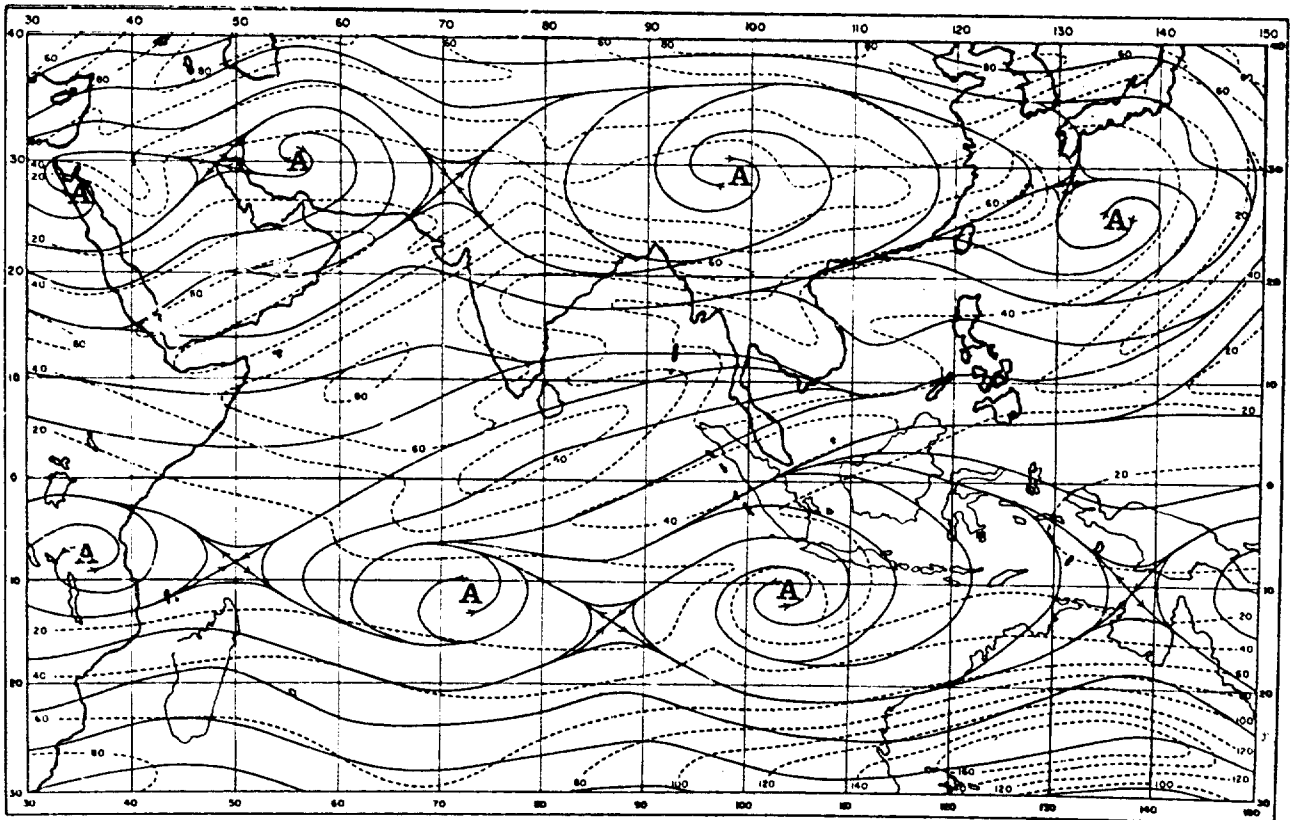


Figure 6. Streamlines at 200 mb., 12Z, 7 July 1963.

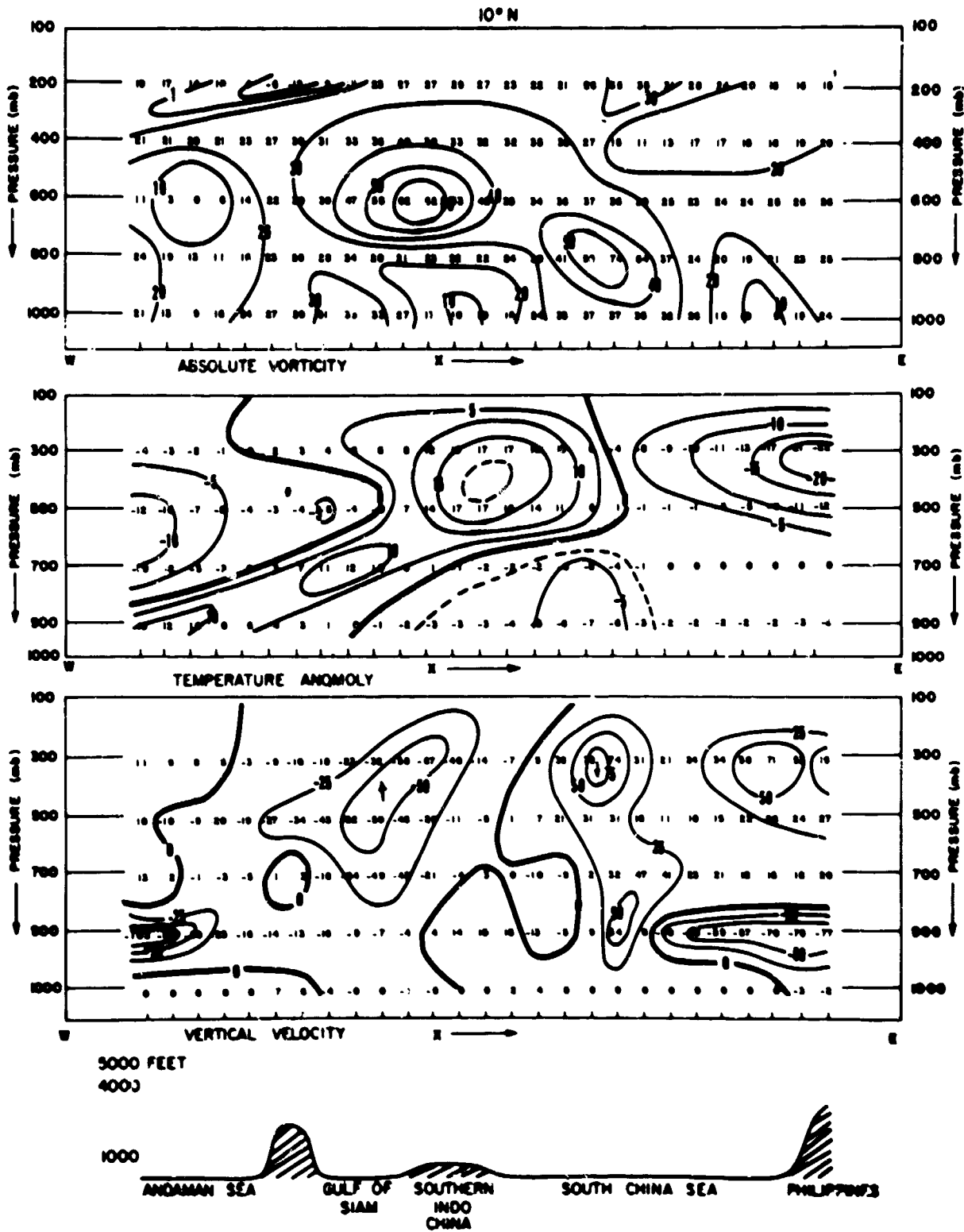


Figure 7. (a) Vertical Cross Section<sup>1</sup> From West to East at 10° N. Through the Mid-Level Cyclone Over Southern Indochina. Top: isopleths of absolute vorticity  $\times 10^{-6} \text{ sec}^{-1}$ . Middle: isopleths of temperature anomaly  $\times 10^{-1} \text{ }^\circ\text{C}$ . Bottom: isopleths of vertical velocity  $\times 10^{-1} \text{ mb./sec.}$  A profile of the smoothed terrain is indicated at the bottom of the cross sections. (001, 17 June 1966).

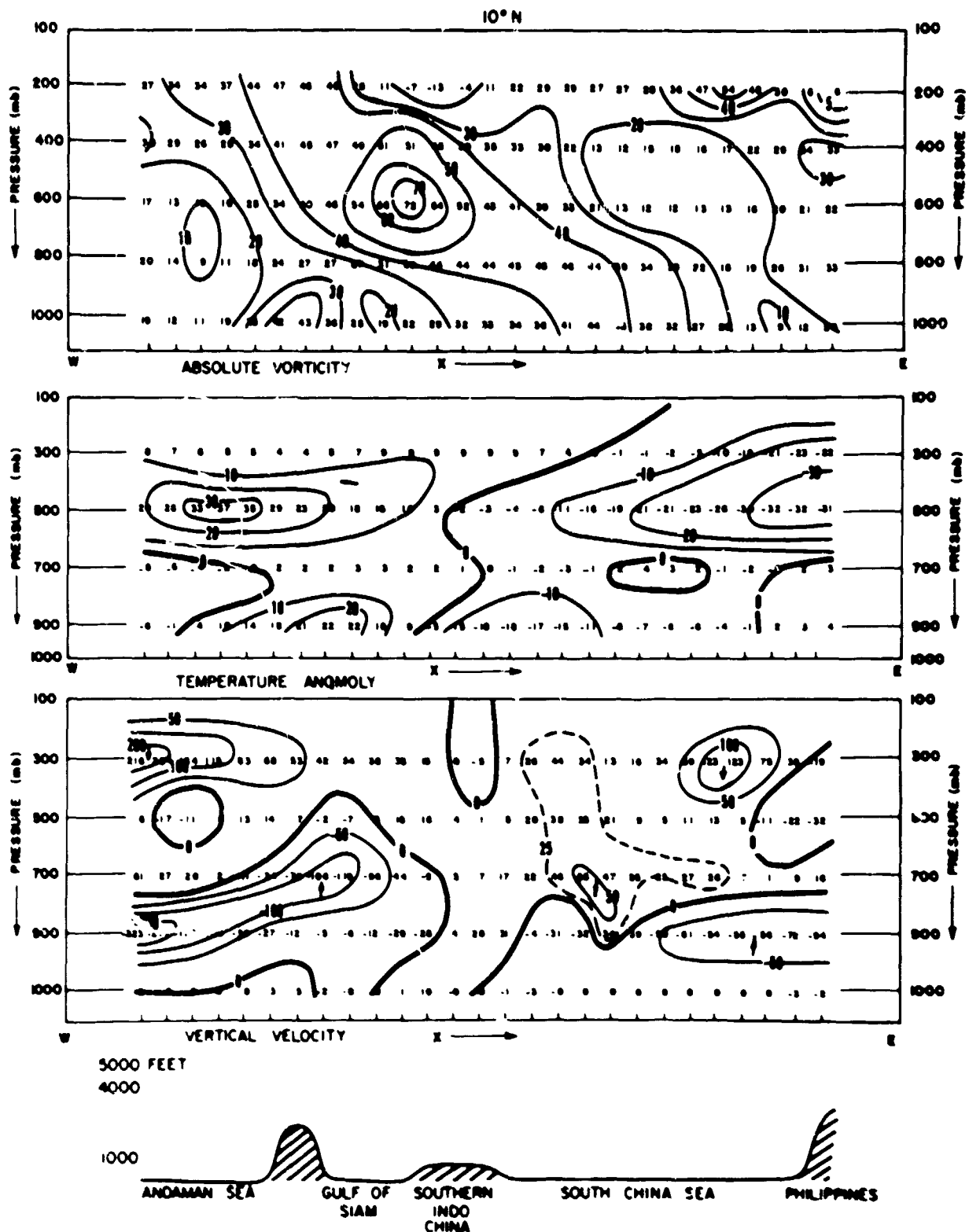


Figure 7. (b) Vertical Cross Section From West to East at 10° N. Through the Mid-Level Cyclone Over Southern Indochina. Top: isopleths of absolute vorticity  $\times 10^4 \text{ sec}^{-1}$ . Middle: isopleths of temperature anomaly  $\times 10^{-1} \text{ }^\circ\text{C}$ . Bottom: isopleths of vertical velocity  $\times 10^2 \text{ mb./sec.}$  A profile of the smoothed terrain is indicated at the bottom of the cross sections. (00Z, 18 June 1966).

20°N

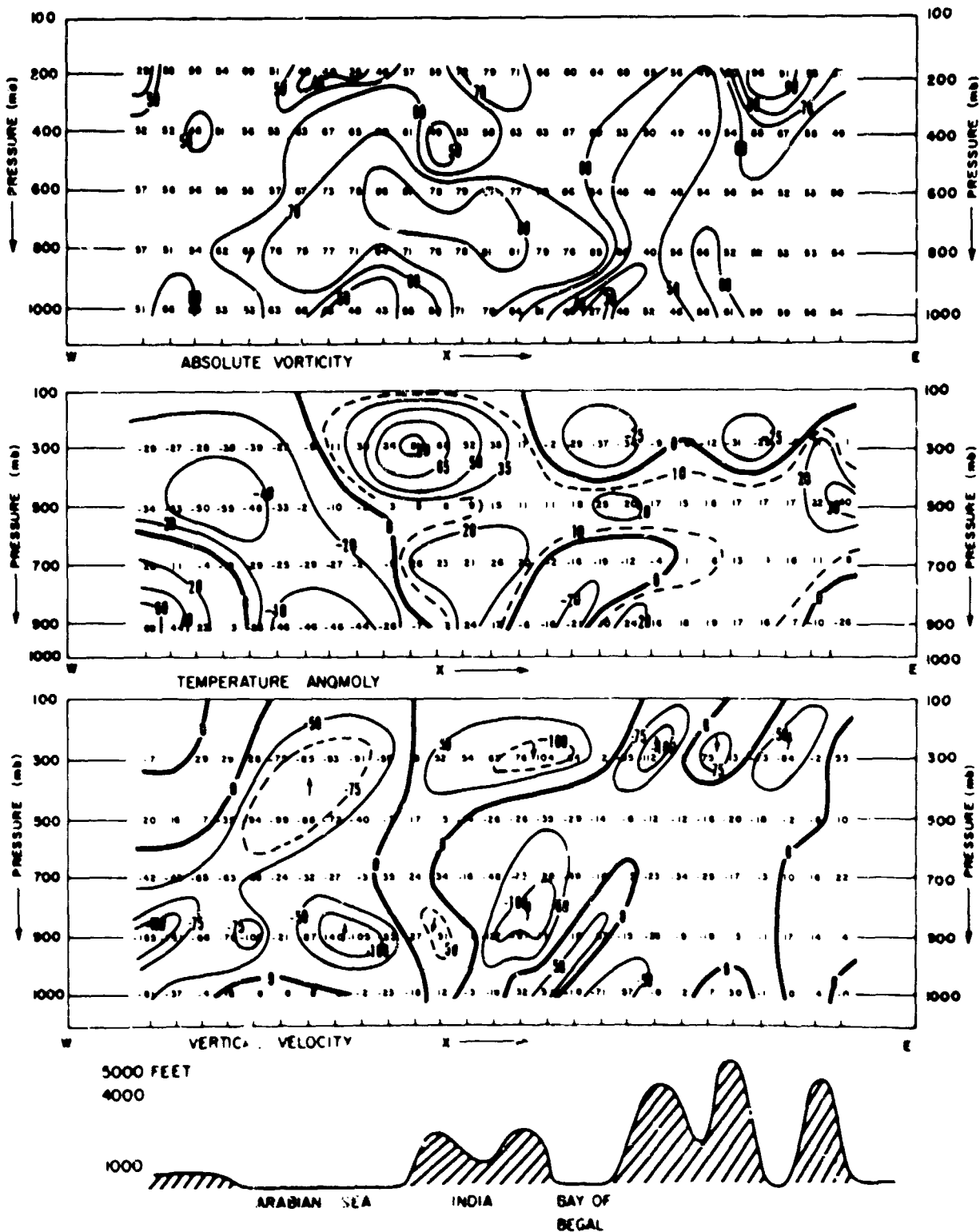


Figure 7. (c) Vertical Cross Section from West to East at 10° N. Through the Mid-level Cyclone over Southern Indochina. Top: isopleths of absolute vorticity  $\times 10^{10} \text{ sec}^{-2}$ . Middle: isopleths of temperature anomaly  $\times 10^4 \text{ }^\circ\text{C}$ . Bottom: isopleths of vertical velocity  $\times 10^3 \text{ mb./sec}$ . A profile of the smoothed terrain is indicated at the bottom of the cross sections. (1200Z, 7 July 1963).

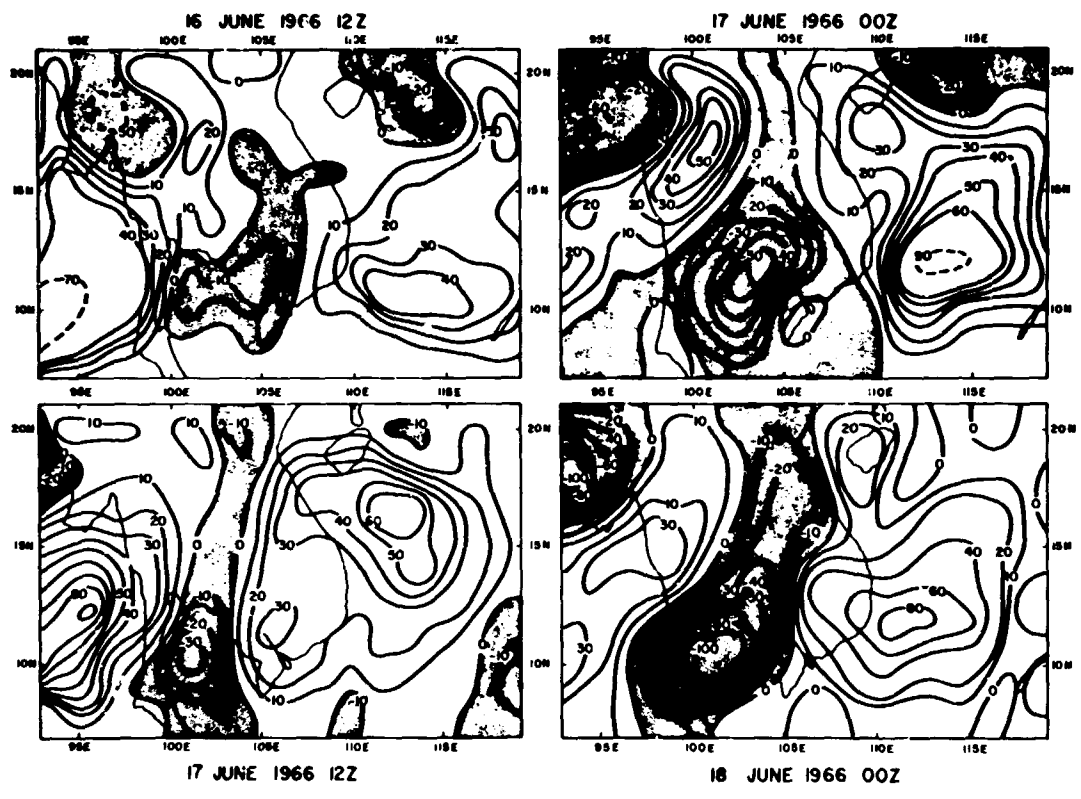


Figure 8. Horizontal Distribution of Vertical Motion (10 mb./sec. ) for Four-Map Times at 700 mb. Shaded areas indicate ascending motion.

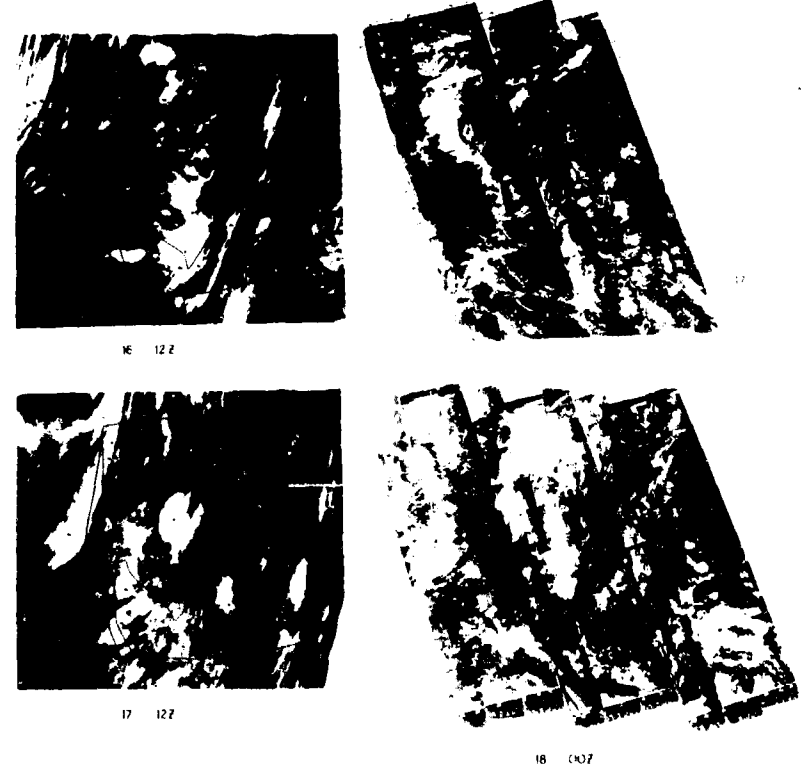


Figure 9. Satellite Cloud Photographs Showing Cloud-Cover at Approximately the Map Time Under Investigation (fig. 4).

primarily due to a systematic change in the distribution of wind vectors and not in the thermal field or its gradients. The primary forcing function in the  $\omega$  equation in the vicinity of the mid-level cyclone is the Laplacian of thermal advection. Its magnitude is reduced during afternoon hours and increased during nighttime due to the changes in the wind speed and direction. These results are in accordance with recent findings of Kreitzberg [8] who used a mesoscale network of roughly 20 aerological stations over southern Indochina. He found marked diurnal changes in the vertical distribution of moisture which he attributed to diurnal changes in the vertical motion field.

Other features of interest found by Kreitzberg include a low-level mesoscale speed maxima of the order of 40 knots with lateral dimensions less than one-degree latitude. He found that regions with active cumulus convection were located roughly over the regions of maximum low-level cyclonic relative vorticity. This is a confirmation of the presence of Ekman-type boundary layer over land areas where the coupling between cumulus-scale and low-level mass convergence seems to be on the mesoscale. Charney [3] has proposed similar ideas in his theory of the intertropical convergence zone. Fujita et al. [6] have used cloud motions from synchronous ATS satellites to show that over oceanic regions of the tropics the low-level wind does exhibit a relative cyclonic vorticity maxima on the mesoscale below organized bands of cumulus convection. It is remarkable that Kreitzberg noted similar structures over land areas.

Lack of mesoscale data makes it very difficult to parameterize cumulus convection properly. An attempt has been made to take this effect into account in a rather rough manner. In general, for larger scale numerical prediction in the tropics, it would be impossible to expect mesoscale data over the entire regions. However, theoretical work on the formation of mesoscale velocity streaks in the boundary layer of a conditionally stable air mass may prove to be important.

## 8. MECHANISM FOR THE MAINTENANCE OF THE UPPER TROPOSPHERIC WARM ANOMALY

The first law of thermodynamics used in this study is expressed by the relation:

$$\frac{\partial T}{\partial t} + \mathbf{V} \cdot \nabla T = -\omega \left( \frac{\partial T}{\partial t} + \frac{R}{C_p p} T \right) + \frac{a(T_c - T)}{\Delta t} \quad (9)$$

The first term on the right represents adiabatic warming or cooling, and the second term on the right gives a measure of the cumulus-scale warming. Quantity  $a$  represents the fraction of the synoptic-scale area covered by convective elements, and  $\Delta t$  is a cloud-time scale.  $\sigma = -\left( \frac{\partial T}{\partial t} + \frac{R}{C_p p} T \right)$ , a measure of static stability, is positive on the synoptic scale.

The warm anomaly above the mid-level cyclone could be maintained by subsidence warming. Several backward trajectories were constructed in order to assess the contribution of this effect. It soon became obvious that large-scale descending motions alone could not account for the observed warm anomalies, e.g.,  $\sigma$  is of the order of  $0.07^\circ \text{ mb}^{-1}$  and  $\omega$  is of the order of  $30 \times 10^{-5} \text{ mb. sec}^{-1}$ .

The order of magnitude of the cumulus-scale warming can be obtained by assuming  $a = 0.01$ ,  $T_c - T \approx 3^\circ \text{ C}$ . and  $\Delta t \approx 15$  minutes. The orders of magnitude of the two terms are:

$$\begin{aligned} \sigma \omega &= 2.1 \times 10^{-5} \text{ sec}^{-1} \\ \frac{a(T_c - T)}{\Delta t} &\approx 3.3 \times 10^{-5} \text{ sec}^{-1} \end{aligned}$$

Over a period of 24 hours parcels moving through this region would experience a warming of the order of  $3^\circ$  to  $4^\circ \text{ C}$ . Both of these mechanisms therefore are important.

Tables 1 and 2 show the distribution of selected computed parameters along backward trajectories based on our solutions of the balanced model. The tables apply to trajectories passing through the mid-level cyclone over southern Indochina and over the Arabian Sea, respectively. These detailed computations confirm our order of magnitude estimates discussed above. The estimates of net radiative cooling in row 9 are taken to be 1.2° C./day, based on values given by London [12]. It may be noted that the location of the center of the mid-level cyclone is close to column 8 in each table.

Table 1. Parameters Along Backward Trajectory Passing Through Mid-Level Cyclone. (Indochina)

Row	Parameters	1	2	3	4	5	6 7 8 9 ↓ Mid-level cyclone ↓				10	11
1	Time in hours along backward trajectory	0	-4	-8	-12	-16	-20	-24	-28	-32	-36	-40
2	Observed temperature at 500 Millibars (°A.)	266.0	266.1	266.3	266.8	267.2	268.6	268.9	269.0	268.7	267.9	267.4
3	Static stability σ (units deg. sec. <sup>-1</sup> mb. <sup>-1</sup> )	.071	.074	.078	.073	.069	.065	.065	.061	.062	.064	.065
4	Calculated vertical velocity ω (units 10 <sup>-3</sup> mb./sec.)	82	67	48	33	27	12	5	2	-19	-38	-49
5	Calculated temperature using adiabatic motions only (°A.)	266.0	265.7	267.2	267.5	267.7	267.3	267.9	267.9	267.8	267.6	267.4
6	Calculated percent area covered by convective clouds	0	0	0	0	0.4	1.2	1.8	1.9	0.6	0	0
7	Temperature difference between cloud T <sub>c</sub> and tropical environment T <sub>e</sub> . (°A.)	0	0	0	0	3.4	3.1	3.3	3.6	3.1	0	0
8	Diabatic warming by cumulus scale (°A./4 hours)	0	0	0	0	0.21	0.58	0.95	1.12	0.29	0	0
9	(Estimated long wave radiative warming °A./4 hours)	-	-0.2	-0.2	-0.2	-0.2	-0.2	-0.2	-0.2	-0.2	-0.2	-0.2
10	Net calculated temperature along trajectory	266.0	266.5	267.0	267.3	267.7	268.2	268.7	268.8	267.9	267.4	267.2

Table 2. Parameters Along Backward Trajectory Passing Through Mid-Level Cyclone (India).

Row	Parameters	1	2	3	4	5	7 8 9 10 ↓ Mid-level cyclone ↓				11	
1	Time in hours along backward trajectory	0	-4	-8	-12	-16	-20	-24	-28	-32	-36	-40
2	Observed temperature at 500 Millibars (°A.)	265.1	266.0	266.7	267.2	267.8	268.7	269.3	268.8	268.2	267.0	266.1
3	Static stability σ (units deg. sec. <sup>-1</sup> mb. <sup>-1</sup> )	.077	.079	.08	.089	.089	.083	.081	.082	.077	.073	.073
4	Calculated vertical velocity ω (units 10 <sup>-3</sup> mb./sec.)	40	43	56	44	32	28	-27	-51	-85	-106	-58
5	Calculated temperature using adiabatic motions only (°A.)	265.1	265.6	266.3	266.9	267.3	267.7	267.4	266.8	265.9	264.8	264.2
6	Calculated percent area covered by convective clouds	0	0	0	0	0.3	1.1	1.7	1.6	0.9	0.5	0.1
7	Temperature difference between cloud T <sub>c</sub> and tropical environment T <sub>e</sub> . (°A.)	0	0	0	0	3.7	3.8	4.1	4.0	3.3	3.6	3.5
8	Diabatic warming by cumulus scale (°A./4 hours)	0	0	0	0	0.18	0.67	1.12	1.02	0.48	0.29	0.06
9	Estimated long wave radiative warming (°A./4 hours)	-	-0.20	-0.20	-0.20	-0.20	-0.20	-0.20	-0.20	-0.20	-0.20	-0.20
10	Net calculated temperature along trajectory	265.1	265.4	266.1	266.7	267.3	268.2	268.3	267.6	266.2	264.9	264.1

Table 3 shows values of  $(T_c - T)$  based on conservation of equivalent potential temperature (i.e., parcel ascent) for Saigon and Bangkok during a 10-day period at 1200 GCT in June 1966. The temperatures of the parcel  $T_c$  are greater than  $T$  below 300 mb. Values of  $(T_c - T)$  over the troposphere, which refer to conditions near sunset, can be as large as  $5^\circ$  to  $6^\circ$  C., and can, under favorable conditions, produce significant warming of the air at upper levels on a synoptic scale. Conditions during the day would lead to even larger values of  $(T_c - T)$ . The present investigation deals with diagnostic calculations of the three-dimensional motion field. Such studies have obvious disadvantages in that only limited conclusions can be drawn regarding the importance of various mechanisms. The manner by which adiabatic warming and cumulus-scale heating couple to produce isolated warm anomalies can only be examined by a prediction experiment. Since these mid-level disturbances are present in the monthly-averaged maps, the role of orography, warm continents and air-sea interaction must be important. These features must be included for a successful simulation of the phenomenon.

Table 3. Time Variation of  $(T_c - T)^\circ\text{C.}$  at Selected Stations in the Vicinity of the Mid-Level Cyclone. June, 1966, 12Z.

Saigon										
Date	9	10	11	12	13	14	15	16	17	18
Pressure										
850	1.7	2.3	3.0	5.3	3.0	1.1	2.3	3.0	2.4	1.4
700	4.4	3.1	3.2	3.1	1.7	1.2	0.7	1.7	1.7	1.0
500	1.9	2.5	-0.2	0.6	3.9	2.4	2.2	0.8	0.6	1.7
400	0.9	1.5	0.1	1.5	1.8	1.0	1.0	1.2	1.2	0
300	1.0	0.6	0.6	0.5	0	-0.2	-0.9	-0.4	0	-0.8
200	-4.4	-5.2	-4.7	-0.3	-5.1	-5.0	-4.2	-4.9	-5.1	-0.4
Bangkok										
850	3.1	9.3	7.5	5.3	1.2	2.4	2.4	3.5	3.1	2.2
700	4.8	4.6	2.7	2.3	1.8	1.8	1.8	3.5	2.3	3.1
500	0.8	4.4	2.9	3.0	1.6	2.9	0.9	3.2	2.2	1.9
400	0	1.2	1.2	1.7	1.9	2.2	2.2	2.0	1.3	1.1
300	-0.	-0.2	0.2	0.2	0.3	0.4	0.1	1.4	-0.2	0.3
200	-5.3	-4.2	-5.2	-4.5	-5.2	-5.0	-	-4.9	-5.2	-4.9

Murakami et al. [15] have made a remarkable start on a two-dimensional formulation of a zonally symmetric monsoon problem. They have produced a reasonably successful simulation of the mean zonal circulation of the Asian summer monsoon by incorporating various features such as eddy diffusion of momentum, heat and water vapor in the boundary layer. They perform a detailed computation of the heat balance of the earth's surface to predict its surface temperature. Cumulus convection is parameterized by a procedure similar to that of Manabe and Smagorinsky [13]. This simulation of the zonally symmetric summer monsoon does not contain any evidence of the mid-level cyclonic vorticity maxima at  $20^\circ$  N. or at  $10^\circ$  N. This, of course, should not be expected because of the symmetry restriction and the scale of this phenomenon. We feel that investigations of mid-level cyclones will be an interesting asymmetric problem of the monsoon circulation. A solution of it could be accomplished by extending numerical models of the type formulated by Murakami and his collaborators and relaxing the symmetry



constraints. Alternatively, one might wish to explain the "trapped" mid-level vorticity maxima as a dynamic instability problem in the presence of horizontal and vertical shear flows.

During the summer season in the middle latitudes zonal winds change from westerlies in the troposphere to easterlies in the stratosphere. Charney and Drazin [2] have shown that such a vertical distribution of zonal currents inhibits a vertical propagation of energy of long quasi-geostrophic waves. There is a close analogy to such a phenomenon in the tropical troposphere over the region of the southwest monsoons. Over southeast Asia a strong belt of surface westerlies decreases with height, and above 500 mb., easterlies are found with an easterly jet near 150 mb. We might speculate that a critical level exists around 500 mb. such that synoptic-scale energy at lower levels is trapped below or around the critical level. This trapping might manifest itself in the form of large mid-tropospheric eddy kinetic energy in these mid-level cyclones. There is an important difference between the monsoon situation and the larger-scale waves considered by Charney and Drazin. This difference is due to the deep cumulus convection which transfers large amounts of energy to very high levels from the boundary layers of the southwest monsoon. This energy is linked to motions on the mesoscale in the boundary layer because of the more direct association of cumulus convection with mesoscale motions rather than with the larger synoptic-scale motion. This analogy appears worth examining in greater detail.

## 9. ENERGY TRANSFORMATIONS BY CUMULUS AND SYNOPTIC-SCALE MOTIONS

If calculations of energetics are to be carried out over the entire globe, a simple formulation of the energy transformation equations can be obtained. In such a problem the generation of eddy kinetic energy can be related to internal barotropic and baroclinic exchanges. On the other hand, when open boundaries are considered, large non-vanishing boundary fluxes are usually present, and a simple interpretation of the energetics of the system is generally not possible. The structure of the mid-level cyclones has been obtained by solving the balance equation over a limited portion of the globe. The results of these computations of energetics are more in the line of, so called, budget studies.

### 9.1 Energy Equations

The local change of kinetic energy per unit mass of air can be written as:

$$\frac{\partial K}{\partial t} = -\nabla \cdot [(K + \phi) \mathbf{W}] - \frac{\partial}{\partial p} [(K + \phi) \omega] - \frac{RT}{p} \omega - \mathbf{W} \cdot \mathbf{F} \quad (10)$$

Upon integration over a mass  $m$  of the atmosphere, this change may be written as:

$$\begin{aligned} \frac{\partial K}{\partial t} = & -\frac{1}{g} \int_p \int_S [(K + \phi) C_n] dS dp - \frac{1}{g} \int_p \int_y \int_x \omega dx dy dp \\ & - \frac{1}{g} \int_p \int_y \int_x \mathbf{W} \cdot \mathbf{F} dx dy dp \end{aligned} \quad (11)$$

where  $C_n$  is an outward normal velocity in the horizontal direction and  $\bar{K}$ , the total kinetic energy, is given by:

$$\bar{K} = \int_m K dm = \frac{1}{g} \int_p \int_y \int_x K dx dy dp \quad (12)$$

Vertical motion is assumed to be zero at 100 mb. in the balanced model used in this study. The contribution to the energetics due to vertical advections at 1000 mb. have been neglected. Frictional dissipation of kinetic energy is expressed in terms of the surface drag (drag coefficient  $C_D = 1.0 \times 10^{-3}$ ) and is roughly proportional to the cube of the surface-wind speed.

### 9.2 Parameterization of Cumulus Convection

In tropical energetics the contribution to 'L-' correlation arises partly from larger-scale and partly from the cumulus-scale motions. It is possible to obtain a measure of the vertical motion that is relevant to the cumulus scale by the following procedure.

The net convergence of flux of moisture into a unit vertical column extending from the top of the friction layer to the top of the atmosphere may be expressed by the relation:

$$l = - \frac{\omega_f q_f}{g} \quad (13)$$

where the subscript  $f$  refers to the top of the friction layer. Units of  $l$  are  $\text{mb. m.}^{-1} \text{sec.}^{-1}$ . For large-scale motions  $l$  is roughly  $10^{-6}$  units in the tropics [10]. Following Kuo, we form a model cloud which requires a net convergence of flux of moisture to replace the tropical sounding  $(T, q)$  by a moist adiabat  $(T_c, q_c)$ . At any level this may be expressed by:

$$-\frac{\partial}{\partial p} \omega_c q_c = C_p \frac{(T_c - T)(q_c - q)}{L \Delta t} + \frac{(q_c - q)}{\Delta t} \quad (14)$$

where  $\Delta t$  is a cloud time scale. Along an undilute cloud element  $\partial \omega_c / \partial p$  equals zero since no entrainment is assumed. We may approximate  $\omega_c$  by the relation:

$$\omega_c = \frac{C_p (T_c - T) + (q_c - q)}{\frac{\partial q_c}{\partial p} \Delta t} \quad (15)$$

This expression for vertical velocity in cumulus scale motion is such that  $\omega_c$  will be zero at the lifting condensation level and at the level where the tropical sounding intersects the moist adiabat. In between these levels there would be rising motion because  $T_c - T, q_c - q$  and  $\partial q_c / \partial p$  are all positive. A typical magnitude of  $\omega_c$  at 500 mb. is roughly  $10^{-1} \text{mb./sec.}$  ( $\approx 1 \text{ m. sec.}^{-1}$ ). The maximum amount of moisture convergence required to produce the model cloud over a synoptic-scale unit area is expressed by the relation:

$$Q = - \frac{1}{g} \int_{p_E}^{p_T} \left\{ \frac{C_p (T_c - T) + (q_c - q)}{L \Delta t} + \frac{(q_c - q)}{\Delta t} \right\} dp \quad (16)$$

The units of  $Q$  are  $\text{mb. m.}^{-1} \text{sec.}^{-1}$ . In a conditionally unstable tropical atmosphere  $Q$  is roughly  $10^{-4}$  units. Since  $l$  is the available moisture convergence, the ratio:

$$a = l/Q$$

may be regarded as a fraction of the synoptic-scale unit area covered by convective model clouds.

There are several limitations in the parameterization procedure and the numerical procedures used for evaluation of the three-dimensional motion field. These limitations are discussed at some length by Krishnamurti [9, 10].

### 9.3 Energy Releases By Convective Scale Motions

A measure of the contribution to the ' $\omega$ ' correlation by the convective scale can be obtained by the integral:

$$-\frac{R}{g} \int_p \int_y \int_x \frac{a \omega_c (T_c - T)}{p} dx dy dp$$

The horizontal distribution of ' $a$ ' is taken into account here; all clouds in each synoptic unit area are alike but they differ from one region to another.

### 9.4 Energy Releases By Synoptic-Scale Motion

Using the synoptic-scale vertical motions, discussed earlier in this paper, a contribution to ( $\omega'$ ) by this scale may be expressed by the integral:

$$-\frac{R}{g} \int_p \int_y \int_x \frac{(\bar{\omega} \bar{T} + \omega' T')}{P} dx dy dp.$$

we assume that  $a \ll 1$  and  $|1-a|=1$ .

It is easy to obtain a rough comparison of the contribution by the two scales within the framework of the parameterization procedure followed here. In an active convective disturbance like the mid-level cyclone,

$$\omega_c = 10^{-1} \text{ mb./sec.}$$

$$\omega' = 10^{-3} \text{ mb./sec.}$$

$$T_c - \bar{T} = 4^\circ \text{ C.}$$

$$T' = 4^\circ \text{ C.}$$

$$a = 1/4$$

and we note that  $\omega_c(T_c - \bar{T}) = \omega' T'$ . This suggests that over active convective regions contributions by the two scales may be comparable.

#### 9.5 Results of Energy Computations

We have evaluated the various integrals of the kinetic energy equation for the four-map times of figure 4. A box with sides along  $7^\circ \text{ N.}$ ,  $19^\circ \text{ N.}$ ,  $95^\circ \text{ E.}$  and  $115^\circ \text{ E.}$  encloses the mid-level cyclone in each case.

The following is a summary of the results of computations. Convergence of flux of potential and kinetic energy into box equals,

$$-12.81 \times 10^{18} \text{ ergs/sec.}$$

Dissipation of kinetic energy by surface friction equals,

$$4.11 \times 10^{18} \text{ ergs/sec.}$$

Generation of kinetic energy by  $(\omega' a')$  synoptic scale equals,

$$-24.76 \times 10^{18} \text{ ergs/sec.}$$

Generation of kinetic energy by  $(\omega' a')$  cumulus scale equals,

$$39.29 \times 10^{18} \text{ ergs/sec.}$$

$$\text{Net imbalance} = -2.39 \times 10^{18} \text{ ergs/sec.}$$

This imbalance is due to several factors such as (1) contribution by  $\bar{\omega} \bar{\alpha}$  which would depend on the size of the box, (2) local changes of kinetic energy in the box, and (3) truncation errors in the estimates and in the averaging processes. For the present we shall not be concerned with an explanation of these imbalances because of the approximation and sources of error in such computations. We find that synoptic scale  $\omega' a'$  contribution transforms eddy kinetic into eddy potential energy. As stated earlier this became obvious when we examined maps of synoptic-scale vertical motions and temperatures. We found that the centers of maximum sinking motions were located closer to the centers of warm anomalies. The important role of the cumulus scale on the energetics becomes clearer from these computations. Part of the kinetic energy released by the cumulus-scale motions is exported out of the box and part of it cancels the synoptic-scale conversions. In the absence of the cumulus scale, this system cannot be maintained in steady state because synoptic-scale energy conversions, friction, and exports would destroy its kinetic energy. It is also very interesting to compare the role of these two scales in maintaining the warm anomaly above the mid-level cyclone as well as an energy conversions.

- (1) Both scales account for warming above the mid-level cyclone.

- (2) Cumulus scale opposes the synoptic scale energy conversion, the former being somewhat larger in magnitude.

We feel that further studies should be carried out to understand the coupling of these two scales of motions discussed in this paper. It would also be worthwhile to see if such a dual role is found in other tropical weather systems.

## DISCUSSION

Southern:

- (1) Do any of these mid-level cyclones develop down to the surface as they move westward into the Bay of Bengal?
- (2) Comment. Since the advent of weather satellites we have noticed a similar occurrence of what appear to be mid-level cyclones (700-600 mb.) over northern Australia which move westward accompanied by a surface isobaric minimum. Generally these dissipate over land west of Darwin at about 15° S. Occasionally, they develop into surface level cyclones over the Bonaparte Gulf. The mid-level cyclones produce widespread rain and flooding, and the inflow area at 700 mb. seems to cover a radius of above 500 miles or so.

RAMAGE:

- (1) There was at least one well documented case of a small intense circulation (60 kts.) extending to the surface near Bombay.

ATKINSON: The temperature anomalies with these mid-level cyclones seem to be much greater over India than those over Indochina. Assuming that large warm departures at 500 mb. during the summer are associated with these disturbances, we may be able to derive a climatology of the frequency of these systems by studying the temperature frequency distributions at individual stations.

KRISHNAMURTI: I agree, this would be highly desirable; this is unfortunately not available at present.

KREITZBERG: Would the mixing and evaporation from the convection up into subsided air produce more evaporative cooling than the preceding warming? That is, doesn't the subsidence do more harm than good by the time you have to moisten that air?

KRISHNAMURTI: I don't think evaporation from falling rain from a small percent of the total synoptic scale area could be all that important. Cumulus convection is very efficient in pumping moisture up as synoptic scale; synoptic changes are known to take place very rapidly when there is cumulus scale pumping.

SADLER: The central portion of the cyclone is apt to be a cloud minimum area and can't contribute cumulus for heating.

KRISHNAMURTI: Cumulus convection is not isolated to the very center of the mid-level low. Convection seems to move to the north and west of the mid-level cyclone. This location will be variable from one case to the next.

NERALLA: Do you have any plans to make diagnostic case studies of heat lows? If so, in which way do they compare with mid-level cyclones?

KRISHNAMURTI: I have no immediate plans for studying heat lows. It is a complicated problem. Dr. Murakami has made a good start on this problem.

## ACKNOWLEDGEMENTS

We would like to express our appreciation to Professor C. L. Jordan for his comments on this work. Financial support for this work was received from the Atmospheric Science Section, National Science Foundation, NSF Grant CA-1480 and Department of Army THEMIS Contract No. DAAB 07-69-C-0062. Computing time was provided by F. S. U. Computing Center.

## REFERENCES

1. BUNKER, A. F., "Interaction of the Summer Monsoon Air With the Arabian Sea." Proceedings of the Symposium on Meteorological Results of the International Indian Ocean Expedition. WMO, Geneva, pp. 3-16, 1965.
2. CHARNEY, J. G. and P. G. DRAZIN, "Propagation of Planetary-Scale Disturbances From the Lower Into the Upper Atmosphere." J. Geoph. Res., 66, pp. 83-110, 1961.
3. CHARNEY, J. G., "The Intertropical Convergence Zone and the Hadley Circulation of the Atmosphere." Proceedings of the Conference on Numerical Weather Prediction sponsored by WMO, pp. III 73-III 79. Japan Meteor. Agency, Tokyo, 1968.
4. \_\_\_\_\_, "A Further Note on Large Scale Motions in the Tropics." J. Atmos. Sci., 26, pp. 182-185, 1969.
5. ERICKSON, C., "Diagnostic Study of an Upper Cold Low." (Abstract) Trans. Amer. Geophys. Union, 50, 179 pp., 1969.
6. FUJITA, T. T., K. WATANABE and T. IZAWA, "Formation and Structure of Equatorial Anticyclones Caused by Large Scale Equatorial Flows." J. Applied Meteor., 8, pp. 649-667, 1969.
7. HAWKINS, H. E. and S. L. ROSENTHAL, "On the Computation of the Streamfunction From the Wind Field." Mo. Wea. Rev., 93, pp. 245-252, 1965.
8. KREITZBERG, C. W., "Mesoscale and Diurnal Variations Deduced From the Saigon Areas Rawinsonde Data." Proceedings of the Conference of Summer Monsoon of Southeast Asia. April, 1969. Univ. of Hawaii, Honolulu. 1969.
9. KRISHNAMURTI, T. N., "A Diagnostic Balance Model for Studies of Weather Systems of Low and High Latitude, Rossby Number Less Than 1." Mo. Wea. Rev., 96, pp. 197-207, 1968a.
10. \_\_\_\_\_, "A Calculation of the Percent Area Covered by Convective Clouds From Moisture Convergence." J. Appl. Meteor., 7, pp. 184-195, 1968b.
11. KUO, H. L., "On Formation and Intensification of Tropical Cyclones Through Latent Heat Release By Cumulus Convection." J. Atmos. Sci., 22, pp. 40-63, 1965.
12. LONDON, J., "A Study of Atmospheric Heat Balance." Final Report to Air Force Cambridge Research Laboratories, 1-67. Dept. of Meteor. New York University. 1957.
13. MANABE, S. and J. SMAGORINSKY, "Simulated Climatology of a General Circulation Model With a Hydrologic Cycle II: Analysis of the Tropical Atmosphere." Mo. Wea. Rev., 95, pp. 155-169, 1967.
14. MILLER, F. R. and R. N. KESHAVAMURTHY, "Structure of an Arabian Sea Summer Monsoon System." East-West Center Press, Honolulu, pp. 1-94, 1967.
15. MURAKAMI, T., R. V. GODBOLE and R. R. KELKAR, "Numerical Simulation of the Monsoon Along 80° E." Proceedings of the Conference of Summer Monsoon of Southeast Asia. April, 1969. Univ. of Hawaii, Honolulu. 1969.
16. NORMAND, C. W. B., "Climatological Atlas for Airmen." Yeravda Prison Press, Government of India, Poona, pp. 1-101, 1943.
17. RIEHL, H., "Tropical Meteorology." New York, McGraw-Hill, 392 pp., 1954.
18. SADLER, J. C., "Forecasting Minimum Cloudiness Over the Red River Delta During the Summer Monsoon." Final Rpt. to Air Force Cambridge Research Laboratories, Contract Report No. AFCRL-68-481, Univ. of Hawaii, Honolulu, pp. 1-104, 1968.
19. YANAI, M., et al., "Power Spectra of Large Scale Disturbances Over the Tropical Pacific." J. Meteor. Soc. Japan, 46, pp. 801-816, 1968.

APPENDIX  
LIST OF SYMBOLS

- L latent heat of vaporization of air
- $H_s, H_l$  sensible and latent heat (respectively) per unit mass of air
- $C_p$  specific heat of air at constant pressure
- $a$  fraction (or percent) of synoptic-scale area covered by convective clouds
- $\theta_e$  equivalent potential temperature
- $R$  gas constant of dry air
- $T_a$  temperature of air at anemometer level, same as  $T$  in this study
- $T_w$  temperature of water
- $V$  total wind speed
- $g$  acceleration of gravity
- $\psi$  streamfunction
- $\zeta, \zeta_a$  relative vorticity and absolute vorticity
- $$V^2 = \frac{\partial^2}{\partial x^2} + \frac{\partial^2}{\partial y^2}$$
- $$\nabla = \frac{\partial}{\partial x} + \frac{\partial}{\partial y}$$
- $\chi$  potential of the divergent part of the wind field, a velocity potential
- $\pi$  Exner pressure  $-\frac{RT}{p^\theta}$
- $\beta$  the beta parameter  $-\frac{\partial f}{\partial y}$
- $\sigma$  static stability parameter  $-\frac{RT}{p^\theta} \frac{\partial \theta}{\partial p}$
- $w$  vertical velocity  $\left(\frac{dp}{dt}\right)$
- $f$  Coriolis parameter
- $T, q$  temperature and specific humidity (respectively) of a parcel raised vertically above the 900-mb. surface with no lateral mixing
- $T, \theta$  temperature and potential temperature of air, respectively
- $V_d$  non-divergent part of the wind
- $I$  net moisture convergence in a unit vertical column extending from 900 mb. to the top of the atmosphere (100 mb.)
- $x, y, p, t$  independent variables
- $K$  kinetic energy  $= \frac{u^2 + v^2}{2}$
- $\phi$  potential energy  $-gz$
- $v$  specific volume
- $q$  specific humidity
- $h$  terrain height (above sea level)
- $i, j, k$  unit vectors along zonal, meridional, and vertical directions

LIST OF SYMBOLS (CONTINUED)

- $\tau_x, \tau_y$  frictional stresses along x and y directions
- $F$  frictional force
- $W$  horizontal wind vector

## USE OF NUMERICAL PRODUCTS IN THE TROPICAL PACIFIC\*

R. E. Hughes  
Fleet Weather Central  
Pearl Harbor

### EXTENDED ABSTRACT

#### PACIFIC TROPICAL WIND ANALYSIS

A majority of USN, USAF and commercial flight operations in the Pacific takes place in the Tropics. To provide real-time environmental support for these operations, a cooperative USN, USAF, ESSA Weather Bureau Tropical Wind Analysis and Forecast Program is in operation at the Fleet Weather Central (FWC), Pearl Harbor. The program is run every 6 hours on one of two CDC 3100 computers. Primary data source is the AWS Automated Weather Network (AWN) from Tinker, AFB relayed from the Fleet Numerical Weather Central (FNWC), Monterey, California. A secondary input is from several weather circuits which terminate in automatic magnetic tape collectors at FWC Pearl. Maximum emphasis is placed on utilization of aircraft reports. RAOBS and PIBALS are used to determine wind shear values by which AIREP winds are spread to the closest standard levels for which analyses are prepared. On the average 550 RAOB/PIBALS and 2200 AIREPS are used in the analyses each day.

Wind analyses are prepared for the 700-, 500-, 400-, 300-, 250- and 200-mb. levels. The analysis technique, developed by Vederman and Bedient [3], is a variation of the correction method. A first guess to the analysis is modified to fit all reasonable data. In areas where the data are sparse or nonexistent the first guess is adjusted toward a climatological mean wind field. The analysis is performed for the area bounded by latitudes 24° S. to 37° N. and longitudes 75° E. to 90° W. The area was recently extended to 60° N. South of 37° N., the first guess is the 6-hour previous tropical analysis. North of 37° N., a prognosis verifying at analysis time is extracted from a hemispheric prognostic chart produced by FNWC Monterey. The two first guess fields are merged, the data are inserted and the analysis is then performed. The analysis produces wind and temperature values at grid points which are separated by a distance of approximately 300 nm.

#### STREAMLINE ANALYSIS

Streamlines are fitted precisely to the analyzed winds. The method has been documented by Davis [1]. Analyzed wind directions are interpolated along selectively spaced lines at 0.1 inch intervals. These line segments are connected to produce each streamline. No subjective modelling constraints are placed on the streamline patterns.

#### WIND FORECASTS

Forecast winds are produced by a statistical technique developed by Lavoie and Weiseranders [2]. Lag correlation coefficients determined for each grid point are used to produce a persistence - climatology mix.

#### SOUTHEAST ASIA WIND ANALYSIS

The Tropical Analysis scheme with minor modifications is used to analyze 850-mb. winds over Southeast Asia. This program produced by Major Joern, USAF, uses a grid spacing of 150 nm. over the area bounded by the equator, 40° N., 75° E. and 140° E.

#### TROPICAL CYCLONE STEERING (TYRACK)

The Tropical Wind Analyses are used in a steering technique to forecast movement of tropical cyclones. The cyclone is treated as a point vortex embedded in a steering flow obtained by smoothing the analyzed winds at several individual levels and at combinations of these levels. For each steering flow, the vortex

\* Un-sponsored



is first steered backward to a point in time for which the storm location has been fixed. The position determined in this manner is compared with the actual storm position. The steering flow which moves the storm backward in the direction closest to the actual movement is selected as the steering flow to be used in the forecast. The difference between the actual position and the position determined by the selected steering flow is added as a bias correction to the forecast positions.

#### REFERENCES

1. DAVIS, R., "A Computer Method to Generate and Plot Streamlines." ESSA Technical Memorandum WBTM PR - 5. 1969.
2. LAVOIE, R. and C. WEIDERANDERS, "Objective Wind Forecasting Over the Tropical Pacific." Scientific Report No. 1, Meteorology Division, Hawaii Institute of Geophysics, University of Hawaii. 1960.
3. VEDERMAN, J. and H. BEDIENT, "Computer Analysis and Forecasting in the Tropics." Monthly Weather Review, Vol. 92, No. 12, pp. 565-577. 1964.

#### DISCUSSION

KREITZBERG: What operational decisions are based on your wind-factor forecast? How close do they limit their fuel based on your wind forecast?

HUGHES: I can't speak for the operational people but I would expect that they use the wind factors for determining fuel load and other necessary flight planning information. I have no information on how close they might limit their fuel load based on our wind forecast.

RENARD: Why are you concerned with eliminating cyclonic outflow and anticyclonic inflow in your streamline analysis--for the scale of your computerized analysis?

Hughes: Only to improve aesthetic appearances. Prof. Ramage noted that under the influence of friction it would be expected that anticyclonic outflow and cyclonic inflow should predominate in the real atmosphere.

ATKINSON: It appears to me that the climatology-persistence mix for the first guess field should be higher than the ratio currently used. Perhaps something like 20 - 80 percent would be better. This would take you back close to climatology at 48 hours which we know is realistic from previous statistical wind studies.

HUGHES: The analysis is performed every 6 hours. Persistence should be the best available 6-hour prognosis.

MANNING: A greater weight was given to climatology in the past but user comments indicated this was undesirable. Our users are more satisfied with the present mix. This is probably because the users are concerned primarily with areas in which data is plentiful. A 20 percent climatology weight might be desirable in sparse data areas. Users were dissatisfied with the smoothing effect of climatology that wiped out features too rapidly in their opinion. Tendency since has been to favor persistence over climatology in the program. We have had no complaints recently on this score as patterns are thus retained longer. In data areas, data are drawn for. In nondata areas, a return to climatology after a few days does not seem to make a noticeable difference.

BRETT: I have a question concerning the 850-mb., 2 1/2 degree grid-computer analysis over Southeast Asia, developed by Major Joerne. Is this product being evaluated as a diagnostic synoptic analysis for operational use, possibly in Southeast Asia? If so, does the 2 1/2-degree product significantly improve the capability of the computer analysis to detect weather producing or suppressing systems?

HUGHES: It is now available for operational use. It can be improved by further evaluation but we are not placing much effort on this product at the present. Other products take higher priority.

# CONVECTION

SUMMER MONSOON STUDIES OF CLOUDS AND WEATHER OVER SEA  
UTILIZING SATELLITE DATA \*

John H. Conover  
Air Force Cambridge Research Laboratories

ABSTRACT

This report summarizes progress over the past 2 1/2 years. Studies range from the development of empirical relationships which can currently be applied in preparing forecasts in the field to more basic studies which are required for understanding the weather there.

A radar weather index, RI, was developed and calculated for each hour to provide a measure of precipitation activity over SEASIA. The index equals the percental coverage of radar echoes within a circle, whose radius is 50 n. mi., centered at the station. Indices were prepared for Tan Son Nhut, a suburb of Saigon, for 1966, 1967, and 1968 and for Pleiku, RVN and Ubon and Udon, Thailand for 1967 and 1968.

Comparison of the heights of pressure levels over Asia and the western Pacific Ocean with activity over the Indochina Peninsula, as represented by the average RI of the four stations, show that activity is first preceded by an increase in the 1000- to 200-mb. thickness over the vicinity of North Korea. This is followed by higher pressures at low levels over China which accentuates the monsoonal trough to the south. Optimum position of the trough for activity 6°-7° north or northeast of the area under consideration. When the trough develops in this position, relative to the station, cloudiness concentrates over or south of the station in a long W. - E. band. For some unknown reason, cloudiness 400 to 500 miles east of the stations, within the band, correlates best with the subsequent radar index. Preceding inactivity, thicknesses are below average over North Korea and the monsoonal trough and cloud band are absent or far removed from the area in question. It is believed that the activity is brought about by stronger winds and zonal shear which develops south of the trough. The significance of the shear lies in the generally accepted fact that deep convection in this part of the world must have its roots at low levels, usually below 900 mb., and ascent at low levels can be caused by convergence which in turn develops from horizontal shear in the Ekman layer. An attempt to prove this using combined gradient-level winds over land and ship surface winds to produce vorticity patterns failed. Suspected causes of failure are that the data were not representative of winds at a constant level within the Ekman layer, and the computer wind analysis smoothed the isotach patterns excessively. On inactive days a broad southwesterly flow is found at low levels over the peninsula. Shear patterns are lacking, and only over the highlands or near coastlines is there sufficient low-level convergence and ascent to set off important shower activity. Superimposed on this synoptic scale of events is the diurnal effect of the Indochina Peninsula. Due to lower diurnal pressure falls inland than on the coast, additional horizontal shear develops in the afternoon in some areas within the prevailing westerly and southwesterly winds. Maximum effect should be on the southeast coast. This, rather than the direct effect of destabilization due to solar heating of the ground, seems to be a logical explanation for the very large diurnal variation in RI at Tan Son Nhut. At that station the maximum RI occurs near 1900 local time and it is 12 to 13 times as large as the morning minimum. At the three inland stations, the diurnal range is significantly smaller although surface afternoon temperatures rise to virtually the same level as temperatures at Tan Son Nhut.

Mean values of kinematically computed vertical motions at five levels, which include the effects of topography, for the most part, yield logical average patterns in relation to the synoptic patterns and diurnal effect just discussed. However, on a day to day basis the observed winds in the form of vertical motions at all levels fail in explaining future cloudiness and RI or even current RI.

On the other hand, some significant forecasting aids have been found in the form of regression equations that employ the noontime, afternoon, or midnight cloudiness at key locations to give subsequent average RI over three or twelve hourly periods for 36 or 48 hours. The cloudiness can be viewed as a more positive manifestation of rising motion, thus avoiding the unsuccessful attempt of utilizing computed vertical motion. Also of anticipated value in forecasting,

\* Research sponsored by Air Force Cambridge Research Laboratory

are maps which show the relative frequency of all radar echoes or new echoes observed from Tan Son Nhut on active or inactive days over the four 6-hourly periods of the day.

An additional point of interest arose with the detection of fast moving (50 - 60 knots) sea-level pressure waves from the east. Although the relation between pressure and weather in SEASIA is far from clear, the pressure waves will be kept in mind in the search for effects that trigger or suppress activity.

## 1. INTRODUCTION

The aim of this study is to improve the forecasting of cloudiness and weather over Southeast Asia (SEASIA) through the supplemental use of data derived from satellites. Studies range from the development of simple empirical relationships which can currently be applied in preparing forecasts in the field, to more basic studies which are required for understanding the weather there.

This work has been underway for about 2 1/2 years. Over the first 1 1/2 years, three progress reports were submitted to the 1st Weather Wing for transmittal to field personnel. This report served as a fourth progress report. However, it differs from previous reports, for the benefit of new workers in the field, in that details of unsuccessful experiments are also discussed. The policy of outlining in this section the findings set forth in earlier reports continues; thereby, eliminating the need for their reference, at least for practical applications. All of the work applies to the months of June, July and August and relates primarily to video satellite data. The application of DRIR data to forecasting is included.

In the first report, dated 24 May 1967, it was noted that subsequent precipitation in the Saigon area was related to cloud patterns in the local noontime satellite photographs. Specifically, precipitation was indexed in the form of a "radar weather index," RI. The RI is equal to the percent coverage by echo within a circle, having a 50 n. mi. radius centered at the radar. In that report the radar used was located at Tan Son Nhut. The RI was computed hourly from coded CPS-9 reports commonly known as "RAREPS." Echo areas reported as "widely scattered" were considered 5 percent covered, as "scattered" 25 percent covered, as "broken," 70 percent covered, as "solid" 95 percent covered and as "cells" 100 percent covered. Each day's cloud photography was subjectively classified as one with or without a band. A band was defined as a major group of clouds which align themselves into a generally straight E. - W. or curved line between NW. - SE. or SW. - NE. Saigon must lie within 3° latitude north of the band. On "band" days subsequent afternoon RI values were high while on "no band" days they were low. Schematic and satellite photographic examples of "band" cases were also shown.

The first report also included information on the lift cycles of radar echoes. It was found that the most frequent lift of broken areas greater than 50 n. mi. in diameter was 3 to 4 hours. Echo duration for cells less than 20 n. mi. in diameter showed a very strong preference for one hour (the normal interval between observations). It was also found that echoes most often drifted with the 700-mb. wind flow at 60 to 70 percent of the wind speed.

The soundings for Tan Son Nhut over the three summer months were examined in respect to stability and subsequent activity. It was found that stability, as indicated by the Showalter index, was not related to subsequent activity. Since then, Bunting (3) found similar results using the Penn State convective cloud model.

It was also noted in the report that work was under way to develop an objective method of determining what areas of cloudiness in relation to Saigon are most important for classifying days as those with or without a band.

In the second progress report dated 23 August 1967 the objective method was presented. It substantiated the point that cloudiness over key areas east and south of Saigon indicates subsequent RI over the Saigon area. Regression equations were given which could be used to successfully predict RI up to 24 hours in advance from cloudiness at the key locations, even though it was warned that these results were based only on one year's data and not were tested on independent days. It was also shown that persistence forecasts fell below the new method after 4 to 5 hours.

The third report, dated 30 June 1968, dealt with new results obtained when an additional year of RI values was included with the data used to develop the previous relationships. These relationships were originally derived by considering 1500 LT<sup>1</sup> satellite data with noon cloud observations and a single season of RI values from Udorn, Ubon and Pleiku.

In past and present work, objective techniques are emphasized because the 1-year tour of duty for most forecasters, in that part of the world, simply does not permit the development of a high degree of skill, whereas objective methods provide a certain amount of "instant experience."

## 2. RELATIONSHIP BETWEEN CLOUDINESS, CURRENT AND SUBSEQUENT RADAR INDICES

### 2.1 Analysis

#### 2.1.1 Cloudiness

Cloud amount was obtained for 1° squares over the area from 3° N. to 25° N. and 94° E. - 125° E. Noontime data were used for the years 1966-1968 and in addition, data near mid-afternoon were used in 1967. Table 1 lists the data sources, median picture times and usable pictures for each season.

Table 1. Sources of Cloud Data, Picture Times and Usable Number of Picture Days.

Satellite	1966	1967		1968
	Nimbus II	Nimbus II	ESSA V	ESSA VI
Mode of data	AVCS	APT	Digital	APT
Median picture time (Z)	0400	0438	0800	0300
" " " (LT)	1200	1238	1500	1100
Usable days	34	43	85	84

NASA gridded the AVCS pictures for 1966; these were then mosaicked and read. For 1967 and 1968 APT tapes recorded at Tan Son Nhut were carefully rerun at the Laboratory and read using master grid overlays especially constructed for the satellite in use and the latitude of interest. Good landmarks provided grid accuracy of about 1/4° of latitude. Cloudiness was read by eye and was coded as follows: 1 = 0 to 0.2, 2 = 0.3 to 0.7 and 3 = 0.8 to 1.0 coverage. Those areas which appeared to consist of transparent cirrus were not counted. More detailed discrimination was not warranted in view of the picture quality and other problems related to the data.

Cloudiness observed at 1500 LT was obtained from the digitized ESSA V satellite data. These data expressed brightness in categories 1 to 5, with 5 representing the brightest. They were processed to give the percentage of categories 4 plus 5 in each 1° square. Experiment showed that a pattern, derived in this way, closely resembled one derived using the technique that was applied to the Nimbus data.

Originally the 1 x 1 degree cloud-code values were smoothed by averaging the four values which covered a 2° square and the average was assigned to the central grid intersection. Recent experiments showed that the correlations significantly improved as the smoothing was increased to 4 x 4 and 5 x 5 degree squares. Since the improvement was about the same for these two smoothing areas, it was decided to smooth all the data over 4 x 4 degree overlapping squares and still assign the

<sup>1</sup>Local time or LT in this report refers to the time used locally. In South Vietnam it equals Greenwich time +8 hours. Throughout the remainder of Indochina, it equals Greenwich time +7 hours. The latter corresponds to the time of the 105th meridian which roughly bisects the peninsula.

value to the central grid intersection. Smoothed cloud values arbitrarily required that at least 14 of the 16 one-degree cloud amounts be known.

The consistency of the cloudiness readings can be shown by (a) comparing satellite pictures before "noise" is removed, (b) comparing smoothed readings of the same picture at different times by one person, and (c) comparing smoothed readings of the same picture by three different people. Results of the first comparison are shown in table 2.

Table 2. Summary of 4° x 4° Smoothed Readings by Three Individuals of a Nimbus II AVCS Mosaic Dated 22 May 1966.

		Average
Individual D		1.69
" E		1.80
" F		2.08
	Std Dev.	Coef. of Variation
D - E	.18	10%
D - F	.18	9%
E - F	.17	9%

The average standard deviation for the entire picture varies  $\pm 0.2$  between individual frames, and the coefficient of variation between smoothed readings is about 10 percent. Comparisons of individual readings are summarized in table 3.

Table 3. Summary of 4° x 4° Smoothed Readings of an APT Picture Obtained On 9 July 1967, Orbit 5590 Frame 4.

		Average
Picture A (Min. of noise, read 7 Mar)		1.496
" B (Noisy, read 20 Feb)		1.685
" C (Min. of noise, same as A, reread 11 Mar)		1.435
	Std. Dev.	Coef. of Variation
A - B	.21	13%
A - C	.15	10%
B - C	.20	13%

It is interesting to note that cloudiness was overestimated on the noisy picture; average values were 15 percent too high. Once again the coefficient of variation between the smoothed readings of the normal picture amounted to 10 percent, an acceptable quantity.

#### 2.1.2 Radar Indices

Radar indices for Tan Son Nhut were computed by hand for 1966. However, due to the large amount of work involved, RAREPS for 1967 and 1968, were card punched and a program was written by Kelley [8] which would compute the percent covered within a 50 n. mi. radius. For 1967 each hourly observation was machine plotted on a scale where 1 in. represented 40 n. mi. The plots were made on transparent paper and bound to permit easy evaluation of changes over three stacked sheets of paper or 3 successive hours. Pertinent data concerning echo motion, tops and intensity accompanied each echo plot. As in 1966 a CPS-9 radar was used to obtain the Tan Son Nhut observations. WSR-57 radars were used at Udorn, Ubon and Pleiku to obtain the 1967 and 1968 data.

Since hourly precipitation measurements were not available, the only comparison between rainfall and RI that could be made had to be done for 6-hourly periods. This was done, using the Tan Son Nhut RI in 1966 and average rainfall from the following stations:

Tan Son Nhut  
 Bien Hoa, about 12 mi. NNE. of Tan Son Nhut  
 Vung Tan, about 40 mi. SE. of Tan Son Nhut  
 Vinh Long, about 55 mi. SW. of Tan Son Nhut

It is obvious that these stations sample the 50 n. mi. radius circle poorly but, for those interested, the correlations are presented in table 4.

Table 4. Correlation, r, and Number of Pairs, n, of Average 6-Hourly Rainfall vs. Average Radar Index, Tan Son Nhut, 1966.

	r	n	$\bar{RI}$
0155-0755 LT rain vs 0230-0730 LT RI	+0.59	80	4.0
1355-1955 LT rain vs 1430-1930 LT RI	+0.51	85	18.0

Correlations of +0.5 and +0.6 were found for respective periods of high and low  $\bar{RI}$ .

In spite of the poor correlations between  $\bar{RI}$  and average precipitation determined by scattered rain-gage stations, the radar index is believed to be a good index of precipitation activity. However, in order to determine the accuracy of RI values computed from RAREPS, a comparison between the computed areas of echoes as shown in the PPI and the coded RAREP during tropical showery conditions is underway.

The average diurnal curves for 1967 and 1968 of RI for June, July and August for Tan Son Nhut, Pleiku, Ubon and Udorn are shown in figures 1 through 4, respectively. These figures show that the noontime picture comes just after the index starts to rise at Tan Son Nhut, Pleiku and Ubon; at Udorn, however, the index is already relatively high at that time. The maximum diurnal variation occurs at Tan Son Nhut, the station nearest the coast, while the lowest diurnal variation is found at Udorn, the northern station, near the center of the peninsula. Afternoon pictures are made when the index has generally reached higher levels.

Figures 5 through 8 illustrate the hour-to-hour and day-to-day variations in the index during the 1967 season for the four locations. These figures dramatically illustrate the day-to-day variation which is precisely the forecast problem under discussion. They also indicate that active periods are generally of several days duration, and, when the action is strong, an index above zero is found throughout the day. Association of the patterns between stations is not particularly strong, although the patterns between Udorn and Ubon show some similarity in mid-June and late July.

Since the hour-to-hour indices vary considerably, the index, for practical purposes, is averaged over 3-hour intervals. These values are used to establish the cloud - RI relationships. The 3-hourly intervals are centered at 1030, 1330 LT, etc. The averages require that all 3 of the 3 hourly values be known, otherwise the average is listed as missing. Averages for 12-hour intervals over the period 1230-2330 LT, the most active period of the day, are also used. Arbitrarily, these averages require at least 9-hourly values out of the 12 for a valid average.

Early in the study days were classified as "active" or "inactive" according to the RI over the period 1230-2330 LT. No classification was made if more than 3 hours were missing. A day was classed as active when 5 or more hours of the 12 were above the monthly hourly averages; remaining days were classed as inactive. On this basis 30 days were active and 44 inactive in the 1966 season.

The classification of days was later changed from active and inactive to tertile 1 and tertile 3 days. The tertiles were determined by ranking all the daily 1230-2330 LT radar averages and dividing the list into highest, medium and lowest thirds. Tertile 1 pertains to the highest in activity while tertile 3 corresponds to the third of lowest activity. Although this reduces the size of the samples, the active and inactive features are more clearly stratified while the cases of middle level activity are eliminated.

## 2.2 Average Cloudiness at 0400Z (1100 or 1200 LT)

Average cloudiness over the 3 months determined from all available pictures in 1966, 1967 and 1968 is shown in figure 9. It should be noted that about half the values used in determining the averages came from the 1968 season. On the other hand, average maps for 1966 and 1967, not shown here, agree closely. The most prominent features relate directly to the topography. Cloud maxima occur over the Annam Mountains and along the windward (western) northern Malaysian coast. A secondary maximum appears along the windward (southwest) coastline of Cambodia. Minima are found to the leeward (east) of the primary maximum, especially along the northeast coast of the peninsula and over the adjacent part of the South China Sea.

## 2.3 Correlations and Their Significance

The technique was simply to perform a correlation between smoothed cloudiness at a grid point and the  $\bar{R}_I$  over some subsequent time interval, using all available days. When this correlation is done at all grid points, a map of correlation coefficients results on which the pattern, maximum value and location of maximum value are clearly shown. These points of maximum correlation and their appropriate regression equations are listed in Section 6, which concerns forecast applications.

The correlations were carried out for  $\bar{R}_I$  periods of 3 hours and the 12 hours of the afternoon up to 7 days after the cloud observations. This was done to determine: (a) how rapidly the coefficients decrease, (b) how the location of the maxima move, and (c) whether any recurrence of patterns is detectable. Only maps showing the correlation with subsequent  $\bar{R}_I$  for the 12-hour period, 1230-2330 LT, beginning just after picture time, are illustrated here to save space.

### 2.3.1 Cloudiness Read Approximately at 0400Z (1100 or 1200 LT)

#### A. Subsequent $\bar{R}_I$ over the period 1230-2330 LT, same day as the picture.

Tan Son Nhut From about 151 days of data over the three seasons, the area of maximum correlation, figure 10, is found some 7° - 8° east of the station with a secondary maximum on the southwest Cambodian coast. Correlations are positive indicating high cloudiness associated with high  $R_I$  throughout a W. - E. band across the map at about 10° N. Far to the north at 23° N. and to the southwest at 5° N., negative correlations signify a decrease of cloudiness with increasing  $R_I$ . The pattern is clearly one of an extensive W. - E. cloud band which runs just south of the station before active afternoons. Why cloudiness 400 miles east of the station correlates best with the subsequent  $\bar{R}_I$  is not understood. Obviously, this cloud mass does not advect to the station vicinity in the ensuing 12 hours.

Pleiku Correlations in respect to subsequent  $R_I$  Pleiku, figure 11, again take the pattern of a large scale W. - E. band, signifying excessive cloudiness with increasing  $R_I$  and vice versa. In this case, however, the maximum is found close to the station.

Ubon The inland station appears to be influenced less by an extensive cloud band, figure 12, although peak values are found along a line from near the station to the Vietnamese coast some 250 miles to the east.

Udorn The other inland station shows maximum correlations, figure 13, near the station and some 600 miles to the east and slightly south. The data do not suggest a large scale continuous cloud band due to the intervening low correlations, but the mysterious positive correlation far to the east is clearly evident.



These patterns show similarities in the form of maxima near the station, which can be interpreted as the effect of persistence, i.e., local cloudiness is followed by precipitation in the area, and a second maximum a considerable distance to the east. A large scale cloud band apparently runs W. - E. near the station and for some reason, far to the east, the variation in cloudiness is directly related to the following  $\bar{R}_I$  at the station. These patterns, along with average cloudiness and gradient-wind patterns on tertile 1 (active) and 3 days (inactive), will be discussed further in section 3.

B. Subsequent  $\bar{R}_I$  over 3-hourly periods the same day and the next day.

A listing of the locations, maximum correlations, number of days used, and regression equations used are given in section 6.

### 2.3.2 Cloudiness Read Approximately at 0700Z (1400 or 1500 T)

A. Subsequent  $\bar{R}_I$  over the period 1230-2330 LT the next day after the picture was reviewed.

Spatial patterns of correlations for radar indices at Tan Son Nhut, Pleiku, Ubon and Udon are not reproduced here. However, significant maxima as discussed in section 2.3.1, are found for each of the stations at locations east of preferred points found for the local noon cloudiness vs. afternoon  $\bar{R}_I$  correlations. Since the correlations are significant, they are listed with appropriate regression equations in section 6. The regression equations have been modified to utilize cloudiness read by eye in coded form in place of original cloudiness in terms of percentages of categories 4 and 5.

B. Subsequent  $\bar{R}_I$  for 3-hourly intervals centered at 1630 LT, 1930 LT, 2230 LT, 0130 LT, 0430 LT, 0730 LT, 1030 LT and 1330 LT.

Before these calculations were made, it was thought that afternoon cloudiness might mask large scale patterns. However, the spatial distributions of correlations continue to display interesting banded patterns which change shape as the  $R_I$  time changes. The correlations are not significantly higher than those found with noontime pictures so they are not listed.

### 2.3.3 Cloudiness Read Approximately at 1600Z (2300 or 0000 LT) from the HRIR or DRIR.

For this correlation the amount of dense high cloud, (DHC) or "light tone" as depicted on HRIR photographs was used. Dense high cloud refers to solid cloudiness having high tops or cloudiness which indicates the greatest degree of "activity." Details concerning the interpretation and reading of the HRIR pictures derived from the Nimbus II satellite have been given by Hawkins [7]. Instructions concerning the reading of DRIR data from the new Nimbus II satellite for forecasting application are given in section 6.

A. Subsequent  $\bar{R}_I$  over the period 1230-2330 LT the next day.

Tan Son Nhut Only 1966 data were available. Therefore, correlations could only be made for Tan Son Nhut. The number of days used in the correlations range from about 50 near the center of the area, to about 30 along the eastern and western edges of the area. These DHC values were originally read over one degree squares centered on degree intersections, therefore, the  $4^\circ \times 4^\circ$  smoothed values are assigned to the  $1/2$  degree latitude and longitude positions. The pattern of correlation coefficients is shown in figure 14. Once again the primary maximum is found 10 degree to the east with a value of +0.60. A secondary maximum is found inland near the center of the peninsula; this is interpreted again as the reflection of persistence. In fact, in section 4, on radar weather climatology, it will be shown that a concentration of echoes is found N. and NW. of Tan Son Nhut in the evening.

B. Subsequent  $\bar{R}_I$  over 3-hourly periods of the next day.

Maps showing the distribution of correlation coefficients are not shown, but the tabular data are included in section 6.

### 2.3.4 Significance and Analysis

It is difficult to assess the significance of the cloudiness - RI correlations and therefore the weight that can be placed on the forecasts which utilize the relationships. This is because of the small and different size data samples and the skewness of both the distributions. Due to the former, a given level of significant correlation will be found at lower and lower correlation coefficients as the number of pairs correlated increases. However, the sample now includes about 100 pairs except near the periphery of the area under study, so this is not considered serious. A more serious problem arises from the fact that the data sample has a skewed rather than normal distribution, and that standard significance tests cannot be used. The skewness of the sample alone provides a "built-in" correlation. To measure this effect the RI values were randomized and the correlations were repeated, thus utilizing the same skewed distributions. Comparison of a randomized correlation,  $r_r$ , with an actual correlation,  $r$ , provided the size of the data sample is about the same, will then indicate improvement. The comparison is made in the form of the difference in the percent reduction of the variance, of  $(r^2 - r_r^2)$ . This calculation was done for the cloudiness versus 12-hourly  $\bar{RI}$  relationships. The percent reduction ranged from 25 to 31 percent for the relationship of noontime cloudiness to 12-hourly afternoon  $\bar{RI}$  of the same day when approximately 38 pairs were correlated. For Tan Son Nhut, which involved 80 pairs, the difference was 24 percent. This decrease in difference is about that expected and is due to the larger data sample. For the 1500 LT cloudiness versus 12-hourly afternoon  $\bar{RI}$  of the next day the reduction ranged from 13 to 21 percent. Here, about 75 pairs were correlated. Since the reductions are consistently positive, even though of moderate amount, they are considered significant and therefore of forecast value.

Maximum correlations of noontime cloudiness with average afternoon RI up to seven days later naturally decrease as the lag increases. At Tan Son Nhut, Pleiku and Udorn the decrease is rapid over the first 24 hours. At Udon the maximum is actually higher at 24 hours (0.43 versus 0.40) than it is on the same day (day 0). For greater lags it too decreases. At lags of 4 or 5 days, i.e., cloudiness versus RI 4 or 5 days later, all of the stations show slightly higher correlations than immediately before or after this lag interval. This suggests a tendency for recurrence of better cloud - RI relationships at this time interval, an indicated periodicity which is also suspected in the sea-level pressure and wind regimes at high levels as discussed later in section 4. Positions of the maximum correlations over the lag period of 2 to 7 days oscillate in a region about 500 miles east of the station. However, since the correlations on days 3 to 7 have very little significance, the above can only be interpreted by saying that the first advance warning of subsequent RI appears about 500 miles to the east one or two days early, depending upon the station. On the next day maxima are found further west and on the same day (day 0) still further west as well as near the station. Thus, a general movement of weather from east to west is evident with continuity, although very weak, over a period of about 2 days.

### 2.4 Relationships Between Simultaneous Cloudiness and RI

This relationship has been computed by using the noontime video picture and and midnight IR picture. The correlation between cloudiness over the 4' x 4' box centered on Tan Son Nhut and the RI for the hour of the picture was found to be 0.56. 42 cases were used. This may be compared with Hawkin's [7] coefficient of 0.71, derived from 53 cases of RI versus the amount of dense high clouds as deduced from the High Resolution Infrared sensor on Nimbus II.

## 3. RELATIONSHIPS BETWEEN WINDS, CLOUDINESS AND SUBSEQUENT AVERAGE RADAR INDEX

A series of tests was made to determine how well the observed winds, convergence and kinematically computed vertical motion agree with the observed cloudiness and radar index. This section describes the results of these tests.

### 3.1 Wind Analysis

These analyses were made to yield winds at one degree grid intersections. A procedure developed by Barnes [1] and modified by Kreitzberg<sup>1</sup> is used. The program weights the observations according to a normal distribution in all directions to a distance of 5 degrees. Three iterations are made in the smoothing process, and final values are not given unless that point comes under the influence of two or more observations. Products of this analysis are considered far more consistent than subjective analysis, at least by those who have not had long experience. However, it is quite possible that the weighting should be made heavier along the wind and lighter across the wind to produce isotach patterns which are elliptical with their major axes parallel to the wind.

### 3.2 Resultant Winds at All Levels on Active and Inactive Days, as Defined in Section 2, in Respect to Tan Son Nhut, 1966

Resultant winds at 1 degree grid intervals from 7° - 25° N. and 95° - 115° E. were computed at 0000Z and 1200Z for each type of day. The patterns are merely described here because details at the gradient level and over a larger area will be shown and discussed later. The 0000Z analysis are emphasized because these correspond to 0800 LT, a map time that would be of some use in forecasting afternoon conditions.

Maps of the surface, gradient and 850-mb. levels at 0000Z show the southeastward extension of the continental monsoonal low as a shift in wind from SW. to S. and SE. On active days the trough line crosses the 105th meridian at 20° N., while on inactive days it is less pronounced and lies a few degrees further north. At these levels the westerlies were found to be stronger on active days than on inactive days over the entire area from 7° N. to 13° N.

700-mb. resultant wind charts were not constructed.

At 500 mb., 0000Z, the trough line, on active days was weak, and it meandered across the map from WNW. - ESE., crossing the 105th meridian at 12° N. On inactive days the trough was not clearly shown, and the anticyclonic circulation on the eastern side of the map had pushed further to the west.

At 300 mb., 0000Z, the area is dominated by the south and southeast flanks of the continental anticyclone. On active days the ridge crosses the 105th meridian at 23° N., while on inactive days it was located clearly off the map or north of 25° N. Winds at this level over Tan Son Nhut were virtually the same on active and inactive days.

Winds at 1200Z, which are measured in the middle of the time period that is used to classify the type of day, show very similar patterns to those just described. In fact, at low levels the trough is more pronounced, and at mid-levels (500 mb.) the same trough is discernible on active days, while on inactive days the trough is weak, and the anticyclone predominates in the east. At the 300-mb. level the patterns are similar but more pronounced.

Thus, the latitudinal positions of these features shift in phase at all levels, averaging somewhat further south or closer to Tan Son Nhut on active days as compared to inactive days.

### 3.3 Resultant Gradient-Level Wind for Tertiary 1 and Tertiary 3 Days 1967

Gray [6] has shown that upward motion must start below 900 mb. to produce deep convection in the western Pacific where conditionally unstable lapse rates predominate. We find the same thermal and moisture structure over Tan Son Nhut, therefore, in the search for the initial forces that lead to general activity, emphasis has been placed on the gradient-level wind in 1967. The area covered for this phase of the study was increased to include 0° - 35° N. and 90° - 125° E. All available ship surface winds were incorporated as "gradient winds" with adjustment. Since radar data were available from Udorn and Ubon, Thailand and Peiku as well as Tan Son Nhut, for this year, maps were made in reference to activity at each of these stations. These maps are shown in figures 15

<sup>1</sup> Formerly of the Satellite Meteorology Laboratory, presently affiliated with Pennsylvania State University, University Park, Pa.

through 18. Since they were also made for comparison with cloudiness, it should be noted that the tertile days apply only for days when pictures were available and therefore, each tertile is made up of only 14 days.

Resultant flow patterns are much alike for the three northern stations, Pleiku, Ubon and Udorn, figures 16 through 18. For tertile 1 days, each figure shows a sharp trough which lies more or less W. - E., extending from the northern Tonkin Gulf, or slightly inland, toward the east. It was consistently located 6° to 7° north of the station. This finding is quite different from the conditions found by Bell [2] for Hong Kong. There, during maximum rainfall the trough averages 1° south of the station, and significant rainfalls are confined to times when the trough is within 4° of the station, either to the north or south. Divergence computations over SEASIA, now shown here, yielded values of  $-1 \times 10^{-3} \text{ sec.}^{-1}$  or more along the trough.

In the case of Tan Son Nhut, figure 15, the trough was about the same distance from the station, but convergence was found to concentrate just south of the trough.

Tertile 3 days, in contrast to tertile 1 days, show that the trough is far to the north, off or nearly off the map, except in the case of Pleiku, figure 16, where it is found 11° north of the tertile 1 position.

These patterns substantiate the findings from the 1966 maps and indicate that, on the average, a large area over the northeast corner of the map experiences southerly and southwesterly winds on tertile 3 days and northeasterly to southeasterly winds on tertile 1 days. Furthermore, on tertile 1 days, when the trough is further south, the westerlies are stronger over the southwest corner of the peninsula. This suggests that differences in the u component of the wind between key points the northeast and southwest would be of forecasting use. Key locations for this purpose were derived from the average u-component charts. They are given in table 5.

Table 5. Key Locations Which Yield Maximum Differences in the u-Component of Wind Between Tertile 1 and Tertile 3 Days. Gradient Level 1967 Nimbus II Cloud Days Only.

Udorn	11 N., 104 E. minus 24 N., 117 E.
Ubon	10 N., 105 E. minus 23 N., 113 E.
Pleiku	9 N., 106 E. minus 22 N., 120 E.
Tan Son Nhut	9 N., 105 E. minus 20 N., 113 E.

To test this relationship, correlation coefficients between the wind differences and subsequent RI's were obtained using the only the days with cloud data. This selection of days was made to facilitate the comparison of additional correlations to be discussed later. Results are given in table 6.

Table 6. Correlation Coefficients Between the Difference in Gradient Level u Component of the Wind at Key Locations at 0000Z (0700 or 0800 LT) versus the RI 1200-2330 LT.

	r	n
Udorn	.34	34
Ubon	.30	34
Pleiku	.39	39
Tan Son Nhut	.24	38

It is clear that on a day-to-day basis these criteria alone would yield poor forecasts of subsequent RI. Furthermore, inspection of the data does not permit the isolation of the extremes of RI according to these wind criteria.

Examination of the daily Hong Kong low-level synoptic charts indicates that the trough discussed above appears to contain a front until about 12 June. Then the front moves northward and gradually the monsoonal trough develops and oscillates around the same position. What significance this may have in regard to the correlations which cover the entire period is not yet known. Further interpretation of these patterns will be found under a later section on large scale constant pressure height patterns.

### 3.3.1 Mean Cloudiness on Tertile 1 and Tertile 3 Days, 1967

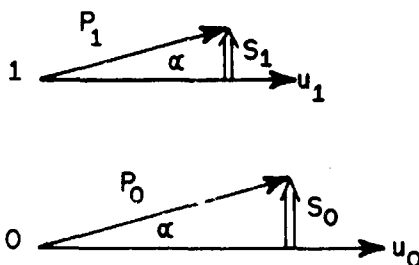
Mean cloudiness at local noontime for the same days is also shown in figures 15 to 18. Dashed lines were drawn where less than ten days data were used. For stations Udorn, Ubon and Pleiku on tertile 1 days cloudiness concentrates in a band south of the trough or from 1 to 5 degrees south of the computed maximum convergence. At Tan Son Nhut, the band of maximum cloudiness is found south of the station and also in poor agreement with the pattern of convergence.

On tertile 3 days the cloud band does not appear, at least south of 35° N., and the patterns are ones primarily of cloudiness over the mountains.

Maps of differences in average cloudiness between tertile 1 and tertile 3 days help to portray the cloud conditions. Figures 19 to 22 show these differences in terms of cloud code numbers for the four stations whose RI areas are shown as hatched ellipses. It should be noted that the E. - W. scale on these maps is about one and one-half times the N. - S. scale, thereby accentuating any E. - W. pattern. At Tan Son Nhut the presence of additional cloudiness, on active days, is clearly shown in the form of a long band centered south of the station. Suggestions of negative differences are shown at the top and bottom of the chart, thus indicating the presence of a large cloud band at a preferred location on tertile 1 days. At Pleiku, Ubon and Udorn similar but less pronounced cloud bands are found over the station on tertile 1 days.

### 3.4 Surface Frictional Induced Convergence

Charney and Eliassen [4] showed that low level vertical motion could develop from frictionally induced convergence. Such convergence develops when horizontal shear is found in the frictional layer as illustrated schematically below.



Let  $u_0$  and  $u_1$  represent gradient-level wind vectors at points 0, and 1. At a middle-level within the frictional layer, respective winds of  $p_0$  and  $p_1$  will be found at an angle  $\alpha$  to the gradient-wind direction. The northward component of shear, within the upper half of the two layers is shown as  $s_0$  and  $s_1$ . Since  $s_0 > s_1$  convergence is present. By similar reasoning under these conditions, convergence develops throughout the entire Ekman layer in the presence of cyclonic vorticity.

#### 3.4.1 Vorticity and Shear versus Subsequent $\bar{R}$

Details of the wind through the Ekman layer cannot be obtained over land and sea, therefore as an approximation, it is necessary to examine the gradient-level winds for horizontal shear. Even this could not be done strictly; winds 3000 ft. above the station were used over land and observed ship winds were used over the sea. These were processed as before, and vorticity was computed over 2° overlapping grid squares. Average relative vorticity maps for tertile 1 and

tertile 3 days in 1966 at Tan Son Nhut are shown in figure 23. About 28 days were used in each average. A major band of positive vorticity lies in a WNW - ESE. band across the maps; if one remembers the resultant wind maps for this level, much of this vorticity can be attributed to curvature of the flow. On tertile 1 days the band of positive vorticity crosses just north of Tan Son Nhut, while on tertile 3 days it is less pronounced and lies further north. On tertile 1 days anticyclonic vorticity averages slightly stronger in a W. - E. band south of Tan Son Nhut, thus causing a stronger gradient of vorticity over the Tan Son Nhut area on tertile 1 days as compared to tertile 3 days. The significance of this feature is not understood. Within the  $3^\circ \times 3^\circ$  local area centered on Tan Son Nhut, the vorticity averages  $+0.5 \times 10^{-5} \text{ sec.}^{-1}$  on tertile 1 days and  $+0.3 \times 10^{-5} \text{ sec.}^{-1}$  on tertile 3 days - a very small difference. It must be concluded that these average vorticity maps, derived from imperfect data, contribute little toward proving that activity follows convergence, which develops through horizontal shear in the lowest levels.

A correlation between average vorticity over a  $2^\circ \times 2^\circ$  square centered at Tan Son Nhut versus the  $\bar{R}_I$  from +3 to -3 hours from the wind-observation time was also poor. The following values were determined:

$$\begin{aligned} \text{Vorticity}_{0800 \text{ LT}} \text{ vs. } \bar{R}_I_{0430-0930 \text{ LT}} & \quad r = +.02 \\ \text{Vorticity}_{2000 \text{ LT}} \text{ vs. } \bar{R}_I_{1630-2130 \text{ LT}} & \quad r = +.33 \end{aligned}$$

The test used 21 - 29 days in June of 1966.

This conclusion was repeated after examination of the 0000Z, 1967 gradient level wind fields. In that case an unsuccessful effort was made to determine optimum paths over which the shear might be indicative of subsequent action.

#### 3.4.2 Pressure Gradient versus Subsequent $\bar{R}_I$

Another way of estimating horizontal shear at low levels is by the pressure gradient across the wind flow. This idea was explored by Dr. William Gray while on Reserve Duty at the Laboratory. Correlations of 0000Z MSL pressure gradients versus Tan Son Nhut  $\bar{R}_I$  1230-2330 LT the next day during the 1966 season were made between numerous coastal stations on the Indochina Peninsula and stations on the Malay Peninsula, islands of the South China Sea, Sarawak, North Borneo and Palawan. On a day-to-day basis, the highest correlation that could be obtained was 0.39 when the pressure gradient between Kuantan (48657) and An-xuyen (48914) was used.

These stations are located near Saigon and on the Malay Peninsula about 300 mi. to the south-southwest, a line which crosses the gradient-level flow at about  $40^\circ$ . A total of 67 days was used. If the  $\bar{R}_I_{0030-2330 \text{ LT}}$  of the next day is forecast, a slightly higher correlation of 0.42, based on 58 days of data, was found.

The observational data prove little toward substantiating the idea that convergence, ascent and activity may result due to cyclonic vorticity in the Ekman layer; however, the theory helps to explain the diurnal distribution of  $\bar{R}_I$  at the four radar stations. Reference to figures 1 through 4 shows that Tan Son Nhut experiences a large diurnal variation in  $\bar{R}_I$  with minima near 0800 LT and maximum near 1900 LT. At Pleiku the diurnal range is about half as large as at Tan Son Nhut but an afternoon maxima still occurs. At Ubon and Udorn minima occur in the morning but afternoon maxima are weak and the diurnal range is still less than at Pleiku. It is proposed that the large diurnal range at Tan Son Nhut is dynamic in nature rather than a result of increased instability due to surface heating. In fact, afternoon surface temperatures rise to exactly the same level at Tan Son Nhut and Udorn. Examination of diurnal pressure fluctuations over the peninsula shows that the smallest afternoon falls occur along the coast, while falls rapidly increase inland to a broad area which covers most of the interior of the peninsula. This difference, or pressure gradient, e.g., between Soc Trang (913), on the coast, and Tan Son Nhut (900) would cause a 20 knot geostrophic westerly wind whereas the pressure gradient between Tan Son Nhut and Ubon (407), located well inland, would cause a mere 8 knot westerly wind. Thus, within the prevailing westerlies at low levels, a zone of horizontal shear normally develops near the southeast coast each afternoon. This shear, as explained earlier, could produce

the "triggering" force which sets off convection and which ultimately leads to the high RI values at Tan Son Nhut in the afternoon. By similar reasoning, the effect should be less pronounced at Pleiku and non-existent at Ubon and Udorn, which corresponds nicely with the observed diurnal patterns of RI.

### 3.5 Relationships Between Cloudiness at Key Locations, Gradient Level Winds and Subsequent Average Radar Index

Although the relation between directly measured gradient-level shear or vorticity to subsequent RI was found to be low, the low-level shear as indicated indirectly from mean sea-level pressure gradients appears to be of some use. In order to seek further improvement, the latter was combined with cloudiness to forecast  $\bar{R}I$  of the next day. To make these correlations compatible, the  $\bar{R}I_{1230-2330 LT}$  instead of the full 24-hour period was forecast for the same sample of 30 days. Table 7 shows a slight improvement when both variables, cloudiness and pressure gradient, are used.

Table 7. Correlations of Pressure Gradient, Cloudiness, and Pressure Gradient Plus Cloudiness vs.  $\bar{R}I_{1230-2330 LT}$  of the Next Day for the Ton Son Nhut Summer of 1966.

- |   |
|---|
| 1) p (station 48914-station 48657) 0000Z vs. $\bar{R}I$ next day: $r = 0.36$  |
| 2) clouds smoothed $4^\circ \times 4^\circ$ (centered $12^\circ N.$ , $11^\circ E.$ ) 0400Z vs. $\bar{R}I$ next day: $r = 0.49$ |
| * 3) (1) plus (2) vs. $\bar{R}I$ next day: $r = 0.54$   |

\* The regression equation for (3) above is:

$$\bar{R}I = 9.6a - 7.9b - 0.8$$

where a signifies cloudiness, read on the scale of 1 through 3 and smoothed over a  $4^\circ \times 4^\circ$  square. The quantity, b, represents pressure gradient in mbs.

Tests of this relationship for 1968 will be discussed in Section 6.

### 3.6 Vertical Motion

In spite of the emphasis that has been placed on the lowest levels of the atmosphere as the layer in which the vertical motion begins, a study of this type would not be complete without further knowledge of vertical motion at all levels. A program to compute vertical motions kinematically from the observed winds at five layers and to include the topography was therefore developed. Winds were analyzed as before and vertical motions were computed twice daily over  $2^\circ$  overlapping squares to give values on a  $1^\circ$  mesh for the 3 months in 1966. Output levels were centered at 900 mb., 775 mb., 600 mb., 400 mb. and 200 mb. To minimize the "blow up" effect at the upper levels, values of vertical motion at 400 mb. were arbitrarily reduced by 40 percent of the unadjusted 200-mb. values the 200-mb. value was reduced to 20 percent of its original value.

#### 3.6.1 Diurnal Patterns of Vertical Motion

As a first approximation in determining the large scale diurnal effect of the Indochina Peninsula, average vertical motion,  $\bar{W}$ , was computed for all days at 0000Z and 1200Z or 0700 LT and 1900 LT (105 meridian time). The average patterns are shown in figures 24 through 26. About 89 days were used over the main part of the mesh to compute the averages. The number of days dropped to about 30 over the peripheral areas. At the 900-mb. level overall patterns, such as descent to the lee (east) of mountains in the Malay Peninsula and to the lee of the Annam Cordillera are similar morning and evening. The major differences

portrayed in figure 30, show that at mid-levels average ascent on tertile 1 days is two to three times as strong as on tertile 3 days. At the lower levels average values are about the same for tertile 2 and 3 days.

### 3.6.3 Active and Inactive Days at 0000Z

Now that reasonable differences in the mean patterns of vertical motion have been found at 1200Z the question arises, are there significant differences at 0000Z, 4 hours preceding the beginning of the defined period of action or inaction that might be used as forecasting aids? Mean maps for this time, based on about the same number of days, are shown in figures 31 through 33.

Examination of all the levels portrayed shows small differences of pattern or magnitude of the values between tertile 1 and 3 days except at the 900-mb. level. At this level the two bands of subsidence that run northwest and southeast on tertile 3 days are essentially crossed by a band of ascent at about 10° N. on tertile 1 days. The feature is barely discernible at the 775-mb. level. This west-east band of ascent agrees closely with the 0400Z cloud band found on tertile 1 days at Tan Son Nhut. In fact, the vertical motions over the sea, east of Tan Son Nhut, differ from upward on tertile 1 days to downward on tertile 3 days. This area is precisely where the highest correlations were found between cloudiness and subsequent RI activity, thus lending credence to the strange position of the maximum correlation.

### 3.6.4 Vertical Motion versus Simultaneous RI

Since it has been shown that the mean patterns of vertical motion are reasonable in relation to precipitation activity, the next logical question concerns the possibility of objectively predicting cloudiness and radar index from the observed vertical motions. In answer to this, several comparisons of the 1200Z (2000 LT) vertical motions over Tan Son Nhut and RI over varying periods of time, but centered at 1200Z (2000 LT) were made with a partial sample of the data. Highest correlations were found when the  $\bar{RI}_{1930-2030 LT}$  was used. It was therefore decided to correlate all days with this RI-time interval. Resulting correlations are shown in table 8.

Table 8. Correlations, r, at Different Levels and the Number of Days Used, n, of Vertical Motion at 2000 LT Over the Tan Son Nhut  $\bar{RI}$  Area vs.  $\bar{RI}_{1930-2030 LT}$  1966.

Level	900 mb.	775	600	400	200
r	.00	+.01	+.08	+.04	+.19
n	84	84	76	62	44

A relationship is conclusively nonexistent and therefore the possibility of predicting RI from vertical motions, at least computed in this way, is out of the question.

The vertical motion-cloud relationship was tested for three areas, each 3° x 3° in size. Vertical motion W was averaged over the 9° square and the central cloudiness value which had been smoothed over a 4 x 4° square was used. A valid vertical motion required that at least 8 of the 9 values be known. The correlations are shown in table 9. At the northern station some significance is found between increasing ascent and a subsequent increase in cloudiness. However, it is clear that these vertical motions cannot be used to predict cloudiness 4 hours later over the southern areas, at least when cloudiness is observed in this fashion.



Table 9. Correlations at Different Heights and Number of Days Used of Vertical Motion at 0000Z vs. Subsequent Cloudiness at 0400Z, 1966.

Area	900 mb.	775	600	400	200
9° - 11° N., 105° - 107° E.	-.05	-.11	-.09	-.11	-.09
(southern tip of peninsula)	43	43	41	36	25
14° - 16° N., 104° - 106° E.	.00	+.16	+.01	+.03	-.37
(centered at Udorn)	39	39	39	33	31
21° - 23° N., 106° - 108° E.	+.13	+.29	+.24	+.41	+.17
(NE of Hanoi)	38	38	26	17	17

To conclude this section, diurnal changes of average vertical motion and average patterns on active and inactive days have been illustrated. However, on a day-to-day basis significant relationships between vertical motion and current RI or cloudiness 4 hours later are all but nonexistent. It is quite possible that the vertical motions could be improved by using a weighting function in the wind analysis that would better portray elliptical isotach patterns oriented along the wind. It was originally hoped that the cloudiness values that may apply to any level would for the most part relate directly to the intensity of the convection. Since this relationship is not particularly high ( $r = +0.56$  for cloudiness versus RI), this also contributed to the poor cloud-vertical correlation.

#### 4. RELATIONSHIPS BETWEEN LARGE SCALE PRESSURE DISTRIBUTIONS AND SUBSEQUENT RI

In Section 3 it was shown that in the mean W. - E. or NW. - SE. trough was present 6° to 7° NNE. of the station on active or fertile 1 days. This trough on inactive days was found, in respect to Pleiku, 11° to the north, and for the other stations was either nonexistent or much further to the north, off the chart. Logical questions that follow are: is the trough really a trough at any one time? Is it the mean of many small lows or vortices positioned along a line? If the latter is true, where do they come from? Are there other pressure patterns more removed from the area covered that are characteristic of active and inactive days on the peninsula? Partial answers to these questions can be given from analysis of pressure over a rectangular area of about 20° x 30° and analysis of constant pressure heights over a much larger area of Asia and the Western Pacific.

##### 4.1 Sea-Level Pressure Analysis, 0° - 20° N., 93° - 120° E.

Day-to-day examination shows that the trough, generally known as the monsoon trough, really is a trough; it comes and goes sometimes in a couple of days, and often small vortices are found in it. These too often form and dissipate in a day or two. In attempting to understand these changes better, sea-level pressure versus time plots were prepared for six stations scattered over the area. These plots shed little light on the movement of vortices, but surprisingly enough, showed a pronounced tendency for minima and maxima at almost the same time over the entire area. Variations were on the order of plus or minus 3 mb. Closer examination hinted that the maxima and minima moved across the area at a high speed; therefore a crude analysis was made. This consisted of noting time differences of maxima and minima (in units of 24 hrs.) and dividing them into the distance between stations to yield an average speed. This overall average speed was 60 kt. from the east! The motion was most evident in the south and the station farthest north, at 16° N. (number 860), did not fit any pattern. A search of the literature showed that Frolov [5] had made a similar analysis over the Caribbean and adjacent areas. He emphasized a 4- or 5-day period, which is also suspected in SEASIA but not proven here, and he chose to call the pressure oscillations synchronous over the area. However, reanalysis of the published times of pressure maxima and minima in respect to Fort-de-France showed an average component from the east of 68 knots. More recent work by Maruyama [9] discusses what may be the same waves although they are most pronounced in the lower stratosphere.

Their wave length is 10,000 km. and they move toward the west at 50 knots. Although the relation between pressure and weather in SEASIA is far from clear, the phenomenon will be kept in mind in the search for effects that trigger or suppress activity.

#### 4.2 Pressure Patterns and Thicknesses Over Asia and the Western Pacific Ocean

In order to examine the large scale pressure patterns, heights of the constant pressure surfaces, 1000 mb., 850 mb., 700 mb., 500 mb., 300 mb. and 200 mb. were employed. Data supplied by the Global Weather Center at alternate grid points or about 400 miles apart were used. Heights at 0000Z each day for the three summer months during 1967 and 1968 were used with the exception of a missing period, 4 through 31 August 1968. All averages, correlations, etc., were referenced to the average  $\overline{RI}_{1230-2130 LT}$  of stations, Tan Son Nhut, Pleiku, Ubon and Udorn combined. This index is believed to be representative of the overall activity over the peninsula.

##### 4.2.1 Mean Height Patterns for Tertile 1 and 3 Days on the Same Day as the Afternoon RI

These average height maps, shown in figures 34 through 39, serve to depict large scale pressure patterns that are not always well known among newcomers to the area.

The primary features at 1000 mb. are the North Pacific high, eastern side of the North Atlantic high, weak polar low and Asian monsoonal low. The monsoonal trough that was discussed earlier in reference to the small charts is clearly shown in the average tertile 1 map; the most important feature that makes it a trough is the extension to the north of the Pacific high toward the west over southern China.

Figures 35 through 37, which depict the 850-mb., 700-mb. and 500-mb. averages, show that the monsoonal trough extends through the 500-mb. level on tertile 1 days, while on tertile 3 days its eastward extension is not discernible at 700 mb. and 500 mb. Patterns at 300 mb. and 200 mb. for each type of day are dominated by the polar low such that they appear to be essentially the same; however, actual heights do differ as we shall soon see.

##### 4.2.2 Average Difference in Heights at All Levels, Tertile 1 Days - Tertile 3 Days

Patterns at 1000 mb., 850 mb. and 700 mb., shown in figures 40 and 41, show relatively higher pressures over China on active days compared to inactive days, and lower pressures extending from India to Indochina and far out into the Pacific. It is interesting to note that the greatest differences, other than over the polar region, are found south of Japan. Difference patterns at 500 mb. and 300 mb., illustrated in figures 41 and 42, show an enhancement over China, while the lower heights on active days shift westward to a position south of China. At very high latitudes the differences indicate the presence of short waves superimposed on the large polar vortex. At the 200-mb. level, shown in figure 42, the differences clearly indicate higher pressure over North Korea and lower pressure over a broad belt extending from India to the Philippines on tertile 1 days as compared with tertile 3 days. These patterns were determined from a total of about 30 days in each tertile from two years of data; however, their significance is indicated by the fact that the same features over China and Indochina were found earlier using the same type of data for 1966 in reference to activity at Tan Son Nhut alone.

##### 4.2.3 Mean Differences in Thicknesses, Tertile 1 - Tertile 3 Days

Further understanding of the patterns just discussed can be attained by examining thicknesses which in turn can be considered in terms of the mean virtual temperature of layers of the atmosphere. Figure 43, the difference in thickness over the layer 200 mb. to 500 mb., shows large positive values (higher temperatures) over North Korea and lesser negative values over an area extending from India to China on active days compared to inactive days. The positive values over North Korea correspond to an excess in temperature of about  $2\frac{1}{2}^{\circ} C.$  and those over Indochina about  $1\frac{1}{2}^{\circ} C.$  on active compared to inactive days. The negative area over India and China that lies north of the low level monsoonal trough in the longitude of Indochina indicates a cooler air column on active than

on inactive days. The lower half of the atmosphere, depicted by the thickness 500 - 1000 mb., also in figure 43, again shows an excess in temperature, now of about 3° C., over North Korea, while the layer is cooler on active than on inactive days in the belt from India to far out in the Pacific. Over the area of RI we, therefore, have on active days, as compared with inactive days, cooler air in the lower atmosphere and warmer air in the upper atmosphere, a reasonable picture of deep convection and the release of latent heat. Differences for the entire column, 200 - 1000 mb. are shown in figure 44. Again on active days, as compared to inactive days, the area of the monsoonal trough is cool while the area near North Korea is warm.

#### 4.2.4 Patterns Preceding the Day of Classification According to RI

The above discussion described conditions on the morning of the same day as the 12-hour period used to classify the day as active or inactive. The logical question is: what patterns are found on preceding days and do they show continuity leading up to an active or inactive day? The data can be examined in at least two ways, by the areal distribution of correlation coefficients between thickness and RI on following days or as differences in thickness, tertile 1 - tertile 3 days on different days preceding the RI. The former has been computed but the magnitude of the correlations (0.3 to 0.4) does not diminish as the lag is increased to 16 days, thus indicating that this magnitude of correlation can be obtained at one place or another by chance. On the other hand, the positions of the maxima correlation do move in reasonable patterns, suggesting some continuity. Changes in the thickness difference patterns are not yet available. Therefore, the question at this time must be left unanswered. However, work along these lines will continue.

## 5. WEATHER RADAR CLIMATOLOGY

With the wealth of weather radar data available, a synoptic climatology can be developed for each station. For example, with maps showing the distribution of echoes at different times of the day, the distribution of new echoes and the tops of echoes are suggested. Furthermore, the above distribution can be made according to synoptic classifications. The work has just started at this writing; therefore, sample data for only one station, Tan Son Nhut using 1967 and 1968 data, will be presented.

A program was developed to provide the frequencies of echoes at 10 n. mi. grid intersections over a 400 x 400 mi. sq. with radar positioned at the center. Counts were built up at each grid point to represent a frequency using the weighting factors for "scattered," "broken," etc., which were discussed in section 1; thus, a grid point that fell within a scattered area was given a count of 0.25. The "frequencies" must therefore be viewed in relative terms.

When frequencies of echoes are tabulated at grid points covering the radar range, the highest frequencies are found near or a short distance from the radar and the numbers decrease to zero in all directions as the range increases. This distribution naturally does not represent the true distribution of echo producing rain; therefore, it would be desirable to make adjustments. Unfortunately, the fall off with range is much different than the theoretical fall off. Therefore, an empirical adjustment like that used by Weldon [10] was tried. The scheme was to derive the average fall off from data in all directions and then normalize to the value found at or near the radar. This process was tried, but the lack of reality became apparent when the overlapping patterns of adjacent, identical radars were normalized. For example, at the mid-point on a line between the two radars the observed frequencies might agree, as they should. However, frequencies near the radar sites might be quite different, a real climatological fact. After normalization, values at the mid-point between radars might differ according to which radar is used. For this reason, Weldon's normalization technique was not used. In its place ratios of the observed frequency/mean frequency at the specified distance from the radar were tried. These numbers tended to blow up where echo frequencies are small, so this type of presentation was also abandoned in favor of the simple listing of the observed frequencies at each grid point.

### 5.1 The Distribution of "New Echoes" and "All Echoes" Over 6-Hourly Intervals on Tertile 1 and Tertile 3 Days at Tan Son Nhut, 1967 and 1968

#### 5.1.1 Period 0000-0500 LT

Total echoes on active days, tertile 1 days, shown in figure 45, during this time interval are highest (41) about 25 miles northeast of Tan Son Nhut. Echoes

are also relatively frequent over the sea, especially over and seaward of the MeKong Delta. New echoes, figure 46, are most common in a band oriented WSW. - ENE. which passes about 70 miles south of Tan Son Nhut. A few echoes also form over the highlands toward the northeast.

In contrast, over the same period on inactive days, tertile 3 days, portrayed in figure 45, the highest frequency is 13 directly over the station. The pattern is more or less concentric over the station and not skewed toward the coastline. New echoes, figure 46, tend to be most common within a circle centered ESE. of the station with maxima still on or 10 - 20 miles southeast of the coastline.

#### 5.1.2 Period 0600-1100 LT

In this time interval the frequencies are minimum. On tertile 1 days, figure 47, they reach 16 and the most active areas are found about 25 miles WSW. of Tan Son Nhut and 30 miles SSE. New echoes are concentrated in a WSW. - ENE. band centered about 20 miles SE. of the station. This places the band parallel with the coastline and 20 - 50 miles inland. Thus, the area of the largest number of new echoes has advanced northward and inland about 50 miles from its earlier position. New echoes, shown in figure 48, are also observed on the western coastlines of the peninsula.

On tertile 3 days, figure 47, the highest frequencies are offshore with values of 10 - 12. New echoes, figure 48, on these days are most common along the coastline and in an area centered 50 miles WSW. of Tan Son Nhut.

#### 5.1.3 Period 1200-1700 LT

On tertile 1 days, depicted in figure 49, the echo frequency is 96 for this time interval. Highest values lie slightly east of the station but in general most of the echoes are over land. New echoes over this period, figure 50, are most frequent over land and just inland to the south and southeast of Tan Son Nhut, while another center of development shows in the foothills northeast of the station.

On tertile 3 days, in figure 49, the maximum frequency is only 24 but the overall area of echoes is about the same as on tertile 1 days. The new echo pattern, shown in figure 50, is also about the same, except about half the number as that found on tertile 1 days.

#### 5.1.4 Period 1800-2300 LT

During this interval echo frequencies are highest on active and inactive days. On tertile 1 days, figure 51, values reach 166, centered 20 miles NNE. of the station. The pattern is nearly concentric about this position, except for a few echoes which are found up to 200 miles away to the north. New echoes during this period, in figure 52, are most frequent 60 - 100 miles northwest and north of the station. On tertile 3 days frequencies, illustrated in figure 51, only reach 18 while the overall area of occurrence stretches from the southwestern tip of the peninsula to 200 miles northeast or well over the mountainous area. New echoes on tertile 3 days, portrayed in figure 52, are also most common in the N. and NNW.

### 5.2 Summary of Echo Patterns

The above observations, in respect to Tan Son Nhut show:

- a. Positions of the most frequent echoes are not very different on a tertile 1 versus tertile 3 days.
- b. Locations of new echoes on tertile 1 days tend to concentrate somewhat (0 - 50 mi.) WSW. or upwind of locations found on tertile 3 days; thus, placing more echoes in position to drift over the 100 mile radar index area as they develop. This conclusion is reasonable in view of the definitions of tertile 1 and 3 days.
- c. Positions of the most frequent new echo areas show a diurnal shift from the coastline over the 0000-0500 LT period to about 25 miles south of the station or slightly inland, for the 0600-1700 LT period to about 50 miles north or northwest of the station for the 1800-2300 LT period.
- d. Positions of the most frequent echoes lag behind (item c) by concentrating near the station at 0000-0500 LT, moving toward the sea for the next 12 hours, then shifting to the north and northwest for the evening period of 1800-2300 LT.

## 6. APPLICATION TO FORECASTING AND CONCLUSIONS

Much of this report has dealt with basic relationships between parameters such as vertical motion and attendant weather, as indicated by cloudiness or the radar index. These relationships have proved to be very poor, at least when the parameters were computed as they might be in the field or with a small computer. Therefore, techniques did not evolve that could be used by the forecaster, but at least the forecaster will realize that tests have been tried and that models must be far more sophisticated to be useful.

On the other hand, synoptic and cloud patterns have been found that characterize activity or inactivity, and objective means of utilizing these relationships for forecasting are presented.

### 6.1 General Synoptic Patterns During Active and Inactive Periods

Prior to activity over Indochina, the Pacific sub-tropical anticyclone appears to have pushed westward slightly; at least the air column from 1000-200 mb. is 2° - 3° C. warmer as compared to inactive days, over an area centered at 45° N., 123° E. or near North Korea. This difference shows as a 10 dkm. increase in heights on active over inactive days at the 200-mb. level. Just when this develops in time, preceding activity is not yet known but it definitely is detectable one to two days in advance. This pattern during active periods is accompanied by pressure rises over China at low levels which in turn accentuate the monsoonal trough. Optimum position of the trough for activity at a particular station is 6° - 7° north or northeast of that station. Along with the pressure trough, which is discernible to about the 500-mb. level, the westerlies increase to the south to create zonal shear. The significance of the higher shear lies in the generally accepted fact that deep convection in this part of the world must have its roots at low levels, usually between 900 mb., and ascent at low levels can be caused by convergence which in turn develops from horizontal shear in the Ekman layer. Mean cloud patterns show that on active days cloudiness concentrates in W. - E. bands south of the trough, or over and south of the stations. From these cloud patterns, a more positive manifestation of rising motion as compared to the kinematically computed vertical motion come the quantitative relationships with subsequent activity expressed in the form of the radar index.

Conversely, during inactive periods the monsoonal trough is absent or displaced far to the north and a broad flow of southwesterly wind is found in the lower troposphere. Shear patterns at low levels are lacking and only over the highlands or near coastlines is there sufficient low-level convergence and ascent to set off important shower activity.

Superimposed on this synoptic scale of events is the diurnal effect of the Indochina Peninsula. Due to larger diurnal pressure falls inland than on the coast, additional horizontal shear develops in some areas within the prevailing westerly and southwesterly winds. Maximum effect should be on the southeast coast. This, rather than the direct effect of destabilization due to solar heating of the ground, is proposed as a logical explanation for the very large diurnal variation in RI at Tan Son Nhut. At that station the maximum RI occurs near 1900 LT while at the three inland stations the afternoon maximum is weak or nonexistent. The geographical distribution of radar echoes as seen by the Tan Son Nhut radar also illustrate the diurnal change. In the early morning most of the activity is near the station. During the day the greatest activity lies between the station and the coastline and in the evening the activity shifts further inland to the north and northwest of the station.

Also oscillations of a global nature appear to be superimposed on the synoptic scale of events. It is quite conceivable that these oscillations enhance or suppress the current synoptic patterns. However, their isolation in the observational data has not yet been achieved.

### 6.2 Objective Aids to Forecasting the Radar Index

#### 6.2.1 The Use of Cloudiness

The cloud - RI relationships were discussed in detail in Section 2. Key cloud areas to be read and equations which use the coded cloud values to give RI for specific times and stations are listed in tables 10, 11 and 12. It is suggested that graphs of the equations be made for the periods of greatest interest, thus facilitating the predictions.

Rules to be followed are:

- a. For daytime pictures read single degree squares then divide by 16 to obtain an average. If more than two 1-degree squares are missing, do not use the equation.
- b. Daytime cloud readings are made according to the code specified in section 2; thin cirrus should be ignored.
- c. Dense high cloud, which corresponds to the "light tone" in the infra-red photography, is defined as having a corresponding radiative temperature of 245° K. or less. In the Nimbus III DRIR photography, the third gray tone from the left in the calibration wedge, on the right hand side of each picture, corresponds to a temperature of 244° K. Therefore, all photography as light as or lighter than the third step from the left is to be counted as dense high clouds.

Table 10. Correlations, r, Number of Pairs, n, and Regression Equations For Predicting Average Radar Index, Y, From Average Coded Cloudiness Over a 4° x 4° Square, x, Read Near Local Noon.

RI Predict Period (LT)	r	n	Center 4°x4° position °N      °E		Regression Eq.
Tan Son Nhut (based on 1966, '67 + '68 data)					
1230 - 1430	.45	136	11	106	Y = 11.9x - 7.0
1530 - 1730	.39	148	10	104	Y = 12.9x - 1.9
1830 - 2030	.51	147	9	113	Y = 20.2x - 7.7
2130 - 2330	.52	147	9	114	Y = 20.9x - 14.2
1230 - 2330	.55	151	9	114	Y = 14.8x - 4.5
0030 - 0230	.49	146	8	112	Y = 13.9x - 11.5
0330 - 0530	.43	130	13	118	Y = 7.5x - 7.0
0630 - 0830	.34	133	13	114	Y = 3.2x - 2.6
0930 - 1130	.27	100	9	119	Y = 2.9x - 1.9
1230 - 1430	.29	138	9	114	Y = 6.0x + 0.6
1530 - 1730	.33	130	11	116	Y = 9.0x + 5.6
1830 - 2030	.31	136	11	116	Y = 10.1x + 4.6
2130 - 2330	.46	108	6	121	Y = 18.6x - 11.5
1230 - 2330	.34	144	12	116	Y = 7.4x + 4.8
Pleiku (based on 1967 + '68 data)					
1230 - 1430	.53	103	13	105	Y = 8.6x - 4.4
1530 - 1730	.51	107	15	109	Y = 9.6x - 3.7
1830 - 2030	.56	116	14	110	Y = 11.2x - 6.6
2130 - 2330	.51	122	13	107	Y = 12.0x - 11.5
	(.62)	118	15	109	Y = 9.7x - 5.5
	(.62)	118	15	110	Y = 9.6x - 4.1
0030 - 0230	.56	118	13	107	Y = 14.5x - 14.8
0330 - 0530	.58	111	15	109	Y = 17.5x - 16.6
0630 - 0830	.53	95	10	115	Y = 10.9x - 9.9
0930 - 1130	.53	82	13	117	Y = 8.8x - 7.8
1230 - 1430	.48	100	11	107	Y = 8.4x - 4.2
1530 - 1730	.43	113	13	108	Y = 9.7x - 4.3
1830 - 2030	.47	104	12	115	Y = 9.3x - 4.2
2130 - 2330	.54	93	13	117	Y = 12.6x - 9.7
1230 - 2330	.535	104	13	116	Y = 8.2x - 2.8

Table 10. Correlation, r, Number of Pairs, n, and Regression Equations For Predicting Average Radar Index, Y, From Average Coded Cloudiness Over a 4° x 4° Square, x, Read Near Local Noon (Continued).

RI Predict Period (LT)	r	n	Center 4°x4° position °N °E		Regression Eq.
Ubon (based on 1967 + '68 data)					
1230 - 1430	.41	105	13	102	Y = 8.2x - 4.5
1530 - 1730	.34	116	16	104	Y = 5.5x - 0.8
1830 - 2030	.29	120	15	104	Y = 6.7x - 1.4
2130 - 2330	.44	113	13	107	Y = 13.4x - 12.6
1230 - 2330	.40	118	13	109	Y = 8.6x - 4.2
0030 - 0230	.37	113	15	107	Y = 12.1x - 11.4
0330 - 0530	.35	105	16	112	Y = 14.2x - 9.4
0630 - 0830	.34	109	14	112	Y = 10.8x - 7.8
0930 - 1130	.43	89	15	110	Y = 11.6x - 9.4
1230 - 1430	.37	96	13	114	Y = 6.1x - 2.0
1530 - 1730	.32	89	16	118	Y = 5.0x + 1.0
1830 - 2030	.45	90	17	118	Y = 12.1x - 6.8
2130 - 2330	.45	99	13	115	Y = 15.0x - 8.4
1230 - 2330	.43	108	13	114	Y = 8.5x - 1.5
Udorn (based on 1967 + '68 data)					
1230 - 1430	.42	104	15	105	Y = 11.7x - 6.4
1530 - 1730	.40	68	7	96	Y = 14.1x - 3.0
1830 - 2030	.38	115	16	105	Y = 8.6x - 3.9
2130 - 2330	.43	112	17	104	Y = 11.2x - 7.9
1230 - 2330	.43	112	16	104	Y = 7.7x - 0.5
0030 - 0230	.38	117	18	104	Y = 10.6x - 8.6
0330 - 0530	.42	111	19	107	Y = 14.8x - 11.1
0630 - 0830	.47	93	12	115	Y = 13.6x - 10.9
0930 - 1130	.35	88	18	108	Y = 10.0x - 7.1
1230 - 1430	.32	81	12	115	Y = 9.6x - 0.1
1530 - 1730	.25	107	23	104	Y = 5.2x + 4.2
1830 - 2030	(.33)	112	13	101	Y = 8.1x - 1.2
	(.33)	112	13	102	Y = 8.5x - 8.5
2130 - 2330	(.34)	94	13	115	Y = 11.1x - 1.7
	(.34)	94	13	116	Y = 10.3x - 1.3
1230 - 2330	.36	98	13	114	Y = 7.0x + 3.0

Table 11. Correlation, r, Number of Pairs, n, and Regression Equations for Predicting Average Radar Index, Y, From Average Dense High Cloud in Tenths Over a 4° x 4° Square, x, Read Just Before Local Midnight From the DRIR.

RI Predict Period (LT)	r	n	Center 4° x 4° Position °N °E		Regression Eq.
Tan Son Nhut (based on 1966)					
0030 - 0130 Next day	+0.76	49	9.5	105.5	Y = 0.47x - 0.20
0330 - 0530 " "	+0.57	46	9.5	106.5	Y = 0.25x + 0.19
0630 - 0830 " "	+0.61	27	11.5	111.5	Y = 0.30x - 0.85
0930 - 1130 " "	+0.64	28	14.5	115.5	Y = 0.45x + 1.4
1230 - 1430 " "	+0.53	37	16.5	113.5	Y = 0.83x + 6.8
1530 - 1730 " "	+0.53	33	9.5	117.5	Y = 0.60x + 14.0
1830 - 2030 " "	( +0.60	34	10.5	116.5	Y = 0.74x + 11.3
	( +0.60	34	11.5	116.5	Y = 0.63x + 12.6
2130 - 2330 " "	+ .40	34	11.5	118.5	Y = 0.25x + 5.6
1230 - 2330 " "	+ .60	35	11.5	116.5	Y = 0.42x + 10.0

Table 12. Correlations and Regression Equations for Predicting Average Radar Index, y, From Smoothed Coded Cloudiness, x, Read Near 1500 LT.

RI Predict Period (LT)	r	n	Center 4° x 4° Position		Regression Equation
Tan Son Nhut					
1230 - 2330 Next day	.43	8	1.	116° E.	y = 4.8x - 4.4
Ubon					
1230 - 2330 Next day	.40	82	N.	116° E.	y = 3.1x + 2.1
Udorn					
1230 - 2330 Next day	.44	66	7° N.	113° E.	y = 5.6x + 2.3
Pleiku					
1230 - 2330 Next day	.40	79	12° N.	115° E.	y = 3.7x + 4.8

- d. Due to the small scale of the DRIR photography on Muirhead recorders, a single reading over a 4° x 4° square will be necessary.
- e. An indication of the expected reliability of the forecast can be judged by the relative values of r, the correlation coefficient, in the table. Values below 0.4 are considered as little better than a crude approximation.

Some results of trial forecasts based on 1966 and 1967 or 1967 data alone to forecast 1968 RI 1230-2330 LT of the same day are given in table 13.



Table 13. RMSE and Number of Forecasts, n, Made For 1968  
 $\bar{R}\bar{I}$  Using Clouds, Persistence and Climatology.

	Clouds		Persistence		Climatology	
	RMSE	n	RMSE	n	RMSE	n
Tan Son Nhut	11.5	75	15.0	86	13.9	89
Pleiku	10.1	79	5.9	91	7.3	92
Ubon	10.5	80	11.6	91	11.2	92
Udorn	11.0	76	11.5	81	10.6	87

Success was scored only at Tan Son Nhut and Ubon while at Udorn the forecasts beat persistence but not climatology, and for Pleiku the method failed. Whether the new equations, based on another year's data, prove more accurate in 1969 remains to be seen.

#### 6.2.2 The Use of a Sea-Level Pressure Gradient

In section 3, a method of forecasting the  $\bar{R}\bar{I}_{1230-2330 LT}$  of the next day at Tan Son Nhut was described. It employed the sea-level pressure gradient, station 48914 - station 48657 at 0000Z as an indicator of low-level convergence, and cloudiness at a key location. When this was tested on 1968 data, the RMSE was 22.9 compared to 9.8 on the dependent data. The method was therefore abandoned in favor of the original method which used the pressure gradient alone to give  $\bar{R}\bar{I}$  for the full 24 hours of the next day.

The equation is:

$$Y = -4.4x + 6.4$$

where  $Y = \bar{R}\bar{I}_{0030-2330 LT}$  next day and

$x = \text{sea level pressure station 48914 minus station 48657 at 0000Z.}$

The 1968 forecasts from 1967 data then had a RMSE of 8.6, persistence gave 9.0 and climatology 7.9. These errors are noticeably lower than those shown in table 13 because they pertain to a 24-hour period and include the normally inactive part of the day. Since climatology gives the lowest errors, further details are not given.

We are therefore left with the fact that the only worthwhile objective aid to forecasting that has come from the study, up to this time, relies on cloudiness as observed from satellites.

## 7. ACKNOWLEDGEMENTS

The author wishes to acknowledge the help and suggestions of Dr. Carl Kreitzberg during the early phases of the studies, Mr. Thomas Keegan for review of the text, and Mr. Francis Valovcin for help in statistical analysis. The services of the following programmers are also acknowledged: Miss Carolyn Mandell, Mr. Edward Conway and Mr. Fred Wiggins, all under the direction of Mr. Donald Armstrong, Mr. Ronald Kelley, Miss Guansezlac Mitchell, Mrs. Helen Patten and Mrs. Elizabeth C. Grady. Mr. Rupert Hawkins supplied the HRIR data and Mr. James Bunting helped with the vertical motion calculations. Tabulations and calculations were performed by Mr. Michael Lorusso, Mr. Dennis Newton and Staff Sgt. John Hart. Thanks are also due to Mr. Richard Sizer who prepared most of the illustrations and Mrs. Helen Angier for typing the report.

## DISCUSSION

HULL: Did you try screening and multiple linear regression techniques on your data? Did you use persistence and attempt to find additional predictors?

CONOVER: I tried multiple regression, but I did not use persistence as one of the variables. Many predictors were attempted.

ATKINSON: What kind of correlation was there between the Radar Indexes at the individual stations?

CONOVER: Generally poor, i.e., 0.3 to 0.4 but it probably would have been higher if the proper lag had been introduced. Until 10 June systems moved from the north. After 15 June they moved from the south.

RAMAGE: In the friction layer, southwest flow along coast near Saigon is diverted more toward low pressure over land than over sea, because of discontinuity in surface friction. This might partly account for lack of correlation between vorticity and RI over Saigon.

CONOVER: It is a possibility, but the observed afternoon average pressure gradient Tan Son Nhut to Ubon would call for an additional 34 knot wouthwest wind so convergence due to shear may still outweigh your suggestion, provided some of the increased wind is over the water and I believe it would be.

KREITZBERG: The land-sea difference in frictional drag may be very small in the afternoon over the delta with southwest flow because of the decrease stability over the land with the daytime heating.

CONOVER: Agreed.

BELL: Two points: First, your correlations with thickness over Japan are a measure of monsoon activity. The Tibetan high forms a downstream trough and a ridge over the Sea of Okhotsk.<sup>1</sup> Second, Yoshino<sup>2</sup> has shown that at 100 mb. the westerlies over Japan are correlated with the easterlies over Bangkok and southeast Asia generally. The correlation coefficient is -0.81. These two references might help explain two of the correlations that you have found.

CONOVER: References are much appreciated.

## REFERENCES

1. BARNES, S. L., "A Technique for Maximizing Details in Numerical Weather Map Analysis." *J. Appl. Meteorol.*, 3:4, 399-409, 1964.
2. BELL, G. J., "The Monsoon Trough Near the South China Coast." *Royal Obs. Hong Kong*, 22 pp., 1969.
3. BUNTING, J. T., "A Note on the Application of a Cumulus Model in SEASIA Sounding Data." *Proceedings of the Conference on the Summer Monsoon of SEASIA, University of Hawaii, 7-9 April 1969, 1969.*
4. CHARNEY, J. G., and A. ELIASSEN, "On the Growth of the Hurricane Depression." *J. Atmos. Sci.* 21:1, 68-75, 1964.
5. FROLOW, S., "On Synchronous Variations of Pressure in Tropical Regions." *Bull. Amer. Meteorol. Soc.*, 23:239-254, 1942.
6. GRAY, W. M., "Global View of the Origin of Tropical Disturbances and Storms." *Atmos. Sci. paper no. 114, Dept. of Atmos. Sci., Colorado State Univ., Ft. Collins, Colorado, 105 pp., 1967.*

<sup>1</sup> Asakura, T., "Dynamic Climatology of Atmospheric Circulation Over East Asia Centered in Japan." *Pap. Meteorol. Geophys.*, 19, 1-67, 1968.

<sup>2</sup> Yoskino, M. M., "Atmospheric Circulation Over the Northwest Pacific in Summer." *Meteorol. Rundsch.*, 20, 45-52, 1967.

REFERENCES (CONTINUED)

7. HAWKINS, R. S., "Interpretation and Application of NIMBUS High Resolution Infrared Radiometer Data." Proceedings of the Conference on Summer Monsoon of SEASIA, Univ. of Hawaii, 7-9 April 1969, 1969.
8. KELLEY, R. G., "Design of a Digital Simulation of the Polar Planimeter for Calculating Areas of Echoes From Radar Weather Observations." Sci. Rpt. No. 2, AFCRL 68-0341, Analysis and Computer Systems, Inc., Burlington, Mass. 01803. Cont. #F19628-67-C-0125, 1968.
9. MARUYAMA, T., "Large-Scale Disturbances in the Equatorial Lower Stratosphere." Jr. Meteorol. Soc. of Japan, 45:391-408, 1968.
10. WELDON, R., "Initial Report, a Mid-Term Report of Personal Research Conducted on SEASIA Weather During June 1967." Prepared 6 May as an assignment for Meteorology #506, Dept. of Meteorology, Penn State Univ., College Park, Pa., 1968.

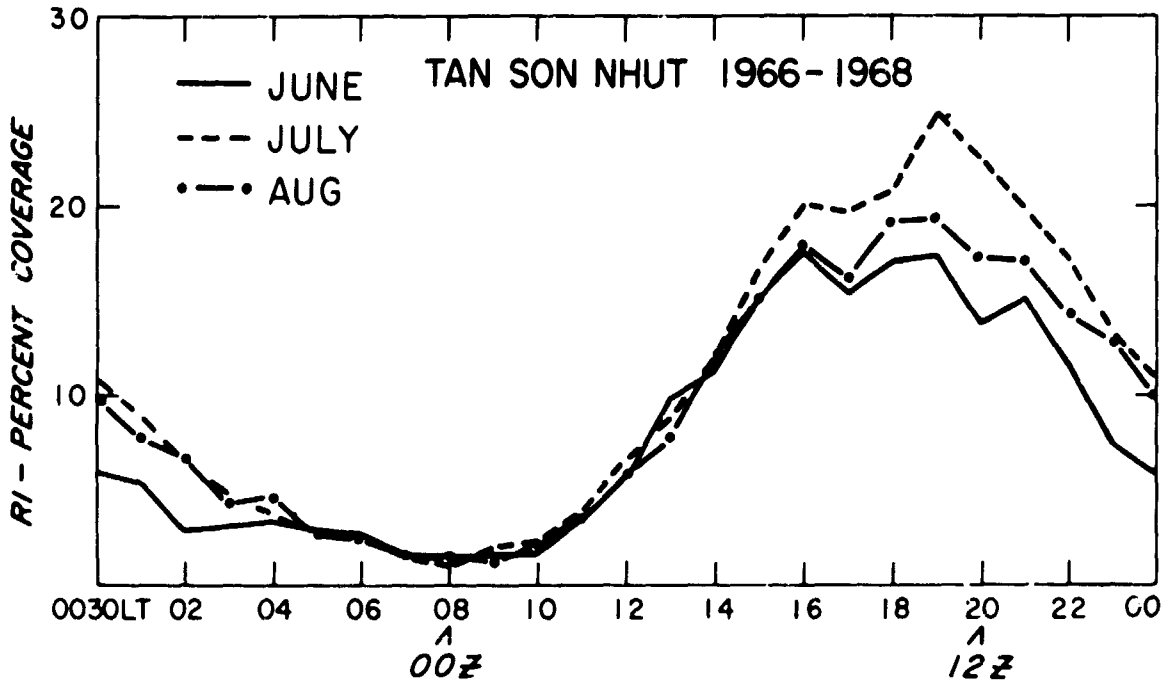


Figure 1. Summer Diurnal Variation of the Radar Index at Tan Son Nhut, 1966-1968.

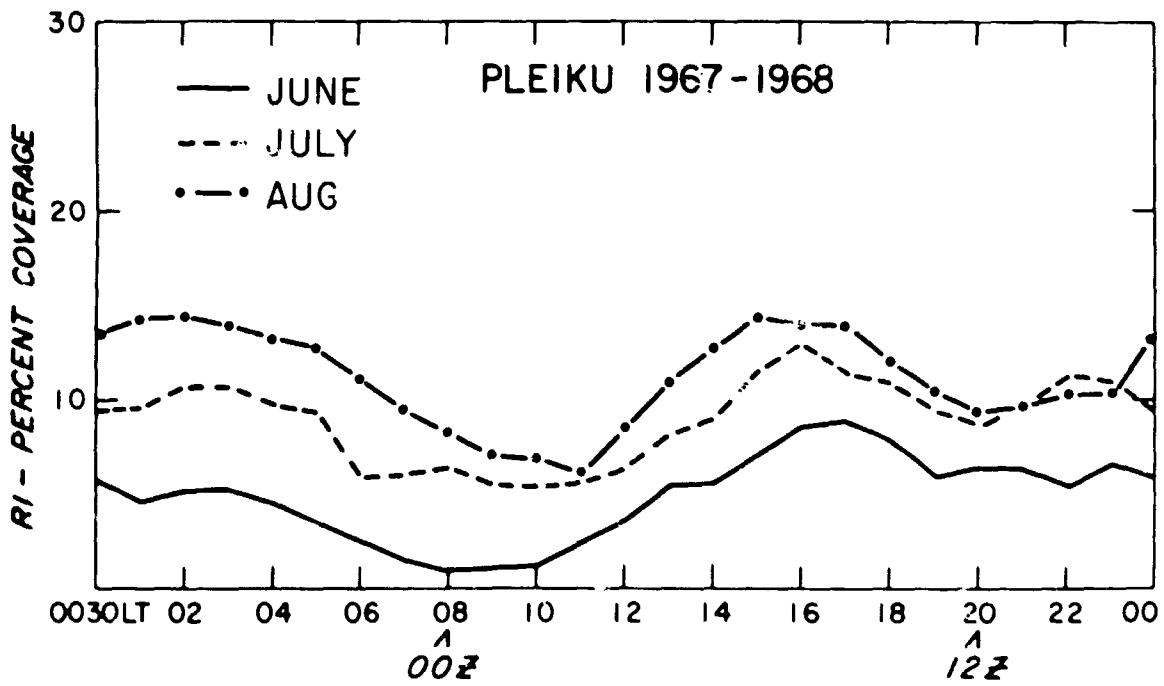


Figure 2. Summer Diurnal Variations of the Radar Index at Pleiku, 1967-1968.

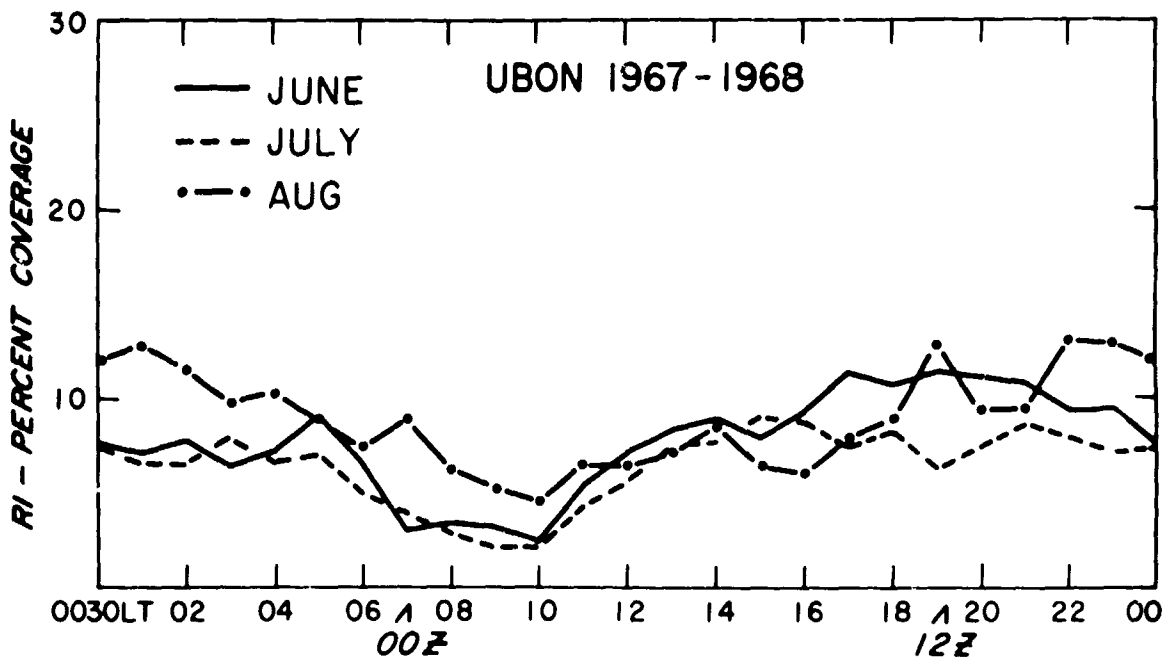


Figure 3. Summer Diurnal Variations of the Radar Index at Ubon, 1967-1968.

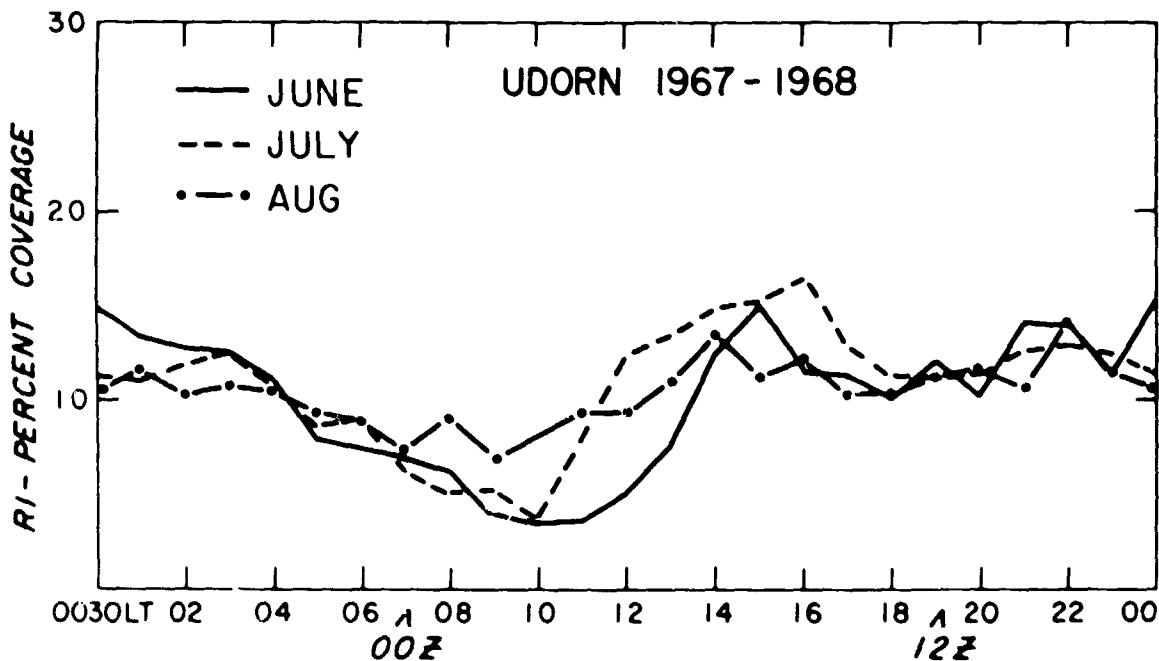


Figure 4. Summer Diurnal Variations of the Radar Index at Udorn, 1967-1968.

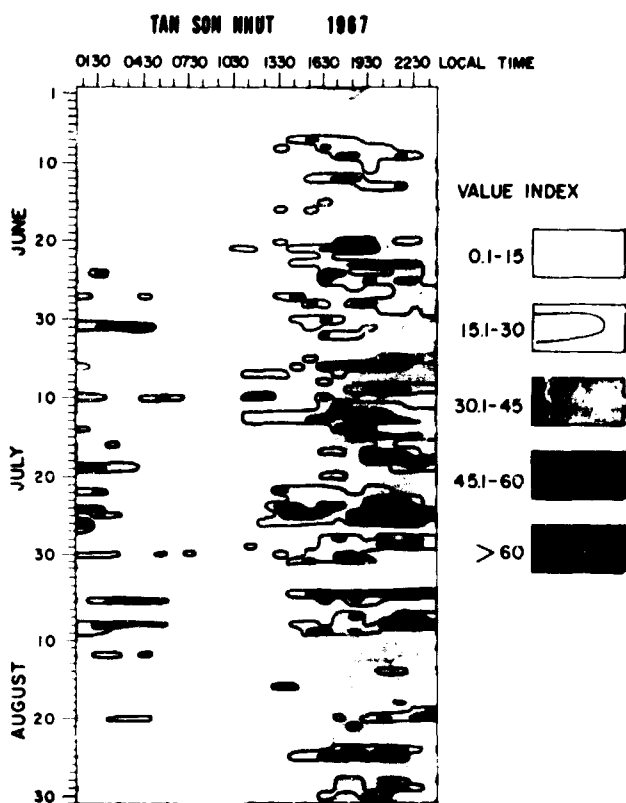


Figure 5. June, July and August 1967 Hourly Radar Index for Tan Son Nhut.

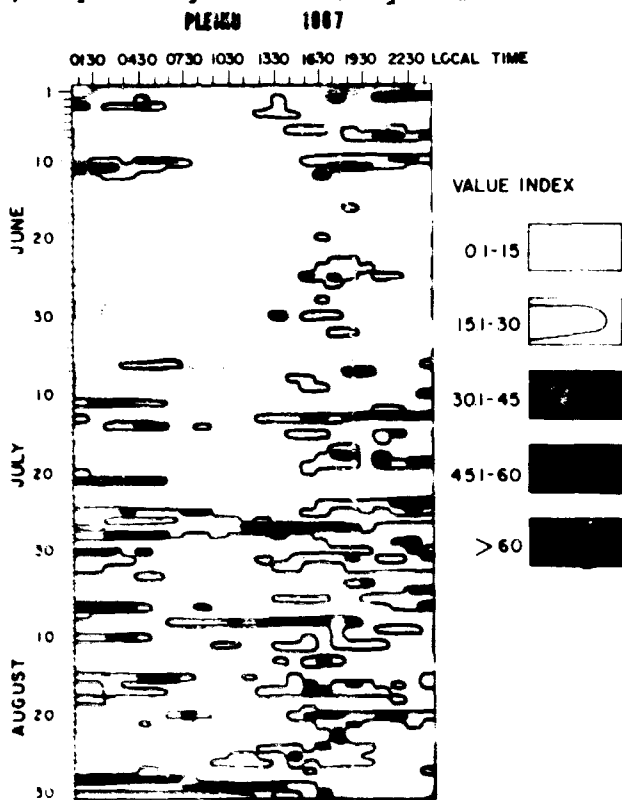


Figure 6. June, July and August 1967 Hourly Radar Index for Pleiku.

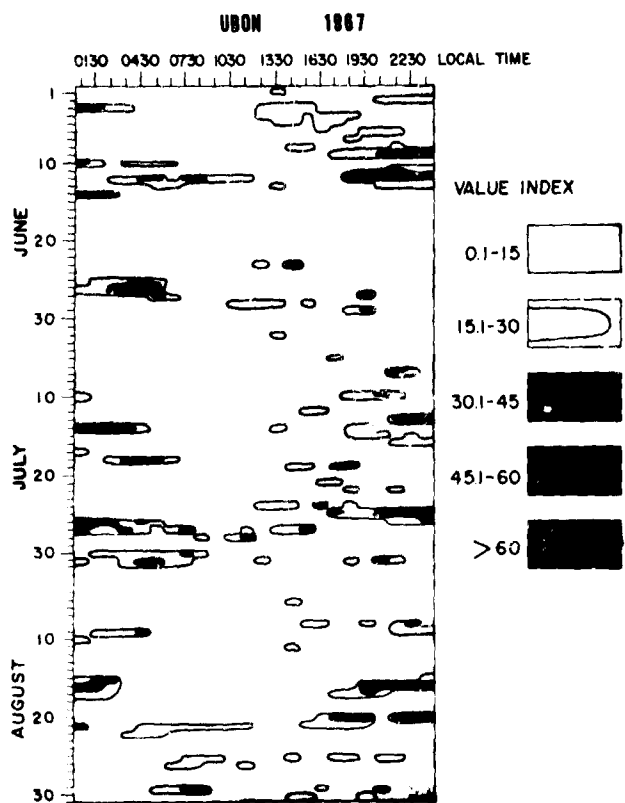


Figure 7. June, July and August 1967 Hourly Radar Index for Ubon.

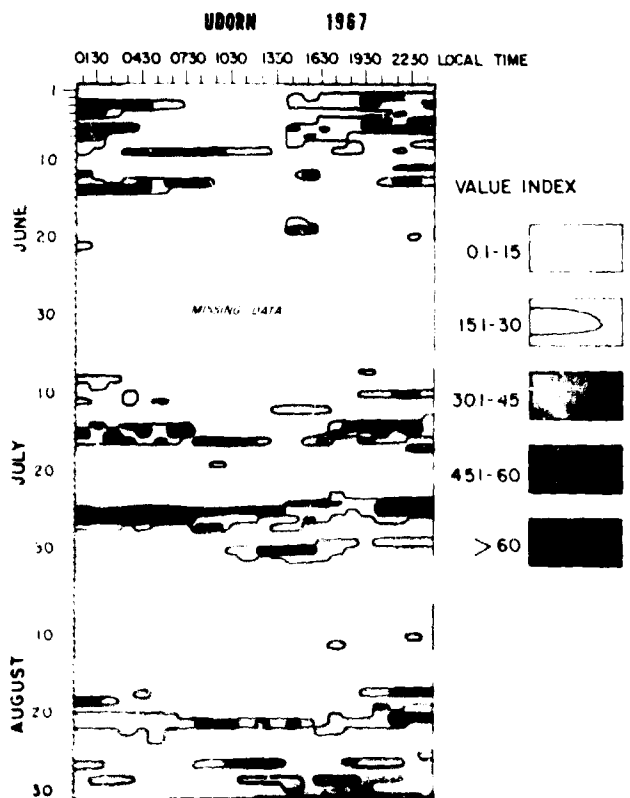


Figure 8. June, July and August 1967 Hourly Radar Index for Udorn.

NOONTIME CLOUDINESS, UNSMOOTHED  
JUNE, JULY AND AUGUST 1966, 67, 68

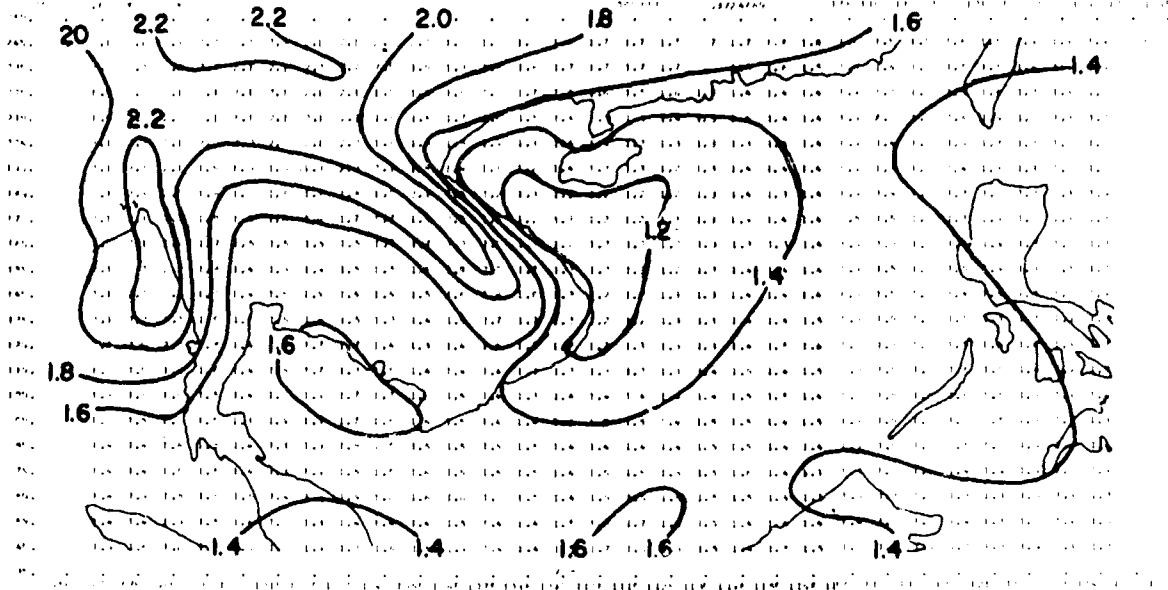


Figure 9. Average Noontime Cloudiness in Cloud Code Units, June, July and August 1966, 1967 and 1968.

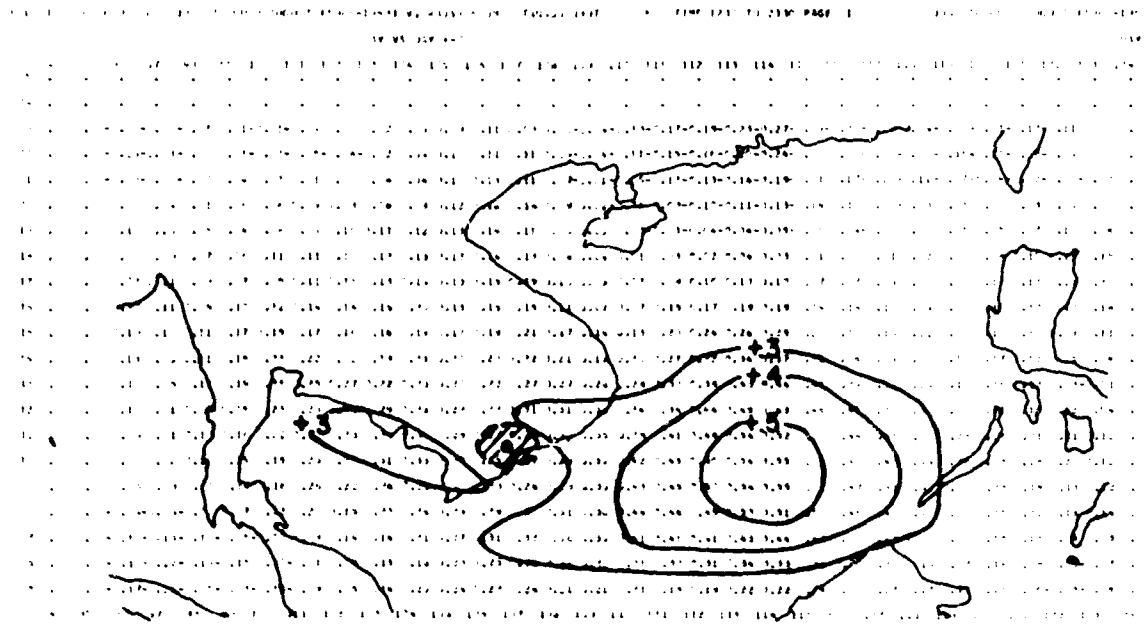


Figure 10. Spatial Distribution of Correlation Coefficients, Noontime Cloudiness vs. RI of the Same Day at Tan Son Nhut, 1966-1968 Data. Area of RI hatched.



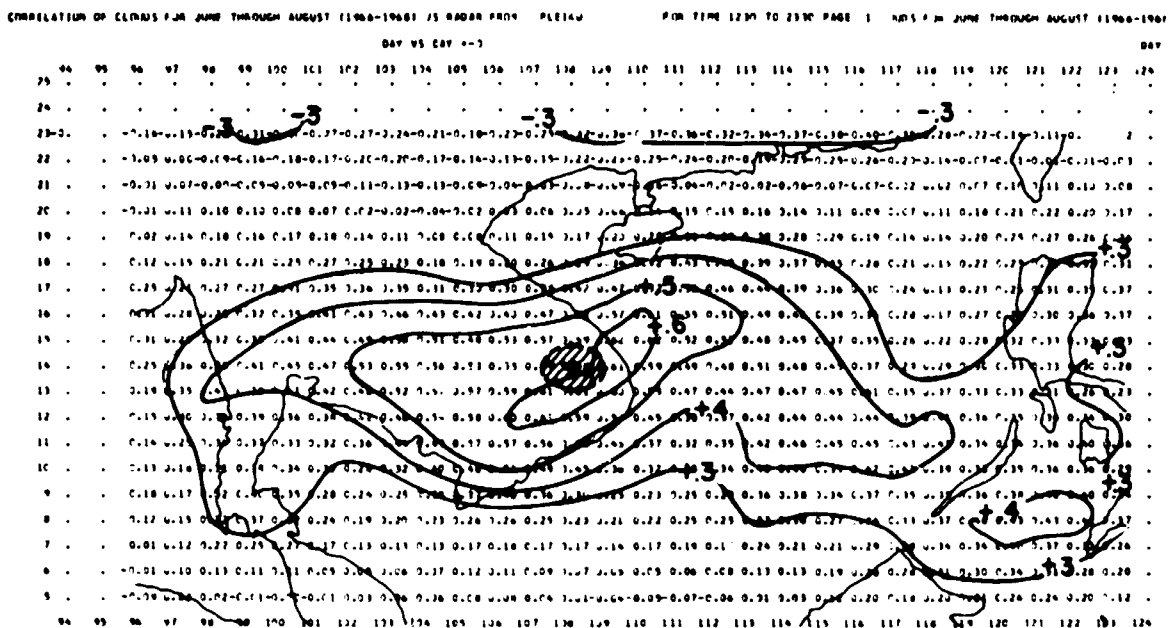


Figure 11. Spatial Distribution of Correlation Coefficients, Noontime Cloudiness vs.  $RI_{1230-2330 LT}$  of the Same Day at Pleiku, 1967-1968 data. Area of RI hatched.

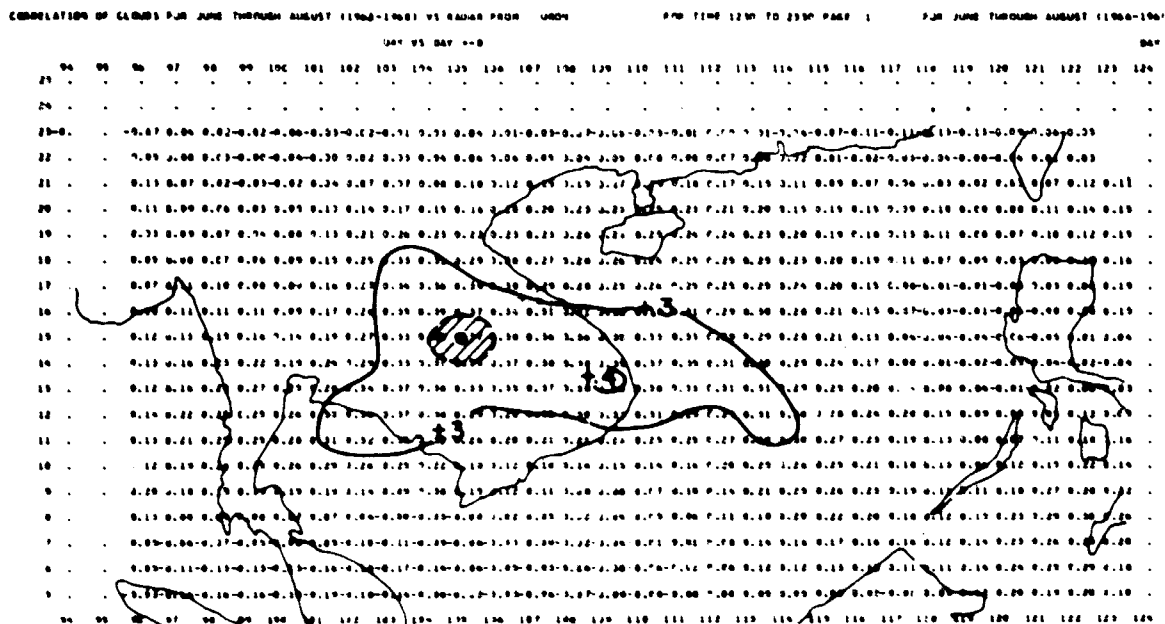


Figure 12. Spatial Distribution of Correlation Coefficients, Noontime Cloudiness vs.  $RI_{1230-2330 LT}$  of the Same Day at Ubon, 1967-1968 Data. Area of RI hatched.

NOT REPRODUCIBLE

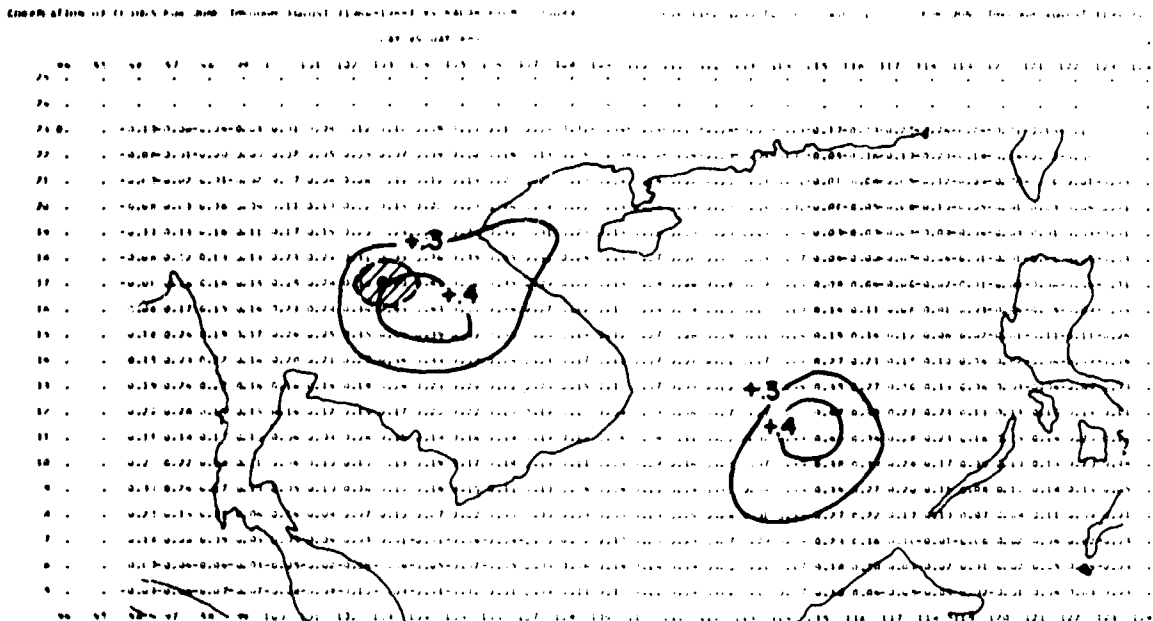


Figure 13. Spatial Distribution of Correlation Coefficients, Noontime Cloudiness vs. RI 1230-2130 of the Same Day at Udorn, 1967-1968 Data. Area of RI hatched.

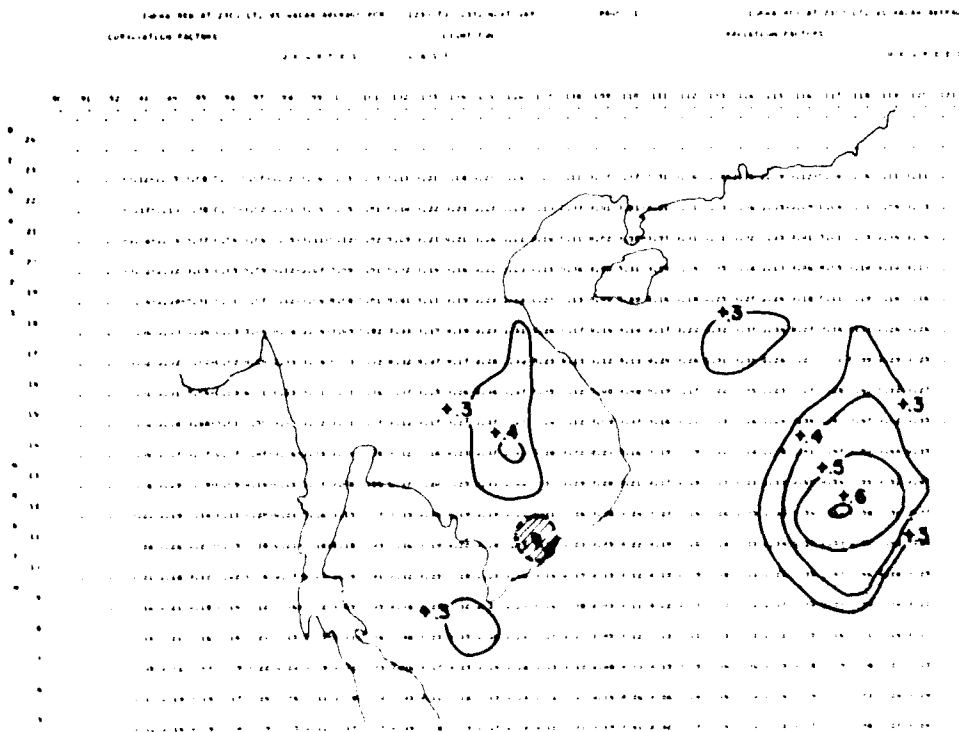


Figure 14. Spatial Distribution of Correlation Coefficients, Dense High Cloud Just Before Midnight, Read From the HRIR, vs. RI 1230-2130 the Next Day at Tan Son Nhut, 1966. Area of RI hatched.

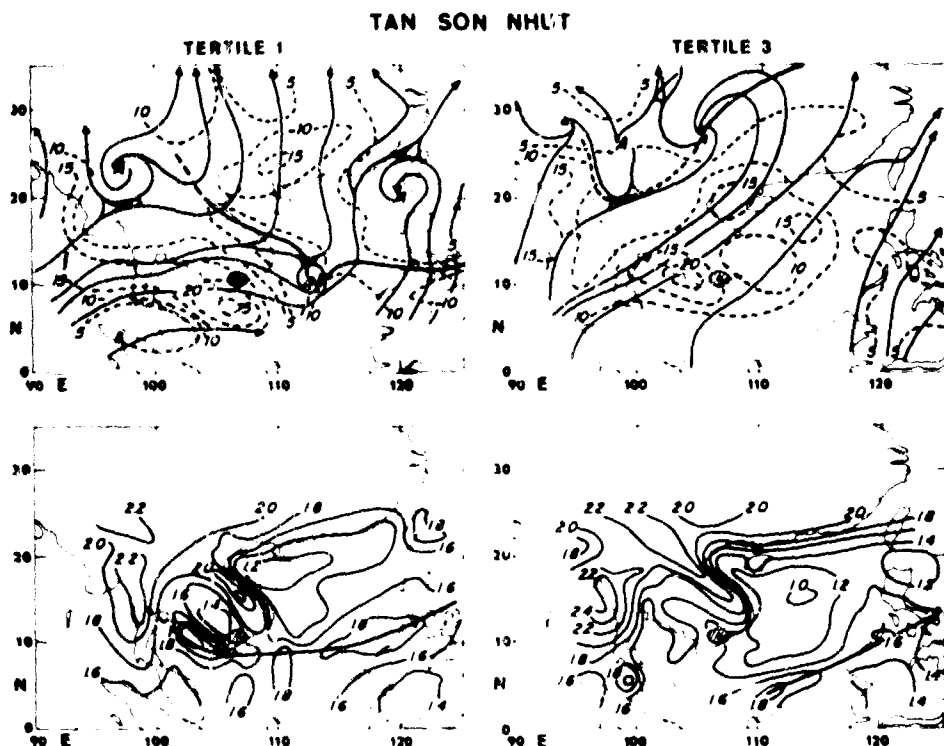


Figure 15. Gradient-Level Resultant Winds, Kts., and Average Coded Cloudiness for Tertile 1 and Tertile 3 Days at Tan Son Nhut, 1967. Monsoonal trough and cloud bands are marked by heavy lines. Area of KI hatched.

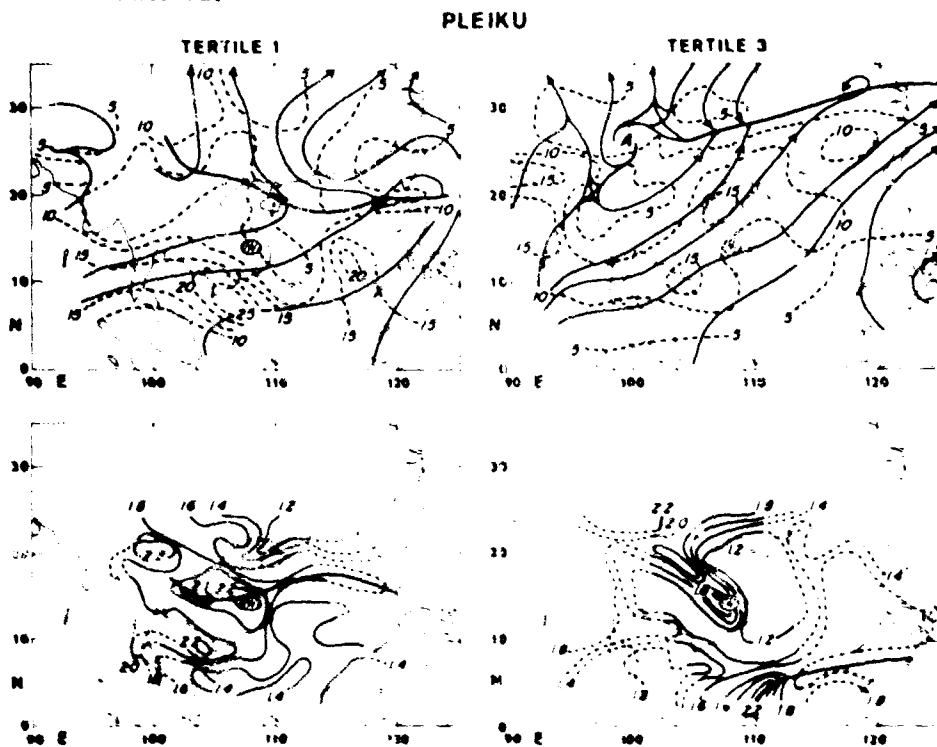


Figure 16. Gradient-Level Resultant Winds, Kts., and Average Coded Cloudiness for Tertile 1 and Tertile 3 Days at Pleiku, 1967 - Monsoonal trough and cloud bands are marked by heavy lines. Area of KI hatched.

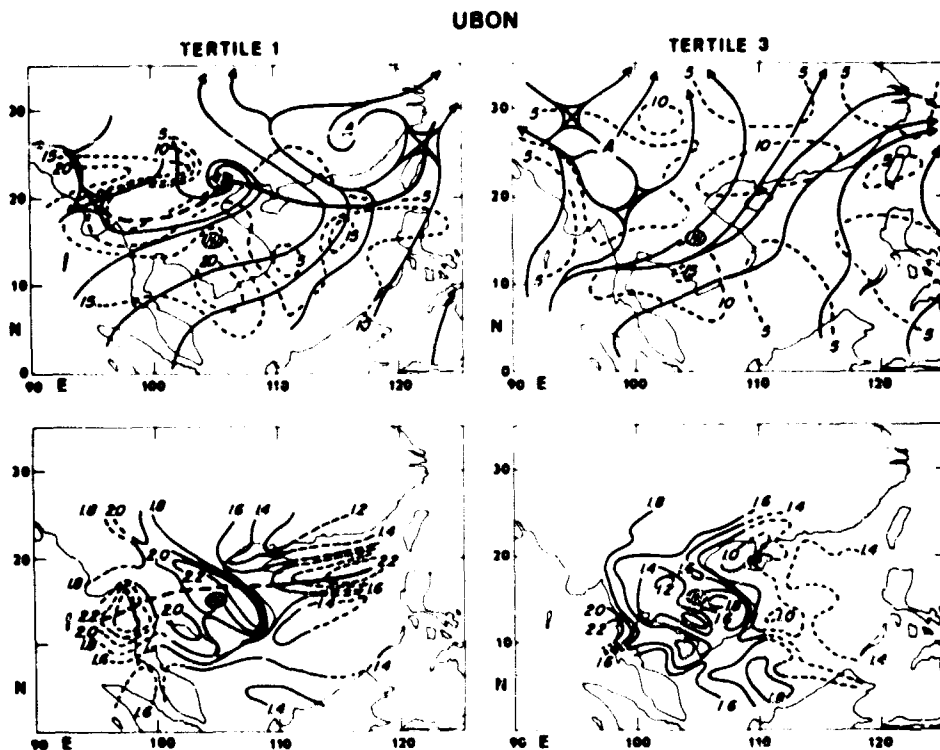


Figure 17. Gradient-Level Resultant Winds, Kts., and Average Coded Cloudiness for Tertile 1 and Tertile 3 Days at Ubon, 1967. Monsoonal trough and cloud bands are marked by heavy lines. Area of RI hatched.

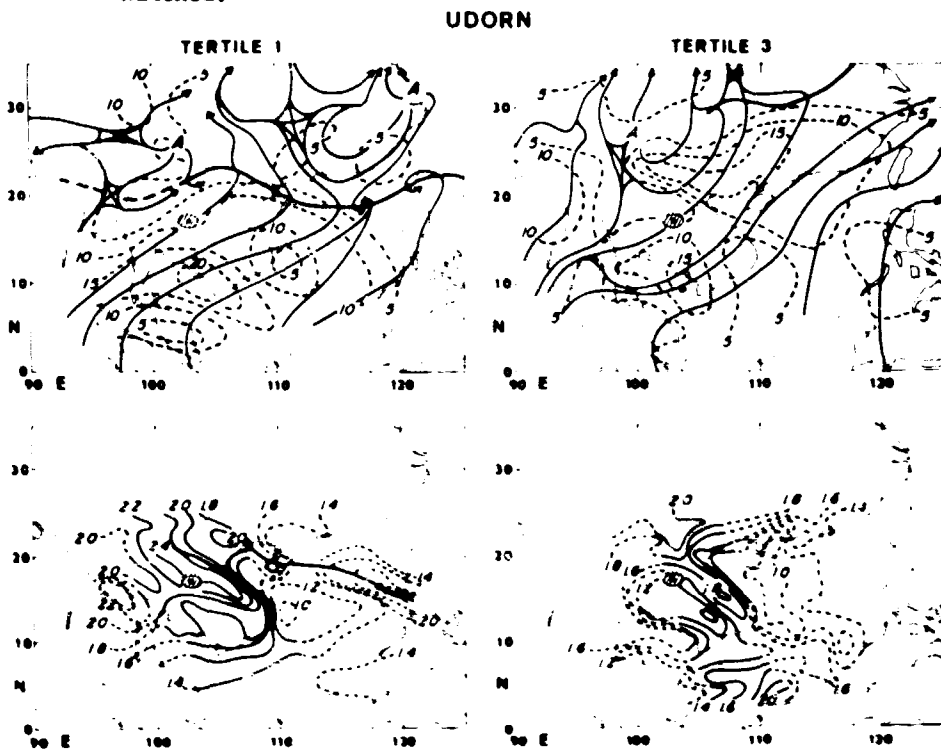
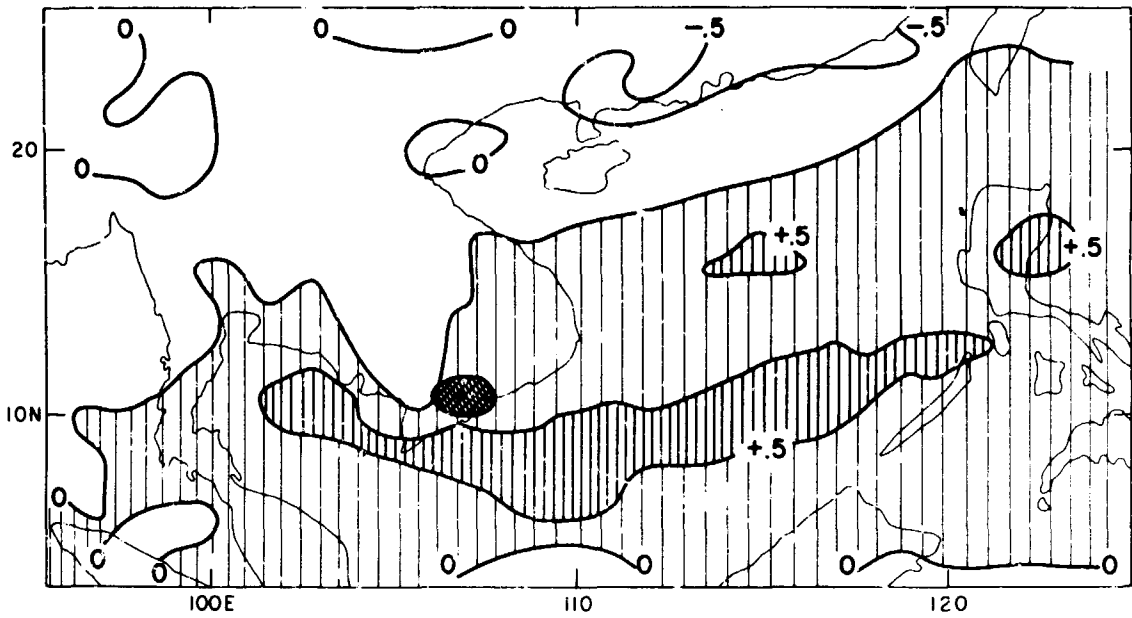
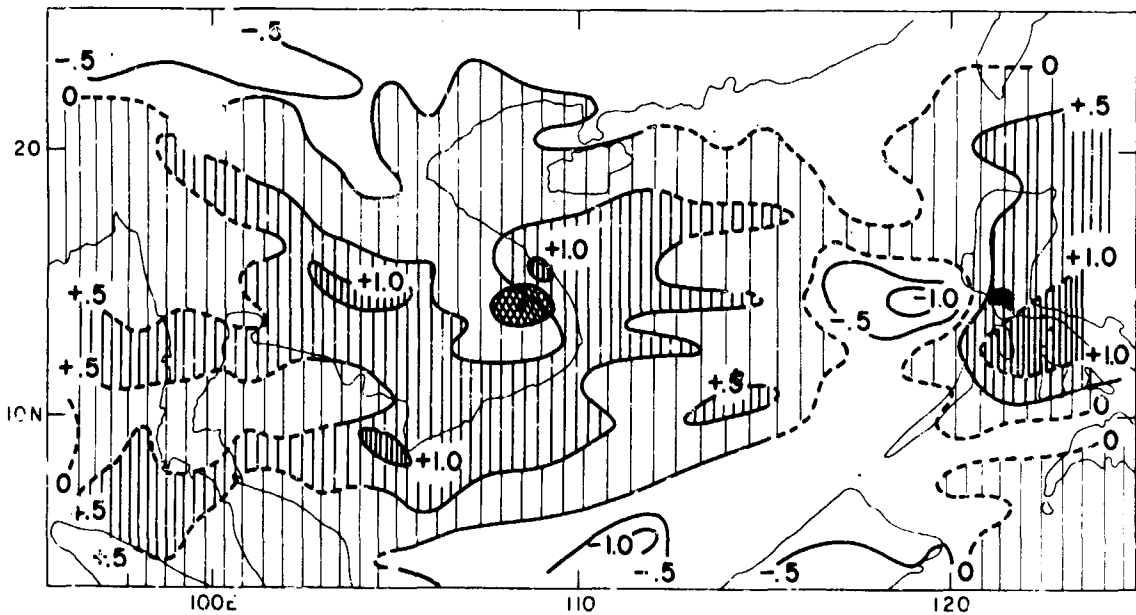


Figure 18. Gradient-Level Resultant Winds, Kts., and Average Coded Cloudiness for Tertile 1 and Tertile 3 Days at Udorn, 1967. Monsoonal trough and cloud bands are marked by heavy lines. Area of RI hatched.



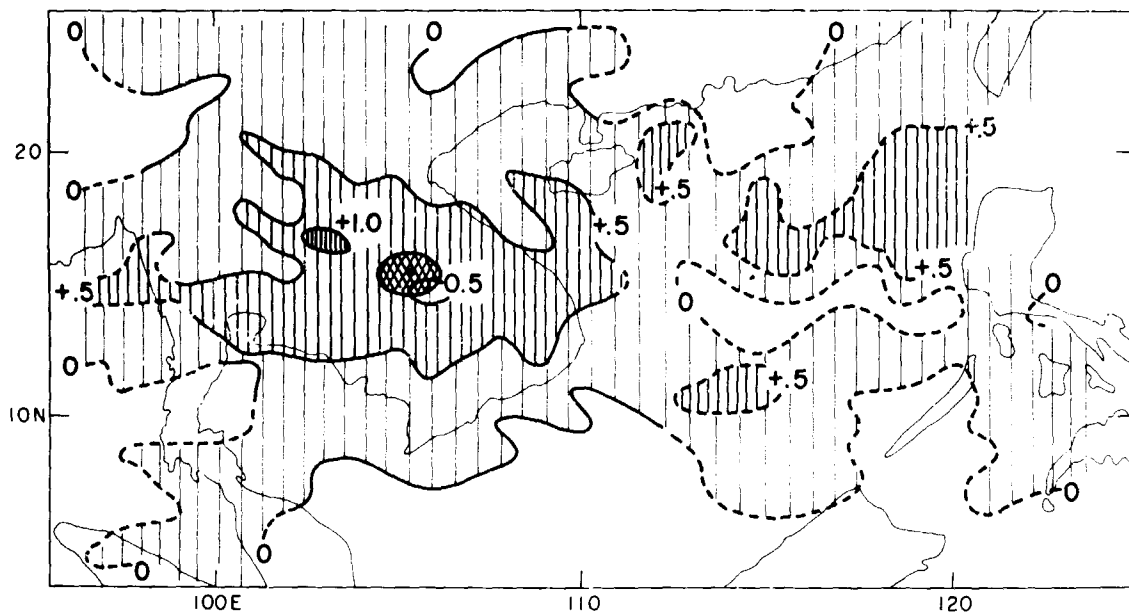
UNSMOOTHED AVERAGE CLOUDS TAN SON NHUT TERTILE 1 MINUS TERTILE 3 DAYS,  
JUNE, JULY, AUGUST 1966 AND 1967 NIMBUS II

Figure 19. Unsmoothed Average Coded Clouds Tan Son Nhut Tertile 1 Minus Tertile 3 Days, June, July, August 1966 and 1967, Nimbus II. RI area hatched.



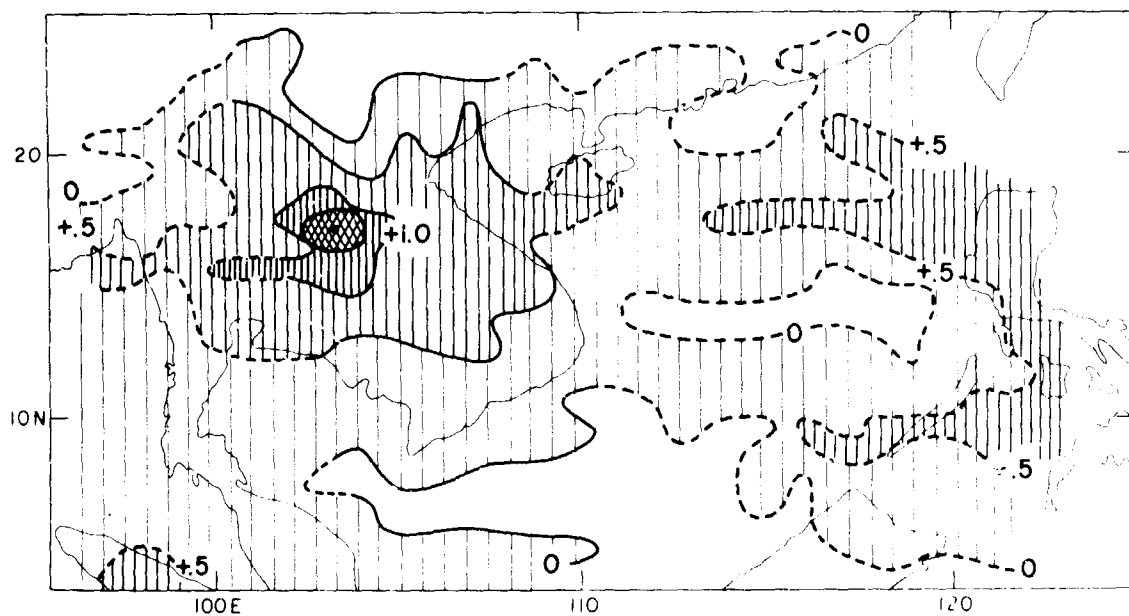
UNSMOOTHED AVERAGE CLOUDS PLEIKU TERTILE 1 MINUS TERTILE 3 DAYS JUNE,  
JULY, AUGUST 1967 NIMBUS II

Figure 20. Unsmoothed Average Coded Clouds Pleiku Tertile 1 Minus Tertile 3 Days, June, July, August 1967, Nimbus II. RI area hatched.



UNSMOOTHED AVERAGE CLOUDS U80N: TERTILE 1 MINUS TERTILE 3 DAYS JUNE, JULY, AUGUST 1967 NIMBUS II

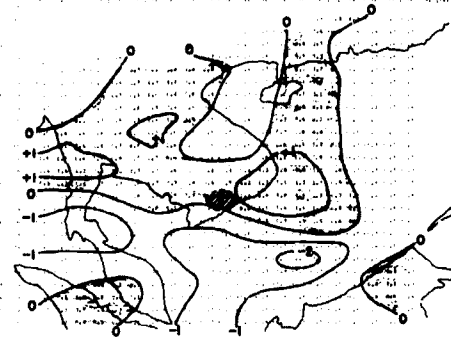
Figure 21. Unsmoothed Average Coded Clouds Ubon Tertile 1 Minus Tertile 3 Days, June, July, August 1967, Nimbus II. RI area hatched.



UNSMOOTHED AVERAGE CLOUDS UDORN TERTILE 1 MINUS TERTILE 3 DAYS JUNE, JULY, AUGUST 1967 NIMBUS II

Figure 22. Unsmoothed Average Coded Clouds Udorn Tertile 1 Minus Tertile 3 Days, June, July, August 1967, Nimbus II. RI area hatched.

00Z RELATIVE VORTICITY-GRADIENT LEVEL - TERTILE 1



00Z RELATIVE VORTICITY-GRADIENT LEVEL - TERTILE 3

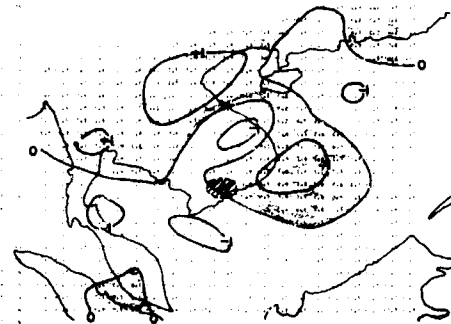


Figure 23. Average Relatively Vorticity ( $\times 10^{-5} \text{ sec.}^{-1}$ ) at the Gradient Level, 00Z, Tertile 1 Days and Tertile 3 Days at Tan Son Nhut, June, July and August 1966. Positive areas are shaded, RI area hatched.

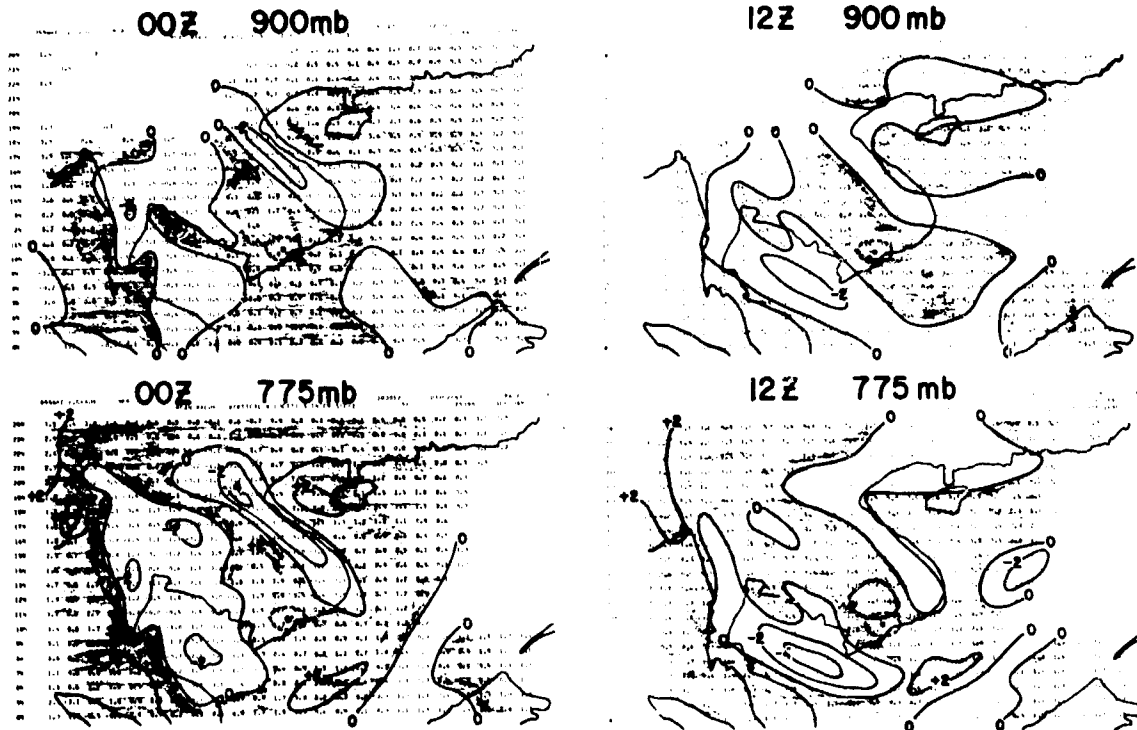


Figure 24. Average Vertical Motion ( $\text{cm. sec.}^{-1}$ ) 900 mb. and 775 mb. All Days 00Z and 12Z, June, July, August 1966. Area of ascent shaded.

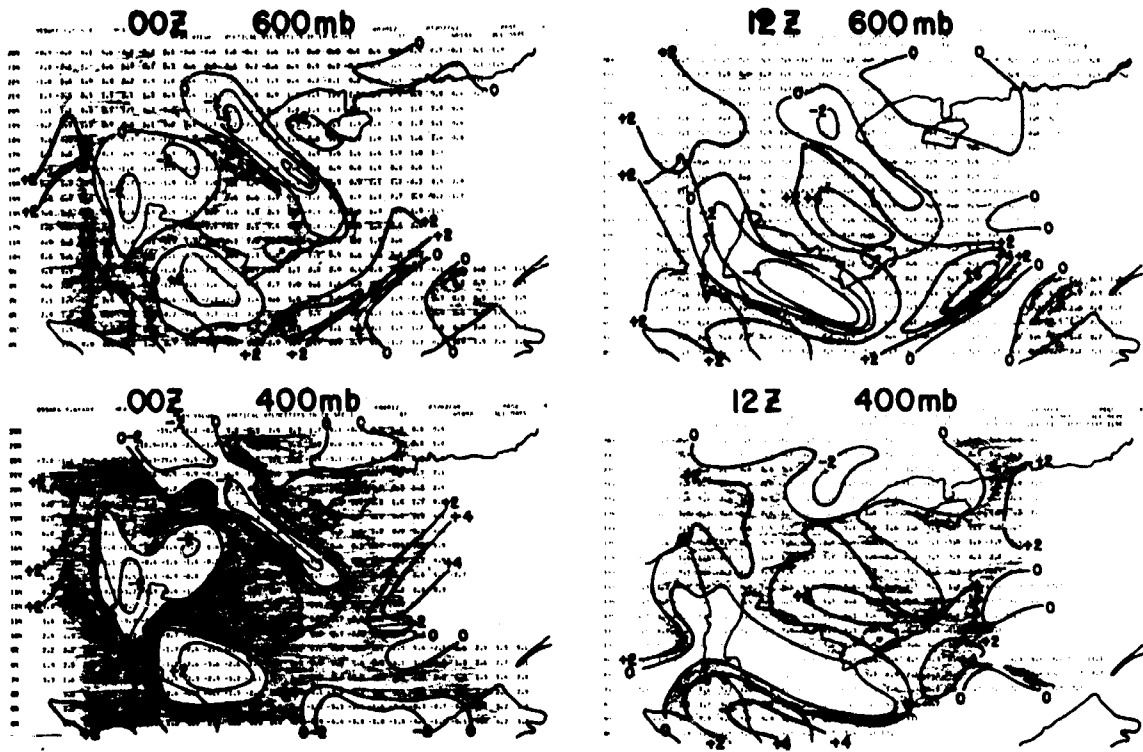


Figure 25. Average Vertical Motion (cm. sec.<sup>-1</sup>) 600 mb. and 400 mb. All Days, 00Z and 12Z, June, July and August 1966. Areas of ascent shaded.

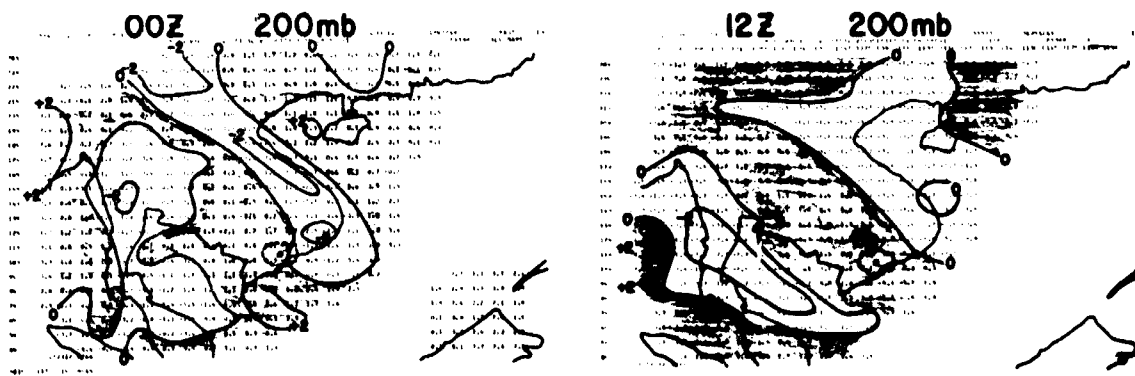


Figure 26. Average Vertical Motion (cm. sec.<sup>-1</sup>) 200 mb. All Days, 00Z and 12Z, June, July and August 1966. Areas of ascent shaded.



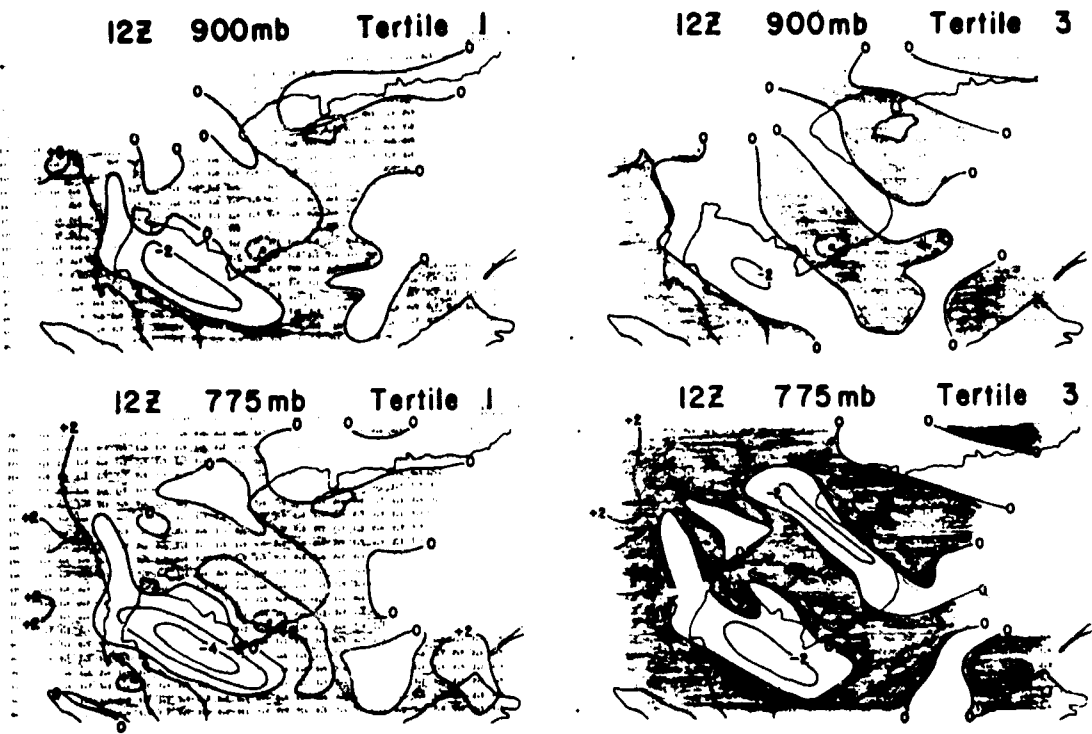


Figure 27. Average Vertical Motion (cm. sec.<sup>-1</sup>) 12Z, Tertile 1 and 3 Days 900 mb. and 775 mb. June, July and August 1966. Areas of ascent shaded.

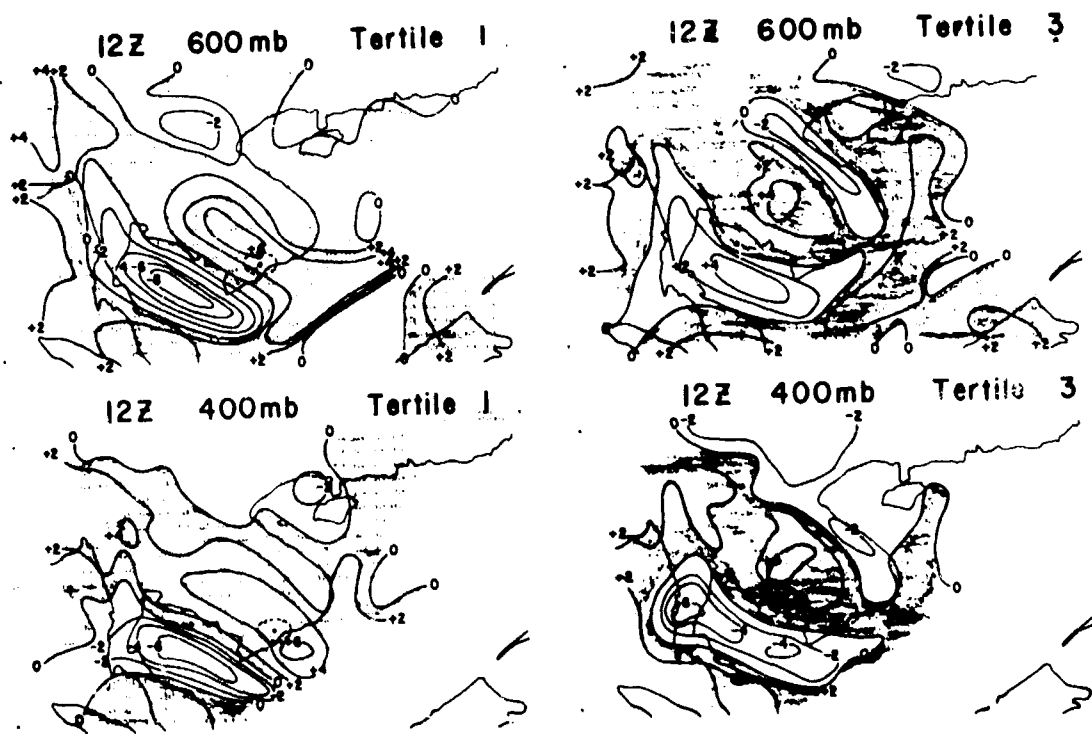


Figure 28. Average Vertical Motion (cm. sec.<sup>-1</sup>) 12Z Tertile 1 and 3 Days 600 mb. and 400 mb. June, July and August 1966. Areas of ascent shaded.

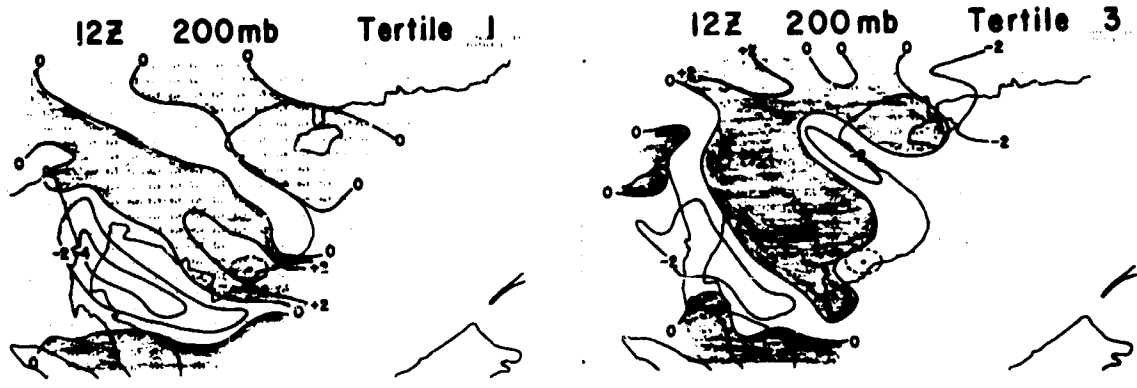
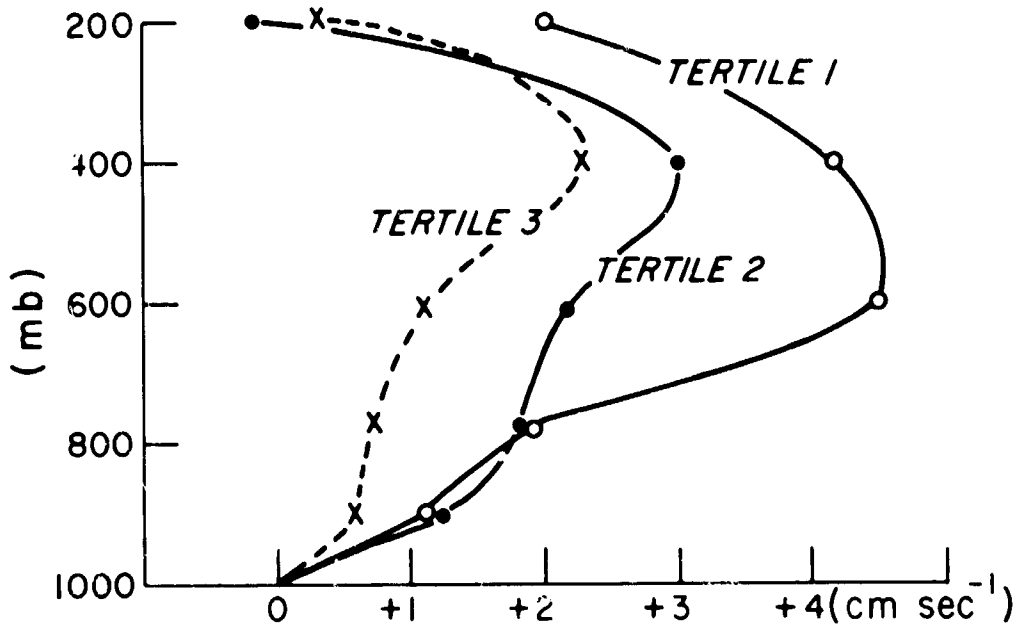


Figure 29. Average Vertical Motion (cm. sec.<sup>-1</sup>) 12Z Tertile 1 and 3 Days 200 mb., June, July and August 1966. Areas of ascent shaded.



AVERAGE VERTICAL MOTION 12Z, 1966 FOR DIFFERENT TERTILE DAYS.  $\bar{w}$  OVER 10-11°N, 106-107°E (4 DEG.<sup>2</sup>)

Figure 30. Average Vertical Motion (cm. sec.<sup>-1</sup>) Over 10° - 11° N., 106° - 107° E. at 12Z, June, July and August 1966 for Different Tertile Days.

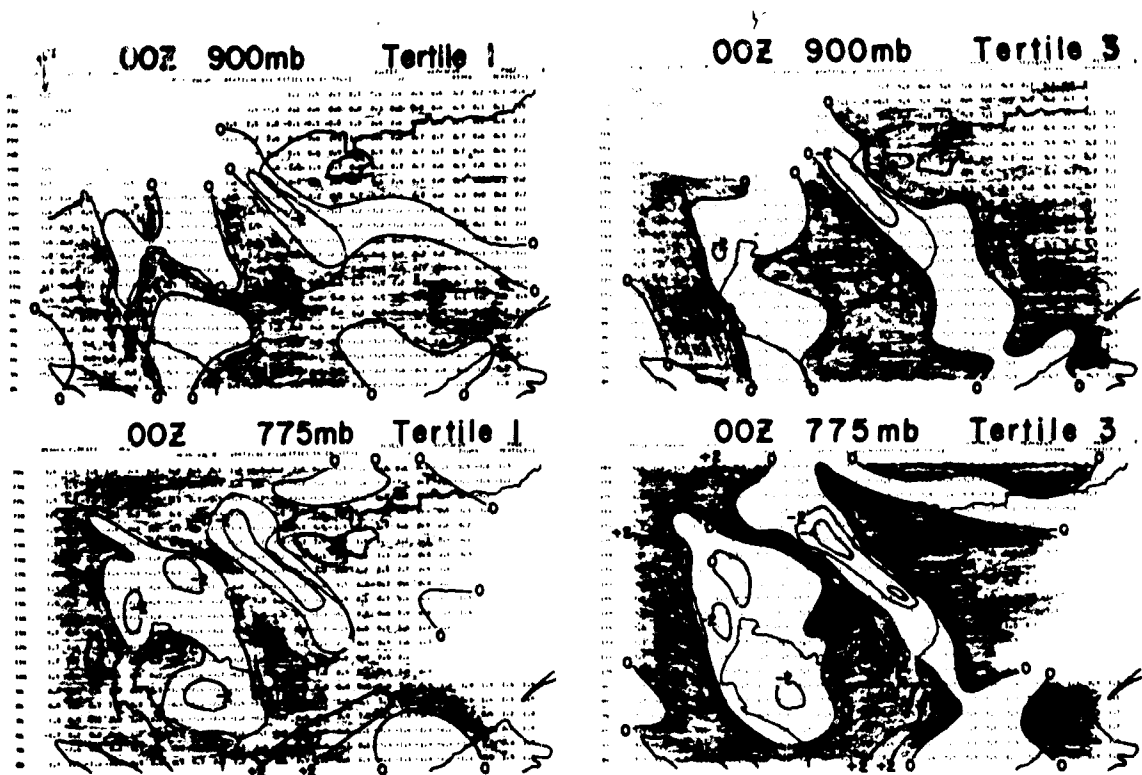


Figure 31. Average Vertical Motion (cm. sec.<sup>-1</sup>) 00Z, Tertile 1 and 3 Days 900 mb. and 775 mb., June, July and August 1966. Areas of ascent shaded.

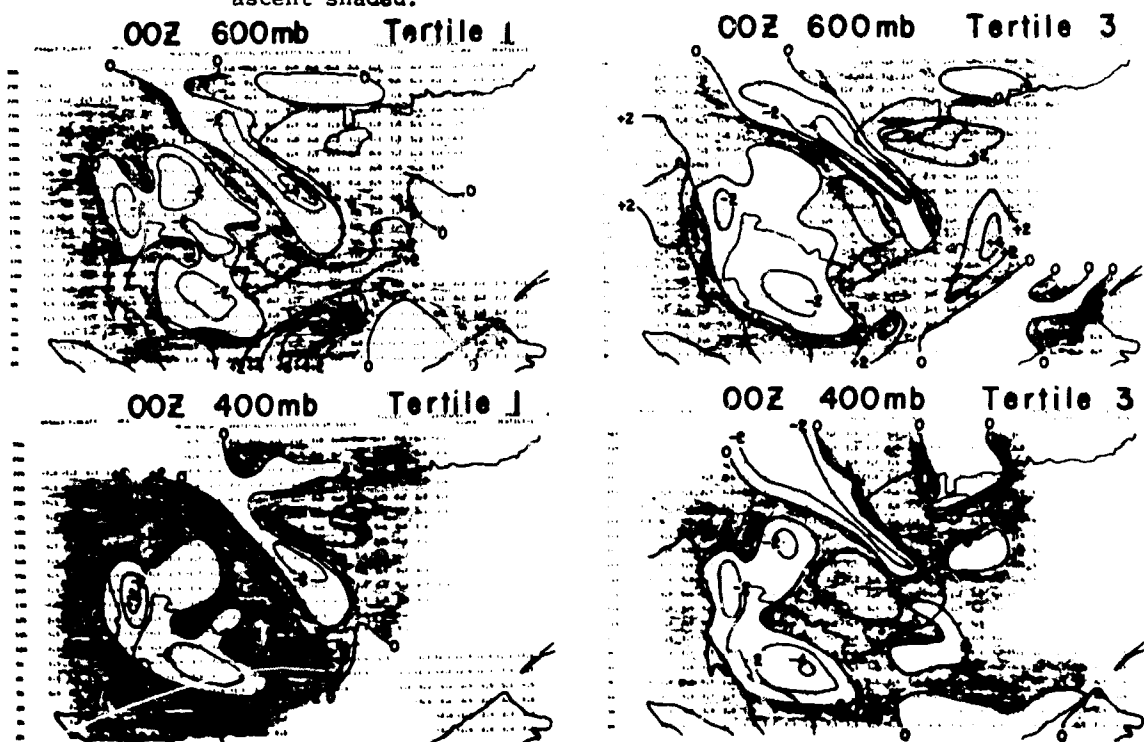


Figure 32. Average Vertical Motion (cm. sec.<sup>-1</sup>) 00Z, Tertile 1 and 3 Days 600 mb. and 400 mb., June, July and August 1966. Areas of ascent shaded.

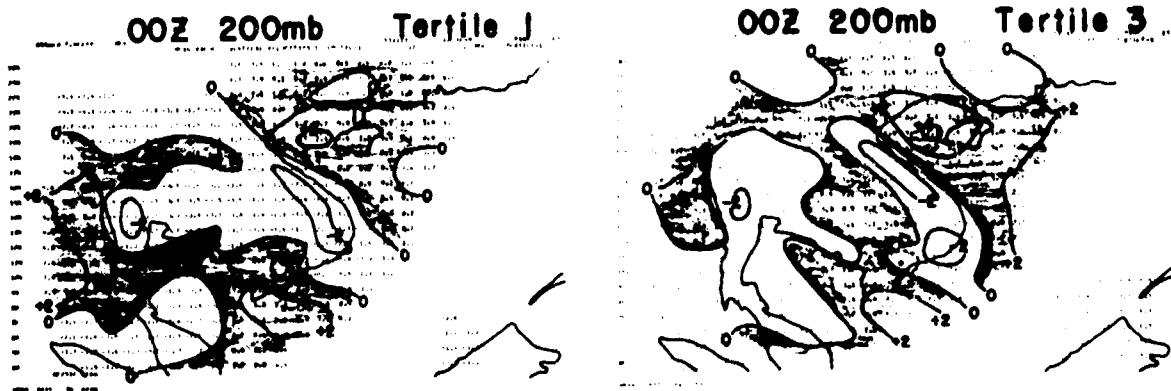


Figure 33. Average Vertical Motion (cm. sec.<sup>-1</sup>) OOZ, Tertile 1 and 3 Days 200 mb., June, July and August 1966. Areas of ascent shaded.

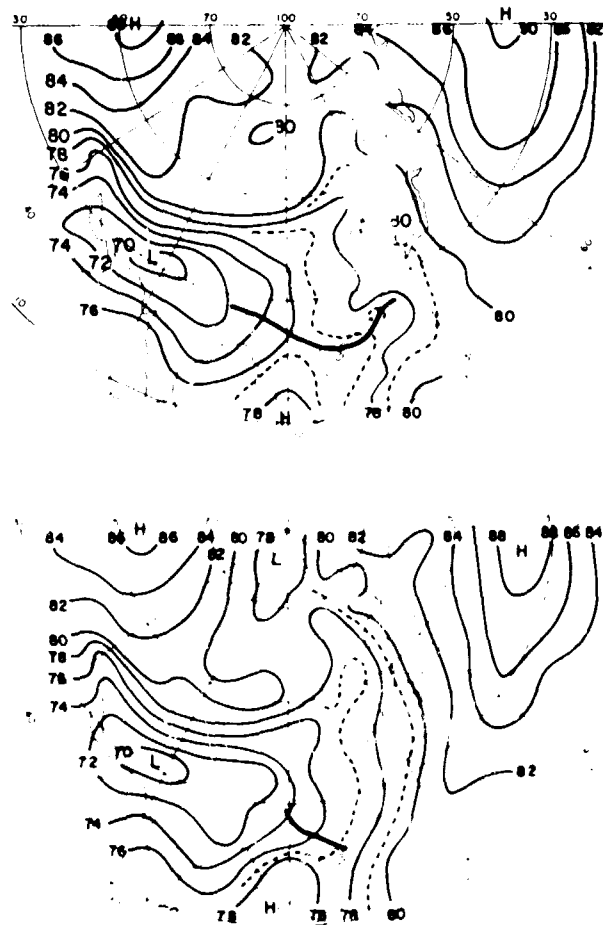


Figure 34. Average Heights of the 1000-mb. Surface. Tertile 1 days upper, tertile 3 days lower. Heavy lines mark trough zones.

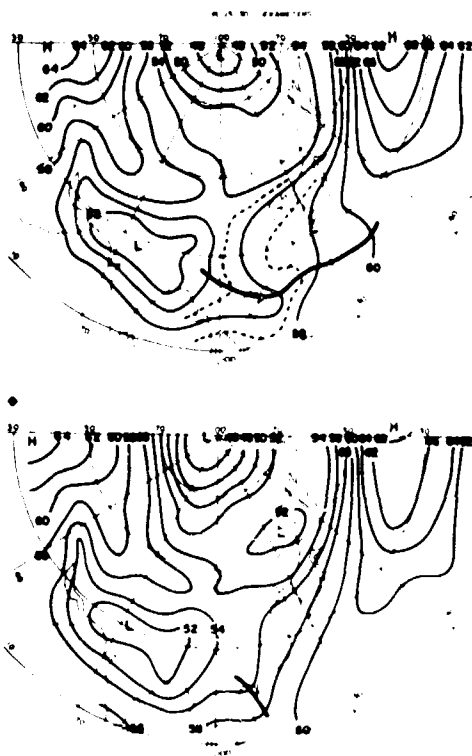


Figure 35. Average Heights of the 850-mb. Surface. Tertile 1 days upper, tertile 3 days lower. Heavy lines mark trough zones.

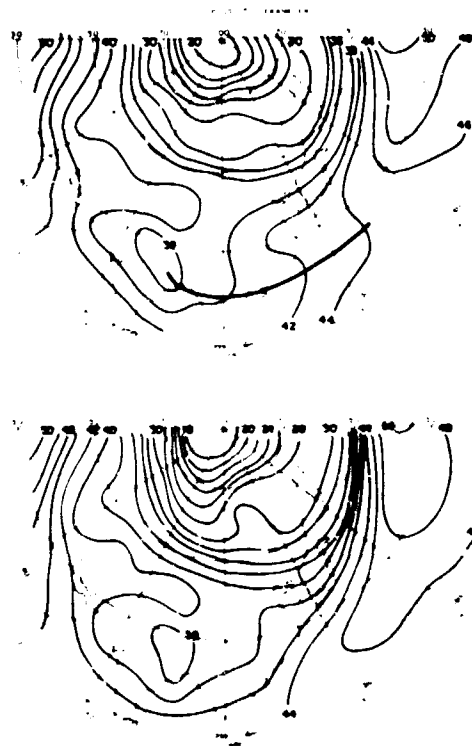


Figure 36. Average Heights of the 700-mb. Surface. Tertile 1 days upper, tertile 3 days lower. Heavy lines mark trough zones.

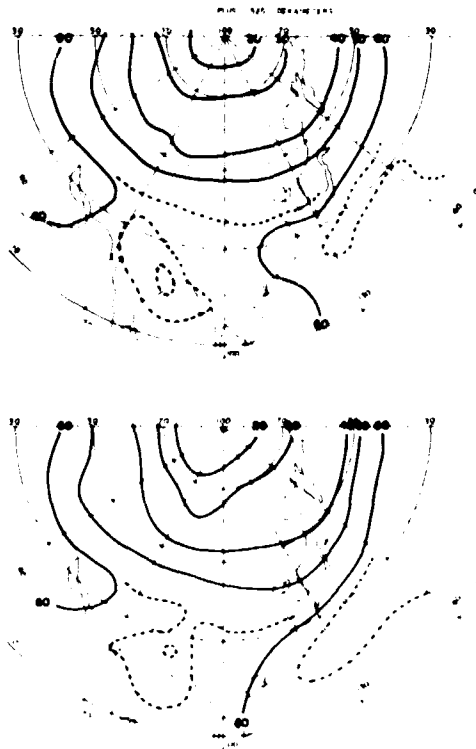


Figure 37. Average Heights of the 500-mb. Surface. Tertile 1 days upper, tertile 3 days lower.

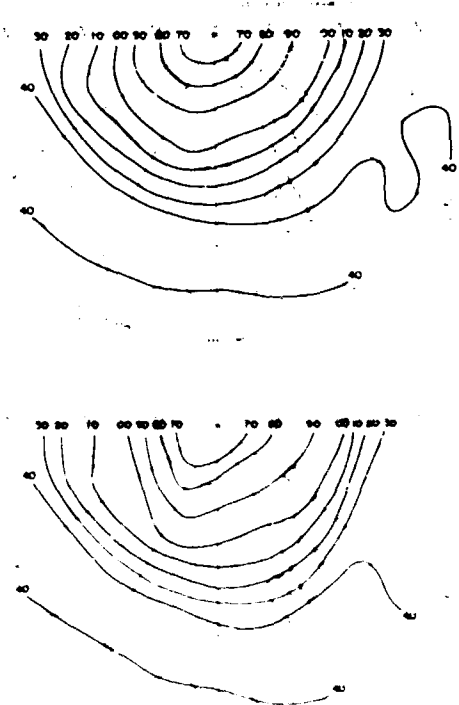


Figure 38. Average Heights of the 300-mb. Surface. Tertile 1 days upper, tertile 3 days lower.

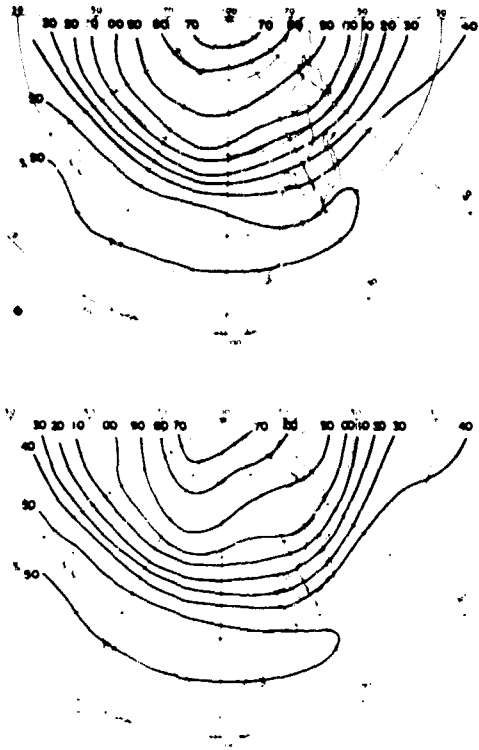


Figure 39. Average Heights of the 200-mb. Surface. Tertile 1 days upper, tertile 3 days lower.

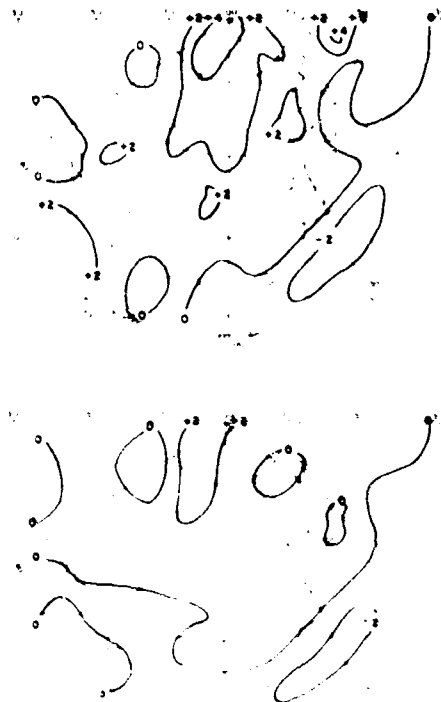


Figure 40. Average Difference in Heights, Tertile 1 Days - Tertile 3 Days. 1000 mb. upper, 850 mb. lower.

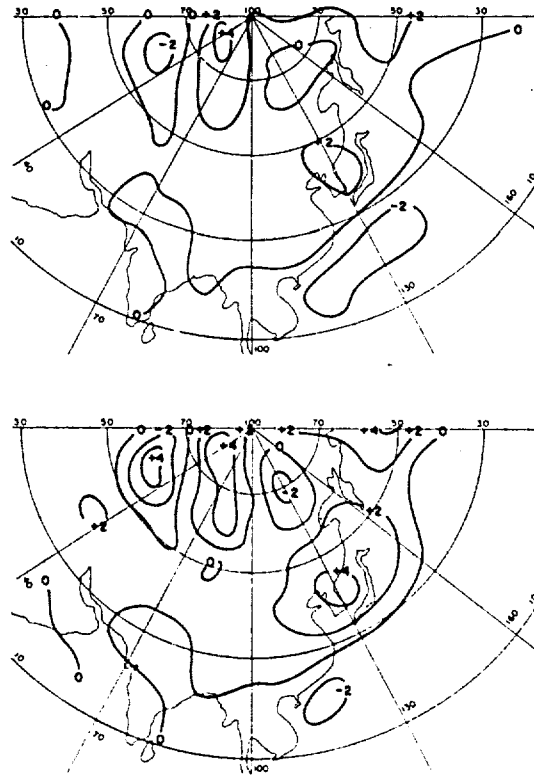


Figure 41. Average Difference in Heights, Tertile 1 Days - Tertile 3 Days. 700 mb. upper, 500 mb. lower.

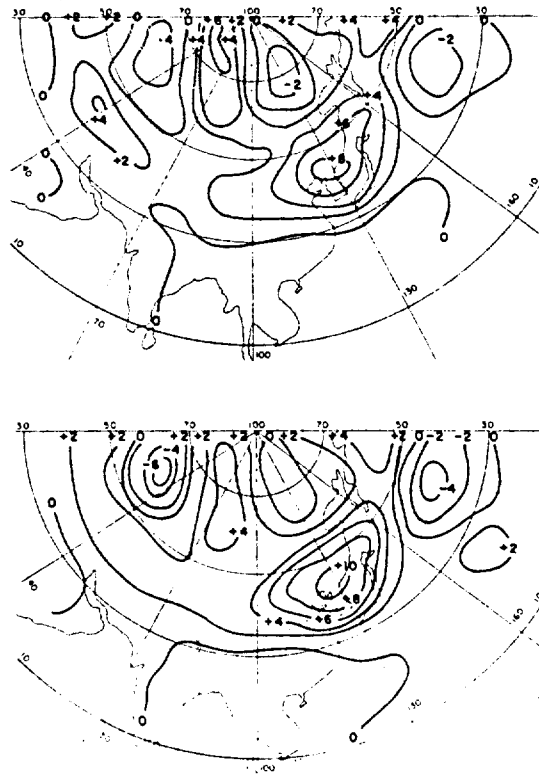


Figure 42. Average Difference in Heights, Tertile 1 Days - Tertile 3 Days. 300 mb. upper, 200 mb. lower.



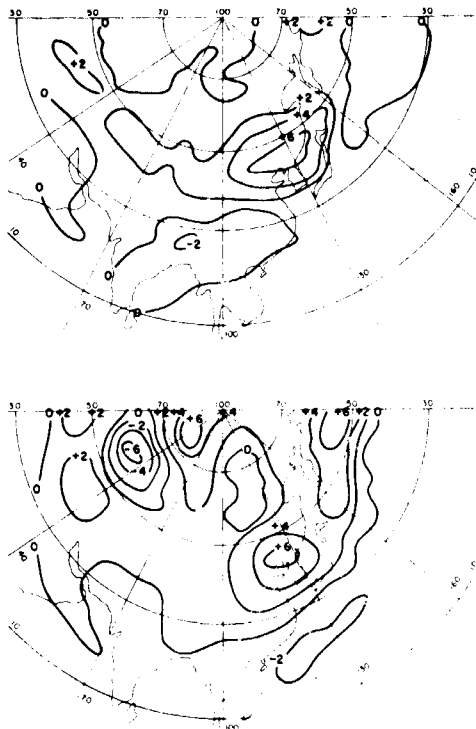


Figure 43. Average Difference in Thickness 200 to 500 mb., Tertile 1 Days - Tertile 3 Days Upper. 500 to 1000 mb., Tertile 1 Days - Tertile 3 Days Lower.

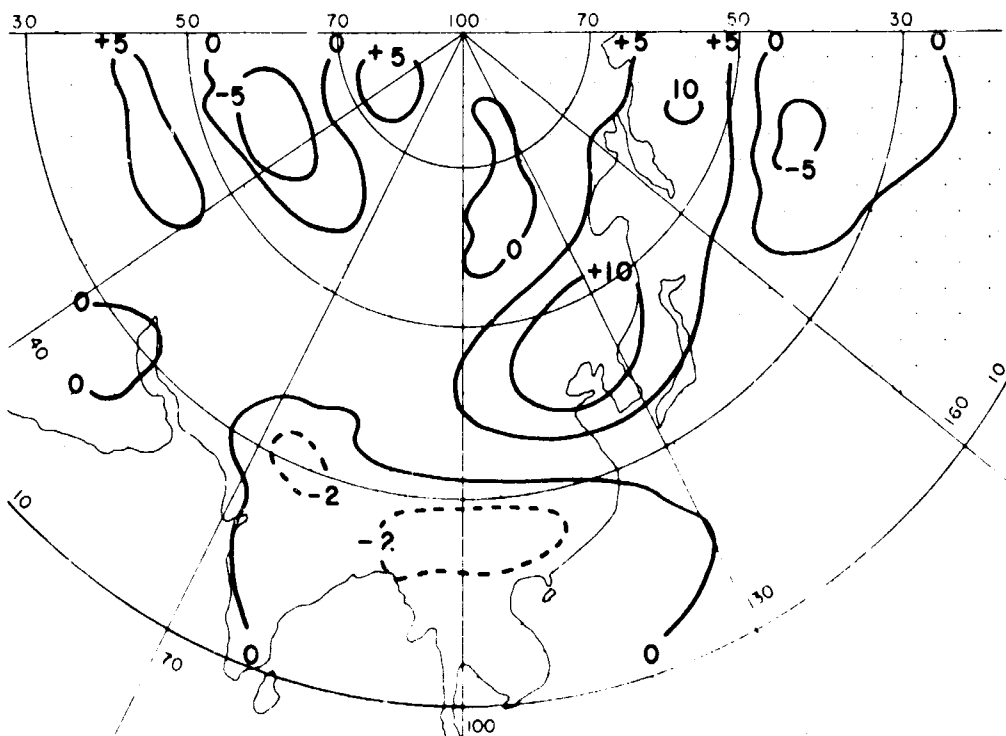


Figure 44. Average Difference in Thickness 200 to 1000 mb., Tertile 1 - Tertile 3 Days.

TAN SON NHUT TERTILE 1 0-5LT ALL ECHOES

TAN SON NHUT TERTILE 3 0-5LT ALL ECHOES



Figure 45. Distribution of All Echoes on Tertile 1 and 3 Days. 00-05 LT Tan Son Nhut. Hilly areas are hatched, radar is located at the dot.

TAN SON NHUT TERTILE 1 0-5 LT NEW ECHOES

TAN SON NHUT TERTILE 3 0-5LT NEW ECHOES

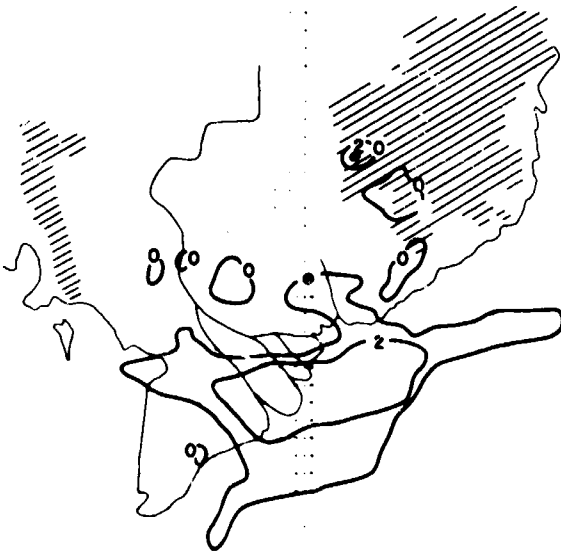


Figure 46. Distribution of New Echoes on Tertile 1 and 3 Days. 00-05 LT Tan Son Nhut. Hilly areas are hatched, radar is located at the dot.

TAN SON NHUT TERTILE 1 6-11 LT ALL ECHOES

TAN SON NHUT TERTILE 3 6-11 LT ALL ECHOES



Figure 47. Distribution of All Echoes on Tertile 1 and 3 Days. 06-11 LT Tan Son Nhut. Hilly areas are hatched, radar is located at the dot.

TAN SON NHUT TERTILE 1 6-11 LT NEW ECHOES

TAN SON NHUT TERTILE 3 6-11 LT NEW ECHOES

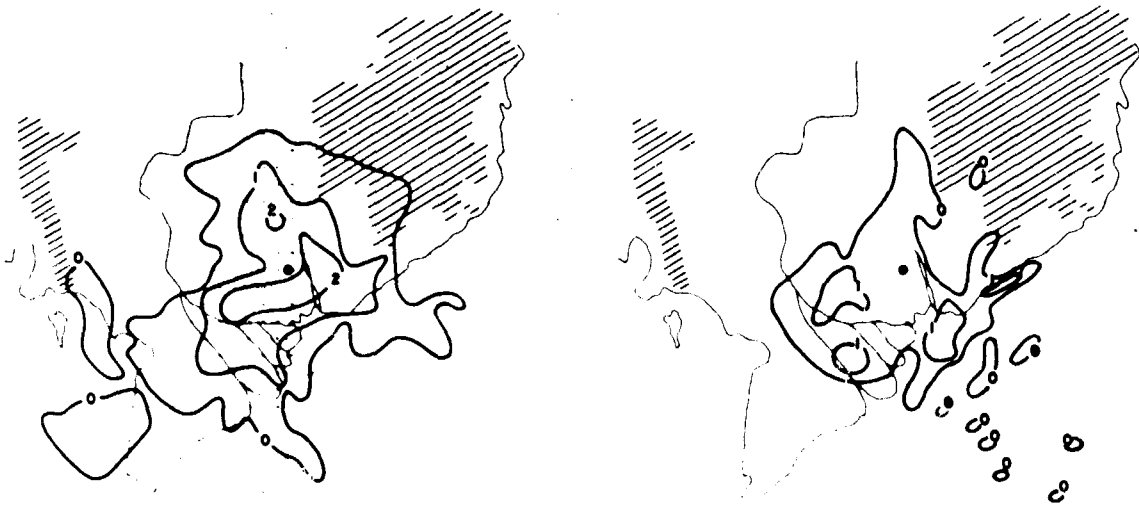


Figure 48. Distribution of New Echoes on Tertile 1 and 3 Days. 06-11 LT Tan Son Nhut. Hilly areas are hatched, radar is located at the dot.

TAN SON NHUT TERTILE 1 12-17LT ALL ECHOES

TAN SON NHUT TERTILE 3 12-17LT ALL ECHOES

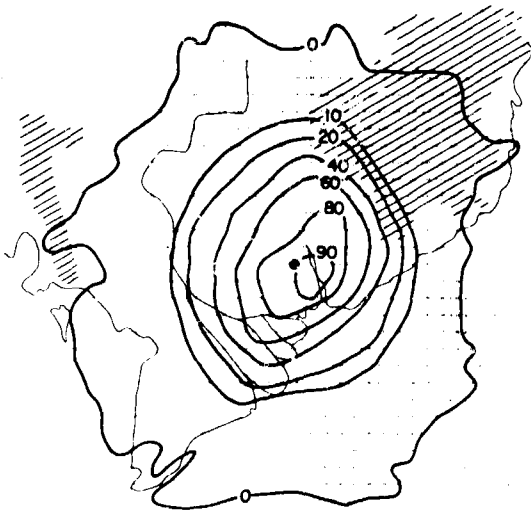


Figure 49. Distribution of All Echoes on Tertile 1 and 3 Days. 12-17 LT Tan Son Nhut. Hilly areas are hatched, radar is located at the dot.

TAN SON NHUT TERTILE 1 12-17LT NEW ECHOES

TAN SON NHUT TERTILE 3 12-17 NEW ECHOES

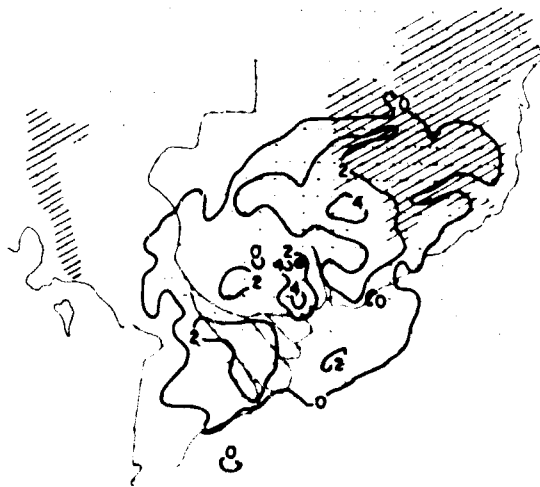
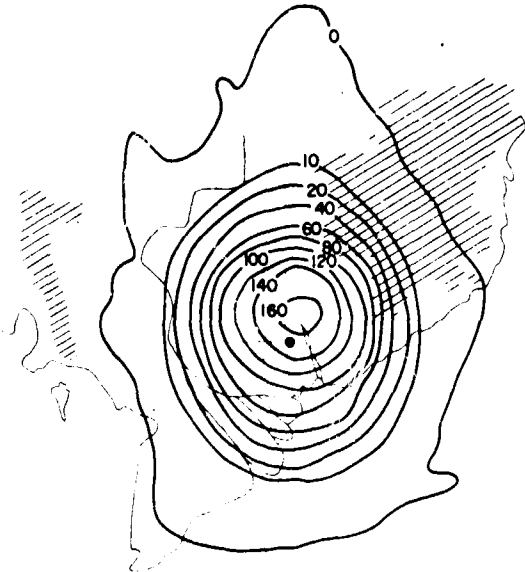


Figure 50. Distribution of New Echoes on Tertile 1 and 3 Days. 12-17 LT Tan Son Nhut. Hilly areas are hatched, radar is located at the dot.

TAN SON NHUT TERTILE 1 18-23 ALL ECHOES



TAN SON NHUT TERTILE 3 18-23LT ALL ECHOES



Figure 51. Distribution of all echoes on tertile 1 and 3 Days. 18-23 LT Tan Son Nhut. Hilly areas are hatched, radar is located at the dot.

TAN SON NHUT TERTILE 1 18-23LT NEW ECHOES



TAN SON NHUT TERTILE 3 18-23 LT NEW ECHOES



Figure 52. Distribution of New Echoes on Tertile 1 and 3 Days. 18-23 LT Tan Son Nhut. Hilly areas are hatched, radar is located at the dot.

## FIFTEEN DAY CYCLES IN SOUTHEAST ASIA RADAR DATA\*

James T. Bunting  
Air Force Cambridge Research Laboratories

### ABSTRACT

Evidence is presented for an oscillation in Southeast Asia radar data with a period of approximately 15 days. The relationship is found when radar data are averaged in lunar time within the lunar synodic month, the period between New Moon and the next New Moon. The semimonthly oscillation which is found, with peaks shortly after both New and Full Moon, is equivalent to 14.8 solar days. Quite similar relationships which have been found by other investigators for other weather elements are discussed.

The application of this relationship to forecasting is limited at present since it is much more pronounced in one year than in the following year for reasons which are not understood. The hypothesis, that the relationship is linked to the tropical semidiurnal pressure oscillation, is examined with negative results in one year and positive results in the following year.

### 1. INTRODUCTION

Recent investigations have found relationships between weather elements and solar and lunar tidal periods. Oscillations have been revealed in at least two different time scales, the solar semidiurnal (two cycles per solar day) and the lunar semimonthly (two cycles per lunar month). These relationships are generally not considered in forecasting; however, they might have some application to forecasts in the tropics, if anywhere, since the magnitude of tidal forces tends to be greatest in the tropics and since tropical weather generally has fewer well-defined systems which might obscure tidal effects. The remainder of this paper considers whether these relationships are present in the southwest monsoon over SEASIA. Evidence for a lunar semimonthly oscillation in radar data is presented and the possibility of its relation to the semidiurnal pressure oscillation is discussed.

Evidence has been published for periodic variation of rainfall within the lunar month, or lunar synodic period (the period between New Moon and the next New Moon). Bradley, et al. [4], working with data for the continental U. S., found that heavy rains occur most frequently in the first and third weeks of the lunar month. This was noted both for individual stations with long records and for the average of all stations in the U. S. Adderley and Bowen [1] revealed a remarkably similar tendency in the Southern Hemisphere, especially for New Zealand. Bradley [3] considered the dates on which tropical depressions intensified to become hurricanes. When the dates were grouped according to time within the lunar month, the distribution of dates peaked near both New and Full Moon, with fewer dates near First and Last Quarters. Brier and Bradley [7] re-investigated U. S. rainfall data and strengthened their statistical arguments for the validity of the lunar semimonthly cycle with peaks a few days after both New and Full Moon. When the data were broken down so that different times of the year and different areas of the U. S. could be examined separately, variation in phase and amplitude of the curves for the lunar month was evident, however. Gerstang and Visvanathan [13] examined extensive rainfall records for the island of Barbados and found a general increase in rainfall frequencies four times during the synodic month: a few days before New and Full Moon, and a few days after New and Full Moon. Berson and Deacon [2] found that heavy rainfall during the monsoon season for Mangalore, India, and Djakarta, Indonesia, was more frequent near New and Full Moon than at other times of the lunar month.

On the other side of the coin, Lund [15] found evidence of a lunar semimonthly period in U. S. observations of sunshine. The first and third weeks of the lunar month had less than average sunshine, while the second and fourth weeks had more than average. This tendency is certainly consistent with the previously mentioned observations for U. S. rainfall.

The previously mentioned observations were extracted from records of data which were necessarily lengthy for several reasons. First of all, events such as heavy rains or hurricane formation are naturally rare and cannot be treated as distributions unless records of many years are available. Secondly, other oscillations of any cause which have periods close to the lunar semimonthly

\* Research sponsored by Air Force Cambridge Research Laboratory

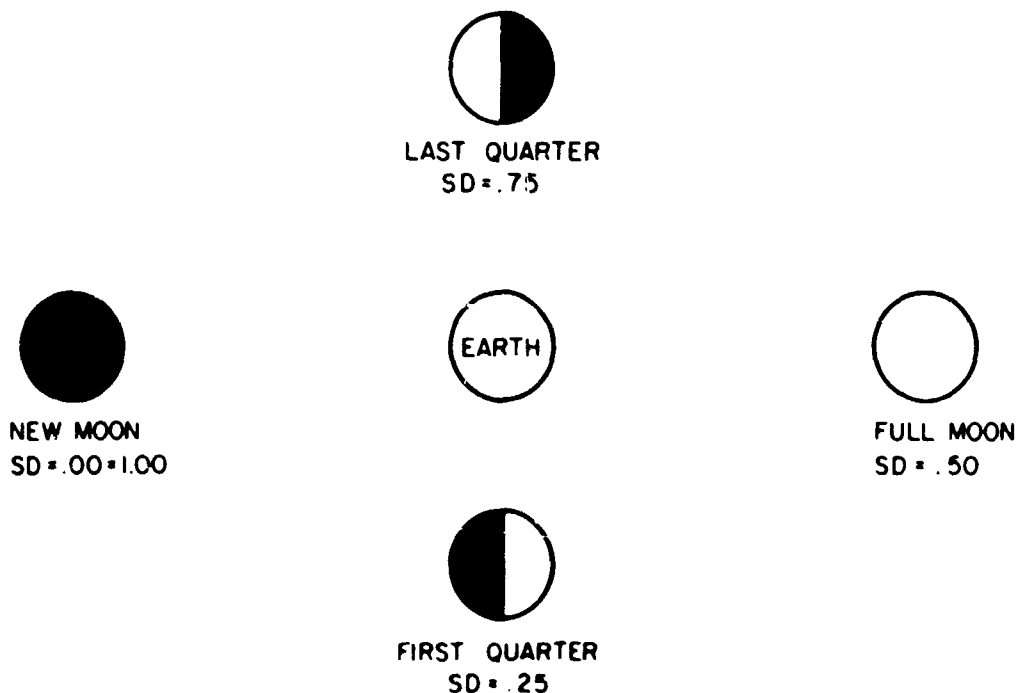
cannot be distinguished in a short data sample. Finally, an excessively lengthy record can be divided into parts which can be analyzed separately. The separate results can be correlated to test the persistence of the lunar semimonthly cycle.

Instead of a long record of rainfall data, radar data from 2 years are used in this study. A semimonthly oscillation might be easier to detect in radar data because a radar samples an enormous space compared to the space sampled by a rain gauge. For the averaging of small-scale effects, the extra space sampled by a radar, might be as useful as the extra time of a longer rain gauge record. Unfortunately, the other advantages of a long record would not apply to our shorter radar record. Oscillations with periods close to the lunar semimonthly cannot be distinguished in our short data sample. With a short record of data, it is possible that errors in observation will obscure the oscillation if it is divided into parts for independent analysis.

## 2. THE RADAR INDEX AND THE SYNODIC DECIMAL

Conover [12] describes radar data processed for two summers (1967 and 1968) for radars in SEASIA, at Tan Son Nhut and Pleiku in South Vietnam, and Ubon and Udorn in Thailand. These data are reduced to the Radar Index (RI), which is defined as the percentage of coverage by radar echoes within 50 n. mi. of the radar. The RI was computed from hourly coded RAREPS. These hourly values of RI for June, July, and August of 1966 and 1967 are used in the following analysis.

Values of RI are recorded for conventional, i.e., solar time. These values are placed in lunar time within the lunar month by means of the Synodic Decimal (SD), which is defined as the angular difference between the apparent longitudes of the moon and sun at Greenwich noon expressed as hundredths of the synodical month of 29.53 days. As displayed in figure 1, the Synodic Decimal has the value .00 at New Moon, .25 at First Quarter, .50 at Full Moon, and .75 at Last Quarter. All data over the whole earth at any time during a particular calendar day are assigned the same value for the Synodic Decimal. The SD for the following day is greater by about .03 to .04, depending on whether the moon is nearest to apogee or perigee.



### *THE SYNODIC DECIMAL*

Figure 1. An Illustration of the Change in the Synodic Decimal During the Lunar Month.

### 3. RELATION BETWEEN RI AND SD

RI data were examined for oscillations within the lunar month as follows: First, for every date and station the 12 observations from 1230 through 2330 LT were averaged to determine the afternoon RI. Each date was assigned an SD according to an ephemeris prepared by Carpenter [9]. Then for each from .01 to 1.00, all corresponding values of afternoon RI were totaled. The sums were smoothed to a .13 running mean of the SD (about 4 days) by dividing the total value of afternoon RI for 13 adjacent SD by the number of entries making up the total value.

Results of the above computation for June, July, and August of 1967 and 1968 are given in figure 2. The decimal point is here omitted from the SD, so that 50 = .50, etc. Two peaks of RI near 15 and 65 are evident. Peak values are about 20 to 30% higher than trough values. The phase of this curve is very nearly the same as for studies of rainfall cited previously, in which peaks were described 3-5 days after New and Full Moon (SD = 10-17 and 60-67) or else excessive values were attached to the first and third weeks of the lunar month (SD = 01-25 and 51-75).

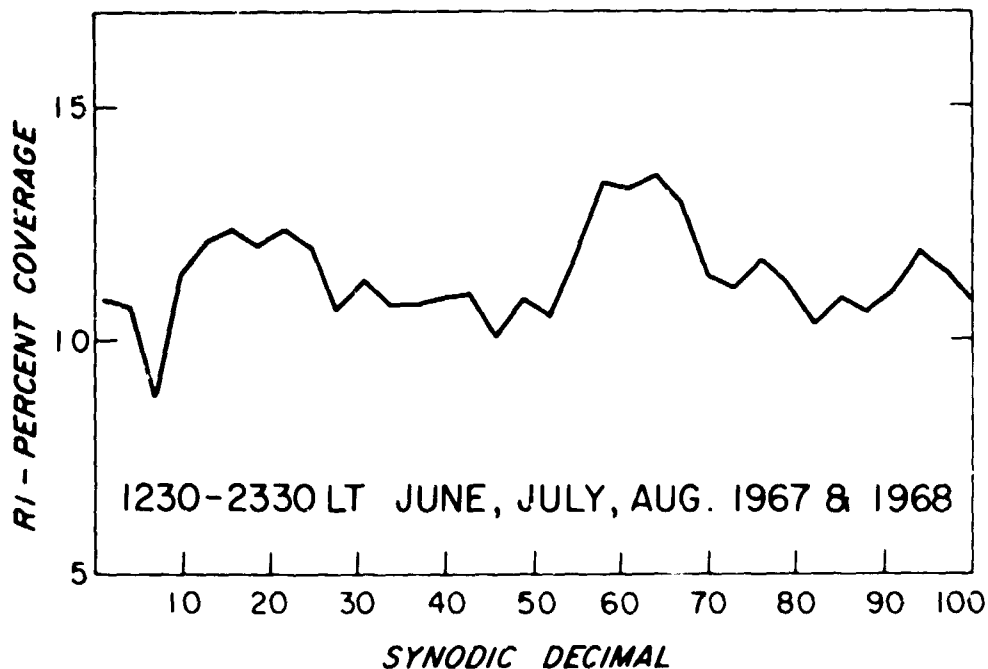


Figure 2. The Afternoon Radar Index (RI) During the Lunar Month Based on Data for 1967 and 1968.

This simple relationship of the afternoon RI during the lunar month suggests an application to forecasting. Even though the amplitude of the relation is small, extremely long-range forecasts could be made since values of the SD can be accurately calculated for many years in advance. Before embarking on such a scheme, however, the relation can be examined for its year-to-year similarity. The data for figure 2 were reworked into separate relations for 1967 and 1968, which are plotted in figure 3. Within the lunar month, the afternoon RI in 1968

A 1230-2330 LT average of RI was chosen initially since Conover had been using the same averages for verification of forecasts. See his paper for this conference.



obviously behaved quite differently than in 1967. For 1967 the two halves of the curve, 01-50 and 51-100, are almost identical. This and the similar day cycles in SZASIA radar data since each half of the lunar month lasts 14.8 days. The peak values for 1967 are 100% greater than the trough values. For 1968 in figure 3, the two halves of the curve are not similar. The RI varies greatly from 01 to 50, but not from 51 to 100. The peaks occur at 31 and 67, and are thus not 15 days apart. From 01 to 50, the 1968 curve bears an inverse relation to the 1967 curve. On the other hand, from 51 to 100, the peak values for both 1968 and 1967 occur over the same range, 58-67.

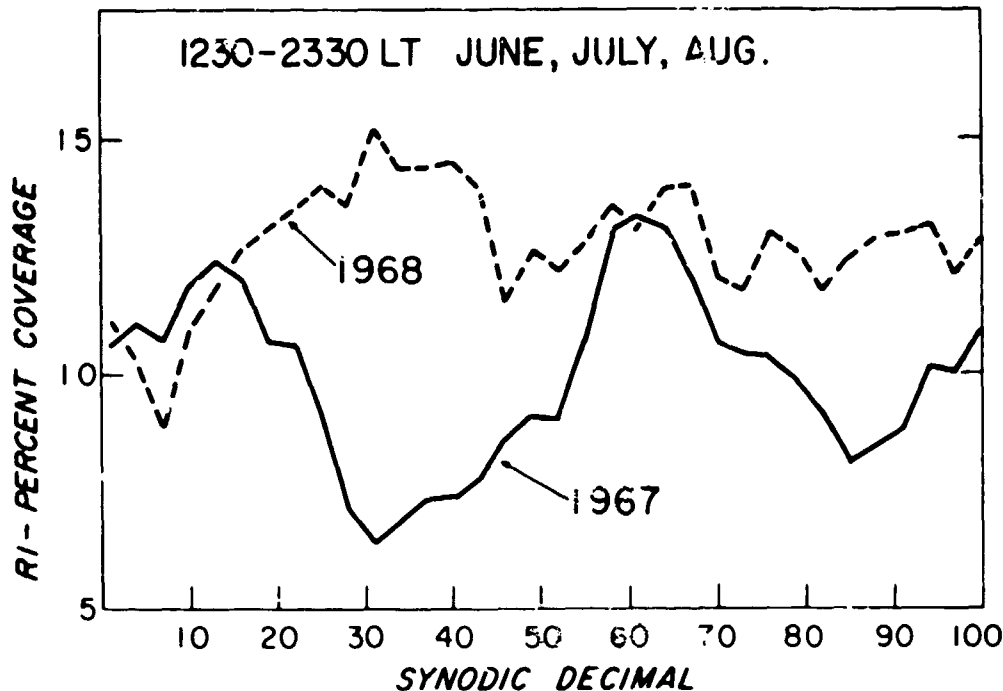


Figure 3. The Afternoon Radar Index During the Lunar Month Done Individually for 1967 and 1968.

The great change in the lunar semimonthly cycle from 1967 to 1968, appears to greatly reduce the value of applications to forecasting. However, arguments are presented in the following section that the choice of different time intervals than the 1230-2330 afternoon hours, would yield different if not better relations.

#### 4. INTERACTION OF LUNAR SEMIMONTHLY AND SOLAR SEMIDIURNAL CYCLES

Solar semidiurnal cycles have received considerable attention in the literature of atmospheric tides. Much lesser attention has been paid to modulation of semidiurnal cycles by lunar tidal periods. The geographical and seasonal variations of the solar semidiurnal pressure oscillation, for example, have been studied in great detail by Chapman and Westfold [10] and by Haurwitz [14]. In the tropics, this pressure oscillation has maxima near 1000 and 2200 in solar time, minima near 0400 and 1600, and accounts for most variation in surface pressure. Brier [6] has evidence that the variation of the amplitude of this semidiurnal pressure oscillation is related to the lunar calendar. Furthermore, Brier and Simpson [8] found relations between the amplitude of semidiurnal surface pressure oscillation and both tropical cloudiness and rainfall. They also demonstrated how the small convergence - divergence field that should be associated with this pressure oscillation might be able to generate the observed cloudiness and rainfall variation. Semidiurnal variation of radar activity would be consistent with their findings.

Conover [12] presents average daily profiles of the RI for each of the four radar locations used in this study. Tan Son Nhut, near the coast, has predominantly diurnal variation. The inland stations, Pleiku, Ubon and Udorn, have semidiurnal variation in some months, not necessarily in phase with the semi-

diurnal pressure variation. In fact, the observed semidiurnal variation of RI inland may have more to do with the geography and local dynamics of the Indochina Peninsula than with the semidiurnal pressure variation itself. However, in this study, only the change in semidiurnal variation during the lunar month is important. Since the semidiurnal pressure variation appears to change during the lunar month, a clue is provided as to how the afternoon RI data may be reorganized.

Separate 3-hour averages of RI were available centered at 1330, 1630, 1930, and 2230 LT. The combination of 1630 and 1930, which includes 1530 to 2030 LT, approximates a time of pressure rise in the tropics. The combination of 1330 and 2230, which is 1230-1430 and 2130-2330 LT, covers times of pressure fall. The two combinations taken together cover the whole afternoon, which was considered earlier. The two combinations taken separately can be used to test the hypothesis that lunar semimonthly oscillation is a function of time in the solar day.

Figure 4 shows this division of afternoon RI data for 1967. The two curves are almost identical. Subjectively, the hypothesis appears to be false. Figure 5 shows the equivalent display of data for 1968. The two curves exhibit highly suggestive differences. First of all, the average RI from 1530-2030 LT is greater for nearly all values of SD. Secondly, most of the two curves can be related by a phase shift of about 15, which supports the hypothesis that lunar semimonthly variation is a function of time in the solar day. If the curves were out of phase by 25 i.e., completely out of phase, the hypothesis that semimonthly oscillation is linked to the semidiurnal pressure oscillation would be strengthened since the behavior of RI during pressure rise time would be the inverse of the behavior of RI during pressure fall time. The possibility remains that a slightly different choice of times might yield two curves more nearly out of phase.

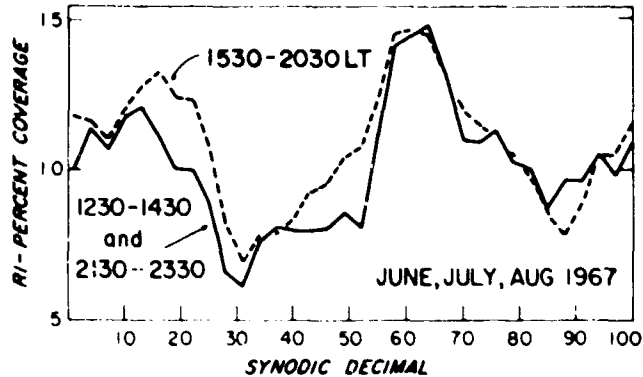


Figure 4. The Radar Index for Separate Periods of the Afternoon During the Lunar Month for 1967 Alone. The Periods of the Afternoon Were Determined From the Semidiurnal Pressure Oscillation in the Tropics. 1530-2030 LT Approximates a Time of Pressure Rise While 1230-1430 and 2130-2330 are Usually Times of Pressure Fall.

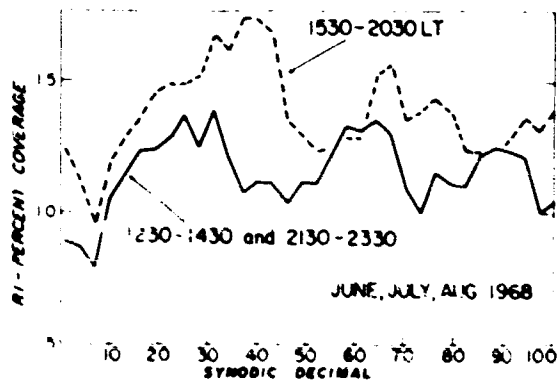


Figure 5. The Radar Index for Separate Periods of the Afternoon During the Lunar Month for 1968 Alone. The Periods of the Afternoon Were Determined From the Semidiurnal Pressure Oscillation in the Tropics. 1530-2030 LT Approximates a Time of Pressure Rise While 1230-1430 and 2130-2330 are Usually Times of Pressure Fall.

## 5. CONCLUSIONS

Radar data for the southwest monsoon in 1967 and 1968 exhibit a semimonthly oscillation in the lunar month, with peaks shortly after New and Full Moon, which is consistent with studies of other weather elements by other investigators. This oscillation is shown to be quite pronounced in 1967 but weak in 1968. When the same data are broken down into different periods of the afternoon according to the semidiurnal pressure oscillation, both afternoon periods for 1967 exhibit the same oscillation during the lunar month; however, the separate afternoon periods for 1968 do not exhibit the same oscillation and seem to be out of phase.

There are a number of possible explanations to the above puzzling relations, assuming that they are real and not due to errors in the data or statistical chance. It is possible, for example, that we have detected cycles of some other cause. Charney [11] and Mak [16] discuss how oscillations of suitable periods might arise in the tropics by dynamic arguments. Another possibility is that not enough aspects of lunar tidal theory have been considered. The anomalistic and nodical cycles of the lunar orbit are found to be necessary in describing the amplitudes of tides in the oceans. There is no a priori reason to exclude them when considering oscillations of the atmosphere. Further data, however, would be necessary to distinguish these other aspects of lunar tidal theory.

## DISCUSSION

ADLER: Working with the 1967 Radar Index data there might be an alternative explanation for the 15-day cycle. At least for the first part of the summer, there is an approximate 15-day variation in the strength of the monsoonal trough.

BUNTING: I have not looked at the RI data in exactly this way before. However, I might point out that I have dealt strictly with RI data and not with other weather elements, which might also vary in a similar manner in lunar time. Also, my cycles are in phase with those found in other investigations.

BELL: It is claimed that an advantage of radar cover data is that it refers to a greater area than individual, conventional reporting stations. Would it not be more profitable to look at satellite cloud cover data for such variations because they cover much greater areas than radar?

BUNTING: This work is in progress.

SOUTHERN:

- (a) What is the monthly variation of the ocean tide around the coast of Vietnam which might just conceivably set up small tidal wind currents on the coast and if it were of sufficient magnitude...?
- (b) I note that the author does not quote other published authorities who have criticized the conclusions of the authors quoted in the paper on statistical grounds, e.g., O'Mahoney of the Commonwealth Bureau of Meteorology.

MILLS:

- (a) 2' to 4' daily about 17° N. on east coast Vietnam; about 6' to 8' (sometimes more) at 10° N.

BUNTING:

- (a) I am not aware of any publications which discuss such a mechanism. In any event, of the four stations I used, only one, Tan Son Nhut, is near the coast.
- (b) O'Mahoney studied data for heavy rainfall at four stations in Australia. He found no evidence for a relation in lunar time throughout the lunar month, except near Full Moon. He also presented noteworthy statistical arguments as to how a smoothing process applied to separate curves might cause them to appear more the same.

ATKINSON: Perhaps we should look further at the semi-diurnal tidal effects on weather at Southeast Asia stations where we have good data, e.g., correlation with Radar Index at Saigon.

RAMAGE: Do you think that this line of work should be pursued to the benefit of Southeast Asia operations? It strikes me as an example of a failing research project--starting out with promise and looking worse and worse as more data are included.

BUNTING: This line of work was begun on the basis of the other investigations which were discussed. It was continued on the basis of the remarkable relation for 1967, which described the RI for that year as well as any other approach. Applications to forecasting are restricted both by the dissimilar results for 1968 and by our lack of knowledge concerning the responsible mechanism and its interaction with other sources of weather. I don't agree that these two years establish a trend of worsening results. More data would be needed to confirm or deny the relationship. In any event, these results can be utilized in a different manner. Even if the relation is small and not large enough to form the basis of a forecast, its presence may be interpreted as a background trend which helps to obscure other sources of weather. This or other periodic relations will have to be removed from tropical data before we can relate weather systems to weather elements with any facility.

#### REFERENCES

1. ADDERLEY, E. E. and E. G. BOWEN, "Lunar Component in Precipitation Data." *Science*, 137, 740-750. 1962.
2. BERSON, F. A. and E. L. DEACON, "Heavy Rainfalls and the Lunar Cycle." *Ind. J. of Meteorol. and Geophysics*, 16, 55-60. 1965.
3. BRADLEY, D. A., "Tidal Components in Hurricane Development." *Nature*, 204, 136-138. 1964.
4. BRADLEY, D. A., WOODBURY, M. A. and G. W. BRIER, "Lunar Synodical Period and Widespread Precipitation." *Science*, 137, 748-749. 1962.
5. BRIER, G. W., "Diurnal and Semidiurnal Atmospheric Tides in Relation to Precipitation Variations." *Monthly Weather Rev.*, 93, 93-100. 1965.
6. \_\_\_\_\_, "Evidence for a Longer Period Tidal Oscillation in the Tropical Atmosphere." *Quart. J. Roy. Meteorol. Soc.*, 92, 284-289. 1966.
7. BRIER, G. W. and D. A. BRADLEY, "The Lunar Synodic Period and Precipitation in the United States." *J. Atmospheric Sci.*, 21, 386-395. 1964.
8. BRIER, G. W. and J. SIMPSON, "Tropical Cloudiness and Rainfall Related to Pressure and Tidal Variations." *Quart. J. Roy. Meteorol. Soc.*, 95, 120-145. 1969.
9. CARPENTER, T. H., "Decimal Ephemeris of Sun and Moon 1848-1974." U. S. Weather Bureau, Washington, D. C. 1965.
10. CHAPMAN, S. and K. C. WESTFOLD, "A Comparison of the Annual Mean Solar and Lunar Atmospheric Tides in Barometric Pressure, as Regards Their Worldwide Distribution of Amplitude and Phase." *J. Atmospheric Terrest. Phys.*, 8, 1-22. 1969.
11. CHARNEY, J. G., "A Further Note on Large-Scale Motions in the Tropics." *J. Atmospheric Sci.*, 26, 182-185. 1969.
12. CONOVER, J. H., "Summer Monsoon Studies of Clouds and Weather Over SEASIA Utilizing Satellite Data." In preparation for Southwest Monsoon Conference, Honolulu, Hawaii, April 7-9, 1969. 1969.
13. GARSTANG, M. and T. R. VISVANATHAN, "Solar and Lunar Influences on Rainfall." Final Report Part 1 to ESSA for Grant No. E-18-67(G), 1-87. 1967.
14. HAURWITZ, B., "Atmospheric Tides." *Science*, 144, 1415-1422. 1964.
15. LUND, I. A., "Indications of a Lunar Synodical Period in United States Observations of Sunshine." *J. Atmospheric Sci.*, 22, 27-39. 1965.
16. MAK, M., "Laterally Driven Stochastic Motions in the Tropics." *J. Atmospheric Sci.*, 26, 41-64. 1969.

## AN OBJECTIVE METHOD OF FORECASTING CHANGES IN CONVECTIVE ACTIVITY IN SEASIA\*

Frank R. Valovcin  
Air Force Cambridge Research Laboratories

### ABSTRACT

The relationship between wind speed at 1.5 km. or 850 mb. and convective activity in SEASIA is examined. Preliminary results indicated that when the wind speed at or near 1.5 km. or 850 mb. is relatively strong, the convective growth and activity within a 50 n. mi. radius of the station is limited. This relationship indicates that a simple objective technique may be used to forecast 4 - 10 hours in advance the type of convective activity that will probably occur between 1200-0000 LST at selected stations in SEASIA.

### 1. INTRODUCTION

The objective of the initial study was to forecast thunderstorm penetrations of the tropopause in SEASIA. As the data were collated and the study progressed, it was decided to investigate the relationship of various parameters with the growth and extent of convective activity and not limit the study to tropopause penetration.

The stations in SEASIA that were investigated were Udorn, Ubon, Pleiku and Tan Son Nhut. Although the results apply to all of the stations, only Ubon and Tan Son Nhut will be discussed in this report. The time schedule for this seminar did not permit the tabulation and verification of the independent data at Udorn and Pleiku.

The purpose of the study was to derive an objective technique to forecast the type of convective activity at the selected stations in SEASIA. Initially stated, the problem was to forecast the occurrence of radar cloud tops  $\geq 45,000$  feet within a 50 n. mi. radius of the station between 1200-0000 LST from June - August. If a radar cloud top was reported 45,000 feet at any time during the 12-hour period, the convective activity was defined as "Active." On the other hand, if radar cloud tops were reported  $< 45,000$  feet during the entire period, the convective activity was defined as "Inactive." An unexpected consequence of this definition is that during an "Inactive" period, that is, when radar cloud tops were  $< 45,000$  feet, there were no radar echoes reported within a 50 n. mi. radius of the station for at least 5 hours at Ubon and 8 hours at Tan Son Nhut on the average. Consequently, a forecast of an "Inactive" period will generally have 4 - 12 hours of no radar echoes reported within 50 n. mi. of the station.

### 2. PRESENT STUDY AND RESULTS

#### 2.1 Data Utilized

Hourly radar weather observations and upper-air data taken during the period June - August 1967 were used as the dependent sample. The independent sample consisted of observations taken during the period June - August 1968. WSR-57 and CPS-9 radars were used respectively at Ubon and Tan Son Nhut.

The hourly radar observations were used to compute a weather radar index. This radar index (RI) is defined as the percent coverage of radar echo on the PPI scope within a 50 n. mi. radius of the station. (Conover, unpublished report to AWS, dated 24 May 1967). Echo areas reported as "scattered" were considered 25% covered, as "broken," 70% covered, as "solid", 95% covered and as cells, 100% covered. Pertinent data concerning echo mode, tops and intensity accompany each echo plot of RI. A tabulation was made of RI and radar cloud tops that were observed at Ubon and Tan Son Nhut during the hours of 1230-2330 LST. This tabulation was then compared to various parameters listed below.

\*Research sponsored by Air Force Cambridge Research Laboratory

## 2.2 Parameters Investigated

The following parameters were screened for possible predictors. Some were thoroughly evaluated with little or no success. Others were partially investigated and will be given further consideration as the study progresses. The radiosonde and wind data were available for Ubon at 0000, 0600, 1200, and 1800Z, but only at 0000Z for the Tan Son Nhut (0000Z corresponds to 0700 LST at Ubon and 0800 LST at Tan Son Nhut).

- (1) Tropopause heights and temperatures.
- (2) Level of the easterly-component of wind direction.
- (3) Change in the level of the easterly component of wind direction.
- (4) Level of the maximum winds in the lower and upper atmosphere.
- (5) 1.5 km. (Ubon) or 850 mb. (TSN) wind speed and direction.
- (6) 12 km. (Ubon) or 200 mb. (TSN) wind speed and direction.
- (7) 24-hour change in wind speed and direction for both 1.5 and 12 km. levels.
- (8) Wind shear between 12 km. and 1.5 km.
- (9) Wind shear between 1.5 km. and surface.
- (10) Daily variation of the u and v component at 1.5 and 12 km. levels.

Initial testing showed a relationship between the wind observation at 1800Z and 0000Z with the occurrence of convective activity during the period 1200-0000 LST. The best relationship appeared at the 1.5 km. or 850-mb. level. Therefore, the effort was directed towards developing an objective technique using the 1800Z or 0000Z wind observations. The parameter selected as a predictor was the wind speed at 1.5 km. for Ubon and 850 mb. for Tan Son Nhut. The reason for this slight discrepancy is that the units used in reporting rawinsonde observations are m./sec. and meters at Ubon and knots and millibars at Tan Son Nhut.

## 2.3 Initial Results

The lower portion of figure 1 shows the daily 1800Z 1.5 km. wind speed at Ubon for the period June - August 1967. Wind speeds  $\geq 9$  m./sec. are shown in black. The "Active" (white) and "Inactive" (black) periods are shown for the same period in the upper portion of figure 1. In order to contrast the "Active" and "Inactive" periods, the number of observations when the RI = 0 was plotted during the "Inactive" period.

Figure 2 shows the same information for Tan Son Nhut except that the 0000Z 850-mb. wind speed was used and wind speeds  $\geq 27$  knots are delineated.

An examination of figures 1 and 2 shows that, at both stations, there appears a relationship between wind speed and convective activity as defined by "Active" and "Inactive" periods. In addition, during "Inactive" periods there will be many observations reporting a RI = 0.

Based on the relationship shown in figures 1 and 2, an objective forecasting technique was developed for Ubon and Tan Son Nhut. In the case of Ubon, the critical value of wind speed is 9 m./sec. Consequently, if the 1800Z (0100 LST) 1.5 km. wind speed is  $< 9$  m./sec. at Ubon, forecast an "Active" period for the afternoon and evening (1200-0000 LST), i.e., Radar Cloud tops  $> 45,000$  feet. If the wind speed is  $\geq 9$  m./sec., forecast an "Inactive" period, i.e., Radar Cloud Tops  $< 45,000$  feet and at least 4 hours or more of a RI = 0. At Tan Son Nhut, the forecasting rule is, if the 0000Z (0800 LST) 850-mb. wind speed is  $< 27$  knots, forecast an "Active" period and if the wind speed is  $\geq 27$  knots, forecast an "Inactive" period between 1200-0000 LST.

In order to evaluate this objective technique, the methods listed in AWS TR 211, dated December 1968, were followed. The three methods used were as follows:

- a. Percent of forecasts correct: The percent correct score is the ratio of the number of correct forecasts to the total number of forecasts.
- b. Heidke Skill Score: The score may vary from -1.0 to +1.0. The Heidke Skill Score compares the number of correct forecasts with the number of correct forecasts expected by chance. From the following contingency array:

		Forecast		
		Yes	No	Total
O B S E R V E D	Yes	A	B	A + B
	No	C	D	C + D
Total		A + C	B + D	A + B + C + D

The Heidke Skill Score is given by the formula:

$$\text{Heidke Skill Score} = \frac{F - D^*}{T - D^*}$$

where  $F = A + B =$  number of correct forecasts

$T = A + B + C + D =$  total number of forecasts

$$D^* = \frac{(A+B)(A+C) + (C+D)(B+D)}{A + B + C + D} = \text{Number of correct forecasts}$$

that can be expected by chance based on the sample.

- c. Appleman Skill Score: This score is similar to Heidke except that a different method is used to measure the number expected by chance and is given by the formula.

$$\text{Appleman Skill Score} = \frac{F - X}{T - X}$$

where  $F$  and  $T$  are the same as Heidke's but  $X$  is either  $(A+B)$  or  $(C+D)$  whichever is larger. Depending on the sample, the Appleman Skill Score may range from a negative value for no skill to +1.0 for perfect skill. In addition, a sample having a predominantly larger occurrence of one predictand may show a positive Heidke Skill Score and a negative Appleman Skill Score.

The contingency array and scores for the dependent sample for Ubon and Tan Son Nhut is shown in table 1.

Table 1. Contingency Table for the Dependent Sample, June - August 1967.

Station:		UBON			TAN SON NHUT				
		Forecast			Forecast				
		Yes	No	Total		Yes	No	Total	
Observed	Yes	39	13	52	Yes	57	11	68	
	No	12	22	34	No	9	14	23	
(Radar Cloud Tops 45,000 Ft.):		Total	51	35	86	Total	66	25	91
Percent of Correct Forecasts		: = 71%			: = 78%				
Heidke Skill Score		: = 0.39			: = 0.44				
Appleman Skill Score		: = 0.26			: = 0.13				

Table 2 shows the contingency array and scores for the independent sample for both stations during the period June - August 1968.

Table 2. Contingency for the Independent Sample, June - August 1968.

Station		UBON			TAN SON NHUT				
		Forecast			Forecast				
		Yes	No	Total		Yes	No	Total	
Observed	Yes	40	18	58	Yes	64	6	70	
	No	15	17	32	No	4	6	10	
(Radar Cloud Tops 45,000 Ft.):		Total	55	35	90	Total	68	12	80
Percent of Correct Forecasts		: = 63%			: = 88%				
Heidke Skill Score		: = 0.22			: = 0.47				
Appleman Skill Score		: = -0.03			: = 0.00				

An examination of table 2 shows a positive Heidke Skill Score and a zero for no skill for the Appleman Skill Score. The percent of forecasts correct are presentable, 63% at Ubon and 88% at Tan Son Nhut. The reason for the Appleman no skill score is due to the population sample of the independent data. However, it is felt that there remains some merit in this simple objective technique. This technique verified over 50% of the "Inactive" periods, i.e., 17 out of 32 at Ubon and 6 out of 10 at Tan Son Nhut. This in itself may have some forecasting merit, since associated with "Inactive" periods are numerous observations with a RI = 0%.



#### 2.4 Suggestion

Many parameters were screened for possible predictors and were listed in section 2.2. Although this study limited itself with the 1.5 km. or 850-mb. wind speed as the final predictor, it is not meant to disclaim or discredit the other parameters. Many of the parameters such as wind shear between 12 and 1.5 km., 24-hour change in wind speed, change in the level of the easterly component of wind direction showed good relationships but none was as good as the 850-mb. or 1.5 km. wind speed.

As the result of this study and the experience gained, it appears that an improvement of the technique may be gained by considering vertical wind profiles, vertical shear and a humidity parameter. On a few occasions an analysis was made of the forecasts that did not verify. It was discovered that the critical wind speed was exceeded in a layer  $\pm 0.5$  km. or  $\pm 50$  mb. of the 1.5 km. or 850-mb. level. Another aspect of the vertical wind profile that should be considered is the maximum shear between levels. The level at which the maximum winds in the lower and upper atmosphere occur should be considered. Finally, a humidity parameter either between the surface and 850-mb. level or between the 850- and 500-mb. level should be incorporated into the objective forecasting technique.

### 3. SUMMARY

An objective technique is derived to forecast "Active" or "Inactive" convective activity during the afternoon and evening hours between 1200-0000 LST at Ubon, and Tan Son Nhut during the period of the southwest monsoon from June - August. The problem is to forecast the occurrence of Radar Cloud Tops  $\geq 45,000$  feet (Active) or  $< 45,000$  feet (Inactive) within a 50 n. mi. radius of the station, based on 1800Z or 0000Z wind observations. The predictor used is the 1800Z 1.5 km. wind speed at Ubon and the 0000Z 850-mb. wind speed at Tan Son Nhut. The objective technique forecasts "Active" periods when wind speeds are  $< 9$  m./sec. at Ubon and 27 knots at Tan Son Nhut. "Inactive" periods are forecast when wind speeds are  $\geq 9$  m./sec. at Ubon and  $\geq 27$  knots at Tan Son Nhut. In addition, "Inactive" periods will generally have from 4 - 12 hours of no echoes being reported at the station.

### DISCUSSION

RENARD: Could you explain the difference between the large percent of "Active" days shown in the contingency tables and the "10% active cases" quoted in the introduction to your technique?

Did you try persistence as a comparator in the skill score relations shown, i.e., use  $\frac{T - P}{R - P}$  where P = persistence?

VALOVICIN:

- (1) Active days are designated whenever there is a report of a radar cloud top  $\geq 45,000$  feet for at least 1 hour in a 12-hour period. However, in the tabulation, each radar cloud top in a 50-mile radius is tabulated for each hour. As many as 65 to 70 radar cloud tops may be tabulated for any 12-hour period. The 10% refers to all tabulated cloud tops and not the number of hours reporting radar cloud tops  $\geq 45,000$  feet.
- (2) Persistence was examined for the 1968 data of the independent sample for both Ubon and Tan Son Nhut. It was not very successful. The number expected by persistence was less than that expected by chance or climatology. Consequently, the skill score was much higher than when persistence was used in the statistical equation. I interpret this as a defeat of persistence as compared to my objective technique.

ADLER:

- (1) Is there a direct relation between your definition of active-inactive days and Conover's RI (scope coverage)? (2) Did you investigate the effect of tropical cyclone activity in the South China Sea on buildups above 45,000 feet over the peninsula?

VALOVGIN:

- (1) No! I define convective activity as a function of the height of radar cloud tops. Mr. Conover defines convective activity as a function of areal coverage of radar activity in a 50 mile radius. On certain days there may be some agreement. On other days, there is no agreement. Correlations between the two is +0.45.
- (2) Not directly, but I did examine some 850-mb. maps and found that in a few cases, especially in August 1967, tropical cyclones were in the area and may be directly or indirectly the cause of the high wind speeds at the stations investigated, especially Tan Son Nhut.

KREITZBERG: It is important to distinguish between forecasting deep convection or heavy precipitation and forecasting scope coverage. They are different problems and the same techniques need not solve both problems. The severe weather cases need not occur when the most area coverage of echoes occur.

VALOVGIN: I agree wholeheartedly.

RAMAGE: I find trouble in reconciling your result that the higher the 850-mb. wind, the lower the CB tops and earlier reports that strong southwesterlies are associated with high radar index.

VALOVGIN: The answer to this question may be found in the comments by Professor Kreitzberg and Mr. Conover. I am in complete agreement with both gentlemen.

HAU: It seems to me that at Tan Son Nhut wind speeds  $\geq 27$  knots is relatively rare at 850 mb. Have you thought about adding some more criteria beside wind speed at one level and lowering your 27 knots to a small value - say, 20 knots for instance - to cover conditions with cloud top  $< 45,000$  ft.?

VALOVGIN: In 1968 they may have been rare, 12 out of 80. In 1967, these were 25 out of 91 which I would not consider rare.

Yes, I would like to see some parameter of vertical wind profiles and humidity included as an additional predictor. I plan to study and evaluate other parameters that may be useful. Finally, by lowering the speed criterion, I feel that in general the percent correct forecasts and the skill scores may be lowered by 10 to 20%. The number of verified "yes" forecasts will be lowered. The number of verified "no" forecasts will be increased.

The total number of correct forecasts will be less than those obtained in the present study. The 27-knot wind speed used in the dependent sample maximized the total number of correct forecasts and the skill scores. This is the reason why the magic number of 27 knots was used for the independent data sample.

BELL: Can you please either explain the radar drill for determining your 45,000 feet tops or give a measure of the accuracy of these observations?

VALOVGIN: The 45,000 feet radar cloud top was arbitrarily used as representing the upper 10% level. It was determined after tabulating some 3,000 hourly RAREPS and computing the cumulative frequency of all the radar cloud tops.

The measurement of the radar cloud top was taken directly from the RAREPS. My experience with radar tops and visual aircraft measurements is that there is good agreement.

CONOVER: In reference to Prof. Ramage's remarks, my data do not really contradict Valovgin's. I show map winds south or southwest of the station and the station is in a region of horizontal shear. Furthermore, our classifications of activity are different; therefore, speeds need not be the same. It is conceivable that activity increases up to a critical speed and above this speed vertical shear tears the cloud apart and activity diminishes.

VALOVGIN: I agree completely.

SOMERVILL: Would someone please relate radar tops, radar index and precipitation amount or intensity (propose Mr. Valovgin, Dr. Kreitzberg, Dr. Ho, or Mr. Conover --all comment).

VALOVGIN: It can't be done without quantitative radar data--which we do not presently have nor do we expect it in the future.

HO: The radar index and rainfall amount are not related one-to-one. Radar index and rainfall amounts reported within the 50 mile radius of Saigon (14 reporting stations) for July 1967 show cases of low radar index in conjunction with high rainfall amounts and vice versa. The number of stations reporting rainfall during the same time indicated that cases of low radar index coincided with widespread rainfall and high index with locally heavy rainfall.

SADLER: We have found in a general sense that the stronger and deeper the westerly monsoon current the greater the area cloud amount from satellite data and also the greater the RI. However, the speed distribution is very important for at times the maximum speed is over the South China Sea and, even though the speed over southeast Asia is high, there is still speed divergence in the area giving less cloudiness and low RI over the area.

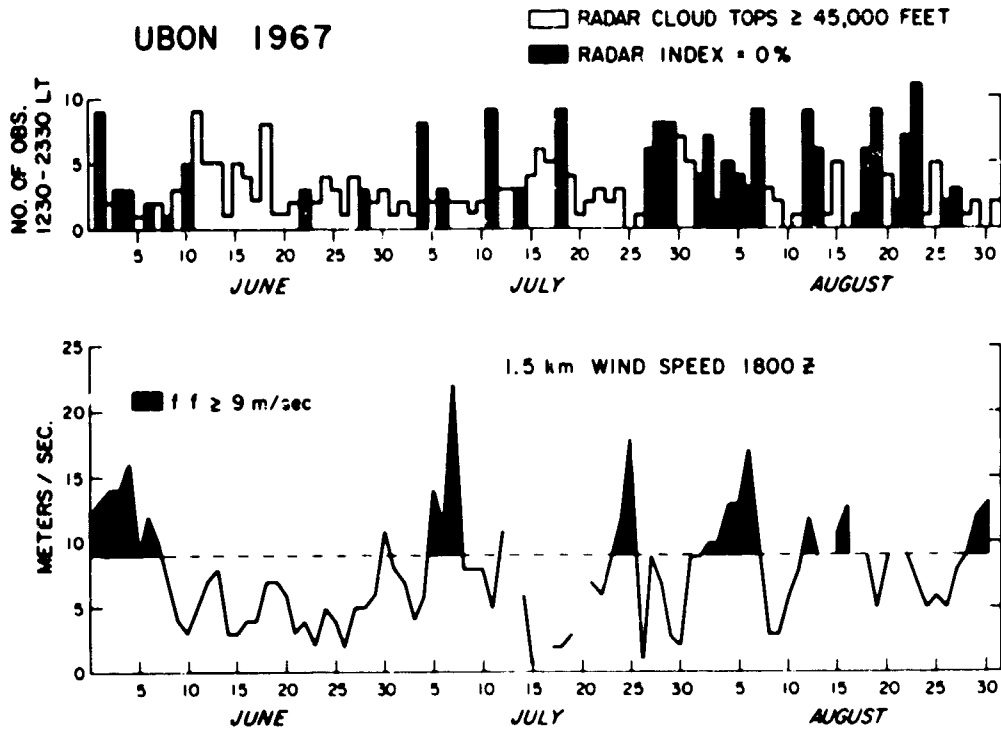


Figure 1. Daily 1800Z 1.5 km. Wind Speed at UBON in Relation to "Active" and "Inactive" Periods.

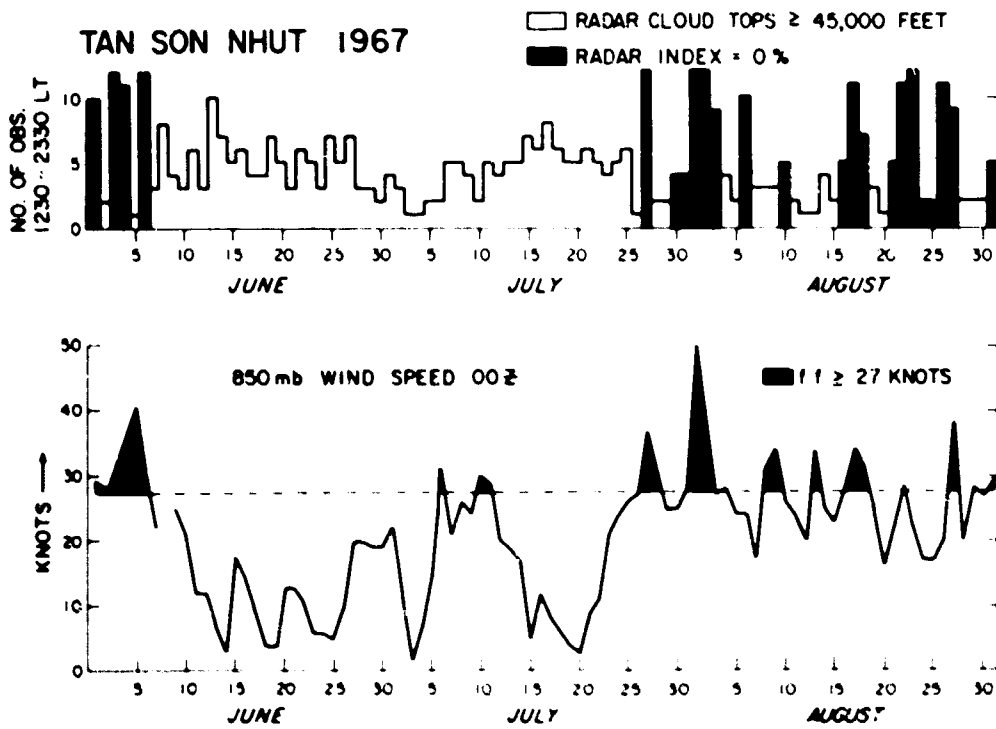


Figure 2. Daily 0000Z 850 mb. Wind Speed at TAN SON NHUT in Relation to "Active" and "Inactive" Periods.

## INTERPRETATION AND APPLICATION OF NIMBUS HIGH RESOLUTION INFRARED RADIOMETER DATA \*

R. S. Hawkins  
Air Force Cambridge Research Laboratories

### 1. INTRODUCTION

This paper has been prepared with the objective of providing both operational and research meteorologists with guidance in the interpretation and application of data from the NIMBUS satellite High Resolution Infrared Radiometer (HRIR) or similar type data. It has been prepared on the basis of studies of NIMBUS I (Aug. - Sept. 1964) and NIMBUS II (May - Nov. 1966) HRIR pictures over Southeast Asia with supporting surface and radar observations. The results will be applicable to a large degree to any satellite system operating in the 4 micron or 8-12 micron atmospheric windows. However, the ability to interpret textures and dark tones (clear or low cloud regions), considered only briefly here, is expected to vary from one system to another. Spacial resolution and sensitivity (grey scale span) are the most important factors contributing to this variation.

The importance of the HRIR data at this time is accentuated due to the scheduled launch of NIMBUS III in April 1969. Also, of operational importance is the fact that near midnight pictures will become available via the Automatic Picture Transmission system of the HRIR. This should prove valuable for planning morning military missions in Southeast Asia.

In section 2 the principal features of the HRIR system are described along with pertinent characteristics of the data. Since this information is available in detail in the references, only the essentials are given. In section 3 comparisons are made with radar and rainfall indices. Section 4 discusses a number of statistical summaries of the data over Southeast Asia.

### 2. CHARACTERISTICS OF THE NIMBUS HRIR SYSTEM AND INTERPRETATION OF THE DATA

This section gives a brief summary of the HRIR system and the fundamentals of interpretation of the data necessary for a clear understanding of the following sections. There is one point that should be kept in mind at all times: the infrared pictures require a different interpretation framework from the daytime video pictures. It should also be mentioned that the direct readout system (Direct Read-out Infrared Radiometer or DRIR) is the same as the HRIR system. The method of readout is the only difference. NIMBUS III will have DRIR capability.

#### 2.1 The NIMBUS HRIR Instrument

The HRIR radiometer measures infrared energy in the 4 micron atmospheric window. The instantaneous field of view is approximately 5 n. mi. directly below the satellite and varies with the angle of view. Scans are made across the earth perpendicular to the motion of the satellite from horizon to horizon. In tropical latitudes, scan lines are oriented roughly east-west. As the satellite advances along its orbit, successive scans are made and from these a "picture" of the earth and its clouds as seen in the infrared is constructed. The HRIR "pictures" are in the form of strips showing an area over 2500 miles wide with the sub-satellite track along its center. The horizons are along the edges of the strips. Examples given here are small portions of these strips.

NIMBUS I and II were launched into sun-synchronous, quasi-polar orbits such that passes occur over an area near local midday and near local midnight. Solar reflection in the wavelength sensed by the HRIR radiometers makes daytime data very difficult to interpret. This report considers only the nighttime data. Subsequent satellite systems operating in the 8-12 micron atmospheric window would remove the daylight problem. In this case, interpretation would be similar to interpretation of the nighttime data.

\* Research sponsored by Air Force Cambridge Research Laboratory

## 2.2 Basic Interpretation of HRIR Type Data

The HRIR radiometer measures radiant energy from the earth, the clouds, and the atmosphere. For all practical purposes, however, the atmosphere is transparent in the HRIR band. The amount of energy emitted by the earth-cloud system depends on temperature and emitting ability (emissivity) of the system. For all practical purposes, the earth and relatively thick clouds emit energy equally well for the wavelength interval of the HRIR system. The emission depends on temperature. Warm surfaces emit more energy than cold ones. Since temperatures normally decrease with altitude in the atmosphere, the earth emits more energy than clouds and low clouds emit more energy than middle clouds and middle clouds more energy than high clouds. An exception is thin high clouds; they allow energy to pass from below and therefore appear warmer and hence lower. The infrared "pictures" are made with black representing the warmest temperatures (land and oceans) and white representing the coldest temperatures (thick high clouds). The greys from black to white denote temperatures from warm to cold. Hence, the HRIR data provide information with regard to cloud cover, cloud types, cloud patterns, and cloud heights. However, it should be mentioned that interpretation is far from clear-cut.

One of the greatest problems is that of spacial resolution. The radiometer field of view looking straight down is about 5 n. mi. circle. With scattered to broken clouds in the field of view, the energy reaching the sensors comes from both warm earth and colder clouds and the resulting temperature corresponds to a level somewhere between the surface and cloud-top temperatures. Thus, a middle-cloud layer could give the appearance of a low-cloud layer. In addition to limitations in determining cloud-top height, resolution restricts cloud type interpretation as well.

The fact that the HRIR "pictures" represent emitted energy around 3.7 microns, while video pictures represent reflected solar energy in the visible part of the spectrum, should always be kept in mind. The greatest difference in the two systems is the appearance of low clouds. In the infrared, low clouds are dark and often indistinguishable from land and ocean but in the video they are, in general, represented by the light greys and whites. In some respects, the de-emphasis of low clouds restricts interpretation particularly in regard to cloud cover. In other cases, such as locating thunderstorm areas and detecting middle- and high-level vortices associated with cyclones, de-emphasis of the low cloud in the HRIR significantly aids interpretation.

Details of Nimbus HRIR system can be found in NIMBUS II User's Guide [1]. Widger, et al. [2], present a variety of information on the system, picture rectification, data interpretation and data application along with numerous case studies.

## 2.3 HRIR Interpretation in Southeast Asia

The HRIR data for NIMBUS II cover the period from 15 May - 20 November 1966 for SEASIA. This includes almost all of the southwest monsoon season. The data from NIMBUS I cover the short period from 30 August - 20 September 1964. Thus, the data, by and large, are for the southwest monsoon season and, to repeat, for approximately local midnight. The results reported here should not be applied to other times of day, particularly for land areas, without regard for diurnal changes.

Comparisons of the video and infrared have been made. In general, advantages of one system are disadvantages of the other and the 12-hour separation in time adds to the problem of comparing the two. Large storm areas appear in both systems but due to diurnal changes and system differences, it is usually impossible to determine what has happened in terms of growth or dissipation. The combination of the two systems has been useful for tracking and determining the presence of major areas of activity.

An example of the HRIR data with several typical features of interest is given in figure 1. Latitude-longitude ticks are given for even 2 deg. (approx. 120 n. mi.) intervals. The young convection complex, figure 1, is made up of individual bright areas of the order of 20 n. mi. diameter. High-level wind shear is indicated by the gradual change in tone of anvils for the large storm area to the southeast. Since the individual bright areas of the young complex are not sheared off by the high-level winds, they either have not reached that

level or have not been at the level very long. A thin cirrus layer spreads over the entire complex. Here, "thin" is used as relative transparency in the infrared. How thick, and how bright these clouds would appear in the video is not known. It is probably safe to assume that semi-transparent cirrus in the infrared is thin, and also semi-transparent in the video wavelengths. A very large and presumably old anvil is located at bottom-center. This cirrus sheet is several hundred miles long and very thin.

Large thunderstorms frequently appear to be made of smaller ones. This is indicated by darker tones between storms or the separating of anvils near the end. Black arrows, figure 1, indicate different thunderstorms inferred from the separation of anvils near the end of the overall anvil. Differences in lengths of the individual anvils probably reflect the relative ages of the individual thunderstorms. In this case, however, the heads of the thunderstorms are not apparent in the picture.

The sharp fall-off of tone from the storms is typical. The tendency for the bright tones (cold clouds) to be elongated east-westerly is also typical. Some of this, if not all, is due to cirrus blowoff by the upper-level easterlies.

A non-cluttered print covering a larger area is given in figure 2. A tropical storm is located just off the picture, top center ( $122^{\circ}$  E.,  $27^{\circ}$  N.). The thunderstorms in the west, figure 2, are over Indochina. The thunderstorms in the center of the picture are located over the South China Sea. Hainan, a good geographical location for grid checking, can be seen faintly in figure 2 at  $110^{\circ}$  E.,  $19^{\circ}$  N. The Gulf of Tonkin is cloud-free with the possible exception of low clouds. However, since the dark tone is solid without irregularities, it is probable that low clouds are absent. Over land this reasoning will not apply since land patterns are usually irregular.

Before quantitative measurements were made, some general conclusions were reached from comparisons of HRIR pictures and radar echo areas. About a dozen orbits in July, August, and September 1966 were compared with radar echo areas for Ubon and Udorn, Thailand and Saigon (Tan Son Nhut), South Vietnam. It was found that the reported echo areas almost invariably fall within bright areas. The echo areas that do not fall within bright areas are usually those with scattered echoes. An example is given in figure 3; a non-cluttered copy of the picture is given in figure 4. The grid points are located about 1.5 deg. to the east and 1 deg. to the south of the true location. The radar station locations are marked (Udorn and Saigon). Use grid tick spacings, 120 n. mi., for judging distance from the stations. A WSR-57 with a 200 n. mi. (approx.) range is located at Udorn and a CPS-9 with a range of about 150 n. mi. at Saigon. The bright clouds about 60 mi. southeast of Udorn gave scattered echoes at 1430 GMT. The non-cluttered print, figure 4, is a typical picture for the summer monsoon season showing a large amount of low stratiform cloud over China, thunderstorms over Indochina, and a band of storms from the Taiwan-Philippine region across the South China and lower Indochina.

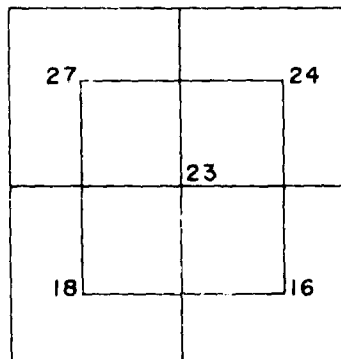
In view of comparisons of bright areas with radar echo areas and surface reports and the definite tone contrast with other tones, bright areas are given the name "Dense High Cloud" (DHC) to differentiate it from high cloud in general.

Dense High Cloud tends to occur in discrete areas, which are subdivisions of larger cloud areas commonly referred to as "blobs" or "clusters." A tally of these areas was made for 24 orbits in the area bounded by  $100^{\circ}$  -  $110^{\circ}$  E.,  $10^{\circ}$  -  $20^{\circ}$  N., the 10 degree block which encompasses most of Indochina. DHC area categories were selected in a manner that would permit easy estimation from the 2 degree grid ticks on the pictures. Thus, areas equivalent to squares with sides having lengths of  $1/4$ ,  $1/2$ , 1, 2, 3, and 4 degrees latitudes were chosen. The respective areas are, of course,  $1/16$ ,  $1/4$ , 1, 4, 9, and 16 deg. In counting merged storms, those attached laterally by more than half the length of the smaller storm were considered one storm, otherwise they were considered two storms. The storm in the center of figure 2 falls into the 3-deg. category. The storm about 50 n. mi. ESE of Udorn in figure 3 falls in the 1-deg. category. The average frequency per day of the storm count derived from 24 orbits is given in figure 5. Also shown are the corresponding frequencies of the mean storm areas per day. The total area of the 1 and 2 deg. size storm (6.7 deg.<sup>2</sup>) is about twice as large as the areas of all the other sizes combined (3.5 deg.<sup>2</sup>).

Figure 6 shows a frequency distribution of the daily amount of DHC (in tenths) over the portion of SEASIA bounded by 100° - 110° E., 10° - 20° N. Cases where this 10° box included 0.40 coverage or more of DHC only occurred 6% of the time. The mean coverage is about 0.15. This figure reiterates the statement made earlier concerning the special nature of DHC; namely, considerably restricted in coverage as compared to cloud coverage in general. Comparisons with radar and rainfall data presented in the next section will emphasize this further.

### 3. DENSE HIGH CLOUD VS. RADAR AND RAIN INDICES

Comparisons of radar echo areas with DHC indicated that rain areas are related to DHC areas. This and the fact that DHC coverage makes up about one-fourth of the clouds over Indochina prompted a quantitative analysis. Saigon radar data were used to obtain radar indices for a 50 n. mi. circle (see fig. 7). Echo areas were weighted (0.25 - scattered, 0.70 - broken, 0.95 - solid, and 1.00 - "cell") to obtain an estimate of the radar rain area. The Radar Index is the radar rain area divided by the total area in the 50 n. mi. circle. DHC (to nearest tenth of 10% of coverage) readings were made for 2 deg. lat. by 2 deg. long. boxes, one centered at Saigon and four overlapping as indicated in figure 7. The mean percent coverage of DHC for 53 cases in June, July, and August 1966 for the five boxes are:



For geographical locations refer to figure 7. The averages for land, except for the Delta box (lower left), are almost 10% of coverage more (40% more DHC) than the ocean box (lower right). The Saigon box is closer to the inland averages than the ocean value. A correlation coefficient of 0.70 was obtained between DHC in the central box and Radar Indices. An independent reading of DHC, to reduce random reading errors, was made; alone it gave the same coefficient and the average of the two readings gave a correlation coefficient of 0.79. The data are given in figure 8 along with the least squares line of best fit.

Some estimates of the probability of rain occurring at a point in DHC can be made. The regression equation gives a Radar Index of 50.4 when Dense High Cloud is 100%. Although it may be representative of large areas of thunderstorms, it is, however, too high for DHC as a whole. If rain occurred only in DHC, the mean percent area would be 47.4 which is the mean Radar Index divided by the mean DHC. As can be seen from figure 8 some rain occurs for cases 0% DHC. The 14 cases with 0% DHC give an average RI of 1.6. Assuming that this value is representative of the entire area without DHC,

$$1.6 (1 - \overline{DHC}) + F (\overline{DHC}) = \overline{RI} \quad (1)$$

where  $\overline{DHC}$  = mean DHC cover,  $F$  = percent of rain area in  $\overline{DHC}$ , and  $\overline{RI}$  = mean Radar Index. Solving for  $F$ ,

$$F = \frac{\overline{RI} - 1.6 (1 - \overline{DHC})}{\overline{DHC}}$$

$$F = \frac{10.9 - 1.6 (1 - 0.23)}{0.23}$$

$$F = 42.0\%$$



Assuming that rain is equally likely at all points in the 50 n. mi. circle around Saigon, the Radar Index is the probability of rain occurring at a point in the area. For the cases under discussion the value of the mean RI is 10.9%, about one-fourth as large as F, which points out the value of knowing whether or not DHC is present.

Another interesting comparison can be made with F. The total cloud coverage, as reported by meteorological stations, is not known for the area and cases under discussion; however, the climatological mean is about 80%<sup>1</sup> for June, July and August at Saigon. In the following discussion, values for 75% and 85% appear in parentheses after the value for 80% coverage. Similar to equation (1), we can write,

$$0 (1 - C) + G (C) = \overline{RI}$$

where, C = cloud coverage and G = percent of rain area in cloud. Solving for G,

$$G = \frac{\overline{RI} - 0}{C} = \frac{10.9}{0.80 (.75, .85)}$$

$$G = 13.6\% (14.5\%, 12.8\%),$$

which is about one-third as large as F.

The HRIR observations were made almost in the center of a 12-hour accumulated precipitation observation. Since precipitation is widely variable in time and space, an arbitrary rainfall index based on the 6 stations shown in figure 7 was devised. The 12-hour rain index which has a scale from 0 to 9 is defined by figure 9. A correlation coefficient of 0.65 was obtained for DHC and the Rain Index. The data points and regression line are given in figure 10. More frequent satellite measurements would undoubtedly improve the relationship.

These results indicate that bright areas (Dense High Cloud) in HRIR pictures are areas of deep cumulus convection. This is an important difference between the video and HRIR systems. Video pictures do not accentuate the difference between bright low stratiform clouds and bright deep cumulus convection as do the HRIR pictures.

#### 4. SOME DENSE HIGH CLOUD SUMMARIES

To get some idea of the small scale geographical distribution and large scale day-to-day variations of DHC, analyses were performed as detailed below.

##### 4.1 Small Scale Monthly Means

In view of the relationships between DHC and the precipitation indices presented in the previous section, one-degree readings of DHC percentage were made for June, July, and August 1966. There were 24 days in June, 14 in July, and 19 in August. Monthly means are presented in figure 11.

In June 1966 the South China Sea was very inactive. In fact, ocean areas, in general, tend to be inactive and land areas active in June. An exception is in the top left corner. The Burma area is low and north Bay of Bengal is high in DHC coverage. The same tends to hold true for July except coverage over the South China Sea has gone up with an active center located at about 11° N., 114° E. This active area is also present in August at 13° N., 116° E. Activity over Indochina is high in August as compared to June and July.

##### 4.2 Large Scale Day-to-Day Variations

Large scale day-to-day variations were investigated by examining the percent coverage of Dense High Cloud over SEASIA between latitudes 10° and 20° N. and longitude 100° and 110° E. as shown in figure 12. These readings indicate a tendency for "pulses" with lengths of a week to ten days.

<sup>1</sup> For a 34-year record Climate of Republic of Vietnam, 20th Weather Squadron, 1st Wea. Wg. (MATS), pg. 94, gives mean cloudiness of 78% for June, 82% for July, and 79% for August.

There is some suggestion that on a night-to-night basis, activity is followed by activity and vice versa. A summary of statistics of 24-hour change in DHC cloud-cover from 15 May to 1 November 1966 for the SEASIA area, 100° - 110° E., 10° - 20° N., is given in figure 13. Figure 13(a) gives the number of cases of various amounts of DHC 24 hours following a given amount of DHC. For instance, two-tenths of DHC was followed by one-tenth 14 times and by zero-tenths 0 times. Three-tenths was followed by three-tenths 5 times. Figure 13(b) shows how the distribution would look if there were no connection (random) between adjacent nights derived from the frequency distribution of DHC, figure 6. Figure 13(c) shows the excess (or deficit) of cases observed over what would be expected if the amounts of DHC occurred at random. For example, there is a tendency for two-tenths to decrease to one-tenth but not to zero-tenths. Zero-tenths is very persistent.

The best forecast based on the observations given in figure 13(a) and for a minimized root-mean-square error is given in figure 14 along with the persistence forecast. The abscissa and ordinate are in tenths of coverage. The greatest difference is on the high end and is about one-tenth at four-tenths coverage. Figure 15 gives the error (percent DHC) with time for the seasonal mean forecast, persistence (subscript one) for readings with random errors and persistence (subscript two) without random reading errors. Notice that the 24-hour RMS error for persistence (subscript one) is about equal to the error for climatology. The point M is for the minimized RMS prediction without reading error. The reading error is based on results of three readings of 200 10 deg. by 10 deg. boxes. These results are, of course, for midnight to midnight. Diurnal changes should be considered to uses at other times.

These results indicate that there are large scale slow moving or varying systems producing areas of activity. We also get this impression from video and infrared pictures of "blobs" and long broad bands of activity. However, studies of synoptic maps in conjunction with satellite pictures have not revealed any definitive relationships.

#### ACKNOWLEDGEMENTS

I wish to thank my coworkers of the Satellite Meteorology Branch for their numerous suggestions. Thanks to Richard Sizer, also of AFRL, for the drafting.

#### REFERENCES

1. STAFF MEMBERS, NASA, "Nimbus II Users' Guide." Washington, D. C. 1966.
2. WIDGER, W. K., et al., "Meteorological Interpretation of Nimbus High-Resolution Infrared (HRIR) Data," NASA Contractor Report CR-312, Washington, D. C. 1966.

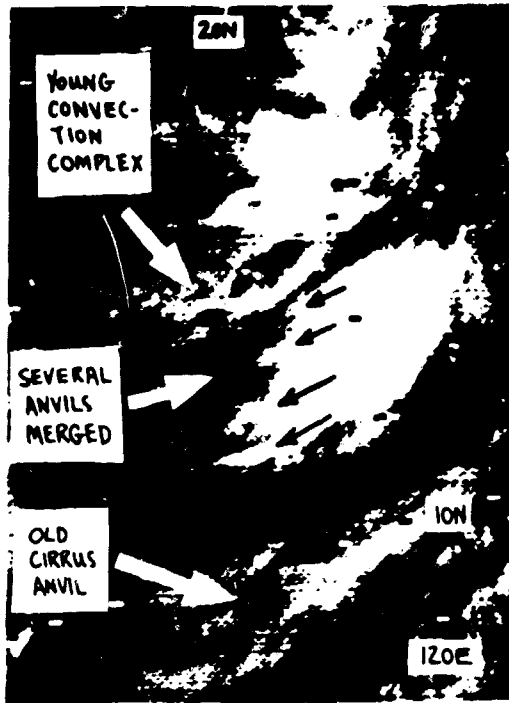


Figure 1. Examples of Several Types of Clouds Including Cumulonimbi, Anvils, and Cirrus. A non-cluttered copy is given in figure 2. Nimbus II, Orbit 1522, 6 September 1966.



Figure 2. Same as Figure 1 but for larger area and without markings.



Figure 3. An Example of Radar Echo Areas Superimposed on the HRIR for Stations Udon and Saigon. Nimbus II, Orbit 777, 12 July 1966, 1650 GMT. Time of radar is 1530 GMT (2330 local time).

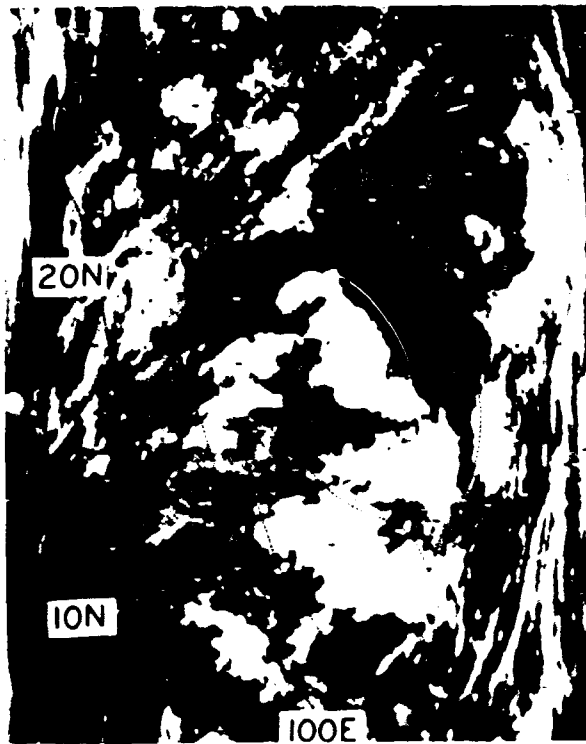


Figure 4. Same as Figure 3 but for larger area and without Radar Echo Areas. The dashed line is geography of Indochina.

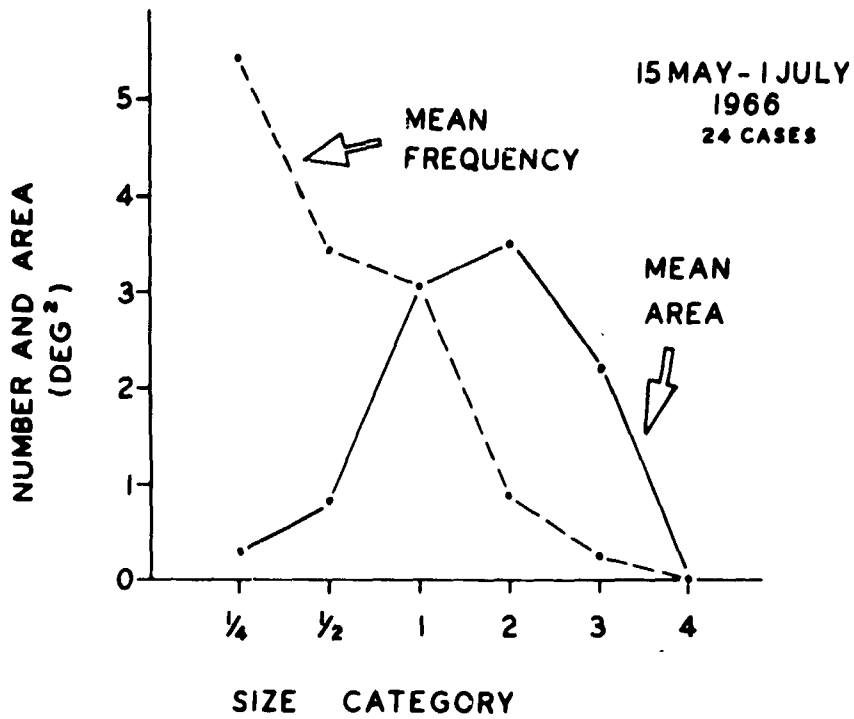


Figure 5. Mean Frequency and Average Area of Coverage for Various Categories of Thunderstorm Areas, 100° - 110° E., 10° - 20° N.

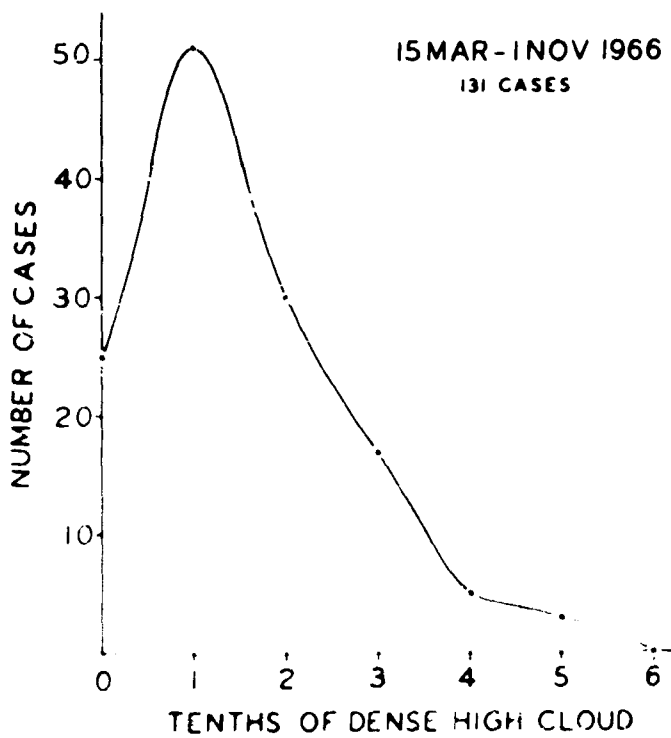


Figure 6. Frequency Distribution of Coverage of Bright Area in Box Defined by 100° - 110° E., 10° - 20° N.

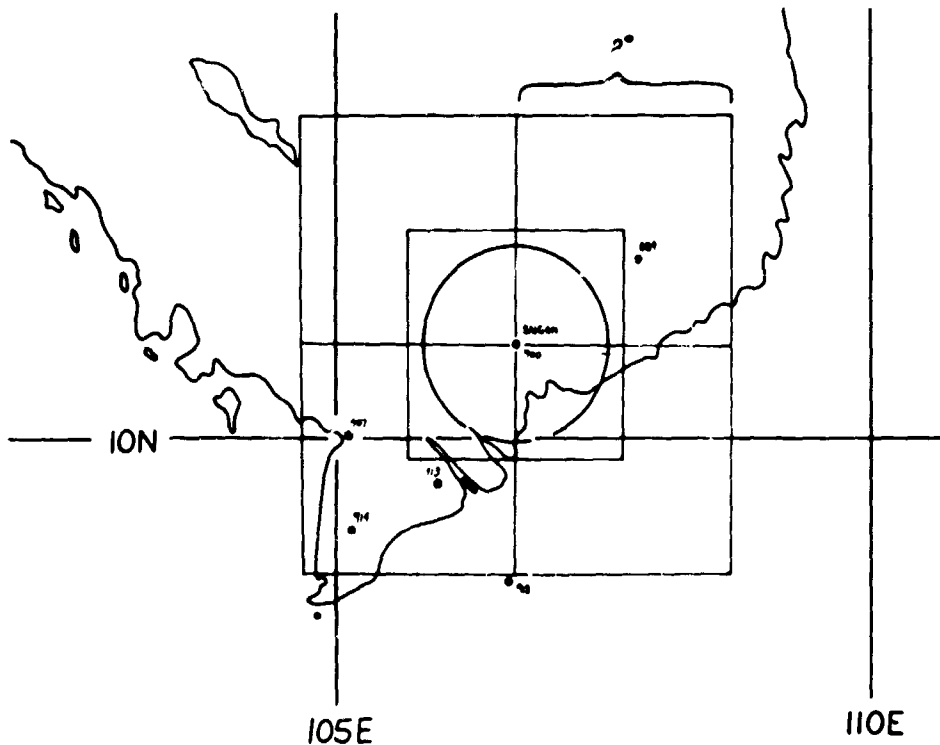


Figure 7. Base Map for Comparisons of Dense High Cloud With Radar and Rain Indices. Boxes are 2° lat. by 2° long. and the circle has a 50 n. mi. radius. The six stations used for the precipitation index (884, 900, 907, 913, 914, and 918) are indicated.

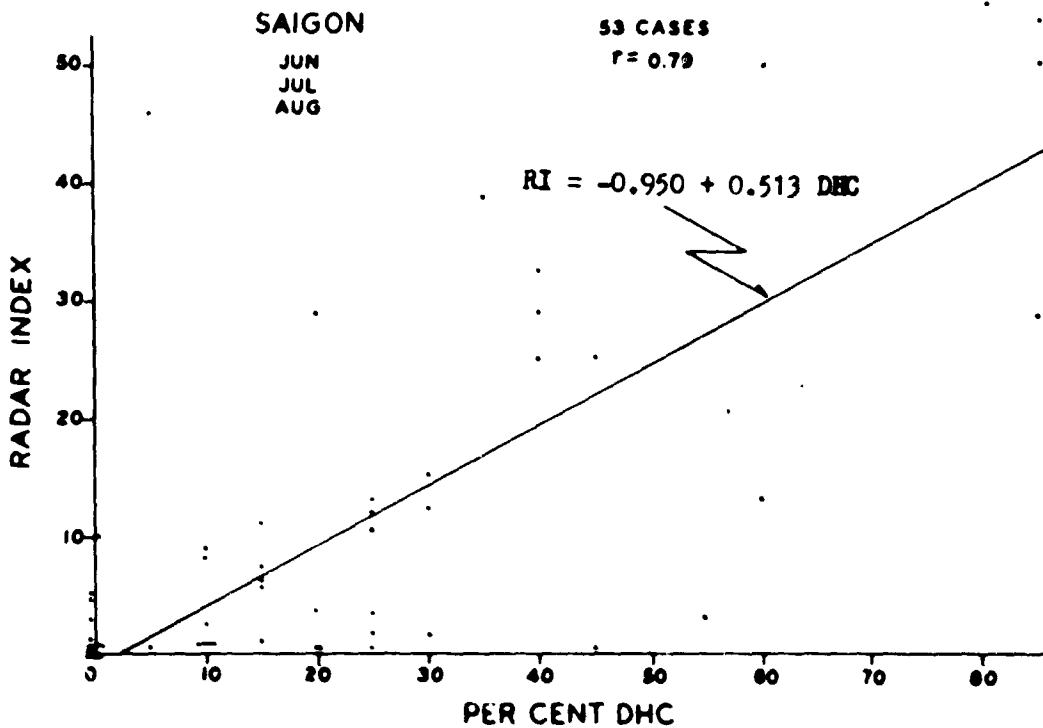


Figure 8. Dense High Cloud Percentage Versus Radar Index and Line of Regression.

Millimeters of Precip. for station with largest amt.

No. of Stations with precip. less than 5 mm	Millimeters of Precip. for station with largest amt.				
	<5	>5 <10	>10 <20	>20 <50	>50
6	0	—	—	—	—
5	—	1	2	3	4
4	—	2	3	4	5
3	—	3	4	5	6
2	—	4	5	6	7
1	—	5	6	7	8
0	—	6	7	8	9

Figure 9. Definition of Six Station Rain Index.

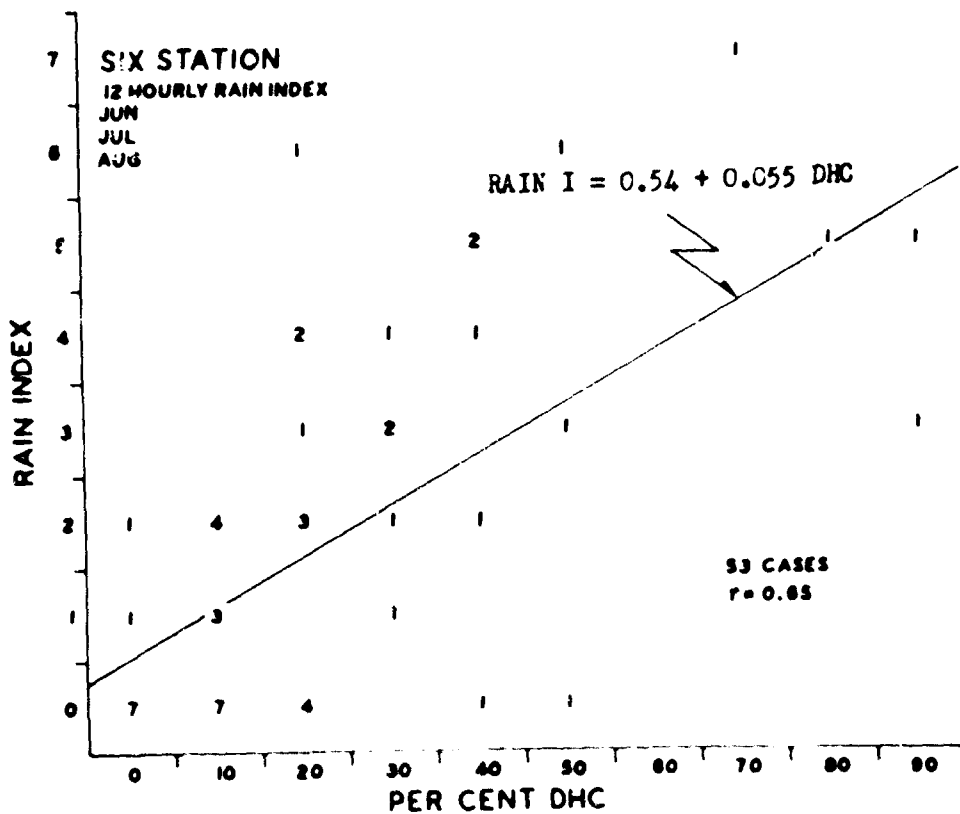


Figure 10. Dense High Cloud Percentage Versus Rain Index and Line of Regression.

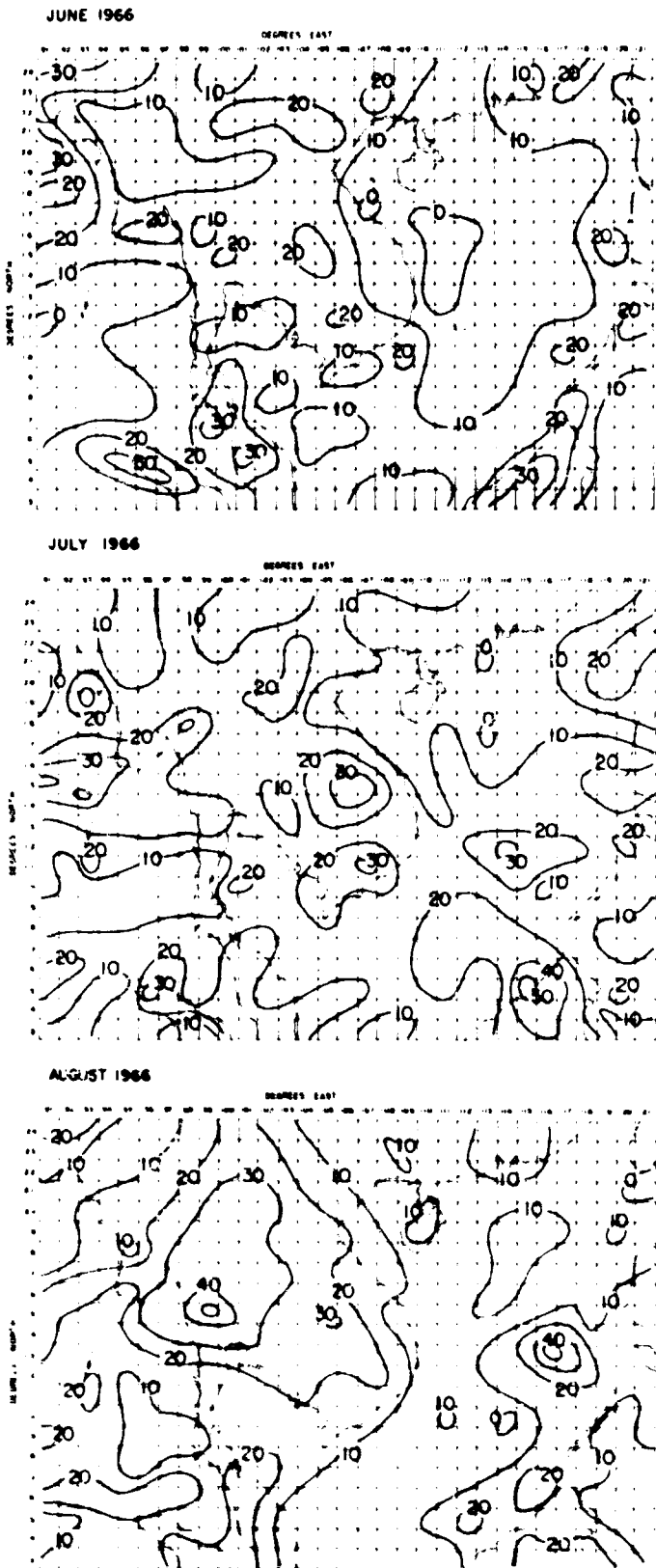


Figure 11. Mean Percent of Dense High Cloud Read for One-Degree Squares for June, July and August 1966.



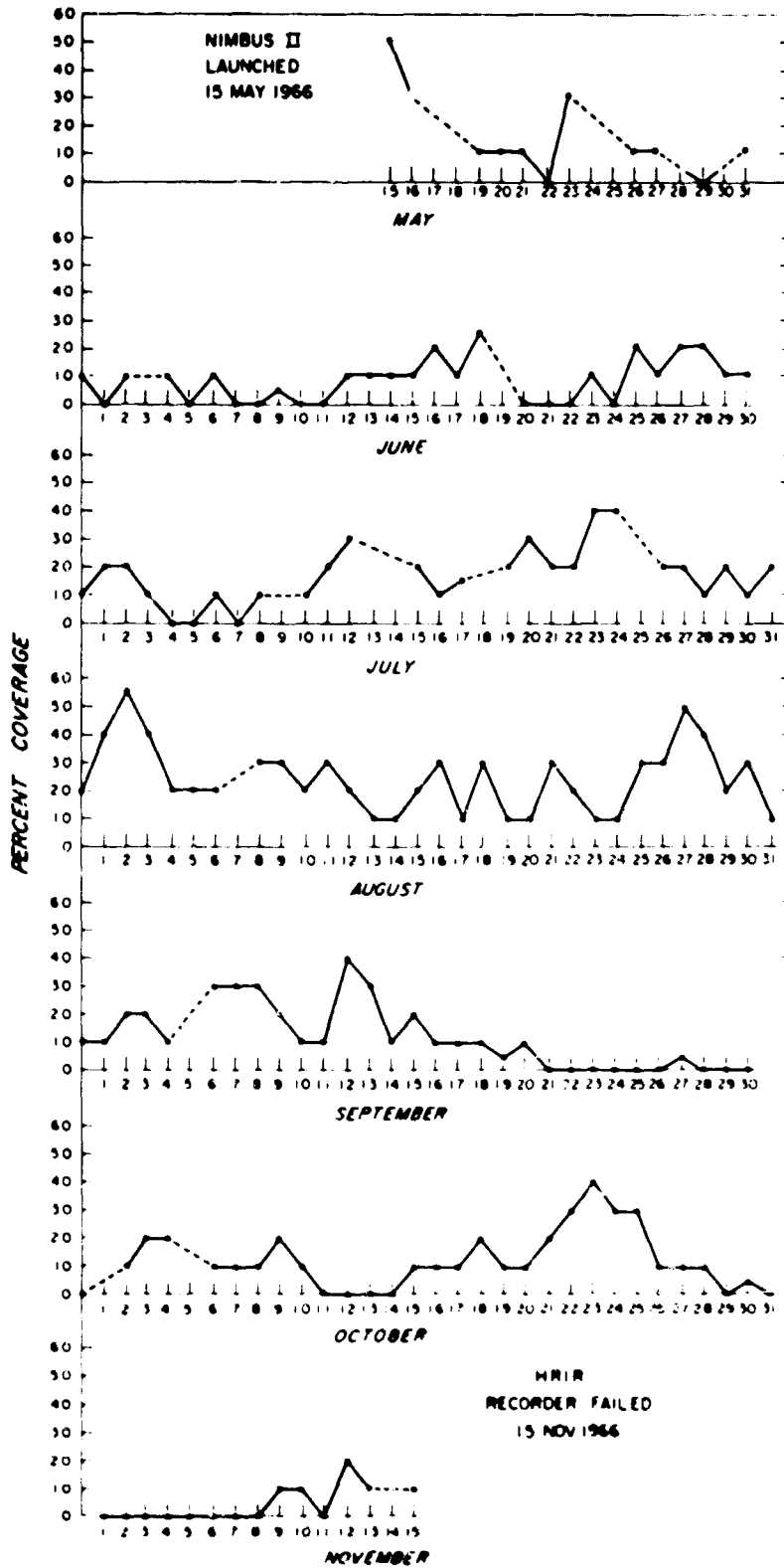


Figure 12. Percent of Dense High Cloud Read for the Area Over Indochina Bounded by 10 and 20 Degrees N. and 100 and 110 Degrees E.

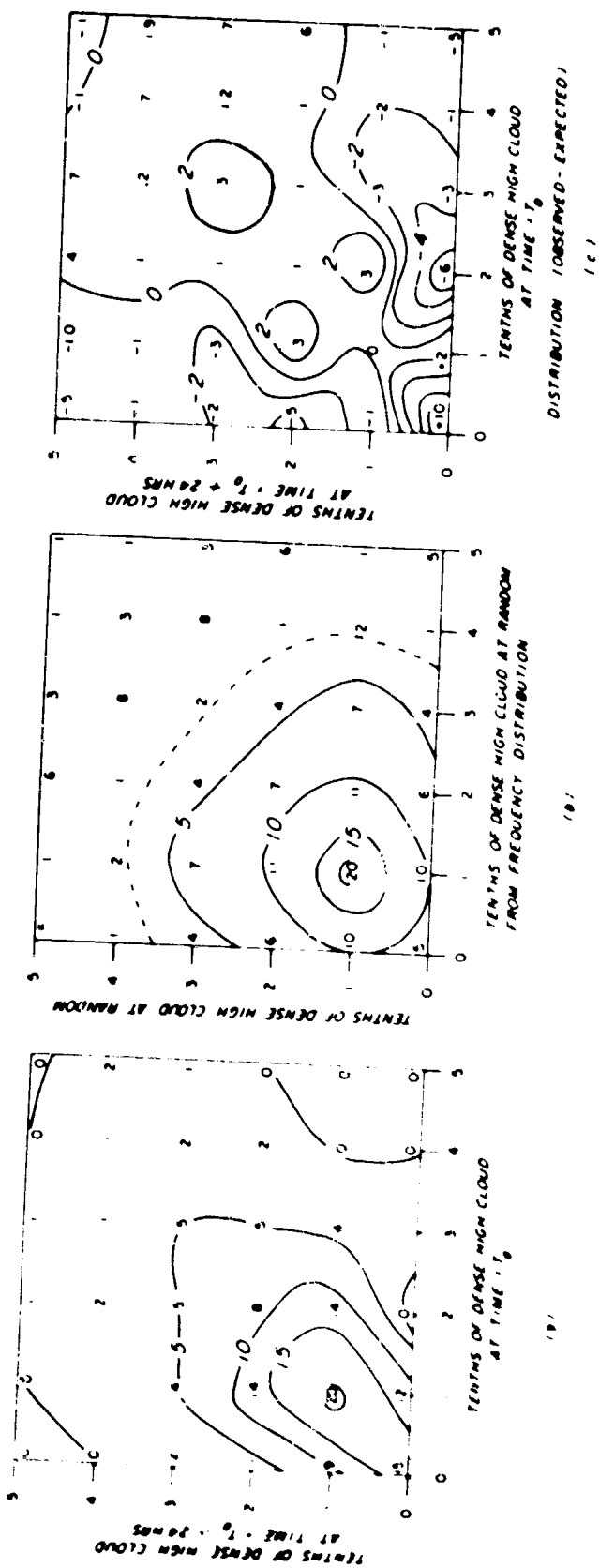


Figure 13. A Summary of 24-Hour Change of DHC for the Area Over Indochina Bounded by 10 and 20 Degrees N. and 100 and 110 E.

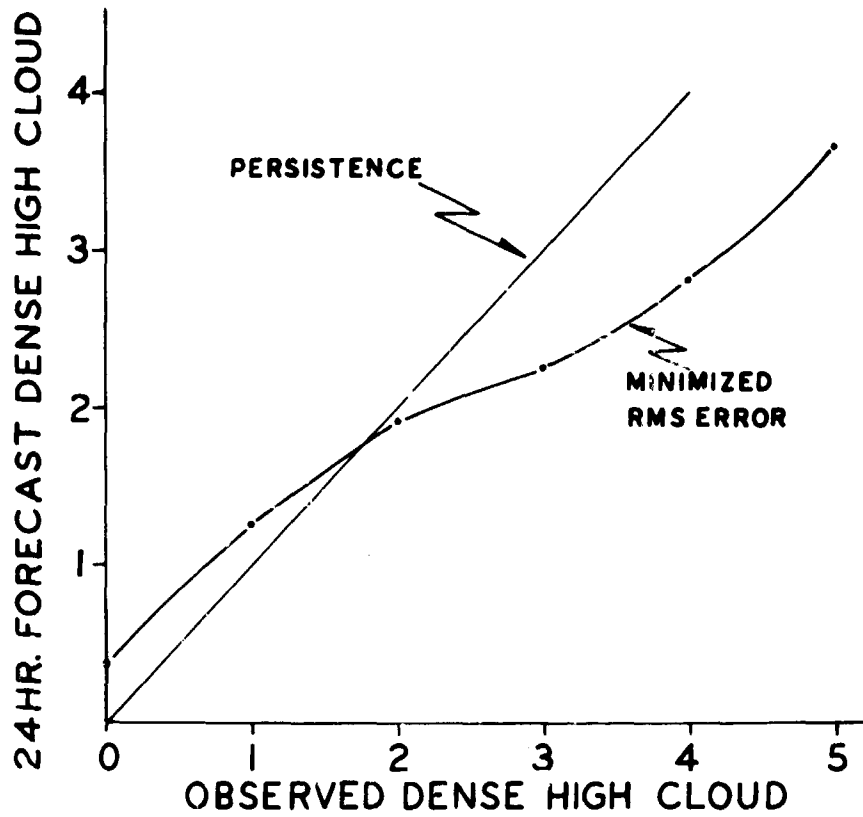


Figure 14. Persistence and Minimized RMS Error Forecast for 24 Hours for DHC in Area Over Indochina Bounded by 10 and 20 Degrees N. and 100 and 110 E.

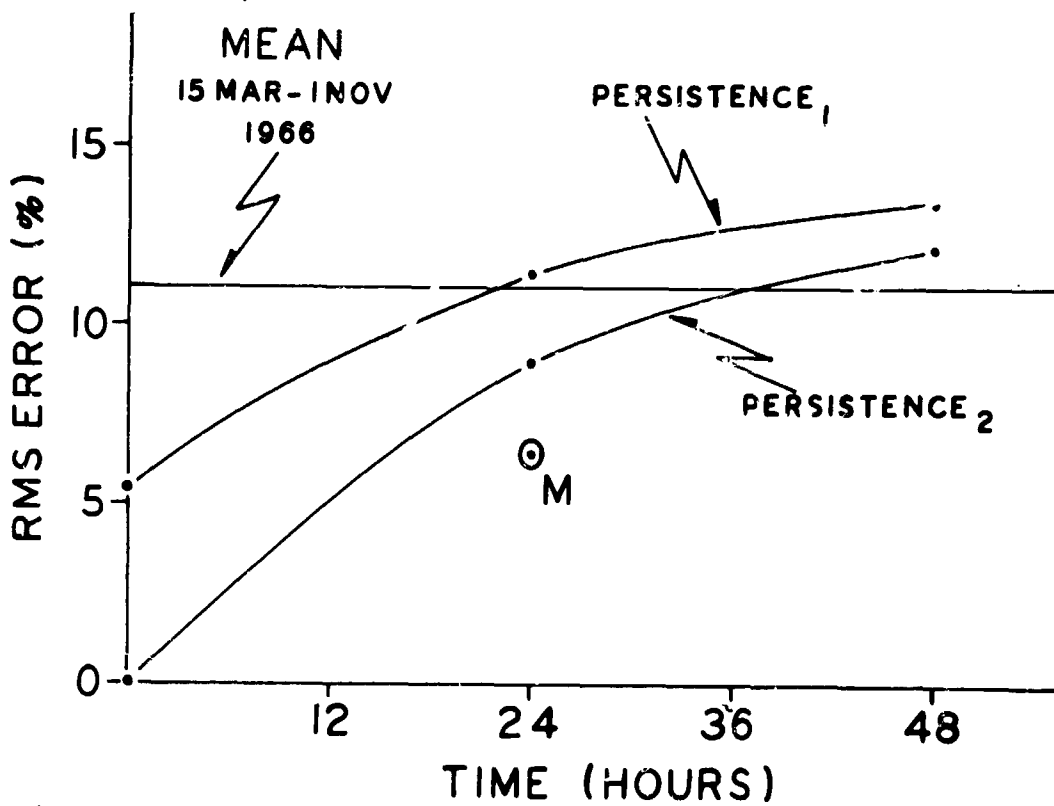


Figure 15. Persistence<sub>1</sub> With Reading Error and Persistence<sub>2</sub> Without Reading Error and Mean DHC With Time.

DERIVATION OF CONVECTIVE FORECASTING MODELS FOR  
NORTHERN AUSTRALIA FROM A CLIMATOLOGY OF LIGHTNING DISCHARGES \*

R. L. Southern, W. R. Kininmonth and N. R. Pescod  
Commonwealth Bureau of Meteorology, Darwin, N. T.

ABSTRACT

The occurrence of ground lightning strikes and of total flashes in the Darwin area has been systematically recorded at five minute intervals over a period of three years.

These measurements are associated with simultaneous daily recorders of precipitation at 20 local rainfall stations during the 1967/68 summer monsoon period to provide a quantitative measure of convection occurring around Darwin. This information provides the basis for nomination of four categories of convective activity ranging from suppressed to very active.

Mean temperature, moisture and wind profiles are then prepared for each category. Significant atmospheric variations between the four categories at Darwin are described. Similar profiles are prepared at Alice Springs for the same Darwin categories to ascertain the extent, if any, of higher latitude interaction. A noticeable relationship between the occurrence of a deep relatively moist layer of low level easterlies and absence of strong upper level westerlies at Alice Springs is noted in the case of "organized" activity at Darwin.

Finally, a sequence of synoptic models incorporating the above relationships is presented as the basis for prediction of convective activity in northern Australia.

1. INTRODUCTION

Continuous objective observations of as many facets of convective activity as possible are essential to enable the successful derivation of descriptive atmospheric models to serve as a basis for prediction. In the past lightning discharge registrations have been inadequately used for this purpose, probably due to the unreliability of operation of registering equipment.

As part of a long term programme in lightning research in relation to the electricity supply industry in Australia a series of studies has been made in the Darwin area. The design, specification and effective operation of lightning measuring equipment and counting registers have been reported on by Prentice and Robson [4]. Professor Prentice and his associates in the Department of Electrical Engineering, University of Queensland, have led such investigations in Australia.

Counts of total flash (cloud to cloud and to ground) within a range of 60 miles and estimates of ground strikes only within a range of 20 miles have been recorded at five minute intervals at Darwin Airport (12° S., 131° E.) over a three year period and are continuing. The effective ranges, although not critical to this study, have been calibrated against a reliable surface network.

This paper utilizes the occurrence of lightning and rainfall over 24-hour periods to break down the wet season months November 1967 through March 1968 into four categories of convective activity; namely, thundery rain days, lightning days with little rain, days of organized or general rain, and "fine" days of much reduced rainfall.

Mean wind, temperature and moisture profiles are then deduced for each of the four categories, and tests are applied to determine the significance of relationships. Finally, mean profiles at Alice Springs (24° S., 134° E.) are examined for each of the Darwin categories to ascertain the extent, if any, of higher latitude interaction, and a series of surface charts is produced of the macroscale features controlling convection in the tropical Northern Territory.

As a prelude to the study a brief discussion of the climatology of convection at Darwin is presented.

\*Research sponsored by Bureau of Meteorology, Australia

## 2. CLIMATOLOGY OF CONVECTION AT DARWIN

The convection cycle at Darwin has been discussed by Hyson, Leigh and Southern [2]. Briefly, the climate is monsoonal with distinct wet (January through March) and dry (May through September) seasons, the remaining months being transitional. Only two percent of Darwin's annual rainfall of 60 inches occurs in the dry season when large cumuloform cloud is rare. The pre-wet transitional months, October through December, are increasingly thundery resulting in 25 percent of the annual rainfall. Agricultural growth is sustained from about mid-November. The wet season inevitably concludes more abruptly than it commences as the atmosphere rapidly stabilizes and dries with the onset of anticyclogenesis over the continent. The remaining post-wet transition month of April produces about five percent of the annual total.

More than two-thirds of the annual rainfall falls in the central wet season months January through March. Of these days, based on a limited synoptic study by Southern [5] for the Darwin-Katherine region for two seasons, about one-third are monsoonal or cyclonic in character, about twenty percent comprise other organized rain days, about one-third comprise days of unorganized rainfall, and the remaining days are quite dry. This variation provides fair scope for forecasting skill.

## 3. CLIMATOLOGY OF LIGHTNING DISCHARGES

Mean daily registrations of total flashes for each month for the years 1966-1968 and mean monthly rainfall for Darwin are shown in figure 1(a). The main features are the increase in total flash activity in the pre-wet transition and the subsequent suppression in February-March in the rather more stable atmosphere with its sometimes stratified monsoonal cloud layers and subdued surface heating.

Figure 1(b) depicts the diurnal variation of total flash for November through March 1967-1968 plotted against the diurnal rainfall distribution for a twelve-year period for reference. A primary maximum of lightning activity in late afternoon in November and December loses ground to a secondary maximum in the early hours of the morning in January through March. A similar shift also occurs in the diurnal rainfall distribution as the monsoonal period develops and the rainfall loses its more noticeable diurnal character.

## 4. CLASSIFICATION OF CONVECTIVE RAINFALL CATEGORIES

As the basis for relating the occurrence of lightning and rainfall in the greater Darwin area during the 1967-1968 wet season, 20 daily rainfall recording stations were selected providing the best spatial distribution permitted by the network. These are shown in locality map, figure 2. Stations probably beyond the effective range of the counters were also included in order to ensure that days of organized or general rain in the area were properly assessed.

Table 1 sets out the mean daily rainfall and lightning registrations for each month considered. The distribution is quite similar to the longer term picture shown previously in figure 1(a). This table serves as the basis for the necessarily somewhat arbitrary nomination of categories of convective activity shown in table 2. The mid-values of the monthly means were used as the boundaries of each of the four classes.

It should be made clear that lightning flash counters respond to both cloud and ground flashes and that a large correction factor must be applied to derive the actual proportion of the counter readings due to ground strikes. For this reason the mean daily ground strikes shown in table 1 should not be considered absolute. To derive ground-flash density, the ratio of effective range for cloud flashes to effective range for ground flashes, and the ratio of cloud flashes to ground flashes are required, as well as the effective range for ground flashes. These ratios, and estimates of ground-flash density are discussed by Prentice and Mackerras [3].

The classification scheme provides that each day must be divided into either of two major conditions (total flashes greater or less than 5000) and at least two of the minor categories shown. If two categories seem equally valid, the

Table 1. Means of the Parameters Used in Determining the Classification of Convective Categories.

Month	Mean Daily Rainfall per Station (inches)	No. Stations Receiving Rain	Mean Daily Total Flash Count	Mean Daily Ground Strikes
November 1967	.12	7	5240	158
December 1967	.20	7	7930	257
January 1968	.52	13	5072	135
February 1968	.82	17	2672	25
March 1968	.24	10	2787	110
Complete Period	.38	11	4959	142
Mid-Value of Monthly Means	.24	10	5072	135

Table 2. Classification of the Convective Categories Used in the Analysis.

No.	Category	Major Condition		Minor Conditions	
		(Total Flash)	Ground Strikes	Rain (inches)	Stations Receiving Rain
1	Thunder	≥5000	≥140	≥.25	≥10
2	Lightning	≥5000	<140	<.25	<10
3	Organized	<5000	<140	≥.25	≥10
4	Fine	<5000	<140	<.25	<10

numerically lower is chosen. The categories are designated as thunder, lightning, organized and fine days respectively for simplicity, but with the following general meanings:

- Thunder: Generally well-distributed rain accompanying considerable lightning and nearby thunder (ground strikes). Common in December.
- Lightning: Considerable lightning between high base cumulonimbus clouds and generally light or well scattered rainfall.
- Organized: Well distributed general rain with below average lightning activity.
- Fine: A day of few lightning counts and little or no rain at most places.

Figure 3 illustrates the number of days allocated to each category and, in accord with expectation, these do, in fact, show the gradual transition from fine to lightning and thunder days and organized rain days as the season progresses.

It is now necessary to relate various atmospheric variables to each of the four categories to ascertain whether interesting or significant relationships exist.

## 5. TEMPERATURE AND FLOW CHARACTERISTICS AT DARWIN AND ALICE SPRINGS

Observations at Alice Springs as well as at Darwin were considered in order to gain an idea of the meridional cross-section. Temperature and flow characteristics for each day were assessed as the mean of the observations at 0900 that day and at 0900 the following day. This period then coincided precisely with the period of the rainfall and lightning registrations used in the classification system.

Temperature and Moisture Profiles. Figures 4(a) and 4(b) provide the mean profiles of temperature and mixing ratio at Darwin and Alice Springs for each category. Median values of mixing ratio were used at levels above 700 mb. in instances where the humidity was too low to be recorded. Where differences between categories appear, marked significance tests were conducted and are included in the figures. A contribution for immeasurable mixing ratios was allowed assuming a normal distribution. At Darwin the principal differences occur in the mixing ratios above 850 mb. and in the more stable temperature sounding on organized rain days. At Alice Springs, where no particular variations had been expected, there is a marked difference in low-level moisture between category 3 and the remainder, and also very noticeable warming above 600 mb. in category 3.

Wind Profiles. The wind profiles at Darwin (figs. 5(a) and 5(b)) provide the mean east-west and north-south components for each category from the surface to above 20 mb. In the zonal flow there is a marked difference in the case of category 3 where a deep layer of westerlies is present in the low levels and a much stronger easterly component exists above 400 mb. In the other categories the low-level flow is generally easterly, then reversing up to 200 m. before strengthening again from the east at greater heights.

Differences are not as marked in the meridional flow although category 3 again shows distinguishing characteristics from the other categories. Here a light northerly component is evident up to 300 mb. changing to southerly below the tropopause.

Corresponding diagrams are shown in figures 6(a) and 6(b) for Alice Springs. Again, category 3 differs strongly from the remainder. The organized rain category at Darwin is accompanied by a much deeper layer of easterlies to 300 mb. and the absence of the strong westerly component associated with the other categories above this height.

The meridional profile also indicates some difference between category 3 and the remainder, the southerly component being weaker through the troposphere while in the stratosphere an interesting, if not significant, stronger northerly component exists.

It is particularly interesting to note the difference in the profiles for categories 1 and 3 in each of the above cases at both Darwin and Alice Springs, both being associated with widespread rain at Darwin but with major differences in the incidence of lightning.

Attempts are now made to relate the above features to synoptic models.

## 6. A SYNOPTIC MODEL FOR ORGANIZED RAINFALL ACTIVITY

A model of the low-level streamline flow for organized rainfall activity at Darwin is shown in figure 7. A deep easterly airflow from the Coral Sea accounts for the relative increase in low level moisture at Alice Springs. When an equatorial trough is located over northern Australia the converging monsoonal air and the relatively moist air of Pacific origin produces general rain in the north. Advection of drier easterly air of a more southerly origin will reduce the buoyancy of the northern air mass inhibiting rainfall.

A deep layer of moist easterlies at Alice Springs is associated with a general weakening and southerly movement of the subtropical westerly jet stream to the vicinity of the Great Australian Bight. This is consistent with the absence of a westerly maximum in figure 6(a) for category 3. Such an effect has been discussed by Troup [6] and corresponds to a similar effect in the Northern Hemisphere noted by Yin [8] and Hutchings [1].

As noted above the only criterion used in separating categories 1 and 3 at this stage is the observed lightning count at Darwin. It can therefore be concluded that the assumption already made that organized monsoonal weather is associated with low lightning counts is well justified. Although no attempt is made to take into account the effect of persistence when conducting significance tests there is close correspondence between the commencement of organized rainfall in mid-January 1968 and the slackening of westerly winds aloft at Alice Springs; in fact, a tropical cyclone developed near Darwin at this time. The correspondence at the end of the wet season is not as marked.

In most cases of organized rainfall activity there is an upper tropospheric easterly regime even though the equatorial trough is not always south of Darwin. This is in agreement with Troup [6, 7]. The absence of the sub-tropical jet stream over central Australia is associated with a reduced meridional temperature gradient in accord with the thermal wind equation. This is consistent with higher temperatures in the upper troposphere at Alice Springs for category 3.

Before discussing rainfall mechanisms in the transition period some thought is given to the thermodynamics of convection at Darwin.

## 7. THERMODYNAMIC CONSIDERATIONS

Figure 4(a) indicates little apparent difference in the temperature soundings for the four categories except for the more stable situation on organized rain days. Experience has shown that the unmodified temperature sounding at 0900 LST is practically useless as a forecasting aid. Modification of the sounding as a means to estimating the buoyancy can be done in two ways, firstly by considering the forecast maximum surface temperature, and secondly by allowing for entrainment.

Earlier results from an unpublished analysis by Kininmonth of January 1967 data indicated that on fine days a shallow layer of westerlies existed in the first five thousand feet of the atmosphere contrasting with the general easterlies of the thunder situation. Kininmonth showed the existence of weak buoyancy on organized rain days, negative buoyancy on fine days and strongly positive buoyancy on thundery days by modifying the sounding in accord with the estimated surface heating. At this stage the sample of data for the month of January is considered too small for significance tests.

In the case of surface westerlies the temperature is prevented from rising unduly by maritime air. However, in the event of surface southeasterly winds prevailing higher inland maximum temperatures will result in greater buoyancy, and convergence with the sea breeze will produce a line of afternoon thunderstorms. These subsequently move northwest in the prevailing flow aloft. This situation eventuates provided the atmospheric moisture content is sufficiently high.

The effect of allowing for entrainment in estimating cloud heights is studied by Hyson, Leight and Southern [2] who show evidence of higher clouds with increasing moisture and more effective buoyancy.

Consideration of the complete five month period of this study shows that there are no longer distinct surface westerlies in the mean for "fine" days. This can be explained by the existence of a second type of "fine" situation in which dry southeasterlies prevail throughout the whole of northern Australia. This, of course, constitutes the normal situation in the dry season when, although there is significant surface heating, lack of atmospheric moisture inhibits thunderstorm activity.

It may therefore be concluded that the major thermodynamic factor necessary for large scale thunderstorm and other rain-producing mechanisms is the presence of adequate moisture in the middle levels. This is illustrated in figure 4(a) which shows that the difference between the moisture traces for categories 3 and 4 is highly significant above 850 mb.

The foregoing comments now lead to transition season models.

## 8. SYNOPTIC MODELS FOR RAINFALL MECHANISMS IN THE TRANSITION PERIOD

The sequence of charts shown in figures 8(a)-(c) combine the ideas presented with concepts reached through forecasting experience in the transition periods.



Figure 8(a) illustrates a situation for suppressed convective activity. The equatorial trough extends across New Guinea and northern Indonesia. A shallow heat low is present over northwest Australia and a weak anticyclone between these two areas of low pressure. Shallow westerlies exist near Darwin. A middle-latitude trough is moving across the Bight resulting in negative isallobars in central Australia thus inducing the region of strong moisture gradient and the associated heat trough to move south.

As the southern trough moves eastward a second anticyclone migrates towards the Bight. By this time the mid-latitude front and associated trough have moved to southeastern Australia as shown in figure 8(b). The continuation of the front into low latitudes can be represented as a surge line or trough which moves northwards with positive isallobars in the south. This movement is associated with strong convergence in the moist tropical air to the north. A trough often extends from northwest Australia to West Irian and this is an ideal situation for thunderstorm activity.

The situation in figure 8(c) occurs irregularly but more frequently in the post-wet transition period. It follows strong anticyclogenesis in the Bight which directs dry southeasterly air over northern Australia where generally fine weather prevails. However in a few cases a rain-producing trough can be traced from the Gulf of Carpentaria westward and sometimes beyond Christmas Island which experiences a renewed rainfall peak at this time of the year.

Frequently the situation in figure 8(b) reverts to that of figure 8(a) as values of the isallobars begin to fall again with the approach of another middle latitude trough and the heat low moves southward again.

The situation in figure 8(b) is favorable for thunderstorm activity for a number of reasons. The first results from local convergence associated with substantial surface heating mentioned above. The second results from formation of a low-level easterly jet stream over land due to differential nocturnal adiabatic cooling along the shores of the Gulf of Carpentaria. This is mainly a winter phenomenon, but is evident to a lesser extent in the transition seasons. The jet reaches a maximum about 0300 LST. Speed convergence occurs as the flow reaches the northern coastline at about the time of the diurnal pressure minimum and this can explain the secondary nocturnal maximum in rainfall and lightning activity.

## 9. SUMMARY

Remembering the limitation of a short period of observations, this investigation shows how counts of lightning can be incorporated into synoptic studies. When a longer series of registrations becomes available, then more rigid models and thermodynamic reasoning relating flow characteristics to convective activity for individual months or lesser periods can be applied.

As far as northern Australia is concerned this study has pointed out significant differences in local and macroscale atmospheric characteristics between days of varying convective activity and postulated the type of synoptic pattern associated with each. The distinguishing features differentiating organized from other activity are especially noticeable. A climatology of radar observations of clouds within a 100 mile radius of Darwin is now being built up to supplement further studies.

In general it might be said that installation of continuously recording lightning counters at other points in the tropics should lead to improved definition of the synoptic processes influencing convection on both macro and meso-scales. Such counters, of course, constitute a very useful alerting system in cases of unsuspected convective activity in the vicinity of aerodromes, especially in the temporary or permanent absence of a radar weather watch.

## ACKNOWLEDGEMENTS

This study would not have been possible without the initiative of Professor S. A. Prentice and his associates at the University of Queensland in establishing a lightning measuring programme at Darwin and elsewhere.

Mr. D. Harrison of the Bureau of Meteorology, Darwin is thanked for his assistance in tabulating data and compiling figures. The comments of meteorologists at Darwin, especially Mr. R. Falls, have been of much value.

## DISCUSSION

CONOVER: Examination of the Tan Son Nhut soundings showed slight differences in dew point between active and inactive days. However, they failed to indicate activity 4 hours later. The difference in the averages was because active and inactive days come in groups. My conclusion was that soundings merely show current conditions and have no predictive value to indicate a coming change. Did you analyse in this respect?

SOUTHERN: We attempt to modify our 0900 LST soundings to account for expected surface heating for mid-afternoon. The 0900 low-level wind profile is used for this purpose. There is a limit to the success of this method and so far it has been attempted for a short period only. We prefer to associate convection with certain typical wind profiles irrespective of the current sounding.

RAMAGE: Mid-tropospheric warming over Alice Springs when organized rain is falling in the Darwin area, corresponds very well to similar events over northwest and west India when presumably air coming up in the rain area spirals north and warms by subsidence.

BELL: Do you get counts on your instrument from fair weather cumulus? We found in Hong Kong that fair weather cumulus with quite low tops would give counts. If the threshold were raised, then it would not count thunderstorms.

SOUTHERN: The minimum threshold of total flash counts on a completely dry day is about 500, but the minimum threshold for ground strikes is virtually zero and so the latter counter provides the best alerting device for convection near the aerodrome. Total flashes go up to 20,000 or so on days of much lightning activity and ground strikes up to 1,000 or 1,250 on days of intense local thunderstorm activity.

SOMERVELL: A comment concerning a similarity between the type of precipitation over Darwin and that over southeast Asia. The heavy thunderstorm activity in both locations occurs just before passage of the so-called monsoonal trough, with the widespread organized precipitation occurring after its passage. It may be equally interesting to note that in point of time, Darwin follows quite nicely in the progression of the organized precipitation maximum southward across southeast Asia and the Philippines, Indonesia and into Darwin. The point of this is that the summer monsoon in both hemispheres does not set in simultaneously throughout the area but follows an orderly progression and extension of the onset of the winter monsoon in the other hemisphere. A further comment with respect to the pronounced January 1967 organized precipitation maximum at Darwin. During January 1967 there was a marked surge in the northeast monsoon over southeast Asia and the South China Sea. This surge was examined by the Working Panel on the southeast Asia northeast monsoon conducted at Norfolk in August 1968, and more recently at the University of Hawaii by Danielsen and Ho. It should prove interesting during the workshop, to investigate any relationship between the Northern Hemisphere surge, and the position and intensity of Southern Hemisphere precipitation characteristics as well as the monsoonal trough.

MILLS: Your example (fig. 8(b)) of a thunderstorm day indicated a cold front trailing from southeast towards Darwin -- is this common (or) normal?

I believe the energy from polar fronts invades the tropics and through the equatorial region. Example: June 1967, southeast Asia.

SOUTHERN: It is common experience that outbreaks of thunderstorms along the northern tropical coast follow anticyclogenesis over central Australia which follows movements of major troughs into southeast Australia. The cold front does not often reach into the tropics but a surge line in the southeasterlies does occur fairly regularly which triggers off convective activity.

FENTON: Since one type of sounding is correlated with organized activity and a different type of sounding with fine weather, in the transitional period between two types the soundings may be similar going from good weather to organized activity and going from organized activity to good weather. It is possible to forecast the trend by preparing a prognostic sounding from the prognostic flow charts for Australia or southeast Asia.

SOUTHERN: The answer should be a qualified affirmative but as long as the prognostic flow pattern is recognized as typical of a certain degree of activity this should be all that is necessary. The object of this study is to build up

a series of synoptic patterns progressing through cycles of suppressed to organized activity and so on. The movements of the surface heat lows, higher latitude troughs and anticyclones and disposition of the subtropical jet stream seem to be the key features.

VALOVICIN: Do you know the relationship between the tropopause heights and the moderately strong echoes that have cloud tops exceeding 50,000 feet.

SOUTHERN: Not offhand, but we can look into this easily enough. The mean height of the tropopause over Darwin is about 54,000 feet, close to 100 mb. and from memory there is not a great deal of variation.

#### REFERENCES

1. HUTCHINGS, J. W., "Proceeding of the W.M.O. Symposium, on Tropical Meteorology." New Zealand Meteorological Service, 1964.
2. HYSON, P., R. M. LEIGH and R. L. SOUTHERN, "Proceeding of the W.M.O. Symposium, on Tropical Meteorology." New Zealand Meteorological Service, 1964.
3. PRENTICE, S. A. and D. MACKERRAS, "Recording Range of a Lightning-Flash Counter." Proc. IEE., Vol. 116, No. 2, 1969.
4. PRENTICE, S. A. and M. W. ROBSON, "Report on Lightning Investigation - Darwin Area." Department of Electrical Engineering, University of Queensland, 1968.
5. SOUTHERN, R. L., "Working Paper 65/3203." Commonwealth Bureau of Meteorology, 1966.
6. TROUP, A. J., "Variations in Atmospheric Flow Associated With the Onset of the Australian Summer Monsoon." Ind. J. Met. Geophys., 12, 1961.
7. \_\_\_\_\_, "Variations in the 200-mb. Flow in the Tropics." Met. Mag., 90, 1961.
8. YIN, M. T., "A Synoptic Aerologic Study of the Onset of the Summer Monsoon Over India and Burma." J. Met., 6, 1949.

Fig. 1a. ANNUAL VARIATION OF LIGHTNING AND RAINFALL

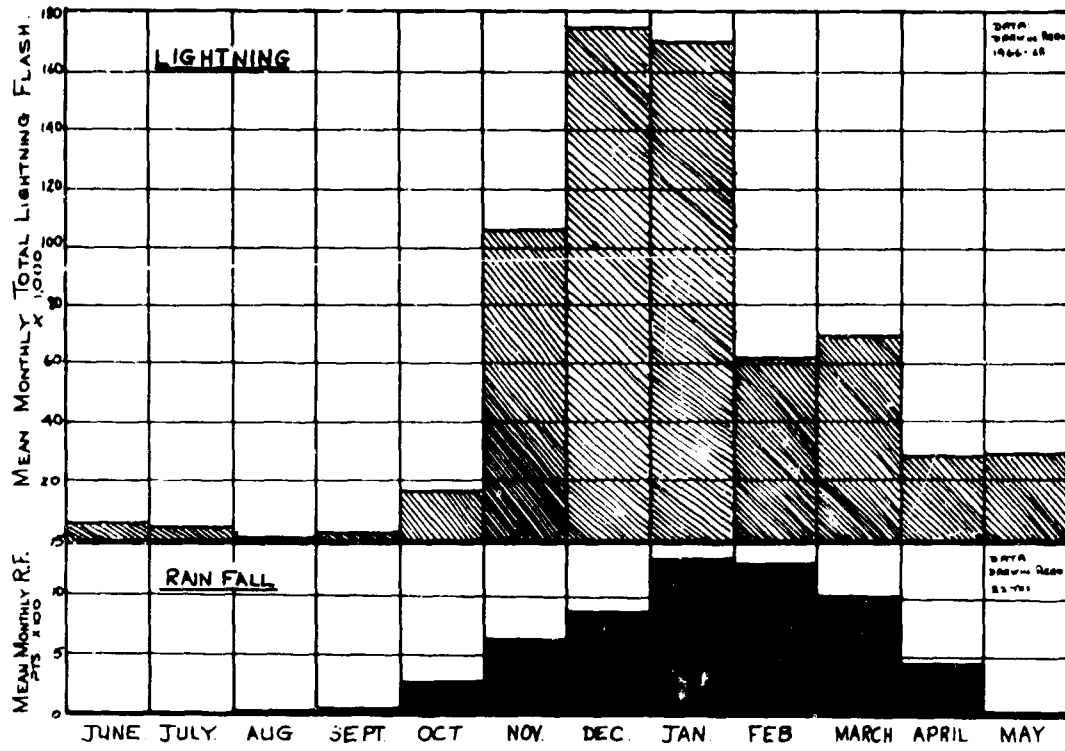


Figure 1a. Annual Variation of Lightning and Rainfall.

Fig. 1b DIURNAL VARIATION OF RAINFALL AND LIGHTNING STRIKES.

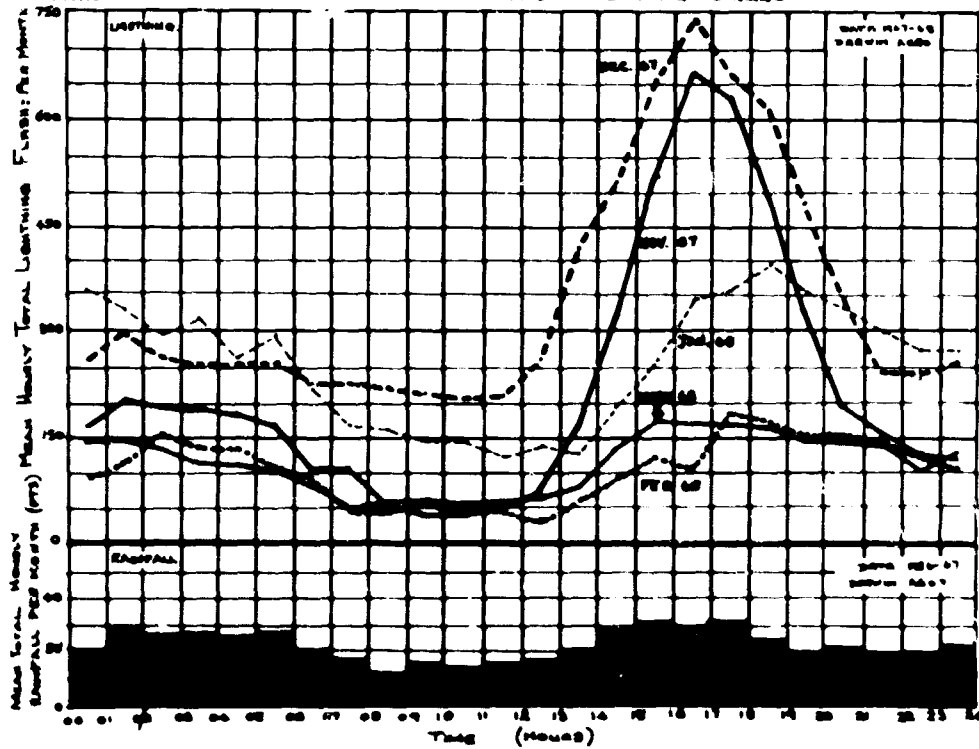


Figure 1b. Diurnal Variation of Rainfall and Lightning Strikes.

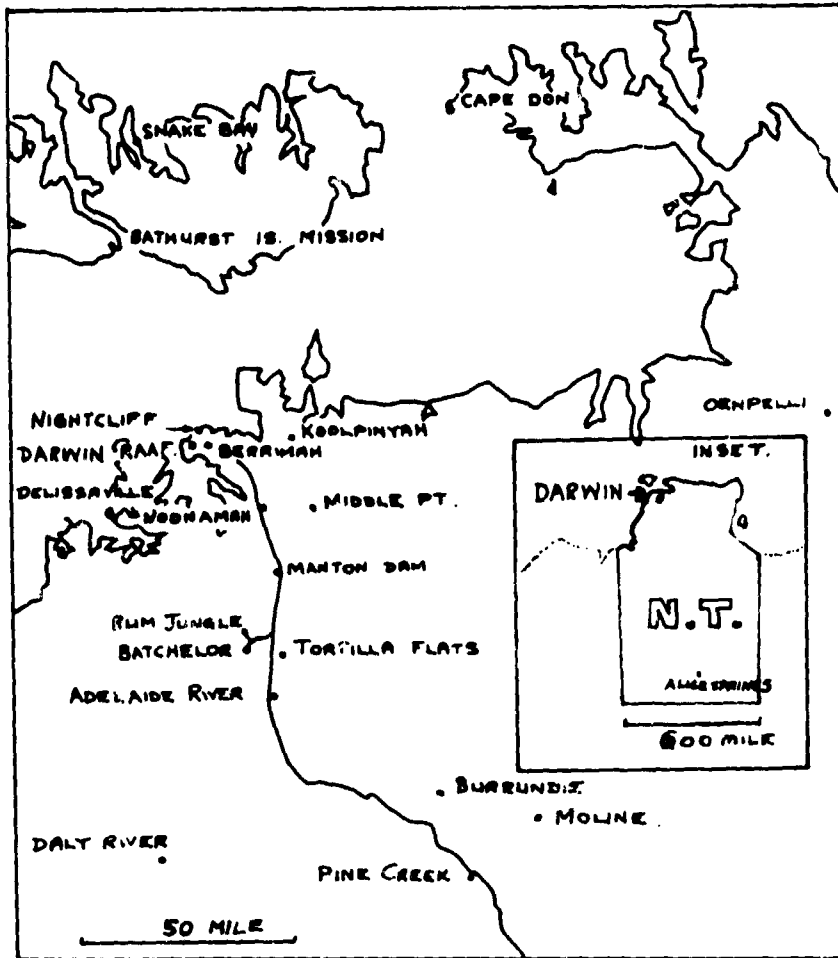


Figure 2. Location Diagram of Rainfall Recording Stations Included in Analysis.

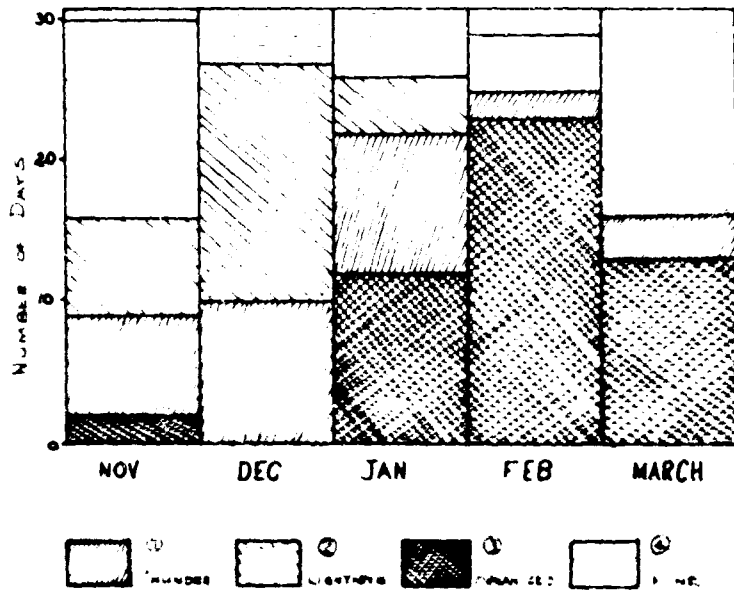


Figure 3. Monthly Distribution of Rainfall Recording Days in Four Categories.

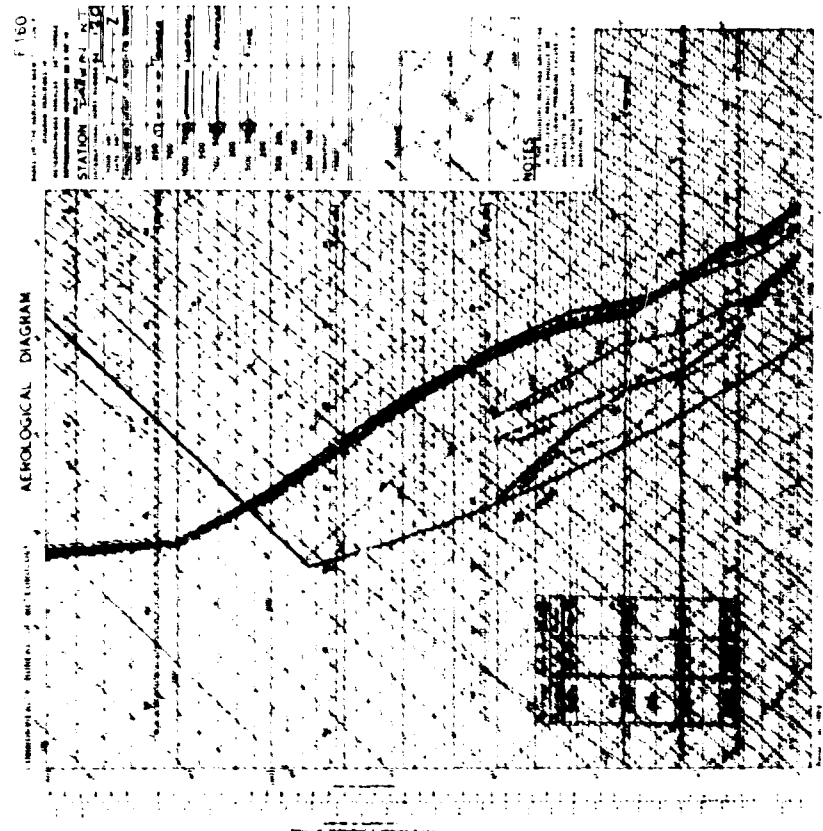
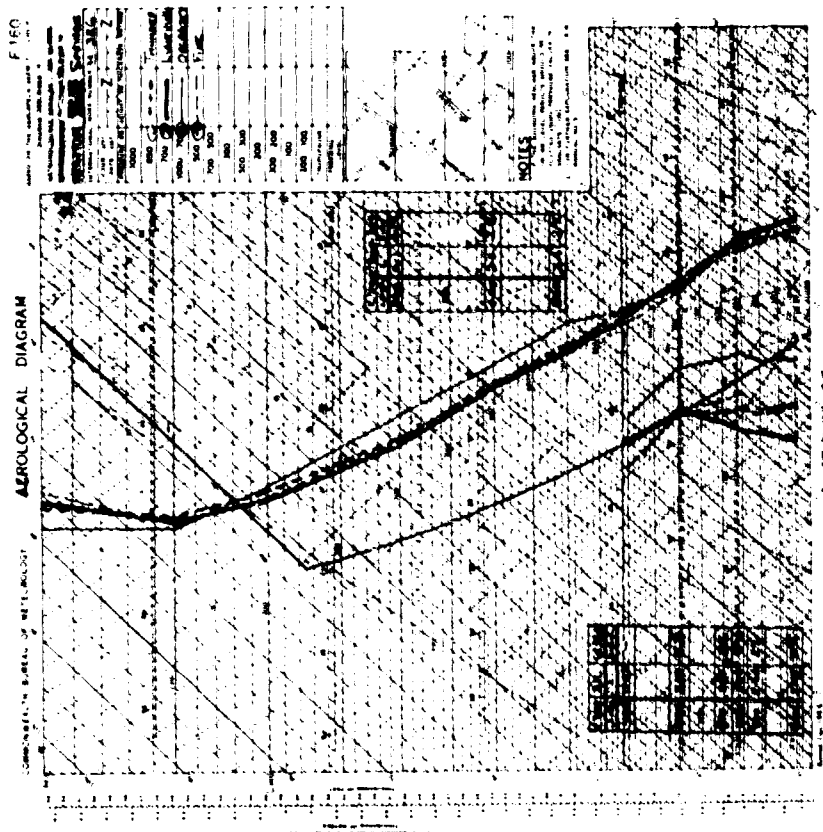


Figure 4b. Mean Temperature and Mixing Ratio Soundings at Alice Springs for the Four Categories of Convection at Darwin.

Figure 4a. Mean Temperature and Mixing Ratio Soundings at Alice Springs for the Four Categories of Convection at Darwin.

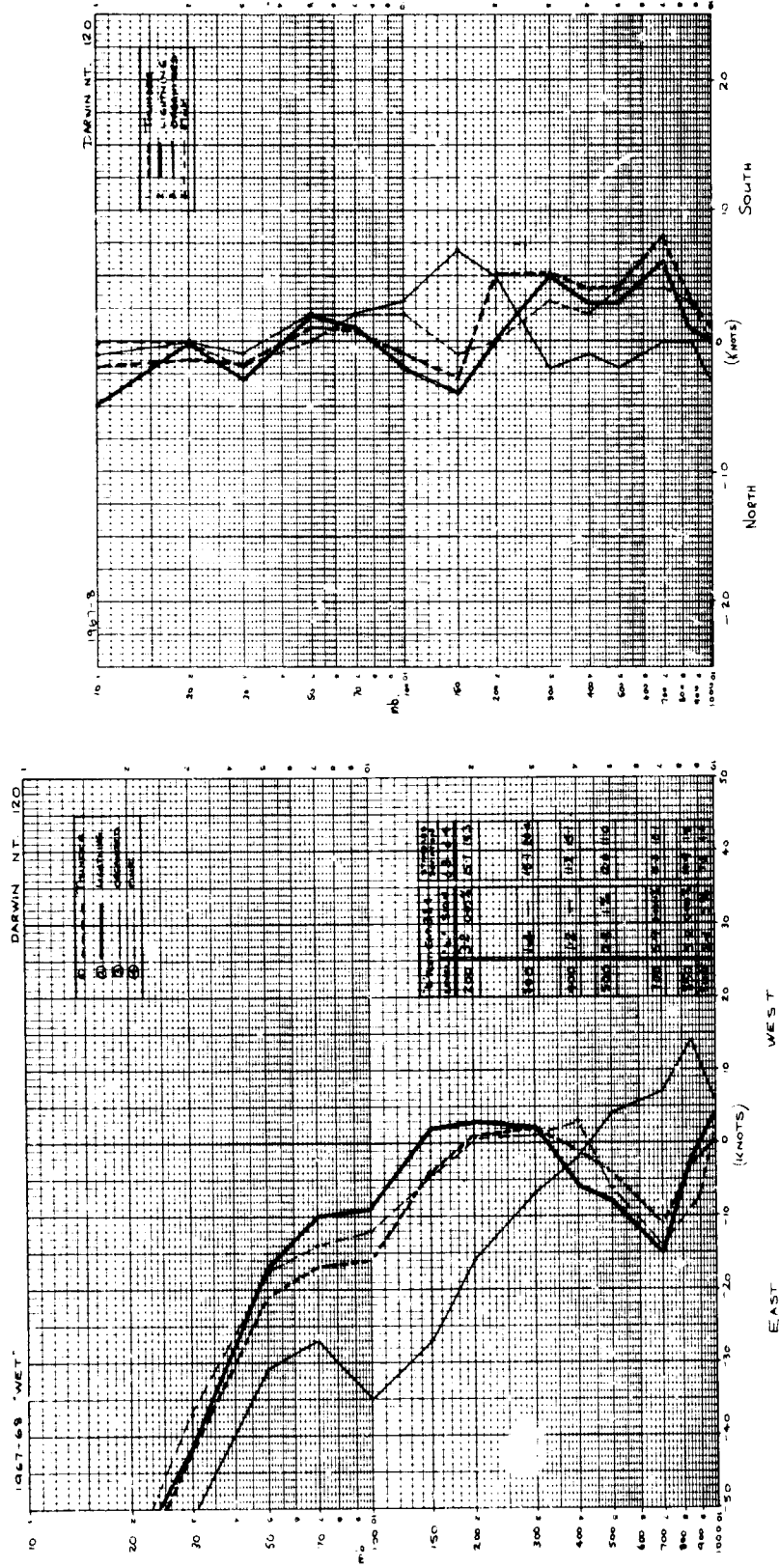


Figure 5a. Mean Zonal Components for the Four Categories of Convection at Darwin.

Figure 5b. Mean Meridional Components for the Four Categories of Convection at Darwin.

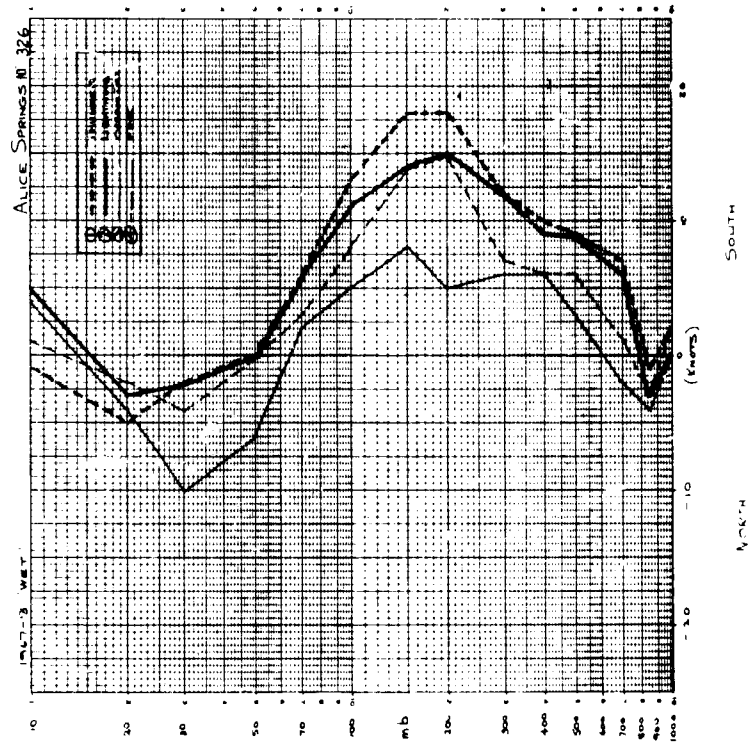


Figure 6a. Mean Zonal Components at Alice Springs for the Four Categories of Convection at Darwin.

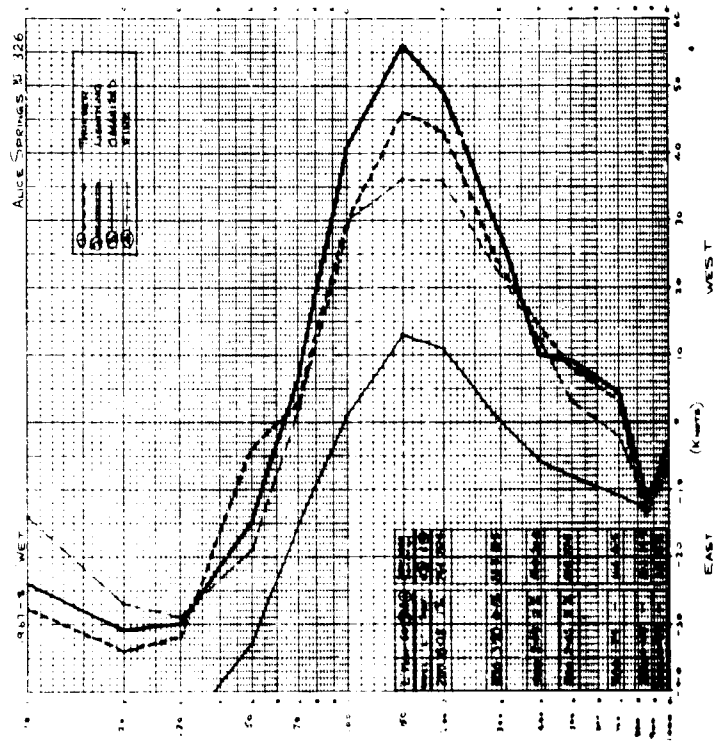


Figure 6b. Mean Meridional Components at Alice Springs for the Four Categories of Convection at Darwin.



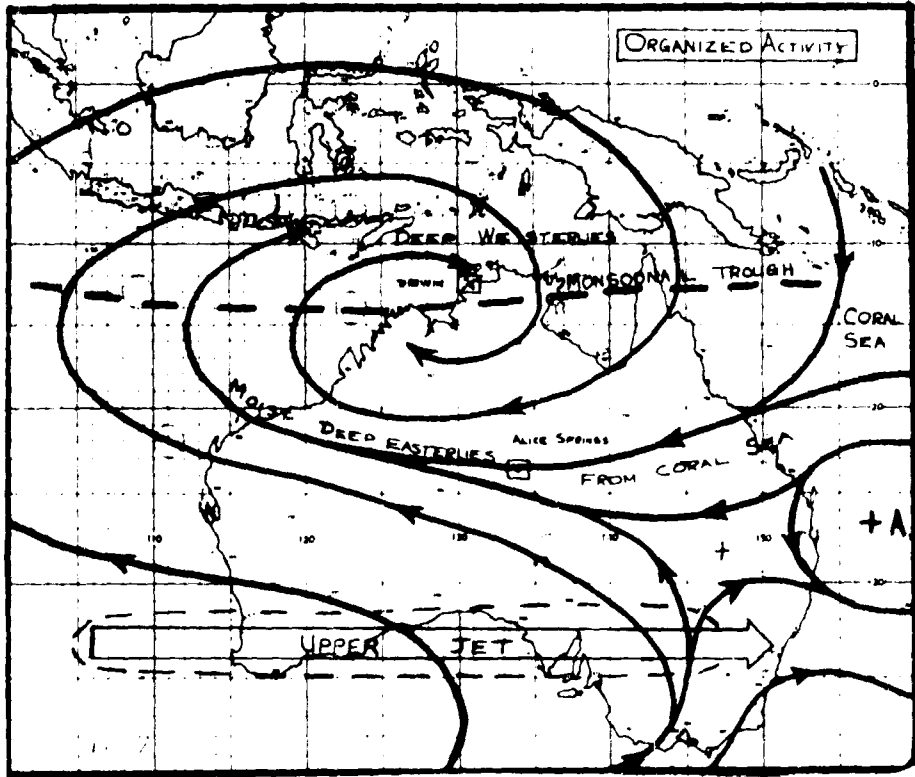


Figure 7. Model of Low Level Streamline Flow for an Organised Pain System at Darwin.

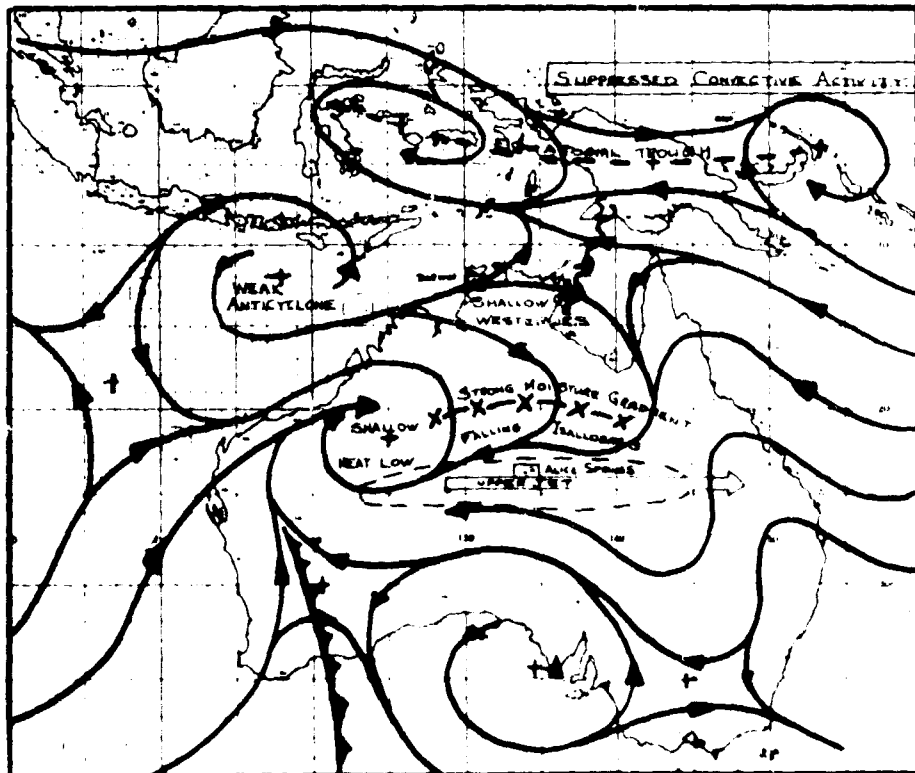


Figure 8a. Model of low level Streamline Flow for Suppressed Convective Activity at Darwin.

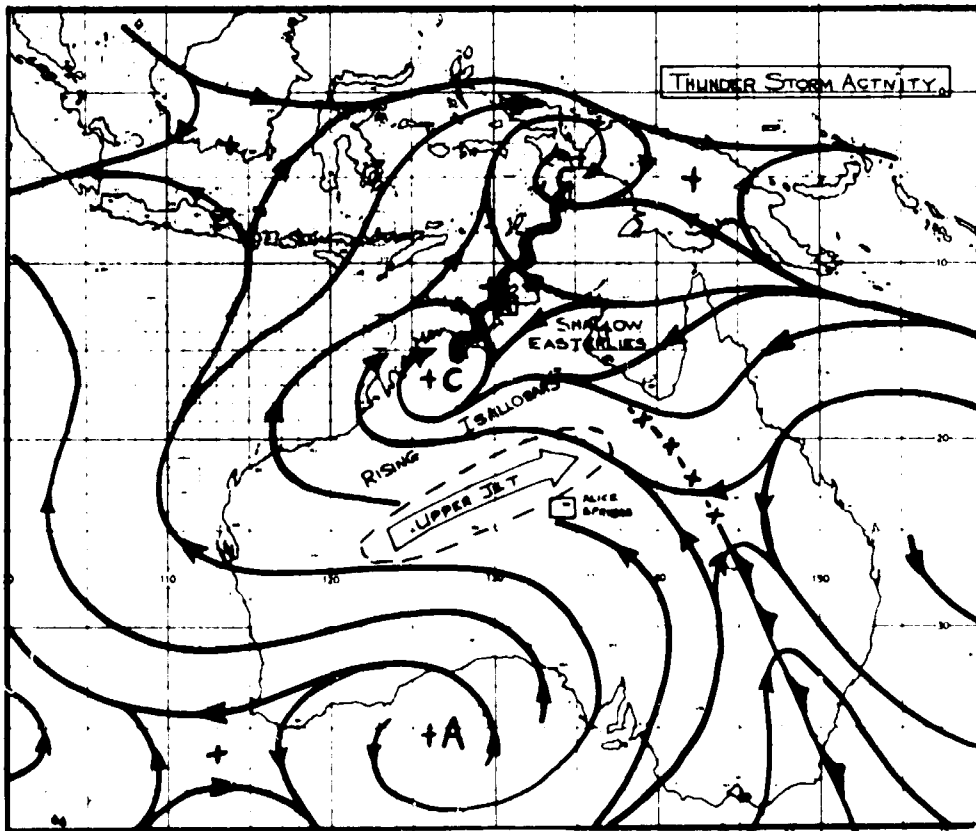


Figure 8b. Model of Low Level Streamline Flow Conducive to Thunderstorm Outbreaks at Darwin.

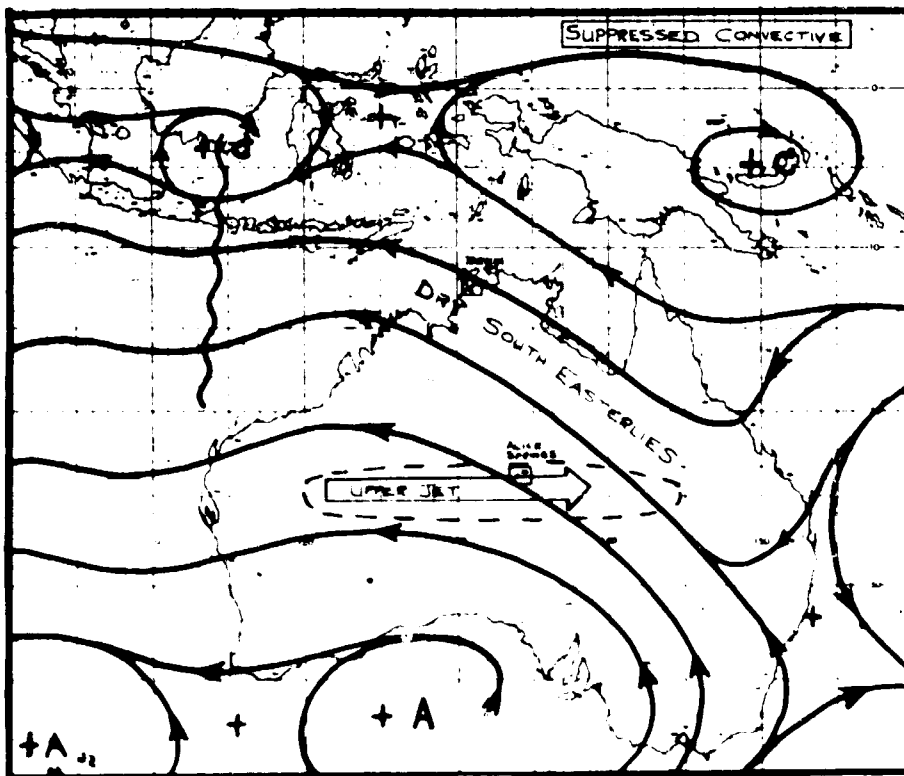


Figure 8c. Model of Low Level Streamline Flow for Suppressed Convection at Darwin.

Preceding page blank

- 255 -

THE INFLUENCE OF THE SYNOPTIC SCALE ON CONVECTION  
OVER SOUTHEAST ASIA DURING THE SUMMER MONSOON\*

Barry E. Harris  
First Weather Wing

and

Gordon Ing and V. R. Neralla  
University of Hawaii

ABSTRACT

Synoptic and climatological evidence indicates the atmosphere over Southeast Asia is routinely convectively unstable and that horizontal advection processes are small compared to vertical advective processes. Coupled with the periodic nature and areal extent of periods of suppressed and increased convection, the evidence indicates variations in convective activity are associated with variations in the monsoon regime. In general, suppressed periods of convection occur during a weak, shallow monsoon regime whereas increased convection occurs with a deep, strong monsoon regime. This evidence suggests that a synoptic-dynamic approach to forecasting convection is desirable.

1. INTRODUCTION

One of the more difficult problems confronting operational meteorologists in Southeast Asia during the summer monsoon season is that of forecasting convective activity. To date efforts toward solving this problem, not only for Southeast Asia, but also for the tropics in general, have been based primarily on the use of stability index concepts. Such concepts were devised for and have been used successfully in mid-latitudes, notably over the central United States; however, their use has been less fruitful in tropical regions.

Although mean aerological data for tropical regions have been available for some time [1, 6, 8], the approach used by operational meteorologists to forecast convective activity over tropical regions, implies a lack of understanding of the structure of the tropical atmosphere. Riehl [9], Garstang, et al. [3], and Harris and Ho [4] have pointed out differences between the thermodynamic structure of the atmosphere over tropical and temperate latitudes. The temperate latitude atmosphere, in the mean, possesses at worst neutral or weak convective instability. In contrast, mean aerological data for all tropical regions reveal an atmosphere possessing strong, convective instability. Further, the mean summer atmosphere over Southeast Asia is more convectively unstable than over the tropical maritime regions of the Bay of Bengal, the western Pacific, and the western Atlantic [4].

Present stability index concepts used in forecasting convection are based on the premise that day-to-day variations in the thermodynamic structure of the atmosphere primarily result from the horizontal advection of moisture and sensible heat. These horizontal advective processes are necessary to increase the convective instability toward some imaginary critical limit beyond which convection is initiated. Within the summer monsoon season, horizontal advection processes over Southeast Asia are immeasurably small on the synoptic scale. Krishnamurti [7] found that, in a large scale sense, in the lower levels convergence of moisture flux is important in furnishing a supply of moisture for convection. Other evidence points to the importance of vertical advection processes through convection in causing the observed variations in the thermodynamic structure of the atmosphere over Southeast Asia.

Mean aerological data for Southeast Asia suggest that the use of conventional stability index concepts for forecasting convection is not applicable to that area. The atmosphere possesses strong convective instability daily and the results obtained from using such indices should and do routinely indicate that day-to-day variations of index values are small and that convection is probable.

\* Research sponsored by Air Force Cambridge Research Laboratory

Despite the evidence of negligible horizontal advection processes and persistent, strong convective instability over Southeast Asia during the summer monsoon, significant day-to-day variations in convective activity do occur. Harris, et al. [5], and Sadler, et al. [11] have shown periods of clearing over Southeast Asia, which were associated with large synoptic scale changes in the monsoonal regime.

Garstang, et al. [3], Riehl and Malkus [10], and Zipser and LaSeur [12] have investigated the interrelationships between the synoptic and convective scales in the tropical atmosphere. These investigators concluded that the synoptic scale largely controls the convective scale in that significant convection is confined to disturbed portions of the synoptic scale patterns. They also found the equivalent potential temperature to be a most useful parameter for portraying differences between the thermodynamic structure of the tropical atmosphere during periods of increased and suppressed convection as well as serving as a measure of synoptic and convective scales in that atmosphere. Further, they found the vertical distribution of equivalent potential temperature varied characteristically with suppressed and increased convective activity.

These findings coupled with evidence of periodic variations in convective activity, failure of stability index concepts, and the basic strong convective instability of the tropical atmosphere suggest that success in forecasting convective activity over Southeast Asia requires a synoptic-dynamic approach rather than a thermodynamic approach.

## 2. THE STRUCTURE OF THE ATMOSPHERE OVER SOUTHEAST ASIA DURING JULY

The mean circulation and cloudiness for the atmosphere over Southeast Asia during July have been presented in these proceedings by Sadler. Suffice it here to emphasize that the basic monsoonal current is convergent and that the maximum of cloudiness is associated with the monsoonal westerlies while a minimum of cloudiness is associated with the easterly flow. The summer atmosphere over Southeast Asia is moist and both conditionally and convectively unstable. Mean virtual equivalent potential temperature ( $\theta_w$ ) data taken at Saigon (fig. 1) for July 1966 and 1967 (fig. 2) reflect strong convective instability on both the early morning and evening profiles. Such intense convective instability is routinely observed over Southeast Asia on a daily basis during the summer monsoon season. The 1200Z profile of  $\theta_w$  shows higher values level for level than the 0000Z profile. The higher values at 1200Z in the lower levels are probably due to radiative heating whereas the higher values at 1200Z in the middle and upper levels are due to a diurnal increase in moisture probably as a result of convection. This implies that convection occurs daily. Convective activity is observed as a routine event over Southeast Asia during the summer monsoon. On any given day one expects to see cumulonimbus, if not overhead, certainly within visual range. This does not mean that there is not a significant variation in convective activity. There are periods, of up to several days duration when convective activity is obviously suppressed below normal and similar periods when convective activity is uncomfortably increased above normal.

## 3. DAY-TO-DAY VARIATIONS IN CONVECTIVE ACTIVITY

Garstang, et al. [3] for the Caribbean and Harris and Ho [4] for Southeast Asia found that the vertical distribution of  $\theta_w$  varied characteristically during periods of suppressed and increased convective activity. During periods of suppressed convection the atmosphere exhibits very strong convective instability while during periods of increased convection the atmosphere possesses weak convective instability (fig. 3). During suppressed periods, synoptic scale subsidence acts to prevent the release of convection. Since no triggering mechanism is activated, moisture is not transported upward from the surface layer. In the absence of cloudiness, radiation received at the surface is increased. Thus,  $\theta_w$  values increase diurnally in the lower layers and remain constant or decrease slightly in the layer of  $\theta_w$  minimum, thereby, increasing the vertical gradient of  $\theta_w$  from the surface to the middle tropospheric minimum.

During periods of increased convection, energy, primarily in the form of moisture, is transported from the lower levels into the layer of  $\theta_{ve}$  minimum, thus increasing the  $\theta_{ve}$  values in that layer. The increased cloudiness reduces the amount of radiant energy reaching the lower levels, thereby serving to reduce the diurnal increase of  $\theta_{ve}$  values in that layer. Consequently, the vertical gradient of  $\theta_{ve}$  is decreased from the surface to the middle tropospheric minimum.

Garstang, et al. [3] found that periods of suppressed convection were correlated with synoptically suppressed conditions while periods of increased convection were associated with synoptically disturbed conditions. The synoptic disturbance served as a framework within which convection was activated and subsequently grew to become the dominant scale. Harris, et al. [5] for Southeast Asia, found that variations in the basic convective activity were associated with large synoptic scale variations in the monsoonal current. Suppressed convective activity was associated with a weak, shallow monsoon whereas increased convective activity was found with a strong, deep monsoonal current.

Day-to-day variations in the structure of the atmosphere are well illustrated by time cross-section analyses of  $\theta_{ve}$ , wind, and moisture (fig. 4) for Udorn during 12-26 July 1967. The Korat Plateau area experienced particularly suppressed convective conditions during 17-21 July 1967 and increased convection during 24-26 July 1967. The daily averaged radar index [2] profile for Udorn during July 1967 (fig. 5) shows definite periodic variations in the convective activity during the entire month of July. The several day duration of the periods of increased and suppressed convection suggest large synoptical scale variations.

The distribution of  $\theta_{ve}$  (fig. 4) exhibits characteristic variations during the suppressed period, 17-21 July 1967. The isopleths in the region below the layer of  $\theta_{ve}$  minimum tend to approach the horizontal, thus resulting in large vertical gradients of  $\theta_{ve}$  and strong convective instability. In striking contrast, the near vertical inclination of the  $\theta_{ve}$  isopleths on 24-26 July 1967 resulting in small vertical gradient of  $\theta_{ve}$  and weak convective instability during that period of intense convection. One might conclude that the horizontal orientation of  $\theta_{ve}$  isopleths imply that the large synoptic scale is dominant while vertical orientation of  $\theta_{ve}$  isopleths indicate that the convective scale is dominant and masks larger scales.

The wind analysis (fig. 4) shows that convection over the Udorn area was related to the depth and strength of the southwest monsoonal regime. During the particularly suppressed period, 17-21 July 1967, the monsoonal westerlies were shallow and weak, while during the increased convection period, 24-26 July 1967, the monsoonal westerlies were deep and strong.

The moisture analysis (fig. 4) reveals that moisture was not transported vertically upward into the layer of  $\theta_{ve}$  minimum during 17-21 July 1967. The dryness in that layer coupled with the strong convective instability suggest synoptic scale subsidence. During 24-26 July 1967 the atmosphere was moist from the surface through 200 mb.

Viewed as a composite, figures 4 and 5 imply that the degree of convective activity, the degree of convective instability, and the depth of the moist layer are related to the strength and depth of the monsoonal current. Suppressed convection--but strong convective instability--and a shallow moist layer are associated with a weak, shallow monsoon. Increased convection--but weak convective instability--and a deep moist layer are associated with a strong, deep monsoonal current.

As noted by Harris, et al. [5] and Sadler (these proceedings) variations in the intensity and depth of the summer monsoonal flow over Southeast Asia may be viewed as expansions or contractions of the mean large scale, monsoonal

circulation. Since the upper boundary of this circulation intersects the 500-mb. surface over Southeast Asia, periodic expansions and contractions of the circulation show well at that level. When the basic circulation weakens and contracts, easterly winds are observed at and below the 500-mb. level over Southeast Asia. Conversely, when the basic circulation strengthens and expands, the westerly current extends above the 500-mb. level over Southeast Asia. Consequently, a weakened or disrupted monsoonal regime will be reflected synoptically at 500 mb. as a ridge intrusion over Southeast Asia, whereas a strengthened monsoonal regime will appear synoptically as an organized westerly current at and above the 500-mb. level. When the monsoonal regime is completely disrupted, the westerly winds may be confined to the lower several thousand feet and pronounced ridging with easterly flow will be observed at and above 850 mb.

#### 4. CASE STUDIES OF PERIODS OF SUPPRESSED AND INCREASED CONVECTION DURING JULY 1967

Using daily averaged radar index profiles and satellite photographs, periods of suppressed and increased convection over Southeast Asia during July 1967 were isolated. Most of these periods have been discussed by Harris, et al. [5]; however, the suppressed period of 3-6 July and the increased convection period of 24-26 July are discussed here.

##### 4.1 The Suppressed Convection Periods of 3-6 July 1967

On 2 July 1967 a tropical depression intensified over the western Pacific Ocean. As is often the case, the subtropical ridge north of the developing cyclone simultaneously intensified and advanced westward over Southeast Asia. By 3 July the 500-mb. flow over Southeast Asia had responded to the ridge intrusion and was southerly with a weak easterly component. By 4 July the flow at 500 mb. was easterly as the ridge became better organized. Ridging effects were apparent at lower levels. On 5 and 6 July pronounced ridging at 500 mb. was apparent as far west as India. The satellite photographs for 3-6 July (figs. 6, 7, 8, and 9, respectively) clearly show the suppressed cloud conditions beneath the ridge and the easterly flow south of the ridge. The photographs also show the westward advance of the suppressed cloudiness across Southeast Asia and through the Bay of Bengal.

Vertical profiles of  $\delta_{\nu}$  for Southeast Asia (fig. 10) during the period of suppressed convection, show strong convective instability both in the morning and evening soundings. It is interesting to note that all stations, although at widely diverse locations over Southeast Asia (see fig. 1), show such strong convective instability. This suggests a large scale suppressing mechanism.

Analyses for 850 mb. (fig. 11) and 500 mb. (fig. 12) for 4 July show a disrupted monsoonal regime. At 850 mb. an anticyclone is shown over the Andaman Sea, and weak southwesterly flow dominates Southeast Asia. At 500 mb. the subtropical ridge is well pronounced near 20° N., and easterly flow dominates Southeast Asia. The minimum of cloudiness occurs beneath the ridge and easterly flow south of the ridge at 500 mb. The strong convective instability in the region of suppressed clouds strongly implies subsidence beneath the ridge and easterly flow at 500 mb.

##### 4.2 The Increased Convection Period of 24-26 July 1967

During the period 17-21 July pronounced ridging again effected suppressed cloud conditions over Southeast Asia. In this instance the ridge intruded westward and moved northward to southern China. In the wake of the ridge the shear and buffer zones and the monsoonal westerlies were reestablished.

By 23 July 1967 the ridge had collapsed, the shear zone had moved north of 20° N., a weak cyclonic vortex had formed in the shear zone and drifted northwestward onto the China coast near Hainan, and a tropical storm had moved northwestward approaching Okinawa. In response to these synoptic scale changes the monsoonal current had strengthened considerably over Southeast Asia. As the increased monsoonal current flowed into the cyclonic systems cloudiness began increasing over Southeast Asia.

By 24 July cloudiness had become intense over Southeast Asia (fig. 3). Photographs for the following two days (figs. 14 and 15) indicate continued intense convection. The photographs show that anvil cirrus had spread as a blanket over the subcontinent by the upper easterly flow.

Vertical profiles of  $\theta_w$  for six widely scattered stations over Southeast Asia (fig. 16) all show weak or nearly neutral convective instability. Again, the areal extent of such instability implies a large scale triggering mechanism.

Analyses for both 850 mb. (fig. 17) and 500 mb. (fig. 18) for 24 July show the strong monsoonal current flowing across Southeast Asia and the South China Sea. Both analyses reflect speed convergence on a synoptic scale over Southeast Asia. Comparison of figure 13 with these analyses shows the more intense cloudiness is confined to the westerly monsoon current.

## 5. CONCLUSIONS

Thermodynamically, the atmosphere over Southeast Asia routinely experiences strong convective instability. The degree of convective instability varies characteristically with periods of suppressed and increased convection. Soundings taken during suppressed periods exhibit strongest convective instability while soundings for periods of increased convection exhibit weakest convective instability. The very strong instability observed with suppressed convection implies the atmosphere is dominated by large synoptic scale subsidence. The weak instability observed during periods of increased convection implies the atmosphere is dominated by convective scale processes which form and grow within the large synoptic scale. These conclusions are substantiated by daily averaged profiles of the radar index which show that variations in convective activity are periodic, with the periods having several days duration, and by the large areal extent of similar convective stability conditions during periods of suppressed and increased convection.

Synoptic analyses reveal that variations in convective activity are associated with variations in the basic monsoonal wind regime. Periods of suppressed convection generally occur in association with a shallow, weak or disrupted monsoonal regime. Increased convection generally occurs in association with a strong deep, monsoonal regime. Since the upper boundary of the basic or mean monsoonal current intersects the 500-mb. surface over Southeast Asia, variations in the intensity and depth of the current are best detected and viewed at some mid-tropospheric level. Synoptically, over Southeast Asia a weak, disrupted monsoonal regime is reflected as a ridge intrusion with convergent, monsoonal westerlies being replaced by a subsiding, easterly current. The strong monsoon condition shows as an organized westerly monsoon current over Southeast Asia extending from the surface into the upper troposphere.

Synoptic evidence indicates that the role of horizontal advective processes is secondary to that of convergence of moisture flux and vertical advection processes in convection over Southeast Asia. When coupled with the strong convectively unstable structure of the atmosphere over Southeast Asia, the evidence implies that a thermodynamic approach to forecasting convection is invalid. The periodic nature of suppressed and increased convection, the characteristic structure of the atmosphere during periods of suppressed and increased convection, the areal extent of the suppressed or increased convection, and the association of areas of suppressed and increased convection with synoptic patterns, strongly suggest a synoptic dynamic-approach to forecasting convection is desirable.

## DISCUSSION

CONOVER: I agree 100% with your conclusions regarding stabilities. For those who might be interested in results of the Penn State cumulus model, Mr. Bunting of CRL tested the 8 driest and 8 wettest days. Results showed no essential differences in cloud top heights for different cloud radii. Determination of the cloud base level is critical to the point that temperatures would have to be read very accurately, i.e., from an aircraft, to indicate a particular area, within a developing cloud area, that would experience the most active clouds.

VEDERMAN: It seems we have to progress from our study of individual raobs to study of synoptic situations and satellite cloud pictures in the tropics. Then we have to begin to develop physical-dynamic models of the tropical atmosphere. If that is done, we may be able to compute vertical motion, amount of clouds precipitation, and motion of trough and ridges.

KREITZBERT: What was the "dynamic" part of the synoptic-dynamic model you favor?

HARRIS: No synoptic or dynamic model was proposed. I suggested that success in forecasting convection over Southeast Asia would probably come through an understanding of the processes of convergence of mass and moisture flux and vertical advection rather than through stability index concepts.

#### REFERENCES

1. COLON, J. A., "The Mean Summer Atmosphere of the Rainy Season Over the Western Tropical Pacific Ocean." Bull. Amer. Meteorol. Soc., 34: 333-334. 1953.
2. CONOVER, J. H., "Studies of Clouds and Weather Over SEASIA Utilizing Satellite Data." AFCRL 3rd Prog. Rept., 24 Aug. 1967 - 30 June 1968. 1968.
3. GARSTANG, M., et al., "Equivalent Potential Temperature as a Measure of the Structure of the Tropical Atmosphere." USNER & DL Rept. No. 67-10, Grant No. DA-AMC-28-043-66-G25. 1967.
4. HARRIS, B. E. and F. P. HO, "The Structure of the Troposphere Over Southeast Asia During the Summer Monsoon Month of July." AFCRL Rept. 69-0081, Contract No. F19628-67-C-0232. 1969.
5. HARRIS, B. E., et al., "The Role of the Synoptic Scale on Convection Over Southeast Asia During the Summer Monsoon." (To be published). 1969.
6. HEBERT, P. J. and C. L. JORDAN, "Mean Soundings for the Gulf of Mexico Area." Monthly Weather Review, 87:317-221. 1959.
7. KRISHNAMURTI, T. N., "An Experiment in Numerical Prediction in Equatorial Latitudes." Sci. Rept. No. 4, AFCRL Contract No. MIPR ES-7-967. 1968.
8. JORDAN, C. L., "Mean Soundings for the West Indies." Jour. of Meteorol., 15:91-97. 1958.
9. RIEHL, H., "Tropical Meteorology." New York, McGraw Hill, p. 45. 1954.
10. RIEHL, H. and J. S. MALKUS, "On the Heat Balance in the Equatorial Trough Zone." Geophysica, 6:503-538. 1958.
11. SADLER, J. C., et al., "Forecasting Minimum Cloudiness over the Red River Delta During the Summer Monsoon." AFCRL Rept. No. 68-0487, Contract No. F19628-67-C-0232. 1968.
12. ZIPSER, E. J. and N. E. LASEUR, "The Distribution and Depth of Convective Clouds Over the Tropical Atlantic Ocean as Determined From Meteorological Satellite and Other Data." Ph. D. Dissertation, Florida State University, 153 pp., unpub. 1967.



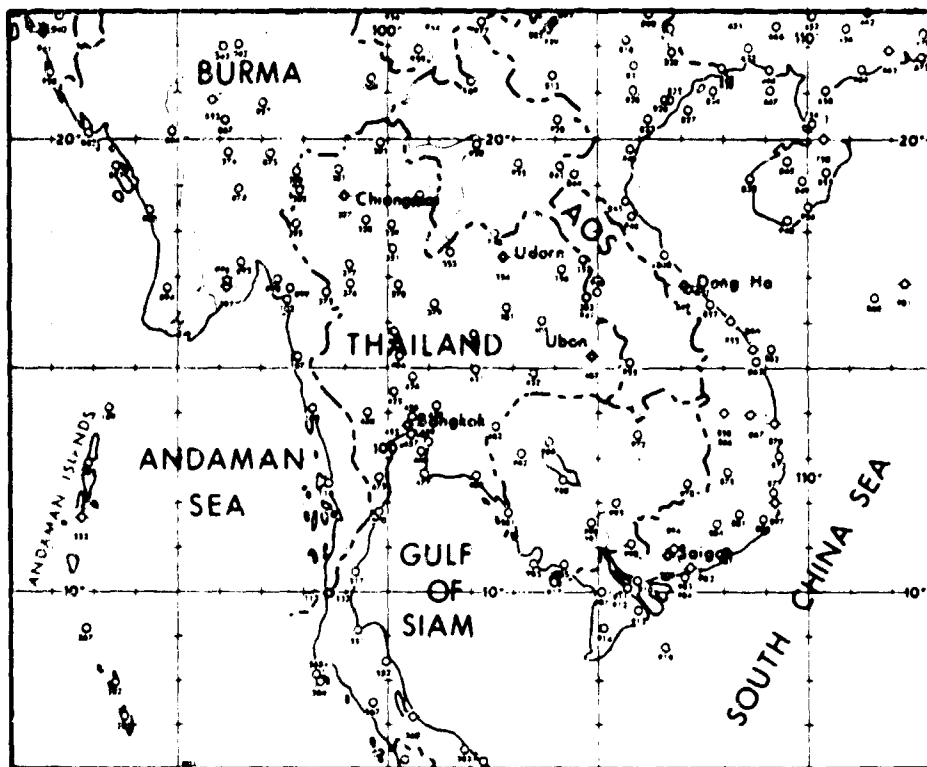


Figure 1. Locator Map of Southeast Asia.

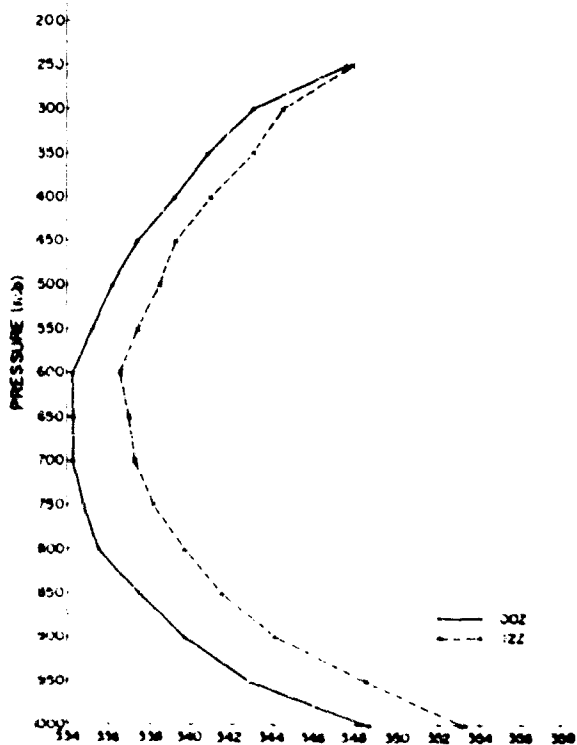


Figure 2. Vertical Profile of Mean Virtual Equivalent Potential Temperature (°A.) at Saigon, July 1966 and 1967.

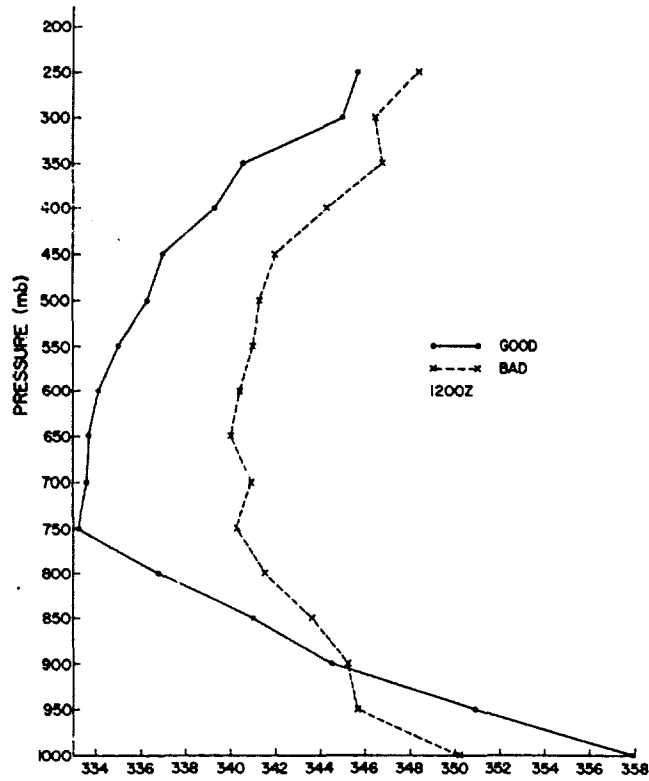


Figure 3. Vertical Profile of Mean Virtual Equivalent Potential Temperature for Saigon During Good and Bad Periods of July 1966.

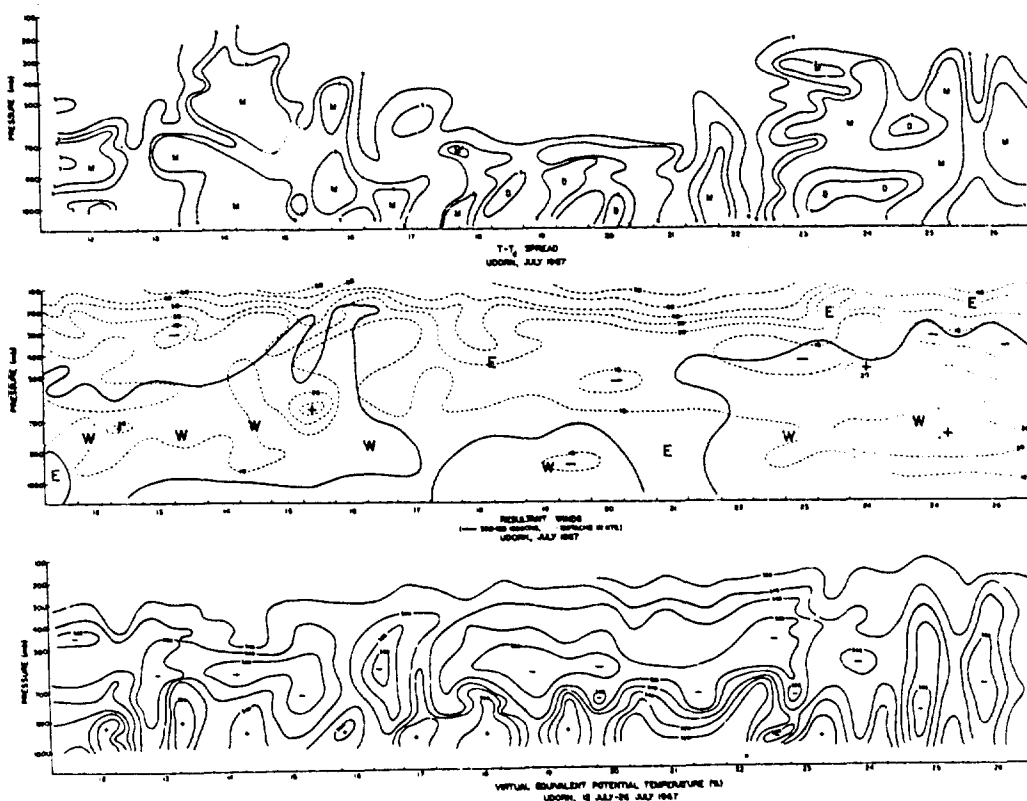


Figure 4. Time Cross-Sections of  $\theta_{ve}$ , Wind and Moisture for Udorn, 12-26 July 1967.

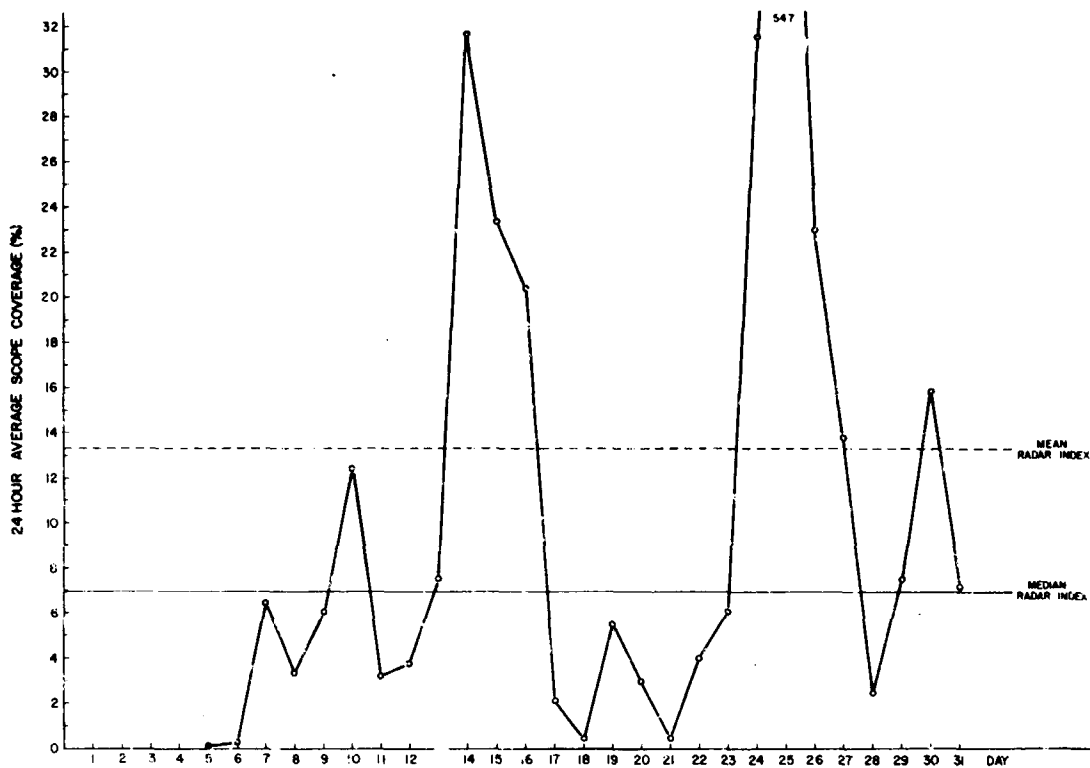


Figure 5. 24 Hour Daily Average of Radar Index Over Udorn for July 1967.



Figure 6. ESSA V Satellite Photographs for Southeast Asia Region on 3 July 1967.



Figure 7. ESSA V Satellite Photographs for Southeast Asia Region on 4 July 1967



Figure 8. ESSA V Satellite Photographs for Southeast Asia Region on 5 July 1967.

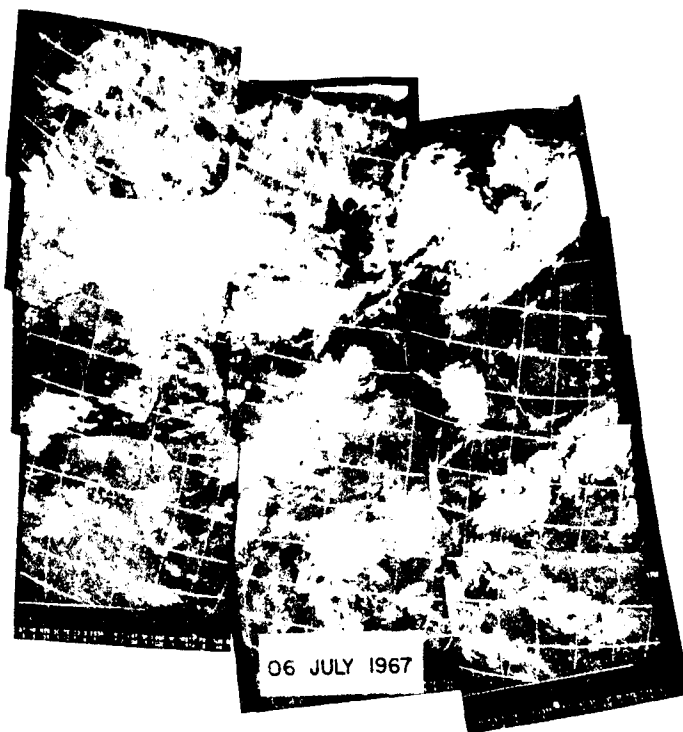


Figure 9. ESSA V Satellite Photographs for Southeast Asia Region on 6 July 1967.

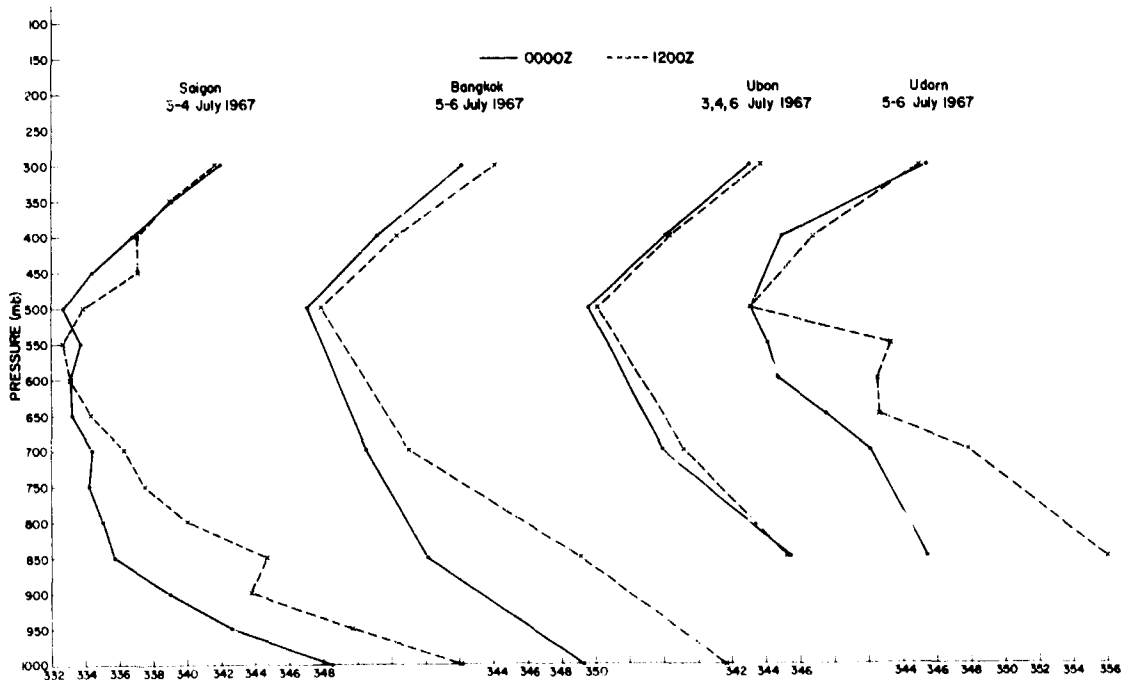


Figure 10. Vertical Profiles of  $\theta_{ve}$  for Southeast Asia Stations During Period 3-6 July 1967.

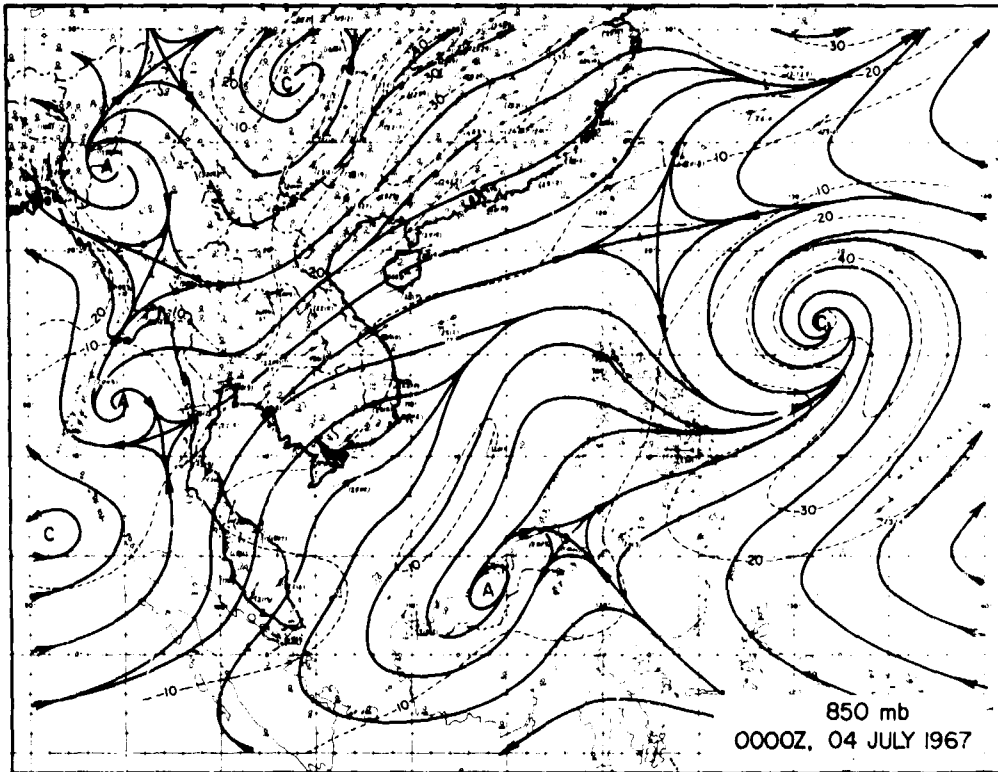


Figure 11. Streamline-Isotach Analysis of the 850-mb. Surface for 4 July 1967.

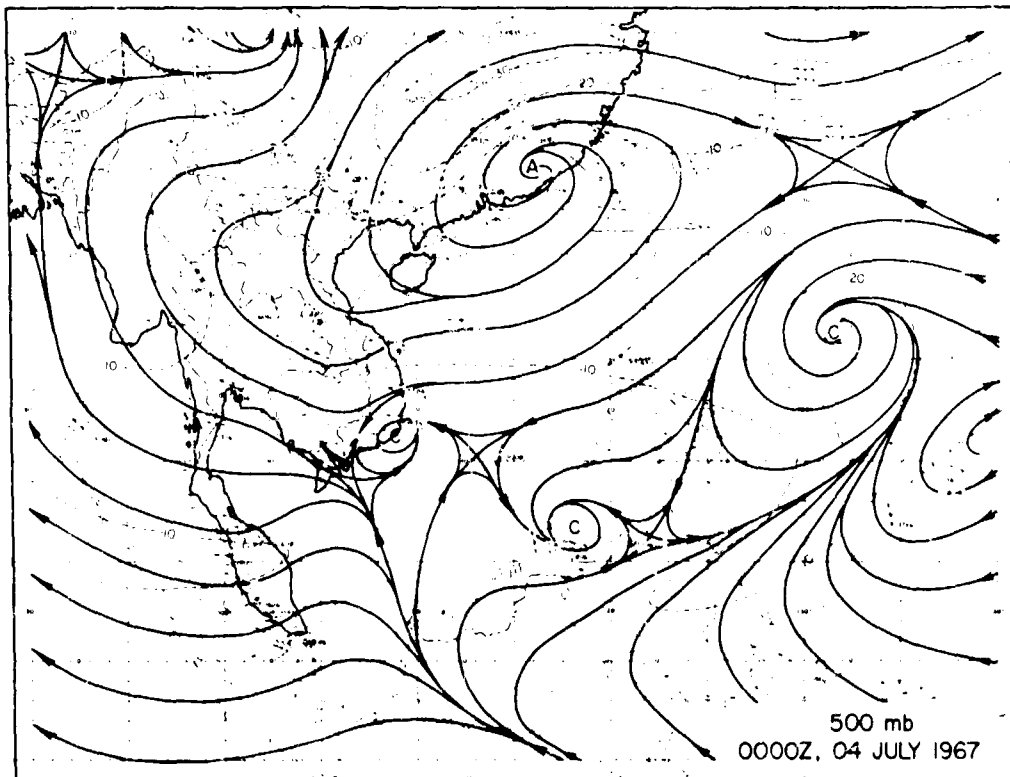


Figure 12. Streamline-Isotach Analysis of the 500-mb. Surface for 4 July 1967.



Figure 13. ESSA V Satellite Photographs for Southeast Asia Region on 24 July 1967.



Figure 14. ESSA V Satellite Photographs for Southeast Asia Region on 25 July 1967.



Figure 15. ESSA V Satellite Photographs for Southeast Asia Region on 26 July 1967.

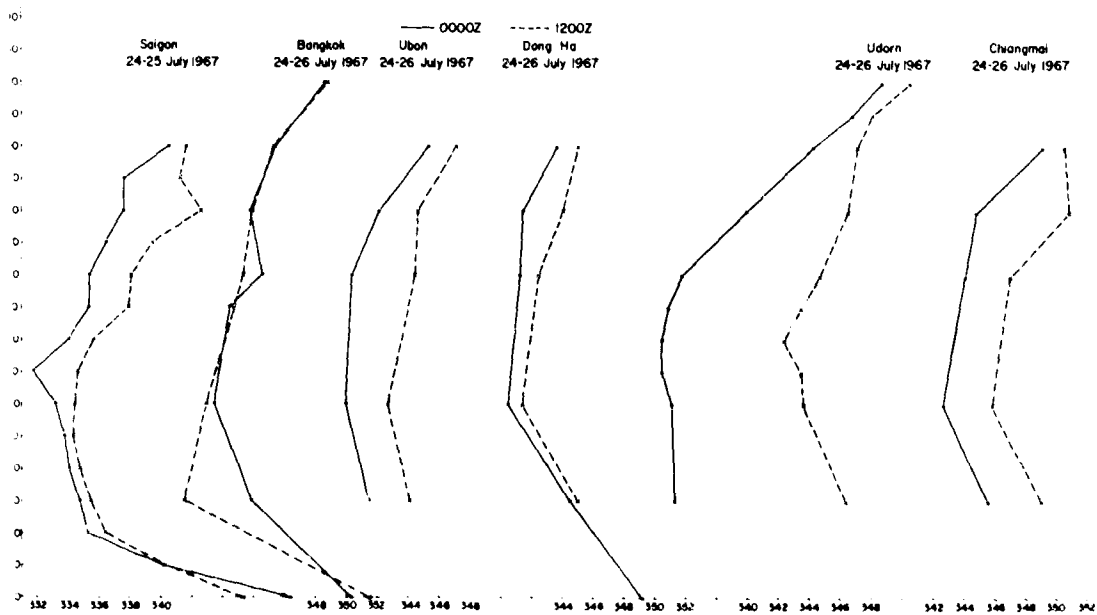


Figure 16. Vertical Profiles of  $\theta_{ve}$  for Southeast Asia Stations During Period 24-26 July 1967.



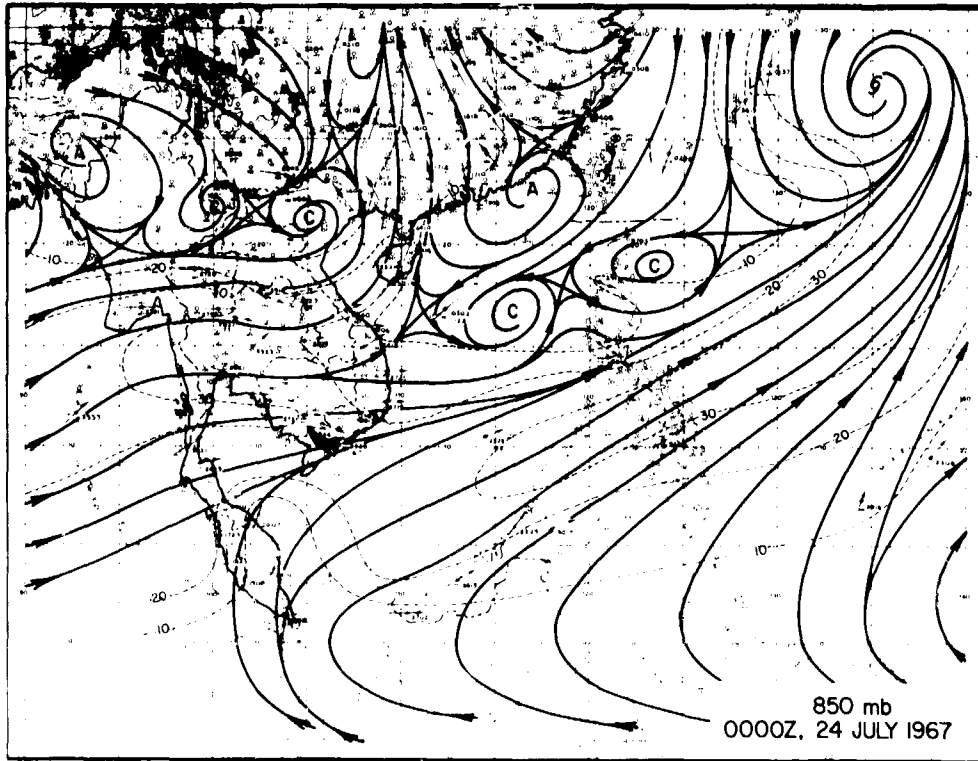


Figure 17. Streamline-Isotach Analysis of the 850-mb. Surface for 24 July 1967.

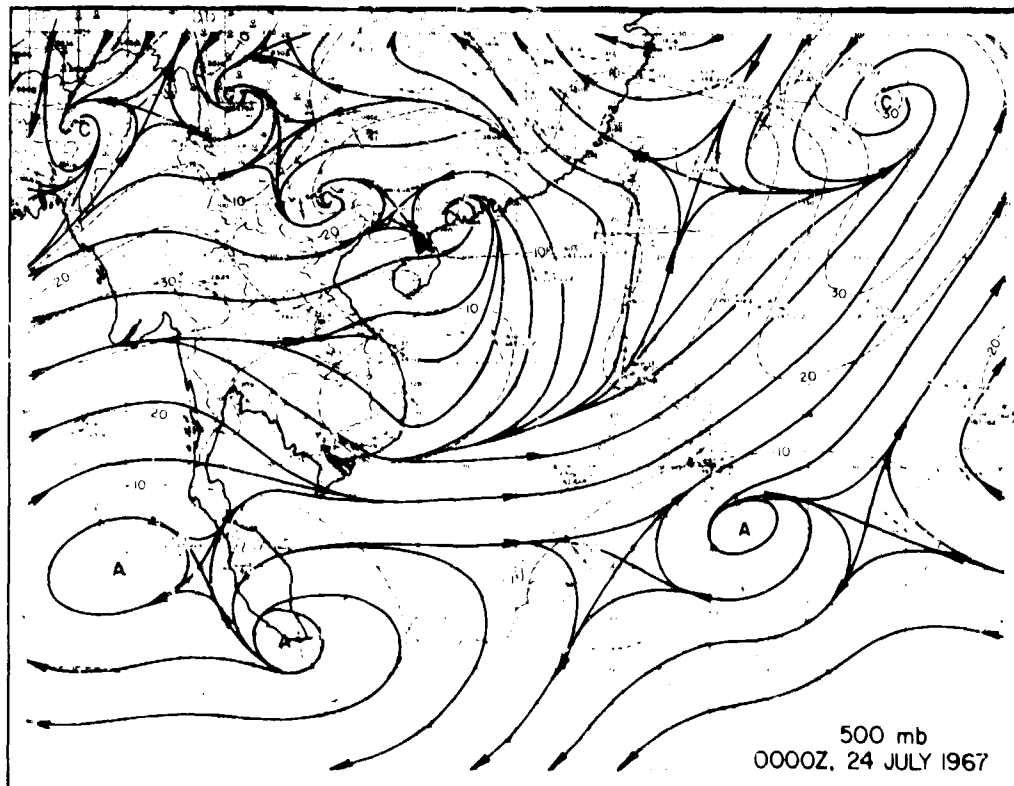


Figure 18. Streamline-Isotach Analysis of the 500-mb. Surface for 24 July 1967.

MESOSCALE AND DIURNAL VARIATIONS DEDUCED FROM  
THE SAIGON AREA RAWINSONDE DATA \*

Carl W. Kreitzberg  
The Pennsylvania State University

Robert W. Endlich, Capt., USAF  
Air Weather Service

John R. Sweeney, Capt., USAF  
Air Weather Service

ABSTRACT

This paper includes the results of two studies that utilized data from the eight Army artillery rawinsonde sites within 60 n. mi. of Saigon.

Large amplitude diurnal changes in specific humidity are observed throughout the middle troposphere over the Indochina Peninsula. Minimum specific humidities are found near noon, and maximum values occur near midnight. Between midnight and noon, observationally significant drying occurs on about 75 percent of the June days as compared with about 12 percent that show significant increase in moisture. The most plausible explanation for the diurnal moisture behavior is widespread subsidence of up to 4 cm. sec.<sup>-1</sup> during the morning hours and ascent during the latter half day. This diurnal circulation appears to be induced by the diurnal change in the surface-pressure gradient due to the thermal low in the interior of the peninsula in the afternoon and the cold high in the early morning.

A case study was made relating mesoscale wind-speed maxima to convective activity in the Saigon area. The convection was located in the region of cyclonic shear on the northern side of a large mesoscale streak of strong westerly winds. It also appeared that small mesoscale-wind maxima moved through the larger scale streak, triggering individual groups of convective cells. Indications were found that strong vertical wind shears at low levels above the south-westerly current are not conducive to heavy showers and thunderstorms.

1. INTRODUCTION

About 20 Army rawinsonde sites in South Vietnam take soundings for artillery ballistic calculations. The original recorder records for the summer of 1967 were reprocessed by computer at the Air Force Cambridge Research Laboratories. About eight of these sites lie within 60 n. mi. of Saigon and take up to four soundings a day. This paper includes the results of some studies made using the June 1967 upper-air data in conjunction with surface, radar and satellite data in the Saigon area.

The most disturbing conclusion of these and previous studies is that disturbed and undisturbed days have essentially identical lapse rates. Dry air in the middle troposphere is effective in limiting convection by entrainment into budding convection. Therefore, the humidity sounding is more important than the temperature sounding in restricting convection. The air within deep convection must originate at levels below 1 or 2 km. to rise to the heights observed by radar. Therefore, one must seek mechanisms inducing low-level convergence beneath a reasonably moist middle troposphere to explain convective storms in South Vietnam.

Examination of the behavior of the moisture field shows that synoptic scale periods of reduced convective activity correspond with similar scale periods of reduction in middle tropospheric moisture. More remarkably, there is a large amplitude diurnal variation in the moisture content and relative humidity in the middle troposphere [3]. For example, the June mean precipitable water in the layer from 3 km. to 8 km. varies from 1.4 cm. at 2300 LT to 1.0 cm. at 1100 LT. This drying can be expected to inhibit convection during the late morning hours unless substantial low-level convergence occurs, permitting convection to progressively moisten the air. The drying during the morning hours occurs in

\*Research sponsored by Air Force Cambridge Research Laboratory

spite of synoptic conditions on more than 75 percent of the June days. The drying occurs throughout layers of southwesterly, nearly calm, and northeasterly flow alike. Thus horizontal advection is unlikely to be the cause, and vertical advection, that is subsidence, appears to be the only feasible mechanism for producing this drying.

Temperature in the middle troposphere also rises during the morning hours much more than would be expected from diabatic effects. The magnitudes of the subsidence required to explain the drying and warming are computed and found to be about  $4 \text{ cm. sec.}^{-1}$ . This phenomenon is observed throughout South Vietnam and Thailand with the largest magnitude and frequency in the center of the Indochina Peninsula.

The cause of this vertical motion is attributed to the diurnal change in the surface pressure gradient force. The monthly mean surface pressures are lower in the afternoon in the interior of the peninsula than along the coast. The opposite pressure differences are found in the morning. Preliminary calculations indicate that the magnitude of the pressure gradients are large enough to produce the low-level divergence and convergence fields required to explain the vertical motions that, in turn, are used to explain the observed diurnal variation in moisture and temperature aloft.

The soundings in the southwest monsoon are systematically potentially unstable such that low-level convergence will produce convection. Consideration of middle level moisture revealed synoptic periods of moist conditions favorable to convection as well as dry periods which hamper convection. The diurnal moisture variation indicates that late morning hours are less favorable for convection than late evening hours. The case study examines a specific disturbed period to determine conditions favorable for production of the low-level convergence and, hence, substantial amounts of convective activity.

In the case examined, a narrow wind streak or isotach maximum in the lower-level southwesterly flow lay on the southern side of the disturbed band. That is, the disturbed region had large cyclonic shear in the low levels which would be conducive to frictional convergence in the Ekman layer [4]. While the entire disturbed band that paralleled the low-level flow drifted southward, cells of convective activity moved through the band. There appear to have been cores of particularly strong wind that moved through the mesoscale-wind streak on the right rear of the cells of showers. Thus the wind-speed field in the boundary layer through the action of friction appears to have been responsible for inducing this band of disturbed weather.

## 2. DIURNAL MOISTURE VARIATIONS

The sites used in this study are shown in figure 1. Included are two sites in Thailand, one on the coast in northern South Vietnam and several in the vicinity of Saigon. It will be shown that drying during morning hours systematically occurs throughout the middle troposphere at all these sites and that the magnitude of the drying is greatest in the interior (Ubon) and at least on the coast.

The consistency of these variations from time to time and layer to layer can be seen in figure 2. The data used were obtained from sites 13 and 15 which are only 24 km. apart. The precipitable water in each 1 km. layer was calculated and averaged at each time of day over all days in June 1967. The percentage variations of the hourly means from the monthly means are graphed in figure 2, top with the height of the middle of the kilometer layer indicated at the left end of the curves.

The noontime minimum in precipitable water is very pronounced and occurs almost simultaneously at all levels. The increase in moisture in the afternoon builds up by 1700 LT at 2.5 km. but it takes until 2300 LT for maximum moisture values to occur at 8.5 km. In figure 2, upper portion, each observed point is shown with smooth lines drawn connecting the points. In this way one can see how consistent the observations are from time to time and layer to layer.

The lower portion of figure 2 shows that the minimum precipitable water per kilometer or minimum specific humidity occurs when temperatures are the highest such that the noontime relative humidity is very low in the monthly

mean. The diurnal variation of temperature is clearly defined, but it is not quite as systematic as that found with moisture. The simultaneous occurrence of warming and a decrease in specific humidity suggests that subsidence may be the cause. Before pursuing the cause of the variations, however, let us examine the frequency of days within the month on which observationally significant drying and warming occurred during the morning hours.

Table 1 shows the frequency of significant departures of noon or near noon observations from a linear interpolation between observations 6 hours earlier and later. The departure is deemed "significant" if it exceeds an estimate of the standard error in observation, namely 0.5° E. and 5 percent RH, and corresponding changes in precipitable water or specific humidity. One sees that the frequency of low humidities and precipitable water is very large when compared with the frequency of days in which the opposite condition occurs.

Site No.	Temperature		Relative Humidity		Precipitable Water		Percentage Variation of Precipitable Water
	Sig. Min.	Sig. Max.	Sig. Min.	Sig. Max.	Sig. Min.	Sig. Max.	
1 + 20	10	49	61	20	62	20	16
3	12	47	61	15	59	18	19
11	11	29	61	27	61	11	17
15	5	48	85	5	74	7	18
16	9	54	75	12	71	12	44
71	10	45	92	1	91	1	41
72	20	48	75	10	74	10	25

Table 1. Percentage Frequencies of Significant Differences Near Noon and the Percentage Variation of Precipitable Water. All Values Are Means From 1-Km. Layers Centered at 4.5, 5.5 and 6.5 Km.

Table 1 also shows the percentage variation of precipitable water at the various sites located in figure 1. The percentage variation is determined from the monthly mean values at each of the four observing times by taking the ratio of the range to the mean. Both the magnitude and the frequency of drying increase with increasing distance from the coast. The exception is that Udon does not show the strong frequent drying shown further down the peninsula at Ubon, presumably because Udon is at the northern end of the peninsula.

This observational evidence indicates that morning drying and warming and afternoon moistening and cooling is a recurring cycle throughout the month of this study. That the phenomenon occurred in regions of southwesterly, very light, and northeasterly flow alike suggests that horizontal advection is not an important cause of these changes. Subsidence appears to be the most important cause of the morning drying and warming. The vertical displacements required to produce the observed diurnal 6-hour moisture and temperature changes have been calculated and appear in tables 2 and 3. The ascending equivalent displacements must be interpreted rather loosely as ascent in the tropics will produce convection with alternating regions of strong ascent and weak descent.

Table 2. Equivalent 6-Hourly Vertical Displacements in Meters Computed From Moisture Changes.

Site HT. (km.)	15 0500- 1100LT	13 0830- 1430LT	15 1100- 1700LT	13 1430- 2030LT	15 1700- 2300LT	13 2030- 0230LT	15 2300- 0500LT	13 0230- 0830LT
	0.5	-320	- 91	169	167	65	102	127
1.5	-230	145	277	51	- 15	- 46	- 18	-118
2.5	-245	- 23	263	80	- 69	23	26	- 90
3.5	-159	+ 65	315	179	- 70	- 58	- 86	-171
4.5	-303	55	458	609	128	-133	-170	-580
5.5	-562	- 56	815	980	143	-430	-391	-520
6.5	-515	38	1040	880	33	-202	-420	-785
7.5	-628	222	880	552	260	0	-418	-880
8.5	-560	410	630	595	276	- 80	-348	-840
9.5	-455	250	485	140	222	-136	-208	-560

Table 3. Equivalent 6-Hourly Vertical Displacements Computed From Temperature Changes.

Site HT. (km.)	15 0500- 1100LT	13 0830- 1430LT	15 1100- 1700LT	13 1430- 2030LT	15 1700- 2300LT	13 2030- 0230LT	15 2300- 0500LT	13 0230- 0830LT
1.5	- 68	- 54	- 56	+120	65	-103	44	38
2.5	- 43	+ 4	- 17	105	11	-147	54	32
3.5	- 56	+ 84	12'	89	37	-125	- 2	- 33
4.5	-235	+ 59	148	170	123	-162	-52	- 81
5.5	-265	- 7	247	306	67	-118	-42	-167
6.5	-277	- 21	165	279	139	- 66	-36	-206
7.5	-397	- 31	111	262	314	+ 15	-30	-238
8.5	-465	-133	78	310	393	+ 96	-14	-325
9.5	-649	-185	198	346	238	+294	+88	-490

The equivalent displacements computed from moisture changes used the relation:

$$\Delta Z = \frac{-\Delta q}{\left(\frac{\Delta q}{\Delta Z}\right)}$$

where  $\Delta q$  is the observed 6-hour change in specific humidity, and  $(\Delta q / \Delta Z)$  is the mean vertical change of specific humidity during that period. This equivalent displacement would explain the observed changes by vertical advection in the absence of horizontal advection, condensation, evaporation or eddy fluxes.

The computation of equivalent vertical displacements from observed temperature changes is more complex because the diabatic changes of temperature,  $(\Delta T)$ , must be removed from the observed local time changes,  $(\Delta T)_{LTX}$ , to obtain the adiabatic,  $(\Delta T)_{ADB}$ , changes from which the equivalent vertical displacements can be determined. That is:

$$\Delta Z = \frac{-(\Delta T)_{ADB}}{\Gamma - \gamma}; (\Delta T)_{ADB} = (\Delta T)_{LTX} - (\Delta T)_{DIA}$$

where  $\Gamma - \gamma$  is the dry adiabatic lapse rate minus the actual lapse rate.

The diabatic changes,  $(\Delta T)_{DIA}$ , were obtained by considering the solar insolation using values extrapolated from Katayama [7]. The infrared cooling was determined from Elsasser diagrams using monthly mean soundings. The monthly mean latent and sensible heating were determined by assuming that they exactly balance the net radiational cooling. The distribution of this latent and sensible heating with time of day was made proportional to the monthly mean convective activity as measured from the percentage scope coverage within 50 miles of Saigon [2].

The displacements shown in tables 2 and 3 are reasonably consistent from time to time, layer to layer, and between moisture and temperature. The displacements required to explain the moisture changes are about twice as large as those required to explain the temperature changes. This relationship is brought out more clearly in figure 3.

Figure 3 shows the equivalent vertical velocities in cm. sec.<sup>-1</sup>, corresponding to the displacements in tables 2 and 3. A vertical velocity of 1 cm. sec.<sup>-1</sup> will produce a vertical displacement of 216 m. in 6 hours. The larger magnitude vertical motions deduced from moisture changes are probably correct. The lower values of vertical motion deduced from the temperature changes are probably underestimated because the monthly mean transport of sensible heat from the tropics is neglected. Net sensible heating most probably occurred principally in the afternoon, meaning that more adiabatic cooling and ascent occurred during the afternoon than was calculated. In the morning hours the export of sensible heat from the region must have been offset by more subsidence and adiabatic heating than was estimated.

To sum up, the observed diurnal moisture and temperature changes imply subsidence of about 2 cm. sec.<sup>-1</sup> from late evening until noon and afternoon and evening ascent equivalent to about 4 cm. sec. of large scale vertical motion. This vertical circulation appears to be more intense inland than on the coast as judged by the magnitude and frequency of the moisture changes.

The cause of the vertical motions deduced from the diurnal moisture and temperature changes over the Indochina Peninsula appears to be the afternoon thermal low and the nighttime high observed over the peninsula. The mean sea-level pressures for each month and each time of day have been prepared by Ing [6] for sites in Indochina. Analyses of these mean sea-level pressures in June at 0500 and 1700 LST are shown in figure 4. The pressure gradients may be larger along the coast than can be determined from the standard surface network.

The diurnal change in the pressure patterns is most probably caused by the larger amplitude diurnal heating and cooling cycle over the land mass as compared with the surrounding oceans. The 0500 LT high cell will drive the low-level air offshore leading to subsidence, drying, and warming over the peninsula during the morning hours. The 1700 LT thermal low will force the low-level air to converge over the peninsula and thence to ascent and increase in moisture at a fixed level. These vertical circulations, suggested by the surface pressure gradient variations, would explain the vertical motions implied by the observed changes in moisture and temperature in the middle troposphere.

Preliminary hand calculations and a simplified particle dynamics type of numerical model provide assurance that the magnitude of the observed changes in pressure-gradient force is adequate to produce the magnitude of the vertical motions deduced from moisture changes. Numerical simulation of the entire process from diabatic heating and cooling to vertical motion remains to be done. Such a study would test the proposed mechanism and permit evaluation of the behavior of the diabatically induced vertical motions for various size land masses, at varying distances from the coast and under different synoptic flow conditions.

### 3. MESOSCALE-WIND STREAKS

The Army artillery sites used standard GMD-1A rawinsonde equipment to obtain density and wind soundings for use in ballistics calculations. In addition to calculating ballistics parameters, the Army teams transcribed the significant level radiosonde data and the rawinsonde data to a meteorologically compatible form for transmission to the Air Weather Service for real time use [5]. The Army rawinsonde data used in this study, however, were recalculated by computer at the Air Force Cambridge Research Laboratories by reevaluating the original recorder records. Significant level data were recomputed and key punched, and azimuth-elevation data were tabulated and key punched at 30-second intervals. While very detailed data were output, the most useful data and the data used in this report were computer-averaged 1-km. mean values of all parameters centered at 0.5, 1.5, 2.5 --- kilometers MSL.

The location of the Army rawinsonde sites in the vicinity of Saigon in June 1967 are shown in figure 5. It can be seen that nine rawinsonde sites are located within about a 50 km. radius but are not necessarily close to surface observation sites. Unfortunately, surface observations are not made at the Army sites and about one-half of the surface sites operate during daylight hours only. Therefore, the detailed comparisons of weather to upper-air winds reported below are restricted to daylight hours. During the southwest monsoon, the low-level flow approaches this region from over the very flat Mekong Delta.

This case study deals with the period 4 - 6 June 1967, with particular emphasis given to the morning of 5 June [9]. The synoptic situation in early June included strong WSW flow at low-levels across Indochina with rather dry air in the middle troposphere and generally less than average convective activity. The satellite data showed WSW - ENE oriented bands of clouds drifting southward down the peninsula. One such band reached the Saigon area on 5 June, and cells of convective activity broke out west of Saigon and drifted ENE. As the morning wore on, cell tracks were located further to the south presumably as the larger scale cloud band drifted ENE.

The large mesoscale 850-mb. flow pattern on the morning of 5 June is shown in figures 6 and 7 (note: 0000Z = 0700 LST = 0800 LDT). The isotach pattern in figure 6 shows a "large mesoscale" wind streak or speed maximum over Saigon (site 900). Strong cyclonic shear is seen on the northern side of this wind streak. The wind data used in the analysis of figure 6 is shown in figure 7 along with regions of strong convergence and divergence. Using the fact that 1 degree of latitude equals 60 nm., the density of the upper air data between 2100Z, 4 June and 0200Z, 5 June and the degree of agreement or variability can be judged in figure 7.

Figure 8 contains a composite vertical time section of the zonal flow in the northern portion of the mesoscale network. There are three periods of strong flow centered about 2200Z, 4 June; 1800Z, 5 June; 1400Z, 6 June. The strength, depth and duration of these strong winds decreased from day to day. The long period of strong winds near 2200Z, 4 June appears on the 1.5-km. or 850-mb. chart at 0000Z, 5 June as the large mesoscale wind streak, figure 6. The shorter period peaks of wind speed, e.g., those at 1600Z, and 2200Z, 4 June and 0300Z, 5 June, will be referred to as small mesoscale-wind maxima, and their relation to individual groups of showers will be discussed later.

The large mesoscale periods of strong wind in figure 8 are sometimes capped by strong shear such as at 2200Z, 4 June and 0300Z, 6 June. It may be difficult for convection to penetrate these layers with strong vertical shear [1]. Strong shear can tear apart a convective column thereby directly preventing deep convection or it can prevent the successive moistening of the middle troposphere by elements from a growing cloud so that each rising bubble will encounter dry air and lose buoyancy by evaporation into entrained air.

Figure 9 shows the percentage occurrence of rain showers and thunderstorms as observed from surface sites in the Saigon area. See figure 5. From 2100Z, 4 June to 1100Z, 5 June the strong shear was located at high levels (around 6 km.) and both showers and thunderstorms were relatively frequent. From 0000Z, to 1200Z, 6 June, the strong shear was located at lower levels (around 3 km.) and showers were common but thunderstorms were rare. These observations suggest that strong winds may be related to low-level convergence but that strong vertical shears in the lower troposphere may prevent deep convection and thunderstorms.

The role of wind shear in driving giant thunderstorms and severe squall lines by providing a dry current that is chilled by evaporation and that sinks in a mesoscale high to scoop up the low-level moist current [8] is another matter and does not apply to everyday tropical thunderstorms.

Having discussed the role of large mesoscale low-level wind maxima and the level of strong shear above them, let us return to the embedded small mesoscale-wind maxima. While the larger wind streak was drifting southward at 10 to 15 knots, smaller maxima appeared to propagate ENE. within the larger streak. Groups of showers also moved ENE. apparently in conjunction with individual wind maxima.

Figure 10 shows a small wind maxima at 850 mb. enclosed by the 45-knot isotach over and south of Saigon (VS). The group of thunderstorms and the area of ceilings lower than 4,000 feet lies just to the north of the peak 850-mb. speed. Actually the rawinsonde data can resolve the large mesoscale-wind streaks, but they can only suggest the nature of the small mesoscale-wind maxima and the indicated relation to the group of thunderstorms.

Doppler equipped aircraft would be required to adequately describe the smaller wind maxima in figures 8 and 10 and their relation to the group of showers that move with the flow on the northern side of the large mesoscale-wind streak shown in figure 6. This case study serves to indicate the nature of the low-level wind field associated with a band of disturbed weather. How frequently this type of mesoscale pattern occurs remains to be seen; certainly other types of mesoscale disturbances also occur in the Saigon area.

## DISCUSSION

HARRIS: In your opinion does the difference in the divergence patterns when the coriolis force is included or omitted in the P.F. model indicate a divergence contribution on the very large scale?

KREITZBERG: Not the very large scale but rather the scale of the Indochina Peninsula.

ALBERS: Were times of calm winds other than 1200 LST tried in P.E. model equations? Use of 0600 LST is suggested to conform with local observations.

KREITZBERG: Yes. 0400 and 1000 LST. Further investigation is in progress - 0600 LST will be tried.

SOMERVELL: The Naval Support Activity Danang reported a low-level wind problem just south of the DMZ on some summer situations during the early forenoon. It appeared that a low-level nocturnal westerly jet was located at about "gradient" - wind level which worked its way down to the ground shortly after sunrise, producing gale-force offshore winds at the surface, and then diminished during the forenoon as the seabreeze set in.

KREITZBERG: We will watch for this phenomenon in the numerical model experiments.

VALOVICIN: The period 4 - 6 June 1967 was one of the driest at Tan Son Nhut according to the radar index. The period also shows the difficulty of trying to relate wind speed with various definitions of convective activity such as radar index, precipitation and radar cloud tops.

MILLS: Did you study 8 through 15 June? You'll possibly find, your 4 through 6 June maximum preceded a cold frontal passage. Note: Follow the history of the 1018 mb. high at 35° N., 105° E. on 6 June 1967 and its associated cold front.

KREITZBERG: We will study 20 - 24 June 1967, and anyone is welcome to work on the 8 - 15 June period.

HAU: Since you are dealing with mesoscale analyses, I would like to ask you about the degree of confidence regarding the input data. Wind measurements, for example, could be greatly different at just one of your sites depending upon where you take them and the type of equipment in use. I don't think that even professional weather observers would reach such a desirable and confident degree of accuracy.

KREITZBERG: These data are from standard GMD-1A equipment and the evaluation angles are high, permitting high accuracy. The original records are converted in detail to punched cards and the winds calculated by computer. The wind accuracy is about 1 to 2 knots, and there are many mesoscale features with much larger amplitudes.

## REFERENCES

1. BLASKARA ROA, N. S. and M. V. DEKATE, "Effect of Vertical Shear on Growth of Convective Clouds." *Quart. J., Roy. Meteorol. Soc.*, 93: 363-367, 1967.
2. CONOVER, J. H., "Studies of Clouds and Weather Over Southeast Asia Utilizing Satellite Data." Fifth Technical Conference on Hurricanes and Tropical Meteorology, Caracas, Venezuela, November 20 - 28, 1967.
3. ENDLICH, R. W., "Diurnal Variations of Moisture Aloft Over Southeast Asia." Master of Science Thesis, the Pennsylvania State University, University Park, Pa., 1969.
4. GRAY, W. M., "Global View of the Origin of Tropical Disturbances and Storms." *Mon. Wea. Rev.*, 96: 669 - 700, 1968.
5. HEADQUARTERS, DEPT. OF THE ARMY, "Artillery Meteorology." Dept. of the Army Field Manual FM 6-15, 1962.
6. ING, G. K. T., "Pressure Data for Stations in Thailand and South Vietnam." Tech. Study 15, Scientific Services, 1st Wea. Wing, 1968.
7. KATAYAMA, A., "On the Radiation Budget of the Troposphere Over the Northern Hemisphere, Part III." *J. Meteorol. Soc. Japan* 45: 26-39, 1967.
8. NEWTON, C. W. and H. R. NEWTON, "Dynamic Interactions Between Large Convective Clouds and Environment With Vertical Shear." *J. Meteorol.*, 16: 483-496, 1959.
9. SWEENEY, J. R., "Mesoscale Wind Streaks in the Tropical Troposphere." Master of Science Thesis, the Pennsylvania State University, University Park, Pa., 1969.





Figure 1. Map of Southeast Asia Showing Sounding Sites (numbered) and Radar Sites (names).

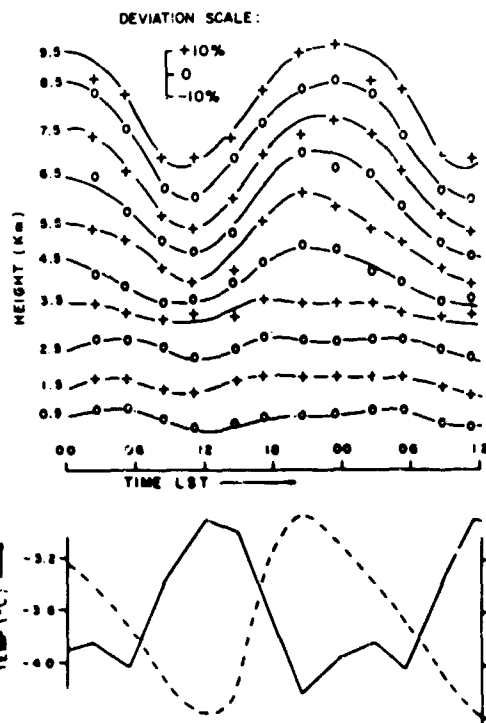


Figure 2. Diurnal Percentage Deviation of Precipitable Water (upper) in Each Kilometer Layer and Diurnal Variation of Relative Humidity (lower, dashed) and Temperature (lower solid) at 5.5 km. for Sites 13 and 15.

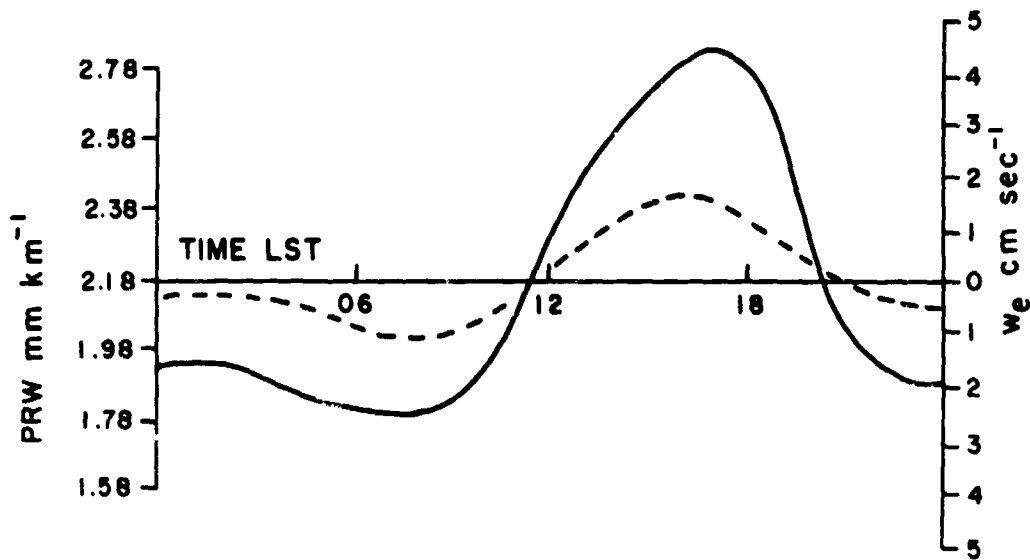


Figure 3. Diurnal Variation of Equivalent Vertical Motions Determined From Moisture Changes (solid) and Temperature Changes (dashed) at 5.5 km. for Sites 13 and 15.

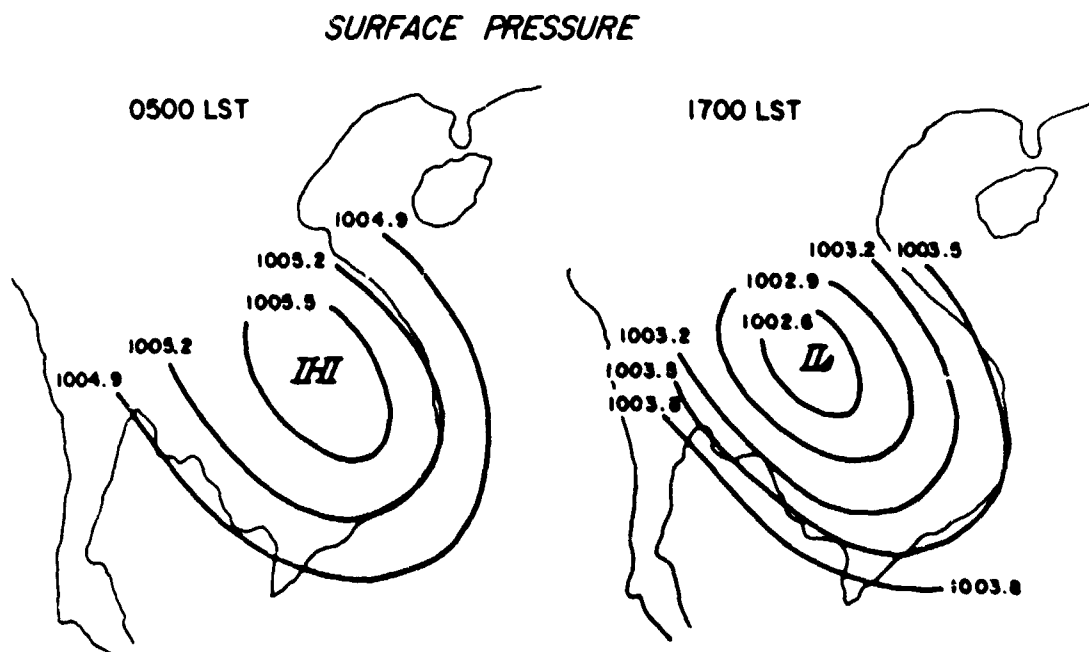


Figure 4. Charts of Mean Sea-Level Pressure (msl) Over Indochina in June at 0500 and 1700 LST.

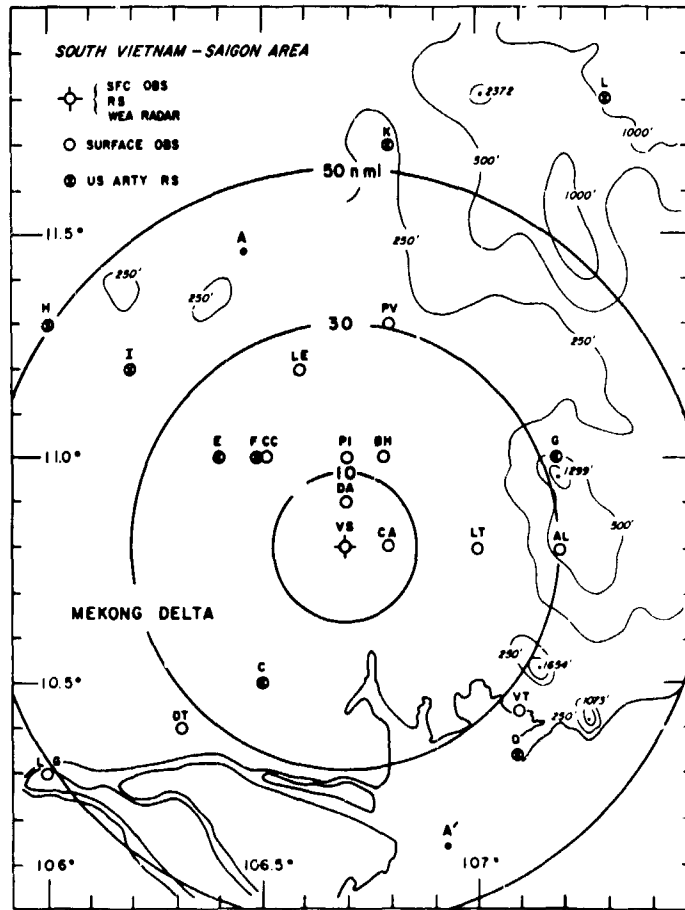


Figure 5. U.S. Army Rawinsonde Sites and U.S. Air Force/Republic of Vietnam Surface Reporting Site Locations Near Saigon.

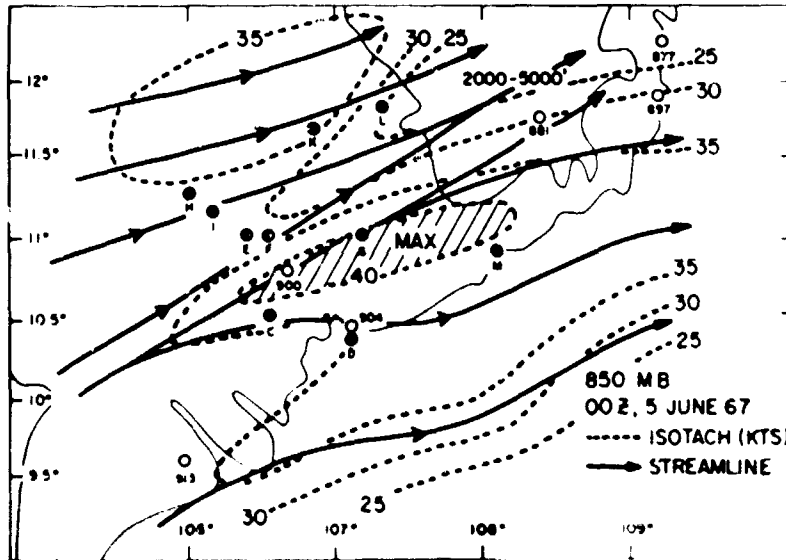


Figure 6. Streamline and Isotach Analysis for 850 mb. at 00Z, 5 June 1967.

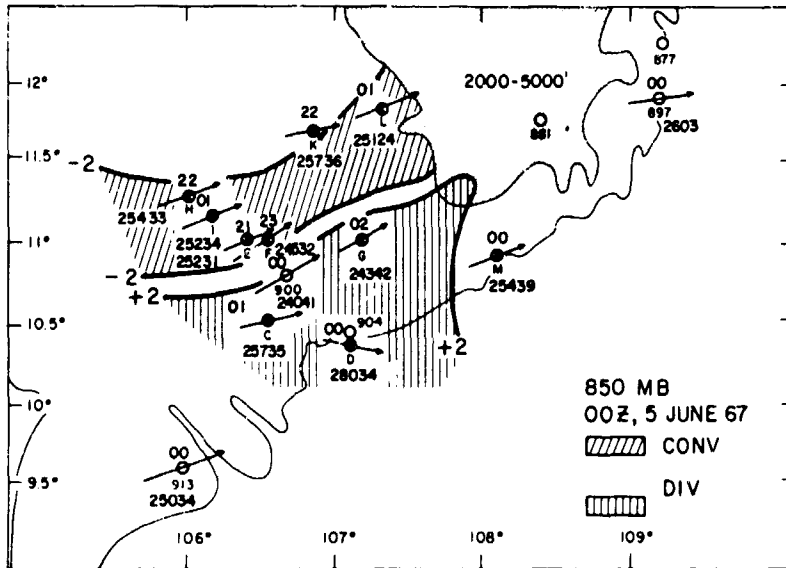


Figure 7. Wind Observations and Divergence - Convergence Patterns for 850. mb. at 0000Z 5 June 1967. Wind direction to the nearest degree and speed in knots are given by the five digit number while the observation time to the nearest hour (Z) is plotted above the station. Divergence values are in units of  $10^{-5} \text{ sec}^{-1}$ .

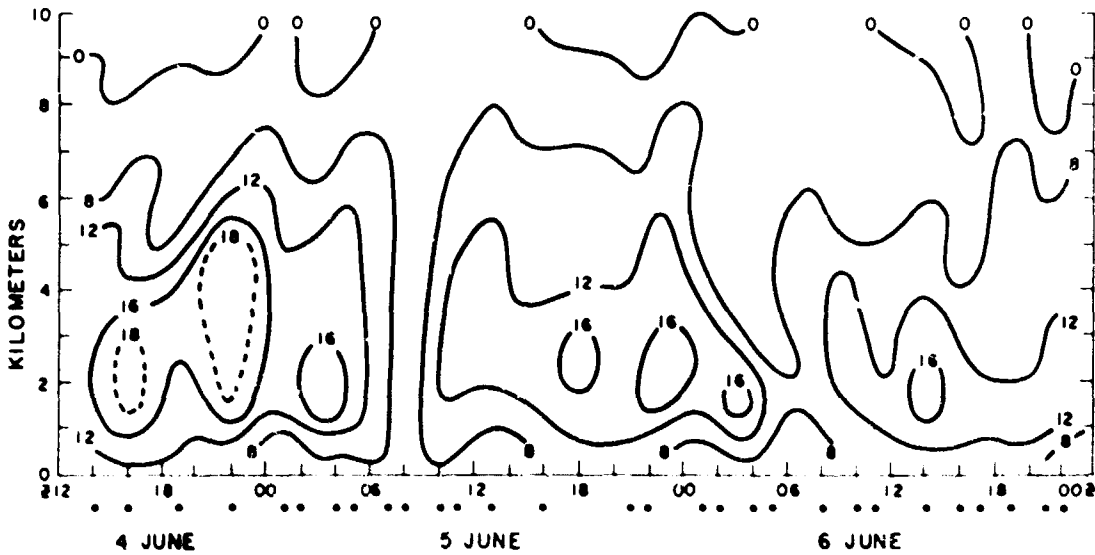


Figure 3. The Percentage Occurrence of Rain Showers (solid) and Thunderstorms (dashed) in the Area Shown in Figure 5. Observations Within :29 minutes of observation time are included. Radar indicus plotted across the top give percent scope coverage.

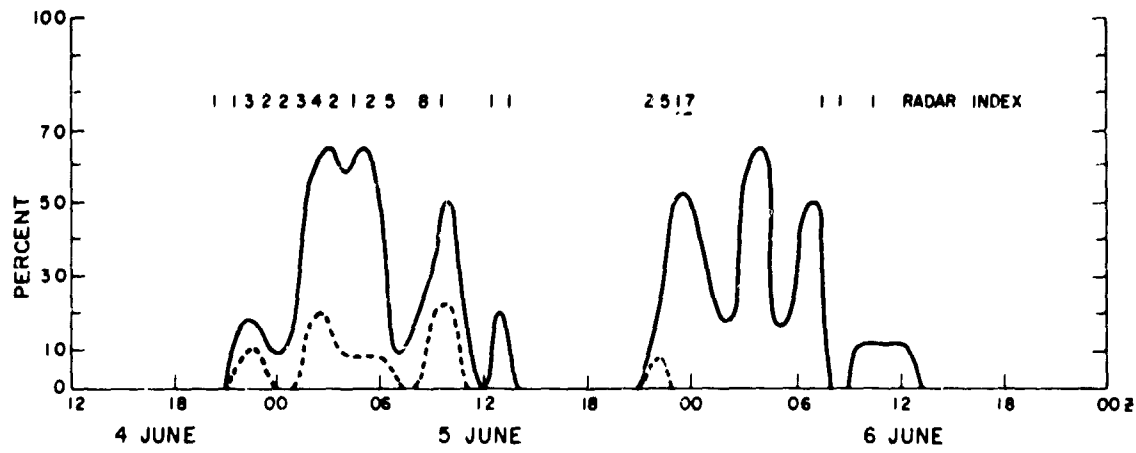


Figure 9. Composite Time Section of the Zonal (east) Wind Component in m. sec.<sup>-1</sup> for the Northern Position of the Mesoscale Network. Sites I, H, K, and L in figure 5 are included. The dots beneath the time scale mark observation times.

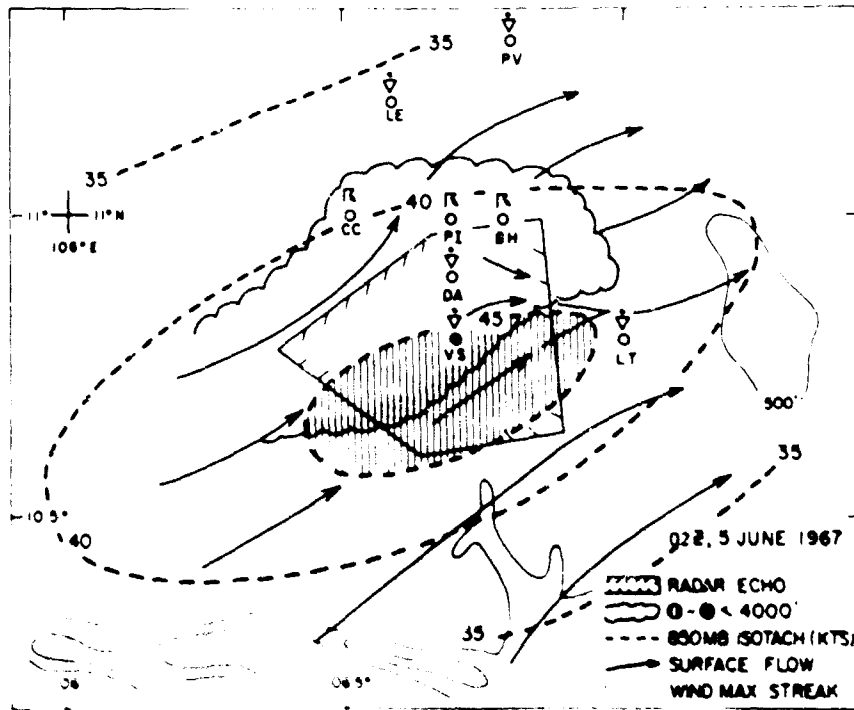


Figure 10. Surface Composite Plane Section for 02Z 5 June 1967.

## VARIATIONS IN CONVECTIVE ACTIVITY OVER SEASIA DURING THE SUMMER OF 1967 \*

R. F. Adler  
Navy Weather Research Facility

### ABSTRACT

Convective activity over the Indochina Peninsula during the summer of 1967 is examined with the aid of radarscope-coverage data, in an attempt to determine the major factors influencing its synoptic variations. Variations in convective activity, as expressed by a radarscope-coverage index (RI), are related to the strength of the tropical trough, measures of stability and low-level moisture, and the presence and location of tropical cyclone activity in the South China Sea.

### 1. INTRODUCTION

The objective of this study is to determine the major factors influencing synoptic variations of convective activity over the Indochina Peninsula during the summer of 1967. The approach is basically a diagnostic one, although the forecasting implications are obvious.

A radarscope-coverage index (RI), giving the average percentage of scope coverage within 50 miles of the station for the twelve-hour period from local noon to midnight, is used as an objective measure of the amount of the convective activity at a station on a particular day. The radar-index data were supplied by Mr. John Conover of AFCRL. The radar indices of three stations, Saigon (48900), Ubon (48407) and Udorn (48354), are used. The locations of these stations are shown in figure 1.

Ubon and Udorn are located on relatively flat terrain in the Korat Plateau of Thailand. Pronounced nearby terrain features include a north-south oriented range of hills (up to around 4000 feet) about one hundred miles to the west, and the Annam Mountains of Laos some 75 miles to the north of Udorn. The east-west oriented Phnom Dangrek Chain (up to around 2500 feet) is located about 50 miles south of Ubon. Saigon is, of course, located in the flatlands southwest of the southern end of the Annam Mountains.

The values of the radar index for each of the stations are shown in the time series of figure 2. The first ten days of June were disregarded because of a frontal passage and a distinctly non-summer type of flow pattern. Breaks in the time series denote missing data.

Although highly oscillatory, as shown by Conover [1] the radar index displays synoptic variability and frequent correspondence among the stations. After 10 July this correspondence is rather good, with peaks and minimums fitting quite well.

To have available an index of the convective activity over the main part of the peninsula west of the Annam Mountains, the three RI's are averaged to obtain a daily  $\overline{RI}$  (fig. 3). Here, the synoptic variability is clearly evident. Relative maxima are present between approximately 23 and 23 June, 10 and 15 July, 22 and 26 July, and a number of peaks in August of lesser duration. Of interest also are the minimums present between 14 and 22 June, 30 June and 4 July, 17 and 21 July, 1 and 3 August, 5 and 6 August, 10 and 15 August, 18 and 19 August, 22 and 23 August.

The usual parameters pertinent to any convection study were considered; i.e., stability, low-level moisture, low-level convergence, and vertical wind shear. In addition, tropical cyclone activity in the South China Sea was studied for its relation to the convection over the peninsula.

The NAVWEARCFAC convection model [3] was used to evaluate the combined effects of stability and moisture. The model is basically a sophisticated approach to parcel mechanics. Change of phase, buoyancy, drag and entrainment are treated through a stepwise lifting process. The microphysics of the cloud is

\* Research sponsored by Navy Weather Research Facility

treated through a set of parameters which specify droplet growth rates. Convective intensity is measured by computing the combined hydrostatic and dynamic pressure change beneath the developed cloud. This pressure change ( $\Delta P$ ) will be used in this study as a measure of the effect of the thermal-moisture structure on the strength of the convection. Soundings from each of the three stations for each day of the three-month period were processed, with the output consisting of various parameters (including  $\Delta P$ ) related mainly to the size of cloud predicted by the model under the conditions prescribed by the sounding data.

Because the low-level convergence field is difficult to compute accurately, another indicator of the convergence field was sought. Since large-scale, low-level convergence has been shown to be associated with the Ekman layer process and regions of positive relative vorticity in the low-level flow [2], a horizontal, zonal shear was selected as an indirect measure of the low-level convergence. The shear was calculated using the 850-mb. wind at Saigon and the average 850-mb. wind in the block formed by 20° N. to 25° N. and 105° E. to 111° E.

Vertical wind shear, which in this study was taken as the magnitude of the shear between 850 mb. and 700 mb., is thought to play a role in the following way. Under relatively low stability conditions, high shear would blow off the tops of the penetrating clouds. This would have the effect of decreasing the convective penetration, and correspondingly reduce the height of the clouds.

## 2. SUMMER OF 1967

As may be seen in figure 3, the summer of 1967 can easily be divided into two periods on the basis of a change in the zonal wind shear. For the first part of the summer, up to 20-25 July, relatively small shears predominate, with west to southwest winds over Saigon and southwest to south winds over South China. The last part of the summer is dominated by large zonal shears, when winds having a significant easterly component are present over South China.

It would be expected that larger shears would be coincident with large RI's, and small and negative shears to be associated with low RI's. However, as can easily be seen in figure 3, this correlation is not evident during the last part of the summer. Rather, the increase in shear is associated with increased tropical cyclone activity in the South China Sea.

During the first part of the summer only one disturbance, Typhoon ANITA, came close to the South China Sea as it passed through Bashi Strait and entered the China mainland east of 115° E. From late July until the end of August, on the other hand, there were two tropical depressions, two storms and one typhoon in the South China Sea, no two on the same day. This tropical cyclone activity had a pronounced effect on the RI over the peninsula. Only short-period oscillations are evident during August, versus longer period oscillations earlier in the summer. In addition, the RI for the last part of the summer did not increase correspondingly to the increase in shear. Whether these two are connected will be discussed later when we will focus on the tropical cyclone problem.

Because of the complications which arose from the tropical cyclone activity beyond 25 July, we decided to confine the major part of our efforts to the period 11 June to 25 July. The first ten days of June were disregarded because of a frontal passage and attendant non-summer type weather.

The relationship of the zonal shear (850 mb.) and the  $\bar{RI}$  (RI averaged over the three stations) for the period 11 June - 25 July is shown in figure 4. Although there is a large scatter, the general trend is obvious. With negative zonal shear,  $\bar{RI}$  is less than 5% in six out of the nine cases. For shears between 0 and 10 knots, nine out of twelve  $\bar{RI}$ 's are between 5% and 10%; and for shears greater than 10 knots eleven out of the seventeen cases have RI's greater than 10%. The correlation between  $\bar{RI}$  and the zonal shear is 0.56. Eliminating the one point where the zonal shear equals approximately -21 knots and the  $\bar{RI} = 14.4\%$  the correlation increases to 0.68. Regardless of the exact magnitude of the correlation, a relation between the shear and the radar index exists. This is not extremely surprising, but emphasizes the importance of the low-level convergence field on the average convection over the peninsula.

Let us now examine the fluctuations of RI at individual stations. Only Saigon and Ubon will be discussed, because Ubon RI data were often missing for the period. For Saigon, figure 5, the RI-zonal shear scatter diagram, shows a distribution not unlike that of figure 4, but with a larger scatter -- especially in the range of zero to ten knots in the zonal shear.

The role of stability and low-level moisture as denoted by the factor  $\Delta P$  is shown in figure 6. Large values of  $\Delta P$  express relative instability, while low values represent the stable end of the spectrum. Two things must be kept in mind when examining the results displayed in figure 6. First, although the left side of the distribution is termed the stable side, almost all the soundings represented were conditionally unstable. Second, cases when the convection model predicted convection "improbable" were plotted with  $\Delta P = 0$ .

By the distribution in figure 6, the stability-moisture structure seemed to have an effect on the Saigon RI during the period studies. For the cases where  $\Delta P < .10$  mb., the median RI was 8%; while for cases where  $\Delta P > .10$  mb., the median value of RI was greater than 17%.

The RI (Saigon) vs. vertical shear (850 mb. - 700 mb.) distribution is given in figure 7. There is a slight preference for higher shears to be associated with high RI's. For vertical shears less than or equal to 10 knots the median RI is 8%; for shears greater than 10 knots the median RI is approximately 13%. However, because there is a positive correlation between the horizontal and vertical shear among these 40 odd points, the physical relationship between vertical shear and convection is clouded. Actually, to determine precisely the relationship between the radar index and any of the parameters studied it would first be necessary to eliminate the effects of the other variables. With the limited number of data in this study this was difficult, and those stratifications carried out did not produce significant results.

To look at the combined effect of the zonal shear and  $\Delta P$  on RI, both the zonal shear and  $\Delta P$  distributions were each divided into three classes, each with approximately the same number of data. For each combination of classes (9 in all) the median RI was noted. This distribution of RI is shown in figure 8. Although some of the boxes have only a few points (the number of points in each box is given by the number in parentheses), there is evidence to show that when either the stability is low or the zonal shear (and presumably then the low-level convergence) is large, large RI's are present. A further representation is given by the number of low, medium, and high RI days in each box. The three classes of RI were set up so that approximately the same number of data points are in each category.

A similar procedure was carried out with the Ubon data. The Ubon RI-zonal shear distribution is given in figure 9. It is noteworthy that though there is a general increase in the RI with increasing shear, there is a large scatter with RI's of 1% present with shears of 20 knots. Unfortunately, the  $\Delta P$  output of the convection model was not applicable at Ubon. The main reason for this is the present lack of a term in the model dealing with the mixing of the lower layers during the daytime. Ubon, with its extremely high afternoon temperatures and often relatively dry lower layers, is unsuited to the model as it stands. As a crude replacement for  $\Delta P$  the dew-point depression at 850 mb. was chosen. The relation of horizontal shear and moisture to the Ubon RI can be seen in figure 10. Of interest here, first of all, is the apparent need for both substantial shear and moisture before incidents of RI's in the high category occur. The effect of the moisture is obvious by looking at each wind-shear category. For zonal shears below 5.5 knots the moisture seems to have little effect. But for the other two classes of shear there is a definite trend toward higher RI as the relative humidity increases.

### 3. SUMMER OF 1968

The radar index data for the summer of 1968 were recently received. Although the corresponding radiosonde data were not available in a form suitable for use with the convection model, in the limited time available a comparison was made between RI and zonal shear (fig. 11). The shear time series in the lower part of the diagram is strikingly similar to the 1967 time series (fig. 3). During early summer the shear varies between about - 15 knots and 20 knots. Throughout this period there is general agreement between the zonal shear and RI. During the last part of summer, especially that period between 19 July and 20 August, the shears again become large and only occasionally drop below 20 knots. However, unlike 1967, the  $\bar{R}_I$  distribution in 1968 increased to values averaging over 20% for much of the period. Of interest also are the sudden drops of  $\bar{R}_I$  after 25 July and 19 August. These will be related in the next section to tropical cyclone activity in the South China Sea.



#### 4. TROPICAL CYCLONE ACTIVITY IN THE SOUTH CHINA SEA AND ITS EFFECT ON THE RADAR INDEX

The possible effect of tropical cyclone activity in the South China Sea on the RI over the peninsula has been mentioned previously in this report. Figure 12 shows three-day running means of  $\bar{R}I$  for the period 20 July - 31 August for both 1967 and 1968. The shaded areas denote periods of tropical cyclone activity in the South China Sea within a radius of 900 nm. of Ubon. The name and classification of the storms are given above the shaded area. Immediately evident is the correspondence of the occurrence of the storms and decreases in the radar index. Only one incident of an increase was noted, that being Tropical Storm IRIS (15 - 16 August 1967).

The cause of these decreases is thought to be twofold. First, outflow from the storm induces subsidence which results in an area of clearing ahead of the storm [4]. This effect is readily observed on satellite photographs. However, the distinct clearing in front of the storm did not always extend to the west of the Annam Mountains and into the area covered by the radar index. In addition, the minimum RI sometimes occurred after the storm had penetrated inland and dissipated. The second part of the cause was found in the movement of the tropical trough at 850 mb. The storms that were associated with the most significant decreases in  $\bar{R}I$  (T.S. FRAN, T.D. #15, Typhoon KATE, T.S. OLIVE and Typhoon NADINE, and Typhoon SHIRLEY) were all coincident with a northward movement of the trough and the appearance of westerly winds over South China. Except for the OLIVE-NADINE combination, all of these storms penetrated the China mainland between 111° E. and 114° E. and continued northward into China. Tropical Storm IRIS also penetrated China at the same geographic location (111° E.), but veered westward along the coast as the trough maintained itself along the coast and did not move north. Thus, it appears that the storms and whatever role they play in the movement north of the trough are significant in the explanation of changes in RI in the presence of tropical cyclone activity in the South China Sea.

#### 5. CONCLUSIONS

1. In the absence of tropical cyclone activity in the South China Sea, the low-level convergence field (as represented by the zonal shear at 850 mb.), stability and low-level moisture combined are related to much of the synoptic variability in convective activity over the Indochina Peninsula during the Summer of 1967.
2. Preliminary analysis shows that low-level convergence (represented by the zonal shear at 850 mb.) was again a major factor in the variability of convective activity during the Summer of 1968.
3. Tropical cyclone activity in the South China Sea had a very pronounced effect on convective activity over the peninsula in the summers of both 1967 and 1968. Especially important is the coincident movement northward of storms crossing the South China coast and the movement northward of the tropical trough. This situation is associated with the most distinct reductions in convective activity noted.

#### REFERENCES

1. CONOVER, JOHN H., "Studies of Clouds and Weather Over Southeast Asia Utilizing Satellite Data, Progress Report - 24 May 1967." Satellite Meteorology Branch, Meteorology Laboratory, Air Force Cambridge Research Laboratories, Bedford, Mass., 1967.
2. GRAY, WILLIAM M., "Global View of the Origin of Tropical Disturbances and Storms." Colorado State University, Atmospheric Science Paper No. 114, 1967.
3. PETERMAN, W. A., "A Model for a Climatology of the Potential of Ice-Phase Modification of Convective Clouds." NAVWEARSCHFAC Tech. Paper No. 8-67, 1967.
4. SADLER, JAMES C., W. R. BRETT, B. E. HARRIS and F. P. HO, "Forecasting Minimum Cloudiness Over the Red River Delta During the Summer Monsoon." Hawaii Institute of Geophysics, University of Hawaii and 1st Weather Wing, 1968.

## DISCUSSION

FENTON: Concerning the 850-mb. shear correlated with the radar index. Is there a time lag, that is, is there a correlation between the 850-mb. shear and the radar index at a later time? It is possible to prepare a prognostic 850-mb. shear for use in forecasting the radar index.

ADLER: There was noted an occasional lag between the changes in zonal shear and RI. However, no systematic lag could be found.

KREITZBERG: Isn't middle level moisture also very important in determining  $\Delta P$  in the convection model as well as low-level moisture and stability?

ADLER: Yes, and the model will take the moisture throughout the cloud layer into account when computing the entrainment effect.

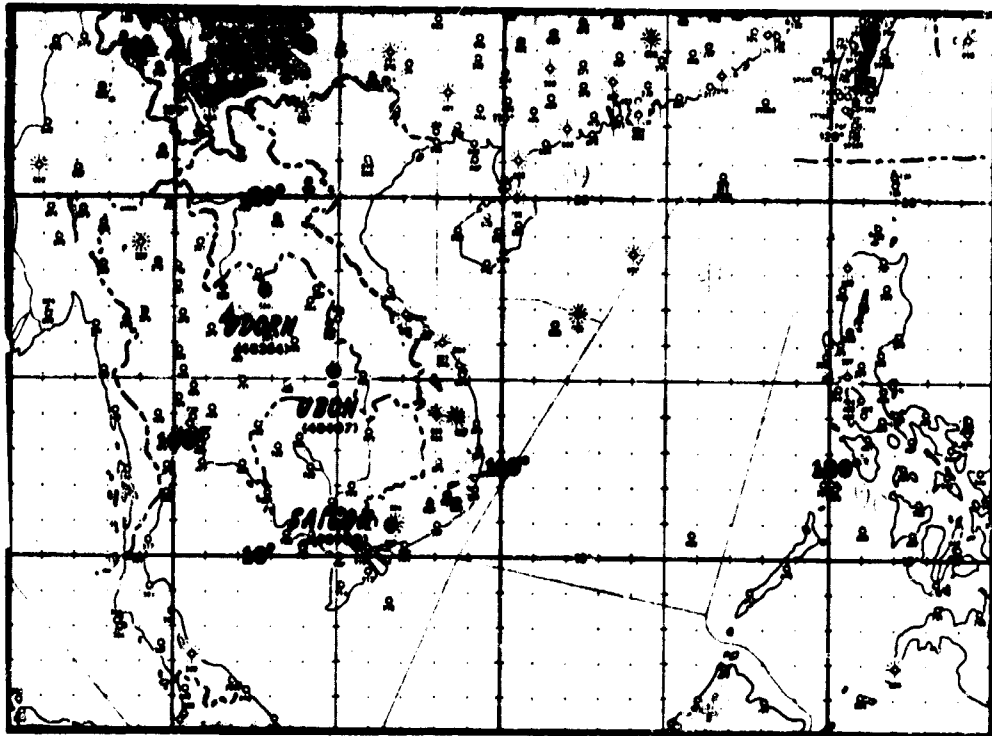


Figure 1. Location of Stations.

### RADAR INDEX (RI)

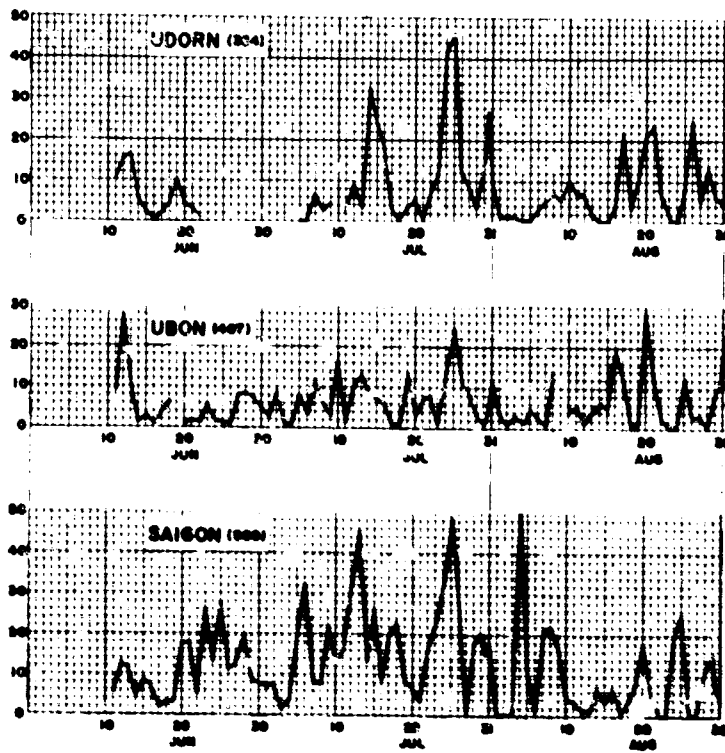


Figure 2. 1967 RI Time Series for Udorn, Ubon and Saigon.

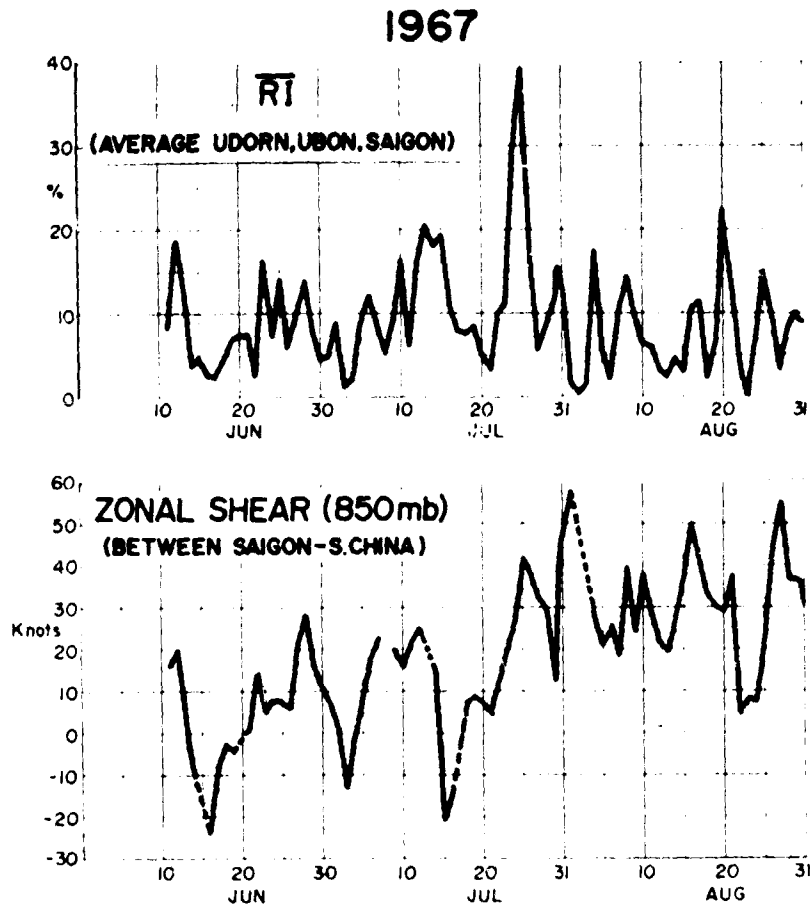


Figure 3. 1967  $\bar{RI}$  and Zonal Shear (850 mb.) Time Series.

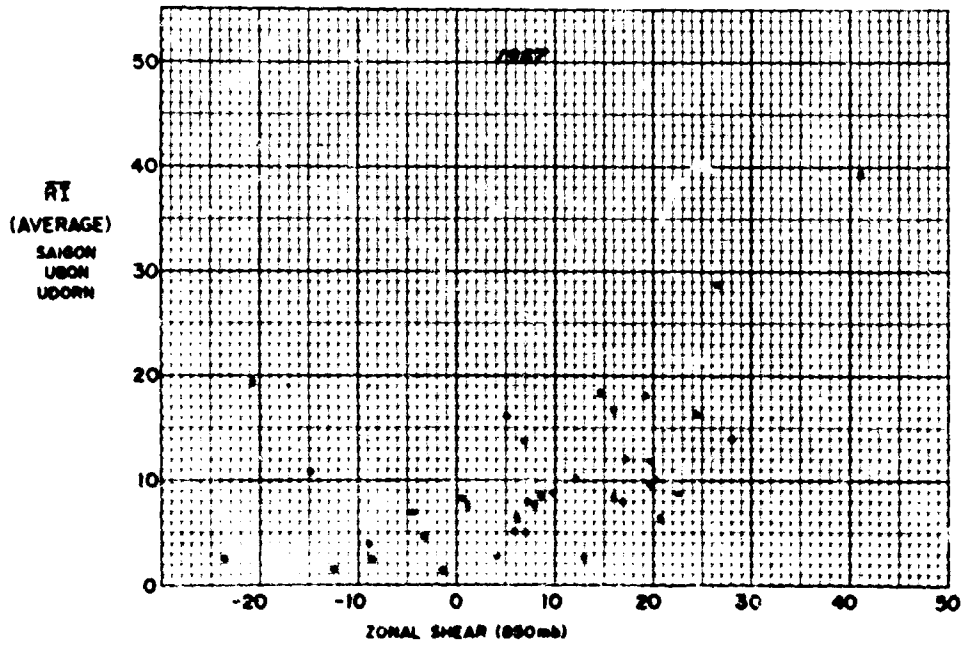


Figure 4. Zonal Shear (850 mb.) vs.  $\bar{RI}$  (11 June - 25 July 1967).

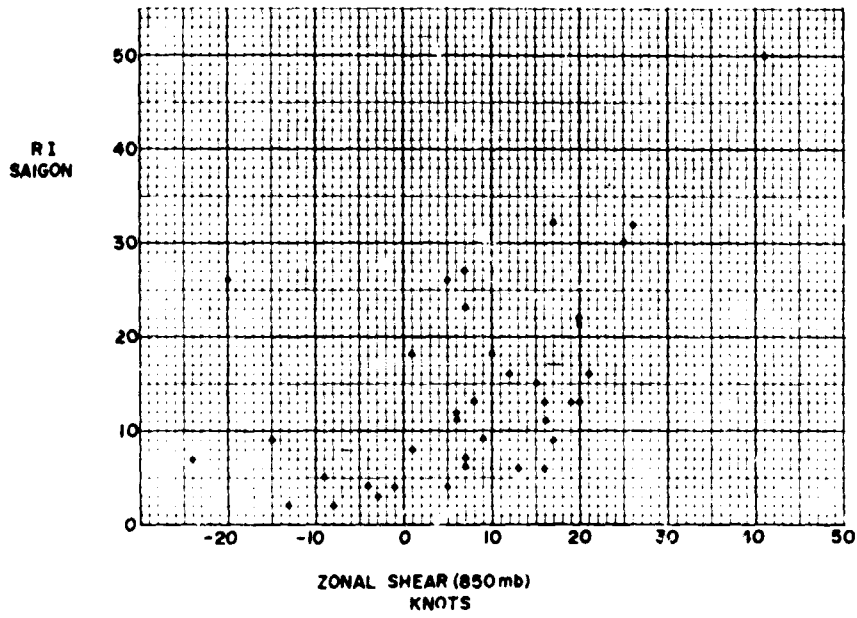


Figure 5. Zonal Shear (850 mb.) vs. RI (Saigon).

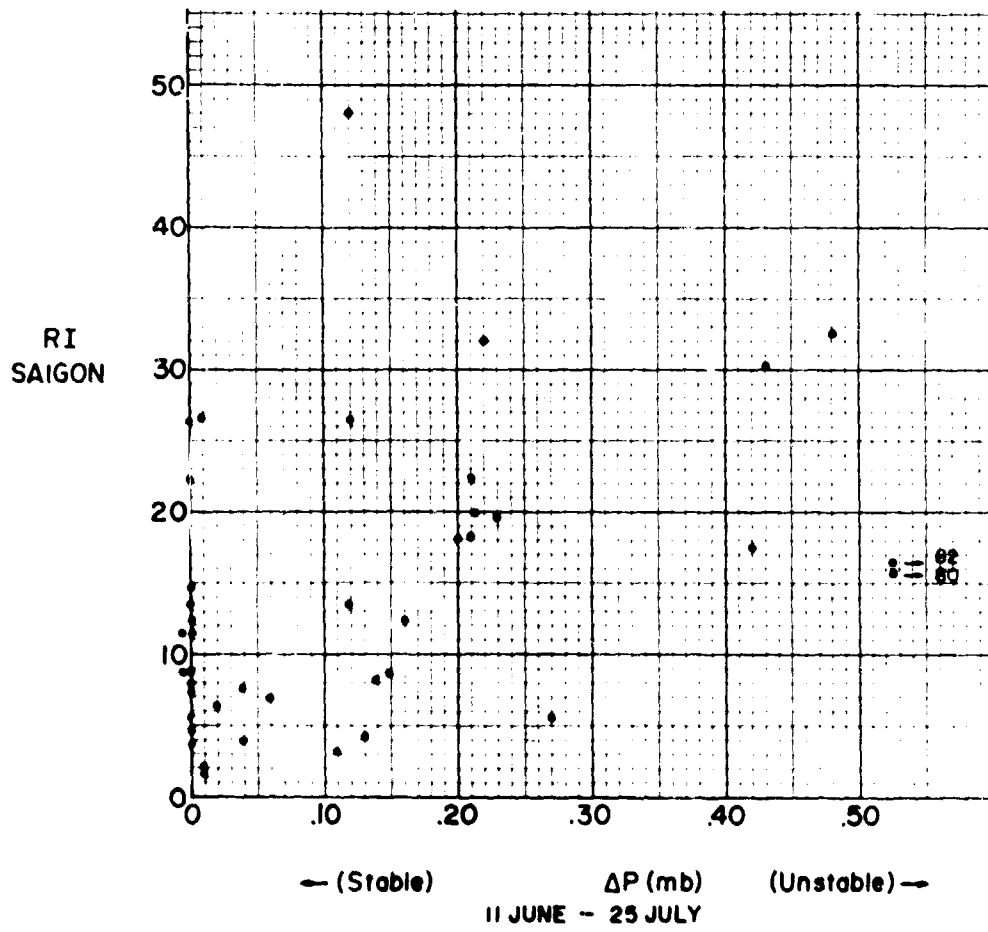


Figure 6.  $\Delta P$  vs. RI (Saigon).

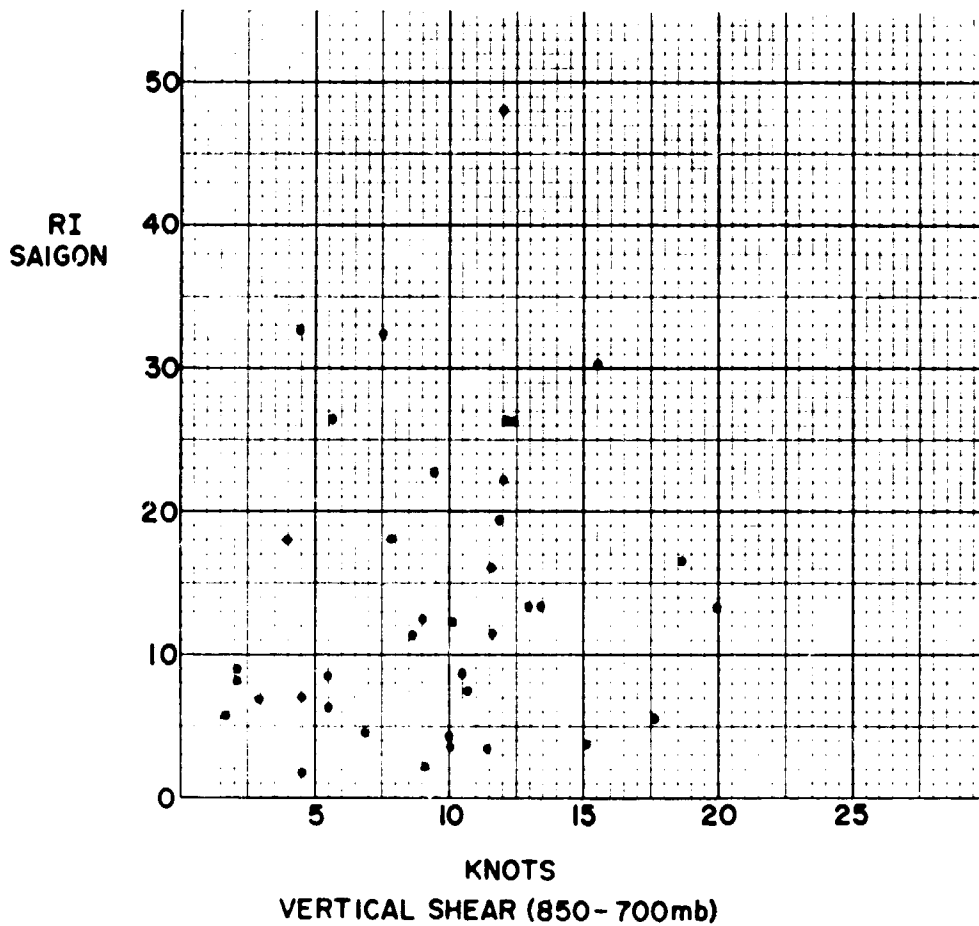


Figure 7. Vertical Shear vs. RI (Saigon).

**HORIZONTAL SHEAR (KNOTS)**

	← stable	$\Delta P$ (mb.)	unstable →
	Improbable 0	$0 < \Delta P < .15$	$\Delta P \geq .15$
SHEAR < 5.5	5.8 (4) L(3) M(0) H(1)	4.0 (8) L(5) M(2) H(1)	18.0 (1) L(0) M(0) H(1)
>5.5 SHEAR < 15.5	11.4 (4) L(0) M(4) H(0)	10.2 (4) L(2) M(1) H(1)	18.2 (3) L(0) M(1) H(2)
SHEAR >15.5	13.5 (3) L(0) M(2) H(1)	48.2 (1) L(0) M(0) H(1)	16.3 (7) L(1) M(3) H(3)

Saigon  
11 June - 25 July

**RI Categories**  
 LOW  $0 < RI \leq 7.2\%$   
 MED  $7.2 < RI \leq 16.3\%$   
 HIGH  $RI > 16.3\%$

Figure 8. Table of RI (Saigon) as Function of Both  $\Delta P$  and Zonal Shear.

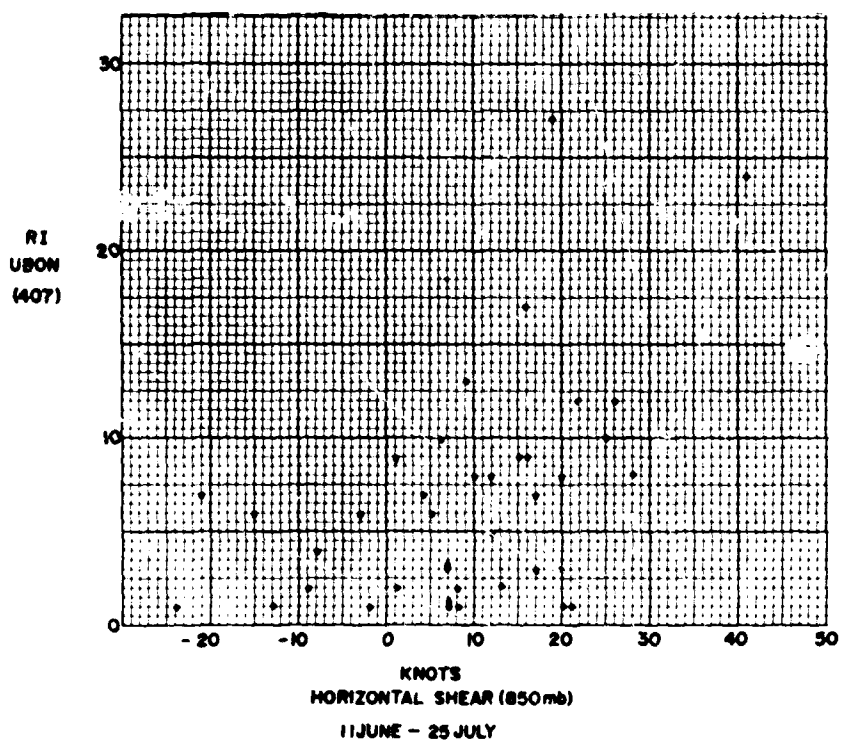


Figure 9. Zonal Shear (850 mb.) vs. RI (Ubon).

UBON

	Temperature-Dewpoint (A50 mb.)		
	T - Td ≥ 4.6°	T - Td ≥ 2.8° ≤ 4.5°	T - Td > 0° ≤ 2.7°
<b>SHEAR</b> < 5.5	5.1 (2) L(0) M(2) H(0)	1.8 (4) L(3) M(1) H(0)	3.5 (4) L(2) M(1) H(1)
<b>SHEAR</b> 5.5 < 15.5	1.8 (5) L(3) M(2) H(0)	6.3 (2) L(0) M(2) H(0)	8.6 (5) L(2) M(0) H(3)
<b>SHEAR</b> > 15.5	3.4 (5) L(1) M(3) H(1)	11.7 (5) L(1) M(1) H(3)	11.5 (4) L(0) M(1) H(3)

RI Categories

LOW 0 < RI < 2.5  
MED 2.5 < RI < 8.5  
HIGH 8.5 < RI

Figure 10. Table of RI (Ubon) as Function of Both (T - T<sub>d</sub>)<sup>850 mb.</sup> and Zonal Shear.

1968

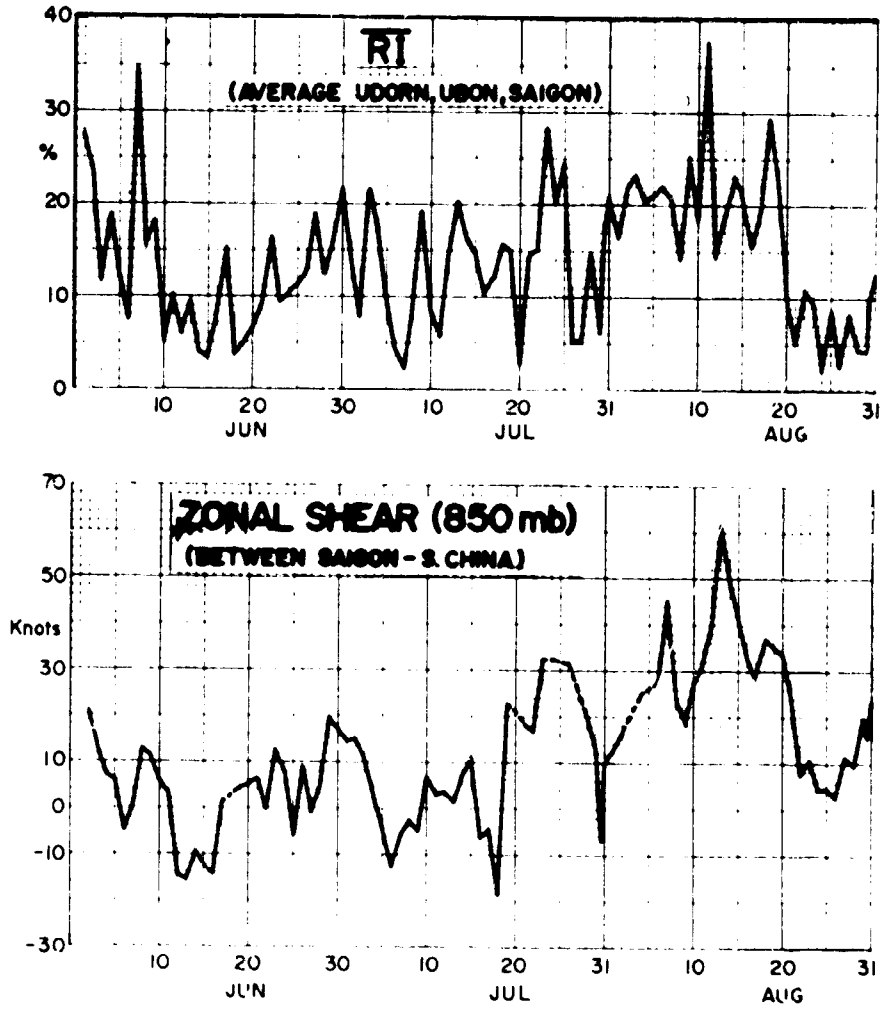


Figure 11. 1968  $\overline{RI}$  and Zonal Shear (850 mb.) Time Series.

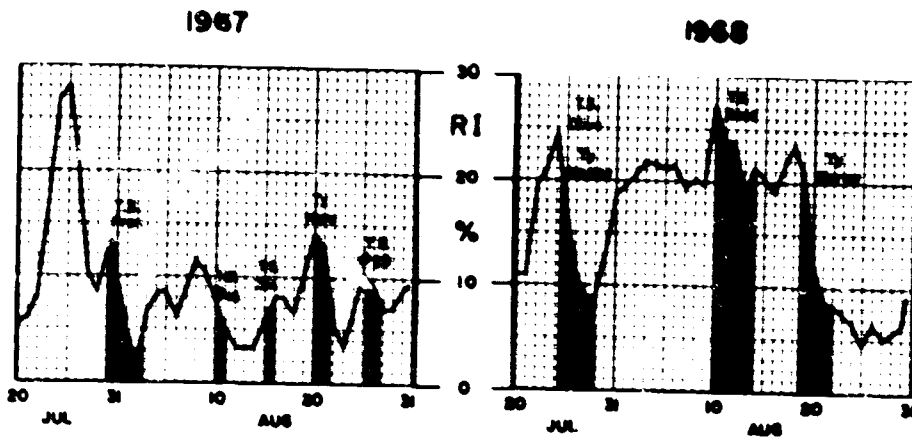


Figure 12. Effect of Tropical Cyclones on  $\overline{RI}$ .



Preceding page blank

- 295 -

## A NOTE ON APPLICATION OF A CUMULUS MODEL TO SEASIA SOUNDING DATA\*

James T. Bunting  
Satellite Meteorology Branch  
Air Force Cambridge Research Laboratories

The following is a brief note describing work with the Penn State Cumulus Model and application to SEASIA sounding data. No attempt is made to elaborate the findings since they are generally inconclusive. It was originally thought that a cumulus model might be a good tool to examine stability in the tropics. As a much more complete model of convection it might succeed where conventional indices of stability failed.

As programmed for the Air Force Cambridge Research Laboratories, the Penn State Cumulus Model uses, as input, cloud base data plus a sounding and computes, as output, radar reflectivities, liquid water contents, incloud temperatures, vertical velocities, cloud top heights, etc., for 10 entrainment rates x 2 different freezing assumptions = 20 different model clouds. The entrainment rate is determined by the cloud radius according to the familiar relation,  $\mu = .2/R$ . This model has been used operationally with some success to forecast the radius of cloud that would experience the greatest potential modification by seeding. This technique requires a cloud base selected by persistence or morning observations. Further, T (cloud base) is assumed equal to T (sounding) and saturated. This approach was used initially and only the cloud top heights were considered as output, since the model seems to predict these well for observed cloud radii and proximity soundings at least in Arizona, Florida, and the Caribbean.

Using the model, nine extremely active days were compared with eight extremely inactive days. The nine active days had a high Radar Index as defined by Conover [1] and are a subset of his tertile 1 days. Henceforth they will be designated "tertile 1" days. Similarly, the eight inactive days had a low Radar Index and come from Conover's tertile 3 days.

Cloud base heights were selected from WBAN's at or shortly before the time of maximum surface temperature. Daily 0000Z soundings were used as input for the cloud environment. All of the above were for Summer 1966 at Tan Son Nhut. Results in terms of a profile of cloud top heights are given in the attached figure for averages of tertile 1 days and of tertile 3 days. The abscissa is cloud radius in kilometers; the ordinate is cloud top in kilometers. Dots are averages for tertile 1 days, crosses are averages for tertile 3 days. Where there are pairs of dots or crosses at the same radius, the results of the different freezing assumptions are evident. The higher dot (cross) is the average cloud top for the "seeded" case, i.e., freezing from  $-4^{\circ}$  to  $-8^{\circ}$  C., while the lower dot (cross) is that for the "unseeded" case, i.e., freezing from  $-15^{\circ}$  to  $-30^{\circ}$  C.

Average cloud top heights for tertile 3 are lower than for tertile 1. Almost all of this difference is due to two tertile 3 days which are suppressed for all radii at low levels. The other six tertile 3 days are rather similar in profile to the tertile 1 days. Further, the suppression of two days can be explained through the assumed cloud bases and the next 150 mb. of the soundings.

The importance of the assumptions at cloud base can be visualized by imagining the process on a thermodynamic diagram. The choice of two different cloud bases usually implies that the model clouds begin their development on different wet adiabats. As the two clouds grow, they receive supplies of buoyant energy which differ by a factor proportional to the area between the wet adiabats, a factor which can be large. In other words, the height and inferred temperature at cloud base are critical parameters for the cumulus model.

There is another reason to be suspicious of the temperature assumption at cloud base. As stated previously, it is usually assumed that T (cloud base) = T (0000Z sounding at cloud base height). However, in computing the LCL or CCL for Tan Son Nhut, T (base) usually is less than T (sounding) at cloud base level. When this is true, an area of "negative" energy is present, for which work must be supplied to lift a parcel to the LFC. The larger the area of negative energy, the less likely is penetrative convection. If the Penn State Model were used with T (base) less than T (sounding) by say  $0.5^{\circ}$  C., the suppression would be almost guaranteed since a 1 m. sec.<sup>-1</sup> updraft is assumed, which would quickly be snuffed out; however, this possibility is generally not considered since the

\* Research report of the Air Force Cambridge Research Laboratory

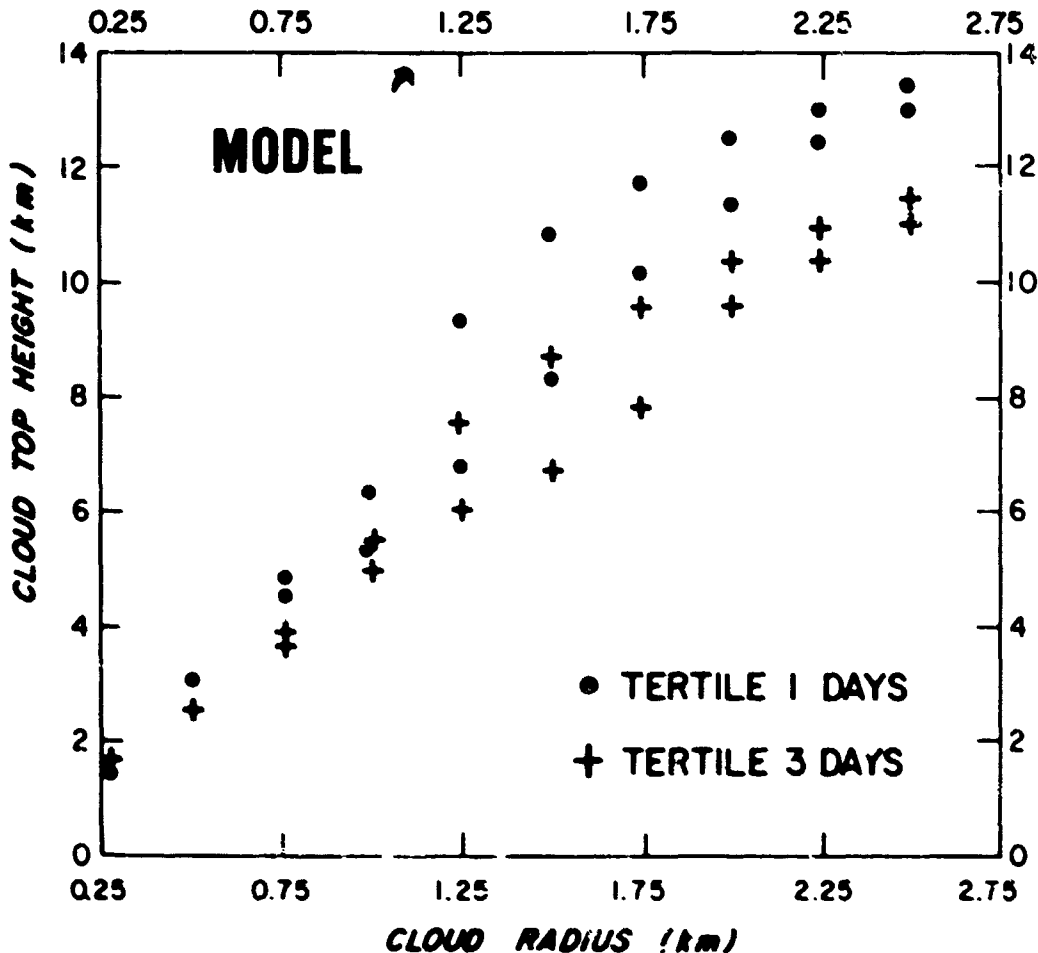
temperature difference is generally not known. In short, not only the temperature of cloud base but also any temperature difference between cloud base and environment is highly critical in the model.

Finally, the limitations of the sounding itself must be considered. The original sounding data necessarily undergo some smoothing when coded for transmission. Also, at least in SEASIA, it may sometimes be risky to extrapolate a sounding over time or space. Kreitzberg (personal communication) has pointed out significant mesoscale variability in temperatures at lower levels using a network of Army rawinsonde sites.

Use of the model has the advantage over simple stability indices since it includes the development of a cloud, instead of just the potential for a cloud. However, like the simple stability indices, it fails to predict convective activity in SEASIA on a day-to-day basis. The failures are attributed to the following reasons. First, dynamic and large-scale factors are not considered. These should be important, particularly in determining the number and radii of incipient convective elements. Secondly, there was confusion as to how to select a cloud base height, particularly when more than one was observed in a WBAN. Finally, the temperature of the cloud base and the temperature distribution of the environment near cloud base are highly sensitive input. The model may still be useful for examining stability in the tropics; however, temperature data substantially more accurate than conventionally reported sounding data would have to be obtained and tested.

#### REFERENCE

1. CONOVER, J. H., "Studies of Clouds and Weather Over SEASIA Utilizing Satellite Data." Proceedings of the Conference on the Summer Monsoon of SEASIA, U. of Hawaii, 7-9 April, 1969.



## GENERAL DISCUSSION

SOMERVELL: There are a few things which I've found disquieting during this conference, and this seems to be my last opportunity to sound off if they're to be considered by this distinguished assembly. However, I'd first like to extend the thanks of the Navy Weather Research Facility; to the invited experts, whose contributions have shed substantial light upon previously ill-defined aspects of the SEASIA Summer Monsoon; to Air Force Cambridge Research Laboratories, without whose wholehearted support and cooperation this conference would not have been possible; to our hosts, Dr. Ramage and the Department of Geosciences of the University of Hawaii, for their excellent arrangements for this conference and their marvellous hospitality; and last but not least, to the Naval and Air Weather Service participants for interjecting liberal doses of real-world meteorology at appropriate points in the discussion by us ivory-tower types.

I've been a rather passive participant thus far, for the reason that I can't pretend to have personally conducted exhaustive and systematic research on the SEASIA area. On the other hand, I did have a 2-year opportunity to acquaint myself with many of the weather features peculiar to the South China Sea and the Indochina Peninsula. I believe this is called learning through experience, a process which can sometimes be inimical to the career prospects of the forecaster involved. Therefore, in attending this conference it was my hope to hear explanations for some of the circumstances which even in retrospect had not always been understood, to play devil's advocate where some suggested solution did not appear to have had the advantage of personal experience, and to propose as fields for fruitful endeavor those features which had seemed troublesome to me at the time but weren't discussed here. Since my impression at the moment is that the last of these has a much larger weighting factor than the other two, it may be that as operational forecasters some of us have been remiss in not providing the research community with timely and well-documented notification of situations which did not seem to be covered by existing meteorological knowledge. Thus, since I was evidently reluctant then to expose myself to risk of ridicule as one uninformed, I now have no one to blame other than myself if the experts here haven't provided solutions to problems of which they're as yet unaware.

This was advertised as a Summer Monsoon Conference, but in the presentation by a number of the speakers views have been expressed concerning the winter monsoon with which I'm not in complete accord. For instance, it has been implied that polar air does not cross the Annams during the Northeast Monsoon. Perhaps the trouble lies in our definition of polar air, but definitions is a subject I'll return to later. At this point I'll merely mention a couple reasons why I find the suggestion intolerable that a piddling little range like the Annams should be insurmountable. During the course of U.S. operations in support of Vietnam, photographic missions have been laid on to document the fact and magnitude of infiltration from North Vietnam into the Republic of Vietnam via the Ho Chi Minh trail. At one time these flights were severely restricted, and our biggest forecasting job was to ensure that on those few instances when aircraft were sent out they didn't return only with pictures of cloud tops. Now, not knowing that cold fronts couldn't cross the Annams, some of us were able to predict that systems leaving China on one day would cause a southwestward moving band of middle clouds to cross Laos into Thailand the next day, and while so doing produce conditions unfavorable for aerial photography. Generally thin and broken, we've since learned that these bands don't show up too well in weather satellite pictures; but there're quite a few aerial photos of them that forecasters who believed what it said in that book may still be trying to explain. Some of those bands, traced all the way from China, even produced rain west of the Annams during fall. Another feature is the sudden and pronounced increases in the lower tropospheric northeasterlies accompanying those bands. During early fall, these wind increases and the attendant cloud bands could top 700 mb; but as the winter progressed they tended to become shallower, and by spring didn't often top 850 mb. A related feature is the pronounced change so evident in satellite photos along the crest of the Annam range, from overcast to the east to clear to the west within an overall northeasterly flow regime. I contend that this clearing is primarily due to subsidence in air of polar origin streaming over the Annams from northeast to southwest. Some 2 years ago we began collecting SEASIA pilot weather reports; and should there be any who seriously doubt the continuity and southwestward movement of these cloud bands throughout most of the winter across the Annams and into Thailand, I would urge them to visit us in Norfolk.

An analogous situation is the manner in which the cloud and precipitation typically associated with the winter monsoon spreads southward across SEASIA during fall and the Indonesian Archipelago during early winter, and then later retreats northward. Additionally, there are those difficult-to-accept denials in the literature of any appreciable exchange of air between the hemispheres. It was suggested during this conference that there can be no feature comparable to the mean polar front of middle latitudes, which moves southward across SEASIA with the onset of winter. Apparently we have another definition problem, and by definition I mean description and explanation for the pronounced southward march of the leading edge of the winter Northeast Monsoon at the surface. A march which is accompanied by a singularly marked southward progress in the seasonal precipitation and cloud maximum, as described in an August 1967 Navy Weather Research Facility report by Dr. Riehl and myself.

In this regard, I found the paper by Mr. Southern extremely interesting, wherein he related Darwin atmospheric electricity data to atmospheric stability and the type of precipitation. It seems more than coincidence, that during the Australian summer with the onset at Darwin of the Southern Hemisphere northwest-monsoon extension of our Northeast Monsoon, there occurred a rather pronounced change from convective showers and generally lesser precipitation amounts to heavier precipitation from predominantly stratiform clouds. I, for one, will be interested to hear whether this is also characteristic of later years.

We're indebted to Dr. Fujita for indisputable proof that pronounced cloud systems move across the equator from one hemisphere into the other; and I believe it was also he who suggested that convective friction over the tropical ocean would slow a lower tropospheric air stream sufficiently, that after having crossed the equator it needn't return to its parent hemisphere via the "duty" inertial circle. Some of us who have contended that the Northeast Monsoon is a polar phenomenon have found the thought attractive that not only air but even weather systems could cross from one hemisphere into the other. We'll now be encouraged to increase the concentration of that with which we fill our pipes. Perhaps in following the succession from "cold front", to "polar air" to "modified polar air", to "air of polar origin", to "non-tropical low-latitude air," etc., we may even find ourselves proposing that some of the weather features observed over SEASIA during the Summer Monsoon originated from Southern Hemisphere middle-latitude influences.

However, there's fortunately no need to hypothesize whether polar air can penetrate into SEASIA during the Summer Monsoon season, unless it's a question as to how one defines summer. It was mentioned earlier, and I'll reiterate now so that there'll be no doubt, that polar surges not only can but do penetrate quite deeply into Vietnam and the South China Sea at least as late as the middle of June and as early as Labor Day, from my personal recollection and that of LT MILLS. We know for a fact that these surges came out of China and got at least as far south as 15° N. Here's another fact -- weak cold fronts with weak eastward moving waves on them are frequent visitors to the northern part of the South China Sea during the first half of June. Those of you now enroute there had better believe it. It was one of these polar surges that produced the clearing which permitted the first Hanoi-Haiphong POL strike in June 1966. I'm hopeful I'll have an opportunity to go back into the files and dig out cases where cold fronts slipped down the eastern slopes of the Himalayas and dipped into northern Tonkin Gulf during late August.

We ran into all kinds of definition problems in our studies of the Northeast Monsoon, and we seem to have even more during the summer season. It's become apparent during this conference: that there's no consensus as to what constitutes the Southwest Monsoon; when it may be considered to have set in; what is an equatorial trough and a monsoon trough -- whether they're the same feature or not; what is the relationship between these troughs, and the often-mentioned here and as often disputed inter-tropical convergence zone; we've a new feature called the buffer zone, which was not completely accepted as to name and nature; something well known along the east coast of Vietnam, the Winds of Laos, was discussed here but not explained to anybody's satisfaction; the once popularly accepted theory that summer precipitation and cloudiness in SEASIA is largely convective was seriously, and in my opinion conclusively, challenged; etc. I certainly hope that these and other like questions will be exhaustively examined by the participants in the work shop to follow, and that as a result we achieve acceptable definitions -- with objective descriptions and physical explanations -- for them. I do not consider this an academic matter. At the moment we're busting too many forecasts wherein we have no understanding of what happened. Research on these problems is handicapped by an inability to communicate with terms which are universally understood. There's still too much of the "that cloud bit there" approach we hear so much of in satellite matters to our research in this area.

WANN: Maybe due to the fact that southeast Asia is a maximum solar energy input area as compared to the rest of the world, the transition (onset) of the southwest monsoon is blurred in this area. This energy input I feel should be considered in the forecasting of the onset of the southwest monsoon.

THORMEYER: The Fleet Numerical Weather Central is currently developing an analog selection technique, which has applicability in forecasting the onset of the southwest monsoon in the South China Sea. Since we don't understand completely the synoptic and dynamic interactions that affect the monsoon, we can take a philosophical approach. If we can find a date in the past that is analogous to the current date, we make the assumption that the same dynamic and synoptic influence that occurred then, even though we didn't understand that influence, will occur again this year with similar weather sequences.

On 24 March 1969 FLENUMWEACEN forecast onset of the southwest monsoon over the South China Sea to commence within a few days of 1 May 1969. "Onset" is defined as the time the predominant wind flow throughout the entire South China Sea ceases to be from the NE-SE quadrant and starts predominating from the SE-SW quadrant.

BUCKMASTER: Too much emphasis being placed upon "Monsoon," "Monsoon Onset" (Dates). If we can't define it in an agreed upon way, then we should de-emphasize the terms.

ATKINSON: The Air Weather Service is preparing a set of monthly mean resultant gradient level (3,000 ft.) streamline-isotach charts for the entire tropical belt from 35° N. to 35° S. The data sources include all climatological winds available at ETAC, wind data from national climatological publications, and mean resultant surface winds summarized from ship reports. These charts will be printed on a 1:20,000,000 mercator projection with two charts (60° E. - 120° W., 120° W. - 60° E.) used to cover the tropical belt. Overlapping analyses will be used at the east and west boundaries so the maps can be put together to cover any part or all of the tropics. Analysis will be completed in June 1969 and the charts will be published sometime this Fall.

SOUTHERN: On a somewhat philosophical note as the Conference is concluding, and bearing in mind the advent of World Weather Watch that will bring to us global analyses in real time, it seems desirable that the major global influences controlling weather be defined. The summer monsoon of southeast Asia has been described as the most significant natural phenomenon on earth recurring annually. It appears reasonable to postulate that its seasonal variations will be determined by other major global features. Maybe we should look for anomalies occurring two or three months prior to its establishment in such systems as the Siberian High, the upwelling off the west coast of South America which leads to stability of the South Pacific anticyclone, radiation or insolation over the polar icecaps, variations in the subtropical jet streams and so on. These may well influence the immense Hadley-type meridional circulations which convey energy to and from the equatorial regions. We must be careful not to obscure global wood by the local trees.

CONOVER: Question to operations people: How badly do you need the detailed type forecasts that it appears may be possible by expansion of the Perm State studies? Are you willing to pay the price for aircraft doppler winds at 850 mb.?

FENTON: Concerning the onset of the monsoon. Since the onset and movement of the monsoon is affected by the continual supply of air from the southern hemisphere, the work being done in the Department of Geosciences of the University of Hawaii concerning trajectories of flow from the southern to northern hemisphere may be useful in estimating the amount of flow from the southern to the northern hemisphere.